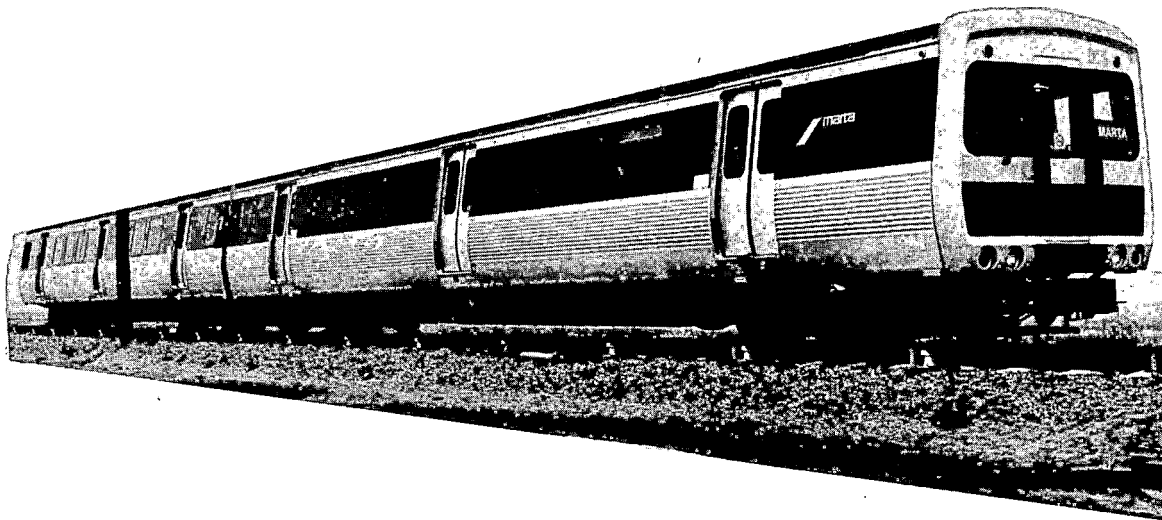


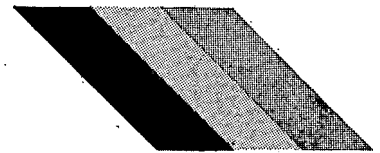
METROPOLITAN ATLANTA RAPID TRANSIT AUTHORITY

TRANSIT VEHICLE ENGINEERING TESTS



U.S. DEPARTMENT OF TRANSPORTATION
TRANSPORTATION TEST CENTER
PUEBLO, COLORADO

marta[®]



401 W. PEACHTREE ST. NE
ATLANTA, GEORGIA

NOTICE

This document is disseminated under the sponsorship of the Department of Transportation in the interest of information exchange. The United States Government assumes no liability for its contents or use thereof.

The United States Government does not endorse products or manufacturers. Trade or manufacturers' names appear herein solely because they are considered essential to the object of this report.

1. Report No. FRA/TTC-81/05		2. Government Accession No.		3. Recipient's Catalog No.	
4. Title and Subtitle Metropolitan Atlanta Rapid Transit Authority Transit Vehicle Engineering Tests				5. Report Date August, 1981	
				6. Performing Organization Code	
7. Author(s) H. Mutter, K. Simmonds, G. Arnold, B. Carter, F. Irani, J. Elkins, B. Swearingen, and R. Dighe*				8. Performing Organization Report No.	
9. Performing Organization Name and Address Transportation Test Center P.O. Box 11449 Pueblo, CO 81001				10. Work Unit No. (TRAIS)	
				11. Contract or Grant No.	
				13. Type of Report and Period Covered FINAL REPORT May 1980 - January 1981	
12. Sponsoring Agency Name and Address U.S. Department of Transportation Urban Mass Transportation Administration Office of Technology Development and Deployment Office of Rail and Construction Technology Washington, D.C. 20590				14. Sponsoring Agency Code	
				15. Supplementary Notes *Boeing Services International, Inc., Operations and Maintenance Contractor, Transportation Test Center, Pueblo, Colorado, 81001, Contract DTFR-80-C-20016 with the Federal Railroad Administration	
16. Abstract <p>This report presents the results of engineering tests conducted on a married pair of rapid transit cars for the Metropolitan Atlanta Rapid Transit Authority (MARTA). The tests were performed at the Transportation Test Center, Pueblo, Colorado, from May 1980 through January 1981. The scope of the test program included evaluation of performance, ride quality, and interior and wayside noise using standardized test procedures; special engineering tests were made to evaluate energy conservation methods, three brake configurations, and three vertical damping configurations. Vehicle curving tests were conducted to investigate the behavior of the vehicle on sharply curved track, to determine the effect of certain modifications to the track, and to derive wheel flange wear indices.</p> <p>The tests showed that the vehicles met the acceleration and time to speed specification requirements. The first two brake configurations evaluated failed to meet requirements in any braking mode. The final brake configuration meets braking rate requirements for friction only and emergency modes but falls short of requirements in the dynamic and blended mode above 40 mi/h. Wheel flange wear indices were developed for variations in axle misalignments and primary suspension longitudinal stiffness.</p>					
17. Key Words Rail Vehicles Rapid Transit Vehicles Noise Curving Brakes Performance Ride Quality Energy Conservation			18. Distribution Statement This document is available to the public through the: National Technical Information Service 5285 Port Royal Road Springfield, Virginia 22161		
19. Security Classif. (of this report) Unclassified		20. Security Classif. (of this page) Unclassified		21. No. of Pages 383	22. Price

ACKNOWLEDGEMENT

The Transportation Test Center wishes to acknowledge the training and maintenance publications of Garrett-Airesearch Manufacturing Company, Rockwell International, and Societe Franco-Belge de Material de Chemin de Fer, and the vehicle procurement specification written by Parsons, Brinkerhoff, and Tudor, which were used to provide information and illustrations for this report.

TABLE OF CONTENTS

<u>Section</u>	<u>Page</u>
EXECUTIVE SUMMARY	xxv
1.0 INTRODUCTION	1-1
1.1 Background	1-1
2.0 TEST PROGRAM SCOPE	2-1
2.1 Purpose	2-1
2.2 Program Summary	2-1
2.3 Test Variables	2-2
2.3.1 Controller Level	2-2
2.3.2 Speed	2-2
2.3.3 Line Voltage	2-2
2.3.4 Vehicle Weights	2-3
2.3.5 Track Type	2-3
2.3.6 Vehicle Configuration	2-3
2.4 Test Program	2-4
2.4.1 Performance	2-4
2.4.2 Ride Quality	2-6
2.4.3 Noise	2-6
2.4.4 Electromagnetic Interference	2-7
2.4.5 Fault Clearing	2-7
2.4.6 Static Truck Tests	2-7
2.4.7 Structural Vibration Response	2-8
2.4.8 Curving and Stability	2-9
2.4.9 Radio Frequency Interference	2-10
3.0 VEHICLE DESCRIPTION	3-1
3.1 General	3-1
3.2 Design Specification	3-1
3.3 Carbody	3-3
3.4 Trucks and Suspension	3-4
3.5 Propulsion and Control System	3-4
3.6 Spin/Slide Protection System	3-8
3.7 Traction Motors and Transmissions	3-8
3.8 Friction Braking System	3-9
3.9 Doors	3-9
3.10 Auxiliary Power Supply	3-10
3.11 Heating, Ventilation, and Air Conditioning	3-10
3.12 Train Controls	3-11
3.13 Vehicle Configurations	3-11
4.0 DESCRIPTION OF FACILITIES	4-1

TABLE OF CONTENTS, CONTINUED

<u>Section</u>	<u>Page</u>
4.1 Transit Test Track	4-1
4.2 FAST Track and Balloon Loop	4-6
4.3 Climatic Conditions	4-6
5.0 INSTRUMENTATION, DATA ACQUISITION, AND DATA PROCESSING	5-1
6.0 PERFORMANCE TESTS	6-1
6.1 Acceleration	6-1
6.1.1 Test Objective	6-1
6.1.2 Test Method	6-2
6.1.3 Test Results	6-2
6.2 Deceleration	6-18
6.2.1 Test Objectives	6-18
6.2.2 Test Method	6-19
6.2.3 Test Results	6-19
6.3 Duty Cycle Tests	6-50
6.3.1 Test Objectives	6-50
6.3.2 Test Method	6-50
6.3.3 Test Results	6-54
6.4 Spin/Slide Tests	6-60
6.4.1 Test Objective	6-60
6.4.2 Test Method	6-61
6.4.3 Test Results	6-61
6.5 Energy Consumption	6-67
6.5.1 Test Objectives	6-67
6.5.2 Test Method	6-67
6.5.3 Test Results	6-70
6.6 Drift Test	6-82
6.6.1 Test Objective	6-82
6.6.2 Test Method	6-83
6.6.3 Test Results	6-83
6.7 Jerk Limit and Control Response Tests	6-91
6.7.1 Test Objectives	6-91
6.7.2 Test Method	6-92
6.7.3 Test Results	6-92

TABLE OF CONTENTS, CONTINUED

<u>Section</u>	<u>Page</u>
7.0 RIDE QUALITY	7-1
7.1 Component Induced Vibration	7-3
7.1.1 Test Objective	7-3
7.1.2 Test Method	7-5
7.1.3 Test Results	7-5
7.2 Speed Effect	7-5
7.2.1 Test Objective	7-5
7.2.2 Test Method	7-9
7.2.3 Test Results	7-9
7.3 Track Section Effect	7-16
7.3.1 Test Objective	7-16
7.3.2 Test Method	7-16
7.3.3 Test Results	7-16
7.4 Car Weight Effect	7-28
7.4.1 Test Objective	7-28
7.4.2 Test Method	7-28
7.4.3 Test Results	7-28
7.5 Suspension Effect	7-28
7.5.1 Test Objective	7-28
7.5.2 Test Method	7-35
7.5.3 Test Results	7-35
7.6 Direction Effect	7-35
7.6.1 Test Objective	7-35
7.6.2 Test Method	7-41
7.6.3 Test Results	7-41
7.7 Acceleration, Deceleration Effect	7-41
7.7.1 Test Objective	7-41
7.7.2 Test Method	7-41
7.7.3 Test Results	7-46
8.0 NOISE TESTS	8-1
8.1 Instrumentation	8-1
8.1.1 Sound Level Indicating Equipment	8-1
8.1.2 Sound Recording Equipment	8-3

TABLE OF CONTENTS, CONTINUED

<u>Section</u>	<u>Page</u>
8.2 Analysis Equipment	8-4
8.3 Test Results	8-4
8.3.1 Equipment Noise Characteristics at Wayside, Car Stationary	8-6
8.3.2 Equipment Noise Characteristics, Car Stationary	8-17
8.3.3 Noise Level Variation with Location Onboard, Car Travelling at 55 mi/h	8-27
8.3.4 Noise Characteristic at a Number of Steady Speeds, Onboard, 0-70 mi/h	8-30
8.3.5 Noise Characteristic Under Acceleration and Deceleration Onboard	8-31
8.3.6 Noise Characteristic with Track Construction	8-33
8.3.7 Noise Characteristic with Steady Speeds, at Wayside 0 to 70 mi/h	8-42
8.4 Conclusions	8-47
8.4.1 External Noise	8-47
8.4.2 Internal Noise	8-49
9.0 DYNAMIC SHAKE TEST AND EQUIPMENT RESONANCE TESTS	9-1
9.1 Dynamic Shake Test	9-1
9.1.1 Test Objective	9-1
9.1.2 Test Method	9-1
9.1.3 Instrumentation	9-1
9.1.4 Test Results	9-8
9.2 Equipment Resonance Tests	9-8
9.2.1 Objective	9-8
9.2.2 Test Method	9-8
9.2.3 Instrumentation	9-13
9.2.4 Test Results	9-13
10.0 CURVING	10-1
10.1 Introduction	10-1
10.2 Test Objective	10-1
10.3 Static Tests	10-3
10.3.1 General	10-3
10.3.2 Test Methods	10-3
10.3.3 Test Results	10-6

TABLE OF CONTENTS, CONTINUED

<u>Section</u>	<u>Page</u>
10.4 Track Tests	10-10
10.4.1 Test Instrumentation	10-10
10.4.2 Test Method	10-15
10.4.3 Test Results and Comparison with Theoretical Predictions	10-23
10.5 Wear Index Predictions	10-38
10.6 Conclusions and Recommendations	10-50
11.0 ELECTROMAGNETIC INTERFERENCE	11-1
11.1 Introduction	11-1
11.2 Test Objectives	11-1
11.3 Test Procedures	11-6
11.3.1 Isolated Carbody, No Return Current Under Car	11-6
11.3.2 Isolated Carbody, Return Current Under Car	11-6
11.3.3 Wheels on Rails, Return Current Under Car	11-8
11.4 Data Analysis	11-8
11.5 Test Results	11-16
12.0 FAULT CLEARING TESTS	12-1
12.1 Test Objectives	12-1
12.2 Test Methods	12-1
12.2.1 Test Locations	12-1
12.3 Test Results	12-1
13.0 RADIO FREQUENCY INTERFERENCE	13-1
APPENDIX A - INSTRUMENTATION, DATA ACQUISITION, AND DATA PROCESSING	A-1
1.0 INSTRUMENTATION	A-2
2.0 DATA ACQUISITION	A-15
3.0 DATA PROCESSING	A-21

LIST OF FIGURES

<u>Figure</u>	<u>Page</u>
3-1 MARTA Cars at the Transportation Test Center	3-2
3-2 Truck Frame, Showing Articulation Joints	3-5
3-3 Truck General Arrangement	3-6
3-4 Truck Primary & Secondary Suspension	3-13
3-5 Bushing Modifications, Configuration C2	3-14
4-1 Transit Test Track	4-2
4-2 Transit Test Track Profile Showing Grades	4-3
4-3 TTC Test Tracks General Layout	4-7
4-4 Layout of the FAST Track	4-8
6-1 Full Power Acceleration Characteristics	6-4
6-2 Effect of Line Voltage and Master Controller Position on Time-to-Speed	6-5
6-3 Effect of Vehicle Weight on Acceleration	6-6
6-4 Effect of Vehicle Weight on Time-to-Speed	6-7
6-5 Tractive Effort/Control Signal Relationship	6-9
6-6 Acceleration--Full Power and P2 Master Controller Position	6-10
6-7 Acceleration Performance--Comparison of BR3 with BR2 Configuration at AW0 and AW3 Weight	6-11
6-8 Acceleration Performance--Comparison of BR3 with BR2 Configuration at AW2 Weight	6-12
6-9 Effect of Vehicle Weight on Time-to-Speed for BR3 and BR2 Configurations	6-13
6-10 Acceleration Performance--Comparison of BR3 and BR2 Configurations at 550 V d.c. and 825 V d.c.	6-14
6-11 Comparison of BR2 and BR3 Configurations with Line Voltage	6-15
6-12 Comparison of BR2 Configuration with BR3 Configuration at P2 Controller Position	6-16
6-13 Blended Braking Deceleration Characteristics, AW0 Weight	6-21

LIST OF FIGURES, CONTINUED

<u>Figure</u>	<u>Page</u>
6-14 Blended Braking Deceleration Characteristics, AW2 Weight	6-22
6-15 Blended Braking Deceleration Characteristics, AW3 Weight	6-23
6-16 Blended Braking--Deceleration Characteristics	6-24
6-17 Blended Braking--Stopping Distance and Time Characteristics, Full Service Braking	6-25
6-18 Friction Braking--Deceleration Characteristics, AW0 Weight	6-26
6-19 Friction Braking--Deceleration Characteristics, AW2 Weight	6-27
6-20 Friction Braking--Deceleration Characteristics, AW3 Weight	6-28
6-21 Friction Braking--Deceleration Characteristics	6-30
6-22 Friction Braking--Stopping Distance and Time Characteristics	6-31
6-23 Dynamic Braking--Deceleration Characteristics, AW0 Weight	6-32
6-24 Dynamic Braking--Deceleration Characteristics, AW2 Weight	6-33
6-25 Dynamic Braking--Deceleration Characteristics	6-34
6-26 Dynamic Braking--Stopping Distance and Time Characteristics	6-35
6-27 Effect of Initial Speed on Emergency Braking, AW0 and AW2 Weights	6-37
6-28 Effect of Initial Speed on Emergency Braking, AW3 Weight	6-38
6-29 Effect of Weight on Emergency Braking	6-39
6-30 Emergency Braking--Effect of Initial Speed on Time and Distance Required to Stop	6-40
6-31 Effect of Brake Mode on Braking Performance, 70 and 35 mi/h Initial Speed	6-41
6-32 Effect of Brake Mode on Braking Time to Stop	6-42
6-33 Effect of Brake Configuration on Blended and Dynamic-Only Braking Modes	6-44
6-34 Effect of Brake Configuration on Friction and Emergency Braking Modes	6-45

LIST OF FIGURES, CONTINUED

<u>Figure</u>	<u>Page</u>
6-35 Effect of Brake Configuration on Time to Stop, Dynamic and Friction Brakes	6-46
6-36 Effect of Brake Configuration on Time to Stop, Emergency and Blended Brakes	6-47
6-37 Effect of Brake Configuration on Distance to Stop, Dynamic and Friction Brakes	6-48
6-38 Effect of Brake Configuration on Distance to Stop, Emergency and Blended Brakes	6-49
6-39 Undercar Equipment Location	6-51
6-40 Undercar Thermocouple Locations	6-52
6-41 Friction Braking--Duty Cycles	6-56
6-42 Blended Braking Duty Cycle Temperature Time Histories	6-58
6-43 Definition of Spin/Slide Efficiency from Vehicle Specification	6-62
6-44 Deceleration with Spin/Slide Protection, Time History	6-64
6-45 Effect of Speed on Energy Consumed by Auxiliary Systems	6-71
6-46 Effect of Line Voltage on Power Demand During Full Service Acceleration	6-72
6-47 Effect of Vehicle Weight and Direction on Power Demand During Full Service Acceleration	6-73
6-48 Energy Consumption, Constant Speeds--Effect of Vehicle Direction	6-74
6-49 Energy Consumption, Constant Speeds--Comparison of Car A and Car B	6-75
6-50 Input Energy Consumption Under Full Service Acceleration to Speed--Effect of Direction of Travel	6-77
6-51 Input Energy Consumption Under Full Service Acceleration to Speed--Comparison of Cars A and B	6-78
6-52 Braking Resistor Energy During Full Service Blended Braking Stops	6-80
6-53 Speed-Time History from Initial Speed of 21 mi/h	6-84

LIST OF FIGURES, CONTINUED

<u>Figure</u>	<u>Page</u>
6-54 Deceleration Characteristics Due to Train Resistance, Brake Shoes in Contact	6-85
6-55 Deceleration Characteristics Due to Train Resistance, Brake Shoes Out of Contact	6-86
6-56 Resistance/Speed Characteristics--Brake Shoes In/Out of Contact	6-88
6-57 Brake Shoe Drag Resistance Characteristic	6-89
6-58 Energy Dissipated by Brake Shoe Drag	6-90
6-59 Control Response and Jerk Limit Specification Requirements	6-93
6-60 Definition of Zero Time Reference for Control Response Evaluation	6-95
6-61 Typical Drive/Brake/Drive Mode Change	6-96
6-62 Jerk Rates for Propulsion System Mode Changes	6-98
6-63 Jerk Rates for Propulsion Mode Change, 750 V d.c.	6-99
6-64 Jerk Rates for Propulsion Mode Change, 550 V d.c.	6-100
6-65 Jerk Rates for Propulsion Mode Changes, 800 V d.c.	6-101
7-1 Ride Quality Accelerometer Locations	7-2
7-2 ISO Weighting Curves	7-4
7-3 Component-Induced Vibration (Vertical)--Forward Floor Centerline (Over Truck Pivot)	7-7
7-4 Component-Induced Vibration (Vertical)--Midfloor Centerline	7-7
7-5 Ride Quality Criteria	7-8
7-6 Carbody Mode Excitation Spectrum	7-10
7-7 Comparison of Vertical Ride Quality to Vehicle Specification, Forward Car Centerline	7-11
7-8 Comparison of Lateral Ride Quality to Vehicle Specification, Forward Floor Centerline	7-12
7-9 Comparison of Vertical Ride Quality to Vehicle Specification, Midfloor Centerline	7-13

LIST OF FIGURES, CONTINUED

<u>Figure</u>	<u>Page</u>
7-10 Comparison of Ride Quality to Specification--Speed Effect	7-14
7-11 Comparison of Ride Quality to Specification--Speed Effect	7-15
7-12 Effect of Vehicle Speed on Ride Roughness	7-18
7-13 Effect of Vehicle Speed on Ride Roughness	7-19
7-14 Comparison of Vertical Ride Quality to Vehicle Specification-- Track Section Effect, Forward Floor Centerline	7-20
7-15 Comparison of Lateral Ride Quality to Vehicle Specification-- Track Section Effect, Forward Floor Centerline	7-21
7-16 Comparison of Vertical Ride Quality to Vehicle Specification-- Track Section Effect, Midfloor Centerline	7-22
7-17 Comparison of Ride Quality to Vehicle Specification--Track Section Effect	7-23
7-18 Lead Truck Bolster Grounding	7-25
7-19 Effect of Track Section on Ride Roughness	7-26
7-20 Effect of Track Section on Ride Roughness	7-27
7-21 Comparison of Vertical Ride Quality to Vehicle Specification-- Weight Effect, Forward Floor Centerline	7-29
7-22 Comparison of Lateral Ride Quality to Vehicle Specification-- Weight Effect, Forward Floor Centerline	7-30
7-23 Ride Quality to Specification Comparison (Vertical)--Weight Effect, Midfloor Centerline	7-31
7-24 Ride Quality Specification Comparison--Weight Effect	7-32
7-25 Effect of Vehicle Weight on Ride Roughness	7-33
7-26 Effect of Vehicle Weight on Ride Roughness	7-34
7-27 Comparison of Vertical Ride Quality to Vehicle Specification-- Suspension Effect, Forward Floor Centerline	7-36
7-28 Comparison of Lateral Ride Quality to Vehicle Specification-- Suspension Effect, Forward Floor Centerline	7-37
7-29 Comparison of Vertical Ride Quality to Vehicle Specification-- Suspension Effect, Midfloor Centerline	7-38

LIST OF FIGURES, CONTINUED

<u>Figure</u>	<u>Page</u>
7-30 Effect of Suspension Configuration on Ride Roughness	7-39
7-31 Effect of Suspension Configuration on Ride Roughness	7-40
7-32 Comparison of Vertical Ride Quality to Vehicle Specification-- Consist Direction Effect, Forward Floor Centerline	7-42
7-33 Comparison of Lateral Ride Quality to Vehicle Specification-- Consist Direction Effect, Forward Floor Centerline	7-43
7-34 Comparison of Vertical Ride Quality to Vehicle Specification-- Consist Direction Effect, Midfloor Centerline	7-44
7-35 Effect of Vehicle Direction on Ride Roughness	7-45
7-36 Forward Floor Centerline--Vertical Vibration During Maximum Acceleration	7-47
7-37 Forward Floor Centerline Lateral Vibration During Maximum Acceleration	7-48
7-38 Midfloor Centerline--Vertical Vibration During Maximum Acceleration	7-49
7-39 Midfloor Centerline--Lateral Vibration During Maximum Acceleration	7-50
7-40 Midfloor Left--Vertical Vibration During Maximum Acceleration	7-51
7-41 Forward Floor Centerline--Vertical Vibration During Full Blended Braking	7-52
7-42 Forward Floor Centerline--Lateral Vibration During Full Blended Braking	7-53
7-43 Midfloor Centerline--Vertical Vibration During Full Blended Braking	7-54
7-44 Midfloor Centerline--Lateral Vibration During Full Blended Braking	7-55
7-45 Midfloor Left--Vertical Vibration During Full Blended Braking	7-56
7-46 Forward Floor Centerline--Vertical Vibration During Full Friction-Only Braking	7-57
7-47 Forward Floor Centerline--Lateral Vibration During Full Friction-Only Braking	7-58

LIST OF FIGURES, CONTINUED

<u>Figure</u>	<u>Page</u>
7-48 Midfloor Centerline--Vertical Vibration During Full Friction-Only Braking	7-59
7-49 Midfloor Centerline--Lateral Vibration During Full Friction-Only Braking	7-60
7-50 Midfloor Left--Vertical Vibration During Full Friction-Only Braking	7-61
8-1 Acoustic Instrumentation	8-2
8-2 Analysis Equipment	8-5
8-3 Wayside Measurement Locations	8-7
8-4 'A' Weighted Wayside Sound Levels 15' from Track Centerline: Cars Stationary, Configuration 1	8-10
8-5 'A' Weighted Wayside Sound Levels 15' from Track Centerline: Cars Stationary, Configuration 1a	8-10
8-6 'A' Weighted Wayside Sound Levels 15' from Track Centerline: Cars Stationary, Configuration 2	8-11
8-7 'A' Weighted Wayside Sound Levels 15' from Track Centerline: Cars Stationary, Configuration 3	8-11
8-8 'A' Weighted Wayside Sound Levels 15' from Track Centerline: Cars Stationary, Configuration 4	8-12
8-9 'A' Weighted Wayside Sound Levels 15' from Track Centerline: Cars Stationary, Configuration 5	8-12
8-10 'A' Weighted Wayside Sound Levels 15' from Track Centerline: Cars Stationary, Configuration 6	8-13
8-11 'A' Weighted Wayside Sound Levels 15' from Track Centerline: Cars Stationary, Configuration 7	8-13
8-12 'A' Weighted Wayside Sound Levels 50' from Track Centerline: Cars Stationary, Configuration 5	8-14
8-13 1/3 Octave Spectrum: Wayside, Car 0109 Stationary	8-15
8-14 1/3 Octave Spectrum: Wayside, Car 0110 Stationary	8-16
8-15 Onboard Measurement Locations, Cars Stationary	8-18
8-16 Onboard 1/3 Octave Spectra: APSE Energized Only	8-21

LIST OF FIGURES, CONTINUED

<u>Figure</u>	<u>Page</u>
8-17 Onboard 1/3 Octave Spectra: Beneath Air Conditioning Fan Outlet	8-23
8-18 Onboard 1/3 Octave Spectra: 'Seated', Location 3 - APSE and TM Fans Energized	8-24
8-19 Onboard 1/3 Octave Spectra: 'Standing', Center of Car, Auxiliary Equipment Energized	8-25
8-20 Onboard 1/3 Octave Spectra: 'Seated', Location 3 - APSE and TM Fans Energized	8-26
8-21 Car Interior Noise Level Limits	8-28
8-22 Onboard Measurement Locations, 'A' Weighted Sound Levels: Car 0109 at Steady Speed of 55 mi/h	8-29
8-23 Onboard 1/3 Octave Spectra: 'Standing', Center of Car - Auxiliaries Energized	8-32
8-24 'A' Weighted Sound Levels vs. Speed: Car 0109 Acceleration	8-34
8-25 Car 0109 (Full Power Acceleration: 0 to 60 mi/h), 'A' Weighted Sound Level Time History	8-35
8-26 'A' Weighted Sound Levels vs. Speed: Car 0109 Deceleration	8-36
8-27 Car 0109, 'A' Weighted Sound Level Time Histories--Braking: Blended and Friction-Only	8-37
8-28 'A' Weighted Sound Level Time Histories at 55 mi/h for Three Track Construction Types, Car 0109	8-39
8-29 'A' Weighted Sound Level Time Histories at 55 mi/h, Showing Change from Coast to Power, and Change Over Switch	8-40
8-30 'A' Weighted Sound Level Time History at 55 mi/h, with Auxiliaries Deenergized	8-41
8-31 Comparison of Pen Writing Speeds Equivalent to Meter Characteristics at Speed of 55 mi/h, Track Section III	8-43
8-32 'A' Weighted Sound Levels 50' from Each Side of Track, 4 Pass-By Speeds	8-44
8-33 Sound Level Time Histories 50' on Inside of Loop, 4 Pass-By Speeds	8-45

LIST OF FIGURES, CONTINUED

<u>Figure</u>	<u>Page</u>
8-34 Sound Level Time Histories 50' on Outside of Loop, 4 Pass-By Speeds	8-46
8-35 1/3 Octave Spectrum, Wayside Pass-By	8-48
9-1 Typical Shake Test Analog Traces	9-2
9-2 Structural Model, Showing Actuators and Accelerometer Measurement Locations	9-6
9-3 Block Diagram of Instrumentation, Signal Conditioning, and Data Acquisition Systems	9-7
9-4 Actuator Locations	9-9
9-5 Actuator Attachment	9-10
9-6 Mode Shapes due to Vertical Excitation, AWO Car Weight	9-11
9-7 Mode Shapes due to Lateral and Torsional Excitation	9-12
10-1 Typical Worn Wheel in Atlanta	10-2
10-2 Gage Face Wear in Avondale Yard	10-2
10-3 Primary Suspension Bush Stiffness Test Rig	10-4
10-4 Measuring Axle Alinement	10-7
10-5 Close-Up of Axle Alinement Measurement	10-7
10-6 Truck Axle Misalignment	10-9
10-7 String Potentiometer, Truck Yaw Angle Measurement	10-11
10-8 Primary Longitudinal and Lateral Displacement Measurement	10-11
10-9 Side View of Truck with Angle of Attack Frames	10-12
10-10 Close-Up of Angle of Attack Probe	10-13
10-11 MARTA Curving Test, Train Consist	10-18
10-12 Wheel Profile, Configurations C1 and C2 Compared with Design Case AAR 1:20 Profile	10-20
10-13 Wheel Profilometer	10-21
10-14 Rail Profilometer	10-21

LIST OF FIGURES, CONTINUED

<u>Figure</u>	<u>Page</u>
10-15 Wheel Profile, Configuration C3 Compared with Design Case CN-A Profile	10-22
10-16 Typical Rail Profiles for Balloon Loop Compared with Design Case 136 lb/yd Rail	10-25
10-17 Lead Axle Angle of Attack vs. Speed (Balloon Loop 7.4° Curve)	10-26
10-18 Truck Angle of Attack vs. Speed (Balloon Loop, 7.4° Curve)	10-27
10-19 Leading Axle Primary Yaw Displacement (Balloon Loop, 7.4° Curve)	10-28
10-20 Trailing Axle Primary Yaw Displacement (Balloon Loop, 7.4° Curve)	10-30
10-21 Truck Curving Diagrams (Balloon Loop, 7.4° Curve, Right Hand)	10-31
10-22 Truck Curving Diagrams (Balloon Loop, 7.4° Curve, Left Hand)	10-32
10-23 Typical Rail Profiles for FAST Section 07 Compared with Design Case 140 lb/yd Rail	10-33
10-24 Leading Axle High Rail Lateral Force vs. Speed (FAST Section 07, 5.2° Curve)	10-34
10-25 Leading Axle Angle of Attack vs. Speed (TTT, 1.5° Right-Hand Curve)	10-35
10-26 Leading Axle Primary Yaw Displacement vs. Speed (TTT, 1.5° Right-Hand Curve)	10-36
10-27 Trailing Axle Primary Yaw Displacement vs. Speed (TTT, 1.5° Right-Hand Curve)	10-37
10-28 Theoretical Lead Axle Angle of Attack vs. Track Curvature	10-39
10-29 Theoretical High Rail Lateral Force vs. Track Curvature	10-39
10-30 Sample Wear Rate vs. Wear Index from Laboratory Experiment	10-40
10-31 Predicted Effect of Primary Longitudinal Stiffness on Wear Index	10-42

LIST OF FIGURES, CONTINUED

<u>Figure</u>	<u>Page</u>
10-32 Predicted Effect of Primary Longitudinal Stiffness on Wear Index	10-42
10-33 Predicted Effect of Radial Axle Misalignment on Wear Index	10-43
10-34 Predicted Effect of Lateral Axle Misalignment on Wear Index	10-43
10-35 Predicted Effect of Radial Axle Misalignment on Wear Index	10-44
10-36 Predicted Effect of Lateral Axle Misalignments on Wear Index	10-44
10-37 Predicted Effect of Carbody Weight on Wear Index	10-46
10-38 Predicted Effect of Carbody Weight on Wear Index	10-46
10-39 Predicted Effect of Wheel Cross-Sectional Profile on Wear Index	10-47
10-40 Effect of Truck Carbody Yaw Pivot Friction Torque on Wear Index	10-47
10-41 Effect of Traction and Braking on Wear Index	10-48
10-42 Effect of Traction and Braking on Wear Index	10-48
10-43 Effect of Cant Deficiency on Wear Index	10-49
11-1 Test Configuration: Isolated Carbody, No Return Current Under Car	11-2
11-2 Test Configuration: Isolated Carbody, Return Current Under Car	11-3
11-3 Test Configuration: Wheels on Rails, Return Current Under Car	11-4
11-4 Loop Positions Relative to Propulsion Components	11-5
11-5 Undercar Induced Voltage, Amplitude and Frequency Distribution	11-7
11-6 Equivalent Search Coil Differential Voltages (400 Hz Component)	11-15
12-1 Traction Motor Armature Fault Protection, Test Circuit	12-5
12-2 Armature Fault Current Profile	12-6
12-3 PCE Blower Motor Fault Protection, Test Circuit	12-7

LIST OF FIGURES, CONTINUED

<u>Figure</u>	<u>Page</u>
12-4 PCE Blower Motor Short-Circuit Current and Voltage Waveforms	12-8
12-5 VLC Output Fault Protection, Test Circuit	12-9
12-6 VLC Output Fault Current and Voltage Waveforms	12-10
12-7 LVPS Output Fault Protection, Test Circuit	12-11
12-8 LVPS Output Fault Current and Voltage Waveforms	12-12
12-9 A/B Car CB Input and Output Side Short Circuit, Test Circuit	12-15
12-10 Third Rail Collector Shoe Grounding Through Shoe Fuse, with Knife Switch Open	12-16
12-11 Voltage and Current Waveforms (Station 33), Third Rail Collector Shoe Grounding Test	12-17
12-12 Voltage and Current Waveforms (Station 30), Collector Shoe Grounding Test	12-18
12-13 Third Rail Collector Shoe Grounding Through Main Fuse, Knife Switch, and Shoe Fuse	12-19
12-14 Voltage and Current Waveforms at Station 30--Third Rail Collector Shoe Grounding Through Main Fuse and Knife Switch	12-20
12-15 Third Rail Collector Shoe Grounding Through Circuit Breaker, Main Fuse, Knife Switch, and Shoe Fuse	12-21

LIST OF TABLES

<u>Table</u>	<u>Page</u>
2-1 Vehicle Weights	2-3
4-1 TTT Construction Details	4-4
4-2 Amplitude and Waveforms of TTT Perturbations, Design Specifications	4-5
6-1 Vehicle Specification Time-to-Speed Criteria Compared with Test Data	6-8
6-2 MARTA East-West Profile, Outbound	6-53

LIST OF TABLES, CONTINUED

<u>Table</u>	<u>Page</u>
6-3 MARTA East-West Profile, Return	6-53
6-4 MARTA Thermal Capacity Profile	6-55
6-5 Friction-Only Braking--Duty Cycle Undercar Temperatures	6-57
6-6 Blended Braking--Duty Cycle Undercar Temperatures	6-59
6-7 Spin/Slide Test Data	6-66
6-8 ACT-1 Simulated Line Profile	6-69
6-9 Consumed Energy Comparisons, Cars A and B vs. MARTA/ACT-1 Profile Runs	6-81
6-10 Propulsion Mode Change Sequence	6-94
6-11 Transition Times for Mode Changes, Configuration BR2	6-102
6-12 Transition Times for Mode Changes, Configuration BR3	6-102
7-1 Equipment in Operation During Measurements of Component-Induced Vibration	7-6
7-2 Carbody Modal Frequencies, AWO Weight	7-17
8-1 Equipment Operating During A Car Wayside Noise Tests	8-8
8-2 Equipment Operating During B Car Wayside Noise Tests	8-8
8-3 'A' Weighted Sound Levels; Interior Noise, Stationary Cars	8-20
8-4 'A' Weighted Sound Levels ('Slow' Meter Characteristic)	8-30
8-5 Hand-Held Meter Readings, Midcar Sound Levels, Track Sections I Through VII	8-38
9-1 Excitation Tests, Data Acquisition and Analysis	9-3
9-2 Accelerometers for Undercar Equipment Analysis	9-14
9-3 Critical Frequencies for Undercar Equipment	9-16
10-1 MARTA Truck Parameters	10-8
10-2 Instrumentation Sensor Listing, Curving/Stability	10-14
10-3 Data for Curved Track Test Sites	10-16

LIST OF TABLES, CONTINUED

<u>Table</u>	<u>Page</u>
10-4 Truck Radial and Lateral Misalignment	10-41
11-1 Search Coil Fundamental and Harmonic Voltages (mV): Case I - Wheels Insulated from Rails and No Return Current in the Rails	11-9
11-2 Search Coil Fundamental and Harmonic Voltages (mV): Case II - Wheels Insulated from Rails and Return Current in the Rails	11-10
11-3 Search Coil Fundamental and Harmonic Voltages (mV): Case III - Wheels in Contact with Rails and Return Current in the Rails	11-11
11-4 Equivalent Differential, Coil Fundamental and Harmonic Voltages (mV) - Case I	11-12
11-5 Equivalent Differential, Coil Fundamental and Harmonic Voltages (mV) - Case II	11-13
11-6 Equivalent Differential, Coil Fundamental and Harmonic Voltages (mV) - Case III	11-14
12-1 Induced Short Circuit Fault Locations	12-2
12-2 Summary of Fault Clearing Test Results	12-4

ACRONYMS

AAR	Association of American Railroads	IRIG-B	Inter Range Instrumentation Group B
ACT-1	Advanced Concept Train-1	ISO	International Standards Organization
ALD	Automatic Location Detector	LVDT	Linear Variable Displacement Transducer
APSE	Auxiliary Power Systems Equipment	LVPS	Low Voltage Power Supply
ATC	Automatic Train Control	MARTA	Metropolitan Atlanta Rapid Transit Authority
B&K	Brüel and Kjaer	NYCTA	New York City Transit Authority
CB	circuit breaker	PBT	Parsons, Brinkerhoff, Tudor (consultants)
CCW	counterclockwise	PCE	Power Control Equipment
CL	centerline	PSD	Power Spectral Density
CN	Canadian National	RDL	Rail Dynamics Laboratory
CTA	Chicago Transit Authority	RFI	radio frequency interference
CTS	Cleveland Transit System	SOAC	State of the Art Car
CW	clockwise	TM	traction motor
DFT	Discrete Fourier Transforms	TSC	Transportation Systems Center
DRS	Data Reduction System	TTC	Transportation Test Center
ECE	Electronic Control Equipment	TTT	Transit Test Track
EMF	electromotive force	UMTA	Urban Mass Transportation Administration
EMI	electromagnetic interference	URB	Urban Rail Building
FAST	Facility for Accelerated Service Testing	VLC	Voltage Limiting Chopper
FFT	Fast Fourier Transform		
FM	frequency modulation		
FRA	Federal Railroad Administration		
Ia	armature current		

ABBREVIATIONS

A	ampere	MCM	thousand circular mils
a.c.	alternating current	MHz	megahertz
°F	degrees Fahrenheit	mi	miles
dB	decibel	mi/h	miles per hour
dBA	decibel, A weighted	mi/h/s	miles per hour per second
d.c.	direct current	min	minutes
', ft	foot	mm	millimeters
g	gravitational force	mrاد	milliradians
GHz	gigahertz	ms	milliseconds
hr	hour	mV	millivolts
Hz	hertz	psig	pounds per square inch gage
", in	inch	rms	root mean squared
kHz	kilohertz	rpm	revolutions per minute
kWhr	kilowatt hours	s	seconds
lb. ft	pounds-feet (torque)	μs	microseconds
lb/in	pounds per inch	v	volts
m	meter	yd	yards

EXECUTIVE SUMMARY

In 1975, technical specifications for 80 new rapid transit cars of the married pair (A and B) type and 20 cars of an autonomous (C) type were released by the Metropolitan Atlanta Rapid Transit Authority (MARTA). The specification featured lightweight cars with aluminum body shells and advanced propulsion systems technology. In May 1976, following an evaluation of bids, MARTA awarded the contract to the Societe Franco-Belge de Material de Chemin de Fer.* In August 1978, MARTA exercised an option for an additional 20 cars of an A and B type mix.

The first two cars arrived in Atlanta in March 1978, and began testing in Atlanta in June 1978. MARTA, in cooperation with the Urban Mass Transportation Administration (UMTA), requested that the Federal Railroad Administration (FRA) conduct engineering tests on a married pair of A and B type production vehicles. These tests were conducted from May 1980 through January 1981 at the Transportation Test Center (TTC). This report documents the results of those tests.

The tests were directed by UMTA, with MARTA providing a full time representative for technical coordination. MARTA retained the engineering consultant firm of Parsons, Brinkerhoff, and Tudor to define special engineering tests to resolve questions arising from MARTA's operation of the cars in revenue service in Atlanta. Dr. Neil K. Cooperrider and Dr. E. Harry Law of Acorn Associates were consulted by MARTA to address specific wheel/rail wear problems and assisted TTC in the formulation of a curve entry, stability, and curving performance test program. Radiation Sciences Incorporated of Skippack, PA, were contracted by the Transportation Systems Center, Cambridge, MA, to conduct wayside radio frequency interference tests at the TTC.

The purpose of the test program was to evaluate the MARTA rapid transit cars in the areas of performance (propulsion, control, braking, and energy consumption), ride quality, and wayside and onboard noise. Special engineering tests included a series of electromagnetic compatibility tests to define the potential influence of the vehicle's direct current (d.c.) chopper propulsion control system on the Automatic Train Control, and an experiment to determine the angle of attack of the truck wheelsets in a curve, as an input to a wear index math modeling program. The wear index provides a significant advancement in the understanding of wheel flange and rail wear characteristics.

The two test vehicles, service numbers 0109 (A type) and 0110 (B type) were built to MARTA specifications.¹ The vehicle bodies are a monocoque structure fabricated from extruded aluminum panels, joined by fusion welding. The trucks, fabricated by Rockwell International, are articulated for wheel load equalization, each truck side frame having a transverse transom arm which terminates in a ball joint assembly in the opposing side frame. Primary suspension is provided by two rubber spring halves which surround each

* Hereinafter referred to as Franco-Belge.

¹ Part II, Technical Provisions for Procurement of Transit Vehicles, Contract No. CQ 310, September 5, 1975.

axle journal bearing. Secondary suspension is provided by two air spring units positioned between the truck frame and the bolster.

Four separately excited d.c. traction motors provide the propulsion and electric braking. Each motor is resiliently mounted to the truck and drives one axle through a gearbox and coupling. A solid-state d.c. chopper system controls the armature and field circuits of the motors in each car. The major braking effort of the car is provided by the dynamic braking capability of the propulsion system, supplemented by pneumatic/hydraulic tread brakes. Dynamic braking is regenerative (returns power to the third rail) or resistive (absorbs power with on-board resistor banks). Slip detection circuits are included in the Electronic Control Equipment to provide spin/slide protection during acceleration and braking.

Track tests were conducted on the Transit Test Track, a 9.1 mile oval of FRA Class 6 track. The married vehicle pair were representative of vehicles used in revenue service in Atlanta. They were tested in a standard configuration (with the exception of onboard instrumentation) and with modifications to the braking system, primary suspension stiffness, and vertical damping of the secondary suspension system.

Standard tests were conducted in accordance with the General Vehicle Test Plan, which defines guidelines and methods for testing and evaluating transit vehicles in the areas of performance, ride quality, and acoustics.

MARTA reported they were experiencing an excessive wheel flange wear rate on the revenue service cars in Atlanta. As a result, a program was initiated at TTC to use mathematical modeling techniques and test data to predict wheel flange wear indices. Theoretical prediction techniques were utilized to show the influence of primary suspension longitudinal stiffness, axle misalignment, wheel/rail coefficient of friction, car weight, wheel profile, yaw pivot friction, balance speed, and propulsion/coast/braking mode on wheel flange wear indices as a function of track curvature. Additional testing will be required under controlled conditions to develop a relationship between the wear indices and actual wheel flange wear rates.

A shake test of the MARTA 'A' car (0109) was conducted in vertical, lateral, and torsional modes in the Rail Dynamics Laboratory to obtain vehicle body mode shape and frequency data for use during the on-track ride quality testing. Additionally, an undercar equipment test was conducted to determine critical resonant frequencies of the equipment which could be used in trouble shooting potential structural problems with equipment bracketry.

Performance acceleration testing was conducted with two vehicle configurations; 1) baseline acceleration data was acquired with 34" (new) wheels and was identified as the BR3 configuration; 2) acceleration data acquired with partially worn (32.5") wheels was identified as the BR2 configuration.

Acceleration test results show that the full rate initial acceleration requirements of 3.0 mi/h/s were obtained with the BR2 and BR3 configurations up to the AW2 weights required by specification. Both configurations met the time-to-speed requirements but the BR2 configuration took less time to speed (10 s less to 60 mi/h).

Control response characteristics were evaluated for a series of propulsion system mode changes from drive to brake and brake to drive. The jerk rates associated with the transition from braking to acceleration are generally below the specification limit requirement of 2.0 to 2.5 mi/h/s² with minimum rates as low as 0.4 mi/h/s² for the application of acceleration tractive effort. The vehicles met the transition time specification requirement of 0.3 s for the mode change from acceleration to braking with consistent times of 0.20 to 0.25 s. However, the mode change from brake to acceleration were consistently in excess of the specification requirement of 0.5 s, with typical transition times in the range of 0.75 s to 1.0 s.

Friction braking duty cycle tests were conducted using simulated revenue service profiles representative of the MARTA East-West line, the New York City Transit Authority, and the Cleveland Transit System (CTS). Brake shoe temperatures stabilized in the 200°F to 270°F range with the CTS profile resulting in the highest brake shoe temperatures. Undercar equipment temperatures remained stable throughout the friction-only braking runs and were typically in the range of 85°F to 110°F. Traction motor temperatures did not exceed 120°F.

A blended brake duty cycle test was conducted to a special revenue profile provided by MARTA. The brake resistor temperatures varied from 400°F to 660°F. Motor case temperatures stabilized at 140°F and 190°F for motors 1 and 3, respectively. Brake shoe temperatures initially in the 190°F to 220°F range fell to 140°F to 150°F at the conclusion of the blended brake duty cycle. The Auxiliary Power Systems Equipment (APSE) bay temperatures increased from 100°F (approximate) to 110° - 130°F.

The original brake configuration (BR1) incorporated a high speed taper in braking rate from 2.0 mi/h/s at 70 mi/h to 3.0 mi/h/s at 50 mi/h. Test results show that the BR1 configuration failed to meet the required brake rates in any of the braking modes. Additionally, examination of the brake cylinder pressure revealed that friction brakes were applied throughout full service braking, which was contrary to specification requirements for electrical braking only at AW2 weights, or less.

The BR2 brake configuration removed the high speed taper and added a low speed taper. Maximum brake cylinder pressure was increased and the constant application of friction braking during normal service brake application at AW2 or less was removed. The BR2 braking performance still failed to meet specification requirements for any of the braking modes.

The BR3 configuration (baseline data in this report) included new Servotrol and variable load valves, recalibrated load weigh system, and modified printed circuit cards. Test results show the BR3 braking rates meet requirements for the friction only and emergency modes but still fail to meet the blended braking rate requirements above 40 mi/h. The BR3 emergency braking rates increase significantly with reduced brake entry speeds (up to 7.0 mi/h/s at 15 mi/h entry speed).

The wheel spin/slide protection system was evaluated for full rate accelerations, full service blended and full service friction braking, at wheel/rail interface coefficients of adhesion of 0.07 to 0.09. Test results show that the required spin/slide efficiencies of 75% were met for all three modes.

A drift test was conducted on the two car train at AW2 vehicle weight to evaluate air and rolling resistance characteristics. Test results show that the normal configuration brake calipers provide a spring-loaded brake shoe drag, adding a retarding force which gives rise to approximately 0.002 g deceleration. This is approximately 20% of the train resistance at 70 mi/h and 50% as it approaches a stop.

Power consumption tests were conducted over a simulated MARTA East-West profile and the Advanced Concept Train profile. Energy consumption rates of 7.5 and 9.7 kWhr/car mile, respectively, were obtained, ignoring potential energy savings from regenerative braking which, under ideal conditions, could improve overall energy consumption for the system with a number of cars operating. Data were obtained to determine the amount of regenerative energy potentially available at the cars during dynamic braking.

Electromagnetic interference tests were conducted on the MARTA car to collect data (induced voltage waveforms - amplitudes and frequencies) for different electromagnetic configurations. Such data were collected successfully and will be used in understanding and troubleshooting electromagnetic interference problems (both wayside and carborne systems) relative to MARTA systems.

Ride quality tests were conducted to determine the vehicle ride characteristics as experienced by a typical passenger and to identify vibration induced into the passenger compartment due to operation of the undercar equipment. Three suspension configurations were evaluated to determine the effect of vertical damping of the secondary suspension system on ride quality. The original configuration (R1) provided hydraulic shock absorbers for vertical damping, but vertical vibrations of 0.15 g were induced into the forward floor at approximately 26 Hz. The second configuration (R2) removed the hydraulic shock absorbers and provided vertical damping by restricting the venturi in the air springs, which reduced the 26 Hz component to .006 g. A third configuration (R3), which combined the hydraulic shock absorbers with the air damping, resulted in vibration levels up to 0.021 g. The R2 configuration was selected for revenue service cars.

Test data showed that ride quality of the MARTA cars (R2 configuration) was within specification for all conditions except the vertical bending mode excitation (6.2 Hz) for the AW3 weight configuration, which exceeded requirements by 0.1 g through curved track sections. This was caused by contact between the truck bolster and the truck frame, due to inadequate roll stiffness and/or leveling valve response. The most significant component-induced vibration was caused by operation of the traction motors, which resulted in 0.008 g rms at 65 Hz (37% of specification maximum).

A series of noise tests were conducted to determine the noise levels inside the cars and at the wayside under normal operating conditions. Car 0110 had an abnormally noisy, out-of-balance APSE blower which influenced the data. As an example, car 0110 average internal noise during equipment operation was 5 dBA above the 65 dBA specification requirements, while car 0109 was 3.2 dBA below specification. The average interior noise level throughout the 0 to 70 mi/h speed range was 4.8 dBA below specification. The interior noise level only increases approximately 3 dBA from 0 to 70 mi/h. The average wayside noise with the car stationary exceeded the specification by

5.8 dBA at 15' and 2.25 dBA at 50' from the track centerline. The average wayside noise at 50' during passby exceeded the specification by approximately 2 dBA.

Eight separate tests (fault clearing) were conducted to evaluate the protection circuits within the electrical system. All protection circuits functioned as designed.

The MARTA cars demonstrated average reliability with approximately 80% availability for the scheduled track time. The vehicles accumulated 5,745 miles during the originally scheduled series of tests. Due to the poor brake performance encountered during the original tests, MARTA modified the brakes to the BR3 configuration, replaced the worn wheelsets (32.5") with new wheel sets (34"), and conducted a special series of tests to evaluate the brake modification. An additional 2,830 miles were accumulated during the follow-up test series.

1.0 INTRODUCTION

This report presents the results of a series of engineering tests carried out on two examples of the Metropolitan Atlanta Rapid Transit Authority (MARTA) rapid transit cars, from May 1980 through January 1981 at the Department of Transportation, Transportation Test Center (TTC), Pueblo, Colorado. The test program was sponsored by the Office of Rail and Construction Technology in the Office of Technology Development and Deployment, Urban Mass Transportation Administration (UMTA), Washington, D.C. The TTC conducted the tests according to established test procedures, developed during a series of transit car test programs at the TTC starting with the State of the Art Cars (SOAC) in 1973.

Special engineering tests to resolve questions arising from MARTA's operation of the cars in revenue service in Atlanta were defined by Parsons, Brinkerhoff, and Tudor (PBT), the consultant engineering company for MARTA. MARTA provided a full-time representative at the Test Center for the duration of the test program to provide liaison in the event of car operational problems. Dr. Neil K. Cooperrider and Dr. E. Harry Law, of Acorn Associates, were consulted by MARTA to address specific wheel/rail wear problems and assisted TTC in the formulation of a curve entry, stability, and curving performance test program. Radiation Sciences Incorporated, of Skippack, PA, were contracted by the Transportation Systems Center (TSC), Cambridge, MA, to conduct wayside radio frequency interference (RFI) tests at the TTC.

1.1 BACKGROUND

Technical specifications were produced in 1975 for a new design of rapid transit car to operate on the MARTA rapid transit system; the specification featured lightweight cars with aluminum body shells and advanced propulsion systems technology. In May 1976, following an evaluation of bids and a visit to France to review the company facilities, MARTA awarded an order to Franco-Belge for:

- 80 rapid transit cars of the married-pair (A & B) type.
- 20 rapid transit cars of an autonomous (C) type, able to operate as independent units.
- A 20-car option which was exercised in August of 1978 for a mix of 20 A and B type cars.

The first two cars arrived in Atlanta in March 1978, 22 months after the award of the contract. These two cars began testing in Atlanta in June 1978, and are now part of a fleet of approximately 70 vehicles presently in revenue service; a fleet of 120 cars is forecast by year-end 1981.

The East-West line of the MARTA rapid transit became operational in December 1979; a North-South line of 24 miles length is now under construction and will link downtown Atlanta with the Hartsfield Atlanta International

Airport. Fleet operating time totalled 120,000 hours in June of 1980, and is forecast at 500,000 hours by year-end 1981.

Following UMTA's policy of extensively testing and evaluating new rapid transit cars at the TTC, a married pair of A and B type cars, serial numbers 0109 and 0110, were shipped to Pueblo in May of 1980. This report describes the test program carried out on those cars and presents the results of a wide spectrum of engineering tests, including vehicle acceleration and braking performance, ride quality, electromagnetic interference, and truck behavior during curve negotiation.

2.0 TEST PROGRAM SCOPE

2.1 PURPOSE

The purpose of the test program was to evaluate the MARTA rapid transit cars in the areas of performance (propulsion, control, braking, and energy consumption), ride quality, and wayside and onboard noise. These tests were conducted according to the guidelines for the standardized test procedures evolved at the TTC. In addition, special engineering tests were designed to evaluate known problem areas and areas of long-term interest to MARTA. For example, a series of electromagnetic compatibility tests were conducted to define the potential influence of the vehicles' d.c. chopper propulsion control system on the Automatic Train Control (ATC); also, an experiment was conducted to determine the angle of attack of the truck wheelsets in a curve, as an input to a wheel wear index math model.

The test data will:

- Validate the acceptance testing carried out on the cars to determine their compliance to the design specification.
- Provide MARTA with valuable information which will aid their long-term maintenance planning and spares provisioning.
- Provide input to a data bank to allow qualitative analysis of comparative vehicle systems.
- Identify technical areas where research and development are desirable.
- Provide information which will advance the state of the art for the mathematical modeling of the rail vehicles as a tool to predict vehicle stability and wheel wear.

2.2 PROGRAM SUMMARY

In the performance domain, three braking system configurations were evaluated; in the ride quality domain, three secondary suspension configurations were tested. Performance and ride quality tests were carried out at three vehicle weights representing empty vehicles, and simulated passenger loads of 21,000 (AW2) and 41,000 (AW3) pounds.

In addition to the above tests, which were carried out to established, standard TTC test procedures for evaluating rapid transit vehicles, special engineering tests were carried out in response to problems relevant to operation of the vehicles on the MARTA property. For example, interference of the vehicle with signals generated by the ATC was observed in certain circumstances in revenue service. The problem was thought to be due to electromagnetic interference from the vehicles' chopper propulsion control system, which can induce alternating current (a.c.) in the running rail, thus generating signals which match, or are harmonics of, the ATC signal; (the ATC

system uses the running rail to transmit its control signals). Tests were carried out at Pueblo to map the electromagnetic field induced by the vehicles, and to identify the prime electromagnetic emission contributors in the propulsion control system.

Rapid wheel flange wear was also a problem identified early in the service life of the vehicles at MARTA, and a wheelset curving and stability test program was designed to evaluate the problem. The program was designed to measure the angle of attack of the wheelsets of one truck during negotiation of a series of curves typical of those encountered in revenue service operation, and compared the curving and stability performance of the standard primary suspension and wheel profiles to alternate configurations. The data from these tests, together with truck stiffness and alinement parameters gathered from a series of static tests, were used as input to a computer math model to predict wheel and rail wear indices.

The curving and stability test program evaluated the curving performance of two primary suspension configurations: (1) with the standard rubber bushes (which surround each axle journal bearing and provide primary springing), and (2) with bushes modified to produce a longitudinal spring rate of approximately one-third of that of the standard bushes. The performance of high conicity wheel profiles was evaluated in conjunction with the soft suspension configuration. Tests were also carried out on tangent track to evaluate truck stability, as truck or wheelset hunting was of concern for the modified configurations.

2.3 TEST VARIABLES

2.3.1 Controller Level

The MARTA cars are equipped with a master controller which is infinitely variable between full power and full service brake; intermediate power and brake positions are indicated on the controller, but there are no positive controller detents. Acceleration performance was evaluated for controller positions P1, P2, P3, and Full Power, and braking performance was determined for controller positions B1, B2, and B3 (full service braking), and for emergency braking activated by a stop button on the wall of the operator cab.

2.3.2 Speed

The vehicles were tested over their speed range of 0-70 mi/h. For those tests requiring constant speed increments, speeds of 15, 35, 55 and 70 mi/h were chosen.

2.3.3 Line Voltage

The ability of the vehicles to operate at other than design line voltages was demonstrated by carrying out acceleration performance runs at line voltages of 550, 750, and 825 V d.c.; the voltages were measured at the input

to the vehicles, with no load on the Transit Test Track (TTT) power distribution system other than the vehicle auxiliaries.

2.3.4 Vehicle Weights

The vehicles were tested at three weights, simulating varying degrees of passenger lading by means of lead ingots placed on the carbody floor. The nominal and actual weights are listed in table 2-1.

TABLE 2-1. VEHICLE WEIGHTS

Condition	Weight Code	Nominal Weight (lb)	Actual Weight (lb)	
			Car 0109	Car 0110
Empty	AW0	76,000	83,280	81,960
AW0 plus 21,000 lbs	AW2	97,000	97,220	96,360
AW0 plus 41,000 lbs	AW3	117,000	117,220	116,360

NOTE: Car 0110 was subjected to a load of approximately 2,500 lb over the rear truck due to the weight of the data acquisition equipment. To provide an equal axle loading throughout, ballast was added over the front truck, and car 0109 was similarly ballasted over both trucks to match the weight of car 0110. Therefore, the actual test weights of the vehicles at AW0 do not match the nominal empty weight.

2.3.5 Track Type

The test program was conducted on the TTT, a nine-mile oval comprising six sections of track representative of typical transit property construction. Details of track construction can be found in Section 4.0, Description of Facilities.

2.3.6 Vehicle Configuration

The vehicle was tested for performance with three braking system configurations; in the ride quality domain, three secondary suspension configurations were evaluated. The curving angle of attack tests evaluated the curving performance of the standard truck primary suspension, and a configuration having a longitudinal stiffness of approximately one-third of the standard primary suspension; tests were also conducted with a high-conicity wheel configuration. These vehicle configuration changes are discussed in detail in Section 3.0, Vehicle Description.

2.4 TEST PROGRAM

2.4.1 Performance

The performance of the MARTA rapid transit vehicles was evaluated in the areas of acceleration; blended, friction-only, and dynamic service braking; and emergency braking activated by the trainline air pressure. Tests were conducted to evaluate the efficiency of the spin/slide protection system, and to evaluate the jerk rate (rate of change of acceleration) and response times of the propulsion control system. Tests were also conducted to determine the energy consumption of the vehicles over two simulated revenue service routes and for a series of acceleration and constant speed modes. The amount of energy that could be regenerated under braking and optimum line receptivity was determined, and a series of drift tests were made to determine the vehicles' train resistance.

2.4.1.1 Acceleration. The acceleration of the vehicles was evaluated at the three vehicle weights, and at line voltages of 550, 750, and 825 V d.c. The recorded voltages were measured at the vehicles, with no load on the line other than the auxiliaries. Test runs were made on level tangent track, accelerating from a stop to maximum speed at master controller settings of P2 and Full Power.

2.4.1.2 Braking. The braking performance of the vehicles was evaluated for blended, friction-only, dynamic-only, and emergency modes of operation at the three vehicle weights. Braking runs were made in clockwise and counterclockwise directions of travel on level tangent track, for initial speeds of 15, 35, 55 and 70 mi/h and master controller settings of B1, B2, and B3; the emergency stop was initiated by pushing the stop button above the vehicle monitor panel, which electrically dumps the trainline air supply. Three braking system configurations were evaluated, as described in Section 3.13, Vehicle Configurations.

2.4.1.3 Duty Cycle. The duty cycle tests evaluated the undercar equipment temperatures and friction brake pad temperatures of the A car during test runs simulating revenue service. The temperatures at 29 locations under the vehicle, including traction motor cases, resistor grids, brake shoes, and electronic equipment bays were recorded using a data logger at each station stop of a series of revenue service simulation runs. The equilibrium temperatures during typical revenue service operation in blended and friction-only braking modes were determined.

Friction brake duty cycle evaluations were carried out, at only the AW2 vehicle weight, using three revenue profile simulations:

- A simulation of the MARTA East-West line round trip from Avondale to High Tower and return.
- A duty cycle typifying New York City Transit Authority (NYCTA) operation; the run comprised a maximum acceleration to 35 mi/h, constant

speed for 30 s and full service braking to a stop, followed by a 30-s station stop; the sequence was repeated for 25 cycles.

- A duty cycle typifying Cleveland Transit Systems (CTS) operation; the run comprised a maximum acceleration to 50 mi/h, constant speed for 55 s and a full service braking application to a stop, followed by a 30-s station stop. Nineteen cycles were completed.

Undercar equipment thermal characteristics for the blended braking mode were evaluated using a profile provided by MARTA; the profile comprised a sequence of four runs controlled by P-signal voltage levels and elapsed time between changes.

2.4.1.4 Spin/Slide. The efficiency of the vehicles' spin/slide protection circuitry was evaluated by carrying out a series of tests at AW2 vehicle weight; operation of the system was examined for acceleration, and for braking modes with blended and friction-only braking. The vehicles were fitted with spray nozzles ahead of each wheel, fed by a pressurized tank with a mixture of liquid soap and water. The nozzles were used to spray the rail ahead of the wheels with soap solution, while the vehicles were driven through the area under maximum acceleration or braking. Data were collected as the vehicles' control systems attempted to correct the resulting spins or slides and reestablish tractive effort.

2.4.1.5 Energy Consumption. The energy consumption of the MARTA vehicles was examined in two ways:

- A series of acceleration, braking, and constant speed test runs were carried out and energy consumption was recorded for each run. The energy dissipated by the brake resistors was also recorded, as it represented a measure of the amount of energy that could be returned to the line in a regenerative mode.
- Simulated revenue service runs were carried out using station stops representative of the East-West line round trip from Avondale to High Tower and return, and a standardized TTC revenue profile known as the ACT-1 (Advanced Concept Train) profile. Energy consumption was recorded incrementally at each station stop and totalled at the completion of the run.

2.4.1.6 Drift. A series of drift runs were carried out at AW0 and AW2 vehicle weights to evaluate the cars' train resistance. The runs were carried out for two vehicle configurations, with the brake shoes held against the wheel treads by the springs inside the brake actuators, and with the brake shoes held clear of the wheels. These test comparisons defined the drag penalty of the constant-contact brake shoe configuration. The tests were carried out by allowing the cars to coast through the level tangent track section from an initial speed of 70 mi/h; successive runs were made in both clockwise and counterclockwise directions to negate wind and gradient effects, with the entry speed of each run approximately 5 mi/h less than the entry speed of the previous run.

2.4.1.7 Jerk Rate and Response Time. The jerk rate (rate of change of acceleration) and response time of the vehicles' propulsion systems were evaluated at AW2 vehicle weight. The tests determined the response and transition times for a series of propulsion mode changes from drive to brake and brake to drive throughout the speed change, and the jerk rates during these mode changes.

2.4.2 Ride Quality

2.4.2.1 Component Induced Vibration. A series of tests were carried out with the vehicle stationary, in which the undercar auxiliary equipment was operated singly and in combinations to identify any potential contributors to carbody vibration. The vibration due to traction motor blowers, evaporator fans, air conditioner compressor, and the brake air compressor were examined separately and in combination. Vertical and lateral accelerations were measured at various locations on the vehicle floor. The tests were conducted at AWO vehicle weight.

2.4.2.2 Effect of Speed and Track Section. The ride quality of the vehicles was examined for the three secondary suspension configurations described in Section 3.4, Trucks and Suspension; i.e., with vertical hydraulic shock absorbers, with venturi in the air springs replacing the shock absorbers, and with both venturi and shock absorbers providing vertical damping. Configurations were evaluated at vehicle weights of AWO and AW3. Tests were conducted at speeds critical to vehicle body modes, and speeds of 15, 35, 55 and 70 mi/h over all TTT sections.

Vehicle interior vibration measurements were taken for vertical, lateral, and longitudinal accelerations at the carbody floor over the front truck, at a midcar location, and over the rear truck. Axle journal vertical and lateral accelerations; sideframe vertical and lateral accelerations; and axle, truck, and bolster displacements were also recorded.

2.4.2.3 Effect of Acceleration, Deceleration. The effects of full service acceleration and braking on ride quality were evaluated on level tangent track for the vehicle configurations and weights described in the previous subsection. Acceleration and braking applications were made from 0 to 70 mi/h and from 70 to 0 mi/h.

2.4.3 Noise

A series of tests were carried out to determine the noise levels at the wayside and onboard the cars, with the vehicles operating over a range of constant speeds and during full rate acceleration and braking. Testing was conducted at the AWO car weight. The effect of component-induced noise on the wayside and interior noise levels was determined by individual and simultaneous operation of the major vehicle subsystems. Wayside measurements were recorded at 15' and 50' from the track centerline.

Wayside noise testing was accomplished on a section of level tangent track with concrete ties and welded rail. Microphone locations were 50' from each side of the track in open, flat terrain, and noise measurements were taken at pass-by speeds of 15, 35, 55 and 70 mi/h. Interior noise measurements were conducted while traversing the tangent portion of Section IV of the TTT at these speed increments at a series of locations in the 0109 car. Additionally, interior data were recorded while the car traveled all sections of the TTT at 55 mi/h to determine the relationship of interior noise level to track type.

2.4.4 Electromagnetic Interference

A series of tests were carried out on car 0109 of the married pair, which was uncoupled from car 0110 for this phase to determine the level, distribution, and frequency content of the electromagnetic flux patterns underneath the car. Tests were conducted to compare the electromagnetic field due to inductive coupling with the running rails, inductive coupling combined with conducted interferences, and the effects of secondary loop paths provided by the wheels and axles of the vehicle. The tests were conducted by disconnecting the traction motors from the vehicle's propulsion system and substituting a load bank to simulate the motors; the car was stationed on a section of isolated track and the propulsion system was operated as though the vehicle was being propelled; electromagnetic emissions were measured by stringing a loop of cable under the car and progressively moving it down the length of the vehicle, measuring the emissions at each location. At each position of the coil, a spectral analysis was obtained for voltage induced in the coil.

2.4.5 Fault Clearing

A series of tests were conducted on car 0109 with the car stationary to determine the ability of the vehicle's propulsion and power supply system to protect itself against armature and ground shorts. The effect of ground faults was evaluated at the following locations:

- Traction motor armature positive terminal.
- Power Control Equipment (PCE) blower positive armature terminal.
- Voltage Limiting Chopper (VLC) output terminal.
- Low Voltage Power Supply (LVPS) output terminal.
- A/B car low voltage circuit breaker (input and output terminals).

2.4.6 Static Truck Tests

Static tests and measurements were carried out on the trucks to determine the alinement of the wheelsets relative to each other and to evaluate the longitudinal, lateral, and vertical stiffness of the truck primary suspension; rotational tests were carried out to determine the breakaway torque

required to rotate the truck in yaw with standard 'Rulon' side bearers and with modified side bearers.

Wheelset alinement tests were carried out using air bearing tables to 'float' the wheelsets and relieve external alinement loads; the alinement of the unrestrained wheelsets was then determined, using an optical transit square to measure the lateral displacement of chord lines across the front faces of the wheels from an optical datum plane.

Vertical and lateral spring rate tests were carried out on the primary suspension of the lead truck of car 0110 by applying forces with a hydraulic actuator with a load cell mounted in series, and measuring the deflection of the primary suspension bushes with dial gage indicators. The lateral test applied a load to the side frame of the truck which was reacted by the rails, thus loading all bushes simultaneously; the vertical test loaded each bush individually by jacking under the truck sideframe journal housing. Longitudinal stiffness measurements were made on the leading axle only; the wheels of that axle were placed on an air bearing table to eliminate friction forces, and the primary bushes were loaded by applying brake pressure incrementally by means of a regulated air supply; a load cell was interposed between one brake actuator and the wheel rim to measure applied force, and the deflection at each journal bearing was measured by means of two dial gage indicators.

The torque required to rotate a truck in yaw was measured by floating the entire truck on an air bearing pad to eliminate friction between the wheels and ground, and applying a couple by means of two chain hoists and cables attached to the corners of the table. The forces in the cable were measured by means of two load cells.

The primary suspension stiffness tests and the wheelset alinement tests described above defined parameters which, in conjunction with the wheelset angle of attack data obtained in the curving tests described in Section 2.4.8, provided input to a curving and wheel wear index math model.

In addition to the truck spring rate tests described above, tests were carried out on an individual primary suspension bush, using an MTS servo-controlled hydraulic load-frame. The tests were used to develop a longitudinally soft primary suspension configuration.

2.4.7 Structural Vibration Response

A shake test program was carried out on car 0110 to determine the rigid body, body bending, and torsional response characteristics of the carbody. A servo-controlled hydraulic actuator was used to provide random noise and frequency sweep excitation in the frequency range 0.5 to 30 Hz with a constant input force of approximately 2,000 lbs. The actuator was attached by removing the 'B' end anticlimber and bolting fixtures directly to the floor structure for vertical and lateral excitation, and by clamping a fixture to a lifting pad at the 'B' end for torsional excitation.

The data were used to determine the resonant frequencies of the carbody and the rigid body suspension modes; further modal analysis may be carried

out at a later date to confirm the accuracy of the finite element model and to determine the complex mode shapes. The structural and rigid body responses were correlated to the ride quality data.

As a result of some observed oscillations of the underfloor auxiliary equipment, further tests were carried out to define the frequency response characteristics of the various systems; accelerometers were mounted on the track signaling coil, the air compressor, the resistor bank, and inductor and blower ballast resistors. The vehicle was then excited over the frequency range in the vertical direction; the data were used to derive the resonant frequencies of the mounted components.

2.4.8 Curving and Stability

One of the vehicle problem areas identified by MARTA related to accelerated wear of the wheels and rails on the Atlanta property. As a result of an examination of the problem, a test program was formulated at the TTC to examine the curving ability of the Rockwell truck, including straight line and curve entry stability. Angle of attack frames were constructed (for the lead truck on car 0110), which measured the angle of attack of each wheelset relative to the rail. The frames were mounted on extensions of the axles and thus followed the yaw attitude of the axles throughout the negotiation of a curve; probes attached to the frame rubbed against the inside face of the rail, and the positions of the probes were measured with displacement transducers. The transducer outputs were used to compute the angle of the wheelset relative to a constant chord of the rail curve. Accelerometers were mounted on the carbody floor and on the truck sideframe and axle journals. These, together with axle/frame and bolster/carbody longitudinal and lateral displacement measurements, were used to examine the stability and ride quality on tangent track and during curve entry. Truck or wheelset hunting was of particular interest for this test mode.

Three vehicle configurations were evaluated:

- Standard primary suspension bushes (longitudinal spring rate of 150,000 lb/in).
- Longitudinally soft primary bushes (longitudinal spring rate reduced to approximately 50,000 lb/in).
- Soft brushes with the addition of high conicity (Canadian National 'A', worn wheel) wheel profiles.

These vehicle configurations are described in more detail in Section 3.0, Vehicle Description.

The test program was conducted over portions of the TTT for the tangent track stability and curve entry objective, and on the FAST (Facility for Accelerated Service Testing) track and Balloon Loop for the wheelset angle of attack objectives. The track sections are described in Section 4.0.

2.4.9 Radio Frequency Interference

RFI measurements were carried out by Radiation Sciences Incorporated, Skippack, PA, at the request of the TSC. The test measurements addressed radiated narrow band and broad band electromagnetic interference (EMI) in the frequency range from 20 Hz to 1 GHz. The test program evaluated the ambient radiated EMI with the substation operational but without the vehicles running, with the cars operational at pass-by speeds up to 70 mi/h, and during acceleration and deceleration.

The appropriate antenna for the frequency range of interest was set up on a tripod and adjusted to a height of approximately 5'. The magnetic loop antennas and dipole antennas were oriented in a horizontal plane and rotated for maximum level indication. The rod antennas were oriented vertically.

The test antennas were located 50' from the center of the level tangent section of the TTT, and were connected via 50-ohm coaxial cable to appropriate interference analyzers or a spectrum analyzer. The data analysis will be conducted by Radiation Sciences Incorporated and will be evaluated by TSC; it is not discussed in this report.

3.0 VEHICLE DESCRIPTION

3.1 GENERAL

The transit cars, manufactured by Franco-Belge, feature lightweight body shells, electronic control of the propulsion system through a d.c. chopper, and a regenerative braking mode which has an energy savings potential estimated at 30%, compared to conventional control methods such as the switched resistor. All of the major systems of the car, comprising 75% of the unit cost, are of American manufacture, with Rockwell International (trucks), Garrett-AiResearch (propulsion system), and WABCO (friction brakes) among the major suppliers.

Three distinct types of cars are used in the MARTA system and are designated 'A', 'B', and 'C' types. A and B cars operate as married pairs with certain equipment shared between them; the A car has the ATC unit, batteries, and battery charger for the pair; the B car has the air compressor. The C type cars are autonomous and can operate independently as a single car. The C cars contain all of the systems that are required on a married pair; many of the components are identical in electrical function but differ in physical size and car location. The C car has two operating cabs and reduced seating capacity compared to A or B cars, which have single operating cabs in each car. The cars can be operated in trains of up to eight cars in any combination of married pairs and single units. The test program at TTC evaluated an A and a B married pair of cars; a photograph of the cars is shown in figure 3-1.

3.2 DESIGN SPECIFICATION

o Carbody Dimensions:

A Car and B Car Length	75'	(max.)
C Car Length	74' 4"	(max.)
Width	10' 6"	(max.)
Width at Threshold	10' 1.25"	(max.)
Height (top of running rail to top of roof).	11' 10"	(max.)

o Weight:

A or B Car (approximately)	76,000 lbs
C Car (approximately)	78,000 lbs

o Passenger Load:

A or B Car	68 (seated)
	140 (full)
	250 (crush)
C Car	64 (seated)
	128 (full)
	235 (crush)

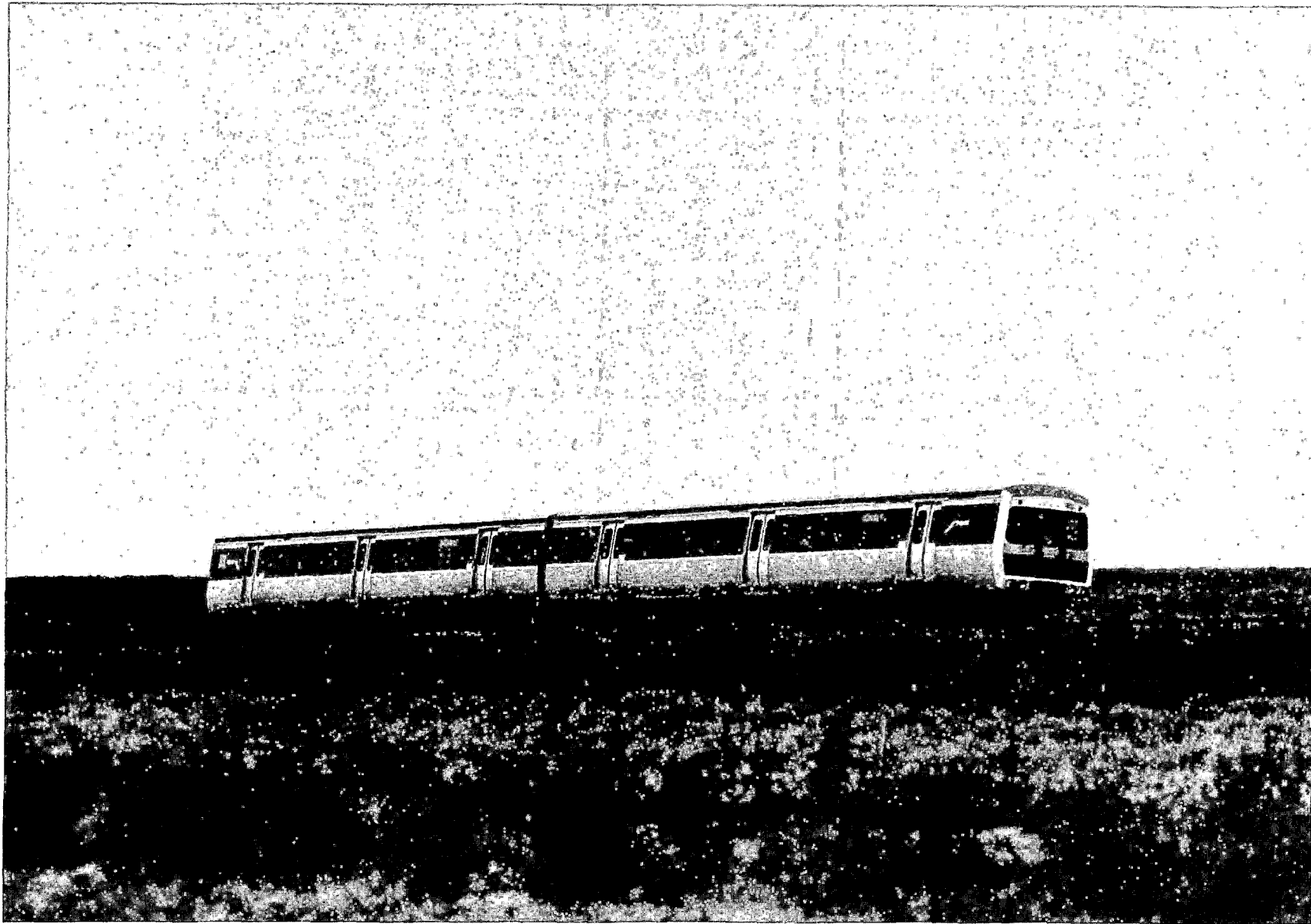


FIGURE 3-1. MARTA CARS AT THE TRANSPORTATION TEST CENTER.

- Third Rail Power Supply:

Maximum	900 V d.c.
Nominal	750 V d.c.
Minimum, full performance	650 V d.c.
Minimum, partial performance	500 V d.c.

- Low Voltage Control Power:

Maximum	42 V d.c.
Nominal	37.5 V d.c.
Minimum	24 V d.c.

- Current Limits:

Maximum Propulsion	1300 A
Maximum Braking	1500 A

- Performance:

Acceleration Rate	3.0 mi/h/s
Maximum Speed	75 mi/h
Normal Top Speed	70 mi/h
Full Service Braking Rate (between 70 & 50 mi/h)	2.0 to 3.0 mi/h/s
Full Service Braking Rate (between 50 & 0 mi/h)	3.0 mi/h/s
Emergency Braking Rate	3.5 mi/h/s

3.3 CARBODY

The vehicle carbody is a monocoque structure fabricated from extruded aluminum panels, joined by fusion welding; this includes the sides, roof, floor, and underframe bolster structure. The floor is designed to isolate the interior materials of the car from an undercar fire for at least one hour.

The carbody underframe is comprised of seven longitudinal sections welded together. These are: two side sill extensions (along the whole length of the underframe, forming the skirt of the body), two side floor extensions, two intermediate floor extensions, and a central floor extension.

The above assembly of sections is reinforced by H-shaped crossbars; longitudinal supports are welded under the sections. The carbody underframe ends consist of the end sill and four aluminum alloy sections assembled transversely. This unit provides, on its lower section, the bracing and the flange on which the coupling is mounted. The bolster-pivot assembly reinforces the underframe at the point of the truck axis. The carbody side structures are curved to provide a greater inside space at the level of the passengers' shoulders. The side structures are formed by the assembly of a grooved section (low part of body) and a stamped panel (at window height). The carbody ends, fabricated from welded aluminum panels, are welded to the carbody sides.

3.4 TRUCKS AND SUSPENSION

The trucks are fabricated by Rockwell International. They are articulated for wheel load equalization, each truck side frame having a transom arm which terminates in a ball joint assembly in the opposing side frame, as shown in figure 3-2. The frames are cast steel type A-65-35. Primary suspension is provided by two rubber spring halves which surround each axle journal bearing and are retained by the frame journal housing and a journal cap. Secondary suspension is provided by two air spring units positioned between the truck frame and a fabricated steel bolster (figure 3-3); the bolster also doubles as an air reservoir for the secondary suspension. The bolster is restrained longitudinally by two radius rods to the truck frame and laterally by a rubber bumpstop. Lateral damping is also provided by an automotive-type hydraulic shock absorber. Vertical damping of the secondary suspension was also provided by two hydraulic shock absorbers. This has been superseded by air damping, provided by restricting venturi in the air springs; both configurations were evaluated. Vertical bumpstops are provided by cylindrical rubber springs inside the air springs (downstop) and by metal-to-metal contact between the bolster and the sideframe in the upstop direction.

The truck wheelbase is 87"; 34" diameter steel wheels are used, with an Association of American Railroads (AAR) 1:20 profile.

3.5 PROPULSION AND CONTROL SYSTEM

The propulsion system provides all drive tractive effort and regenerative/resistive braking for the vehicle, and generates control signals for the friction braking system.

A d.c. chopper system controls the armature and field circuits of the motors in each car. A d.c. chopper is a device which converts a d.c. voltage of one level into a d.c. voltage of another, lower level. A simplified chopper circuit can be thought of as analogous to a mechanical switch placed between a d.c. voltage source and a load. By opening and closing the switch rapidly, d.c. voltage pulses are applied across the load. The average value of the load voltage can be varied (or regulated) by varying the frequency at which the switch is operated (constant on-time), the duty cycle of the switch (ratio of on- to off-time) or both.

A solid-state chopper uses power thyristors in place of the mechanical switch to perform the chopper function. The advantages of a thyristor over the mechanical switch or another electronic device are its large power handling capabilities, low power dissipation, and high speed of operation. The thyristor-controlled chopper operates in the same manner as the mechanical switch-controlled chopper. The thyristor's voltage output to the load is controlled by adjusting the frequency and/or duty cycle of the thyristor. A filter is added between the thyristor and the load to suppress the fluctuations in the chopper output. The electronic control regulates the motor torque (in the drive mode) and the power output (in the dynamic braking mode, when the motor is operating as a generator).

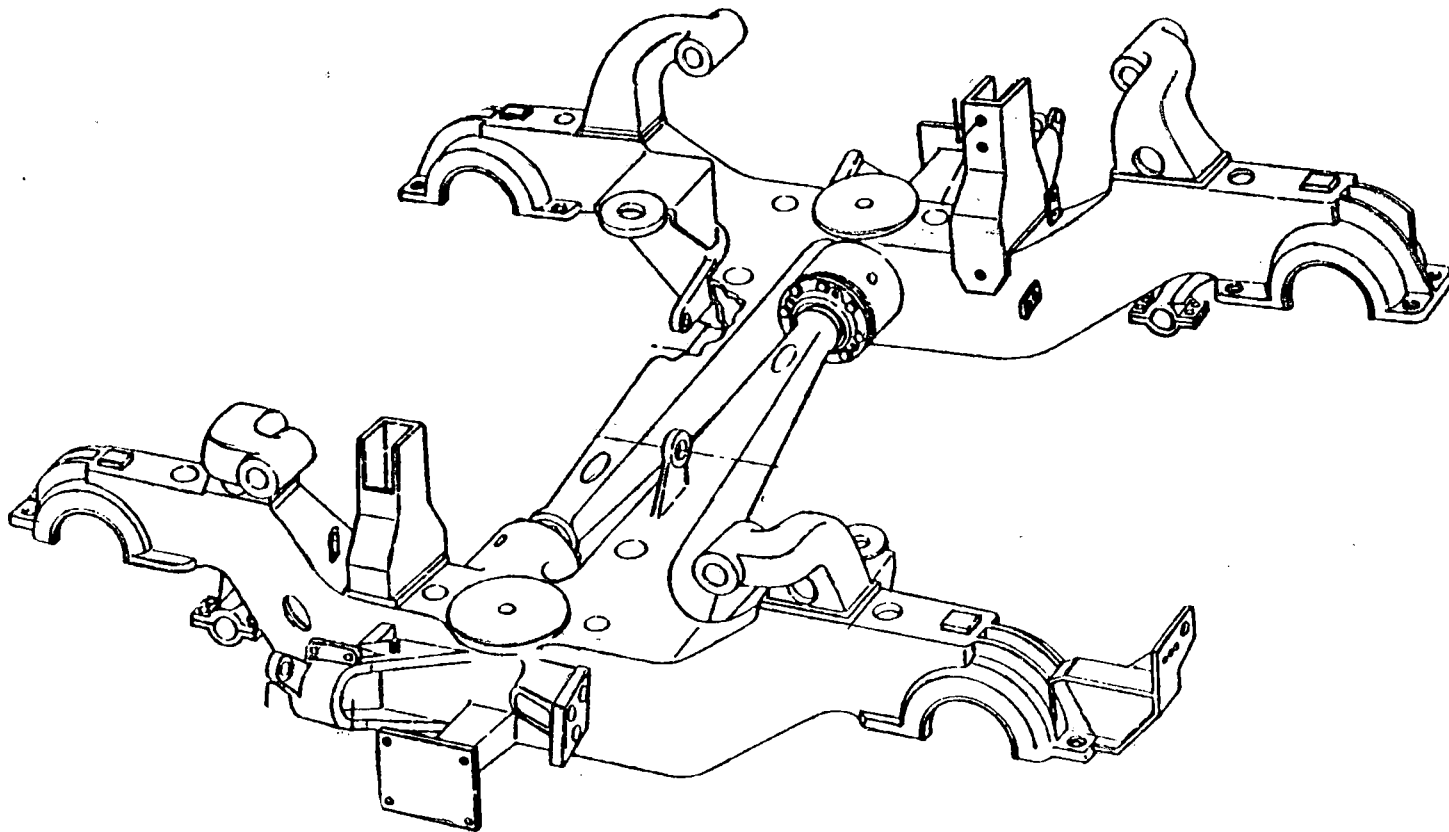


FIGURE 3-2. TRUCK FRAME, SHOWING ARTICULATION JOINTS.

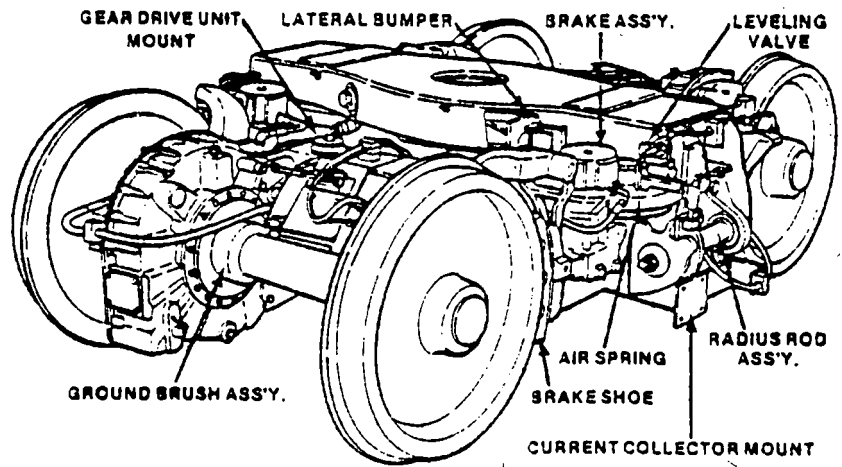
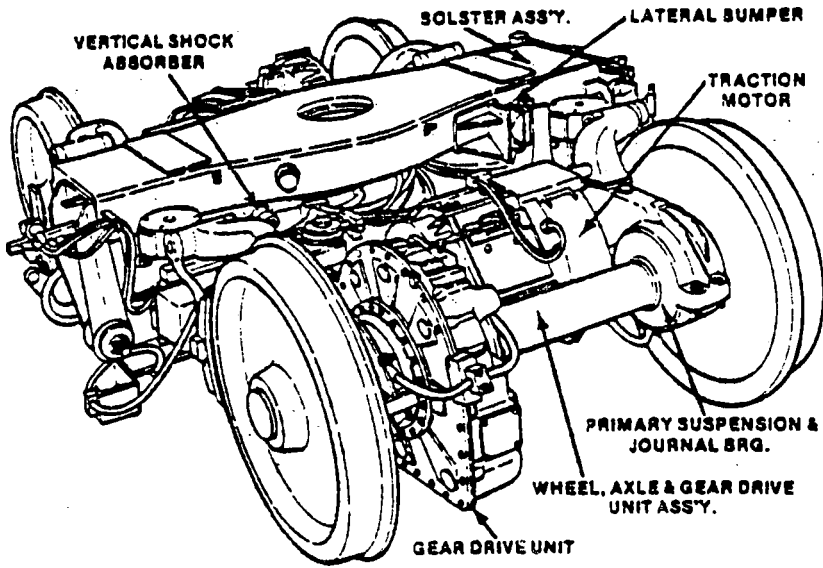


FIGURE 3-3. TRUCK GENERAL ARRANGEMENT.

Energy from dynamic braking is regenerated into the line when the line voltage is below 850 V d.c.; the line is then said to be 'receptive'. If the line is above 850 and below 900 V d.c. when a braking application is made, only a portion of the braking energy can be returned to the line, and it is termed 'partially receptive'. Above 900 V d.c., no braking energy is returned to the line and the system is said to be 'non-receptive'; the braking energy from the motors is then dissipated in conventional braking resistors installed on the car. The control system automatically apportions the braking energy between regenerative dynamic braking (wherein the electrical energy produced by the traction motors is returned to the third rail), resistive dynamic braking (where the electrical energy is dissipated by the on-board resistor grid), and conventional friction braking (provided by the vehicle's tread brakes). The system responds to a braking command in a manner that automatically maximizes regenerated energy and minimizes brake shoe wear; each brake command is satisfied by blending the braking options together in the priority sequence, (a) regenerative braking, (b) resistive braking and (c) friction braking.

In the drive mode, initial acceleration is accomplished by using the chopper to limit the armature current and voltage. However, at a standstill, the back-EMF (electromotive force) on the armature is zero and operation of the chopper at its minimum frequency and pulsewidth (approximately 80 Hz and 200 μ s, respectively) would result in too much torque being developed by the motors. Therefore, initial starting torque is regulated by controlling the field flux on the traction motors and operating the chopper at its minimum output. As the speed (and the back-EMF) on the motors builds up, the flux is increased to its maximum value (full fields). Control of motor torque now reverts to the chopper.

As speed increases, the frequency of the chopper is increased from its minimum frequency to 400 Hz. This results in a controlled increase in the average voltage applied to the armatures such that the armature current is constant in spite of the increasing back-EMF. During this variable frequency mode of chopper operation, the pulsewidth (on-time) of the chopper is maintained at the minimum value.

The operating frequency of the chopper stops increasing when it reaches 400 Hz, but the chopper output continues to increase by increasing the pulsewidth (on-time). Again, the motor torque remains constant while speed and back-EMF build, since the average chopper output voltage is increased with increased pulsewidth.

The chopper pulsewidth is increased until the chopper reaches the full-on state. At this point, the full line voltage is applied to the motors. This operating point is the base speed of the motor. Motor base speed is defined as that motor speed at which the back-EMF becomes equal to the applied line voltage.

To continue acceleration above base speed, the field power supplies are regulated to reduce the field flux. Decreasing the flux reduces the back-EMF, thereby maintaining armature current and increasing motor speed. In other words, above base speed, field weakening is used to control tractive effort and speed.

The acceleration control scheme can be summarized as follows:

<u>CHOPPER</u>	<u>FIELD</u>
Minimum Frequency, Minimum Pulsewidth	Increasing Field Flux
Increasing Frequency, Minimum Pulsewidth	Full Field Flux
Maximum Frequency, Increasing Pulsewidth	Full Field Flux
Maximum Frequency, Maximum Pulsewidth (Base Speed)	Full Field Flux
Chopper Full-On	Decreasing Field Flux

The control system senses passenger load and compensates both the propulsion and braking commands to provide constant acceleration and deceleration regardless of weight. Passenger load is sensed by a pressure transducer that monitors the secondary suspension air spring pressure.

3.6 SPIN/SLIDE PROTECTION SYSTEM

Protection against inadvertent wheel spins or slides is provided. By definition, whenever the tangential speed of the wheel differs from the linear speed of the vehicle, a wheel slip occurs. When such a slide or spin occurs, the available acceleration or deceleration of the vehicle is greatly diminished. Slip detection circuits are included in the Electronic Control Equipment (ECE) to maximize the available tractive effort in acceleration and deceleration. Detection of wheel slip is determined on a per-axle basis. In the drive mode, if a spin is detected on any one of the four axles, tractive effort is reduced on all axles until the spin is corrected. Upon correction, tractive effort is reapplied on a jerk-limited basis, to the commanded value. In the brake mode, detection of a slide on any axle causes the electrical braking effort to again be reduced on all axles. At the same time, the friction brake air dump valve is energized on the truck where the wheel is sliding, and friction braking effort is applied (increased) on the other truck.

Detection of a wheel slip is accomplished by comparing the actual wheel rate-of-change of rpm (either acceleration or deceleration) with a maximum predetermined rate. Detection of a slip requires that wheel acceleration or deceleration exceeds the predetermined limit of 8 mi/h/s. In addition to this detection method, a speed difference excess of 5 mi/h between any two axles also triggers the slip correction circuitry.

3.7 TRACTION MOTORS AND TRANSMISSIONS

Four separately-excited d.c. traction motors provide the propulsion and electric braking for the vehicle. Each motor is resiliently mounted to the truck and drives one axle through a gearbox and coupling. The two traction

motors on each truck are electrically connected in series. The total developed torque of the four traction motors is regulated as a function of speed by the series chopper and field power supplies. All the traction motors are identical and completely interchangeable. Each pair of motors is force-ventilated by filtered air. The motors are rated at 120 kW, 360 V, 365 A, at 3,989 rpm continuous. Maximum acceleration and braking currents are 637 and 720 A, respectively. Maximum speed (worn wheels, worst case) is 4,239 rpm. Power is transmitted to the axles through a single reduction, parallel-drive gearbox with a gear reduction ratio of approximately 5.8:1.

3.8 FRICTION BRAKING SYSTEM

As previously discussed in Section 3.5, Propulsion and Control System, the vehicles are retarded by three modes of braking; these are regenerative and resistive dynamic braking, in which the traction motors operate as generators and the braking energy is returned to the rail or absorbed by the onboard resistor banks, and friction braking by conventional brake shoes operating against the wheel treads. For a normal service brake application, the control system responds to a braking command and apportions the braking effort between dynamic braking and friction braking, with priority given to dynamic braking. The friction brakes are brought into operation to fill voids in the dynamic braking effort (such as occur as the vehicle comes to a stop and dynamic braking effort falls below the requested level) and to supplement dynamic braking at the higher passenger loads. The friction brakes are also designed to provide the full service braking effort in the event of a failure of the dynamic braking system, and to provide the total braking effort for emergency stops.

The friction braking system, manufactured by WABCO, operates a tread brake shoe at each wheel. Each brake shoe is actuated by air pressure operating through an air/oil hydraulic intensifier which produces a force at the brake shoe of approximately 121 times the brake cylinder air pressure; typical maximum normal forces are of the order of 9,000 pounds per shoe.

The friction brakes, as currently configured, are unique to the transit industry in that they are constantly held in contact with the wheel treads by a spring inside the brake actuator. Thus, the friction brakes produce a small retardation force at all times. This is an important factor in the context of evaluating the performance data, in that any change in the brake actuator configuration, brake shoe clearance (or brake shoe wear), or primary suspension stiffness can affect the total spectrum of vehicle performance. For example, acceleration rates, train resistance, energy consumption, energy available for regeneration, and duty cycle brake temperatures can all be affected by variation of the pressure of the brake shoes against the wheel.

3.9 DOORS

Each car is equipped with three electrically controlled doors per side. The doors are of the sliding, bi-parting leaf type, retracting into pockets in the carbody sidewall. The door operators are electromechanical actuators

which operate the doors through extension arms; in the closed position an over-center locking feature of the extension arm linkage prevents the door from being opened manually except through the operation of the emergency release. A push-back feature is provided by a spring loaded linkage on the extension arm which allows the doors to be pushed back a total of 3" to allow extraction of clothing and small articles. The doors are equipped with obstruction-detection systems, and interlocks prevent the starting of the car with a door open; full service braking is applied by the interlocks if the doors are opened beyond the push-back feature with the car in motion.

3.10 AUXILIARY POWER SUPPLY

The auxiliary power supply system provides regulated 650 V d.c. for the high voltage auxiliaries, and 37.5 V d.c. for the low voltage control circuits and for battery charging. The components of the auxiliary power supply system are the Auxiliary Power Systems Equipment (APSE) and the battery box. The battery box is mounted only on A and C type cars. (B cars operate only with A cars, in married pairs, and share the A car battery power; C cars are designed to operate independently).

The APSE contains two chopper circuits, the VLC and the LVPS. The VLC is a variable frequency, constant pulse width chopper circuit and provides a regulated 650 V d.c. at up to 116 A (continuous), from input voltages varying between 650 and 900 V d.c.; maximum chopper firing rate is 1.58 kHz. For input voltages from 500 V d.c. to 650 V d.c. the auxiliary supply is unregulated.

The LVPS circuitry also operates as a variable frequency, constant pulse width chopper with a continuous rating of 215 A at 37.5 V d.c. nominal; the maximum firing rate of the LVPS chopper is 500 Hz.

The battery box contains a 240 ampere-hour, 25 cell nickel-cadmium battery set, and provides start-up and emergency low-voltage d.c. power for the vehicle control circuitry; it is sized to provide one hour of operating time for essential low-voltage systems.

3.11 HEATING, VENTILATION, AND AIR CONDITIONING

The air comfort system consists of two separate subsystems, each rated at 9 tons refrigeration effect, which are independently regulated by a common temperature control unit. Each system is comprised of an in-line, air-cooled condenser and compressor assembly mounted undercar, and an evaporator and blower assembly mounted overhead at the end of a centerline air distribution duct. Electric heat assemblies are located downstream of the evaporator coils. Two stages of heat, 6 kW and 2.5 kW, are provided at each overhead unit, together with one stage of floor heating from radiant units.

In service, the system functions automatically to control the cooling and heating cycles in response to preset interior temperature requirements and outside conditions.

The vehicles are integrated into the MARTA rail system by an ATC. Each cab is equipped with an automatic train control system that will start the train upon the pressing of a 'proceed' button, maintain the train at the maximum safe speed, and stop the train at each platform. The operator need only operate the proceed button, open and close the doors, and make public address announcements. The cars also can be operated manually.

The vehicle configurations evaluated during the test program can be classified as:

- Those changes to the vehicle that affected the braking and general performance of the vehicle.
- Those which affected the ride quality.
- Those that were evaluated as part of the curving and stability test.

Three braking system configurations were tested; also tested were three secondary suspension configurations affecting ride quality, two primary suspension configurations, and a modified wheel profile affecting curving performance and stability. For convenience, each group has been given a prefix letter and then numbered sequentially; thus R1, R2, and R3 are configurations affecting ride quality. BR1, BR2, and BR3 represent changes to the braking system, and C1, C2, and C3 represent modifications affecting curving performance and stability. These prefixes have been correlated with the data presented so that test runs, data, and configuration can be readily related. The unique aspects of each configuration are described in detail below:

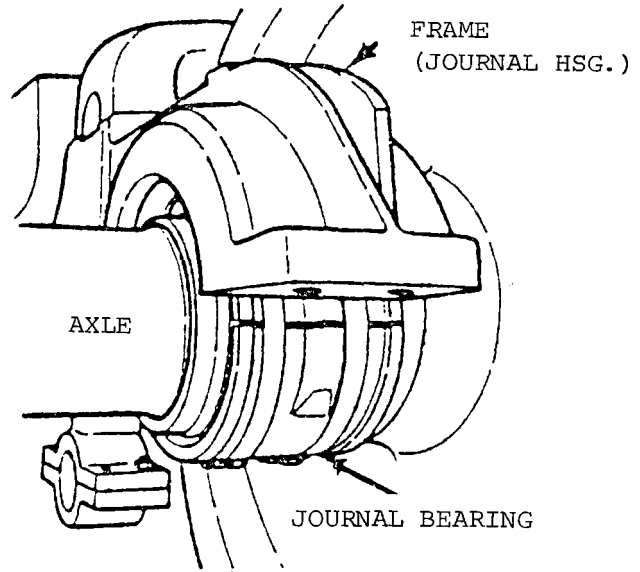
- BR1. Vehicles with braking systems in a standard configuration representative of the MARTA fleet. A high speed 'taper' was incorporated in the braking command signal, which increased the brake cylinder pressure in a linear ramp between 70 mi/h and 50 mi/h, proportional to decreasing speed and independent of master controller position; the object of the taper was to comply with the specification requirement that full service braking be initiated at a deceleration level of 2.0 mi/h/s at 70 mi/h, increasing linearly to 3.0 mi/h/s at 50 mi/h, and maintaining a 3.0 mi/h/s level to a complete stop.
- BR2. The vehicles' friction braking system was modified to a standard detailed by MARTA and WABCO. The existing Servotrol valves were replaced with new units supplied by WABCO; modified A30 and A31 printed circuit boards were installed in the ECE; H-5 Relay air valves were replaced with H-7 type; the variable load valves were modified by replacing the diaphragms and springs with parts supplied by WABCO.

The total effect of the modifications was to remove the high speed taper described in configuration BR1 above, and to add a low speed

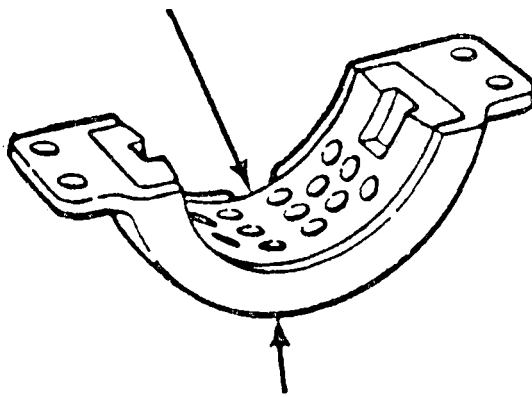
taper; maximum brake cylinder pressure was increased and a small constant application of friction braking which had been present throughout blended braking stops with the BR1 configuration was eliminated.

- BR3. New Servotrol valves with revised command signal/brake cylinder pressure characteristics were installed; new variable load valves, adjusted to provide 48 psig of brake cylinder pressure with 60 psig air spring pressure (corresponding to an AW0 load condition), and 82 psig at 110 psig air spring pressure (AW3) were fitted; the load weigh system within the ECE was recalibrated to correspond with the 60-110 psig air spring pressure range. The low speed taper effect was retained to provide a reduction in brake cylinder pressure below 20 mi/h; this had the effect of reducing the pressure proportionately to speed from 100% at 20 mi/h, to 60% at zero mi/h. The high speed taper between 70 and 50 mi/h was also retained. Internal gains were modified on the A30 and A31 printed circuit boards, resulting in a minimum Servotrol current of 0.202 A at AW0 load conditions and 0.049 A at AW3. The A11 printed circuit board was recalibrated; the original output from this board was 11.0 V at test point 1. After recalibration, the output was 11.40 V. This modification increased the electrical braking demand by 3.6%.
- R1. Ride quality tests were initially carried out with the secondary suspension configured as illustrated in figure 3-4. Motion between the truck bolster and the truck frame was damped by vertical, automotive-type shock absorbers, two per car.
- R2. The vertical shock absorbers described in the R1 configuration were thought to transmit vibrations to the carbody in the frequency range 25-50 Hz; the shock absorbers were removed for this configuration and replaced with a venturi in the air springs, which provided a restriction to airflow and therefore some measure of viscous damping in the vertical direction.
- R3. A third secondary suspension configuration was evaluated in which both the vertical shock absorbers and the air spring venturi were used to provide vertical damping.
- C1. The primary truck suspension is provided by two semi-cylindrical rubber bushings which surround each axle journal bearings and are retained in split journal housings (figure 3-4); longitudinal spring rate of the primary suspension was measured in the truck, and found to be 150,000 lb/in (the rubber bushings were part numbers 3280-P-7452 and 3280-N-7450, lower and upper bushings, respectively). Initial curving and stability tests were carried out on this configuration of primary suspension.
- C2. The rubber bushings described in C1 were subsequently modified at the TTC by removing material near the horizontal axis to reduce the longitudinal spring rate. Further curving and stability tests were carried out, which was expected to have improved curving performance over the standard bushings. The longitudinal spring rate was reduced from 150,000 lb/in to approximately 50,000 lb/in by removing material in the manner illustrated in figure 3-5.

Upper Half of Journal
Housing.
Primary Suspension.



LOWER RUBBER HALF



Lower Half of Journal
Housing and Primary
Suspension Bush.

Lateral Snubber

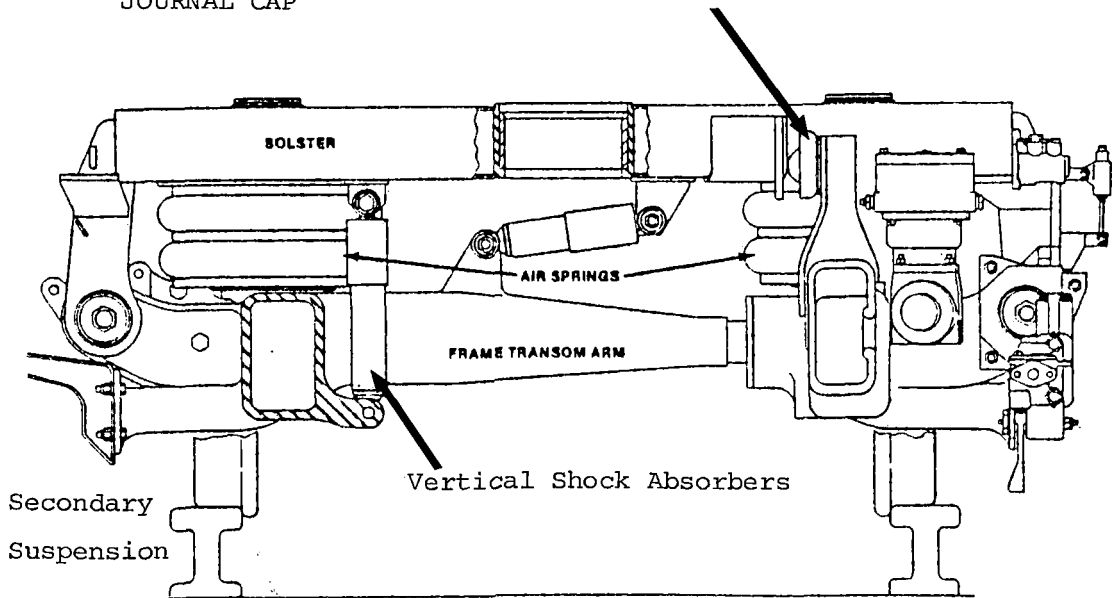
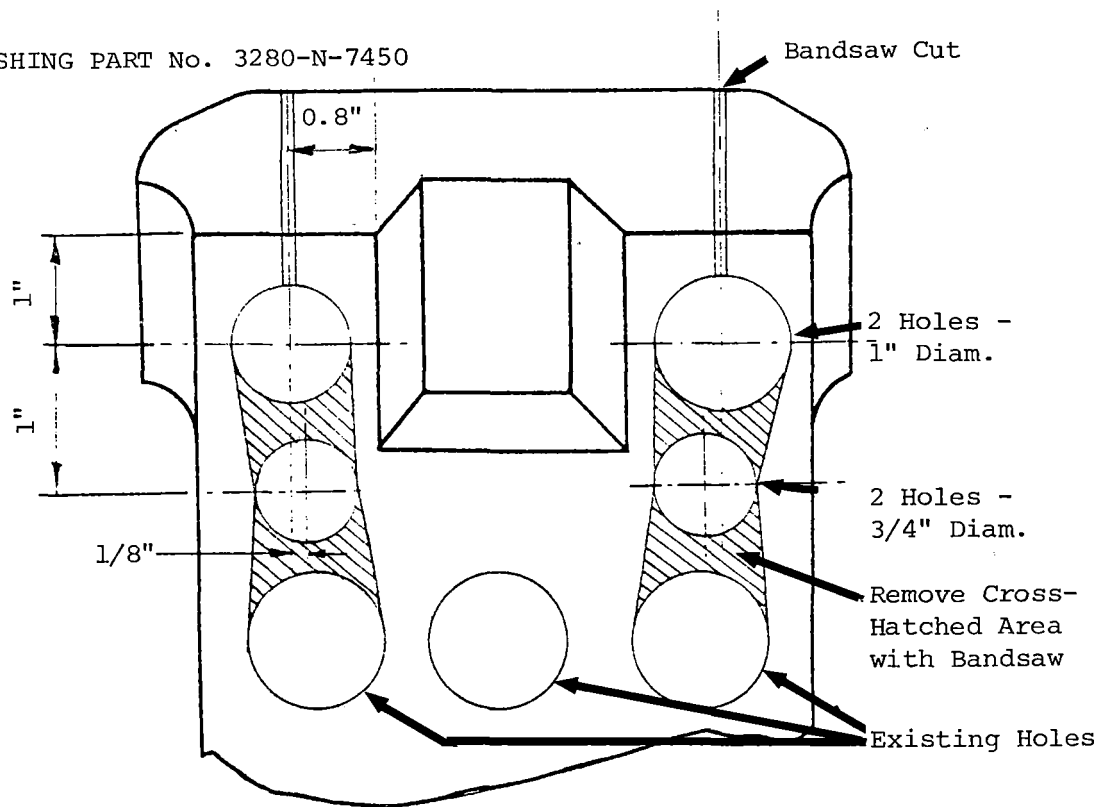


FIGURE 3-4. TRUCK PRIMARY & SECONDARY SUSPENSION.

LOWER BUSHING PART No. 3280-N-7450



UPPER BUSHING PART No. 3280-P-7452

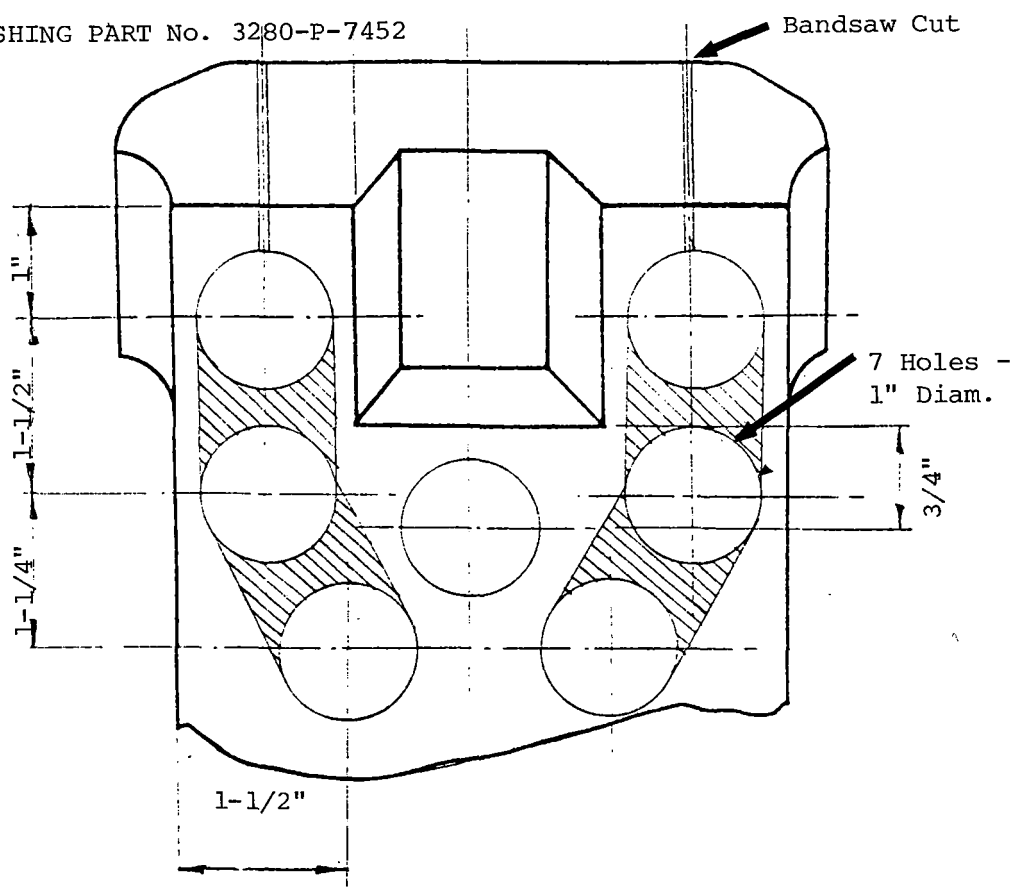


FIGURE 3-5. BUSHING MODIFICATIONS, CONFIGURATION C2.

- C3. A third configuration was evaluated in the curving and stability test program in which the primary suspension bushing modifications described in C2 were combined with high conicity wheel profiles. The profiles were cut on the lead truck of car 0110 only, to a Canadian National 'A' worn wheel profile.

4.0 DESCRIPTION OF FACILITIES

4.1 TRANSIT TEST TRACK

The performance, ride quality and noise tests were conducted on the TTT, a 9.1-mi oval incorporating six typical types of transit track construction. The TTT includes a perturbed section, typical grade crossings and switches, and a 4,000-ft level tangent section that is used for all performance testing and for instrumentation calibration prior to each day's testing.

Track orientation and plan are shown in figure 4-1, and track profile is shown in figure 4-2. Table 4-1 shows the characteristics of each of the six track sections. The perturbed section is located between stations 11.2 and 14.8. The perturbations were made only to the outer rail in profile and alinement; wavelength varied between 14 and 56 ft. Table 4-2 details the amplitude and waveforms of the perturbations. The level tangent section of track between stations 30.0 and 34.0 was used for all brake, acceleration, and tractive resistance tests.

The track is designed for sustained 80 mi/h vehicle operation with the exception of the perturbed track section, which is subject to a speed limit based on ride quality test requirements and safety considerations. For this program, the test speed limit for the perturbed section was 65 mi/h.

Power is provided by a conventional third rail and by a section of overhead catenary cable; the third rail was constructed to NYCTA specifications.

Two alternate sources of electrical power were employed:

- A rectifier station, purchased from the Chicago Transit Authority (CTA), with no-load line voltage preset from 620-780 V d.c., which provided nominal, no-load line voltage of 750 V d.c. (current limit 7,500 A, 2 hrs) at the third rail shoe.
- One of two newly-commissioned rectifier stations, which were built to meet the test requirements of TTC. The voltage can be varied infinitely from 400 to 1,000 V d.c. with a current limit of 11,000 A. The stations each feed from one bus to all of the TTT and are designed to operate in several alternate modes, including computer control. Voltage can be controlled at a constant level at the substation, or sensed at the position of the vehicle on the track and held within the above constraints to a constant value at the vehicle regardless of demand or voltage drop through the rails; in alternate modes of operation the test vehicle can be subjected to a voltage profile or a voltage step as might occur in revenue service at the transition between one substation and another. For the test program, the substation was manually controlled and the voltage was regulated to maintain a nominal no-load level at the substation.

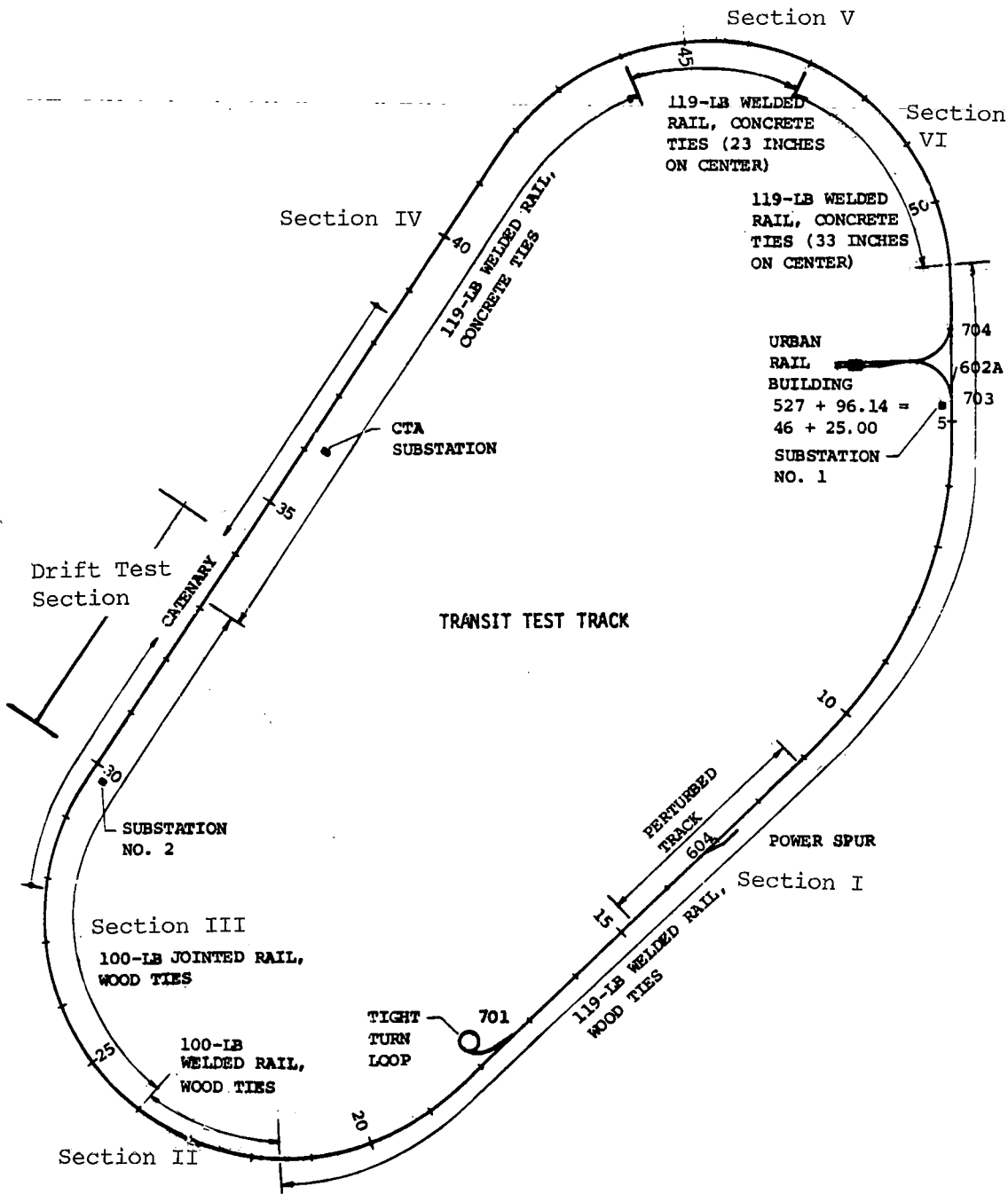
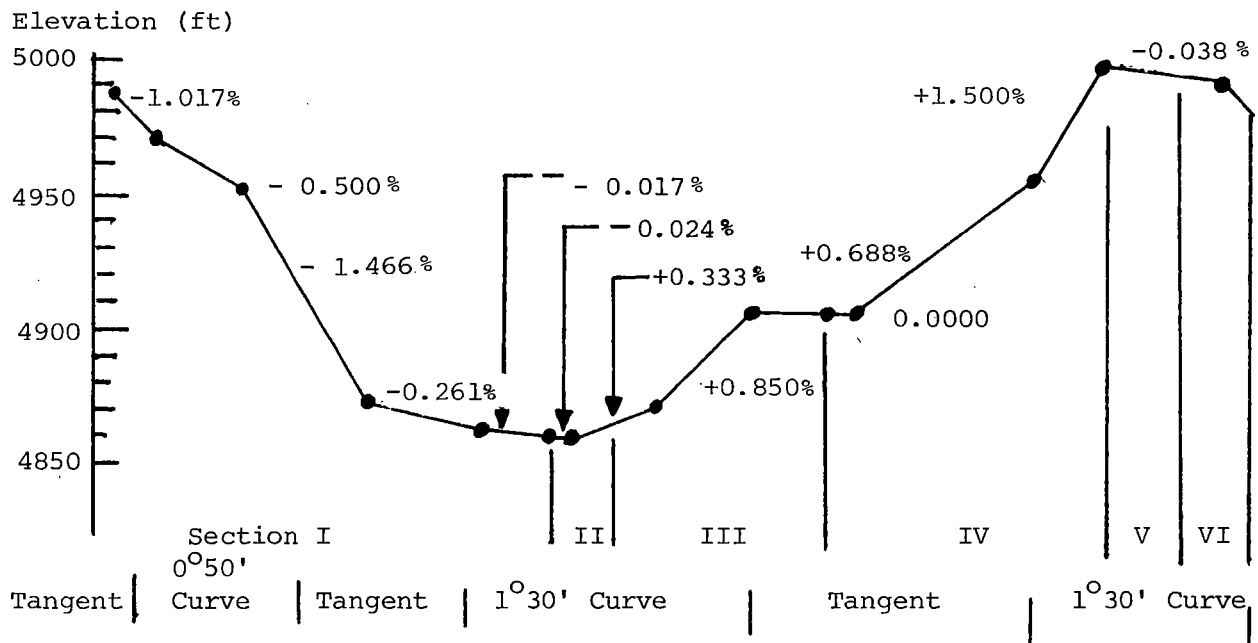


FIGURE 4-1. TRANSIT TEST TRACK.



NOTES:

Track Curvature:

Sta.	to	Sta.	Degree of Curve
55.3		10.3	0° 50'
18.9		29.4	1° 30'
41.8		50.8	1° 30'

Curve Superelevation:

1°30' curves are superelevated a maximum of 4.5". The maximum superelevation on the 0°50' curve is 2".

Elevation:

Minimum - 4,863 ft. at Sta. 22.0.

Maximum - 5,003 ft. at Sta. 46.0.

FIGURE 4-2. TRANSIT TEST TRACK PROFILE SHOWING GRADES.

TABLE 4-1. TTT CONSTRUCTION DETAILS.

Section	Location (Sta to Sta)	Alinement	Trackage	Fastener	Rail
I	51.0 - 17.4	Tangent and 0° 50' curve	Wooden ties 24" on center	Spike	119 lb/yd Welded
	17.4 - 21.5	1° 30' curve	Wooden ties 23" on center		
II	21.5 - 24.0	1° 30' curve	Wooden ties 23" on center	Spike	100 lb/yd Welded
III	24.0 - 29.0	1° 30' curve	Wooden ties 23" on center	Spike	100 lb/yd Jointed
	29.0 - 33.0	Tangent	Wooden ties 24" on center		
IV	33.0 - 40.5	Tangent	Concrete ties 30" on center	Spring Clip	119 lb/yd Welded
	40.5 - 44.0	1° 30'	Concrete ties 27" on center		
V	44.0 - 47.0	1° 30'	Concrete ties 23" on center	Spring Clip	119 lb/yd Welded
VI	47.0 - 51.0	1° 30'	Concrete ties 33" on center	Spring Clip	119 lb/yd Welded

TABLE 4-2. AMPLITUDE AND WAVEFORMS OF TTT PERTURBATIONS, DESIGN SPECIFICATIONS.

Profile					Alinement			
Sta 11.8	Sta 12.0	Sta 12.2	Sta 12.4	Sta. 12.6	Sta. 13.6	Sta 13.8	Sta 14.0	
1.5"	0.38"	0.38"	0.75"	1.5"	0.75"	0.38"	0.75"	
1.48" ± 1 tie	0.30" ± 1 tie	0.36" ± 1 tie	0.71" ± 1 tie	1.43" ± 1 tie	0.74" ± 1 tie	0.30" ± 1 tie	0.71" ± 1 tie	
1.42" ± 2 ties	0.15" ± 2 ties	0.30" ± 2 ties	0.61" ± 2 ties	1.22" ± 2 ties	0.71" ± 2 ties	0.15" ± 2 ties	0.61" ± 2 ties	
1.34" ± 3 ties	0.02" ± 3 ties	0.23" ± 3 ties	0.46" ± 3 ties	0.92" ± 3 ties	0.67" ± 3 ties	0.02" ± 3 ties	0.46" ± 3 ties	
1.22" ± 4 ties	0" ± 4 ties	0.15" ± 4 ties	0.29" ± 4 ties	0.58" ± 4 ties	0.61" ± 4 ties	0" ± 4 ties	0.29" ± 4 ties	
1.70" ± 5 ties		0.07" ± 5 ties	0.14" ± 5 ties	0.28" ± 5 ties	0.54" ± 5 ties		0.14" ± 5 ties	
0.92" ± 6 ties		0.02" ± 6 ties	0.04" ± 6 ties	0.07" ± 6 ties	0.46" ± 6 ties		0.04" ± 6 ties	
0.75" ± 7 ties		0" ± 7 ties	0" ± 7 ties	0" ± 7 ties	0.38" ± 7 ties		0" ± 7 ties	
0.58" ± 8 ties					0.29" ± 8 ties			
0.42" ± 9 ties					0.21" ± 9 ties			
0.28" ± 10 ties					0.14" ± 10 ties			
0.16" ± 11 ties					0.08" ± 11 ties			
0.07" ± 12 ties					0.04" ± 12 ties			
0.02" ± 13 ties					0.01" ± 13 ties			
0" ± 14 ties					0" ± 14 ties			
Wave Length	56'	14'	28'	28'	28'	56'	14'	28'

- Notes:
1. Only outer rail is perturbed.
 2. Alinement accomplished by perturbing rail towards outside of oval.
 3. Perturbations are symmetrical around station number; distance from station number is indicated in number of ties.

4.2 FAST TRACK AND BALLOON LOOP

A curving and stability test program was carried out to determine the behavior of the trucks and wheelsets during curving and to relate this information to a mathematical prediction of wheel wear. As the TTT curves are limited to $1^{\circ} 30'$ (the angle subtended by a 100-ft chord), the test program was carried out by using a locomotive to push a vehicle along sections of the FAST track and the Balloon Loop, where curves typifying rapid transit revenue service are to be found. A general map of the TTC, showing the locations of the Transit Test Track, the Balloon Loop, and the FAST track is shown in figure 4-3; a detailed layout of the FAST track is shown in figure 4-4. The test program employed FAST track sections 03 (5° curve), 07 (5°), 13 (4°), 17 (two curves of 3° and 5°), and 22 (tangent track section) and the Balloon Loop (7° curve).

4.3 CLIMATIC CONDITIONS

The TTC is located on semiarid rangeland, subject to large daily temperature variations, bright sunlight, and low humidity. Average daily temperatures range between a minimum of 15°F in January and a maximum of 92°F in July. The lowest temperature on record is -31°F and the highest is 105°F . Freezing temperatures occur during 152 days of the year. Annual precipitation averages 12". The sun shines during about 73% of the daylight hours. At ground level, there is typically 25% to 75% more solar radiant energy than along the northeast coastal regions of the United States.

In general, the dry and sandy conditions with minimal industrial pollution result in high wheel/rail adhesion. The elevation (4,950 ft) gives a lower air density than is usual at most transit properties. Average barometric pressure is 25.2" of mercury.

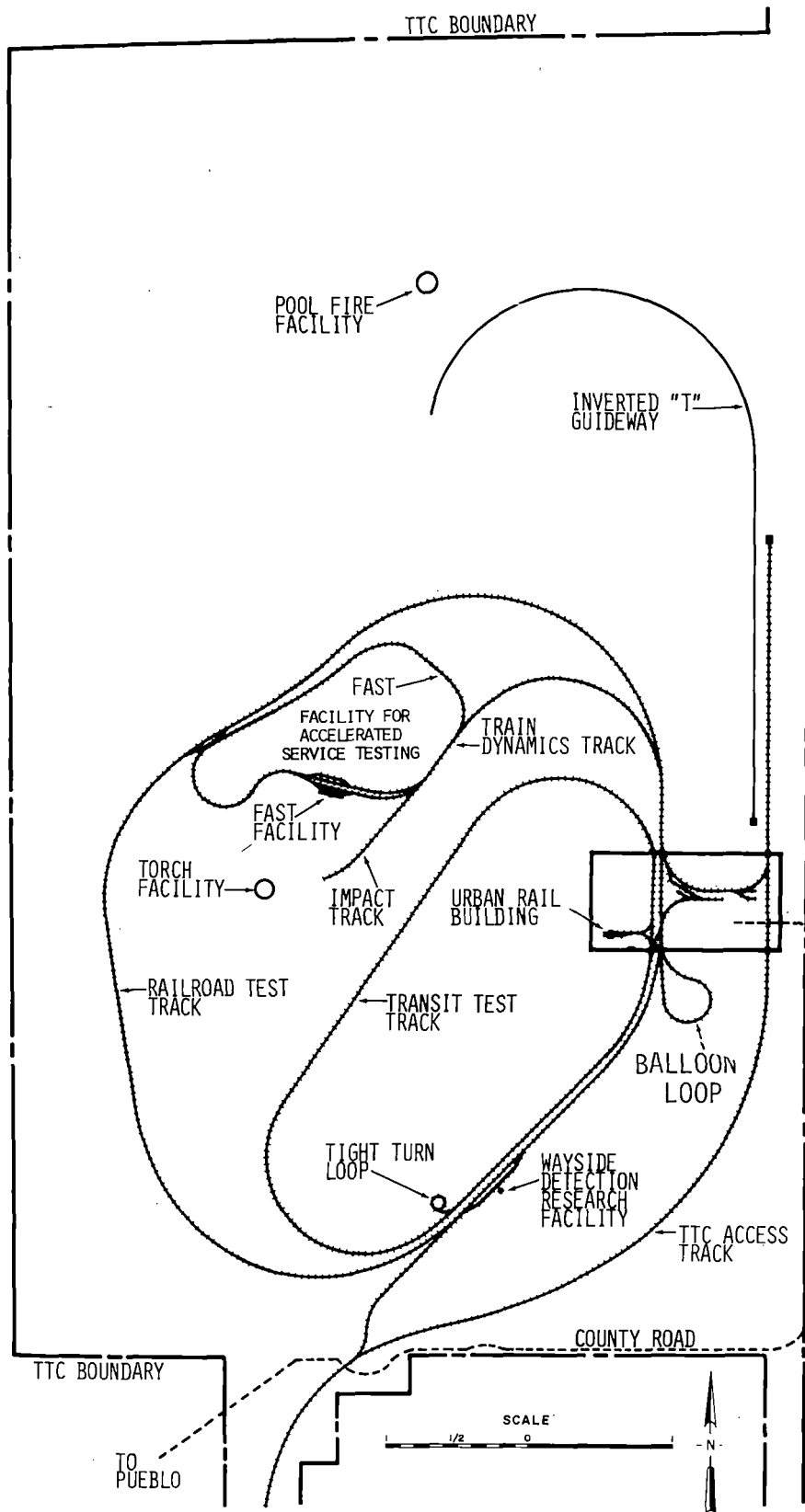
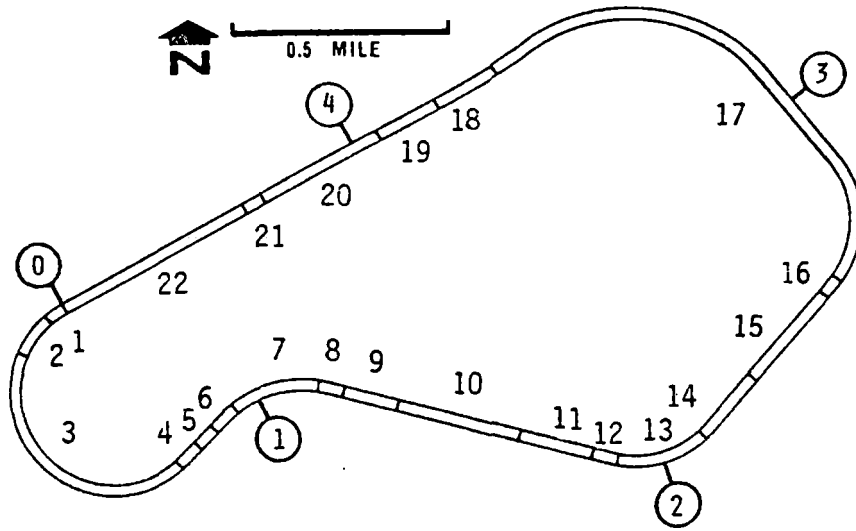


FIGURE 4-3. TTC TEST TRACKS GENERAL LAYOUT.



THE FAST TRACK

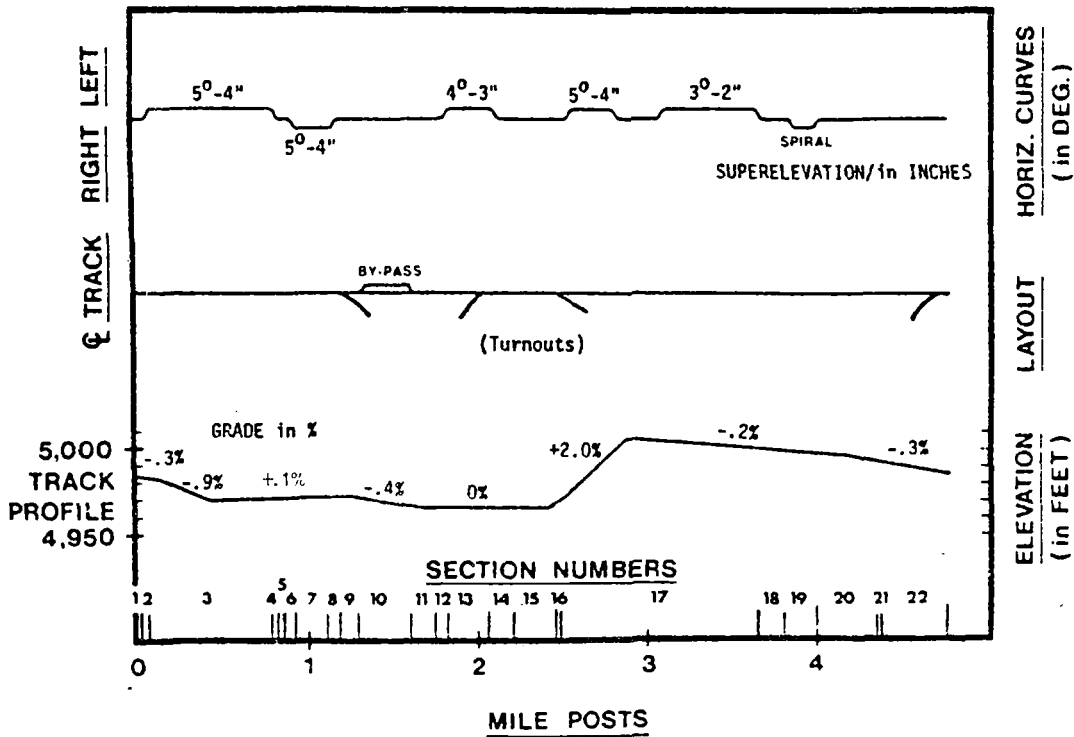


FIGURE 4-4. LAYOUT OF THE FAST TRACK.

5.0 INSTRUMENTATION, DATA ACQUISITION, AND DATA PROCESSING

A detailed discussion of the data acquisition process, a description of the instrumentation used, and the data processing methodology and equipment are included in appendix A. Pertinent aspects of data acquisition, instrumentation, and data processing for each test are included in the following sections (6.0 through 12.0).

6.0 PERFORMANCE TESTS

The purpose of the performance tests was to characterize the operational capabilities of the vehicles. Performance characteristics were defined for acceleration, braking in all modes of operation (i.e., blended, friction-only, dynamic-only modes of service braking, and emergency braking), train resistance, energy consumption, spin/slide protection, and duty cycle thermal characteristics. The vehicle performance was compared to the design specification requirements, wherever applicable, as detailed in Metropolitan Atlanta Rapid Transit Authority, Specifications for the Procurement of Transit Vehicles, Contract No. CQ 310, prepared by Parsons, Brinkerhoff, and Tudor (PBT) for MARTA.

The performance of two vehicle configurations is described in the following test program discussion. The final brake configuration evaluated has been used as the baseline configuration in describing the performance characteristics of the vehicles. This configuration was incorporated in the vehicles by MARTA/PBT at the conclusion of the test program, and is described as configuration BR3 in section 3.13, Vehicle Configurations. It represents a prototype configuration unique to the test vehicles at TTC, and was chosen to represent the acceleration and braking performance because, at the time of reporting, it was the latest vehicle improvement attempted in this area.

The performance characteristics of the vehicles with the braking system set up to the BR1 and BR2 configurations are compared to the baseline data at the conclusion of each test results discussion in the Acceleration and Deceleration test program sections (6.1 and 6.2, respectively). The reader should note the baseline data (i.e., configuration BR3) were obtained with new 34" diameter wheels; the BR1 and BR2 configuration tests were made with partially-worn 32½" diameter wheels.

6.1 ACCELERATION

6.1.1 Test Objective

The test objective was to determine the overall acceleration characteristics of the test vehicles as affected by master controller position, weight, direction of travel, and line voltage; and to compare these characteristics with the specification requirements. The requirements are:

- Tractive effort shall be directly proportional to the trainline P-signal, adjusted on each vehicle to compensate for the gross weight.
- The propulsion system shall provide an initial acceleration of 3.0 mi/h/s from zero speed to a preselected speed such that the following time to speed criteria are met:

<u>Speed (mi/h)</u>	<u>Maximum time to achieve speed (s)</u>
15	6
24	9
50	32
70	91

- The performance specified shall be achieved at all weights up to AW2, with new wheels, on level tangent track and with all voltages between 650 and 900 V d.c. at the current collector.
- The P-signal proportioning shall be such that at a P-signal amplitude of 80% (50% of the propulsion range), the propulsion system shall provide an initial acceleration of 1.5 mi/h/s such that the following time-to-speed criteria are met:

<u>Speed (mi/h)</u>	<u>Maximum time to achieve speed (s)</u>
15	11
24	17
30	23
50	92

6.1.2 Test Method

The vehicles were positioned on the level, tangent track section between stations 30.0 and 34.0. Acceleration runs were made from a standing start to 70 mi/h or maximum speed at master controller settings of P2 and full power; three vehicle weights, AW0, AW2, and AW3, and three line voltages of 550, 750, and 825 V d.c. were tested with control from the cab of each car.

The voltage was limited to 825 V d.c. by an over-voltage protection device which was not readjusted for the test and prevented operation of the cars at higher voltages. The requirement to demonstrate the specified level of performance at voltages up to 900 V d.c. was therefore not addressed. The 550 V d.c. voltage case was chosen to demonstrate the ability of the vehicles to operate at low voltages; below this voltage level, a low voltage trip would occur whenever an acceleration was attempted, and so the ability to operate at 500 V d.c. line voltage was not evaluated.

6.1.3 Test Results

6.1.3.1 BR3 Configuration, 34" diameter Wheels. In general, the vehicles met the intent of the specification requirements for an initial acceleration of 3.0 mi/h/s and the time-to-speed criteria, quoted in Section 6.1.1 for full power acceleration, at nominal line voltages of 750 to 825 V d.c. and at vehicle weights up to AW2.

Performance was shown to be independent of vehicle direction of travel or operating cab. The full power acceleration characteristics as affected by line voltage and direction of travel are shown in figure 6-1; the plots show some deterioration in the acceleration level for the low voltage (550 V d.c.) case, which is also evident in the time-to-speed plot, figure 6-2. This is not significant since the specification requires only that the performance be maintained over the voltage range of 650 to 900 V d.c. at the third rail pickup.

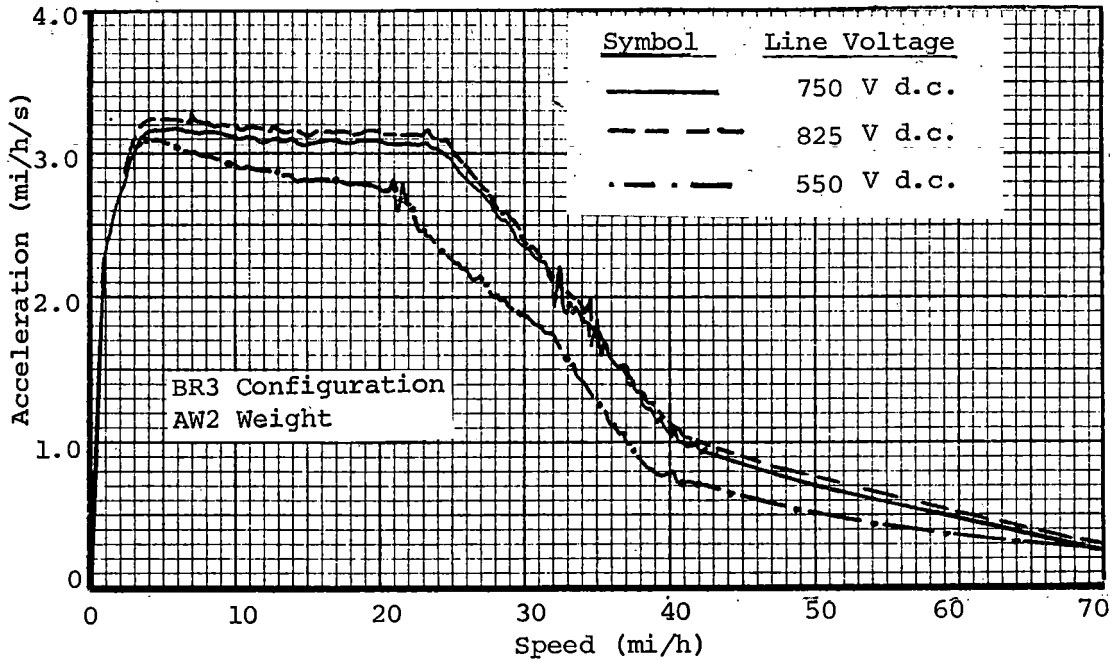
Full power acceleration levels were shown to be independent of vehicle weight up to AW2 (the specification requirement) with some deterioration in performance up to 40 mi/h above this weight (figure 6-3); this is also illustrated in the time-to-speed plots for various vehicle weights, figure 6-4, and in table 6-1 which compares vehicle specification time-to-speed criteria with the test data. The vehicles met the time-to-speed criteria to within one or two seconds at speeds up to 50 mi/h, with a slight performance degradation at the higher weights.

The time-to-speed data at 70 mi/h should be treated with some caution since the marginal levels of acceleration available at higher speeds (approximately 0.3 mi/h/s) cause small changes in acceleration (from curve entry, gradient, or surface wind effects) to give rise to large changes in the time-to-speed data. Where these data were considered to be inaccurate due to any of the above circumstances, they have been omitted from the test data tabulation.

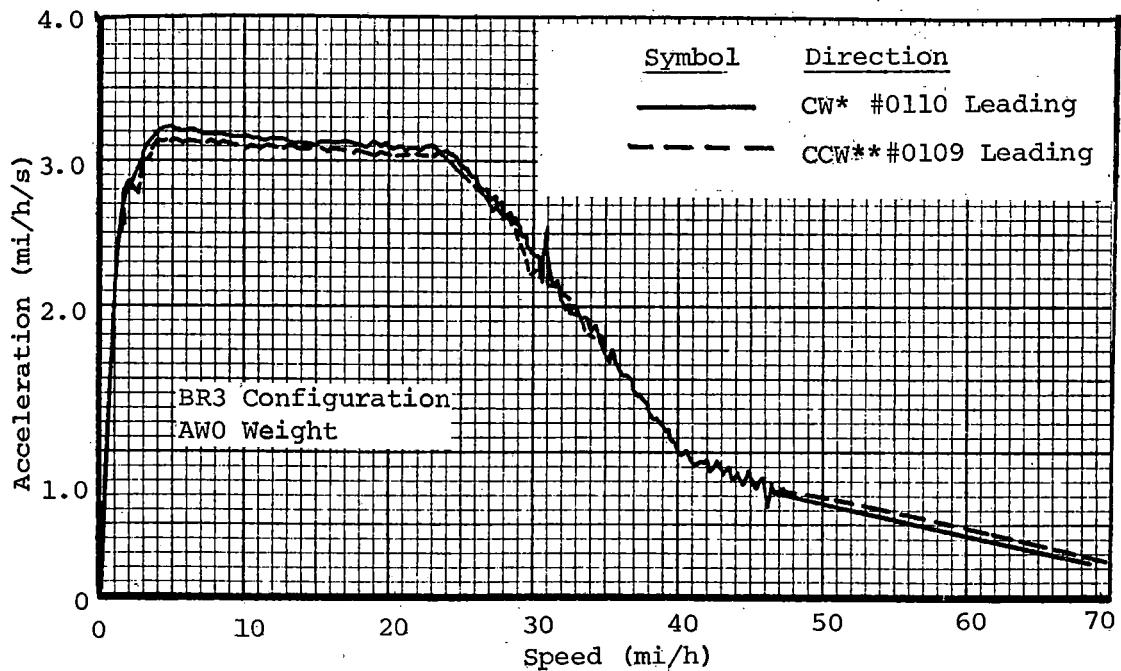
Compliance with the specification acceleration criteria at the 50% propulsion level was evaluated by carrying out acceleration runs at the P2 master controller position. This controller position gave a P-signal output of 8 V at the vehicle monitor panel, compared to 10 V for a full power controller position; i.e., 80% of P-signal amplitude (which corresponds to a propulsive effort demand of 50% of maximum). This can be seen in figure 6-5, which illustrates the P-signal/tractive effort demand characteristics. Acceleration levels at the P2 controller position fell below the specification requirement of 1.5 mi/h/s, at 1.2 -1.3 mi/h/s, as shown in figure 6-6, and the times-to-speed were also in excess of the specification criteria by approximately 5 s up to 30 mi/h (table 6-1); at 50 mi/h, the vehicles met the time-to-speed criterion of 92 s.

The acceleration tests reported herein were carried out with new wheels. Time-to-speed data were taken by measuring the elapsed time from the first motion of the master controller; approximately 1½ seconds of control response time can be subtracted from the times presented, if information is required on time-to-speed from the first motion of the vehicles.

6.1.3.2 BR2/BR3 Configuration Comparison. Acceleration performance characteristics for the BR2 vehicle configuration with 32½" diameter wheels are compared to the baseline (BR3 configuration with 34" diameter wheels) characteristics in figures 6-7 through 6-12. Figures 6-7, 6-8, and 6-9 compare the effect of vehicle weight on acceleration and time-to-speed on each configuration at the full power controller setting. BR2 configuration data have been overlayed on the BR3 baseline plots as a series of discrete data points for clarity. In general, the BR2 configuration and the BR3 configuration had



a. Acceleration. Effect of Line Voltage.



b. Acceleration. Effect of Direction of Travel.

* Clockwise

** Counterclockwise

FIGURE 6-1. FULL POWER ACCELERATION CHARACTERISTICS.

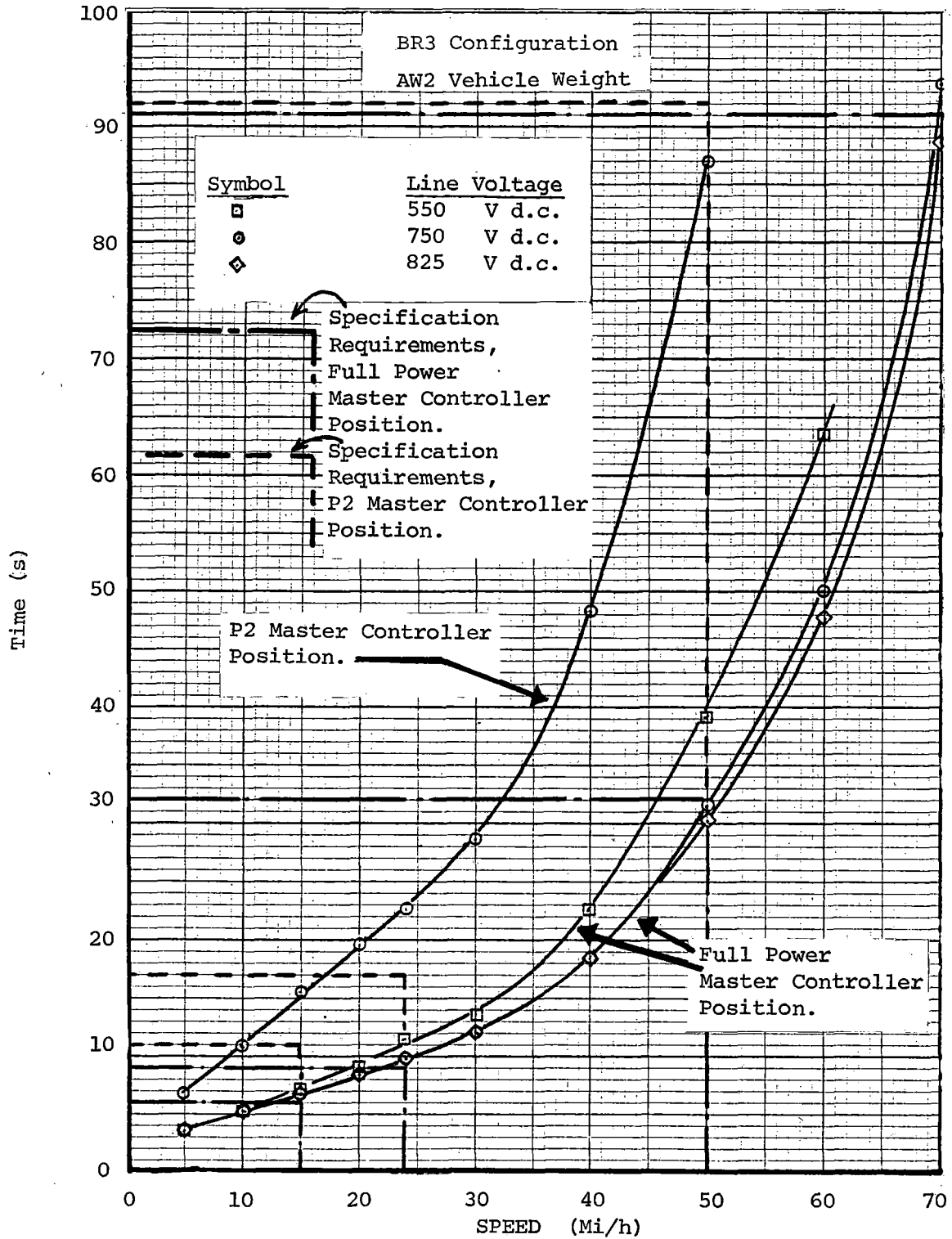


FIGURE 6-2. EFFECT OF LINE VOLTAGE AND MASTER CONTROLLER POSITION ON TIME-TO-SPEED.

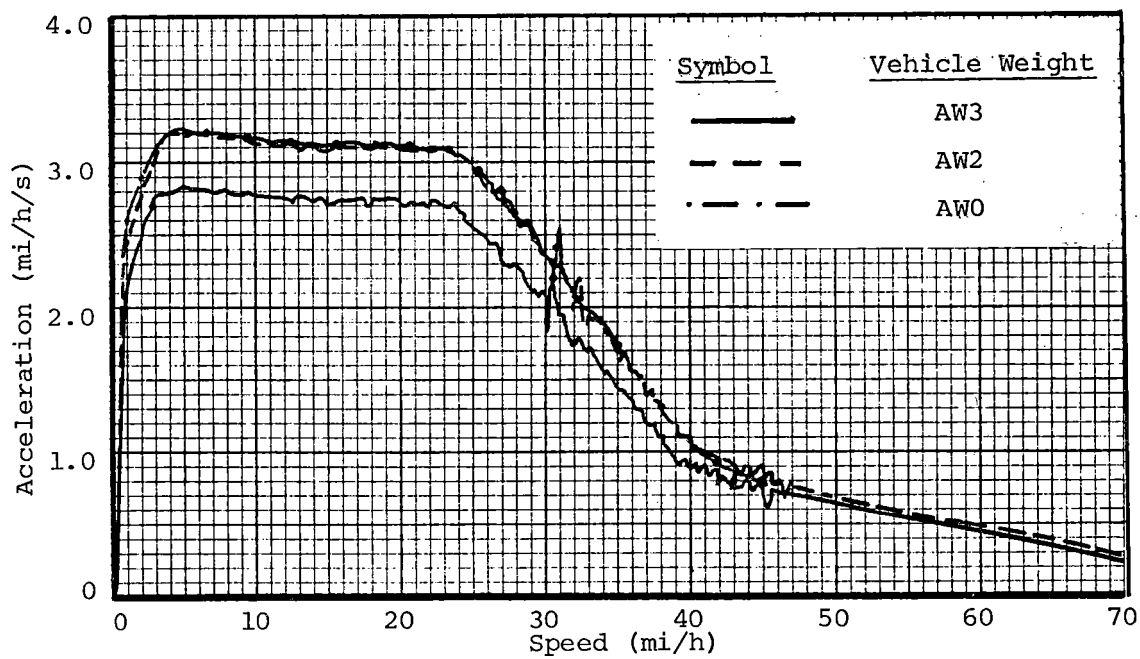


FIGURE 6-3. EFFECT OF VEHICLE WEIGHT ON ACCELERATION.

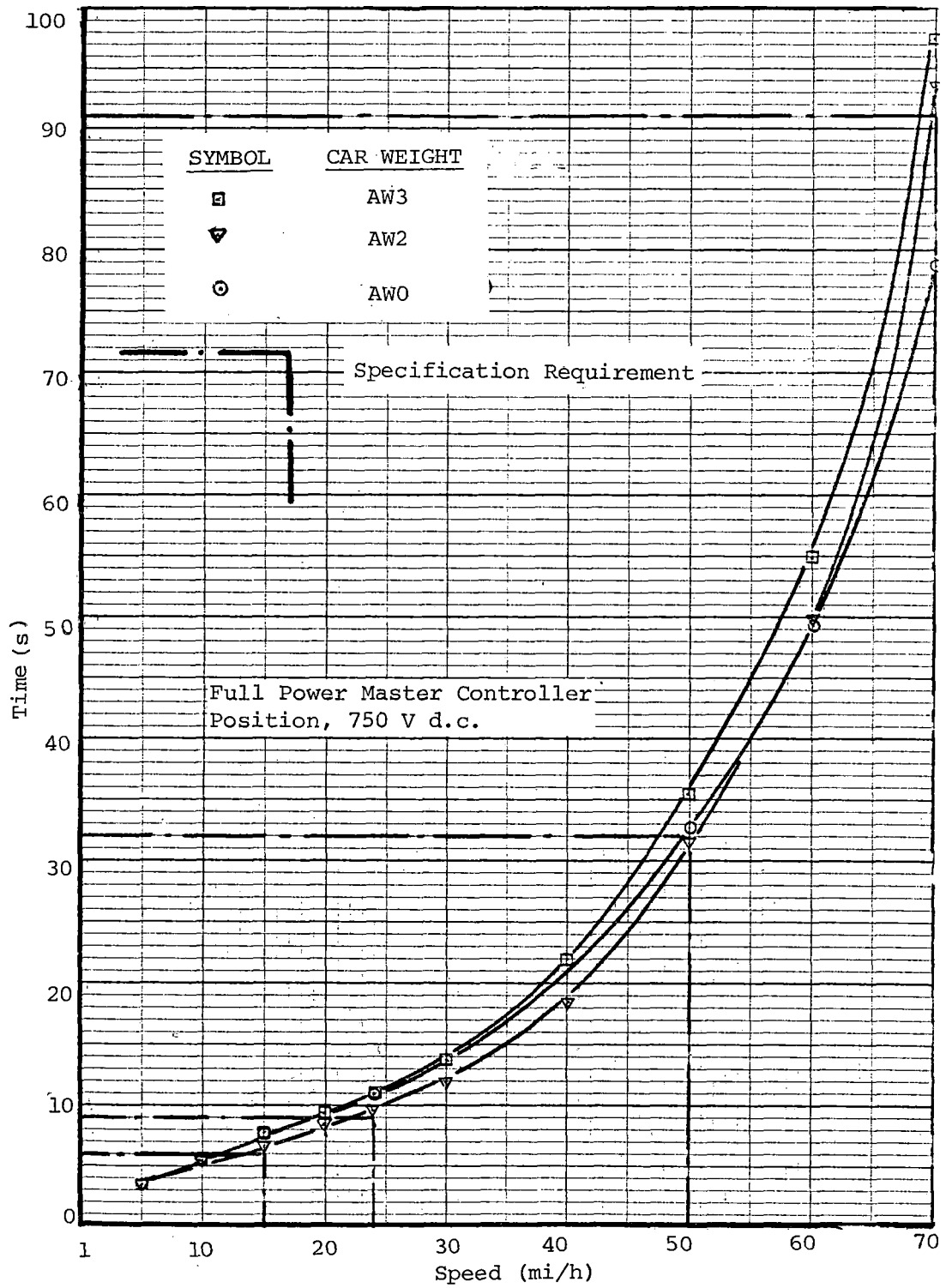


FIGURE 6-4. EFFECT OF VEHICLE WEIGHT ON TIME-TO-SPEED.

TABLE 6-1. VEHICLE SPECIFICATION TIME-TO-SPEED CRITERIA
 COMPARED WITH TEST DATA.

Specification Requirement*			Test Data (Time to Achieve Required Speed, s)**				
Master Controller Position	Speed (mi/h)	Max. Time to Achieve (s)	550 V d.c. AW2	750 V d.c. AW0	750 V d.c. AW2	750 V d.c. AW3	825 V d.c. AW2
Full	15	6	7.2	6.6	6.8	7.4	6.8
"	24	9	10.7	9.7	9.7	10.9	9.9
"	50	32	39.4	31.6	31.2	34.2	29.6
"	70	91	----	----	93.8	97.6	88.6
P2	15	11		16.1	15.5	15.8	
"	24	17		23.5	22.6	23.8	
"	30	23		29.9	28.7	29.8	
"	50	92		----	87.0	84.3	

* At vehicle weights up to AW2 and line voltages from 650 to 900 V d.c.

** BR3 Configuration

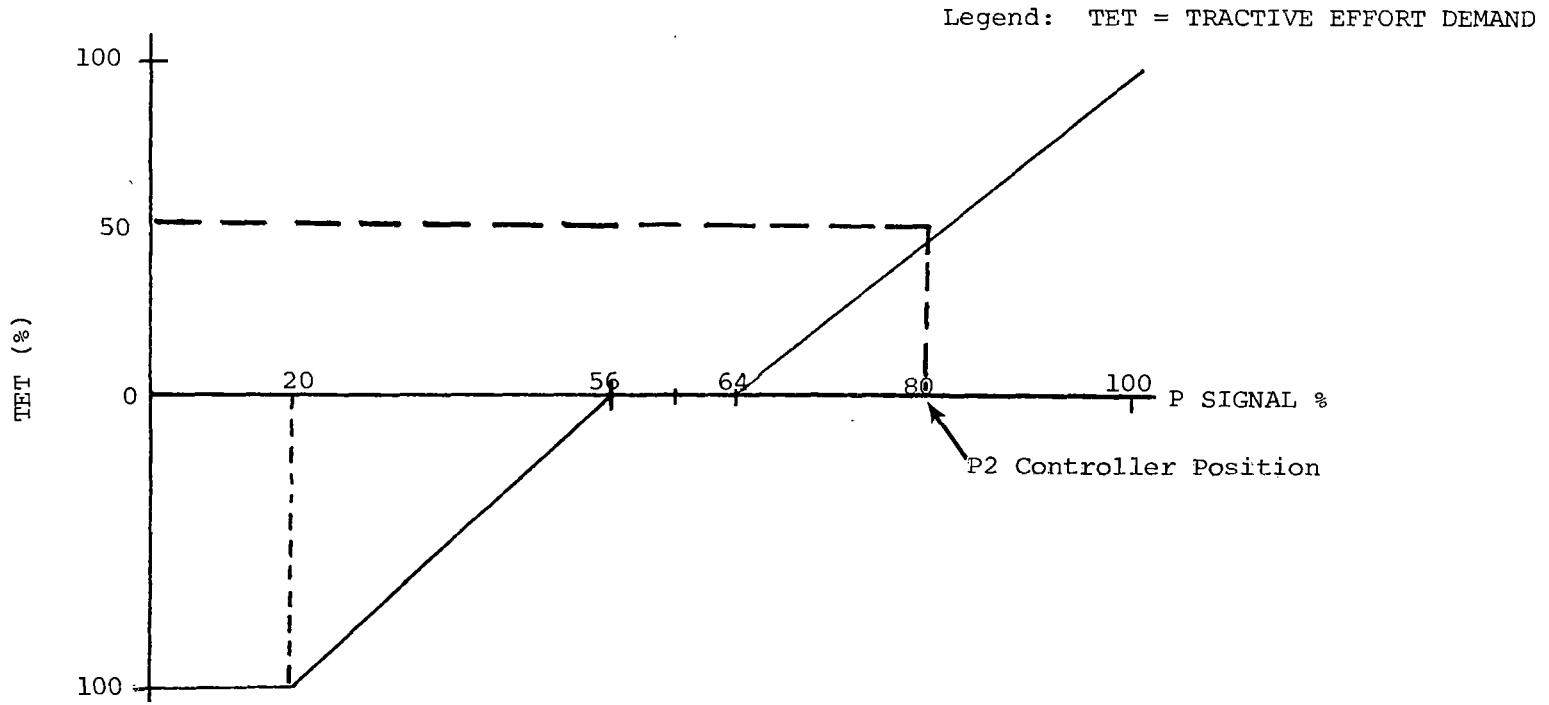


FIGURE 6-5. TRACTIVE EFFORT/CONTROL SIGNAL RELATIONSHIP.

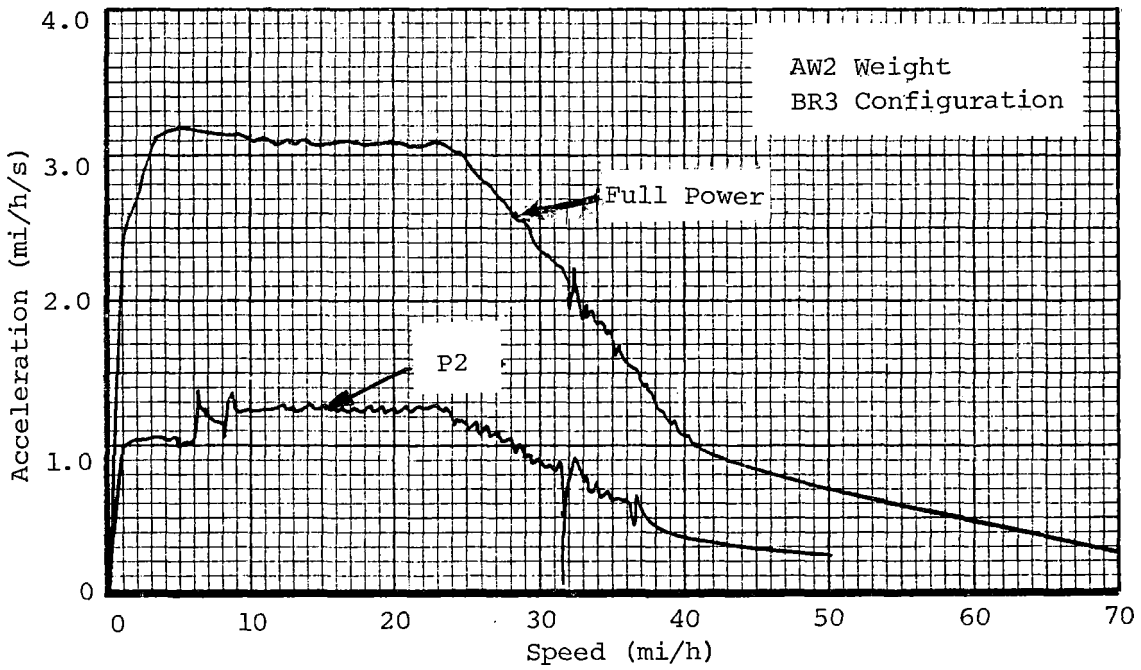


FIGURE 6-6. ACCELERATION - FULL POWER AND P2 MASTER CONTROLLER POSITION.

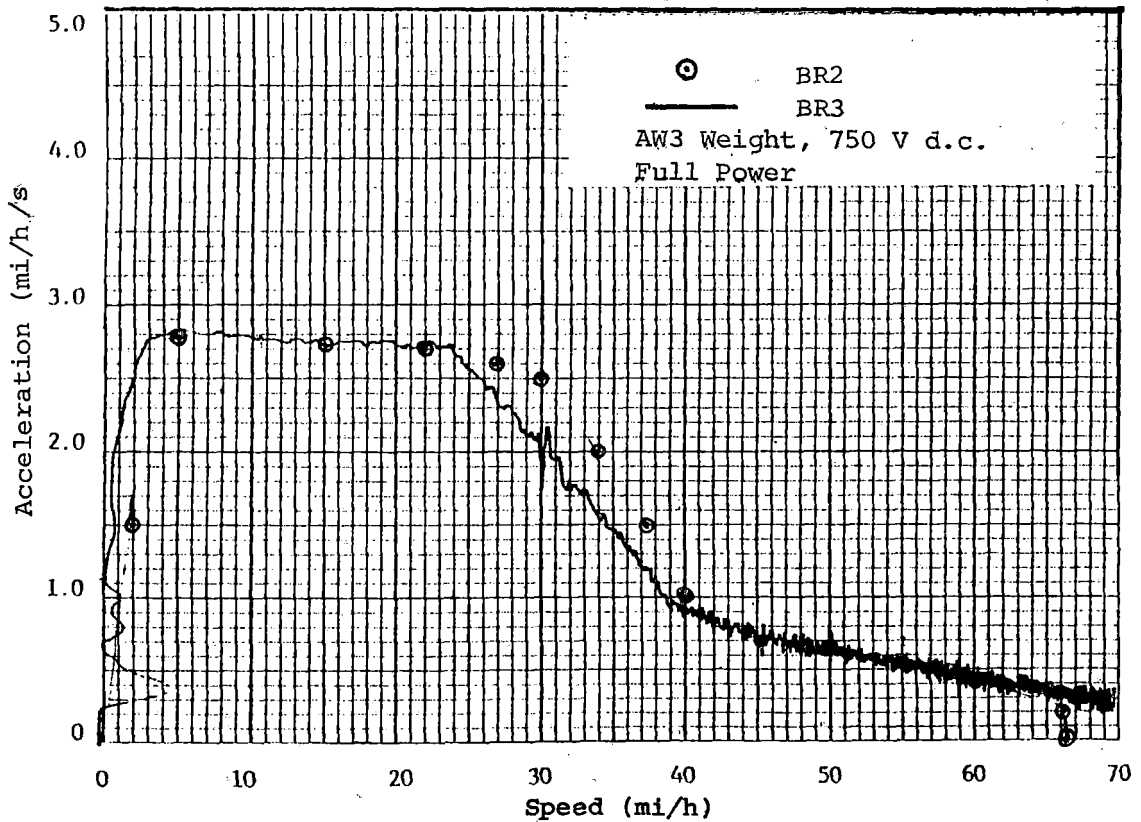
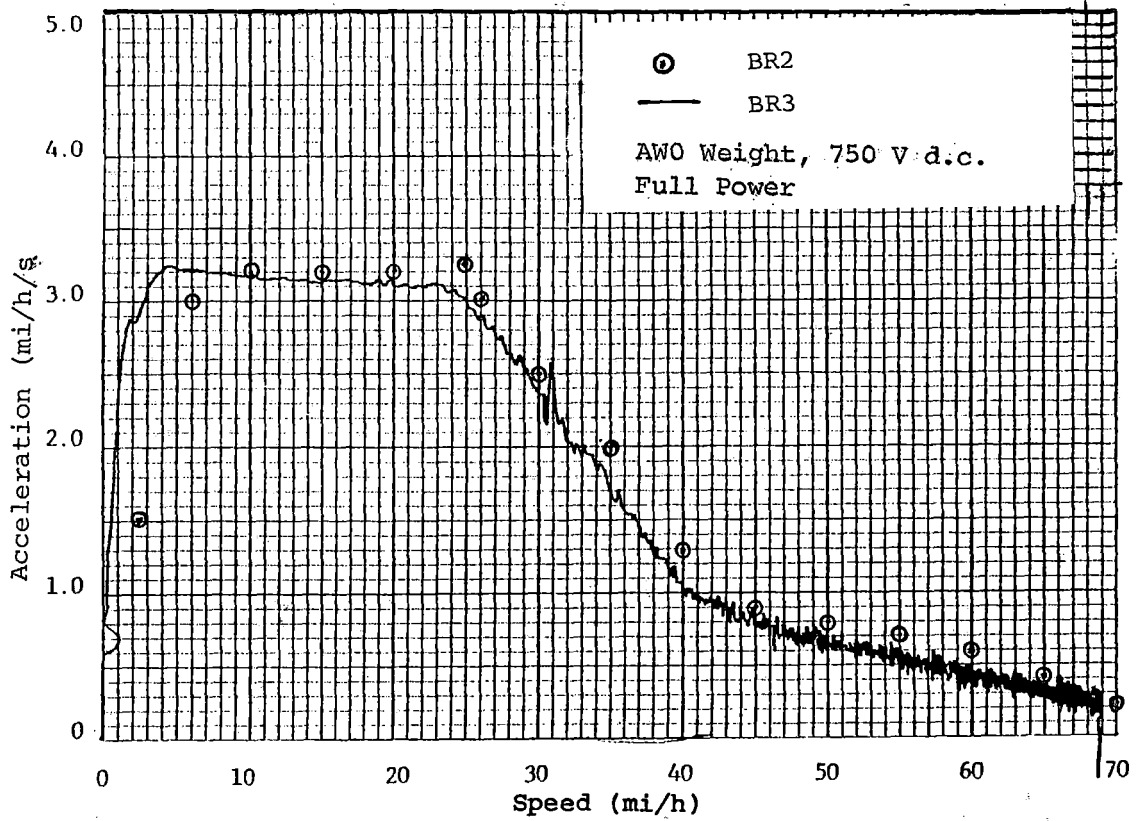


FIGURE 6-7. ACCELERATION PERFORMANCE - COMPARISON OF BR3 WITH BR2 CONFIGURATION AT AW0 and AW3 WEIGHT.

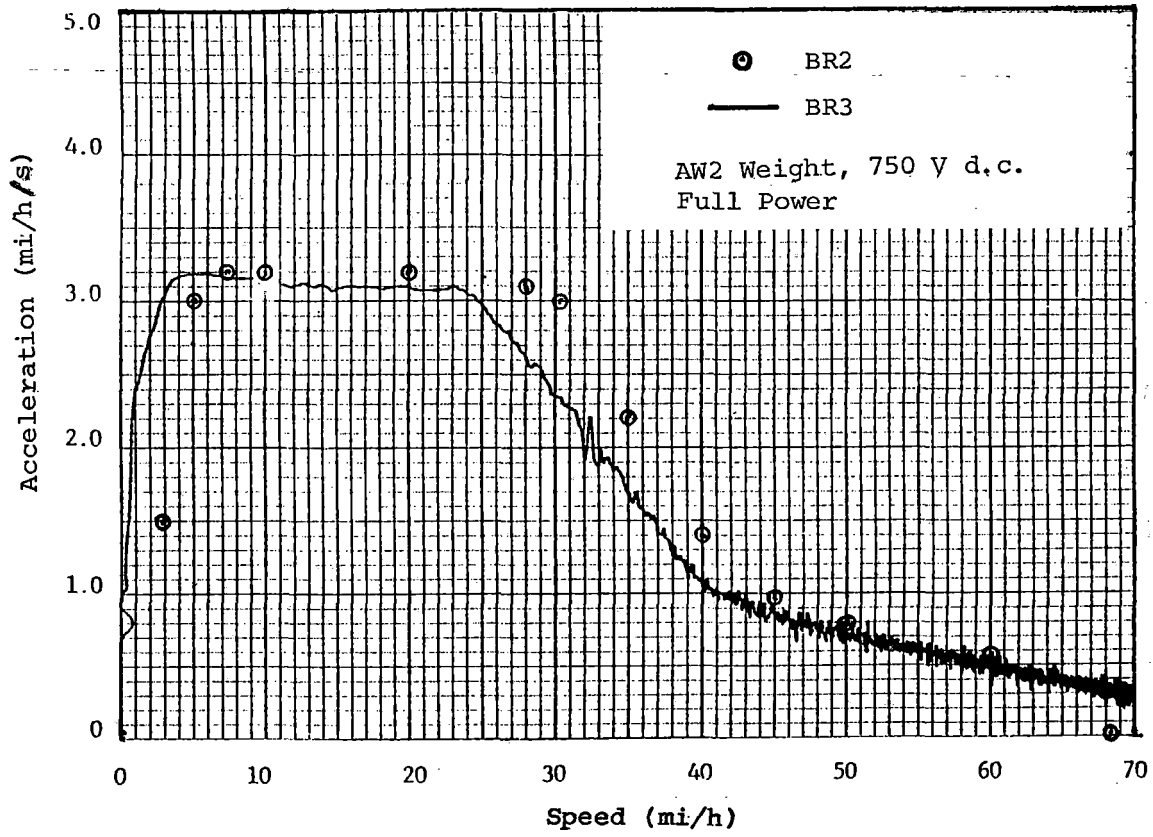


FIGURE 6-8. ACCELERATION PERFORMANCE - COMPARISON OF BR3 WITH BR2 CONFIGURATION AT AW2 WEIGHT.

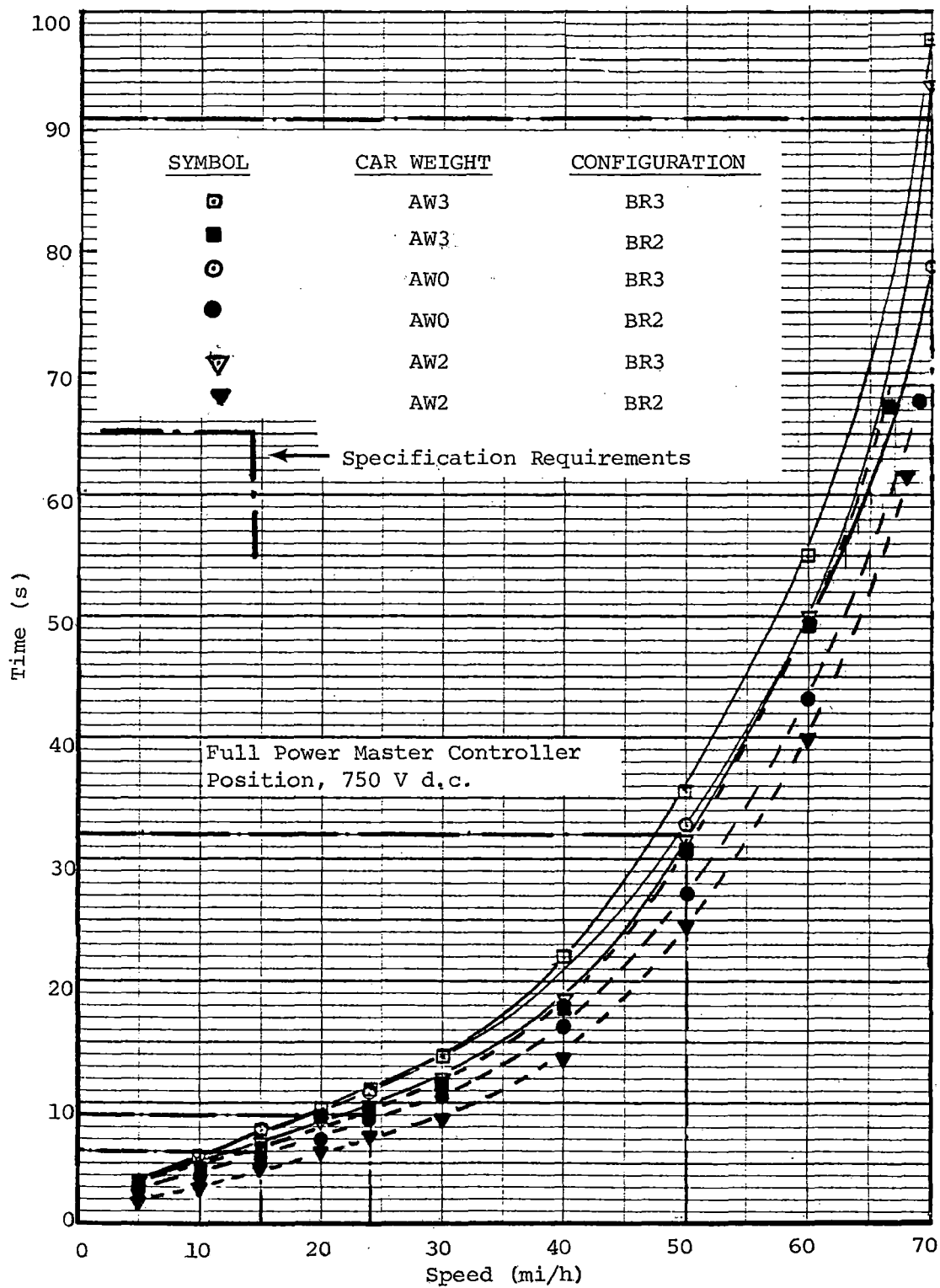


FIGURE 6-9. EFFECT OF VEHICLE WEIGHT ON TIME-TO-SPEED FOR BR3 AND BR2 CONFIGURATIONS.

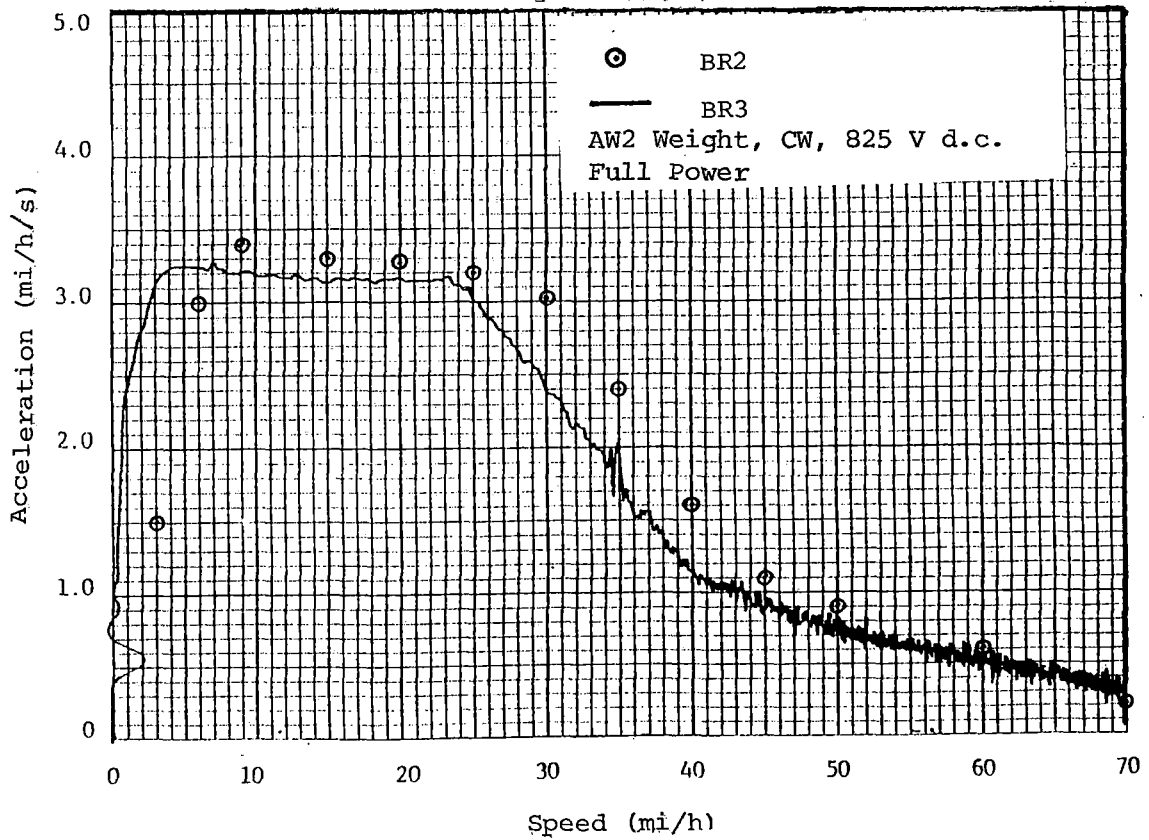
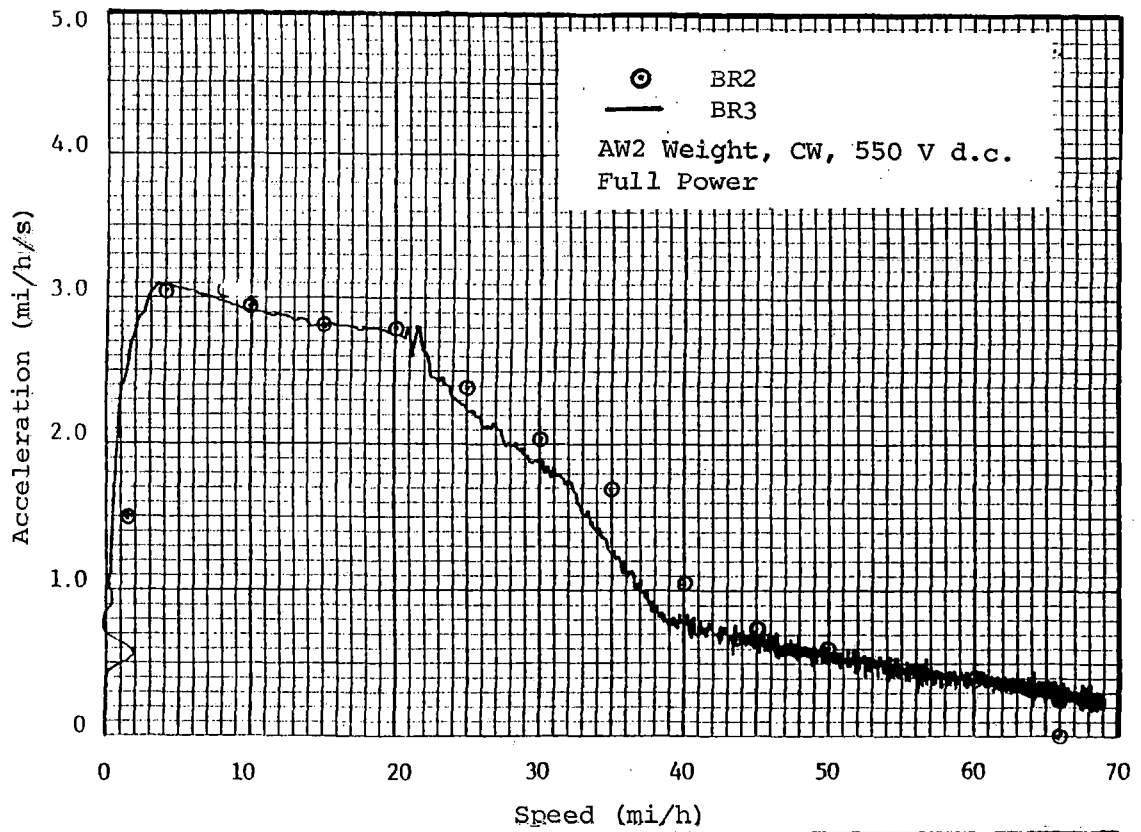


FIGURE 6-10. ACCELERATION PERFORMANCE - COMPARISON OF BR3 AND BR2 CONFIGURATIONS AT 550 V d.c. AND 825 V d.c.

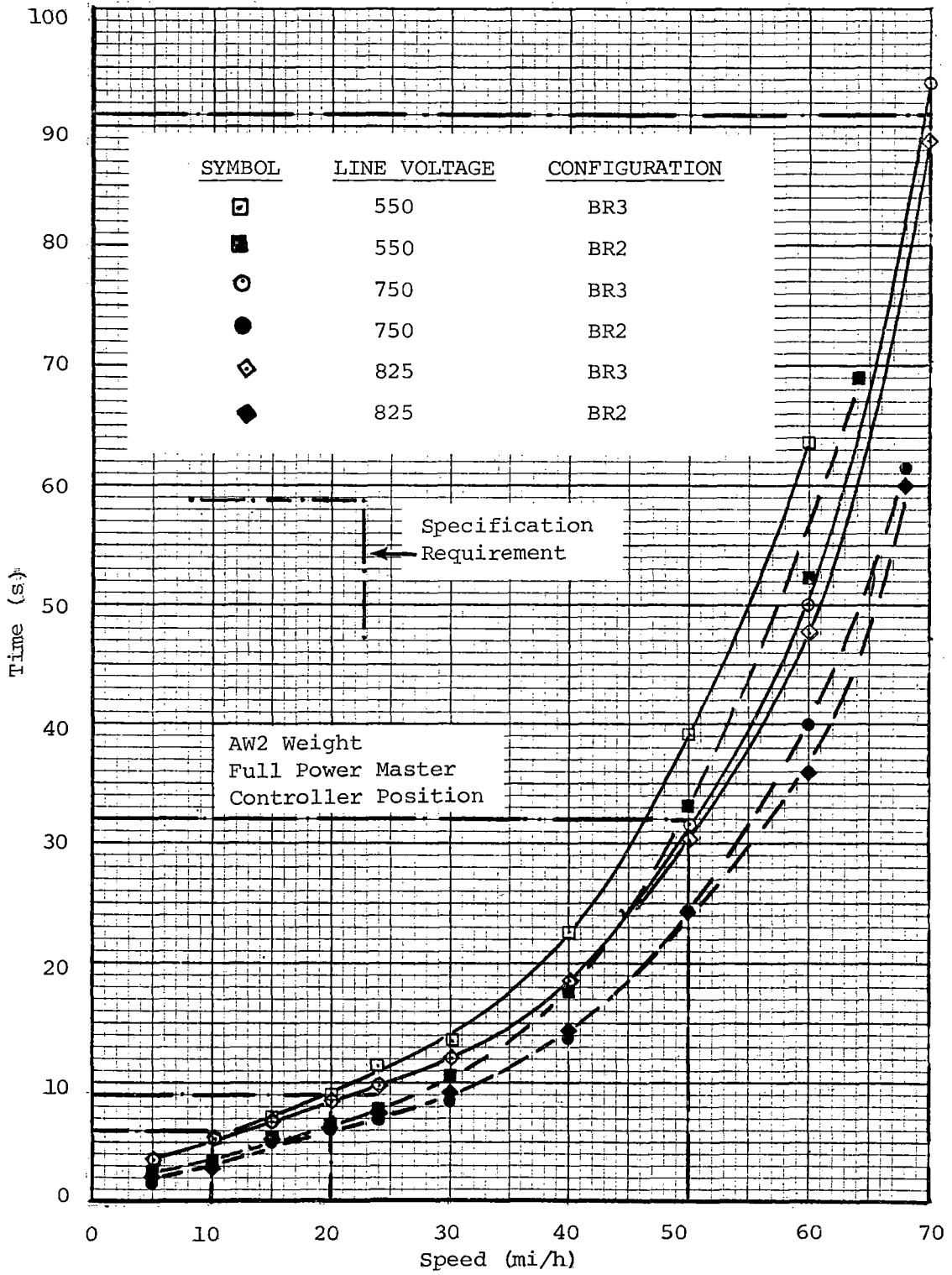


FIGURE 6-11. COMPARISON OF BR2 AND BR3 CONFIGURATIONS WITH LINE VOLTAGE.

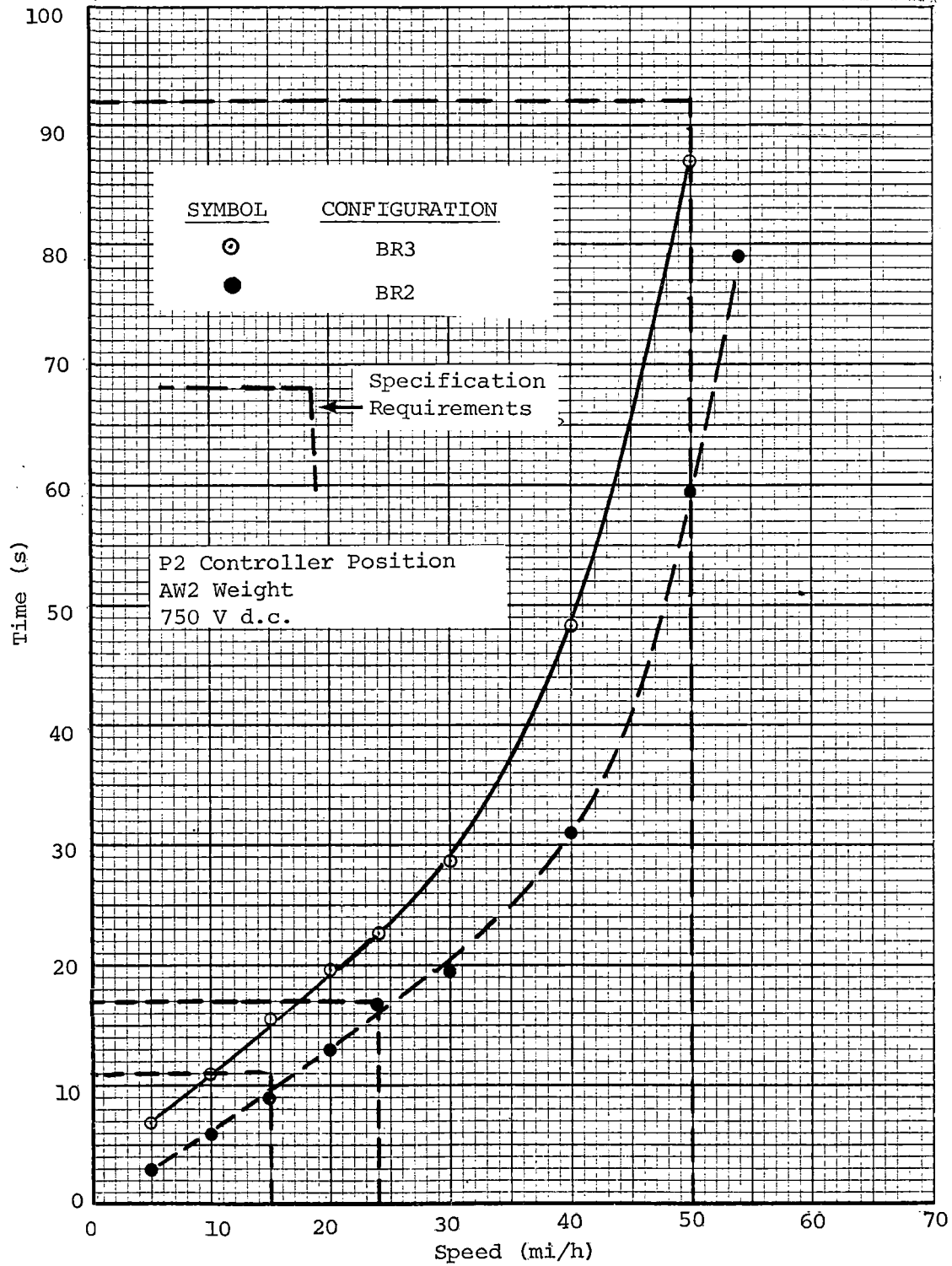


FIGURE 6-12. COMPARISON OF BR2 CONFIGURATION WITH BR3 CONFIGURATION AT P2 CONTROLLER POSITION.

similar maximum acceleration levels for full power acceleration from a standing start. The maximum acceleration is, however, sustained to higher speeds for the BR2 configuration at AW2 and AW3 vehicle weight, approximately 30 mi/h at AW2 compared to 24 mi/h for the BR3 configuration. Comparing the performance of the two configurations at AW0 weight, a much closer correlation is evident, leading to the conclusion that the sustained maximum acceleration at higher weights is due to differences in the propulsion system characteristics and may be a function of the load weigh compensation.

The effect of reduced wheel diameter has been considered. The traction motor performance curves show that the motors provide constant torque up to base speed, the rpm at which the line voltage is fully applied across each pair of motors. Above this speed, field weakening is used for further increases in rpm, and the available torque diminishes rapidly. The effect of a smaller wheel diameter (in this case $4\frac{1}{2}\%$ smaller) is to increase motor rpm for a given vehicle speed by the same proportion. Therefore, the speed at which the transition to field weakening occurs and acceleration level decreases will be $4\frac{1}{2}\%$ lower with $32\frac{1}{2}$ " diameter wheels than with 34" wheels, an opposing trend to the one shown in these comparisons.

The acceleration performance of the BR2 vehicle configuration is compared to the BR3 configuration at three line voltages: 750, 550, and 825 V d.c. in figures 6-10 and 6-11, respectively. At 750 V d.c., the maximum acceleration level achieved was approximately 0.1 mi/h/s higher for the BR2 configuration at 3.2 mi/h/s, and was sustained to a higher speed (30 mi/h) than for the BR3 configuration (24 mi/h). At 825 V d.c., the acceleration characteristics for the BR2 configuration show that maximum acceleration levels are 0.15 mi/h/s higher and sustained to 30 mi/h compared to 25 mi/h for the BR3 configuration. For the 550 V d.c. case the BR2 acceleration levels were similar to the BR3 baseline configuration levels, with some decrease in the rate of change of the BR3 acceleration in the 25 to 45 mi/h speed range.

Time-to-speed data are presented in figure 6-12 for the P2 controller position at 750 V d.c. line voltage; the BR2 configuration data are compared to BR3 configuration test results. The BR2 configuration showed improved time-to-speed performance at the P2 master controller position. At P2 master controller, the BR2 configuration met the time-to-speed criteria of the vehicle specification, whereas the BR3 configuration did not.

6.2 DECELERATION

6.2.1 Test Objectives

The test objectives were to determine the overall deceleration characteristics for the available modes of brake operation, as affected by master controller position, vehicle weight, direction of travel, initial speed, and brake configuration, and to compare the actual performance with the following vehicle specification requirements for braking:

- Blended braking deceleration with 34" wheels at all weights up to and including AW3 shall be:

<u>Vehicle Speed</u>	<u>Braking Effort</u>
70 mi/h	2.0 mi/h/s
70 to 50 mi/h	linear increase from 2.0 to 3.0 mi/h/s
50 to 0 mi/h	3.0 mi/h/s

- Any deviation above or below the called for braking level shall not exceed $\pm 10\%$ with the average deceleration not deviating greater than $\pm 7\%$.
- The braking effort listed above shall be available with the electrical brakes inoperative. During stops made with only the friction brakes, any deviation from the commanded effort shall not be greater than $\pm 20\%$, and the average deviation over the stop shall not exceed $\pm 10\%$ except during spin/slide operation.
- For vehicles with 34" wheels at any weight up to and including AW2, the braking effort listed above shall be required from the electrical brakes, except at speeds below the electrical brake fade out speed of approximately 3 mi/h. Above a vehicle weight of AW2, or under conditions which result in the inability of the electrical brakes to provide the commanded braking effort, friction brakes shall be blended on a per vehicle basis to maintain the commanded effort.
- Under emergency stop conditions, a single unit or multi-unit train shall maintain an irretrievable braking effort of not less than 3.5 mi/h/s over the entire speed range for weights up to and including AW3. The braking effort includes train resistance. Emergency brake application shall be via the friction brake system only. Spin/slide and load weigh systems shall be active. Electrical braking blending functions shall be inactive.

6.2.2 Test Method

Braking tests were carried out on level, tangent track between rail stations 30.0 and 34.0. The vehicle was driven into the test section at a predetermined speed and braked to a stop at a defined master controller position. Initial speeds of 15, 35, 55, and 70 mi/h were used for master controller positions of B1, B2, and B3 (full service braking), and test runs were made in both clockwise and counterclockwise directions of travel. The effect of vehicle weight on braking performance was evaluated by testing at weights of AW0, AW2, and AW3. Blended, friction-only, dynamic-only, and emergency braking modes were evaluated.

For the friction-only braking tests, the brakes were evaluated at stable temperatures; a series of friction-only stops were made prior to the test runs to stabilize brake temperature and simulate operational conditions. The brakes were maintained between 200° and 260°F by monitoring thermocouples attached to the brake shoes; when the temperatures exceeded these values, several 'cooling down' laps were made of the test track.

Emergency braking performance was evaluated with the friction brake shoes at ambient temperatures as this was considered to be more representative of real world emergency braking conditions. Brake pad temperatures were typically in the range of 100° to 120°F throughout the emergency braking tests.

6.2.3 Test Results

The discussion of the braking data contained herein centers around the final brake configuration evaluated at the TTC: this is described (in Section 3.13, Vehicle Configurations) as brake configuration BR3. This configuration was chosen for presentation as the prime configuration. Although it was an experimental configuration not in revenue service, it did represent the latest attempt at the time of writing, by PBT and the brake system manufacturers, to make the system performance comply with the vehicle specification requirements.

Other brake system configurations, evaluated earlier in the MARTA test program at the TTC, are compared briefly to the BR3 configuration at the conclusion of this discussion. In the following test results discussion, the data from the modes of brake operation tested for the BR3 configuration are evaluated. For each mode of operation, plots are presented of (a) the deceleration characteristics from initial speeds of 70, 55, 35, and 15 mi/h; (b) the effect of master controller position for an intermediate initial speed of 35 mi/h; and (c) plots of time and distance required to stop at full service braking. These plots are presented for AW0, AW2, and AW3 vehicle weights. Dotted lines representing the full service braking specification requirement, plus and minus the allowable deviation of 10% for blended and dynamic braking and 20% for friction braking, have been superimposed on the deceleration plots to illustrate the acceptability of the vehicle performance.

6.2.3.1 Blended Braking. At AW0 vehicle weight, the deceleration levels for full service braking fell within the required $\pm 10\%$ deviation band. The

specification requirement is for a deceleration rate of 2.0 mi/h/s at 70 mi/h, ramped linearly to 3.0 mi/h/s at 50 mi/h and maintained at this level until stopped. The effect of initiating the stop at different speeds was minimal with the vehicles achieving the same deceleration level for a given speed (figure 6-13a).

As the weight was increased, the deceleration levels deteriorated, and at AW3 vehicle weight (crush passenger load), the achieved deceleration level was 0.2 to 0.5 mi/h/s below the -10% allowed deviation level over most of the full service stop from 70 mi/h. Figures 6-14a and 6-15a show AW2 and AW3 deceleration characteristics, respectively. At the higher vehicle weights, a large magnitude (0.5 to 0.7 mi/h/s at AW3) deceleration spike was observed at the initiation of braking at the intermediate speeds (see figure 6-15a).

Tests at B1, B2, and B3 master controller positions at 35 mi/h initial speed showed that controller linearity was acceptable at speeds down to 20 mi/h. Below 20 mi/h at the B1 controller position, and 8 mi/h at the B2 position, the deceleration levels increased dramatically, giving rise to large braking effort/controller position non-linearities at low speeds.

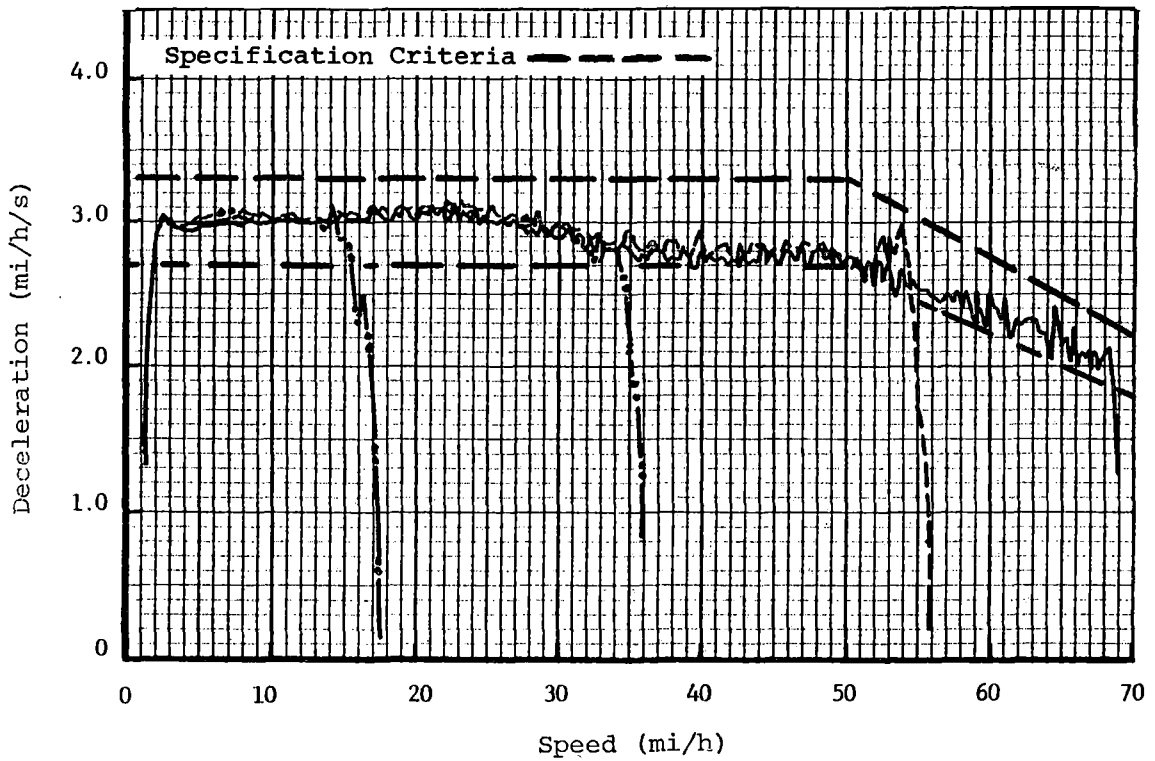
A comparison plot (figure 6-16a) shows data for a full service stop from 70 mi/h in a clockwise direction of travel (car 0110 leading) compared to similar data for a counterclockwise direction (car 0109 leading); it shows that direction of travel and lead car have a minimal impact on braking performance.

The effect of car weight on blended braking rates shown in figures 6-16b and 6-17 indicate a general reduction in braking rates with increased weight. At AW0 weight the vehicle marginally meets blended braking specification requirements while, at AW2 and AW3 weights, the vehicle falls short of the requirements. The specification requires that braking rates be met at all weights for the blended braking mode. (Please note that the time-to-stop data presented in figure 6-17a include control response time and therefore the plots do not go through the time axis origin.)

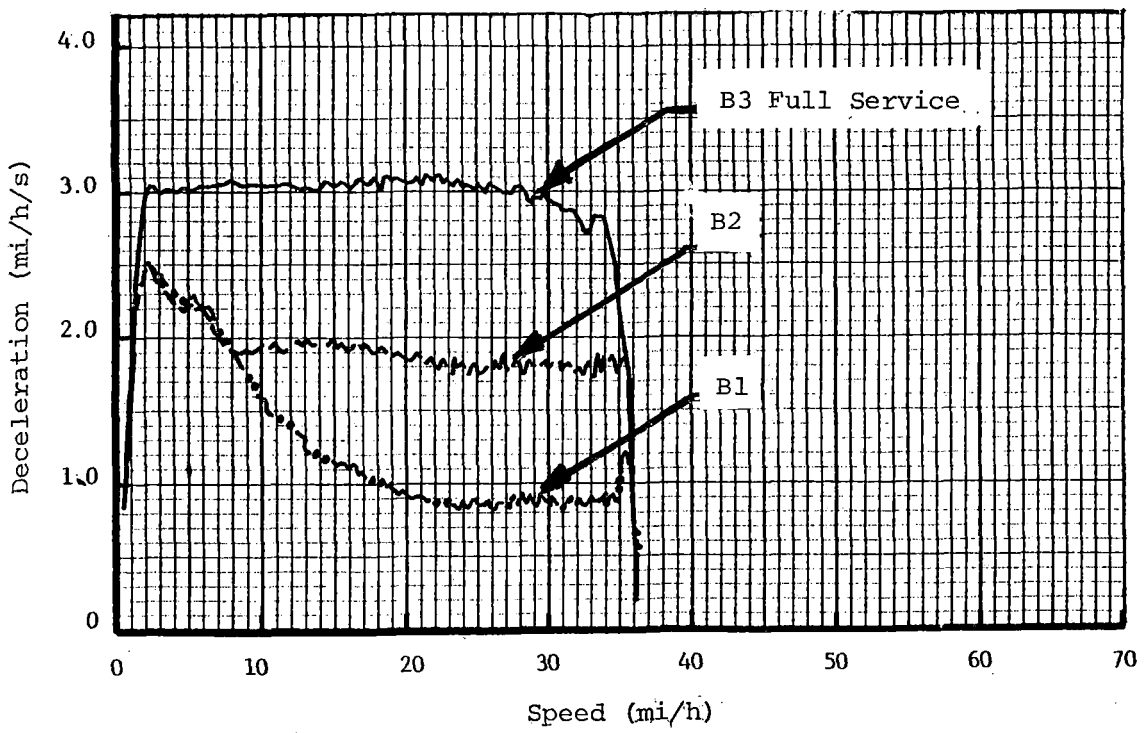
6.2.3.2 Friction Braking. The effects of initial brake entry speed on full service friction braking performance are presented in figures 6-18a through 6-20a for vehicle weights of AW0, AW2, and AW3, respectively. The data show that initial speed has a large influence on the deceleration levels attained in full service friction braking, with the levels increasing markedly with decreasing initial speed. The most significant change in deceleration level occurs at the 35 mi/h initial speed case where the deceleration increased by an average of 0.8 mi/h/s over the stop compared to similar data from 55 mi/h initial speed.

The friction braking deceleration data is characterized by a transient longitudinal vibration in the 25 to 5 mi/h speed range, with a maximum amplitude of ± 0.3 mi/h/s at a frequency of approximately $\frac{1}{2}$ Hz: this phenomenon, while not apparent to the rider, can be seen in all the friction braking deceleration plots--figure 6-18b, for instance.

The friction braking deceleration levels meet the requirements of the vehicle specification throughout the range of vehicle weights, for initial brake entry speeds of 70 and 55 mi/h. For initial brake entry speeds of

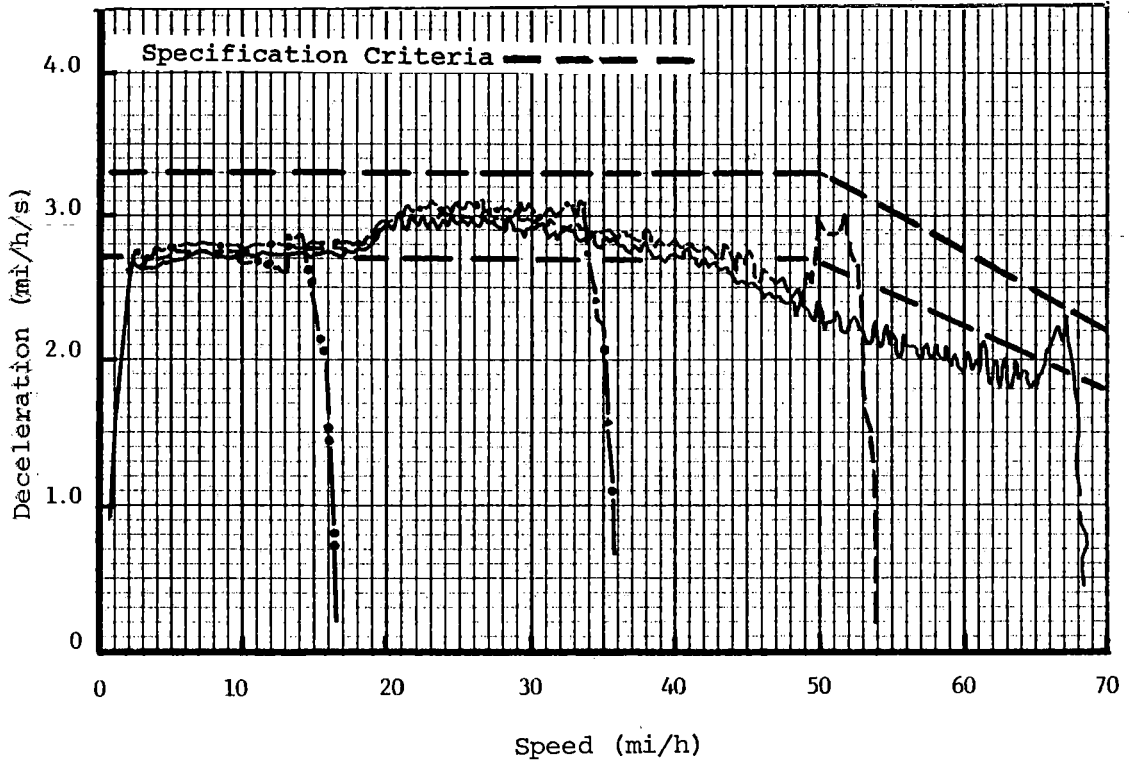


a. Effect of Initial Speed on Full Service Braking.

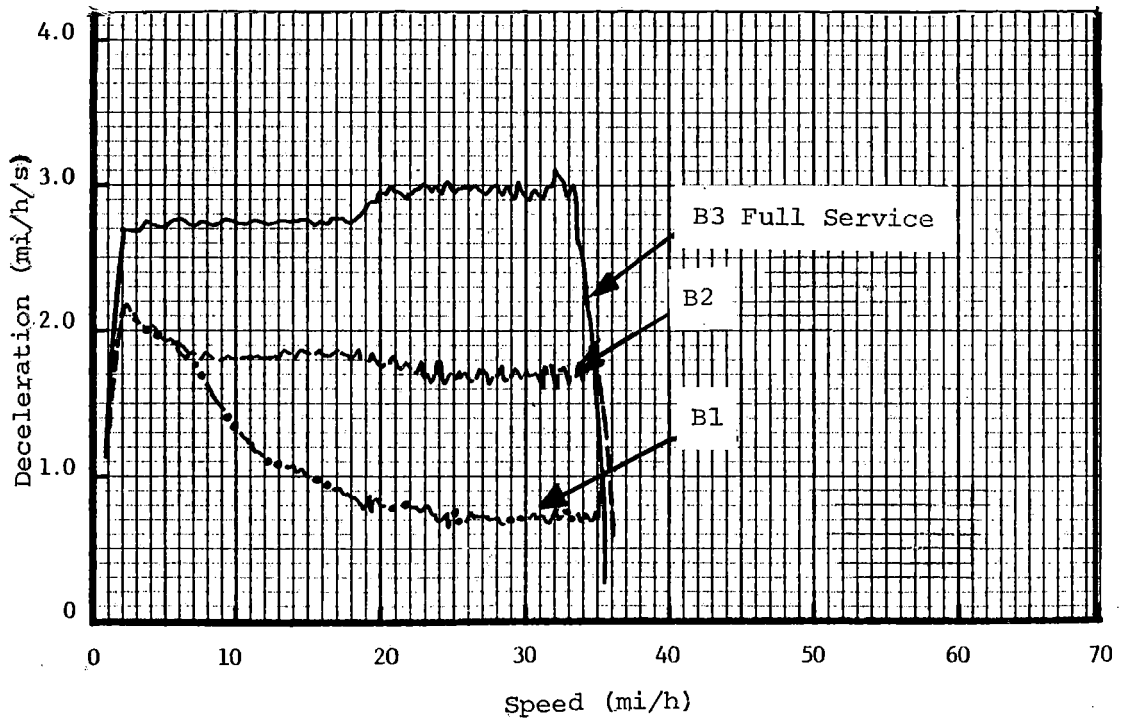


b. Effect of Master Controller at 35 mi/h.

FIGURE 6-13. BLENDED BRAKING DECELERATION CHARACTERISTICS, AWO WEIGHT.

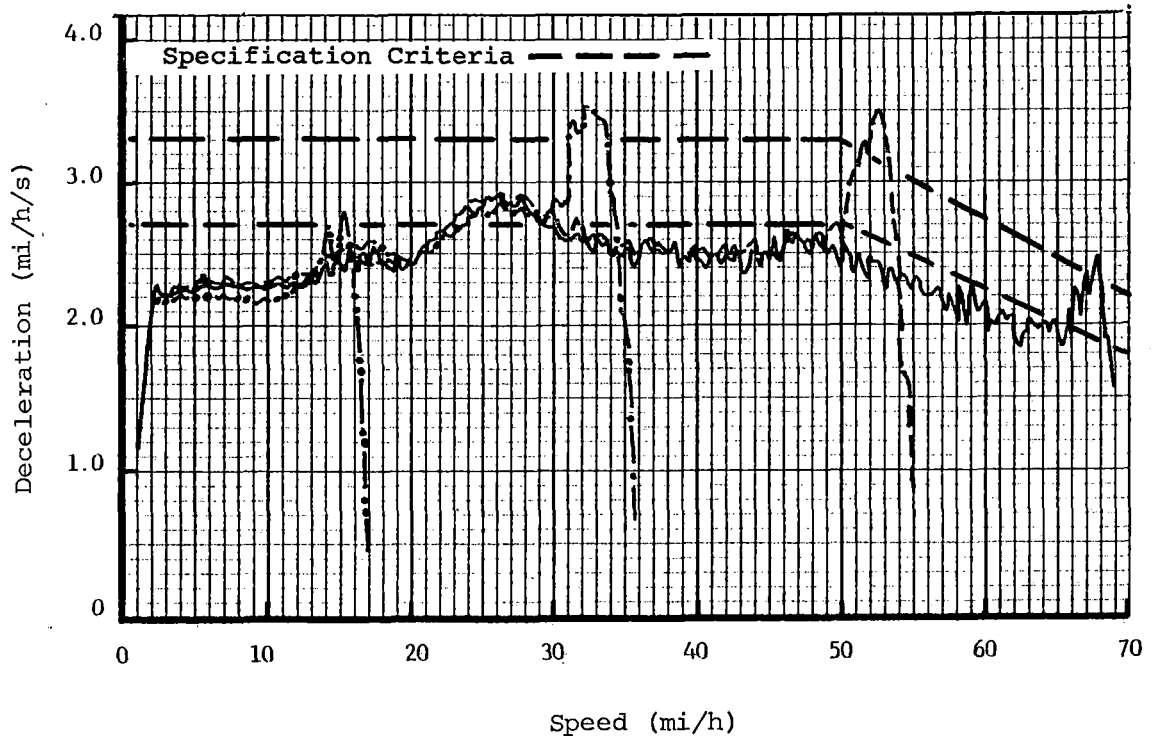


a. Effect of Initial Speed on Full Service Braking .

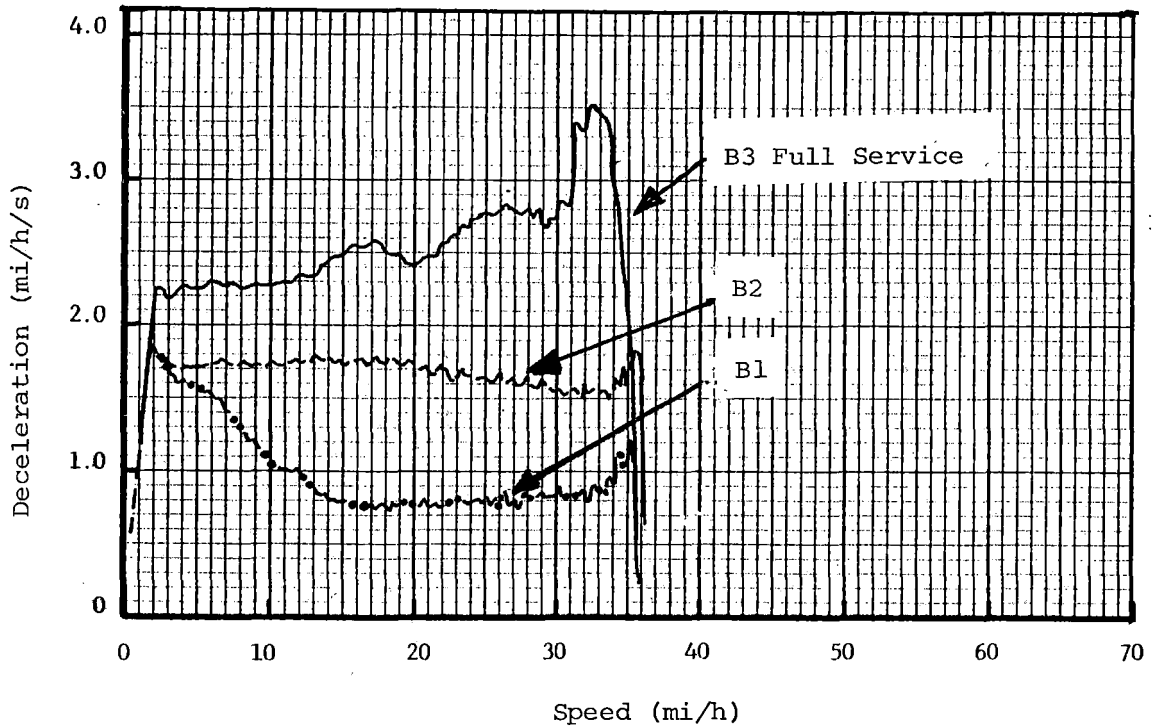


b. Effect of Master Controller at 35 mi/h .

FIGURE 6-14. BLENDED BRAKING DECELERATION CHARACTERISTICS, AW2 WEIGHT.

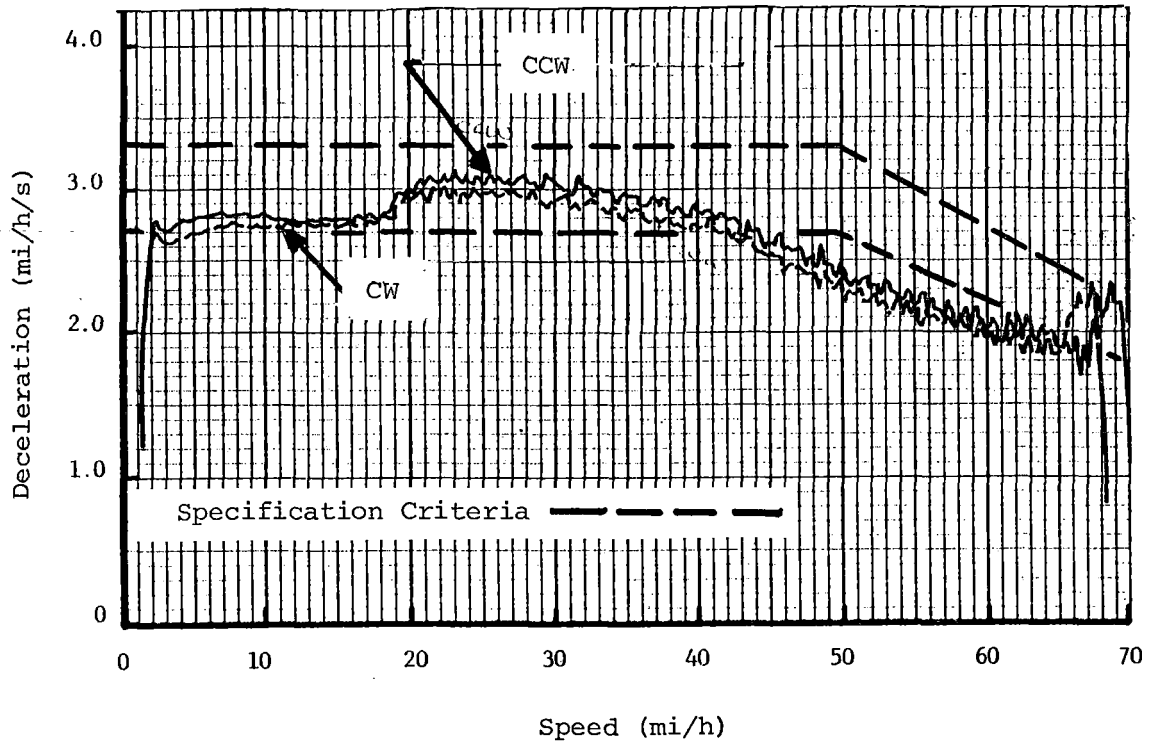


a. Effect of Initial Speed on Full Service Braking.

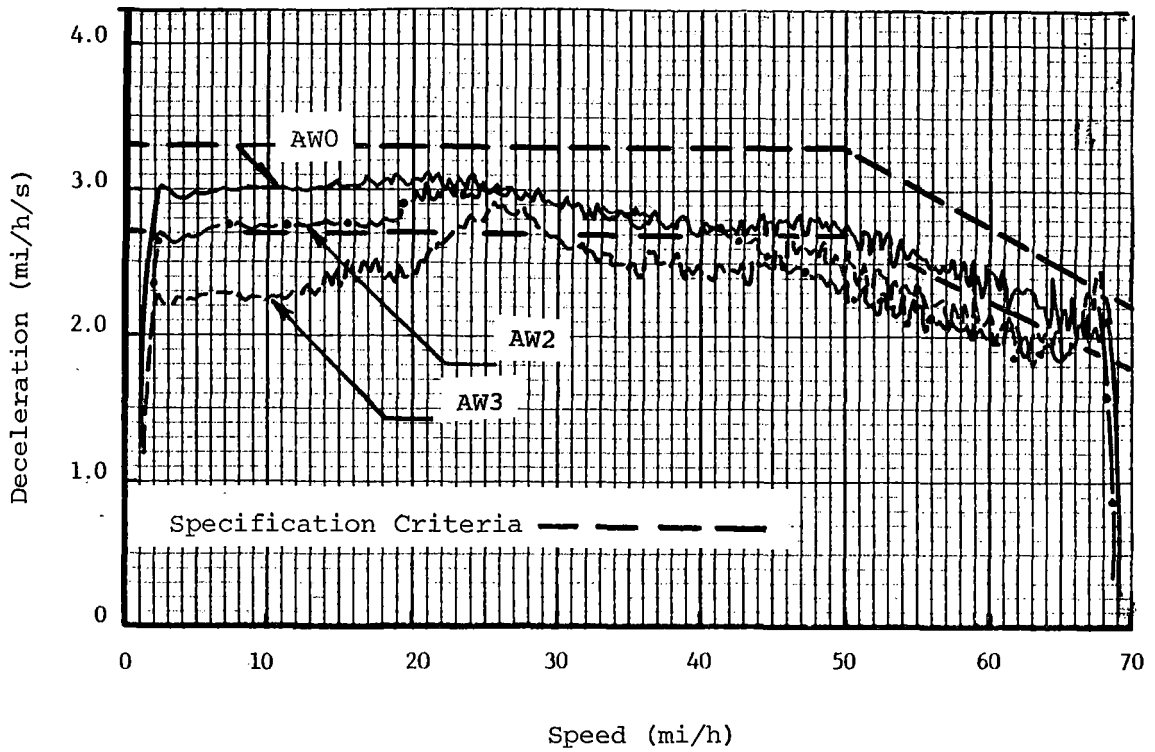


b. Effect of Master Controller at 35 mi/h.

FIGURE 6-15. BLENDED BRAKING DECELERATION CHARACTERISTICS, AW3 WEIGHT.

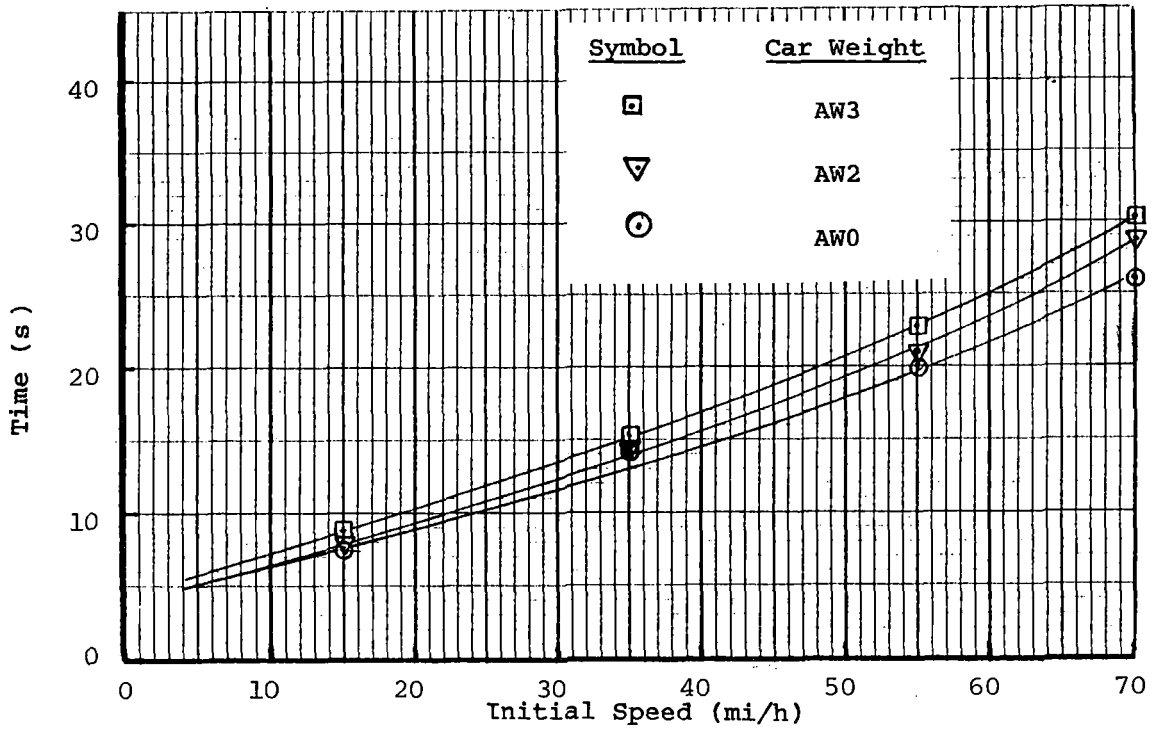


a. Effect of Direction on Full Service Braking -AW2.

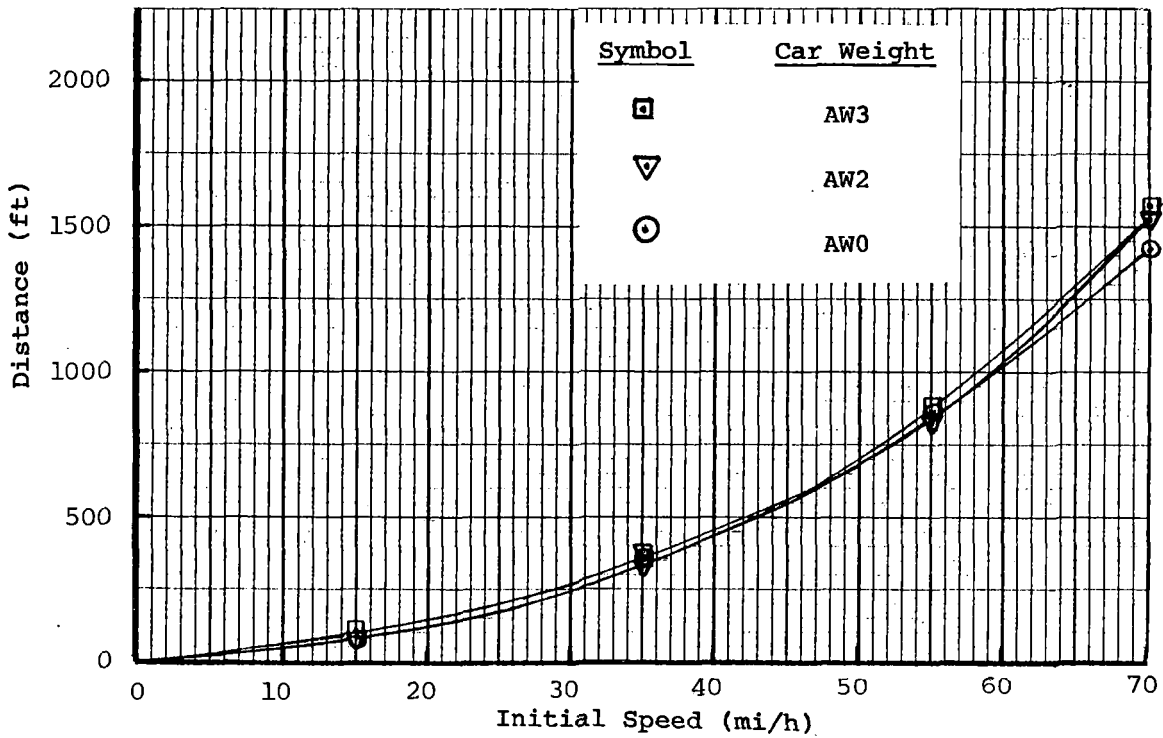


b. Effect of Weight on Full Service Braking.

FIGURE 6-16. BLENDED BRAKING - DECELERATION CHARACTERISTICS.

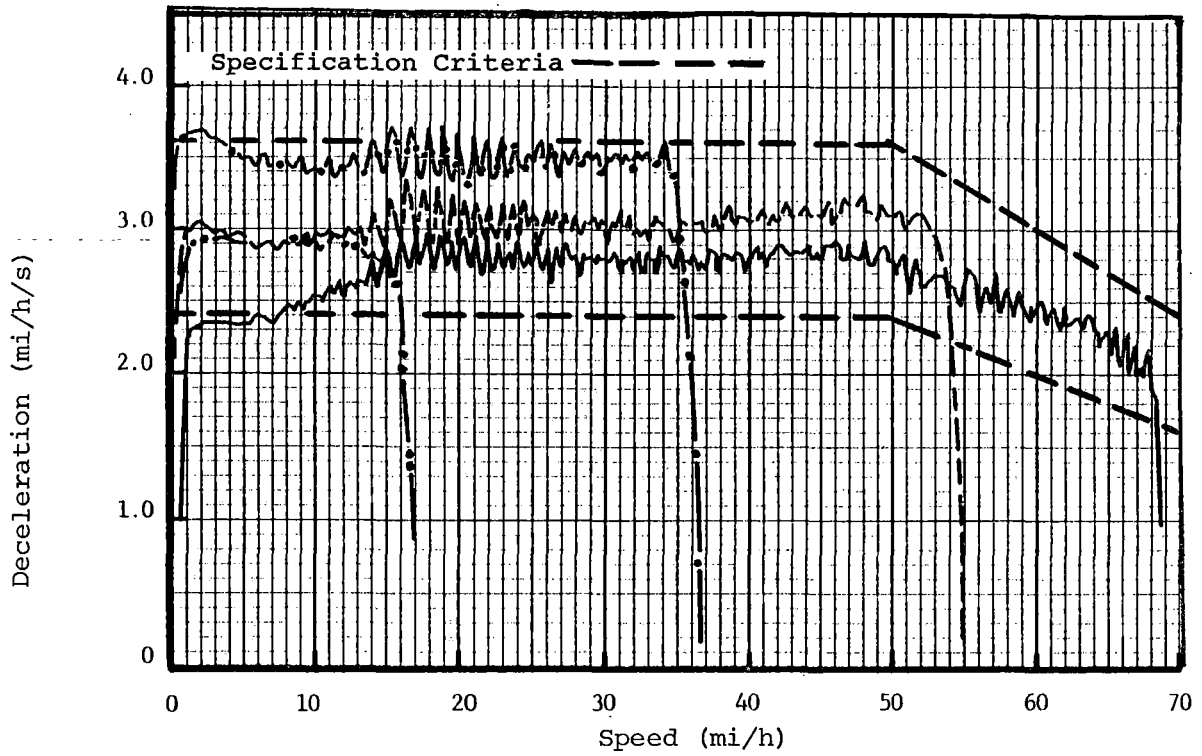


a. Time to Stop from Initial Speeds.

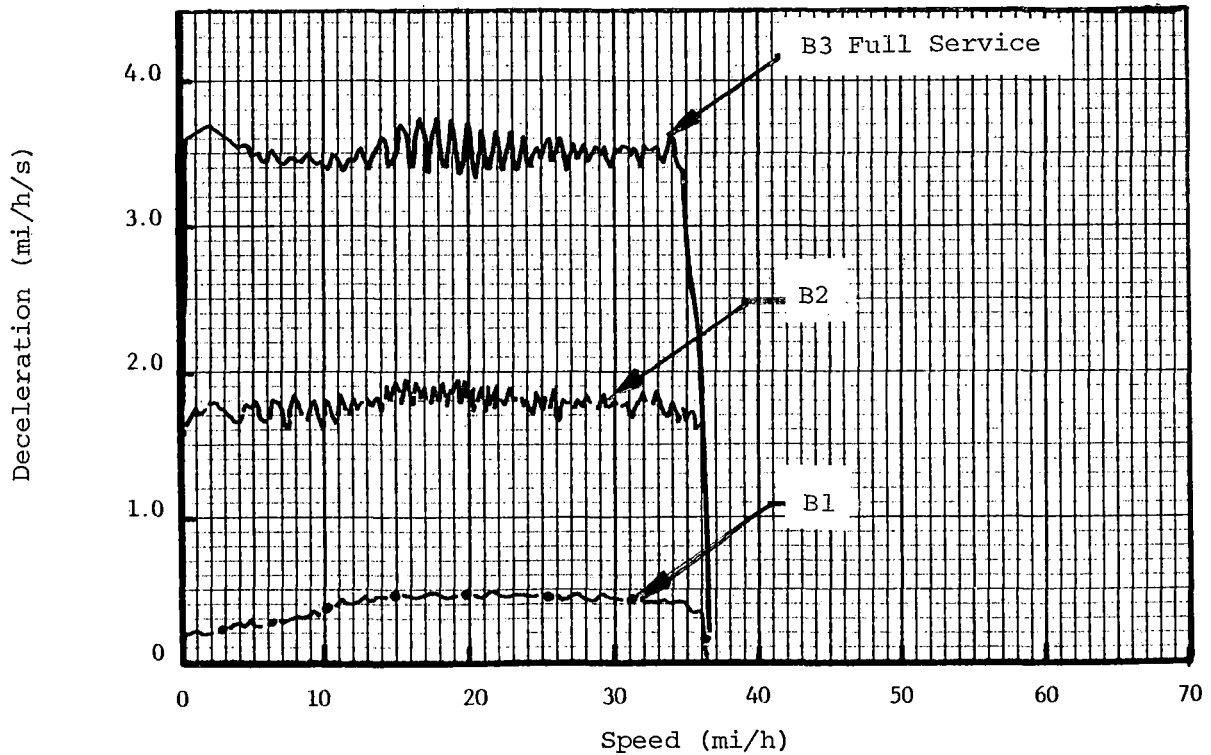


b. Distance to Stop from Initial Speeds.

FIGURE 6-17. BLENDED BRAKING - STOPPING DISTANCE AND TIME CHARACTERISTICS, FULL SERVICE BRAKING.

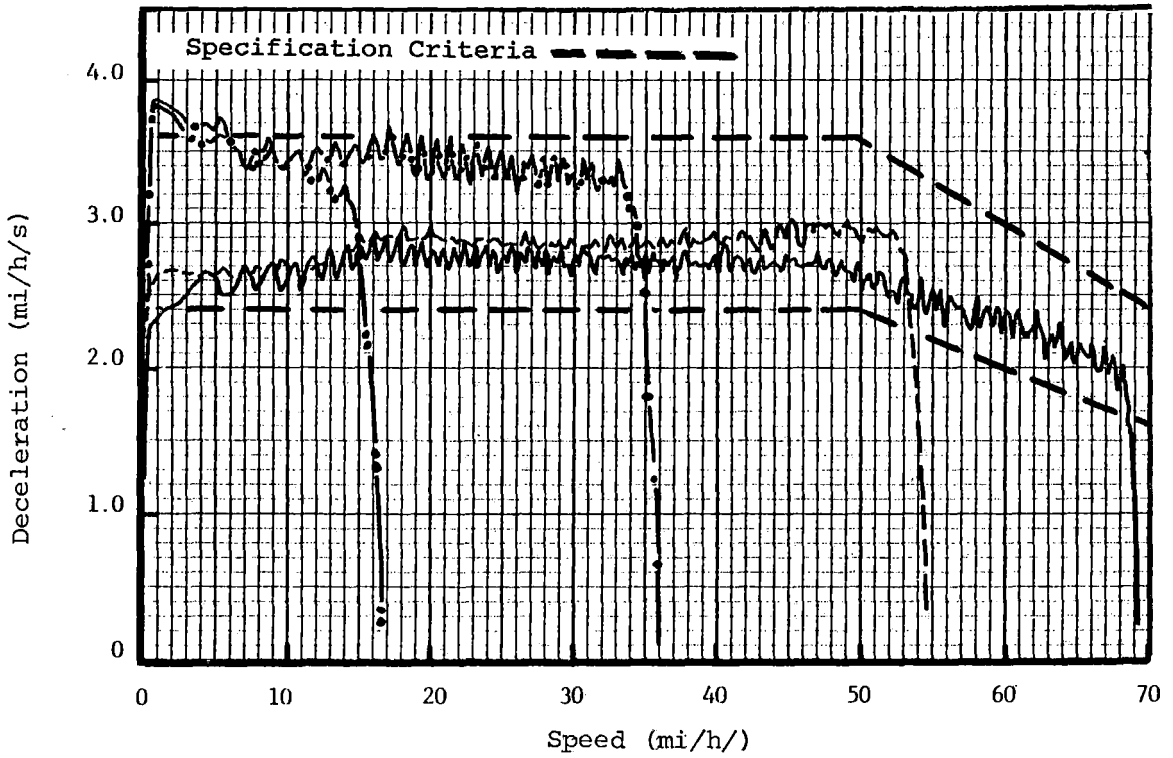


a. Effect of Initial Speed on Full Service Braking.

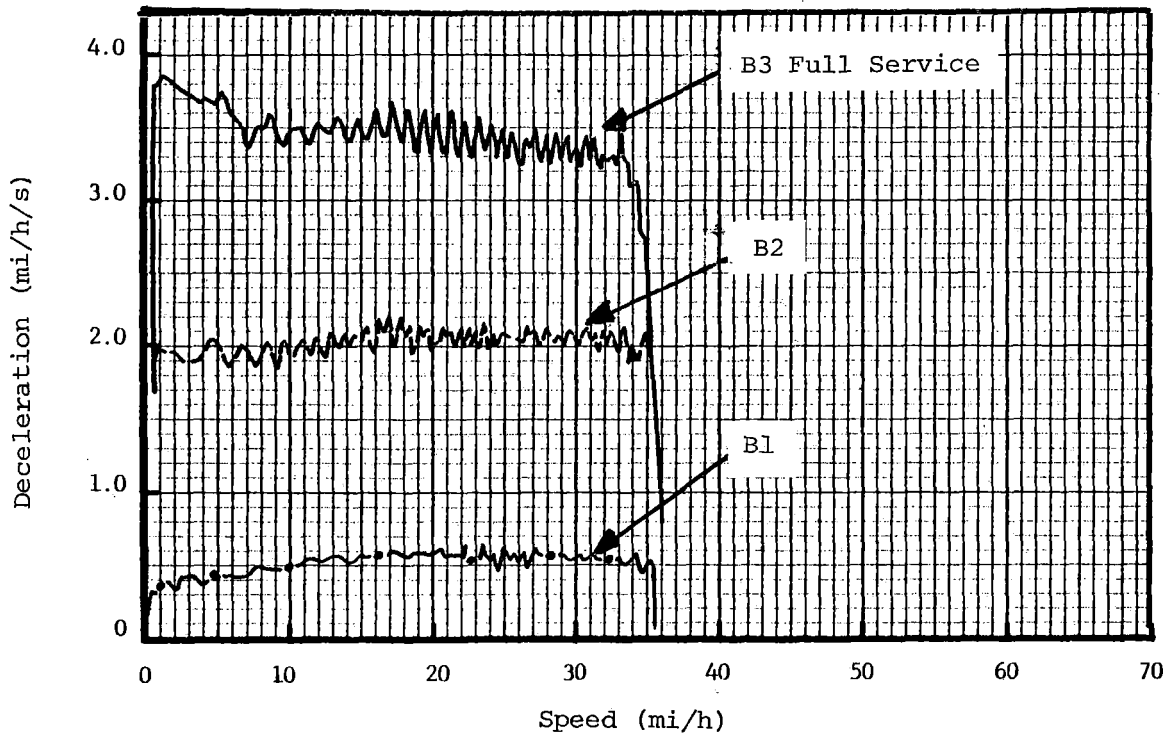


b. Effect of Master Controller at 35 mi/h.

FIGURE 6-18. FRICTION BRAKING - DECELERATION CHARACTERISTICS, AWO WEIGHT.

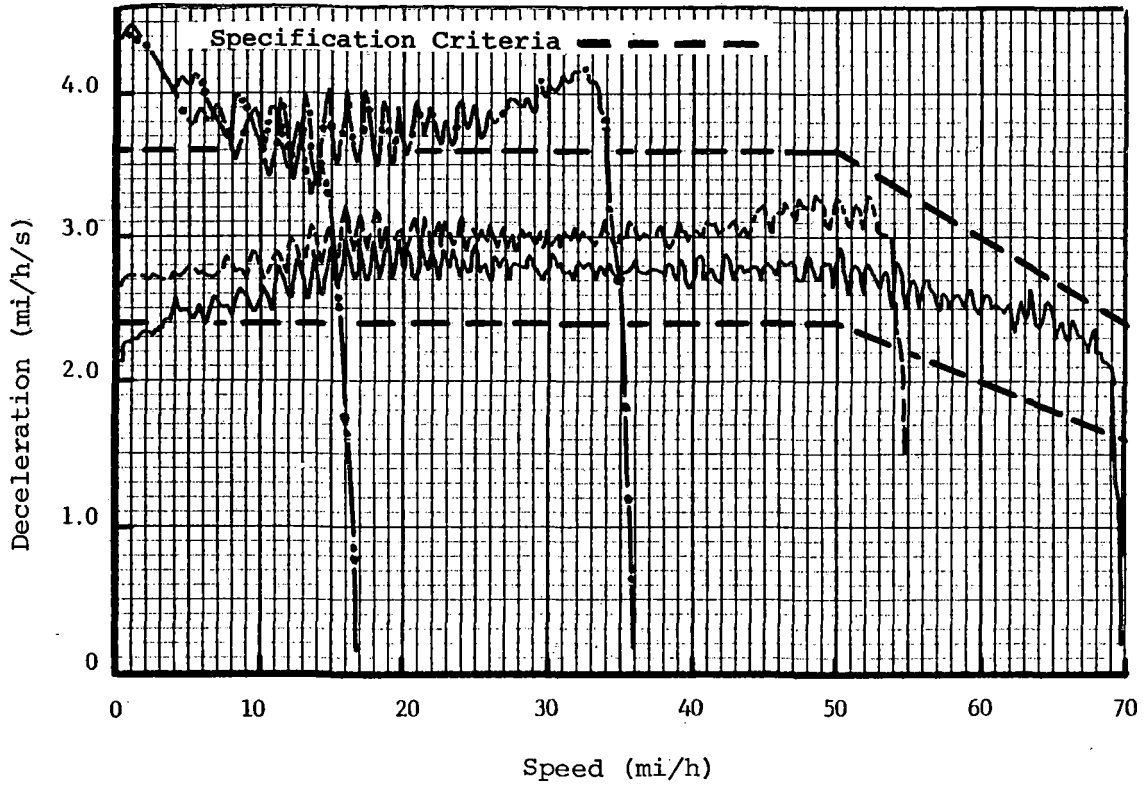


a. Effect of Initial Speed on Full Service Braking .

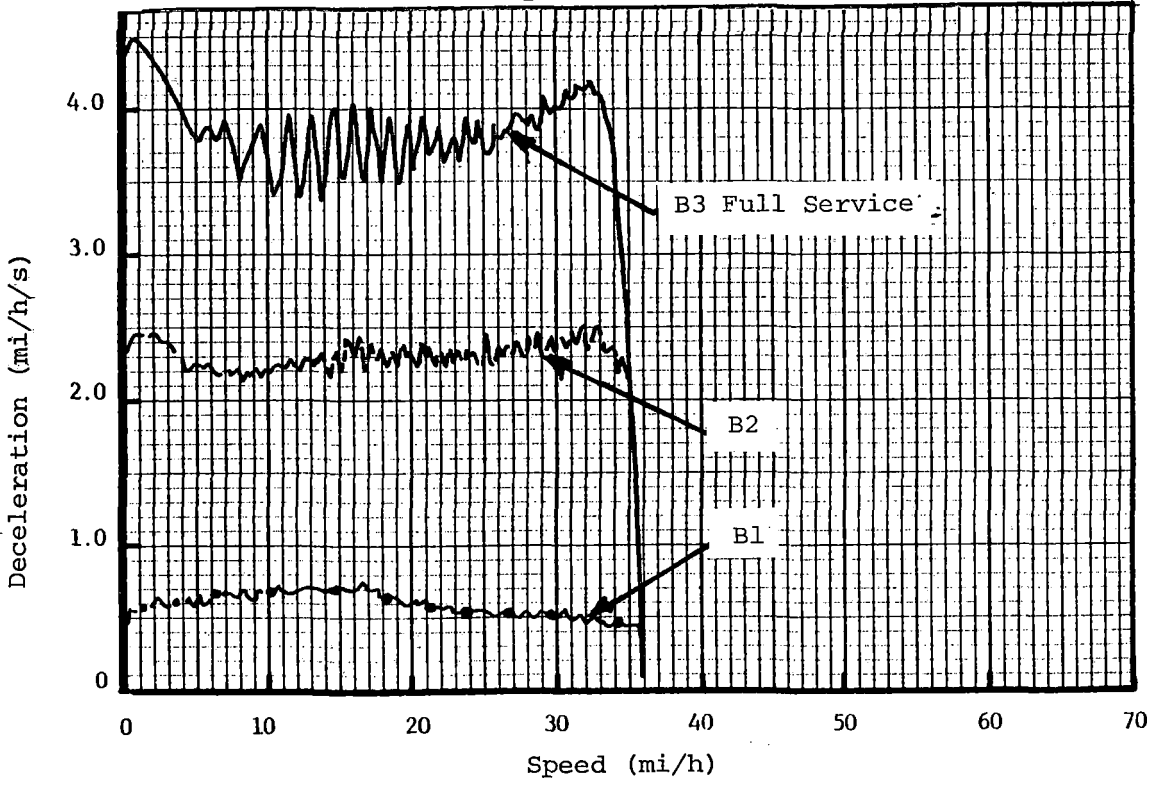


b. Effect of Master Controller at 35 mi/h.

FIGURE 6-19. FRICTION BRAKING - DECELERATION CHARACTERISTICS, AW2 WEIGHT.



a. Effect of Initial Speed on Full Service Braking.



b. Effect of Master Controller at 35 mi/h.

FIGURE 6-20. FRICTION BRAKING - DECELERATION CHARACTERISTICS, AW3 WEIGHT.

35 mi/h and lower, and vehicle weights of AW0 and AW2, the friction brakes generally meet the requirements of the specification, with minor deviations outside the allowable $\pm 20\%$ limits. Average deceleration levels over the stop, computed from stopping distance and time required to stop records, are within the required $\pm 10\%$ of the nominal 3.0 mi/h/s level.

For initial speeds of 35 mi/h and below and a vehicle weight of AW3, the friction brakes do not meet the specification requirements. Deviations to the deceleration level exceed the allowable variation of $\pm 20\%$ of 3.0 mi/h/s, and the average deceleration over the stop, again computed from distance and time, exceeds the allowable level of 3.0 mi/h/s $+10\%$. Deceleration peaked at 4.5 mi/h/s for the AW3, 35 mi/h case.

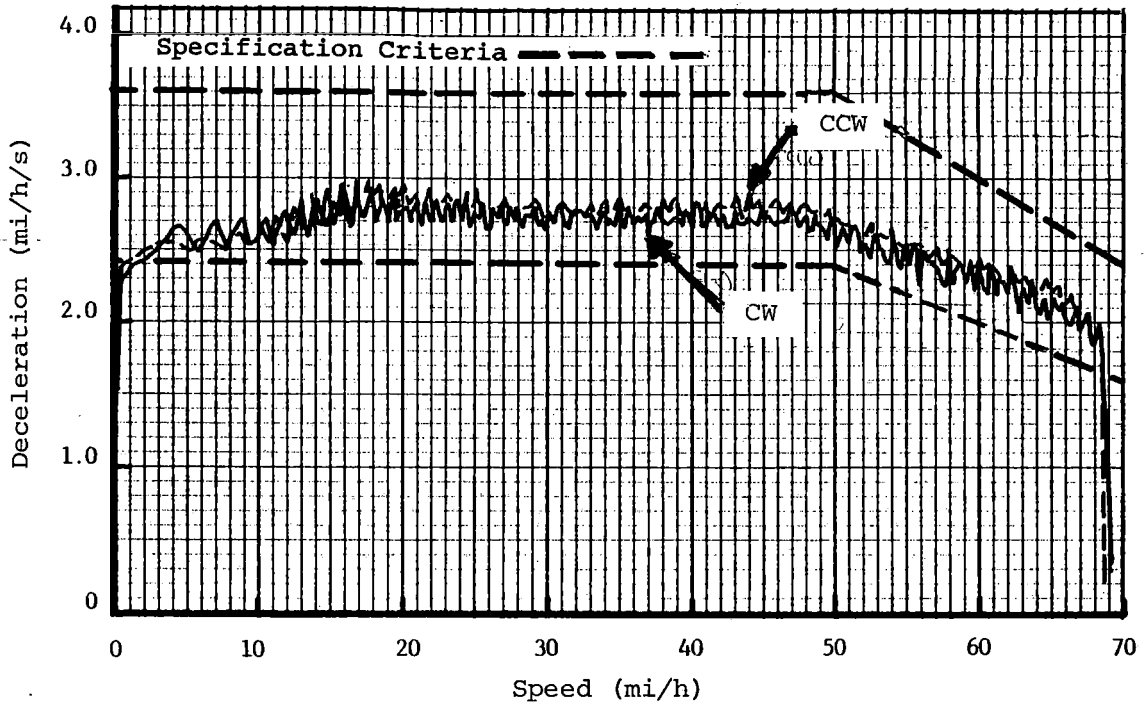
Master controller linearity was considered good in the speed range 35 mi/h to zero at all weights, as evidenced by the plots showing deceleration levels for master controller positions (figures 6-18b through 6-20b).

The effects of direction of travel and vehicle weight on friction braking deceleration levels are summarized in figure 6-21. Direction of travel (or lead car) can be seen to have a negligible effect on full service friction braking from 70 mi/h. The effect of vehicle weight was minimal for the 70 mi/h initial speed, full service brake application case, but had a considerable influence at the lower initial speeds, as seen in the 15 mi/h data which show increasing deceleration levels with increasing weight. Time and distance to stop data are presented in figure 6-22 for all three vehicle weights.

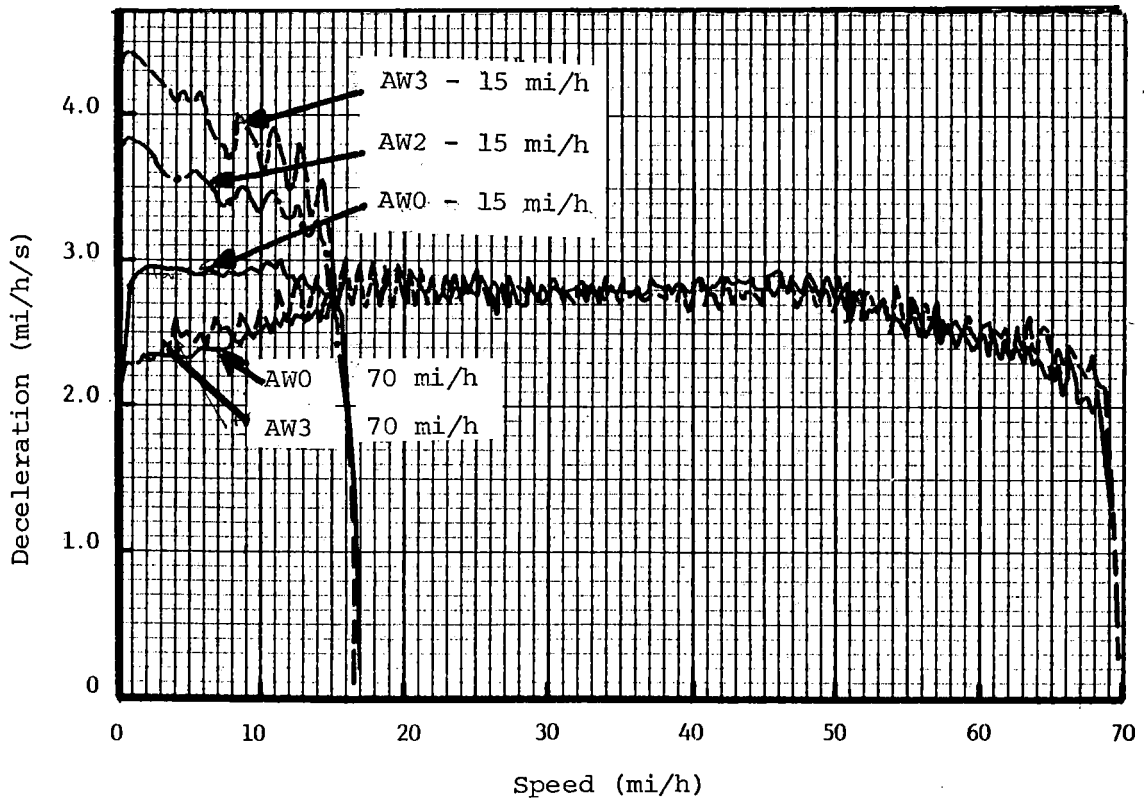
6.2.3.3 Dynamic Braking. The dynamic braking characteristics are presented in figures 6-23 through 6-26. The full service dynamic braking characteristics can be seen to be independent of initial brake entry speed. The dynamic braking system met the vehicle specification requirement for deceleration levels at AW0 vehicle weight and at AW2 weight below 40 - 45 mi/h. Above this speed, the deceleration was approximately 0.5 mi/h/s below the minimum acceptable level. There is no specification requirement for dynamic braking above a vehicle weight of AW2. At these weights dynamic braking may be blended with friction braking to achieve the required braking effort. The test data at AW3 vehicle weight (figure 6-25) show that the dynamic braking alone cannot maintain the desired levels of deceleration in full service braking at maximum vehicle weights, and must be assisted by blending friction braking.

The effect of master controller position on deceleration characteristics for an initial speed of 35 mi/h is also shown in figures 6-23b and 6-24b. As with blended braking, the system showed good linearity of response to controller input from 35 mi/h down to approximately 20 mi/h. Below this speed, the response to a B1 controller setting (and to a B2 setting below 5 mi/h) increased dramatically with the deceleration level. Typically it rose from 0.8 mi/h/s at 20 mi/h to 2.2 mi/h/sec at 2 mi/h for the B1 controller setting at AW2 vehicle weight.

The effect of car weight on dynamic braking characteristics in figures 6-25b and 6-26 indicates a reduction in braking performance with increasing weight.

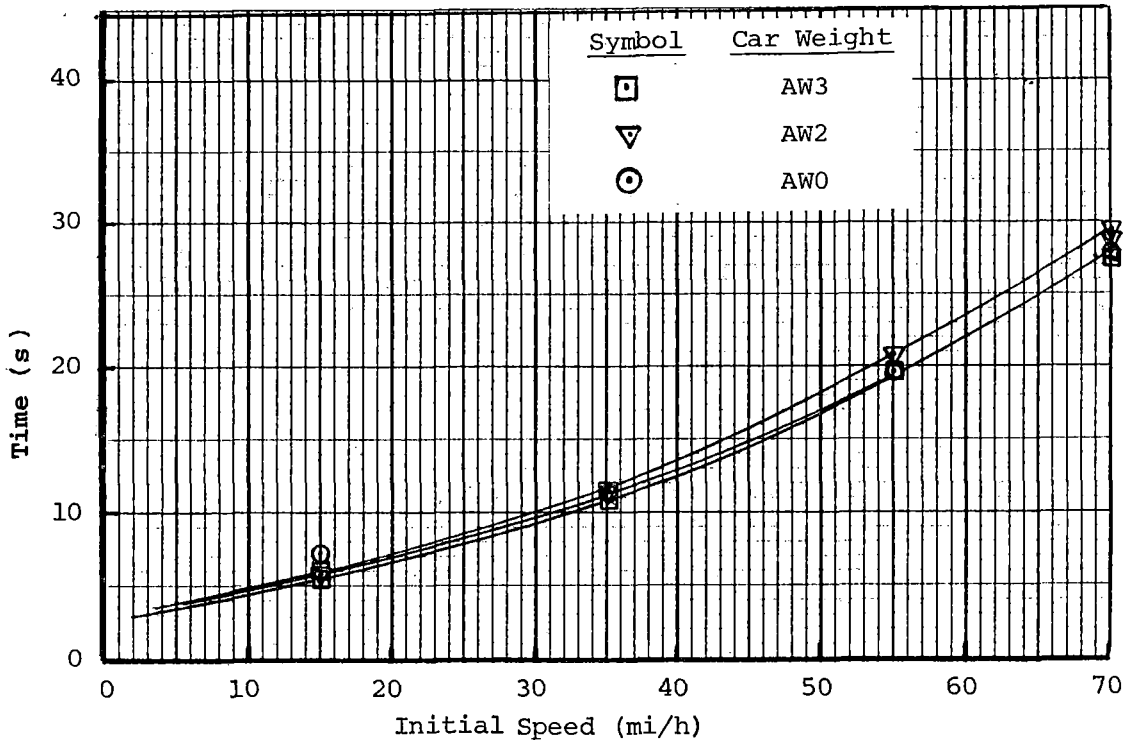


a. Effect of Direction on Full Service Braking-AW2.

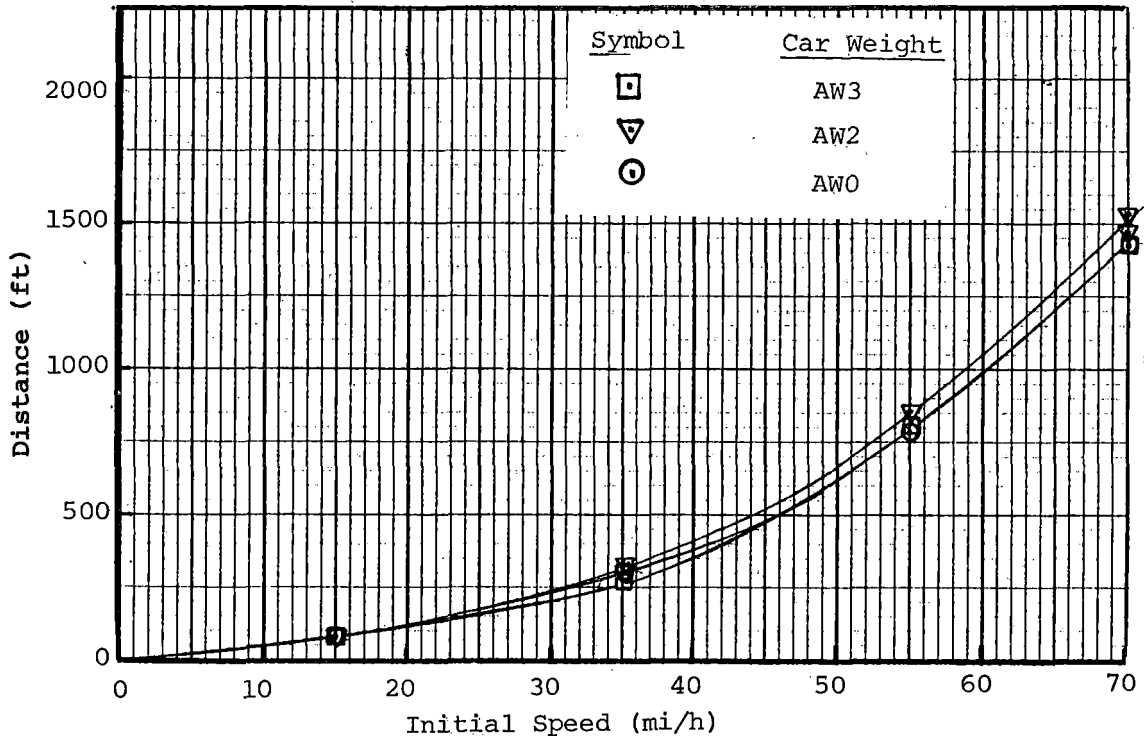


b. Effect of Weight on Full Service Braking.

FIGURE 6-21. FRICTION BRAKING--DECELERATION CHARACTERISTICS.

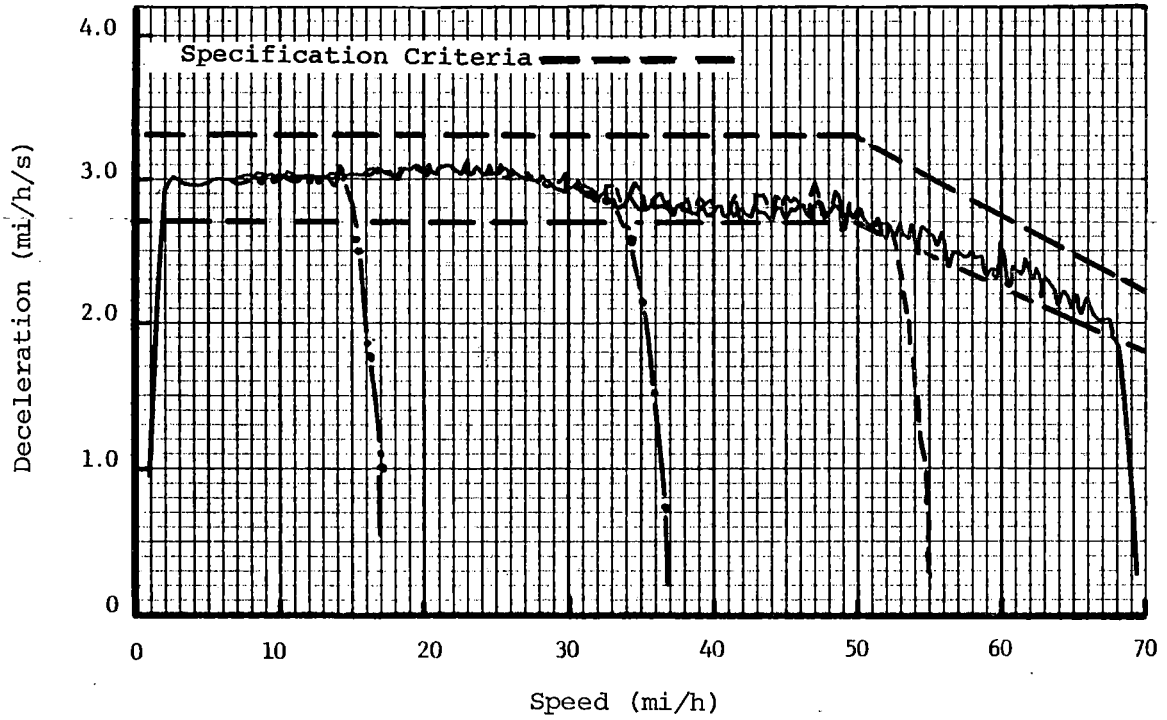


a. Time to Stop from Initial Speeds.

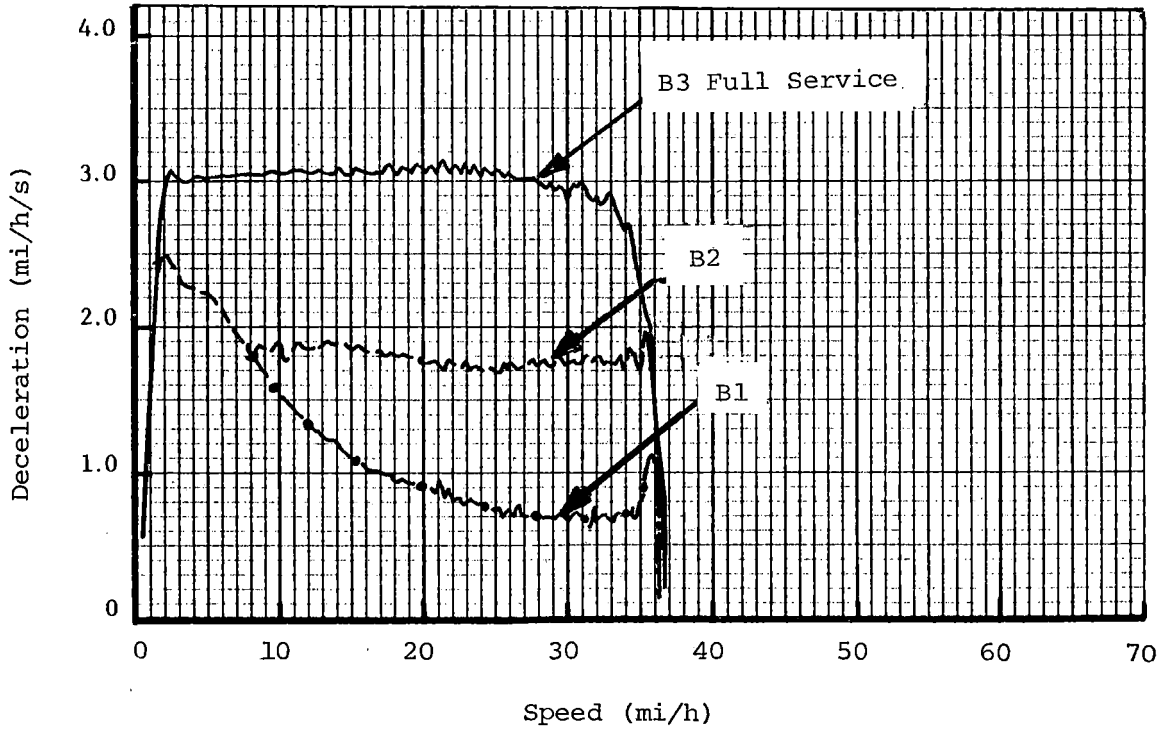


b. Distance to Stop from Initial Speeds.

FIGURE 6-22. FRICTION BRAKING-STOPPING DISTANCE AND TIME CHARACTERISTICS.

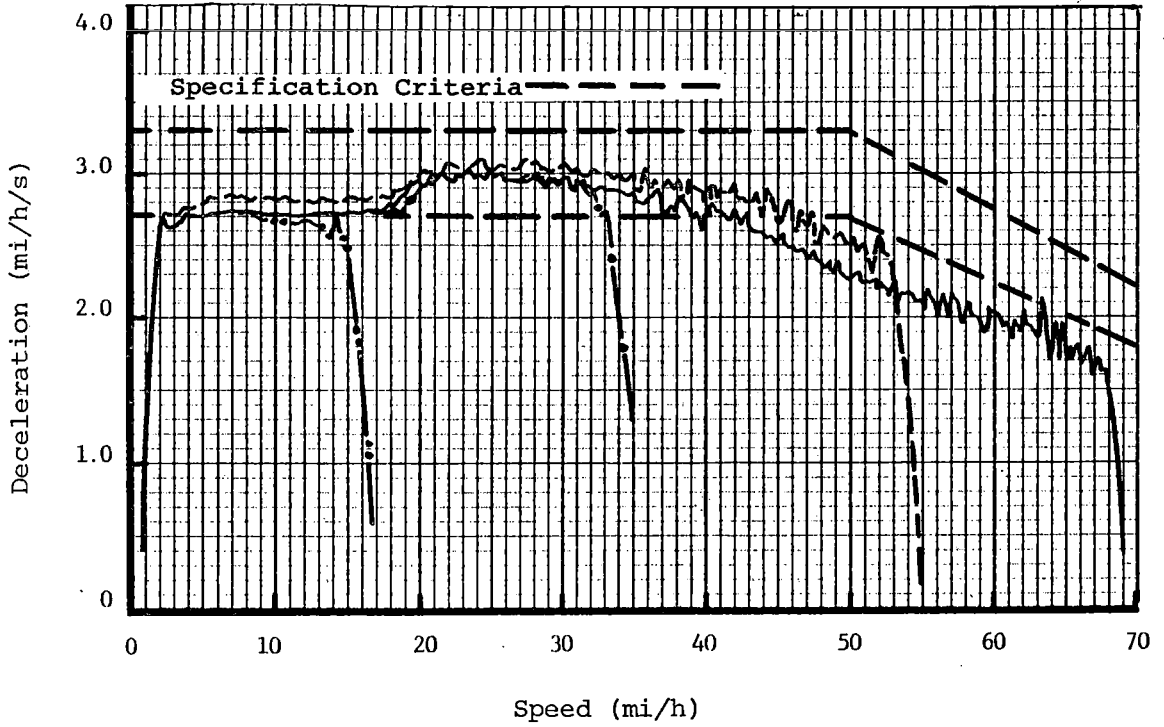


a. Effect of Initial Speed on Full Service Braking.

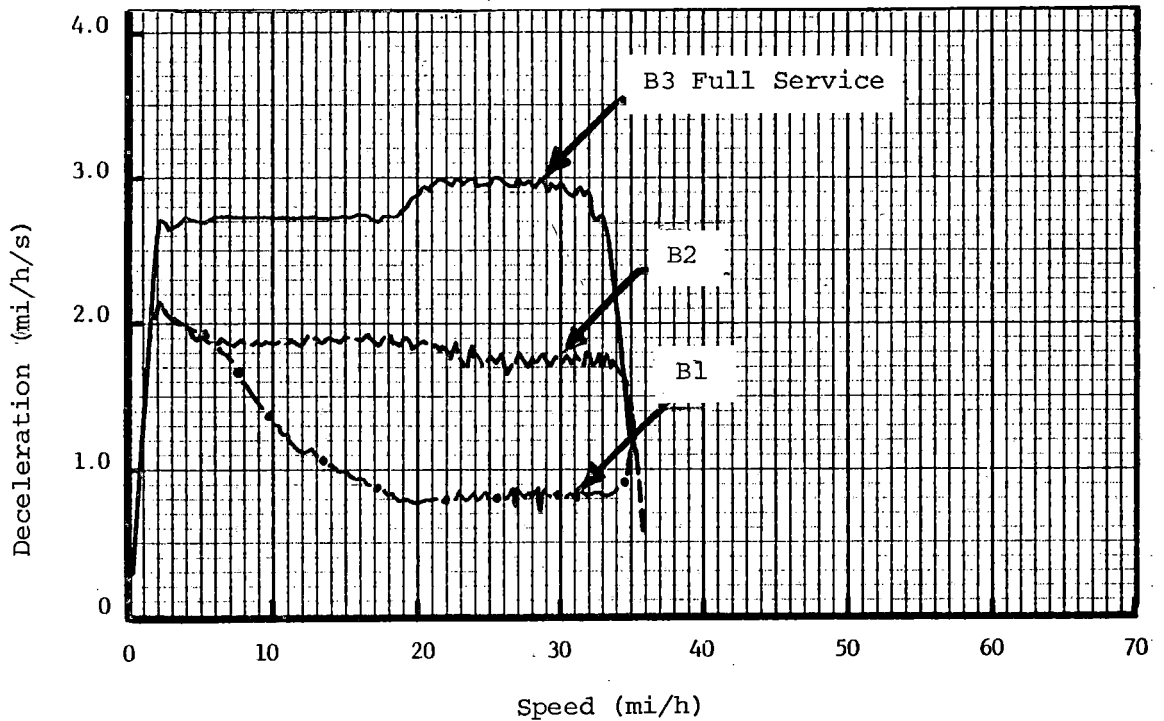


b. Effect of Master Controller at 35 mi/h.

FIGURE 6-23. DYNAMIC BRAKING--DECCELERATION CHARACTERISTICS, AWO WEIGHT.

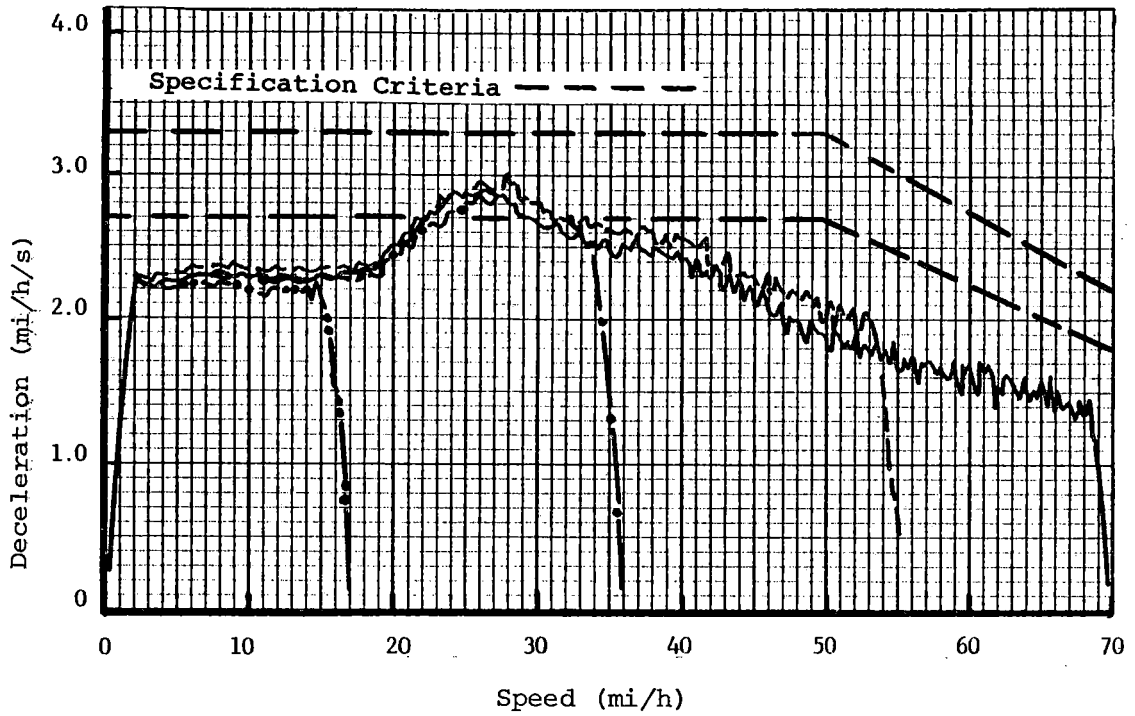


a. Effect of Initial Speed on Full Service Braking.

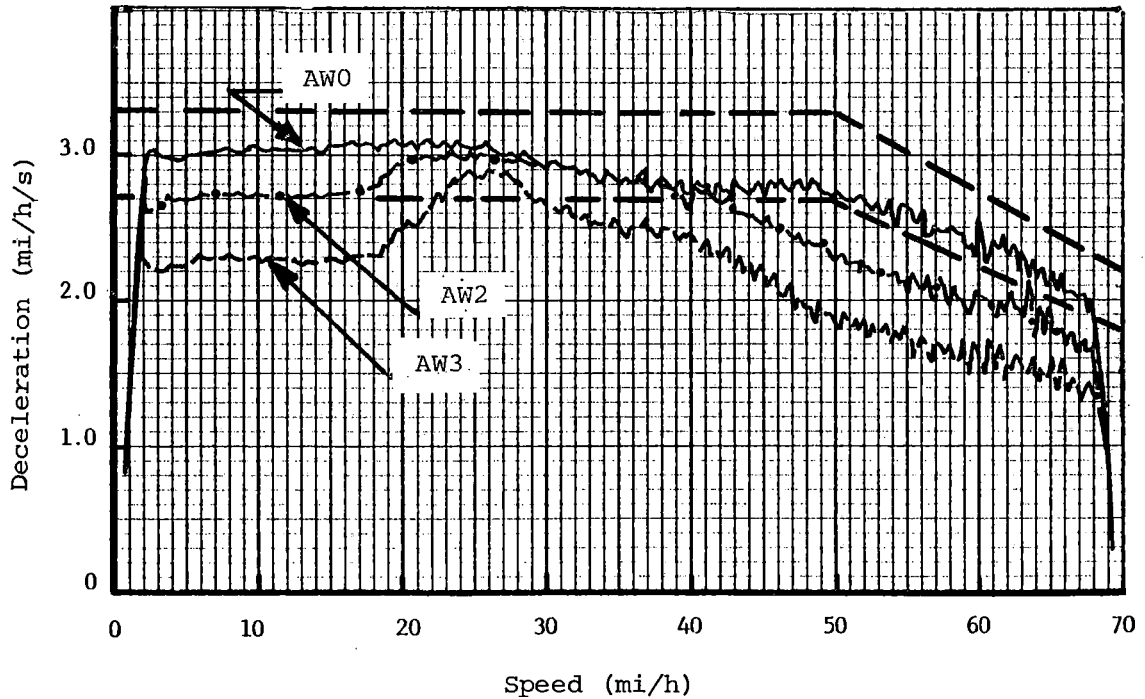


b. Effect of Master Controller at 35 mi/h.

FIGURE 6-24. DYNAMIC BRAKING--DECELERATION CHARACTERISTICS, AW2 WEIGHT.

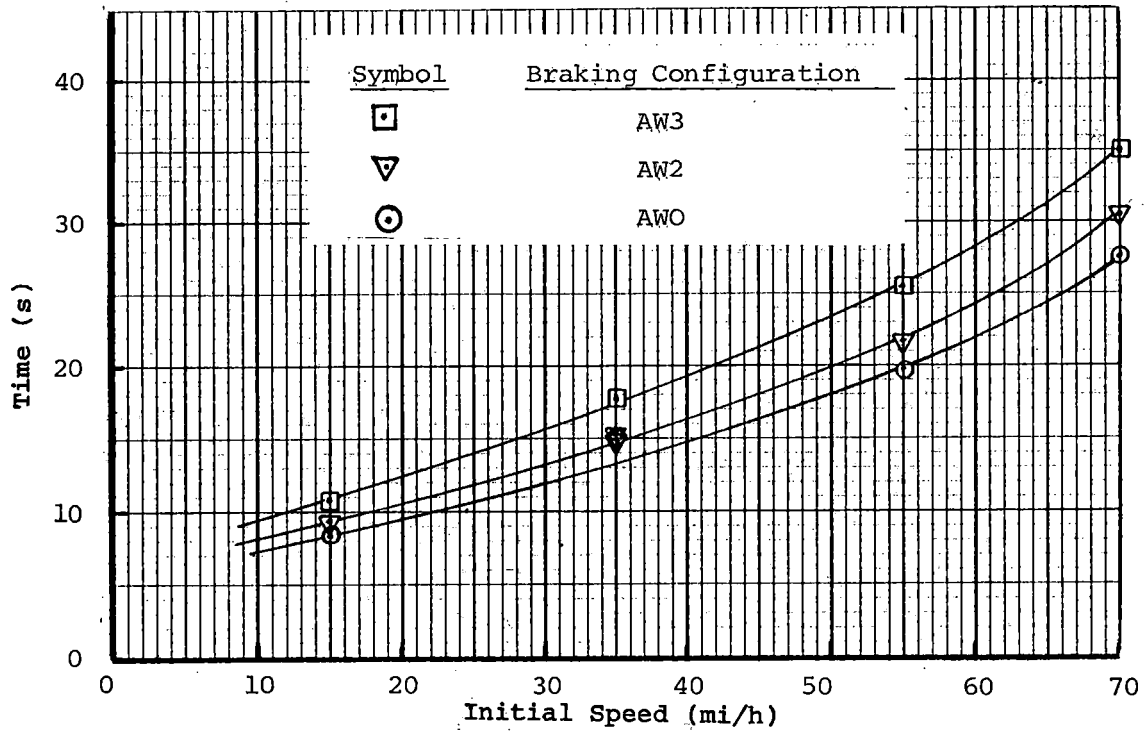


a. Effect of Initial Speed on Full Service Braking, AW3

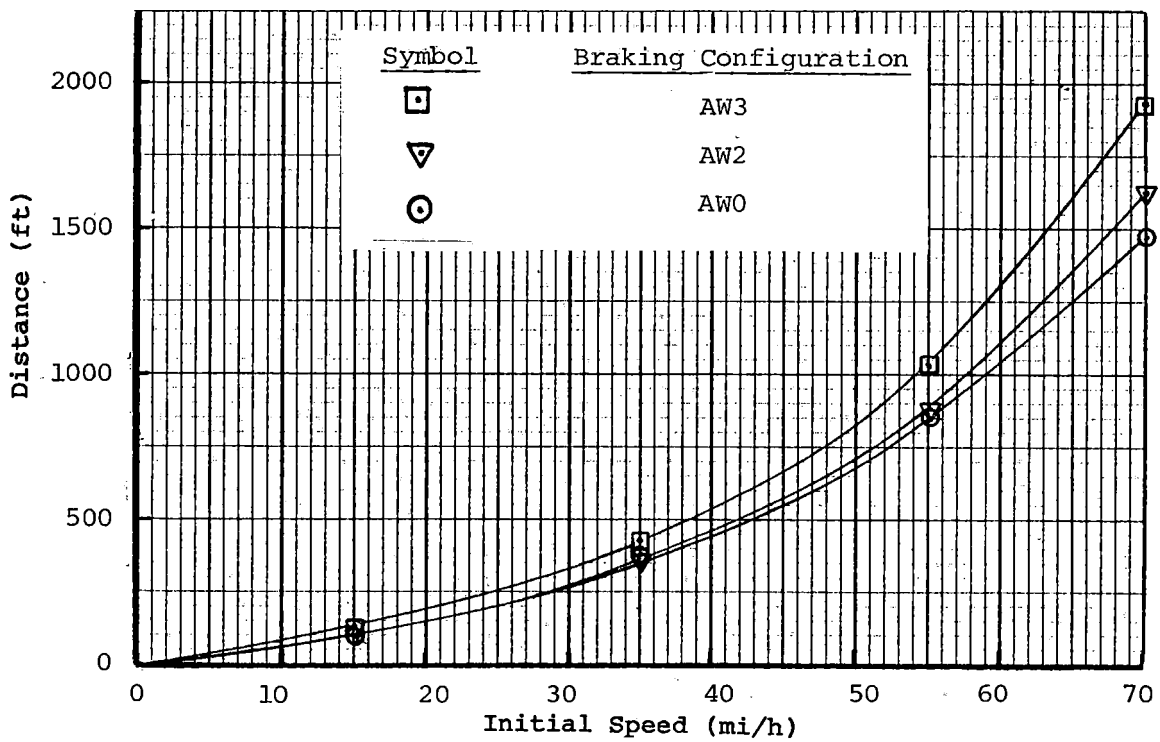


b. Effect of Weight on Full Service Braking.

FIGURE 6-25. DYNAMIC BRAKING--DECELERATION CHARACTERISTICS.



a. Time to Stop From Initial Speeds.



b. Distance to Stop from Initial Speeds.

FIGURE 6-26. DYNAMIC BRAKING--STOPPING DISTANCE AND TIME CHARACTERISTICS.

6.2.3.4 Emergency Braking. Emergency braking deceleration characteristics are presented in figures 6-27, 6-28, and 6-29 for each vehicle weight. Superimposed on the plots are dotted lines representing the minimum emergency braking deceleration criterion in the vehicle specification, of 3.5 mi/h/s over the entire speed range. The plots show that the emergency braking deceleration characteristics exhibit the same trends with initial brake entry speed as was observed in the full service friction braking data; the deceleration levels achieved increase with lower initial brake entry speeds.

The emergency braking characteristics all show rapidly increasing deceleration levels below 20 mi/h regardless of initial speed with the worst cases occurring at maximum vehicle weight; the deceleration from a 15 mi/h initial speed peaked at 7.0 mi/h/s for AW3 vehicle weight.

The high braking effort demands resulted in several wheel slide occurrences, in each case on the rear trucks of one or both cars. The results of activation of the spin/slide protection system can be seen in the deceleration levels for the 35 mi/h initial speed case, AW0 weight, at 4 and 1½ mi/h, where there are momentary losses of deceleration as the brakes respond to the spin/slide system.

Figure 6-29 shows the effect of vehicle weight on emergency braking for the 70 mi/h initial speed case, showing some deterioration of deceleration with increasing weight. Average deceleration levels for these three emergency braking conditions, computed from stopping distance and time-to-stop, show the same trends, with average values of 3.55, 3.49, and 3.35 mi/h/s for AW0, AW2, and AW3 vehicle weights, respectively.

However, the vehicles met the requirement for a minimum deceleration level of 3.5 mi/h/s throughout the stop at all vehicle weights and initial speeds, with the exception of the 70 mi/h initial speed emergency braking cases at AW2 and AW3, which fall 0.2 to 0.3 mi/h/s below the specification level between 40 and 10 mi/h. Emergency braking time-to-stop and distance required to stop data are plotted (figure 6-30) versus initial brake entry speed for all vehicle weights.

6.2.3.5 Comparison of Braking Mode Performance. A comparison of the blended, dynamic-only, and friction-only braking modes is made in figures 6-31 and 6-32, which compare the deceleration characteristics and distance/time required to stop with full service braking at AW2 vehicle weight. Deceleration characteristics are presented for the 70 and 35 mi/h initial brake entry speed cases. The data show close correlation of deceleration levels between blended and dynamic-only modes of operation, which is to be expected, as the friction brakes are applied only momentarily during the blended braking stop at AW2 weight. The inherent initial speed effect of friction brakes, discussed in section 6.2.3.2, wherein the deceleration levels for a given brake application increase with decreasing initial brake entry speed, affects the matching of friction braking performance with blended and dynamic modes of operation. While there is reasonable correlation between friction and blended modes for the 70 mi/h initial speed case (within 0.3 mi/h/s), the friction-only mode deceleration levels are higher at the 35 mi/h initial speed. Typically differences in the range 0.7 to 0.9 mi/h/s occur due to the friction brake characteristics.

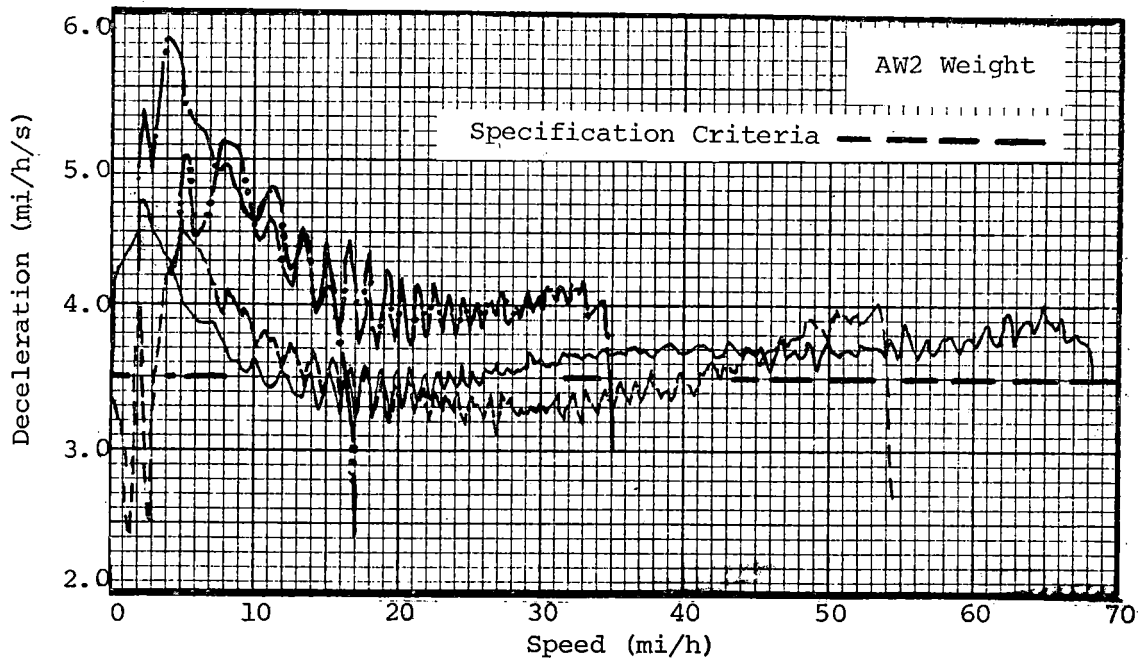
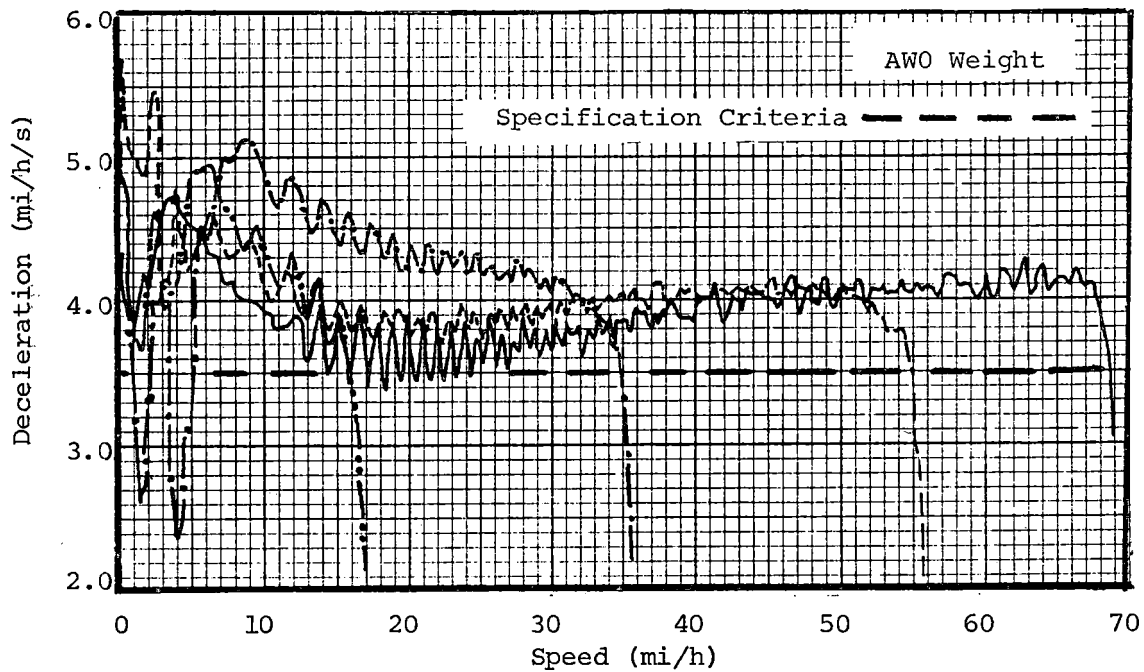


FIGURE 6-27. EFFECT OF INITIAL SPEED ON EMERGENCY BRAKING, AWO AND AW2 WEIGHTS.

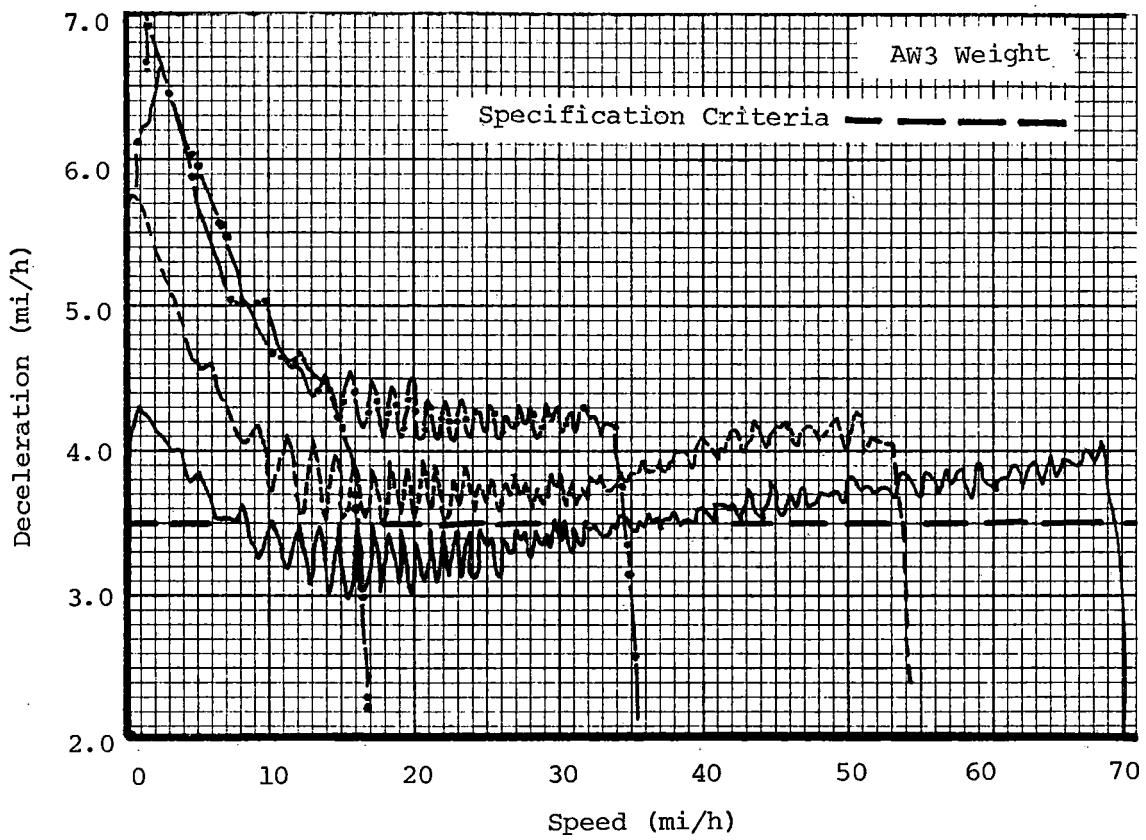


FIGURE 6-28. EFFECT OF INITIAL SPEED ON EMERGENCY BRAKING, AW3 WEIGHT.

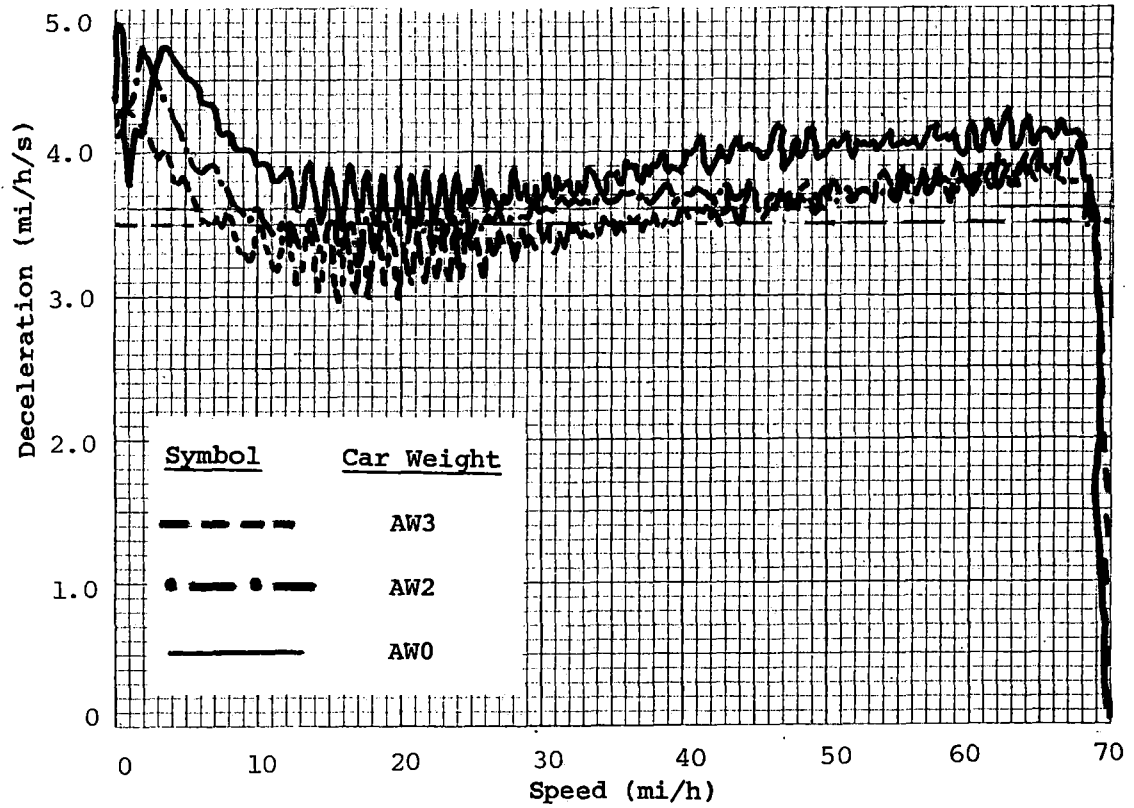


FIGURE 6-29. EFFECT OF WEIGHT ON EMERGENCY BRAKING.

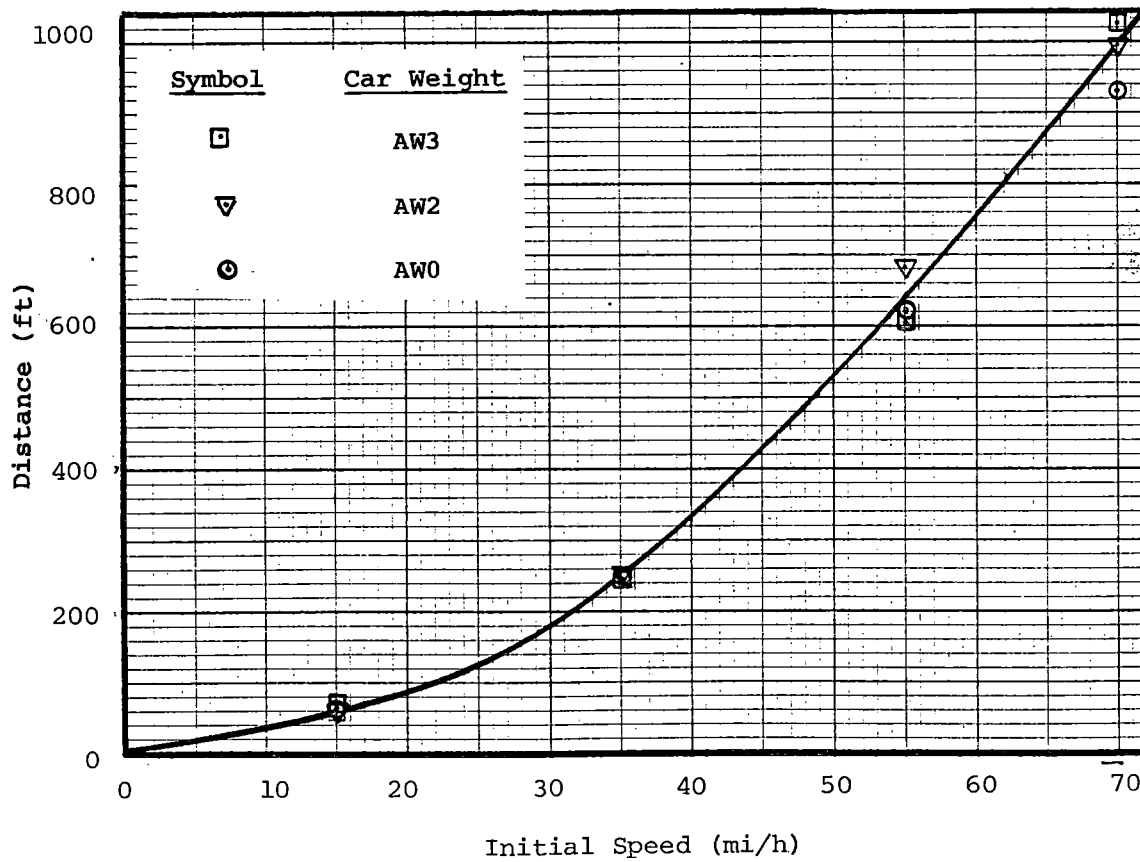
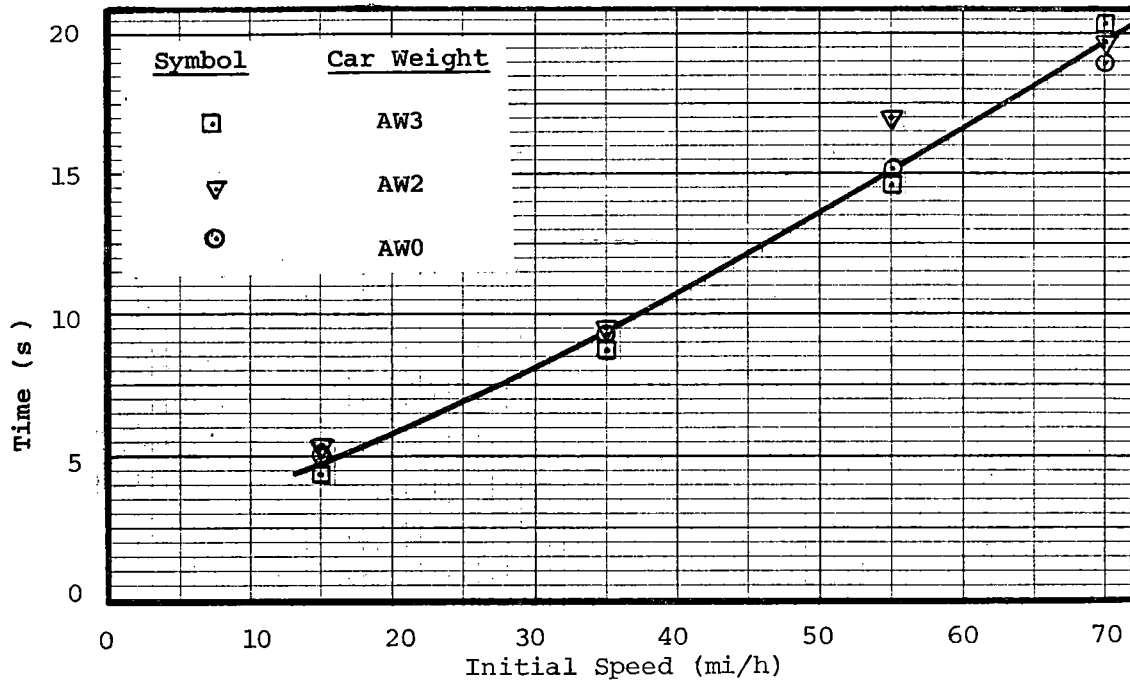


FIGURE 6-30. EMERGENCY BRAKING - EFFECT OF INITIAL SPEED ON TIME AND DISTANCE REQUIRED TO STOP.

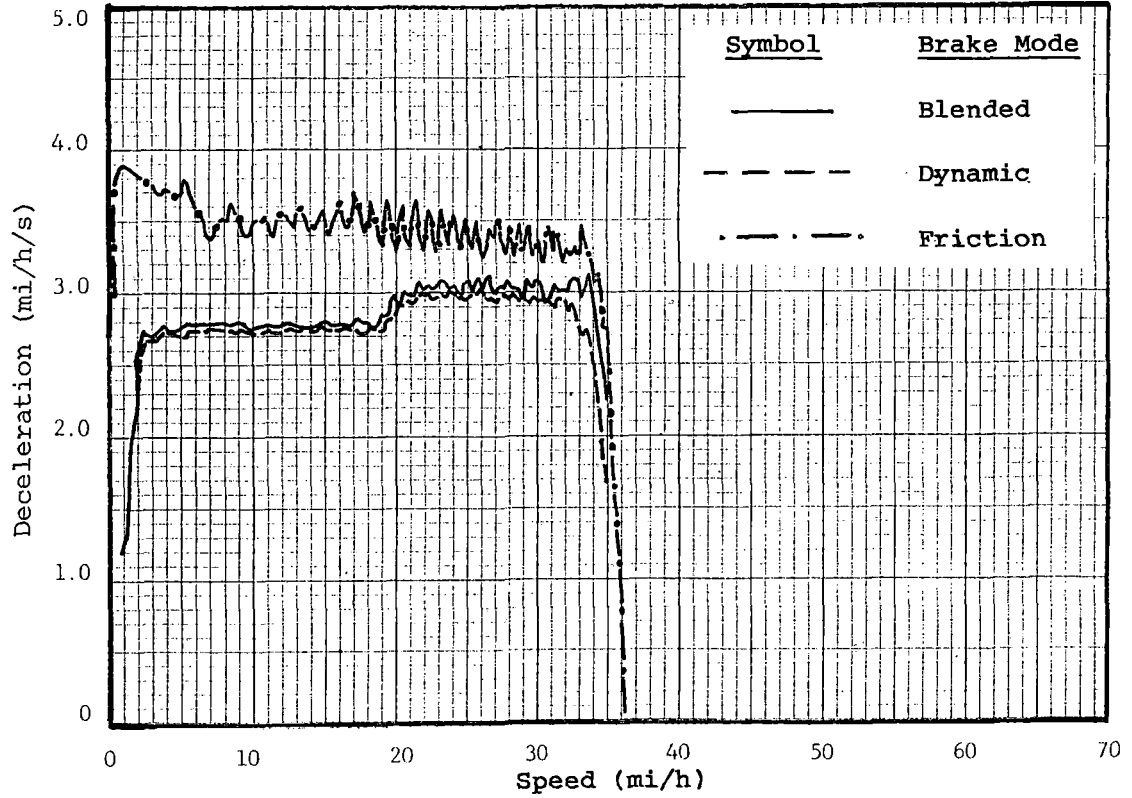
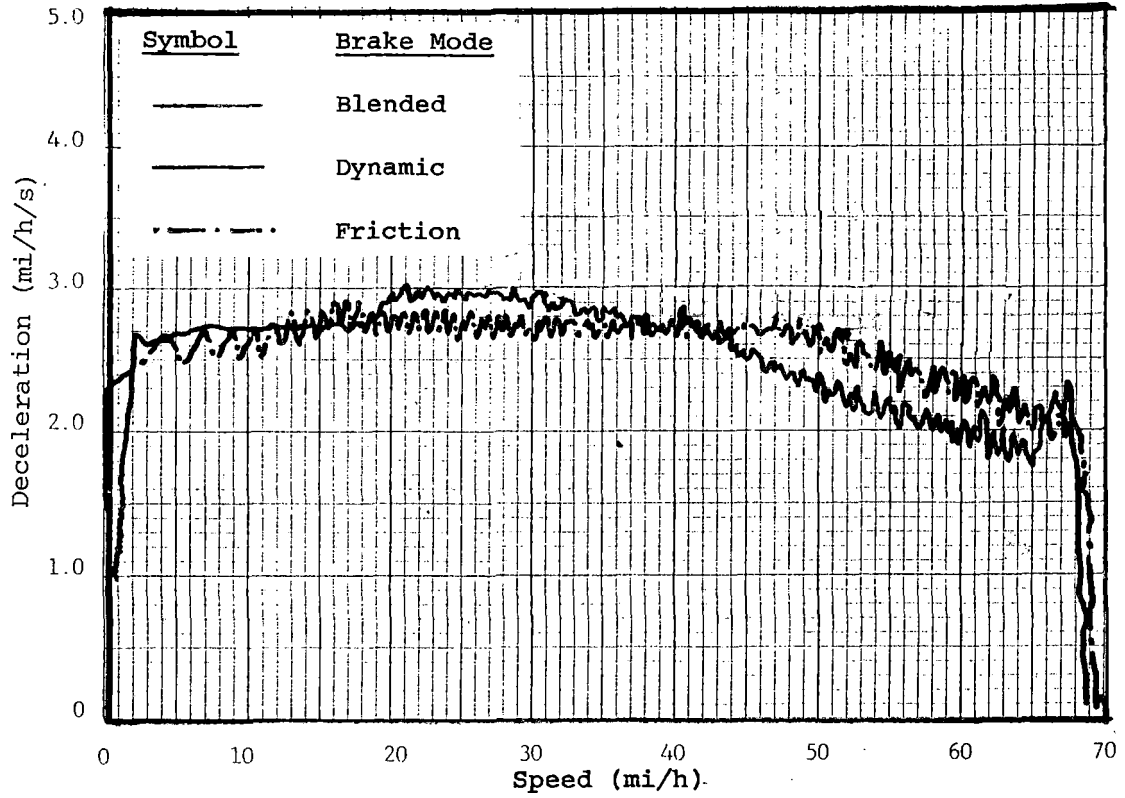


FIGURE 6-31. EFFECT OF BRAKE MODE ON BRAKING PERFORMANCE, 70 AND 35 mi/h INITIAL SPEED.

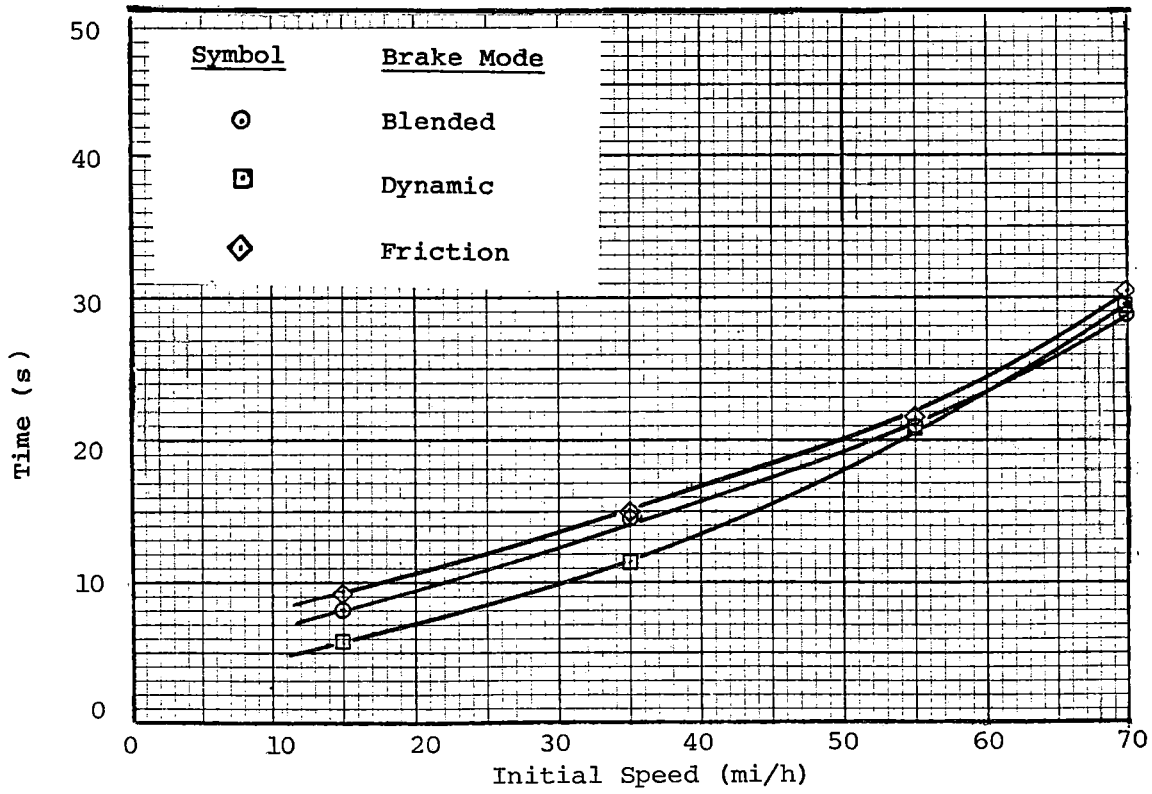
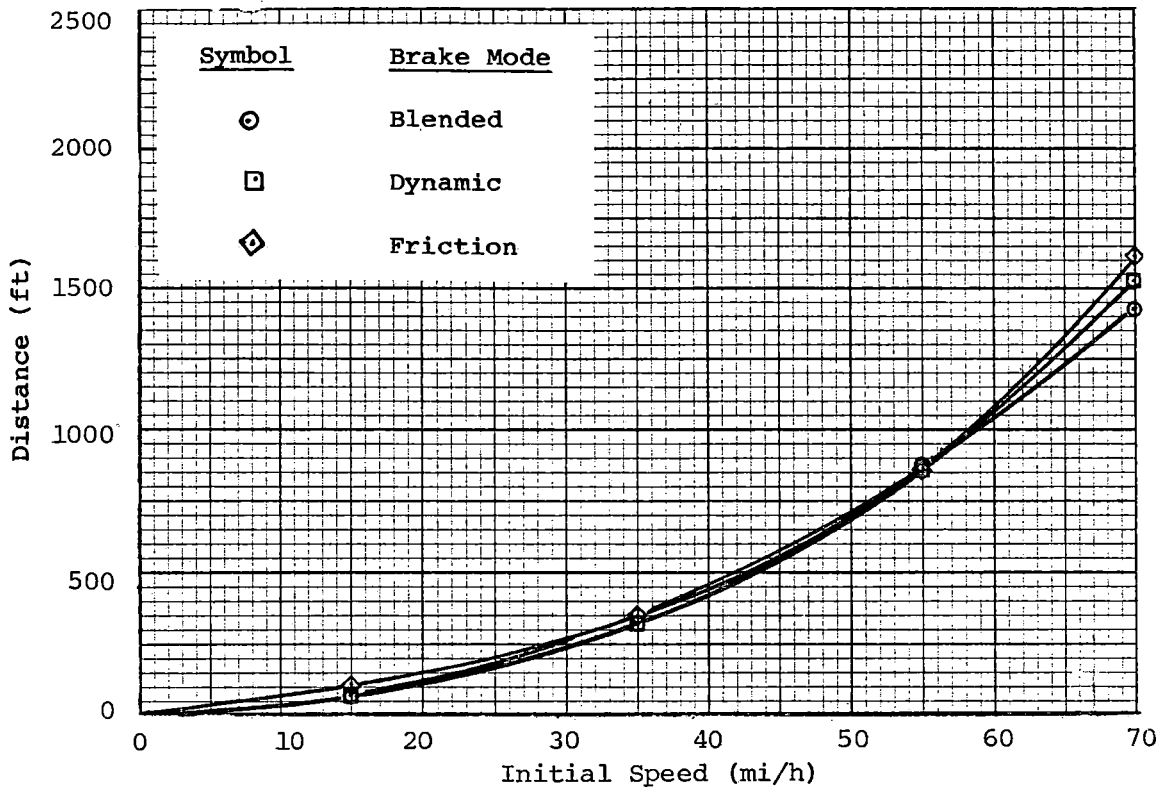


FIGURE 6-32. EFFECT OF BRAKE MODE ON BRAKING TIME TO STOP.

6.2.3.6 Comparison with Brake Configurations BR1 and BR2. The performance characteristics of two earlier brake configurations (BR1 and BR2, described in Section 3.13, Vehicle Configurations) evaluated at the TTC are compared to the baseline characteristics in figures 6-33 through 6-38. The deceleration characteristics of the three configurations are compared in figures 6-33 and 6-34 for a full service brake application from 70 mi/h initial speed at AW2 vehicle weight. Data for blended, dynamic-only, friction-only, and emergency modes of operation are presented for each configuration; the data points for the BR1 and BR2 configurations have been taken from chart records and overlaid on the analog deceleration plots of the baseline BR3 configuration.

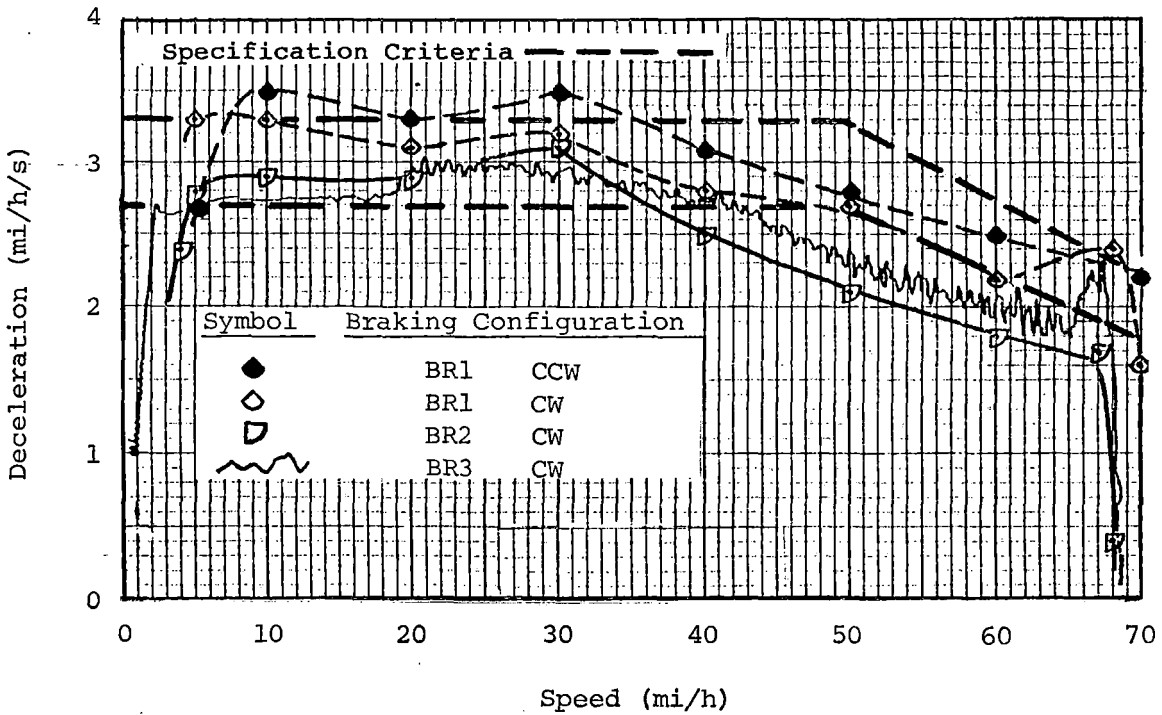
The data show that the BR1 configuration outperforms the BR3 baseline configuration throughout the 70 mi/h blended braking stop with typical deceleration values 0.3 to 0.5 mi/h/s higher than the BR3 configuration levels. Note that data in figure 6-33a are plotted for both clockwise (car 0110 leading) and counterclockwise (car 0109 leading) direction of travel for the BR1 configuration. The deceleration levels attained were dependent on which car the test was conducted from, with car 0109 leading giving superior deceleration levels by up to 0.3 mi/h/s. This was a characteristic of the BR1 configuration.

Examination of the BR1 brake cylinder pressure data shows that the friction brakes were applied throughout the full service braking; this is not in compliance with the vehicle specification which states that the braking effort is required from the electrical brakes (except at speeds below the point of dynamic brake fade-out) at vehicle weights up to AW2. For this reason the BR2 configuration incorporated modifications to eliminate the continuous friction brake application in blended braking. Figure 6-33a shows that the BR2 configuration achieved maximum deceleration levels comparable to the final BR3 configuration evaluated, but was inferior in the 70 - 40 mi/h speed range. Both BR2 and BR3 configurations perform below the specification requirement in this area.

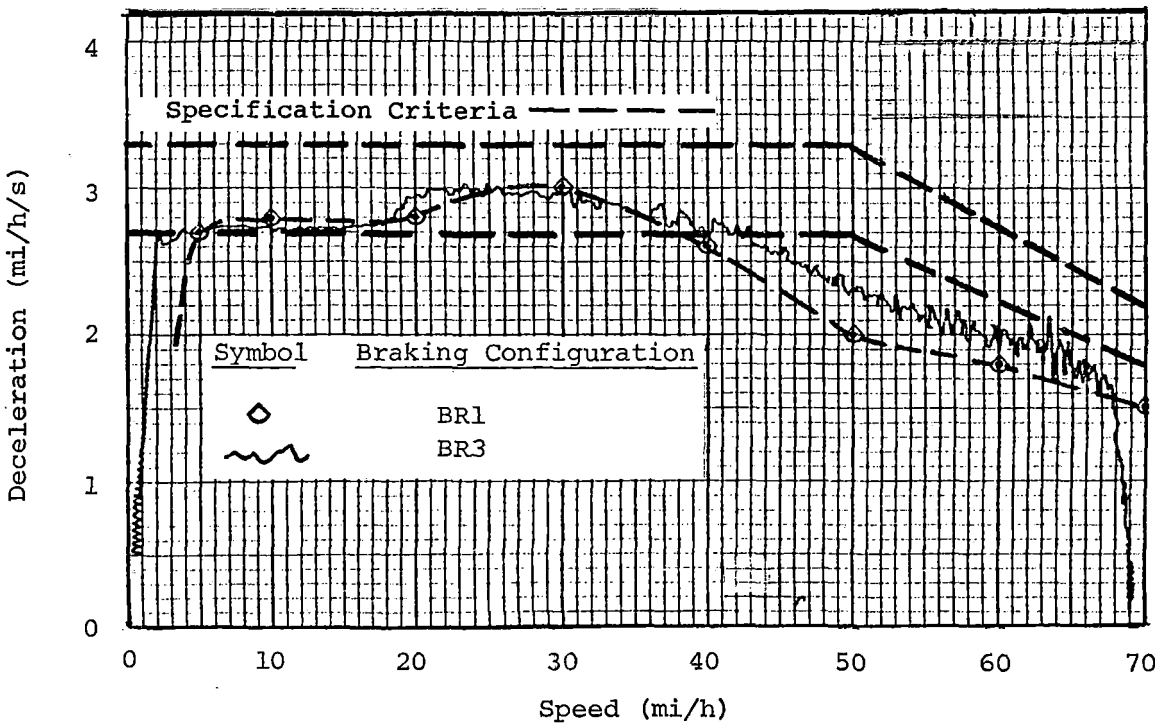
The dynamic braking characteristics are illustrated in figure 6-33b for the BR1 and BR3 brake configurations. The BR1 deceleration performance was similar to the BR3 baseline configuration and again both configurations' performance fell below the specification requirement in the 70 - 40 mi/h speed range. The dynamic braking characteristics of the BR2 configuration were not evaluated as the configuration was considered to be electrically the same as that of BR1.

A review of the friction-only and emergency braking modes, figure 6-34, shows that both configurations are generally inferior to the final BR3 configuration throughout the speed range; emergency braking deceleration levels for the BR1 configuration fell as low as 2.3 - 2.5 mi/h/s over the speed range 65 - 20 mi/h; a sustained emergency braking deceleration of 3.5 mi/h/s is required throughout the speed range.

The trends of stopping distance and time required to stop from initial brake entry speeds for full service braking at AW2 vehicle weight are plotted in figures 6-35 through 6-38 comparing the brake configurations in each mode of operation.

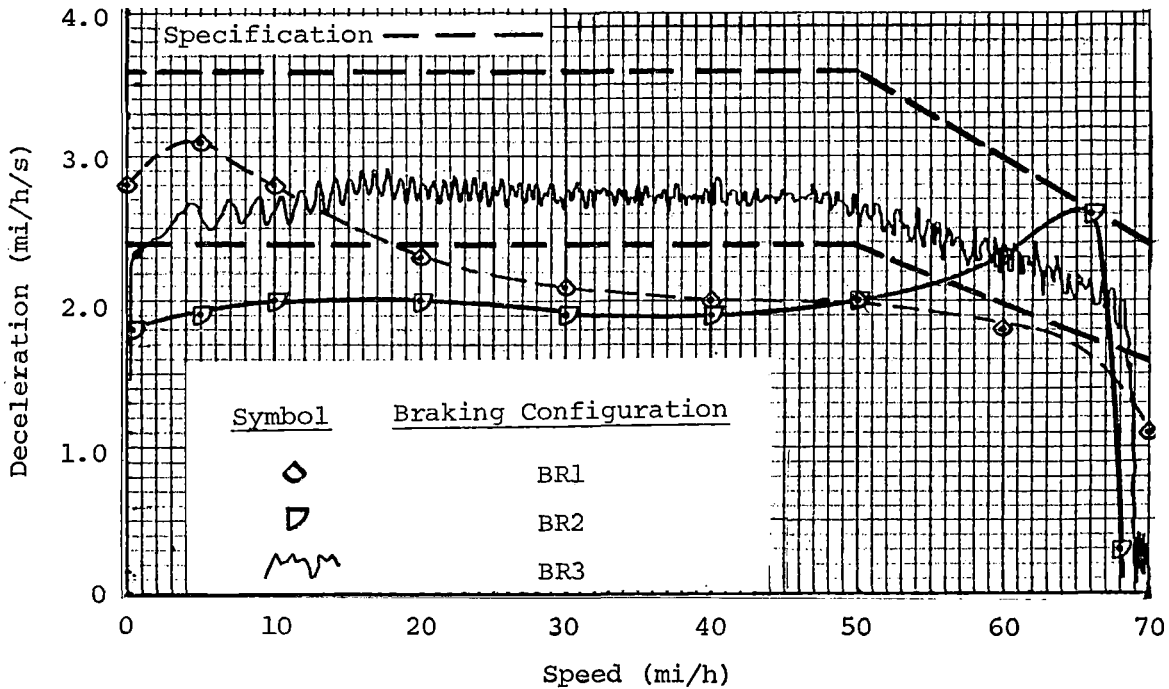


a. Full Service Braking, AW2 Weight, Blended Brakes

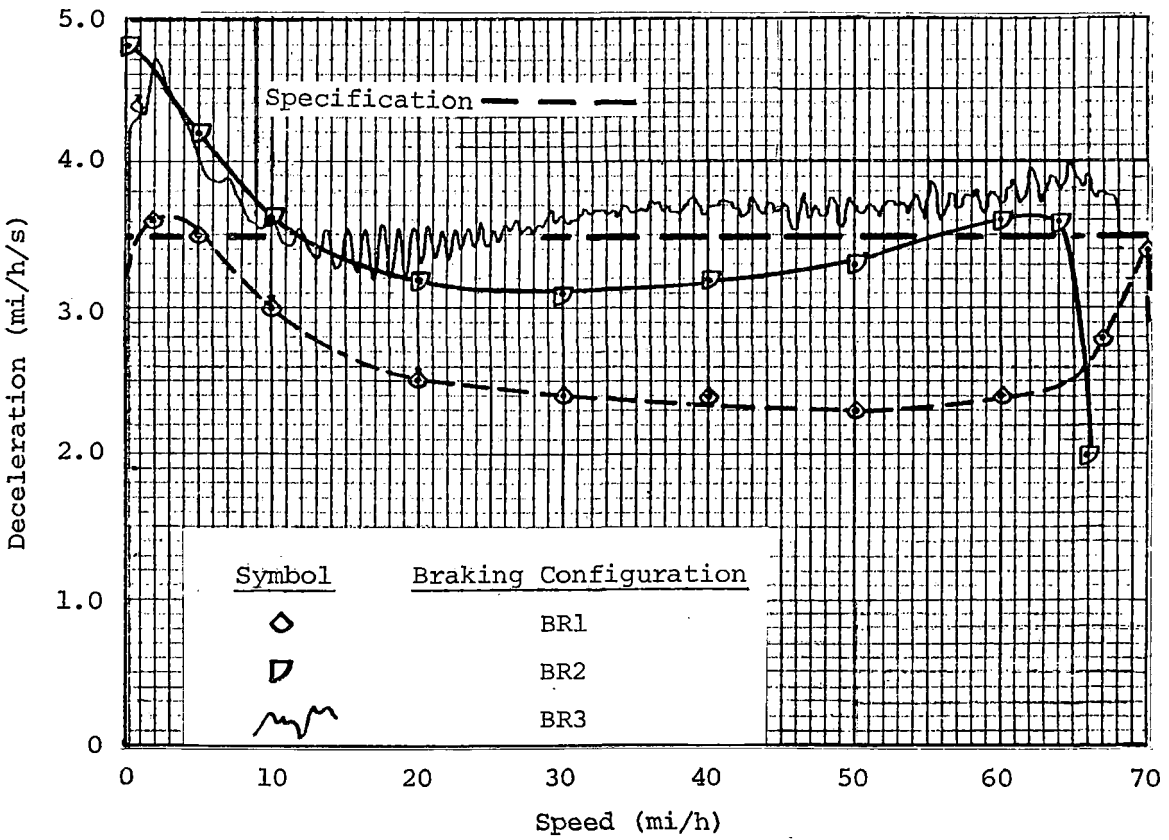


b. Full Service Braking, AW2 Weight, Dynamic Brakes

FIGURE 6-33. EFFECT OF BRAKE CONFIGURATION ON BLENDED AND DYNAMIC-ONLY BRAKING MODES.

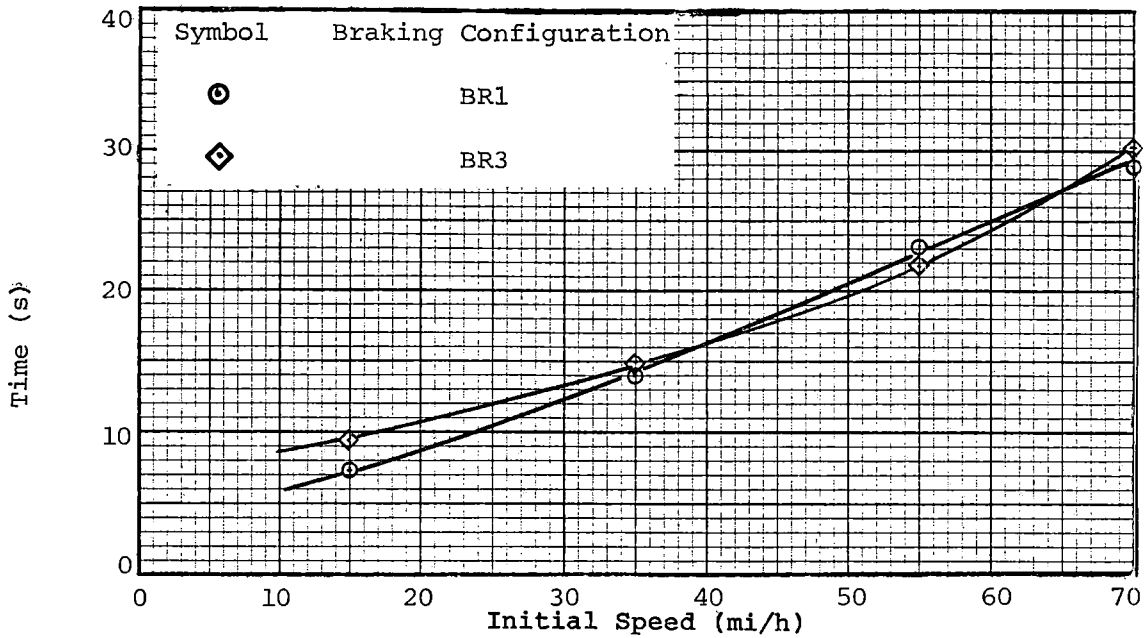


a. Full Service Braking, AW2 Weight, Friction Brakes

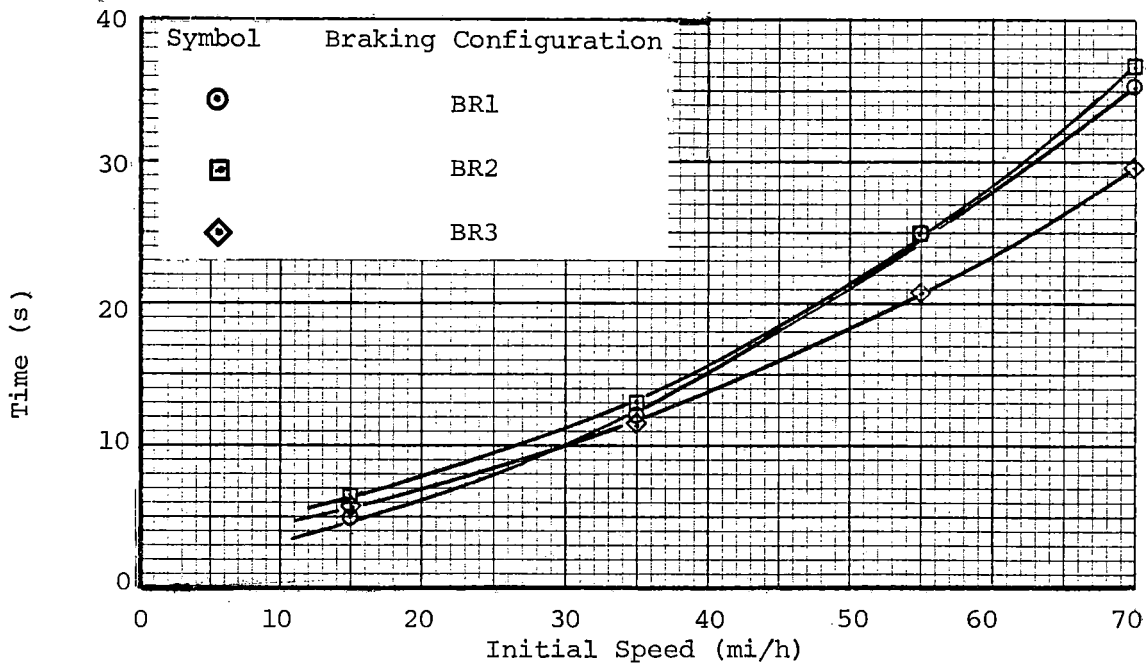


b. Full Service Braking, AW2 Weight, Emergency Brakes

FIGURE 6-34. EFFECT OF BRAKE CONFIGURATION ON FRICTION AND EMERGENCY BRAKING MODES.



a. Full Service Braking, AW2 Weight, Dynamic Brakes.



b. Full Service Braking, AW2 Weight, Friction Brakes

FIGURE 6-35. EFFECT OF BRAKE CONFIGURATION ON TIME TO STOP, DYNAMIC AND FRICTION BRAKES.

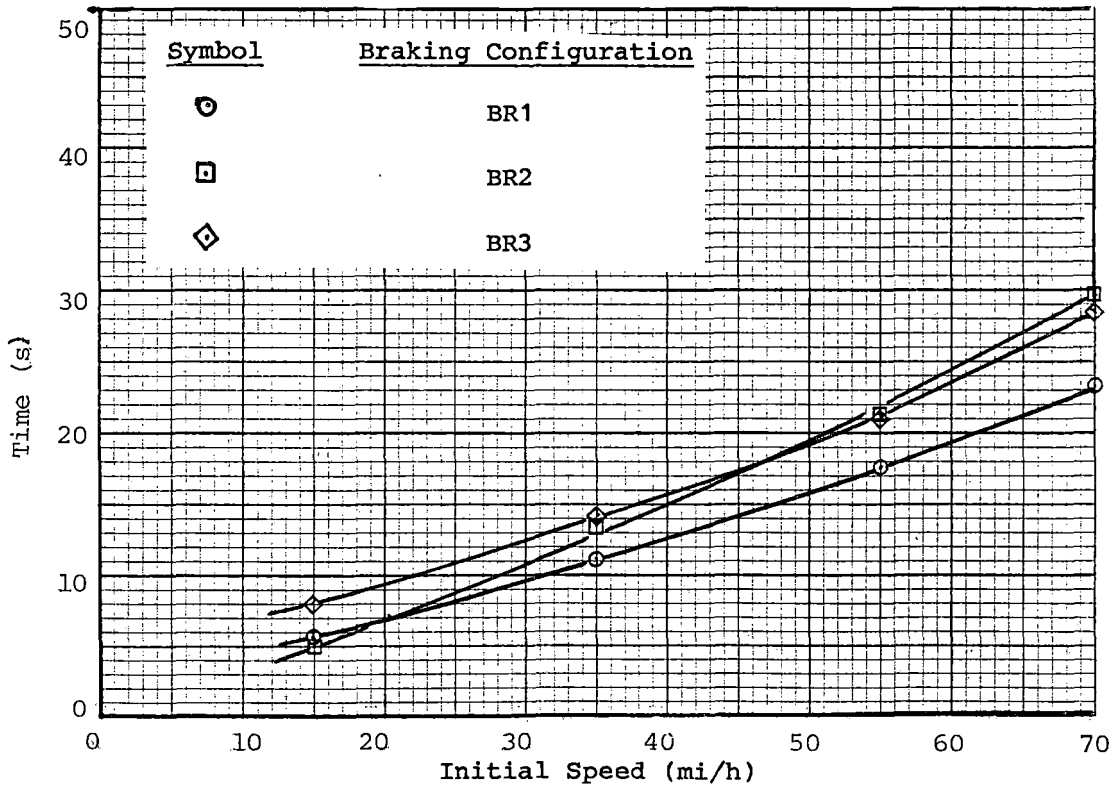
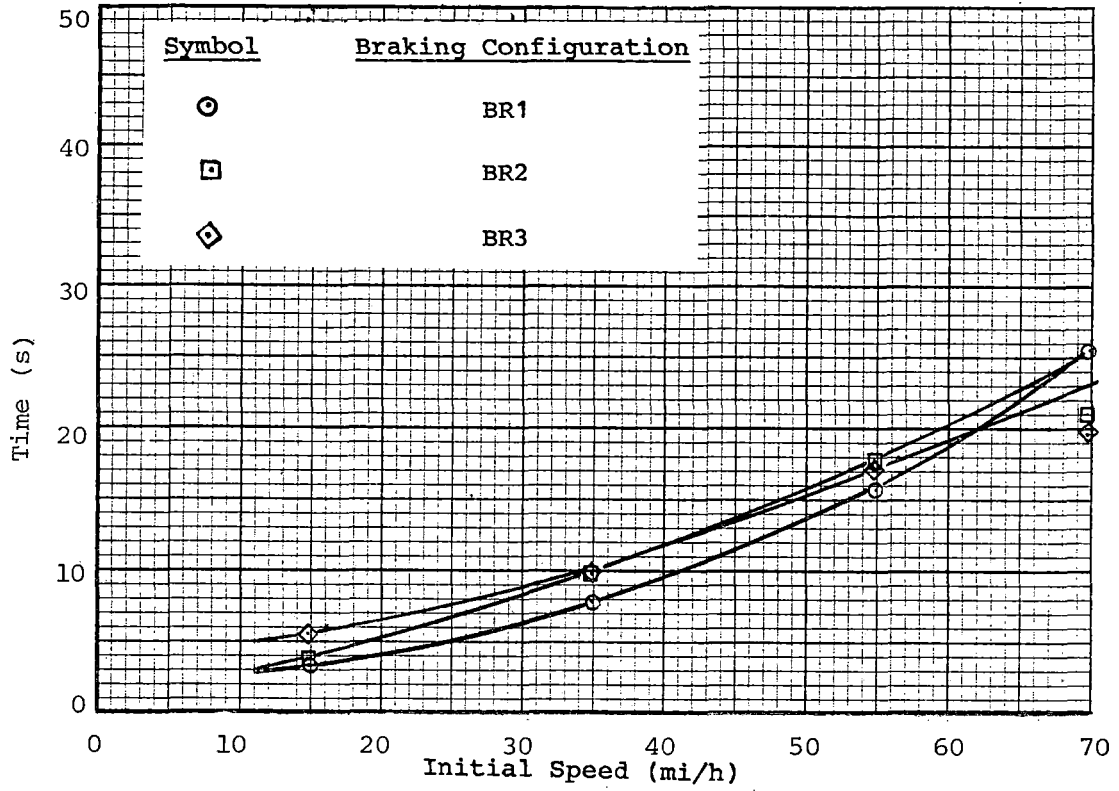
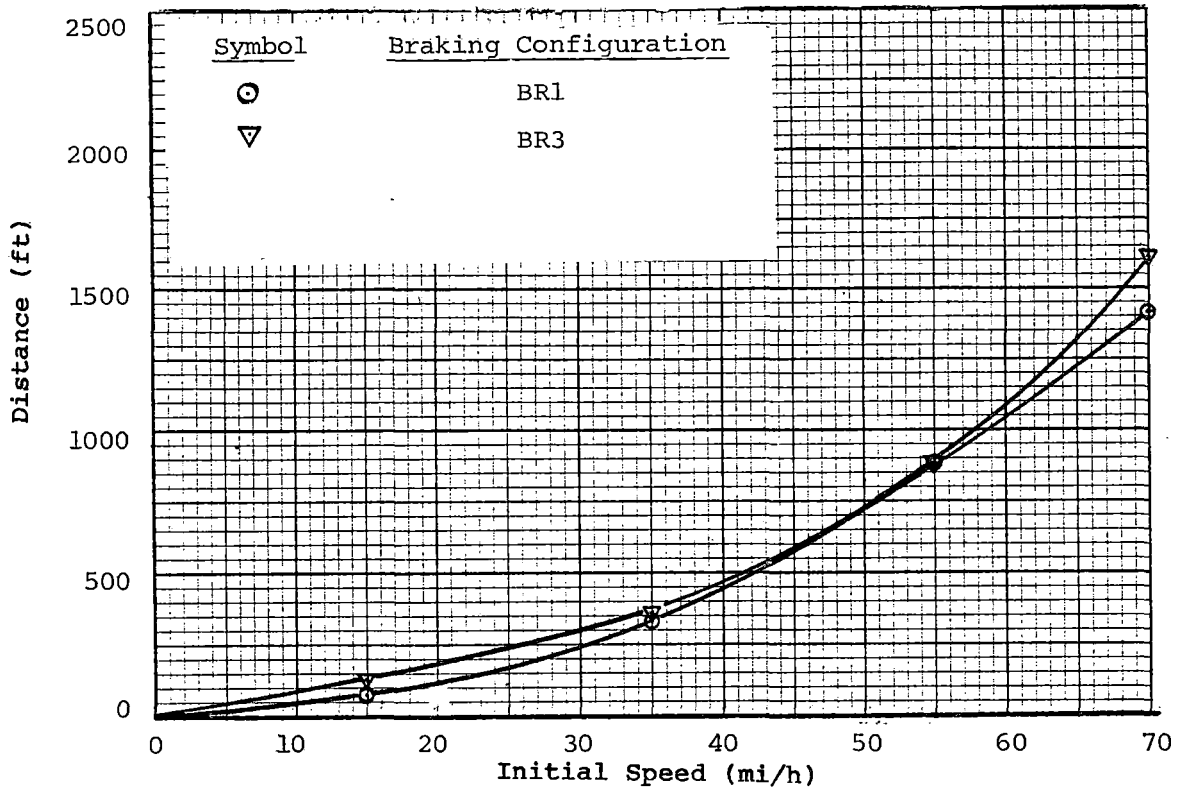
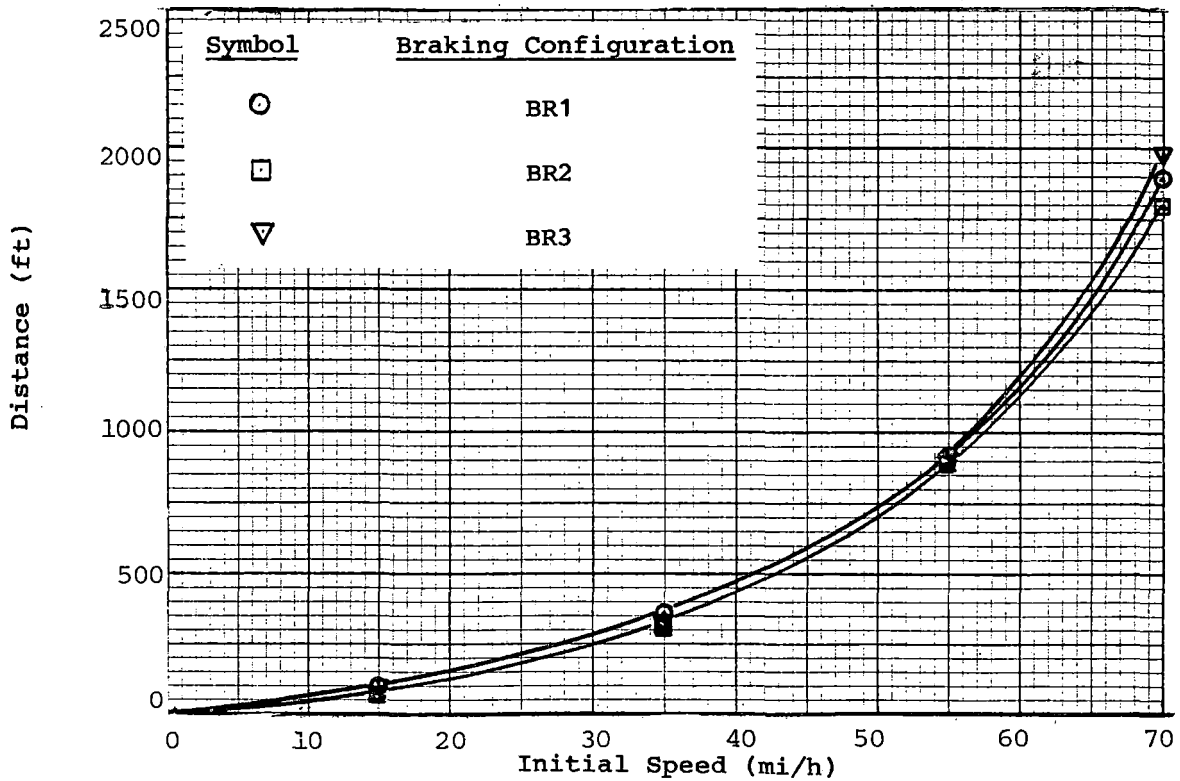


FIGURE 6-36. EFFECT OF BRAKE CONFIGURATION ON TIME TO STOP, EMERGENCY AND BLENDED BRAKES.

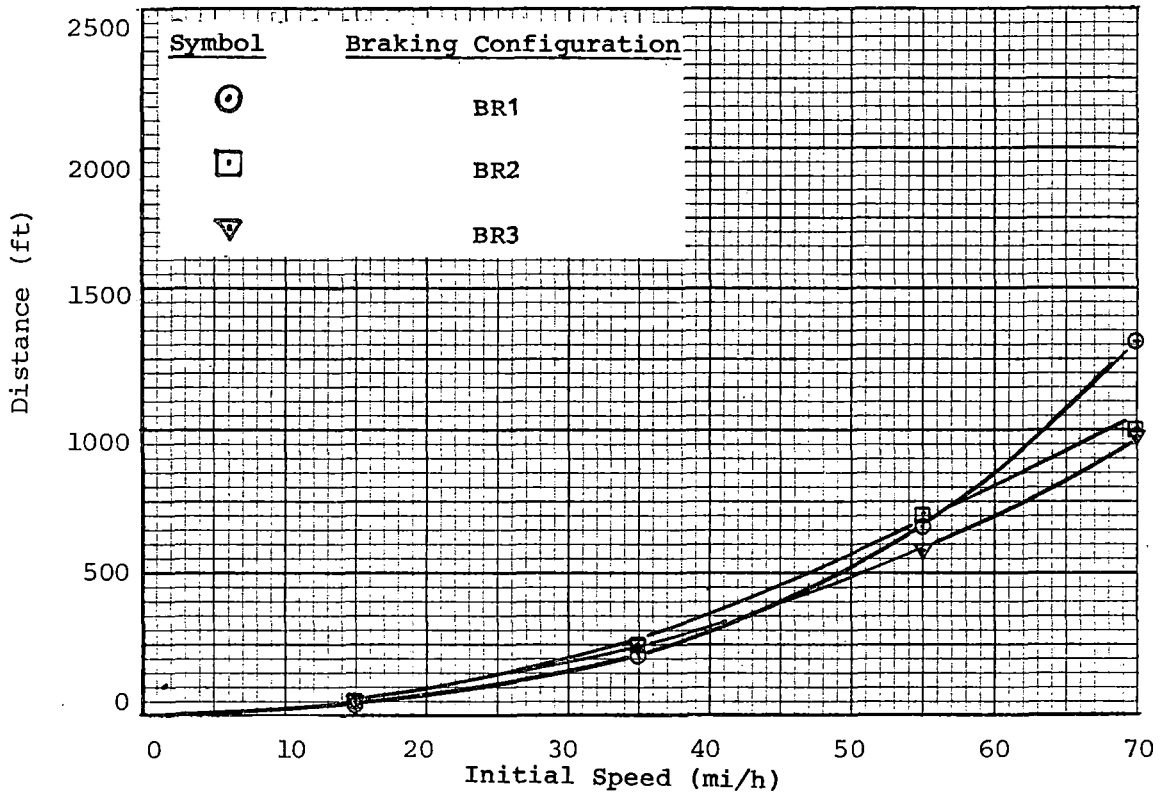


a. Full Service Braking, AW2 Weight, Dynamic Brakes .

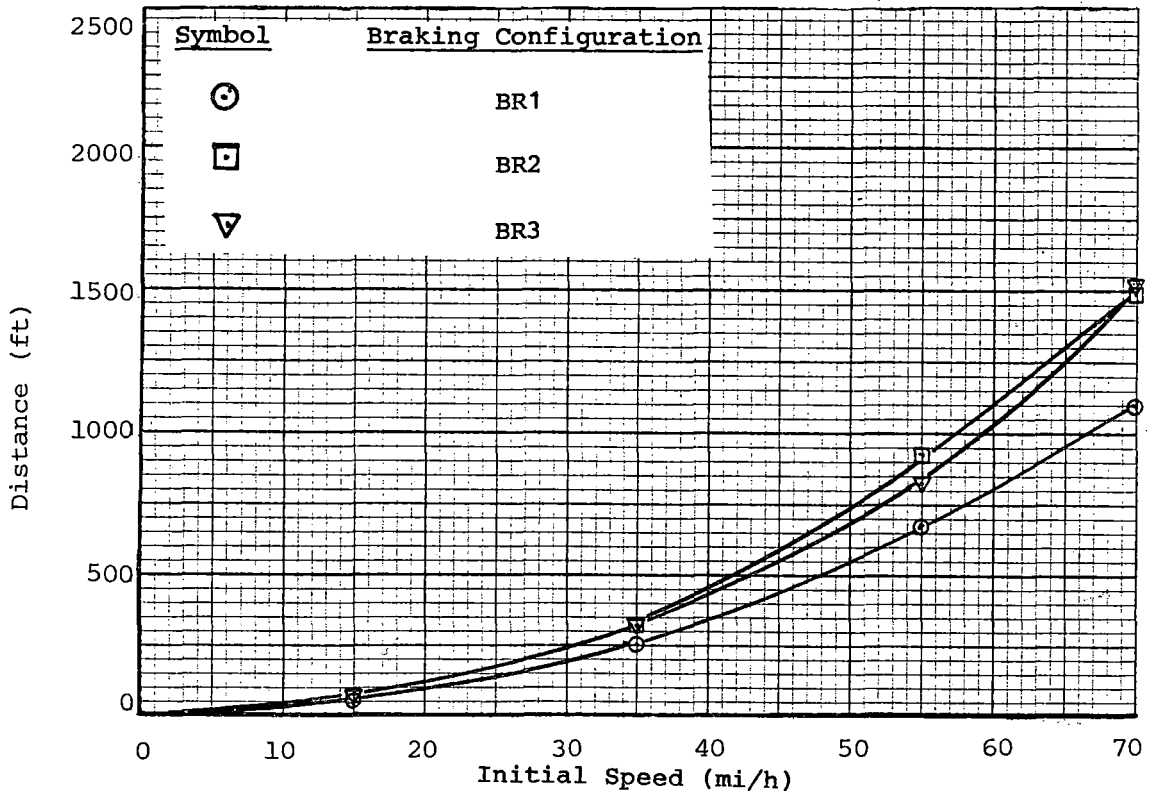


b. Full Service Braking, AW2 Weight, Friction Brakes.

FIGURE 6-37. EFFECT OF BRAKE CONFIGURATION ON DISTANCE TO STOP, DYNAMIC AND FRICTION BRAKES.



a. Full Service Braking, AW2 Weight, Emergency Brakes.



b. Full Service Braking, AW2 Weight, Blended Brakes.

FIGURE 6-38. EFFECT OF BRAKE CONFIGURATION ON DISTANCE TO STOP, EMERGENCY AND BLENDED BRAKES.

6.3 DUTY CYCLE TESTS

6.3.1 Test Objectives

The objectives of the test were:

- To determine the equilibrium temperatures of the braking systems, when operating on a continuous duty cycle representing revenue service operation, in a friction-only and a normal blended braking mode.
- To determine the stabilized temperatures of the undercar equipment when operating on continuous duty cycles representing revenue service; the data are intended to provide information to assess the thermal adequacy of the equipment design and location.

6.3.2 Test Method

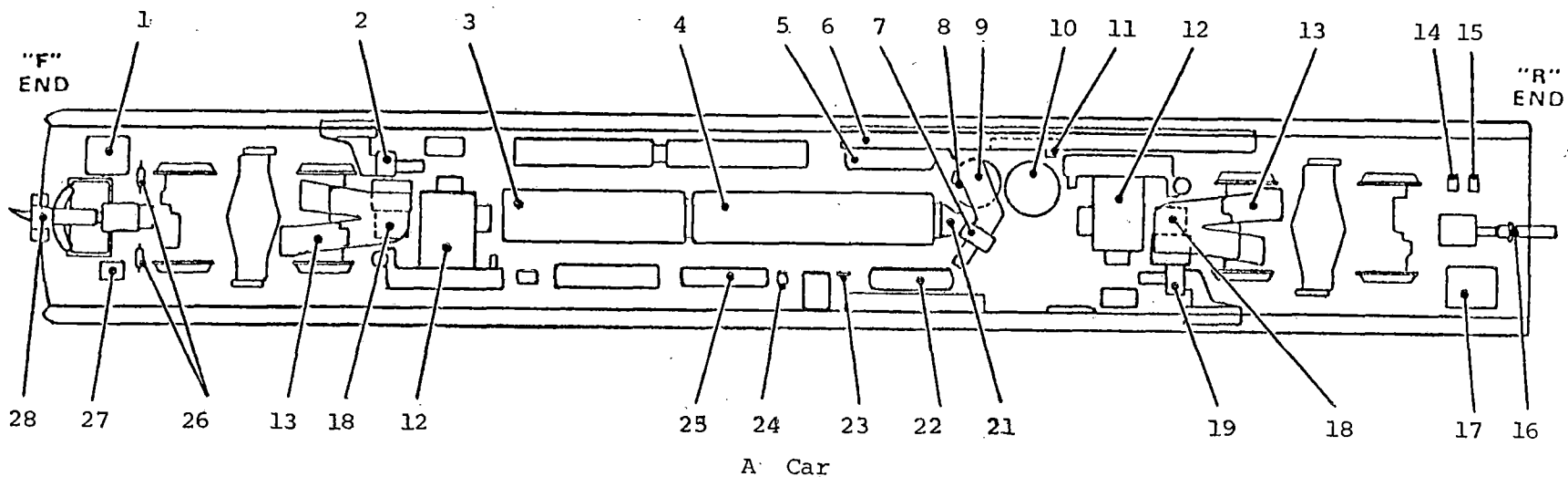
The cars were operated in a series of test runs simulating actual revenue service profiles. Temperature data from thermocouples in twenty-nine locations under the A car (0109), including traction motor cases, resistor grids, electronic equipment bays, and two locations on the left lead axle brake shoe, were recorded at each station stop. The data were recorded immediately after the vehicles came to rest at each stop, by means of a data logger which scanned the thermocouples sequentially and printed the temperatures, in degrees Fahrenheit.

The location of the undercar equipment for a MARTA A car is shown in figure 6-39. Corresponding thermocouple locations chosen for these tests are illustrated in figure 6-40.

The equilibrium temperatures of the friction brake shoes, operating in a friction-only braking mode, were evaluated using three revenue service profile simulations. These were:

- A simulation of the MARTA East-West line round trip from Avondale to High Tower and return; the profile is shown in detail in tables 6-2 and 6-3.
- A duty cycle typifying NYCTA operation. The cycle comprised a maximum acceleration to 35 mi/h, a period of constant speed for 30 s, followed by full-service braking to a stop, and a 30-s station stop; the sequence was repeated for 25 cycles.
- A duty cycle typifying CTS operation. The run comprised an acceleration to 50 mi/h, constant speed for 55 s, and full-service braking to a full stop, followed by a 30-s station stop. The sequence was repeated for 19 cycles.

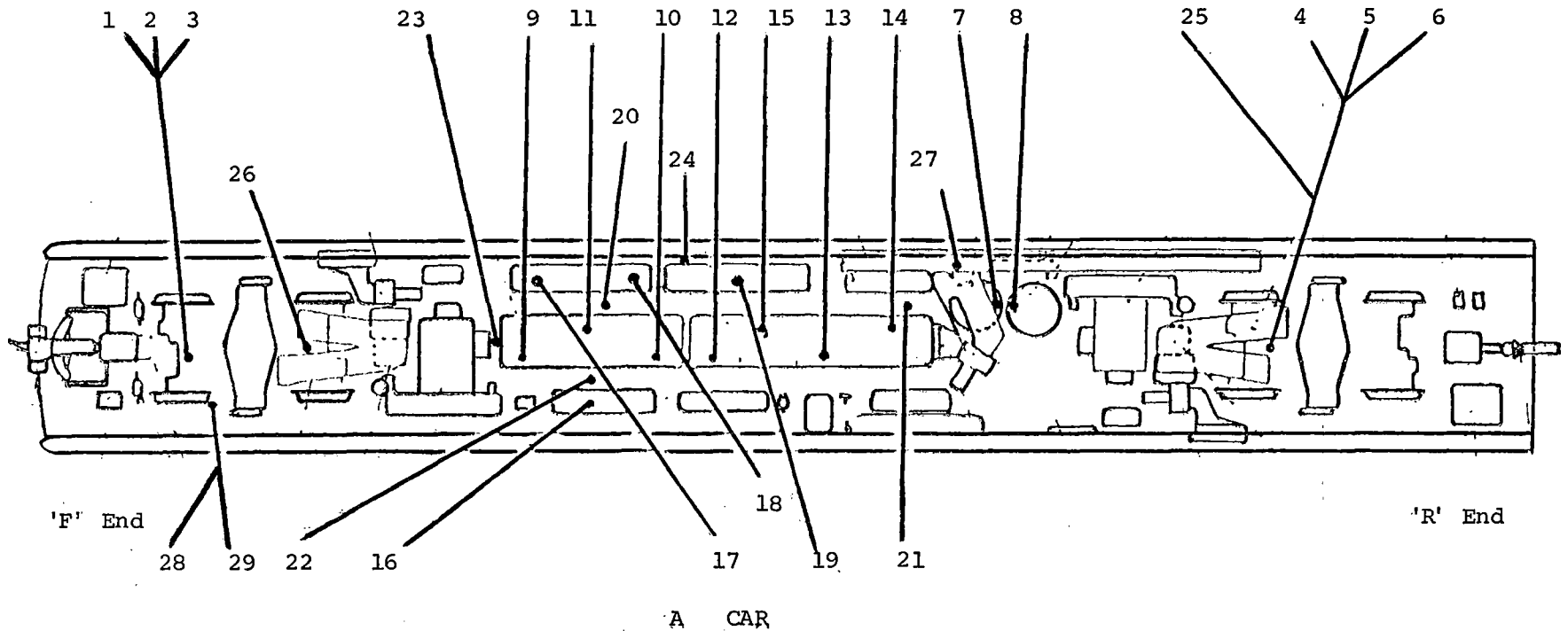
The equilibrium temperatures of the brake grid resistors and undercar equipment operating in the normal blended braking mode were evaluated using a special revenue profile provided by MARTA. The profile was comprised of a



NOMENCLATURE

1	Train Line Junction Box	15	Low Voltage Junction Box
2	Traction Motor Blower	16	Semi-Permanent Coupler
3	Auxiliary Power System Equip.	17	R-End Low Voltage
4	Power Control Equipment	18	Body/Truck Junction Box
5	Air Supply Reservoir	19	Traction Motor Blower
6	PCE Cooling Air Duct	20	Air Compressor Unit
7	Equipment Cooling Blower	21	PCS Air Duct
8	Smoothing Inductor	22	Main Reservoir
9	PCE Blower Air Duct	23	Ground Plate
10	Input Inductor	24	Vent Valve
11	Thermostat	25	Air Conditioning Control Box
12	A/C Compressor and Condenser	26	ATP Pick-up Coil
13	Traction Motor Cooling Air Duct	27	Antenna Junction Box
14	High Voltage Junction Box	28	ATO Antenna Junction Box

FIGURE 6-39. UNDERCAR EQUIPMENT LOCATION.



CHANNEL	LOCATION/DESCRIPTION
0	Outside Ambient (Open Air)
1	Top of traction motor #1 case
2	Bottom of traction motor #1 case
3	Internal traction motor #1 (Brush Area)
4	Top of traction motor #3 case
5	Field Coil of traction motor #3
6	Internal traction motor #3 (Brush Area)
7	Surface of smoothing inductor (adjacent to input inductor)
8	Surface of input inductor (adjacent to smoothing inductor)
9	APSE Bay #1 internal (Open Air)
10	APSE Bay #3 internal (Open Air)
11	APSE Bay #5 internal (Open Air)
12	PCE Bay #1 internal (Open Air)
13	PCE Bay #3 internal (Open Air)
14	PCE Bay #5 internal (Open Air)
15	PCE Bay #7 internal (Open Air)
16	Battery box internal (Open Air)
17	Brake Resistor grid fwd. end fwd. unit (Open Air)
18	Brake resistor grid rear end fwd. unit (Open Air)
19	Brake resistor grid middle rear unit (Open Air)
20	Undercar Midway ASPE Bay #5 & resistor grid (Open Air)
21	Undercar midway PCE Bay #5 & reservoir (Open Air)
22	Undercar midway APSE Bay #2 & battery box (Open Air)
23	Undercar midway APSE and A/C unit (Open Air)
24	Undercar floor contact above brake resistor bank
25	Undercar floor contact above #3 traction motor
26	Undercar traction motor #2 positive armature lead (Contact)
27	PCE cooling duct intake (approximately 3 inches in)
28	L1 brake shoe stationary (Note #1)
29	L1 brake shoe rotational (Note #2)

NOTES:

- 1) Bonded to the side of the brake shoe.
- 2) Mounted in a hole drilled in the brake shoe, 1/8" from the wheel/shoe friction face.

FIGURE 6-40. UNDERCAR THERMOCOUPLE LOCATIONS.

TABLE 6-2. MARTA EAST-WEST PROFILE, OUTBOUND.

Depart Station	TTT Sta. No.	Speed (mi/h)	TTT Sta. No.	Speed (mi/h)	TTT Sta. No.	Speed (mi/h)	TTT Sta. No.	Speed (mi/h)	TTT Sta. No.	Speed (mi/h)	Arrive Station	Dwell Time (s)
Avondale	5.000	25	5.340	50	9.210	0					Decatur	15
Decatur	9.210	50	10.240	60	13.950	50	15.990	0			East Lake	15
East Lake	15.990	50	17.080	60	17.670	70	22.800	50	24.830	0	Candler Pk	15
Candler Pk	24.830	50	29.060	0							Inman Pk	15
Inman Pk	29.060	50	30.060	60	35.790	50	36.790	0			King Mem.	15
King Mem.	36.790	50	37.140	37	40.210	0					Ga. State	15
Ga. State	40.210	37	42.290	0							Five Points	15
Five Points	42.290	37	42.830	50	44.310	0					Omni	15
Omni	44.310	50	46.400	0							Vine City	15
Vine City	46.400	50	50.260	0							Ashby	15
Ashby	50.260	50	51.110	60	9.910	50	10.910	0			West Lake	15
West Lake	10.910	50	12.040	60	17.760	50	18.780	0			High Tower	60

TABLE 6-3. MARTA EAST-WEST PROFILE, RETURN.

Depart Station	TTT Sta. No.	Speed (mi/h)	TTT Sta. No.	Speed (mi/h)	TTT Sta. No.	Speed (mi/h)	TTT Sta. No.	Speed (mi/h)	TTT Sta. No.	Speed (mi/h)	Arrive Station	Dwell Time (s)
High Tower	18.780	50	17.860	60	12.040	50	10.920	0			West Lake	15
West Lake	10.920	50	9.920	70	51.880	50	50.270	0			Ashby	15
Ashby	50.270	50	46.410	0							Vine City	15
Vine City	45.410	50	44.670	37	44.320	0					Omni	15
Omni	44.320	37	42.300	0							Five Points	15
Five Points	42.300	37	40.270	0							Ga. State	15
Ga. State	40.270	37	36.850	0							King Mem.	15
King Mem.	36.850	37	36.500	50	35.850	60	30.110	50	29.120	0	Inman Pk	15
Inman Pk	29.120	50	24.890	0							Candler Pk	15
Candler Pk	24.890	50	23.900	60	17.130	50	16.050	0			East Lake	15
East Lake	16.050	50	13.020	60	10.290	50	9.280	0			Decatur	15
Decatur	9.280	50	6.060	37	5.400	25	5.060	0			Avondale	60

sequence of four runs, described by P-signal voltage levels (i.e., master controller position) and elapsed time between master controller position changes. The sequence of four cycles was repeated ten times. The P-signal voltages and times are tabulated in table 6-4. They represent what was considered to be the most arduous part of the MARTA North-South route. A digital display of P-signal voltage and a stopwatch were used for maintaining the desired speed and schedule profile.

Undercar equipment temperatures were recorded for the revenue service profiles described above. All duty cycle testing was conducted at the AW2 vehicle weight.

6.3.3 Test Results

- Friction Brake Duty Cycles. Friction brake temperatures measured at the brake shoe of the left No. 1 axle are presented in figure 6-41 for the MARTA East-West line simulation, and for simulations of the NYCTA and CTS revenue service profiles. At each station stop the temperatures were measured for two thermocouples mounted on the brake shoe, one bonded on externally, the other mounted in a hole drilled in the brake shoe and located 1/8" from the wheel/shoe interface. Brake shoe temperatures stabilized in the 200° to 270°F band, with the CTS profile resulting in the highest brake shoe temperatures.

Undercar equipment temperatures remained stable throughout the friction-only braking runs and were typically in the range 85° to 110°F; traction motor temperatures were somewhat higher but did not exceed 120°F. Due to the lack of significant temperature trends, the data were not plotted on a station-stop basis, but are presented as temperatures at the start and conclusion of each revenue profile in table 6-5. Ambient temperatures on the test days were 75° to 80°F for the MARTA and NYCTA profiles and 80° to 90°F for the CTS profile.

- Blended Brake Duty Cycles. The significant temperature trends from the MARTA simulated revenue service duty cycle for blended braking are shown in figure 6-42 for each station stop. Initial and final temperatures, after 40 station stops, are tabulated in table 6-6 for those locations where there were no significant temperature trends. As might be expected, the brake resistor grids (thermocouples 17, 18, and 19) showed the most variation in temperature throughout the duty cycle. Brake resistor temperatures stabilized in the 400° to 660°F range, with the highest temperature recorded at the midsection of the rear brake resistor, after 27 station stops.

The effects of replacing the friction-only braking (of the revenue service profiles discussed earlier) with blended braking, incorporating resistive dynamic braking, can be seen in a comparison of the data for the traction motors and the friction brake shoes. Motor case temperatures, which were initially in the 110° to 120°F range, rose steadily throughout the run and stabilized at 140° and 190°F, respectively, for motors 1 and 3. This compares to maximum temperatures of approximately 120°F for the friction-only braking case.

TABLE 6-4. MARTA THERMAL CAPACITY PROFILE.

Run No.	P Signal (V)	Elapsed Time (s)	P Signal (V)	Elapsed Time (s)	P Signal (V)	Elapsed Time (s)	P Signal (V)	Dwell Time (s)
1	10	28	7.0	32	6.0	33	0.8	20
2	10	28	7.0	48	6.0	49	0.8	20
3	10	28	7.0	35	6.0	36	0.8	20
4	10	28	7.0	31	6.0	34	0.8	60

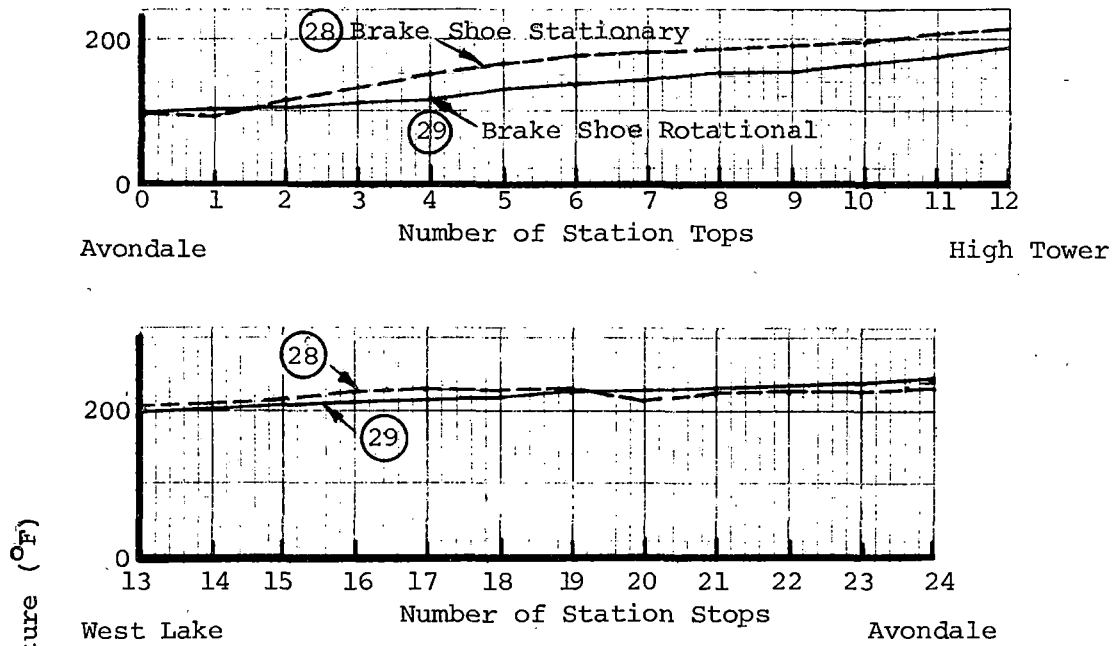
6-55

NOTES: The 'P' signal of 0.8 volts was held until the vehicle came to a complete stop.

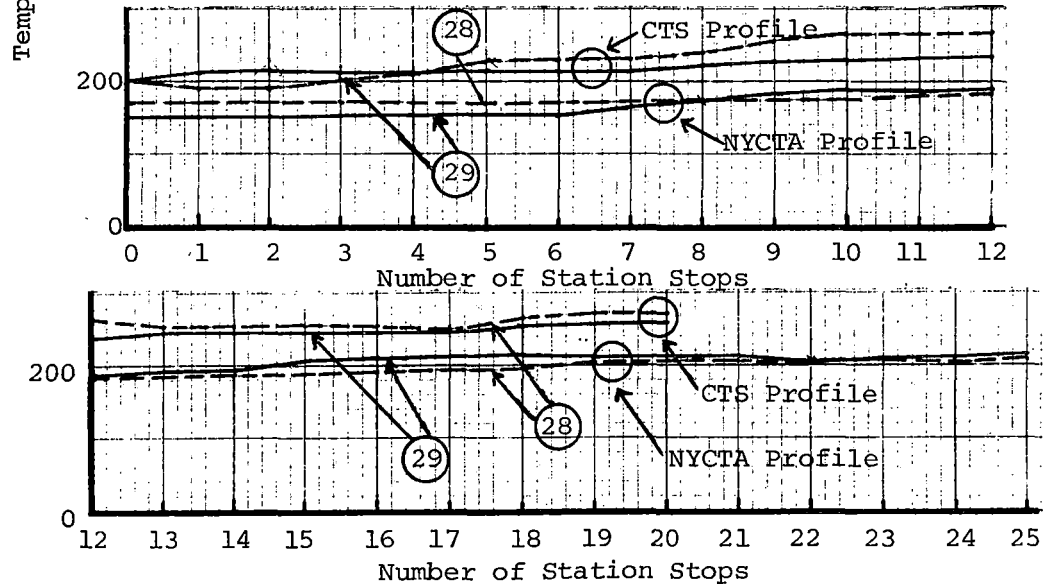
The dwell time was started at the time the vehicle came to a stop.

This sequence of runs was repeated until all thermocouples stabilized; 10 repeats of the above sequence were made.

MARTA EAST-WEST LINE ROUND TRIP SIMULATED PROFILE



NYCTA AND CTS REVENUE SERVICE PROFILES




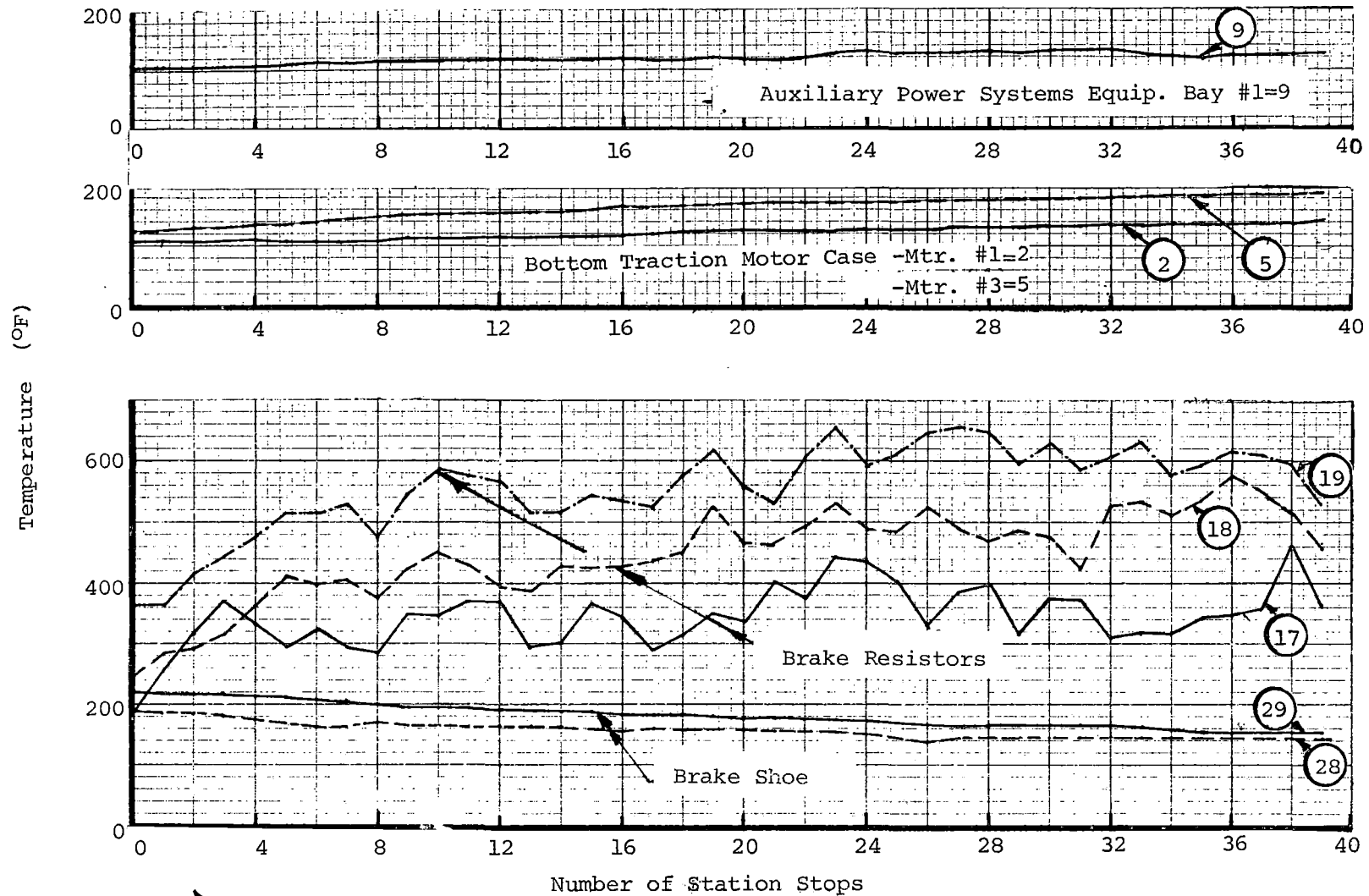
NOTE:  Denotes Termocouple Location, Detailed in Figure 6-40.

FIGURE 6-41. FRICTION BRAKING - DUTY CYCLES.

TABLE 6-5. FRICTION-ONLY BRAKING - DUTY CYCLE UNDERCAR TEMPERATURES.

Channel	Location/Description	MARTA E-W, Round		NYCTA		CTS	
		Initial (°F)	Final (°F)	Initial (°F)	Final (°F)	Initial (°F)	Final (°F)
0	Outside Ambient (Open Air)	75	75	83	80	80	90
1	Top of traction motor #1 case	91	93	108	108	109	112
2	Bottom of traction motor #1 case	93	96	111	112	112	114
3	Internal traction motor #1 (Brush Area)	85	90	95	97	96	98
4	Top of traction motor #3 case	90	100	110	109	110	112
5	Field Coil of traction motor #3	119	126	117	117	117	119
6	Internal traction motor #3 (Brush Area)	85	97	99	101	99	104
7	Surface of smoothing inductor (adjacent to input inductor)	93	96	101	103	103	105
8	Surface of input inductor (adjacent to smoothing inductor)	82	99	95	104	100	106
9	APSE Bay #1 internal (Open Air)	87	103	97	106	101	101
10	APSE Bay #3 internal (Open Air)	91	96	100	102	103	105
11	APSE Bay #5 internal (Open Air)	92	96	102	103	104	106
12	PCE Bay #1 internal (Open Air)	90	94	100	102	102	103
13	PCE Bay #3 Internal (Open Air)	86	93	99	103	99	101
14	PCE Bay #5 internal (Open Air)	84	85	91	92	91	90
15	PCE Bay #7 internal (Open Air)	84	85	98	101	100	101
16	Battery box internal (Open Air)	85	83	88	88	88	90
17	Brake resistor grid fwd. end fwd. unit (Open Air)	111	86	88	92	88	85
18	Brake resistor grid rear end fwd. unit (Open Air)	100	85	90	92	90	88
19	Brake resistor grid middle rear unit (Open Air)	111	85	90	92	90	86
20	Undercar midway ASPE Bay #5 & resistor grid (Open Air)	88	88	90	97	90	90
21	Undercar midway PCE Bay #5 & reservoir (Open Air)	84	87	88	96	89	87
22	Undercar midway APSE Bay #2 & battery box (Open Air)	90	87	88	95	88	92
23	Undercar midway APSE and A/C unit (Open Air)	96	99	102	106	104	109
24	Undercar floor contact above brake resistor bank	85	86	89	93	92	93
25	Undercar floor contact above #3 traction motor	86	92	91	94	94	100
26	Undercar traction motor #2 pos. armature lead (Contact)	90	104	100	107	101	113
27	PCE cooling duct intake (approximately 3 inches in)	76	78	86	86	86	84
28	L1 brake shoe stationary (Note #1)	96	233	154	217	194	271
29	L1 brake shoe rotational (Note #2)	99	243	171	211	211	259

NOTES: 1) Bonded to the side of the brake shoe.
 2) Mounted in a hole drilled in the brake shoe, 1/8" from the wheel/shoe friction face.




NOTE:  Denotes Termocouple Location, Detailed in Figure 6-40.

FIGURE 6-42. BLENDED BRAKING DUTY CYCLE TEMPERATURE TIME HISTORIES.

TABLE 6-6. BLENDED BRAKING - DUTY CYCLE UNDERCAR TEMPERATURES

Channel	Location/Description	Initial (°F)	Final (°F)
0	Outside Ambient (Open Air)	80	91
1	Top of traction motor #1 case	101	131
2	Bottom of traction motor #1 case	107	141
3	Internal traction motor #1 (Brush Area)	93	103
4	Top of traction motor #3 case	105	128
5	Field Coil of traction motor #3	123	187
6	Internal traction motor #3 (Brush Area)	104	120
7	Surface of smoothing inductor (adjacent to input inductor)	99	113
8	Surface of input inductor (adjacent to smoothing inductor)	102	117
9	APSE Bay #1 internal (Open Air)	104	127
10	APSE Bay #3 internal (Open Air)	99	113
11	APSE Bay #5 internal (Open Air)	99	113
12	PCE Bay #1 internal (Open Air)	96	113
13	PCE Bay #3 Internal (Open Air)	97	110
14	PCE Bay #5 internal (Open Air)	91	91
15	PCE Bay #7 internal (Open Air)	98	109
16	Battery box internal (Open Air)	86	95
17	Brake resistor grid fwd. end fwd. unit (Open Air)	180	363
18	Brake resistor grid rear end fwd. unit (Open Air)	245	459
19	Brake resistor grid middle rear unit (Open Air)	363	528
20	Undercar midway ASPE Bay #5 & resistor grid (Open Air)	104	200
21	Undercar midway PCE Bay #5 & reservoir (Open Air)	94	89
22	Undercar midway APSE Bay #2 & battery box (Open Air)	95	115
23	Undercar midway APSE and A/C unit (Open Air)	101	118
24	Undercar floor contact above brake resistor bank	95	130
25	Undercar floor contact above #3 traction motor	95	104
26	Undercar traction motor #2 positive armature lead (Contact)	106	127
27	PCE cooling duct intake (approximately 3 inches in)	81	80
28	L1 brake shoe stationary (Note 1)	188	142
29	L1 brake shoe rotational (Note 2)	223	154

- NOTES:
- 1) Bonded to the side of the brake shoe.
 - 2) Mounted in a hole drilled in the brake shoe, 1/8" from the wheel/shoe friction face.

Brake shoe temperatures, initially in the 190° to 220°F range, fell to 140° to 150°F at the conclusion of the blended braking test; the data for the initial temperatures may have been influenced by earlier friction braking stops. This compares to equilibrium temperatures of 200° to 260°F at the conclusion of the friction-only braking profiles. Temperatures in the APSE bays increased from approximately 100° to 110°-130°F, throughout the blended braking profile, with the #1 bay location showing the highest equilibrium temperature.

The duty cycle testing shows that resistive braking, with all of the dynamic braking energy being dissipated in the form of heat by the onboard resistor grids, subjects the undercar equipment to the most extreme thermal duty cycle. Other modes of braking, whether friction-only or dynamic/regenerative, require less energy to be dissipated by the resistor grids with consequently lower undercar temperatures. The tests, though relatively limited in scope, suggest that temperatures in excess of 600°F can be expected as the norm at the resistor grids, during operation of the vehicles with ambient temperatures of 80° to 90°F. Radiant heat from the resistor grids may influence the temperatures of surrounding equipment; for example, the equilibrium temperatures at the locations of thermocouples 20 and 24, midway between APSE bay #5 and the resistor grid and on the floor above the resistor bank were 200° and 130°F, respectively, at the conclusion of the blended braking profile.

All of the undercar locations that were instrumented, with the exceptions of areas in the immediate vicinity of the brake resistor grids, stabilized at temperatures below 130°F during the revenue service simulations. The undercar thermal environment appears to be well within the temperature limitations for the types of electrical cable insulation used; these are Fluorinated Ethylene Propylene and Ethylene Tetra Fluorethylene, with maximum allowable temperatures of 392°F and 302°F, respectively.

The stabilized brake shoe temperatures of 200° to 270°F were thought to be typical of friction-only brake shoe temperatures over the simulated revenue profiles tested. Similar tests carried out on the Massachusetts Bay Transportation Authority Blue Line cars gave brake shoe temperatures at the second axle of the lead truck of 190° to 212°F for the NYCTA and CTS simulated profiles, respectively. The temperatures were recorded with an embedded thermocouple mounted in a manner similar to that of channel 29 of the MARTA test program.

6.4 SPIN/SLIDE TESTS

6.4.1 Test Objective

The objectives of the spin/slide test program were:

- To determine the acceleration characteristics of the vehicles under poor wheel/rail adhesion conditions; and to derive the efficiency of the spin/slide protection system for full service blended, friction-only brake applications, and full-power accelerations.

- To compare the spin/slide performance efficiencies determined from the test data with the vehicle specification criteria. Specification spin/slide requirements are summarized as follows:
 - The wheel spin/slide protection system shall detect slips whether they are random or synchronous.
 - The system shall not allow braking to be removed for more than three seconds. If this limit is exceeded, the system shall be bypassed and full braking effort restored.
 - At coefficients of adhesion of 0.06 or greater at the wheel/rail interface, the efficiency of the system shall be at least 75% during acceleration or blended braking over the speed range of 3 to 70 mi/h. The friction brakes alone shall achieve an efficiency of at least 75% with a coefficient of 0.1. The efficiency shall be calculated as indicated in figure 6-43.
 - Spin/slide protection shall be active for all modes of braking, including emergency brake applications.

6.4.2 Test Method

Both cars were equipped with spray nozzles, arranged to spray a mixture of water and soap solution directly into each wheel/rail interface, for every wheelset. The soap solution reduced the adhesion to the point where spins and slides could be sustained; the solution was made by adding approximately 16 fluid ounces of liquid soap and eight ounces of mineral oil to 40 gallons of water. The spray nozzles were fabricated by drilling a standard pipe union blank with a number 60 drill (0.040" diameter); the resulting flow rate when spraying was approximately 1 gallon/minute per car. The nozzles were connected by means of ½" I.D. flexible plastic tubing to a 40-gallon tank containing the soap solution; the tank was pressurized to approximately 80 psig by a small portable air compressor.

Prior to the test runs, a series of slow passes were made through the test section, spraying soap solution on the rail head to precondition the track. Test runs were then conducted on the preconditioned rail. Full power acceleration runs were made from a standing start, with data collection being terminated when wheel spin activity ceased; braking runs with both blended and friction-only modes of operation from initial speeds of 15, 35, 55, and 70 mi/h were terminated at the end of the preconditioned track. Spin/slide protection was not examined for the emergency braking case.

6.4.3 Test Results

In order to provide the reader with an understanding of the data analysis rationale for evaluation of the spin/slide protection system, the test results discussion has been divided into three sections describing the operation of the system, the data analysis methods, and a presentation of the test data.

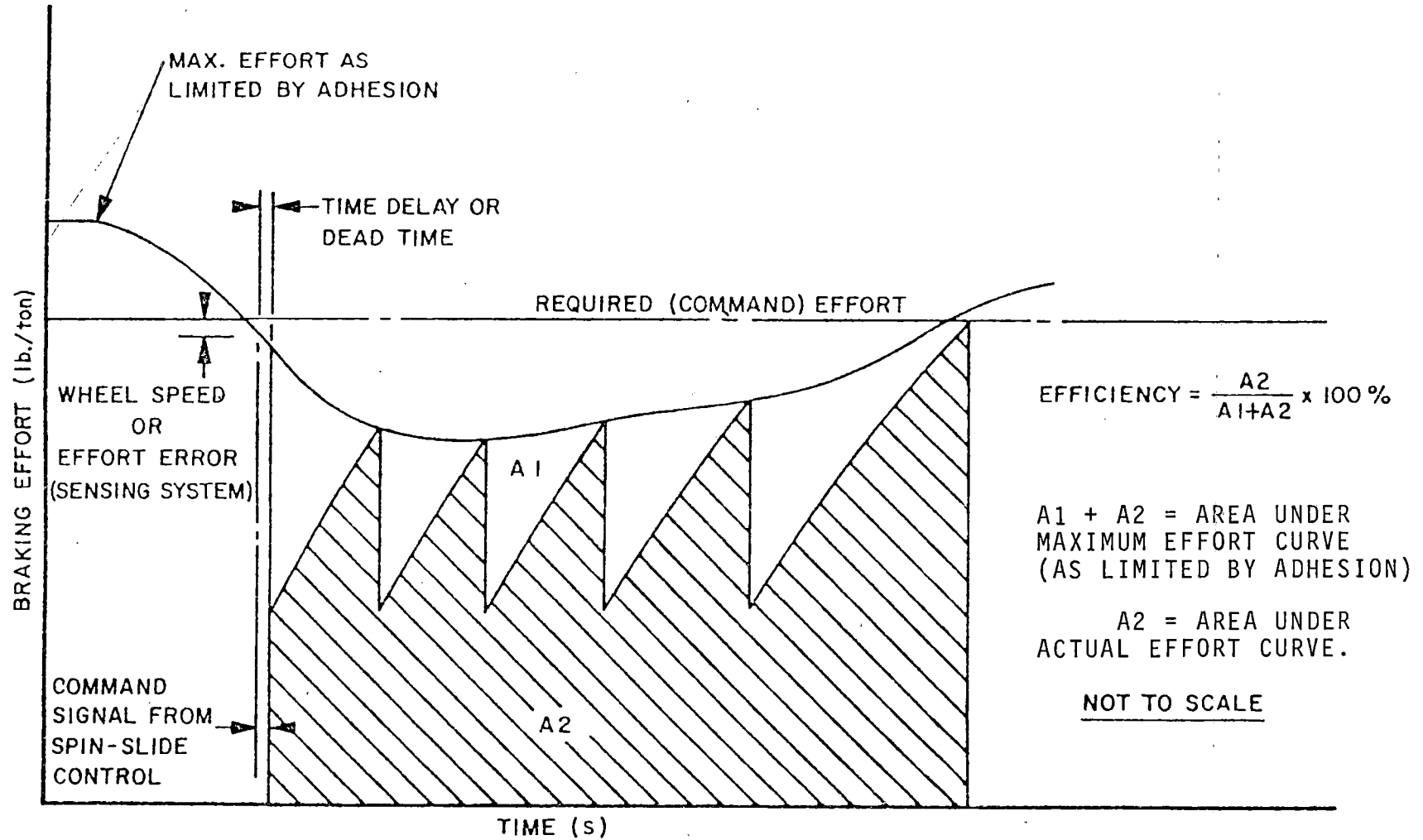


FIGURE 6-43. DEFINITION OF SPIN/SLIDE EFFICIENCY FROM VEHICLE SPECIFICATION.

6.4.3.1 The Spin/Slide Protection System. The car control system includes speed and slip detection circuitry which monitors motor speed sensor outputs from the four traction motors. Detection of a wheel slip is accomplished by comparing each wheel acceleration derived from these sensors (i.e., rate of change of rpm) with a maximum predetermined rate.

A slip occurs, by definition, whenever the tangential speed of the wheel differs from the linear speed of the vehicle; the slip is defined as a spin whenever the tangential speed of the wheel exceeds the speed of the vehicle, and as a slide whenever it is less than the speed of the vehicle. A slip is detected by the system when the wheel tangential acceleration (or deceleration) exceeds the predetermined limit of 8 mi/h/s or when a speed differential in excess of 5 mi/h exists between any axles. Detection of a wheel slip is determined on a per axle basis.

In the drive mode, if a spin is detected on any one of the four axles, tractive effort is reduced on all axles until the spin is corrected. When the slip detection circuits determine that the axle has regained synchronism with the linear speed of the vehicle, tractive effort is reapplied on a jerk-limited basis to the commanded value.

In the brake mode, detection of a slide on any axle causes the electrical dynamic braking effort to be reduced to zero on all axles. Simultaneously, the dump valve is energized on the truck where the wheels are sliding, reducing the friction braking effort on this truck to zero, and friction braking effort is applied (or increased) on the other truck. Upon correction of the slide, dynamic braking is reinstated on a jerk-limited basis to the commanded value.

6.4.3.2 Data Analysis Methods. The test runs were examined for wheel slips by reviewing the chart records of individual wheel speeds. Runs most suitable for analysis were selected on the basis of exhibiting the highest number of simultaneous wheel slips throughout the train during the test period. The data were analyzed using the definition of spin/ slide efficiency contained in the vehicle design specification document (figure 6-43). Spin/slide system efficiency is defined as the area (A2) under the tractive effort time history curve during a period of wheel slips, divided by the area under a line faired through points of peak tractive effort, (A1 + A2). This line represents the maximum available tractive effort as limited by wheel/rail adhesion. If the propulsion system was able to detect incipient slides and modulate tractive effort to follow this line, then a spin/slide efficiency of 100% would result.

The spin/slide efficiencies were calculated on a 'per-train' basis, using the longitudinal acceleration as an indicator of achieved tractive effort, since acceleration is proportional to tractive effort from the simple 'Force equals Mass times Acceleration' relationship. Areas A2 and (A1 + A2) were calculated by numerical integration of the longitudinal acceleration trace, using 1-s time elements from the first detected slip to the resumption of full traction; the reduction in tractive effort command signal was used as an indicator of system slip detection. An example of the time history traces for a typical brake application with wheel slides occurring is illustrated in figure 6-44.

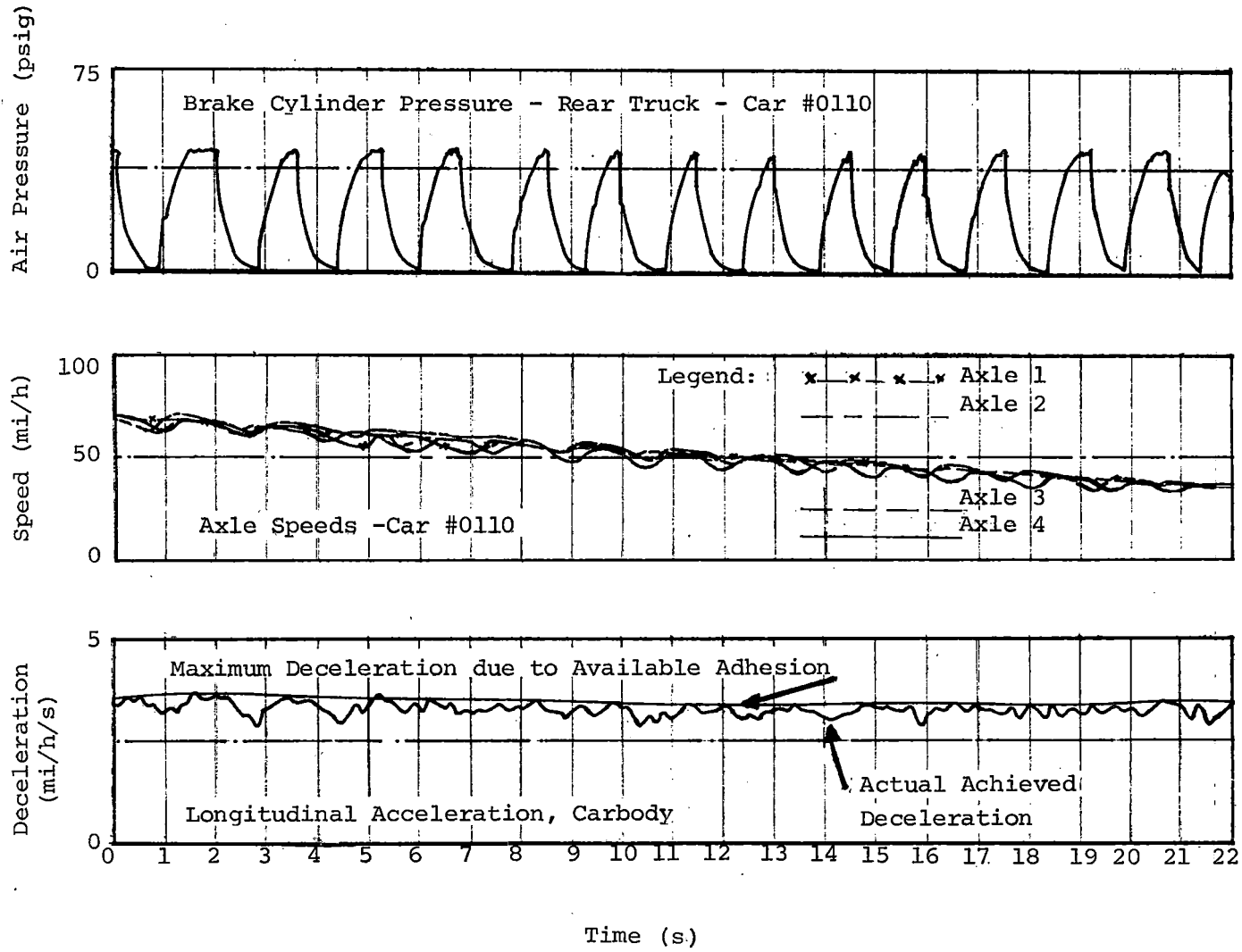


FIGURE 6-44. DECELERATION WITH SPIN/SLIDE PROTECTION, TIME HISTORY.

Table 6-7 is a summary of the data obtained from the analyzed runs. The initial and final velocities were taken from the analog output of ninth-wheel speed and are not influenced by wheel slips; the ninth wheel is a spring loaded, damped wheel which rides on the rail head and provides a pulsed rpm input to the data acquisition system, where it is conditioned as speed and integrated with time as a distance output. The distance traveled during the spin/slide period was obtained from the distance trace where it is displayed as a step function with a resolution of 10 ft/step. The spin/slide efficiency values presented in the table were computed using the previously described numerical integration of the acceleration/deceleration trace. The efficiency values were then calculated from the area under the actual acceleration curve and divided by the area under the maximum available acceleration curve, which was described by a line drawn through the acceleration peaks. The efficiency values are expressed as a percentage: $100 [A2/(A1 + A2)]$.

The coefficients of adhesion (table 6-7) are average values for the period of wheel spin/slide computed from the maximum available acceleration curve. An average maximum acceleration for the period of wheel slip was computed from the area under the maximum available acceleration curve divided by the elapsed time for the period. An average coefficient of available adhesion for the period of the slip was then computed by dividing this value by g , the acceleration due to gravity.

The effects of train resistance on the calculation of spin/slide efficiency and average available adhesion levels were considered and discarded as insignificant. Train resistance effects emanating through the rail, such as journal bearing friction and motor windage, are overcome by the vehicle tractive effort and do not influence the calculation of spin/slide efficiency or coefficient of adhesion. Aerodynamic train resistance effects provide an incremental retarding force to the vehicle as a function of velocity squared, which is not applied through the wheel/rail interface. This affects the accuracy of the calculation of the coefficient of adhesion from average maximum acceleration, since an incremental force affecting that acceleration is derived from a source other than the available adhesion. The aerodynamic contribution to train resistance was therefore estimated for the vehicles over the speed range 0 to 70 mi/h in order to assess its influence on the adhesion calculation. This was accomplished using the aerodynamic drag portion of the Davis formula specified in the vehicle specification document. The aerodynamic train resistance, at 40 mi/h, was calculated to be approximately 1% of the tractive effort values obtained during the spin/slide tests. Since the aerodynamic effects are proportional to velocity squared, the influence on calculated values of average available adhesion will be 1% or less and can be ignored.

6.4.3.3 Test Data. The data presented in table 6-7 show that the spin/slide protection system met the specification criteria to achieve an efficiency of 75% during acceleration, blended or friction-only braking, with the exception of one acceleration run which achieved a value of 73%. Average available adhesion values varied from 0.07 to 0.09. No instances were observed in which the braking effort was removed for three seconds or more, and so the requirement for the spin/slide system to be bypassed and full braking applied in this event was not evaluated. Operation of the spin/slide protection system during emergency braking was not evaluated by these tests,

TABLE 6-7. SPIN/SLIDE TEST DATA.

Mode of Operation	Initial Velocity (mi/h)	Final Velocity (mi/h)	Distance Traveled (ft)	System Efficiency (%)	Average Maximum Acceleration (mi/h/s)	Average Available Adhesion
Maximum Acceleration	4	38	1130	79	1.90	0.09
Maximum Acceleration	10	42	1635	73	1.64	0.07
Full Service Blended Brake	35	3	1260	83	1.60	0.07
Full Service Blended Brake	55	26	2730	77	1.63	0.07
Full Service Blended Brake	68	39	4110	80	1.49	0.07
Full Service Friction Brake	32	10	700	88	1.85	0.08
Full Service Friction Brake	50	12	1970	79	1.98	0.09
Full Service Friction Brake	64	34	3020	78	1.92	0.09

although operation of the system has been observed during emergency braking performance tests; the data are not suitable for spin/slide efficiency calculations due to the lack of simultaneous wheel slides on all trucks.

6.5 ENERGY CONSUMPTION

6.5.1 Test Objectives

The objectives of the energy consumption tests were to determine the electrical demands placed upon the third rail for various operating conditions.

Specific objectives of the tests were:

- To determine the energy consumption of the auxiliary power systems under steady state conditions.
- To measure the maximum power demand of the vehicle.
- To measure the energy requirements, per car mile, of the vehicle at constant speed.
- To measure the energy required to accelerate the vehicle to various speeds from a standstill.
- To determine the energy regenerated by the dynamic braking system, that could be returned to the third rail.
- To measure the energy requirements for propulsion and other onboard systems during round-trip simulated profile runs.

6.5.2 Test Method

The tests were run in two phases, between which there was a change in car wheel diameter and a change in substation type. During phase one, the cars were equipped with 32½" diameter 'half-worn' wheels. For phase two, the cars were refitted with 34" 'new' wheels. In addition, for phase two, a new substation was brought on line, which did not let the voltage drop as much under heavy load as did the first substation. The maximum power demand tests were run during phase two. All others were carried out during phase one.

Total consumption was measured by means of watt-hour meters on the input to each car. In addition the following information was recorded on strip chart:

- Input line voltage.
- Input line current to each car.

- Voltage and current across the motor armatures of each truck in both cars (the motors in each truck are wired in series).
- Elapsed time.
- Train speed.
- Distance traveled.

All clockwise test runs were with car 0110 leading, starting at station 30. All counterclockwise runs were with car 0109 leading, starting at station 34.

Steady state energy consumption of the auxiliary onboard power systems was determined by measuring the total energy consumption of each car over a finite time period whenever the train was at a standstill. This consumption was assumed to be constant with time whether or not the train was moving.

The maximum power demand for car 0110 was determined by accelerating the cars from 0 to 70 mi/h on level tangent track at a maximum acceleration rate for the following conditions:

- 550, 750, 825 V d.c. at AW2 weight, clockwise direction.
- AW0 and AW2 weight at 750 V d.c., clockwise direction.
- AW2 weight at 750 V d.c., counterclockwise direction.

The power requirements at constant speeds were determined by operating the cars at AW2 weight, 750 V d.c. nominal line voltage at constant speeds of 25, 37, 50, 60, and 70 mi/h on level tangent track. Three runs in each direction were made for each speed except 70 mi/h, for which only 2 runs in each direction were made.

The power required to accelerate the cars from standstill to speed was determined by accelerating AW2 weight cars at full service acceleration through tangent level track to speeds of 30, 40, 50, 60, and 70 mi/h at 750 V d.c. Three acceleration runs were made to each speed in each direction.

Brake energy regeneration tests were conducted by operating the cars through level tangent track at AW2 weight and 750 V d.c. nominal line voltage at entry speeds of 70, 60, 50, and 37 mi/h. When the cars entered the test section full service blended braking was initiated and the cars were braked to a standstill. Two braking runs for each entry speed were made in each direction.

Energy consumption requirements were determined for the MARTA East-West line simulated profile from Avondale to Hightower (table 6-2) and the ACT-1 profile (table 6-8). The cars were operated clockwise around the TTT following the maximum speeds and distances between stations and station stop times prescribed. A stop of one minute was made at the end of the line and the train was then run counterclockwise back to the beginning following the reverse profile, completing one round trip.

TABLE 6-8. ACT-1 SIMULATED LINE PROFILE.

Start Station	Station Marker	Maximum Speed(mi/h)	Stop Station	Station Marker
A	52.170	60	B	7.960
B	7.960	65	C	13.250
C	13.250	50	D	15.800
D	15.800	60	E	19.840
E	19.840	50	F	22.450
F	22.450	40	G	23.860
G	23.860	40	H	25.120
H	25.120	50	I	27.760
I	27.760	65	J	35.680
J	35.680	65	K	42.280
K	42.280	40	L	43.600
L	43.600	50	M	46.240
M	46.240	40	N	47.560
N	47.560	65	O	52.840
O	52.840	65	N	47.560
N	47.560	40	M	46.240
M	46.240	50	L	43.600
L	43.600	40	K	42.280
K	42.280	65	J	35.680
J	35.680	65	I	27.760
I	27.760	50	H	25.120
H	25.120	40	G	23.860
G	23.860	40	F	22.450
F	22.450	50	E	19.840
E	19.840	60	D	15.800
D	15.800	50	C	13.250
C	13.250	65	B	7.960
B	7.960	60	A	52.170

Two MARTA round-trip profiles and one ACT-1 round-trip profile were run. All profiles were run at AW2 weight with 750 V d.c. nominal line voltage.

6.5.3 Test Results

Results, unless stated otherwise, are per car.

6.5.3.1 Steady State Energy Consumption. The steady state energy consumption rate of the auxiliary power systems was found to be 0.0125 kWhr/s (a constant draw of 45 kW) while standing still, accelerating, braking or operating at constant speed. Therefore, the energy consumed per mile by these auxiliary systems is a function of car speed as shown in figure 6-45.

Because of the air brake compressor onboard, the B car was expected to consume slightly more energy than the A car; however, no difference was discernable.

6.5.3.2 Maximum Power Demand. Figures 6-46 and 6-47 show the power demand for the 'B' car under full acceleration to 70 mi/h from standstill. These plots show that the maximum power demand under full acceleration occurs between 23 and 25 mi/h for all the tested configurations of different weights, line voltages, and directions. The data were obtained by multiplying together the instantaneous line voltage and current that were recorded on strip charts for car 0110 to give the kW power values shown.

The results in figure 6-47 follow predictable trends. Heavier cars demanded more power to maintain a given level of acceleration, and direction of travel had no significant effect.

In figure 6-46, car 0110 can be seen to demand the same power at 825 V d.c. as at 750 V d.c., while maintaining full service acceleration. At 550 V d.c., power demand is limited by the lower line voltage and the train is unable to maintain full service acceleration.

6.5.3.3 Energy Requirements at Constant Speed. Figures 6-48 and 6-49 show the total energy consumed per car-mile for traveling at constant speeds of 25, 37, 50, 60, and 70 mi/h. Figure 6-48 shows the effect on car 0110 of traveling in different directions, while figure 6-49 compares the two cars with each other. The energy consumed was determined from analog strip chart data by performing a numerical integration of the line voltage and line current input value for each car.

Choice of voltage and current data for the calculated values was made by finding the average of the 'measured' power demand values for each car for the three runs in each direction. That run which came closest to the averages for both cars was chosen as being representative for that speed in that direction. Current and voltage data for that run were used in the numerical integration. The data were taken over a 4,000' test section and have been scaled to represent kWhr per car mile.

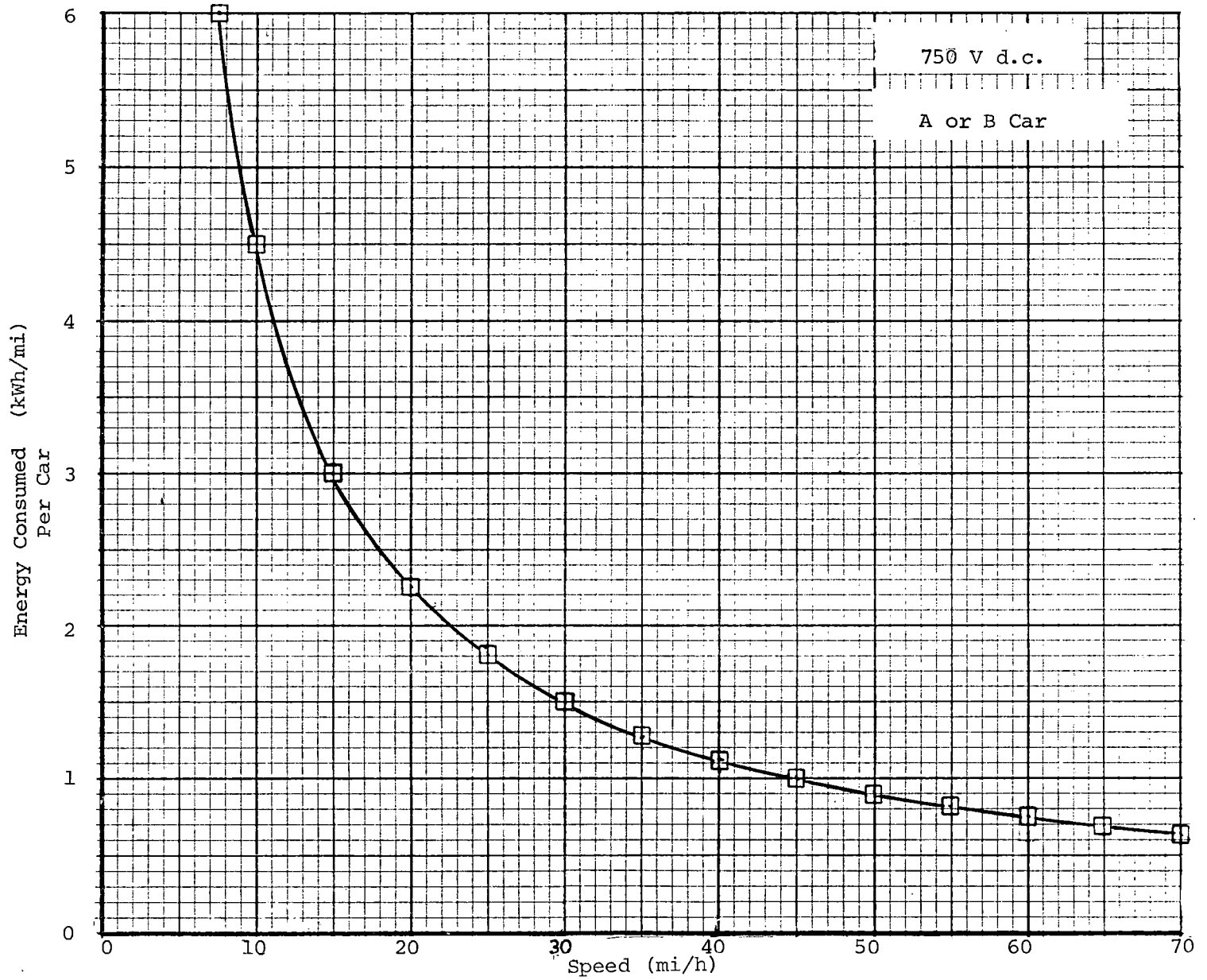


FIGURE 6-45. EFFECT OF SPEED ON ENERGY CONSUMED BY AUXILIARY SYSTEMS.

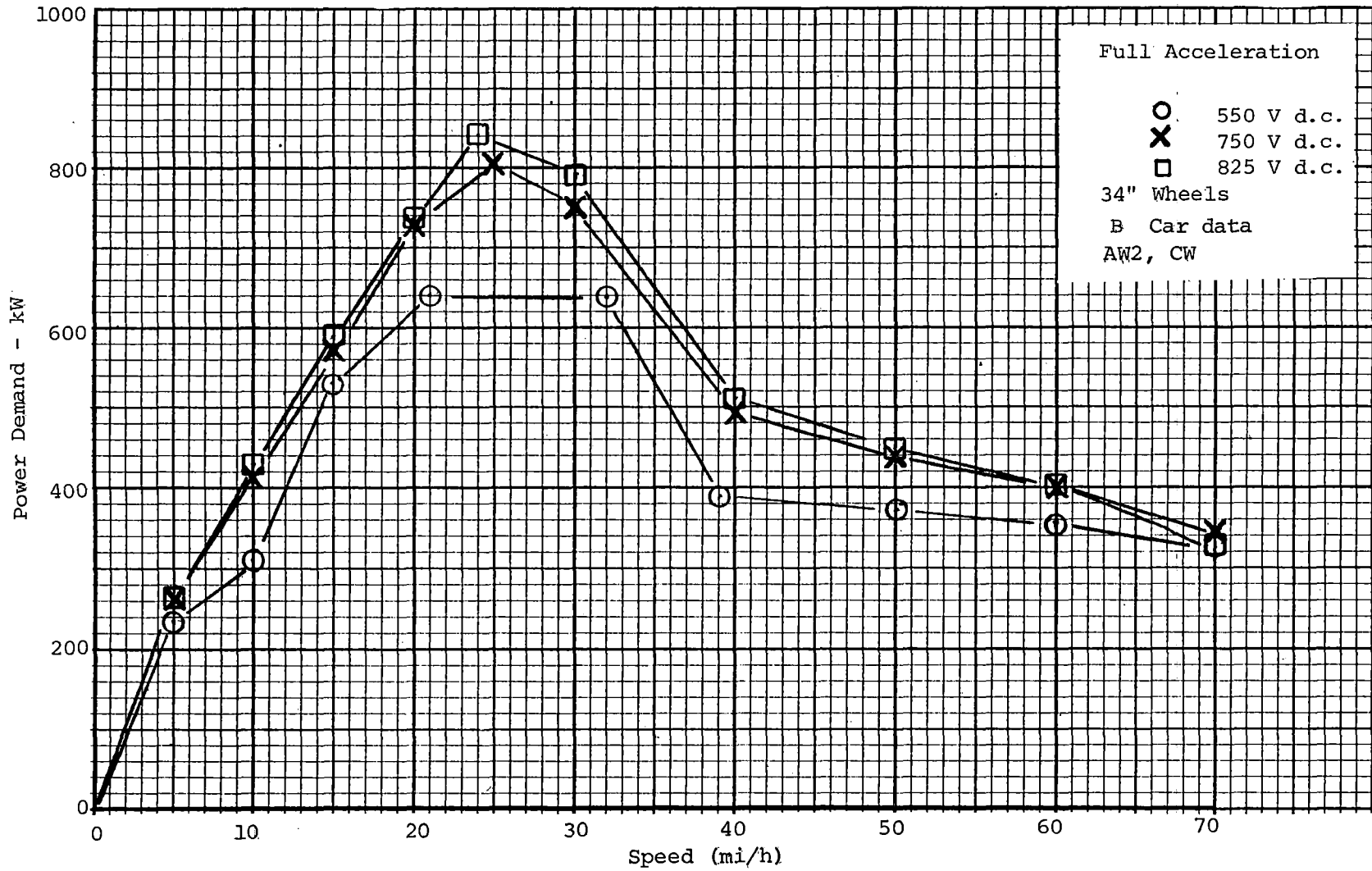


FIGURE 6-46. EFFECT OF LINE VOLTAGE ON POWER DEMAND DURING FULL SERVICE ACCELERATION.

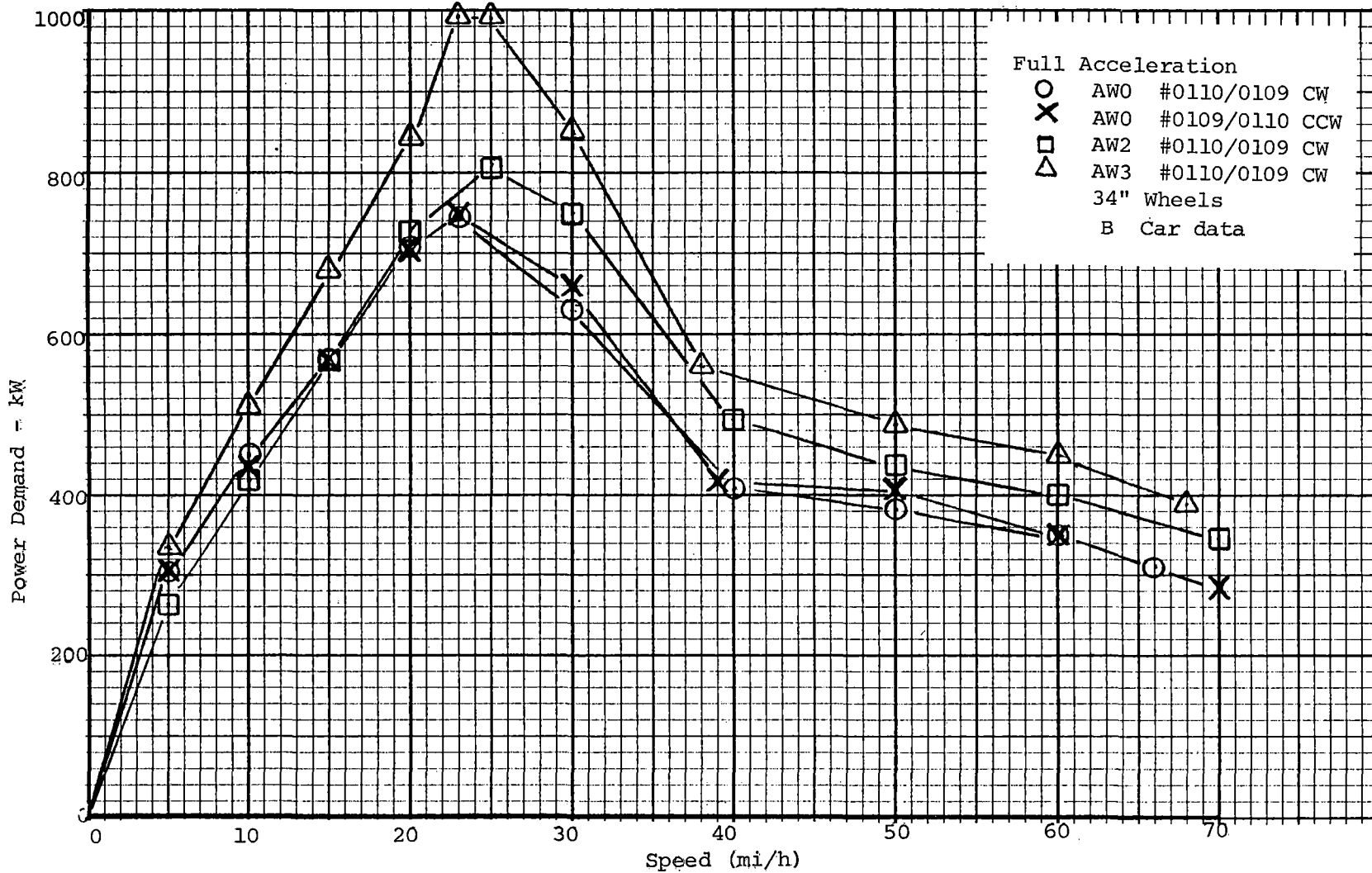


FIGURE 6-47. EFFECT OF VEHICLE WEIGHT AND DIRECTION ON POWER DEMAND DURING FULL SERVICE ACCELERATION.

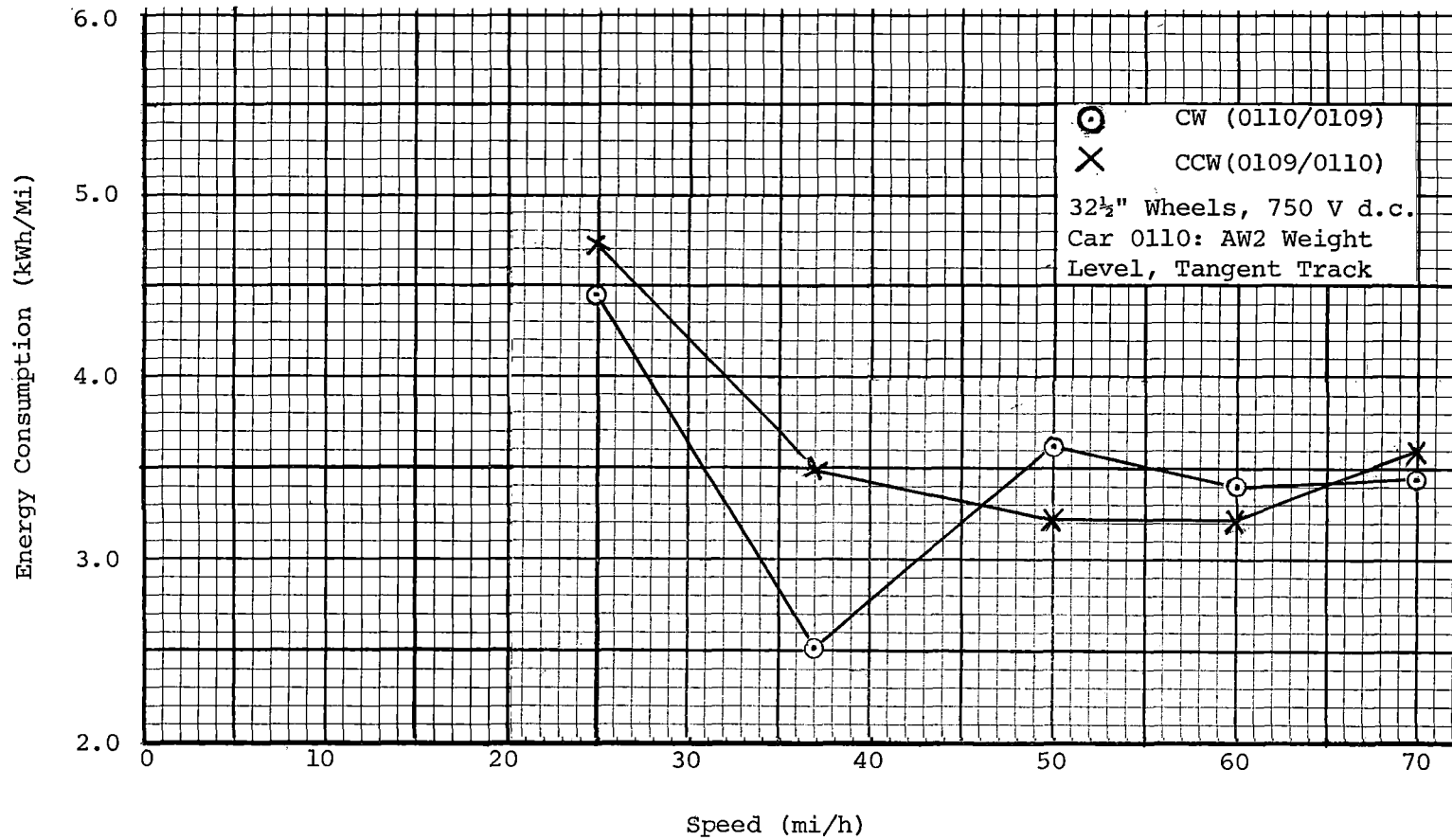


FIGURE 6-48. ENERGY CONSUMPTION, CONSTANT SPEEDS - EFFECT OF VEHICLE DIRECTION.

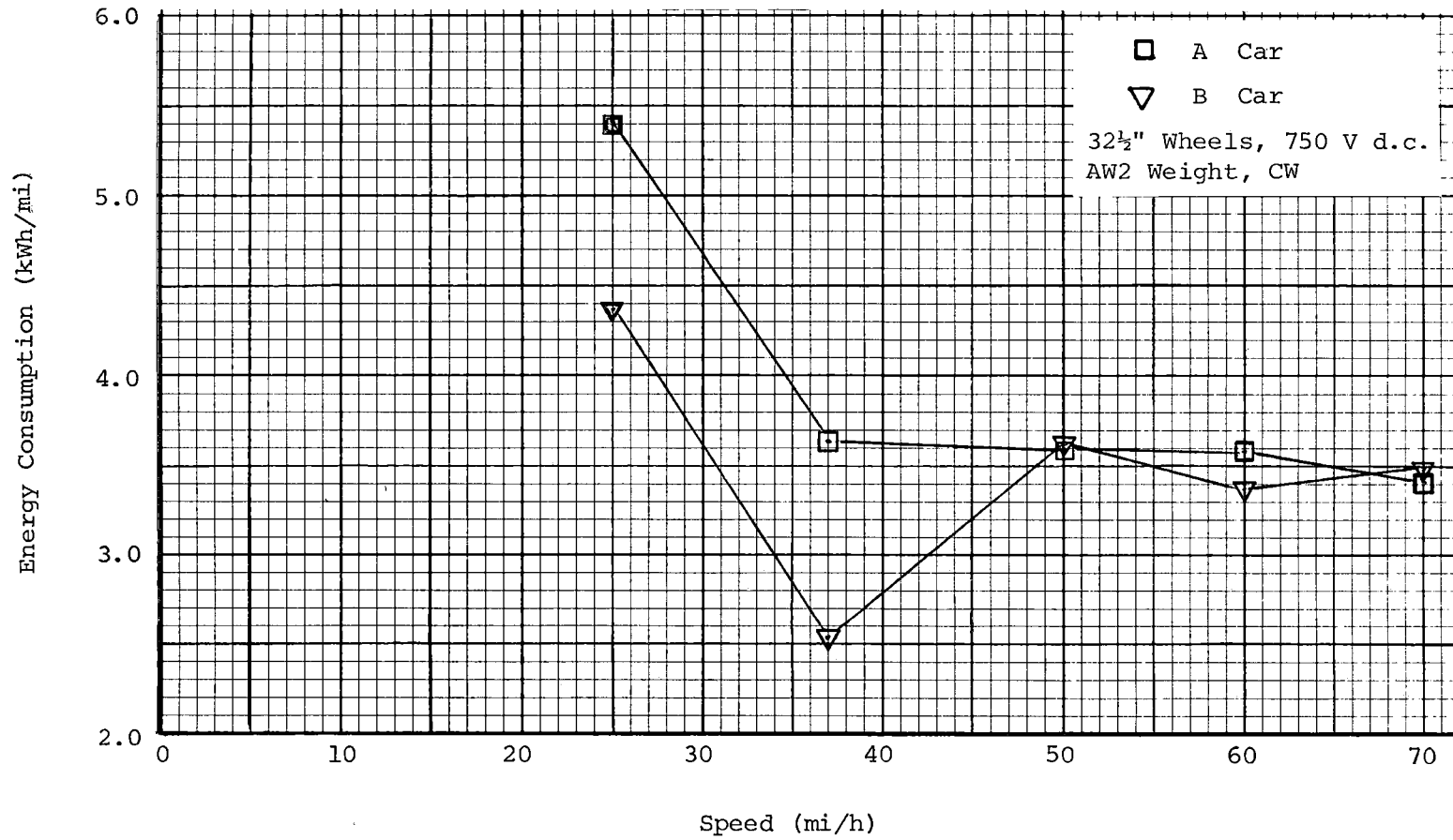


FIGURE 6-49. ENERGY CONSUMPTION , CONSTANT SPEEDS - COMPARISON OF CAR A AND CAR B.

As can be seen in both figures, both cars consume more power per mile below 35 mi/h than at the higher speeds. This is mostly attributable to the fact that at low speeds the auxiliary systems are consuming more energy per mile than at higher speeds, due to the longer time required to cover any given distance (see figure 6-45).

Considerable scatter can be observed in both figures 6-48 and 6-49, which tends to mask trends in the data. This scatter is due to the difficulty in maintaining constant speed, since the speed was controlled manually by the motorman who had to continually move the controller from acceleration to coast. The position of the controller at the moment of entering the test section would also have a big effect, especially at the higher speeds. Thus, if the cars were entering just after changing to a coast mode, less energy would probably be consumed than if they entered just after changing to the acceleration mode.

The expected trends in both figures 6-48 and 6-49 would have the highest energy consumption per car mile at very low speed, with the lowest consumption between 37 to 50 mi/h, rising again at 70 mi/h. This is reasonably duplicated by the counterclockwise data for the B car. This expected trend was obtained by using the Davis formula to estimate the drag of the vehicles (outlined in section 6.6.3.5) and adding the energy consumption of the auxiliary systems.

6.5.3.4 Energy Consumed Under Maximum Acceleration. Figures 6-50 and 6-51 show the energy consumed under full acceleration to various speeds, comparing cars A and B, and the effects of direction of travel. The data are from a numerical integration of line voltage and current recorded on strip charts for each car.

The particular data shown were chosen as 'average' by taking the average value recorded by the watt meters for each car for three runs in each direction. That run which came closest for both cars to the average was chosen as representative for that direction and maximum speed. In the case of the 30 mi/h data, since no watt-meter data were available, the first run in each direction was chosen.

In figure 6-50 it can be seen that travel in the clockwise direction increased the energy consumption of car 0110 up to 14% over counterclockwise travel, with the apparent increase being greatest at highest speed.

6.5.3.5 Regenerated Energy Available During Braking. Tests were conducted to determine the capability of the cars to regenerate energy back to a receptive line. The term receptive line means that on a 750 V (nominal voltage) system, the line voltage must be between 650 and 850 V before all of the braking energy can be returned to the rail. Between 850 and 900 V, the conditions are classified as 'partially receptive'; i.e., some energy may be returned to the line. Above 900 V, the system is nonreceptive. Since the TTT is not a receptive line, in that it has no means for absorbing electrical energy and holding the line voltage below 900 V, the energy dissipated by the brake resistors was calculated as a measure of the available regenerative energy.

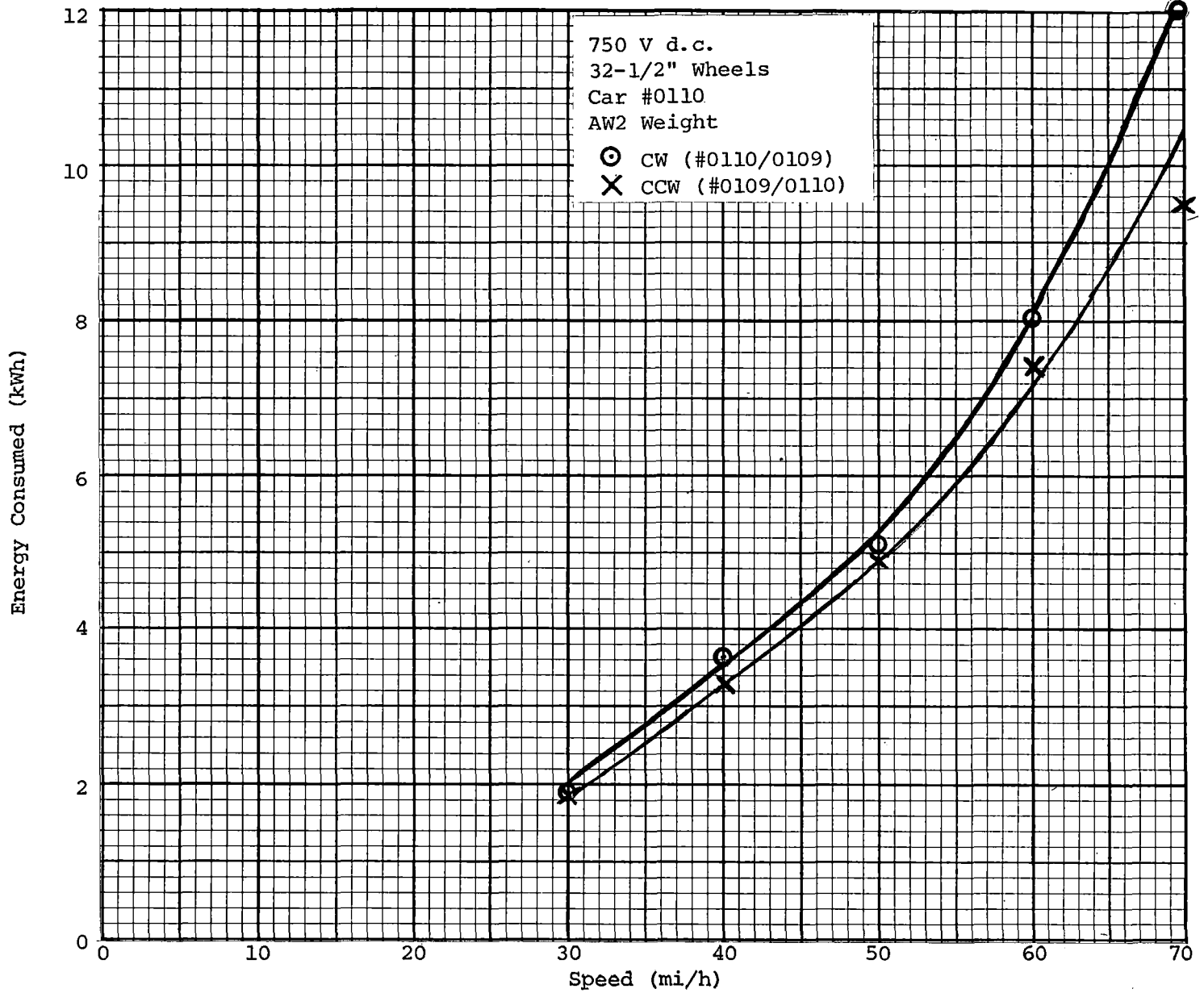


FIGURE 6-50. INPUT ENERGY CONSUMPTION UNDER FULL SERVICE ACCELERATION TO SPEED - EFFECT OF DIRECTION OF TRAVEL.

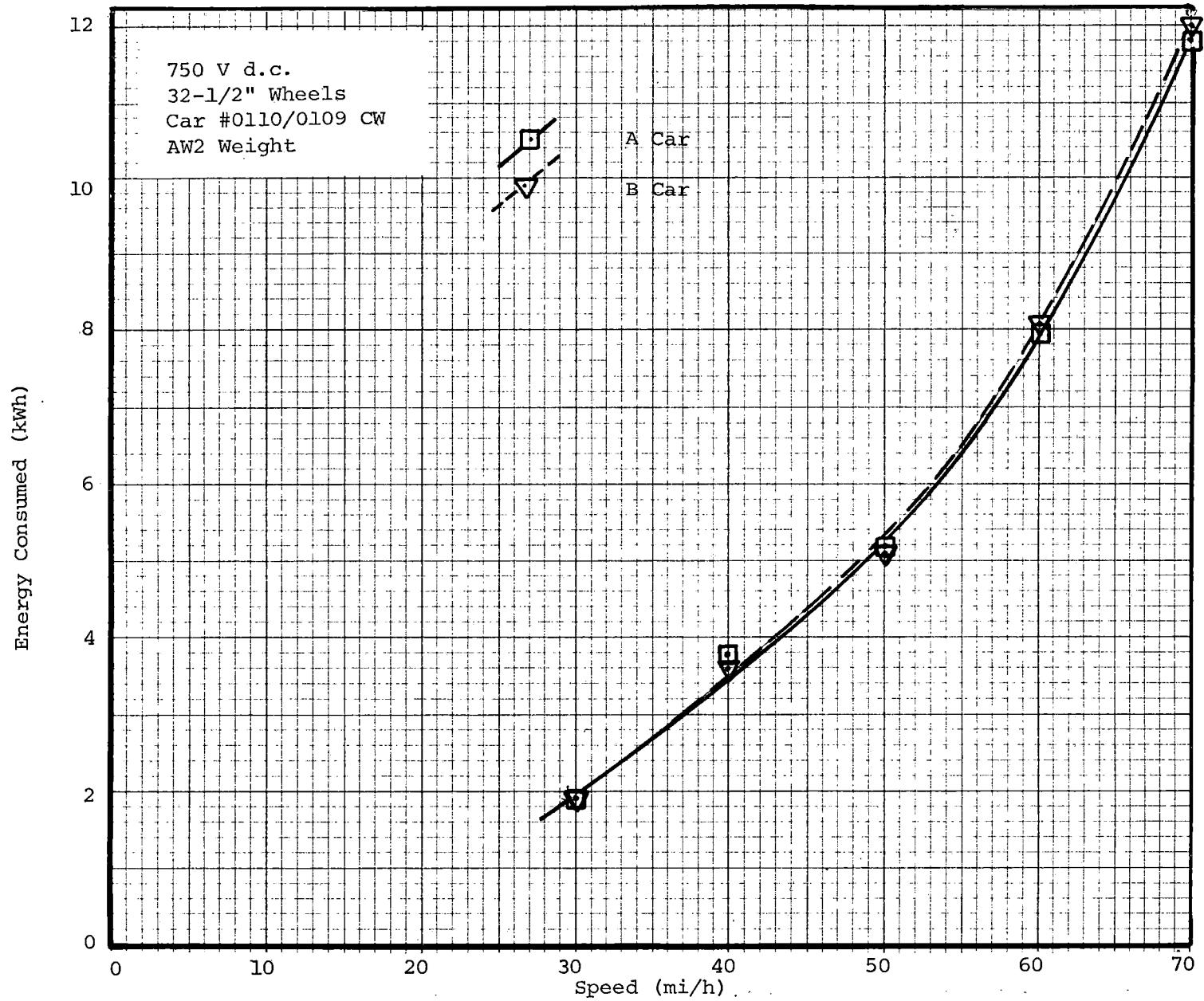


FIGURE 6-51. INPUT ENERGY CONSUMPTION UNDER FULL SERVICE ACCELERATION TO SPEED - COMPARISON OF CARS A AND B.

The reader should note that the term 'available regenerative energy' refers to the energy generated at the car during dynamic braking and available to power other vehicles. In order for energy savings to be realized in practice, other vehicles must be operating on the system at the same time as the vehicle is braking, and demanding sufficient energy to maintain a receptive line. In this situation, line losses are experienced between the vehicle regenerating the energy and those absorbing it so that, even under ideal conditions, all of the available energy is not regained.

Figure 6-52 shows the calculated regenerative energy available. The data were reduced by numerical integration of the traction motor armature voltage and current when operating in a full service blended braking mode. The energy required to operate the auxiliary systems (which is provided by the traction motors in blended braking) was subtracted (0.0125 kWhr/s/car) to yield the available regenerative energy.

As can be seen in figure 6-52, the regenerative energy data were very consistent with no significant difference being apparent between cars or direction of travel. This consistency could be noted over many successive runs, with full service braking from a given speed to a stop producing very similar results.

6.5.3.6 Energy Consumed for a Typical Round Trip Transit Profile. Table 6-9 shows the results of the MARTA and ACT-1 round-trip profile runs. Data for each of the parameters were measured or calculated as follows:

- Total Energy Consumed (A) was measured by means of watt-hour meters on the input lines to both cars.
- Energy Used for Propulsion (B) was calculated by subtracting the Energy Supplied by 3rd Rail for Auxiliary Systems (D) from the Total Energy Consumed (A), or:

$$(B = A - D)$$

- Total Energy Used by Auxiliary Systems (C) equals Energy Supplied by 3rd Rail for Auxiliary Systems (D) plus Energy Supplied by Traction Motors for Auxiliary Systems (E), or:

$$(C = D + E)$$

- Energy Supplied by 3rd Rail for Auxiliary Systems (D) equals 0.0125 kWhr/s times the time when NOT in braking mode.
- Energy Supplied by Traction Motors for Auxiliary Systems (E) equals 0.0125 kWhr/s times the time when IN braking mode.
- Total Energy Dissipated by Brake Resistors (F) is the result of a numerical integration of the Traction Motor Armature Voltage and Current minus (E); (F) is, therefore, a measure of the energy potentially available for return to the system in a regenerative braking mode.
- Distance Traveled (G), Time for Round-Trip (H), Time in Motion (I), and Time Stopped (J) are data from the strip charts.

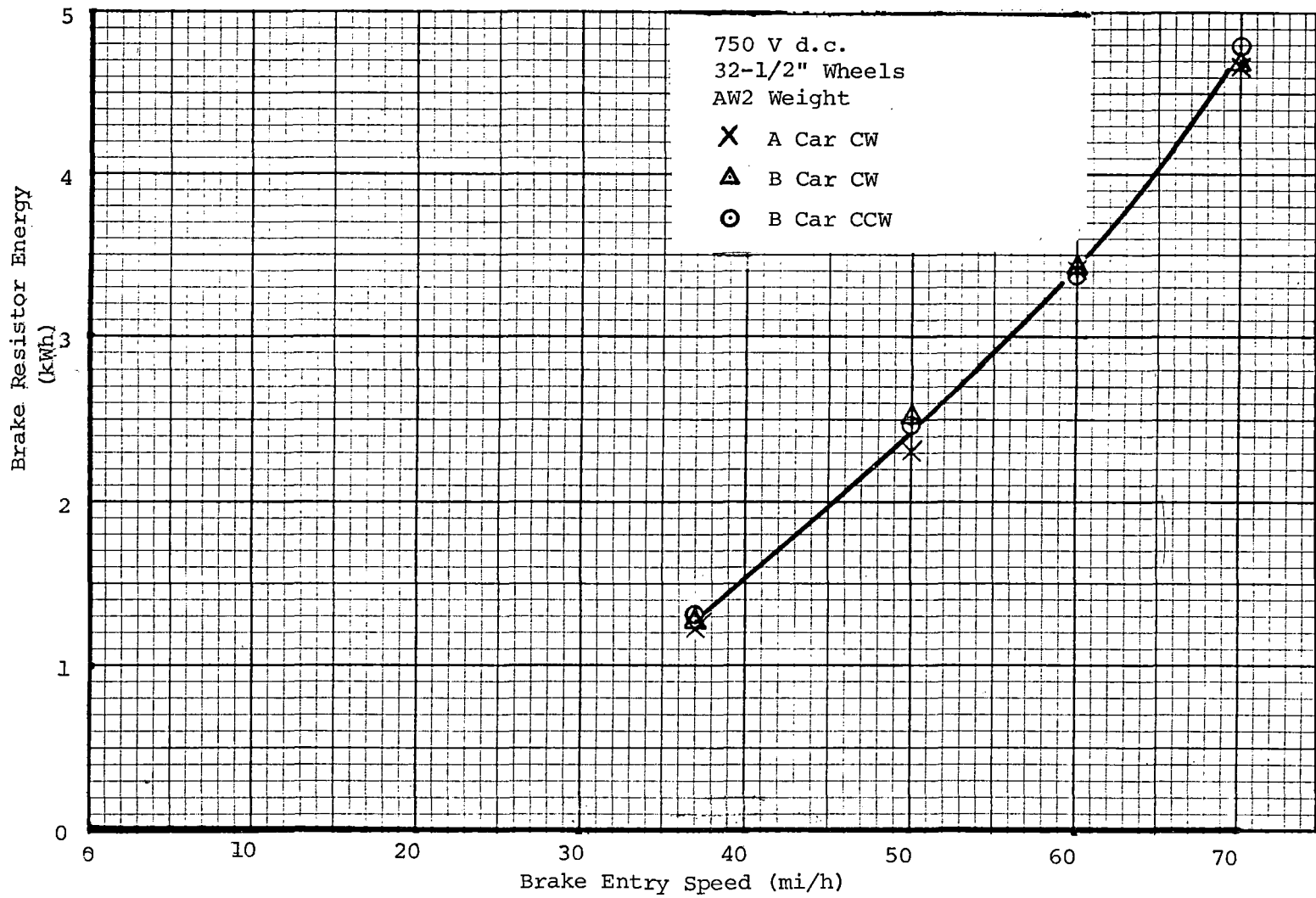


FIGURE 6-52. BRAKING RESISTOR ENERGY DURING FULL SERVICE BLENDED BRAKING STOPS.

TABLE 6-9. CONSUMED ENERGY COMPARISONS, CARS A AND B VS. MARTA/ACT-1 PROFILE RUNS.

Energy Consumption in Profile Runs		MARTA Profile		ACT-1 Profile	
		A Car	B Car	A Car	B Car
A	Total Energy Consumed (kWhr)	174.4	173.7	176.0	175.1
B	Energy Used for Propulsion (kWhr)	147.9	147.2	153.0	152.1
C	Total Energy Used by Auxiliary Systems (kWhr)	32.3	32.3	29.5	29.5
D	Energy Supplied by 3rd Rail for Auxiliary Systems (kWhr)	26.5	26.5	23.0	23.0
E	Energy Supplied by Traction Motors for Auxiliary Systems (kWhr)	5.8	5.8	6.5	6.5
F	Total Energy Dissipated by Brake Resistors	62.5	65.7	72.1	74.2
G	Distance Traveled (mi)	23.3		18.1	
H	Time for Round Trip (min:s)	43:02		39:19	
I	Time in Motion (min:s)	37:01		30:48	
J	Time Stopped (min:s)	6:01		8:31	
K	Average Speed in Motion (mi/h)	37.8		35.3	
L	Energy Consumed per Mile with No Regeneration (kWhr/mi)	7.49	7.45	9.72	9.67

AW2 weight
 750 V d.c.
 32½" wheels
 MARTA profile average of two runs

- Average Speed in Motion (K) equals Distance Traveled (G) divided by Time in Motion (I), or:

$$(K = G/I)$$

- Energy Consumed per Mile with NO Regeneration (L) equals Total Energy Consumed (A) divided by Distance Traveled (G), or:

$$(L = A/G)$$

In addition, as requested by MARTA engineers, the average motor current was determined for a typical motor on a MARTA profile. In choosing data, the motor pair which consistently drew the most current was evaluated. This was determined to be the pair for the rear truck of the B car. A numerical integration of the armature current record was performed, integrating from the start of the round trip to the finish, including stops. This result was then divided by the time required for that run. This yielded a 296.2 A average current, which is 80% of the maximum traction motor rating of 365 A continuous.

A considerable amount of the total energy consumed was found to be available as regenerated energy. For the MARTA profile, 36.8% of the total energy used is dissipated in the brake resistors, while on the ACT-1 profile, 41.7% of the energy is dissipated. Thus, a greater percentage of total energy consumed is available for regeneration on the ACT-1 profile. This is due to there being more stops and shorter distances between stops on the ACT-1 profile.

These same reasons also cause the ACT-1 profile to have a higher energy consumption per mile, since more periods of acceleration are required due to the increased numbers of stops.

Although a greater percentage of total energy was regenerated during the ACT-1 profile, given equally receptive third rails for both MARTA and ACT-1 profiles, the ACT-1 profile would still have a greater energy consumption per mile (after accounting for the regenerated energy). This is caused by the greater percentage of low speed running and acceleration required on the ACT-1 profile--at low speeds the propulsion system is less efficient due to operation of the armature current chopper.

For both round-trip profiles the B car consumed less energy than the A car, the difference being approximately 0.5% in both cases. This tends to show that any significant differences shown between the cars in the previous sections get 'smoothed' out over the long run.

6.6 DRIFT TEST

6.6.1 Test Objective

The test objective was to evaluate the MARTA car open air train resistance characteristics. The tests were conducted at an AW2 vehicle weight,

but were expanded to include two vehicle configurations, the normal mode of operation with the brake shoes held against the wheel treads by the springs inside the brake actuators, and in a modified mode of operation, with the brake shoes held clear of the wheels. It was intended that these two configurations would enable the drag penalty of the constant contact brake shoes to be evaluated. A further objective was to compare the drift characteristics obtained experimentally with those predicted by the empirical modified Davis formula.

6.6.2 Test Method

The tests were carried out by allowing the cars to coast through the 4,000' level tangent track section, during which time the vehicles lost approximately 8 mi/h from the initial entry speed. Entry speeds to the tangent section were set at 5 mi/h decrements from the initial 70 mi/h maximum. Both clockwise and counterclockwise runs were made to compensate for wind effects.

Two vehicle configurations were tested, both at a vehicle weight of AW2: in the normal mode (brake shoes in contact with the wheel treads), and in a modified mode (brake shoes held clear). Speed was recorded from the vehicle's own speed signal.

6.6.3 Test Results

6.6.3.1 Data Processing and Analysis. The speed signal was filtered at 1.0 Hz low pass to reduce noise, and then digitized at 32 samples per second. Engineering unit listings of speed at each second were made for each pass through the tangent section.

The forces retarding the vehicle were very small in comparison to the vehicle mass, resulting in low deceleration (approximately 0.005 g). A typical speed/time history is shown in figure 6-53. To calculate the deceleration rate, the slope of the speed/time history was calculated by a straight line fit, using the least squares method. A time window of 21 s was selected, and this window was moved down the time history at one-s intervals to produce a number of deceleration values. Each deceleration value was paired with the corresponding speed value at the middle of the time window.

Data pairs of deceleration and speed were then merged for successive runs through the tangent section for both clockwise and counterclockwise directions, and were plotted. This is illustrated in figure 6-54 for the normal mode of operation with the brake shoes in contact with the wheel treads. The data pairs were fitted with a 2nd order polynomial curve by the least squares method. The corresponding deceleration/speed plot for the abnormal mode (brake shoes free of the treads) is shown in figure 6-55, again fitted with a 2nd order polynomial curve.

The deceleration data were used to calculate train resistance using Newton's Law ($F=ma$). The effective vehicle weight used in the calculations

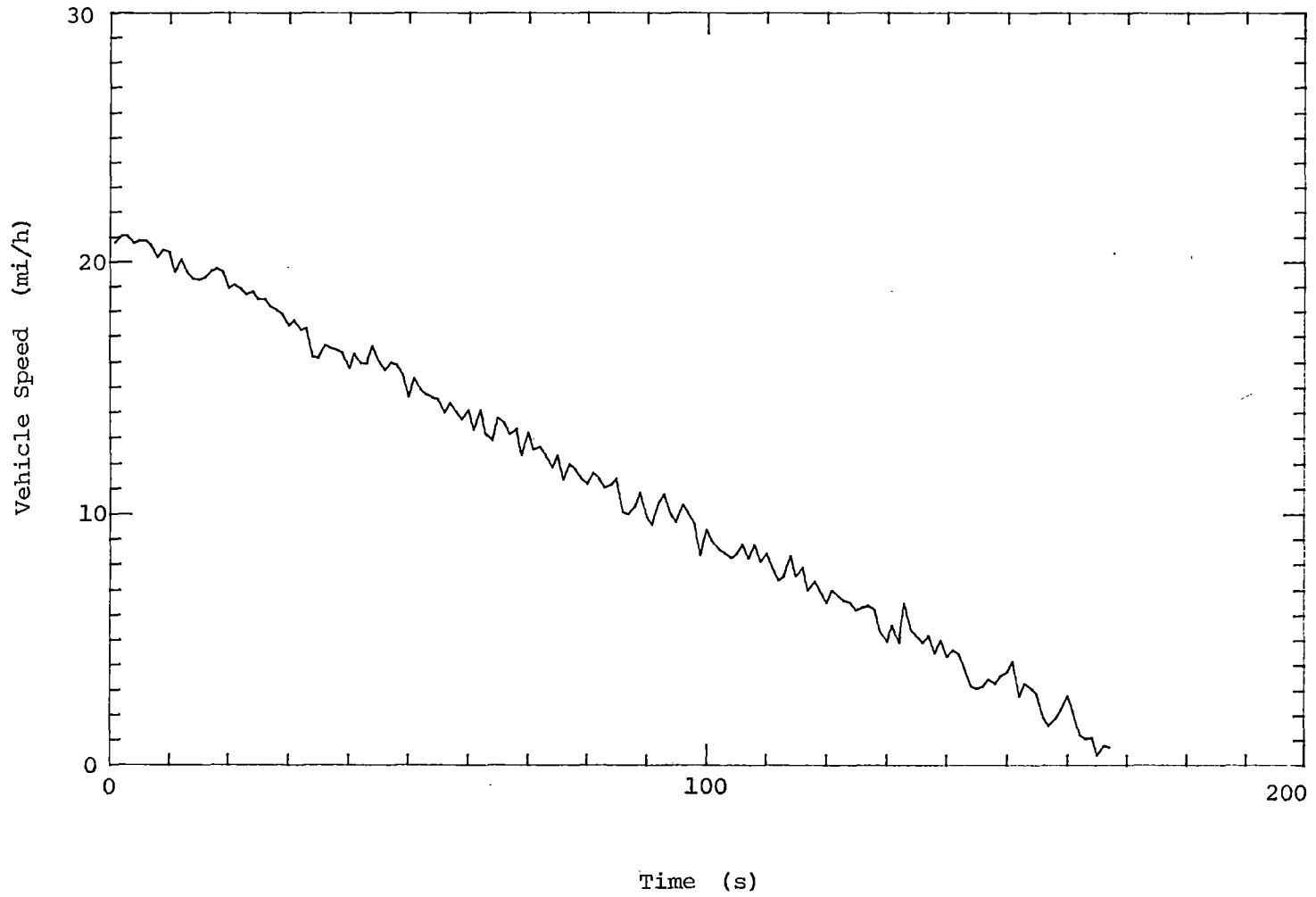


FIGURE 6-53. SPEED-TIME HISTORY FROM INITIAL SPEED OF 21 MI/H.

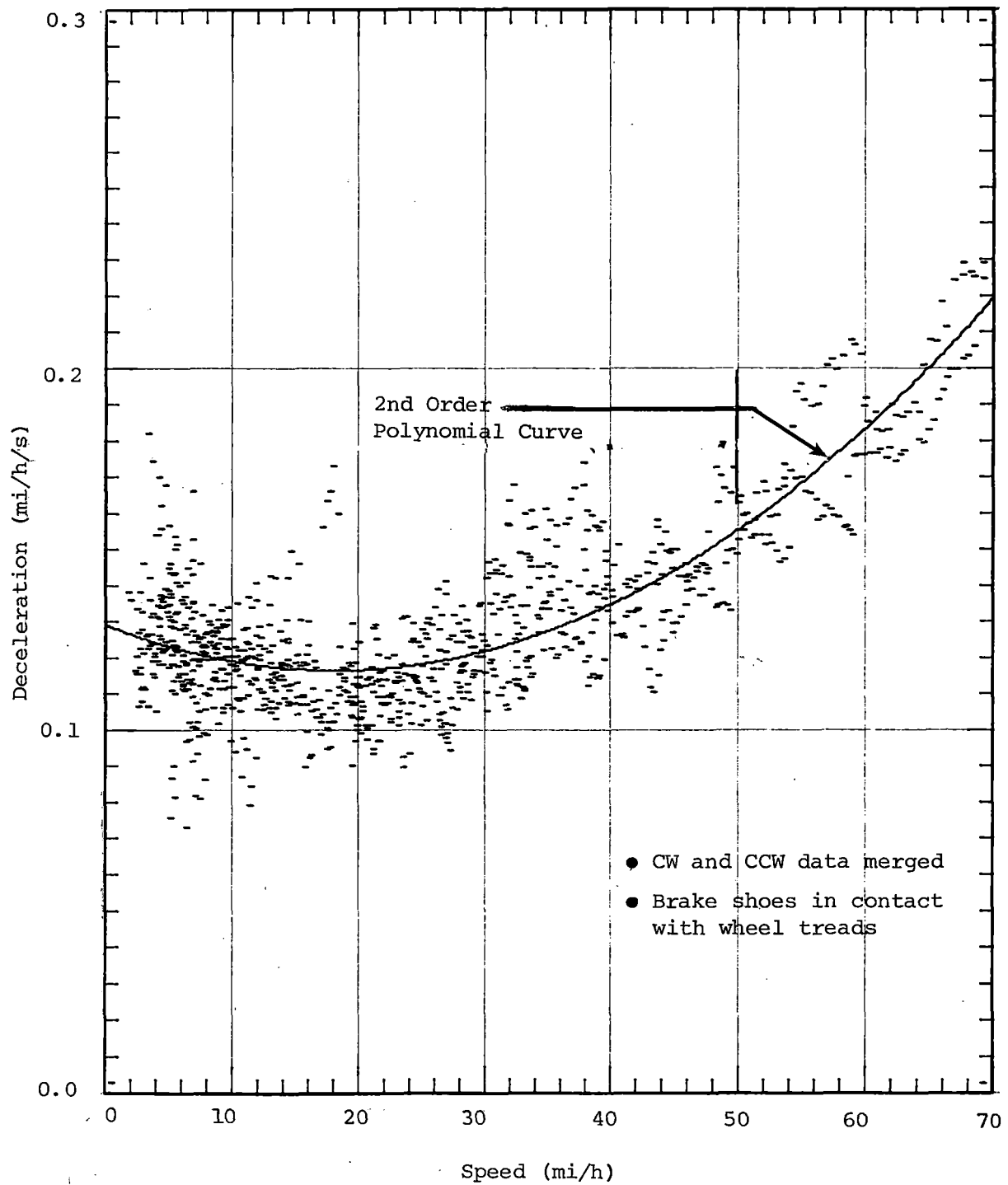


FIGURE 6-54. DECELERATION CHARACTERISTICS DUE TO TRAIN RESISTANCE, BRAKE SHOES IN CONTACT.

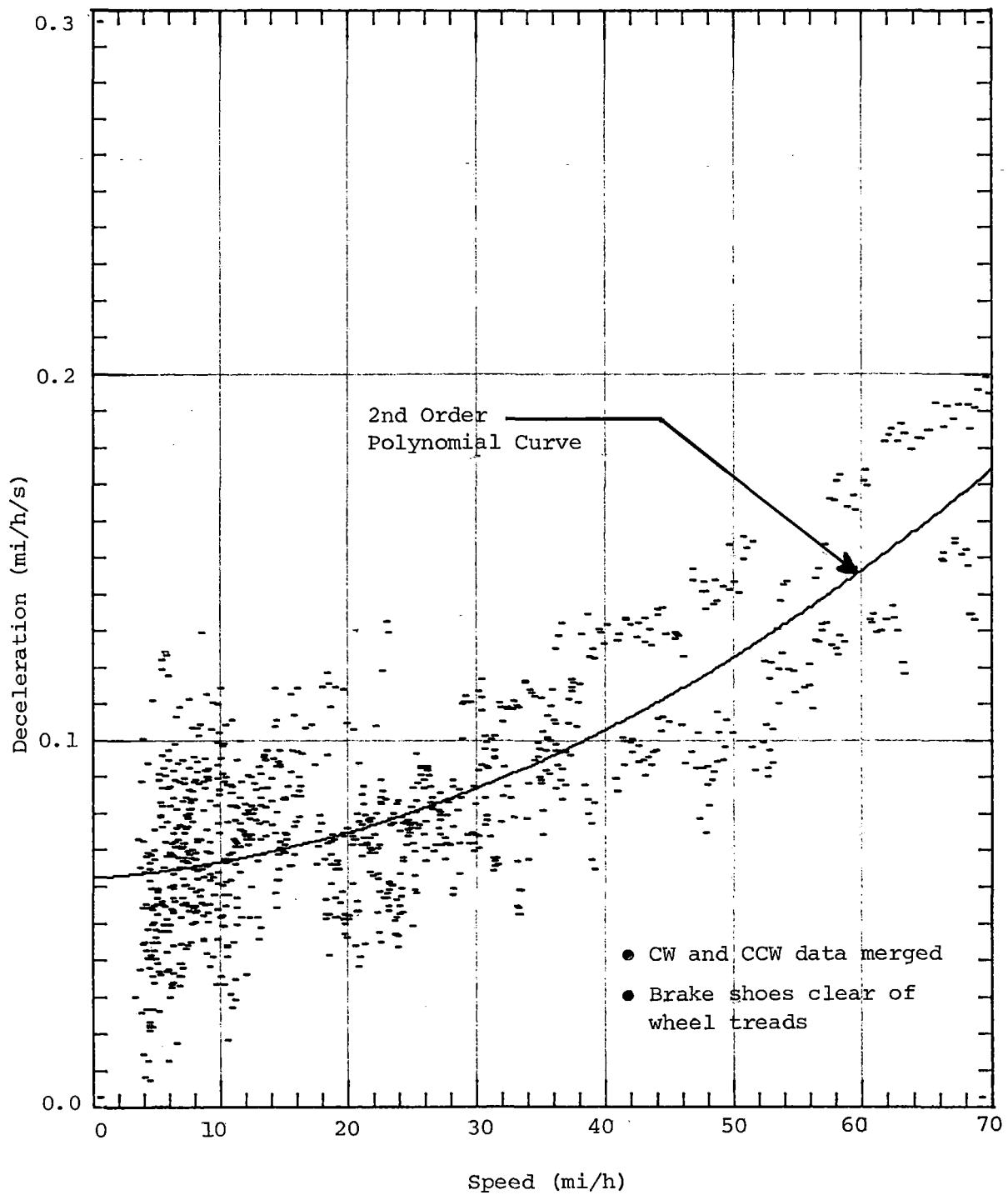


FIGURE 6-55. DECELERATION CHARACTERISTICS DUE TO TRAIN RESISTANCE, BRAKE SHOES OUT OF CONTACT.

included an estimated 10% of the AWO weight to account for the rotational inertia of the motors, wheels, gearing, etc. Therefore, the total effective AW2 weight was 210,000 lb for the two-car train consist.

6.6.3.2 Resistance with Brake Shoes in Contact. The average train resistance with the brake shoes held in contact against the wheel tread is shown in figure 6-56 as a function of speed. This train resistance is for the two-car consist averaged in clockwise and counterclockwise directions, and includes brake shoe, air, gearing, motor, and rolling resistance in the coasting mode. This configuration is representative of normal vehicle operation.

6.6.3.3 Resistance with Brake Shoes Out of Contact. The average train resistance with the brake shoes completely out of contact with the wheel tread is also shown in figure 6-56 as a function of speed. This is not a normal vehicle operational configuration. The difference in resistance provides an estimation of the brake drag penalty caused by constant brake shoe contact.

6.6.3.4 Brake Drag Characteristics. The constant brake drag is present during vehicle acceleration as well as during coasting and therefore provides an energy consumption penalty. Figure 6-57 shows the brake drag/speed characteristic estimated from the drift data of figure 6-56. The data show an upward trend in drag at the lower speeds. This is attributed to the braking characteristics of the friction brake pads. Similar trends can be observed in the friction-only braking performance data where, typically, the deceleration levels increase with decreasing speed, even though brake cylinder pressures are maintained constant. An estimate of the energy dissipated by the brake shoe contact was made by multiplying the brake drag force at a given speed by the speed and converting to kW as shown in figure 6-58. These data could be used by an analyst to calculate the energy-consumption penalty associated with dragging brakes through an operational profile.

6.6.3.5 Comparison of Experimental and Predicted Drift Performance Prediction. The experimental train resistance performance data gathered in these tests were compared to calculated train resistance values obtained from the empirical Davis formula, using the coefficients defined in the vehicle specification for flanging losses, bearing and seal losses, and aerodynamic losses.

The modified Davis Formula for train resistance is

$$TR = 1.3 + \frac{29}{W} + bV + \frac{cAV^2}{WN}$$

In this empirical formula, the first term (1.3) represents rolling resistance (lb/ton); the second, bearing and seal losses; the third, flanging losses; and the fourth, aerodynamic losses where,

TR = train resistance, lb/ton,

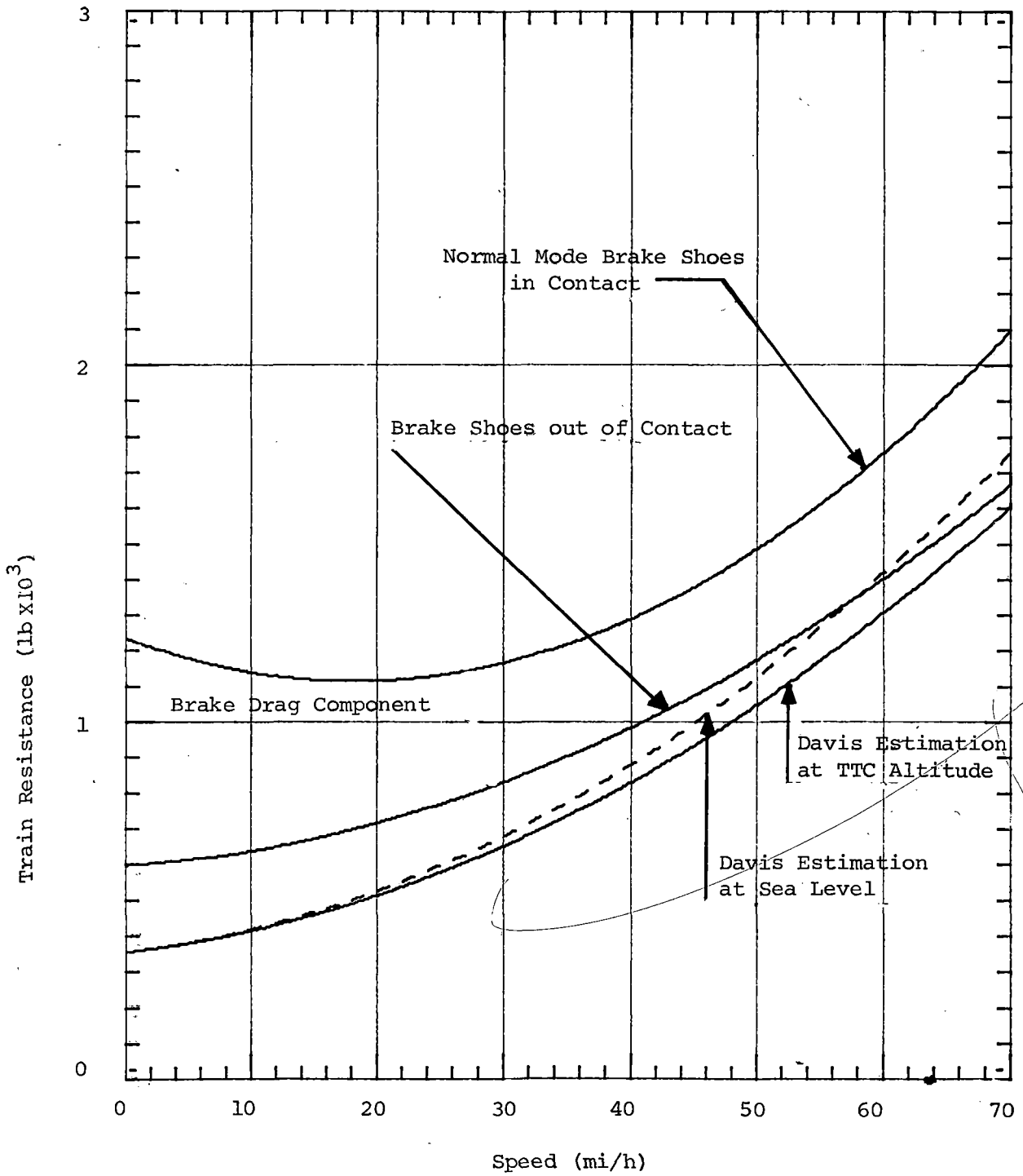


FIGURE 6-56. RESISTANCE/SPEED CHARACTERISTICS--
BRAKE SHOES IN/OUT OF CONTACT.

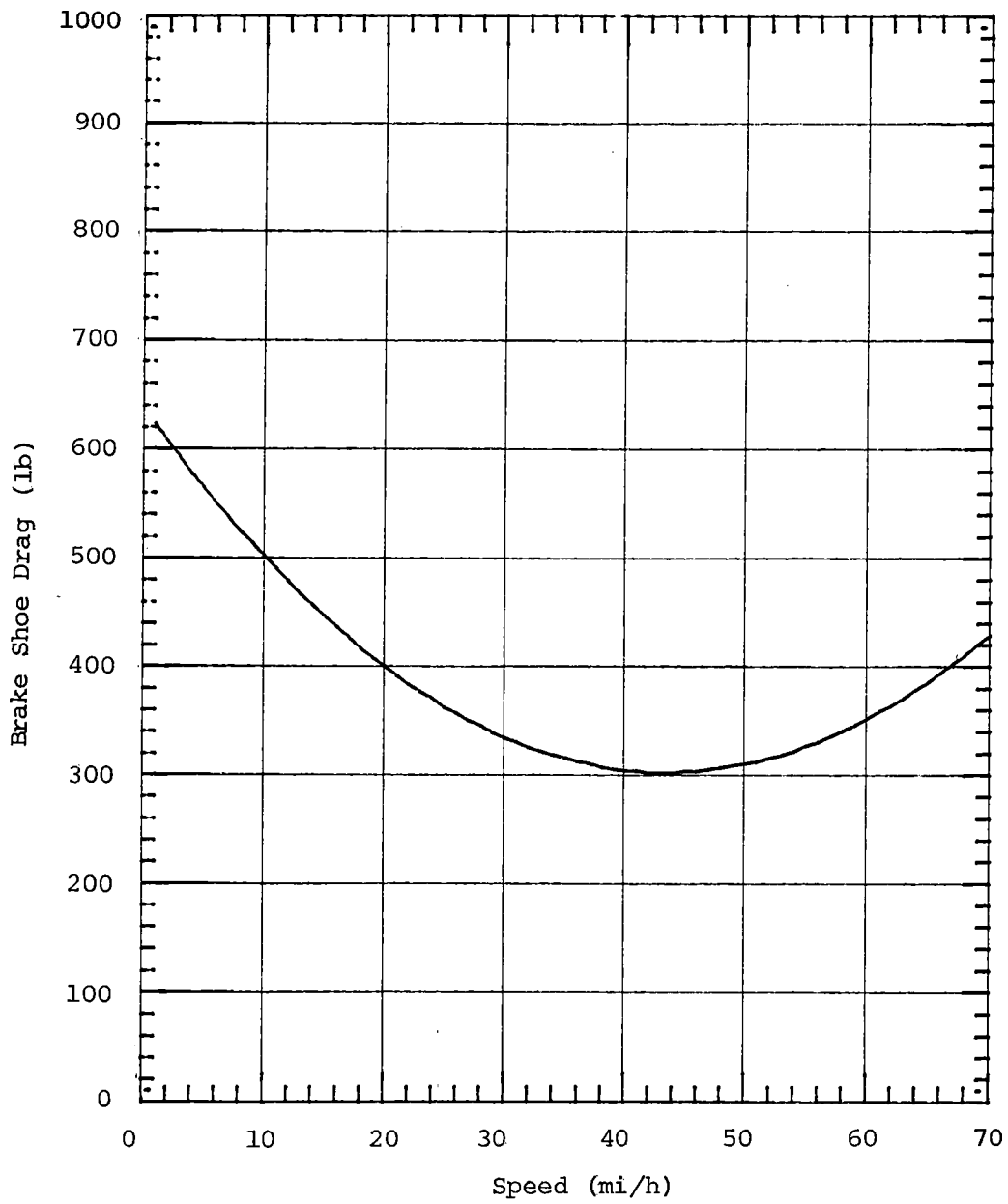


FIGURE 6-57. BRAKE SHOE DRAG RESISTANCE CHARACTERISTIC.

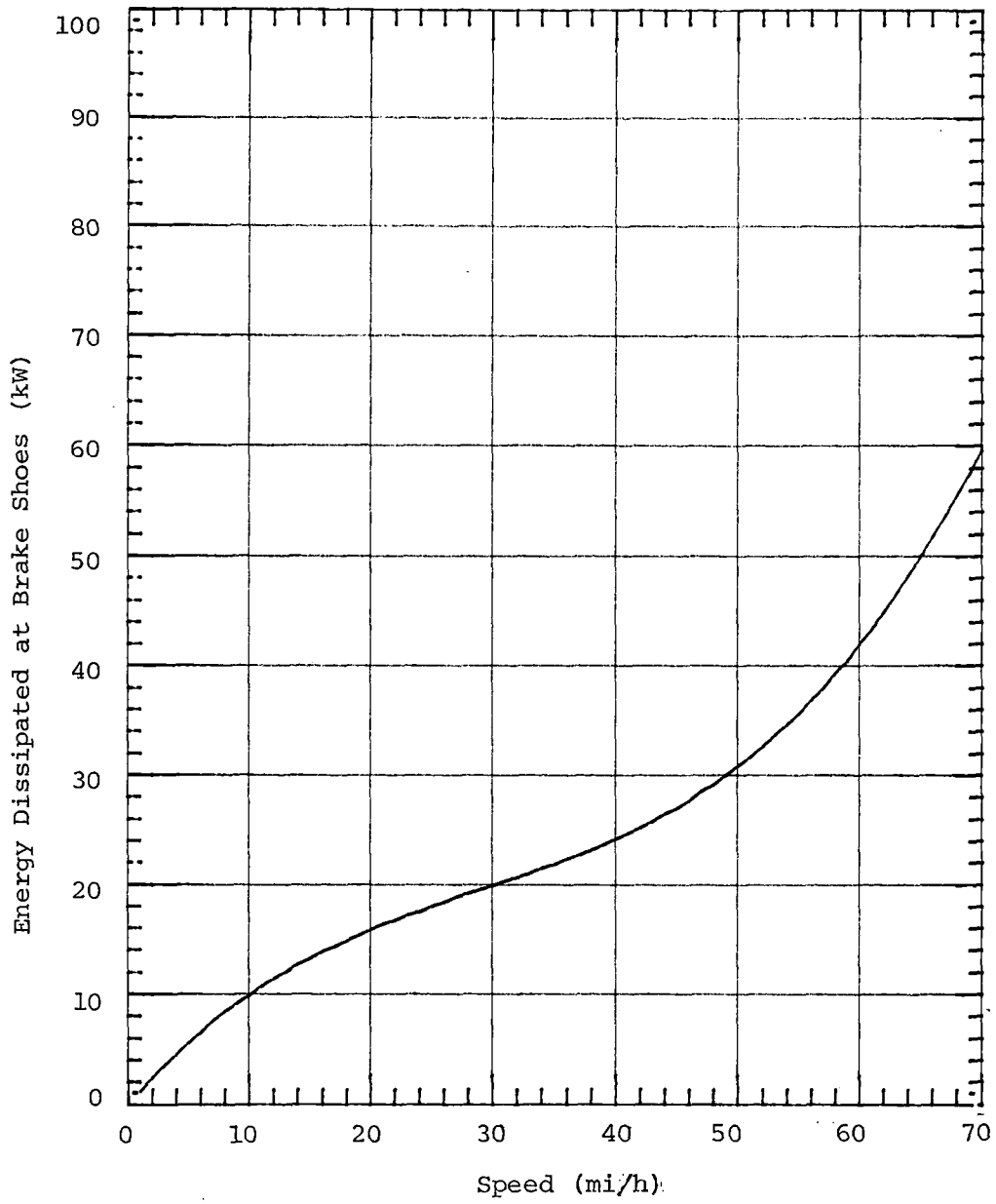


FIGURE 6-58. ENERGY DISSIPATED BY BRAKE SHOE DRAG.

W = weight per axle, tons,
b = flanging losses coefficient,
N = number of axles,
V = train speed, mi/h,
c = air resistance coefficient, and
A = frontal area of train, ft².

Applying the formula with the values quoted in the specification:

Flanging coefficient, b = 0.04
Leading vehicle aerodynamic loss coefficient, c = 0.0020
Trailing vehicle aerodynamic loss coefficient, c = 0.0003
Frontal area, A = 100 ft²

and also applying an altitude correction factor of 0.864 to the aerodynamic loss term to allow for the low air density at the test site (4,950 feet above sea level). Figure 6-56 compares the experimental train resistance data with the Davis formula estimation, corrected for the altitude of the test site and also shown for the sea level case.

The estimated train resistance is calculated for the train under the power mode and does not include gearing and motor windage losses. As such it falls below the experimental characteristic for the coasting, brakes free mode.

6.7 JERK LIMIT AND CONTROL RESPONSE TESTS

6.7.1 Test Objectives

The objectives of the tests were:

- To determine the jerk rates and transition times for a series of propulsion system mode changes from drive to brake and brake to drive over the vehicle speed range.
- To compare the data gathered with the vehicle specification requirements for jerk rate and transition time which are as follows:
 - "The rate of change of acceleration or deceleration shall be 2.0 mi/h/s². The tolerance on this limit value shall be minus zero to plus 0.4 mi/h/s².

- Jerk rate limits shall apply to all changes in service brake and power tractive effort changes, except that, during the function of the wheel spin/slide protection system, the release of positive or negative tractive effort shall not be jerk limited. The jerk rate limitation shall not apply to emergency brake applications.
- Control response times for changes in and within modes shall be as indicated in figure 6-59."

6.7.2 Test Method

Control response and jerk rate were evaluated by making a series of propulsion mode changes over the speed range, alternately accelerating and braking the vehicles to a fixed schedule. These parameters were evaluated in full for the BR2 brake configuration using the test sequence shown in table 6-10, and were checked for the final BR3 brake configuration for full power acceleration at 0, 30, and 60 mi/h and full service braking at 45 and 70 mi/h.

The tests were conducted for each car with clockwise and counterclockwise directions of travel on the track, at AW2 vehicle weight. The effect of line voltage was assessed by testing at three voltage levels of 550, 750, and 800 V d.c.; the tests were intended to be carried out at an upper line voltage of 900 V d.c., but over-voltage protection circuitry prevented operation at this voltage, and 800 V d.c. was found to be the highest voltage at which the tests could be conducted.

6.7.3 Test Results

Test data analysis was conducted directly from the chart records, using the definitions for zero time reference, response time, and jerk rate illustrated in figures 6-59 and 6-60. An evaluation of two typical mode changes is illustrated in figure 6-61, which is a reproduction of a section of traces, and shows analog signals representing master controller position, longitudinal acceleration, vehicle speed, and motor armature current for a 10-s period. For this particular example, the cars were accelerated at a P2 master controller position to approximately 35 mi/h, braked at a B2 master controller position to 30 mi/h, and then accelerated once again at a P2 setting.

The zero time reference and transition points were determined from the definitions of figures 6-59 and 6-60 and were drawn on the traces; the time intervals were measured directly from the chart using the known paper speed of 10 mm/s. The paper speed was checked against 1-s timing marks input by the data system, and was found to be accurate to 1/10th of a second over a 30-s time period.

The mean slopes of the acceleration/deceleration ramps were determined by inspection, and the jerk rates were computed by dividing the change in acceleration of the mean slope by the time required for the change ($\Delta A / \Delta t$).

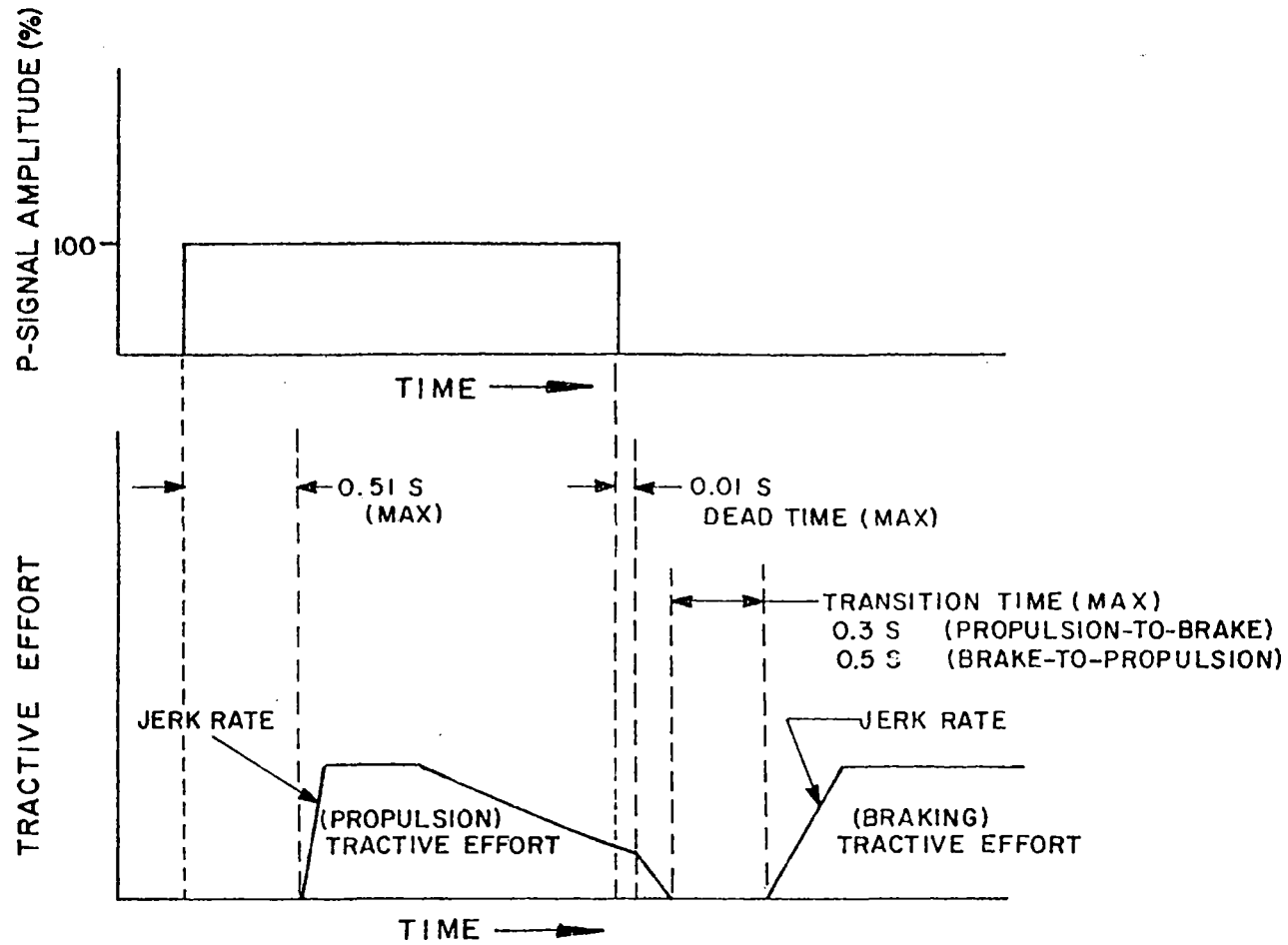


FIGURE 6-59. CONTROL RESPONSE AND JERK LIMIT SPECIFICATION REQUIREMENTS.

TABLE 6-10. PROPULSION MODE CHANGE SEQUENCE.

<u>Speed (mi/h)</u>	<u>Master Controller Position</u>	<u>Action</u>	<u>Next Speed (mi/h)</u>
0	P1	Accelerate	15
15	B1	Brake	10
10	P1	Accelerate	25
25	B1	Brake	20
20	P2	Accelerate	35
35	B2	Brake	30
30	P2	Accelerate	45
45	B2	Brake	40
40	P3	Accelerate	55
55	B3	Brake	50
50	Full	Accelerate	65
65	B3	Brake	60
60	Full	Accelerate	70
70	B3	Brake	0

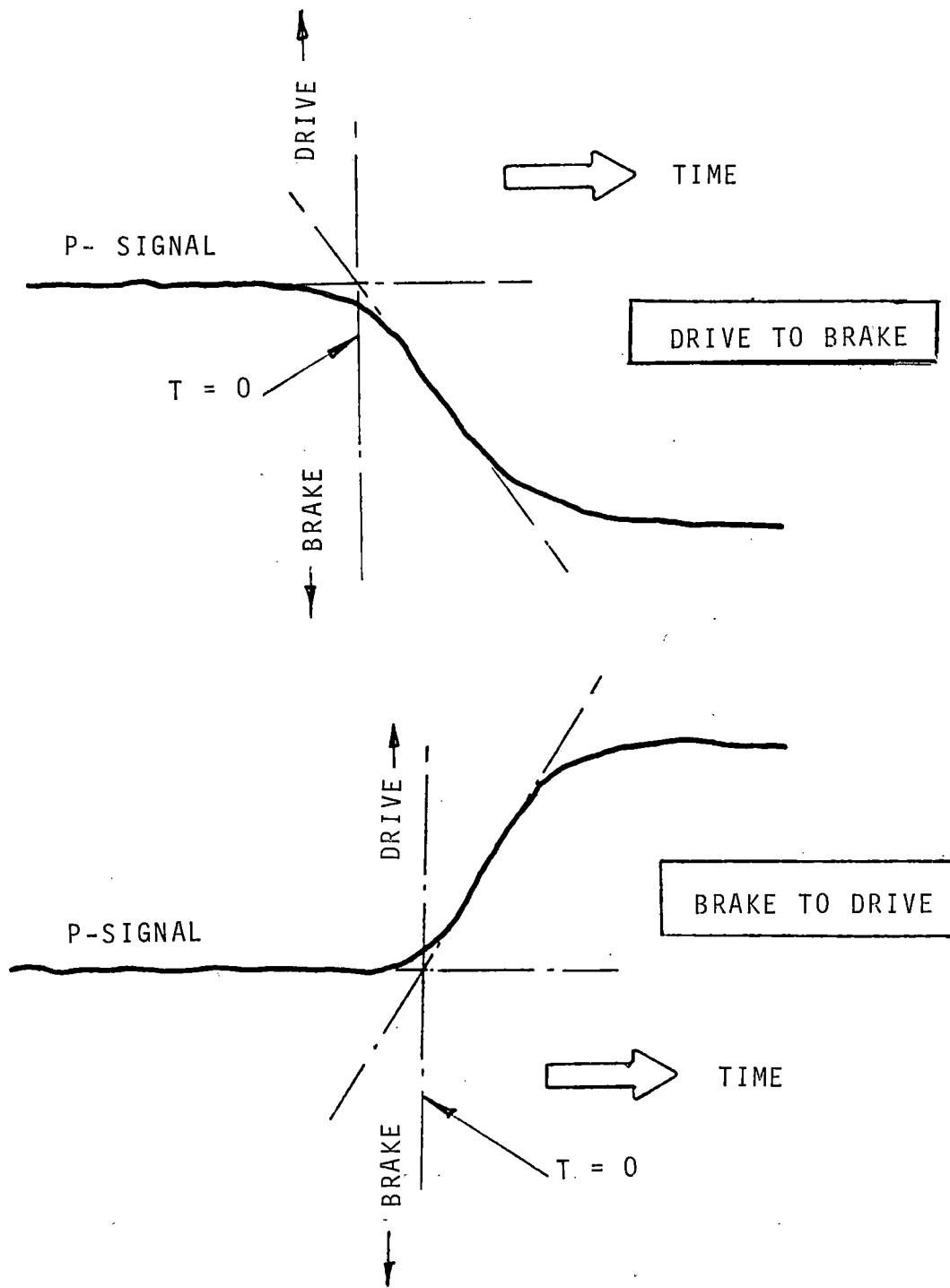


FIGURE 6-60. DEFINITION OF ZERO TIME REFERENCE FOR CONTROL RESPONSE EVALUATION.

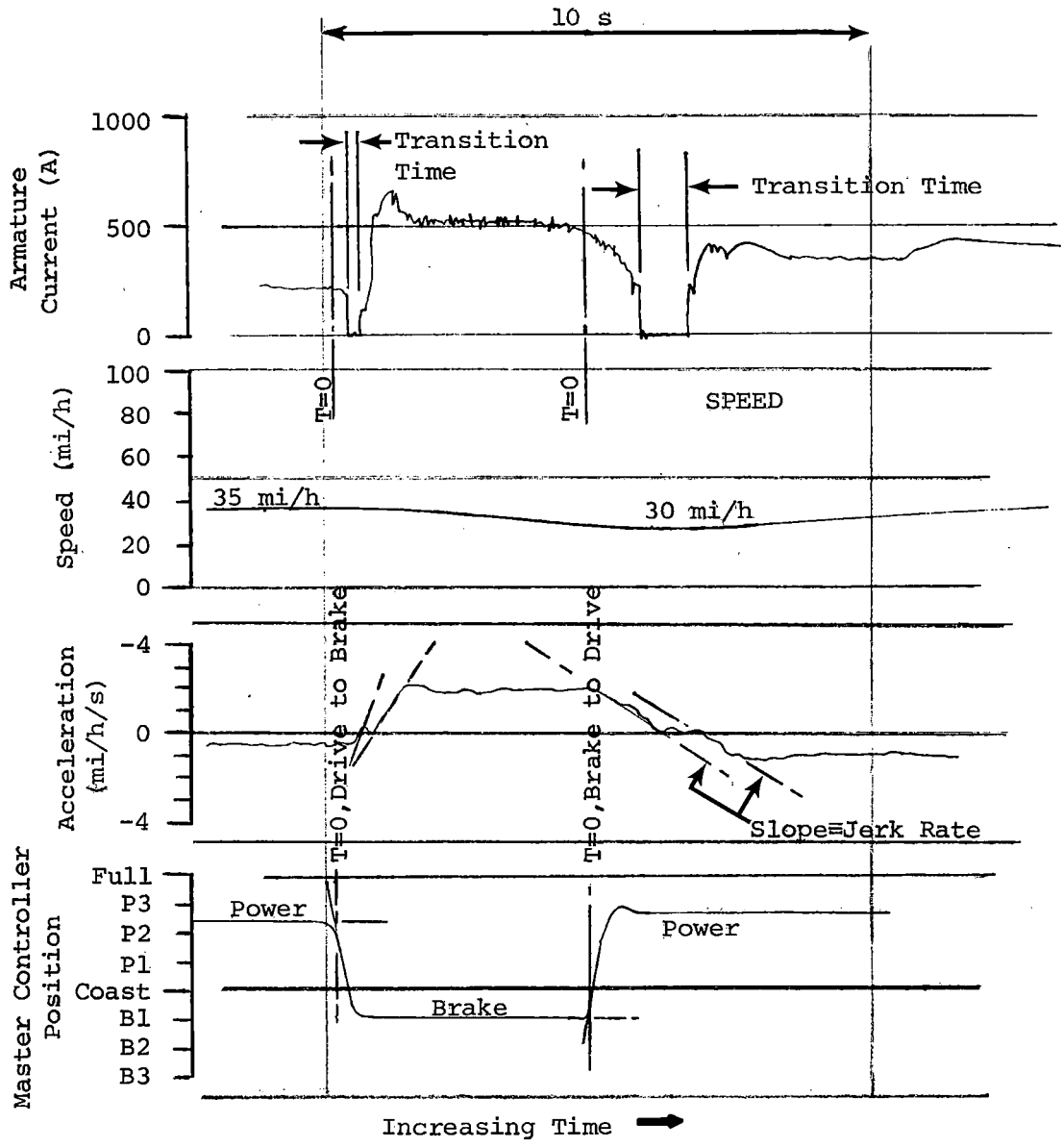


FIGURE 6-61. TYPICAL DRIVE/BRAKE/DRIVE MODE CHANGE.

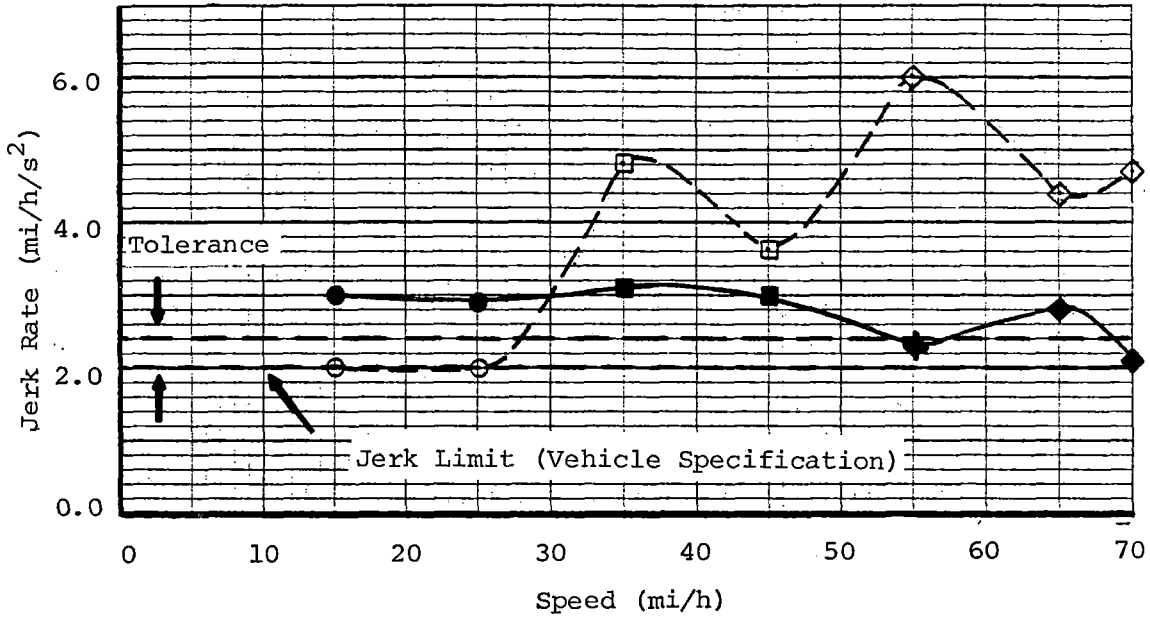
Inspection of the traces shows that there are two jerk rates associated with each mode change, one due to the removal of tractive effort and one due to the application of tractive effort of the opposite polarity, after a delay due to the transition of the propulsion system. For example, in the case illustrated in figure 6-61, a change from an acceleration at P2 master controller setting to a deceleration at B2 controller position, there is a jerk associated with the removal of power and another with the application of braking tractive effort. Jerk rates and transition times were evaluated for four control response test runs at the BR2 brake configuration; the effect of operating from each car and the effect of line voltage on jerk rate are presented in figures 6-62 through 6-65. Data from the BR3 configuration check runs have been superimposed on figures 6-63 through 6-65.

Three general trends are apparent from the data plots:

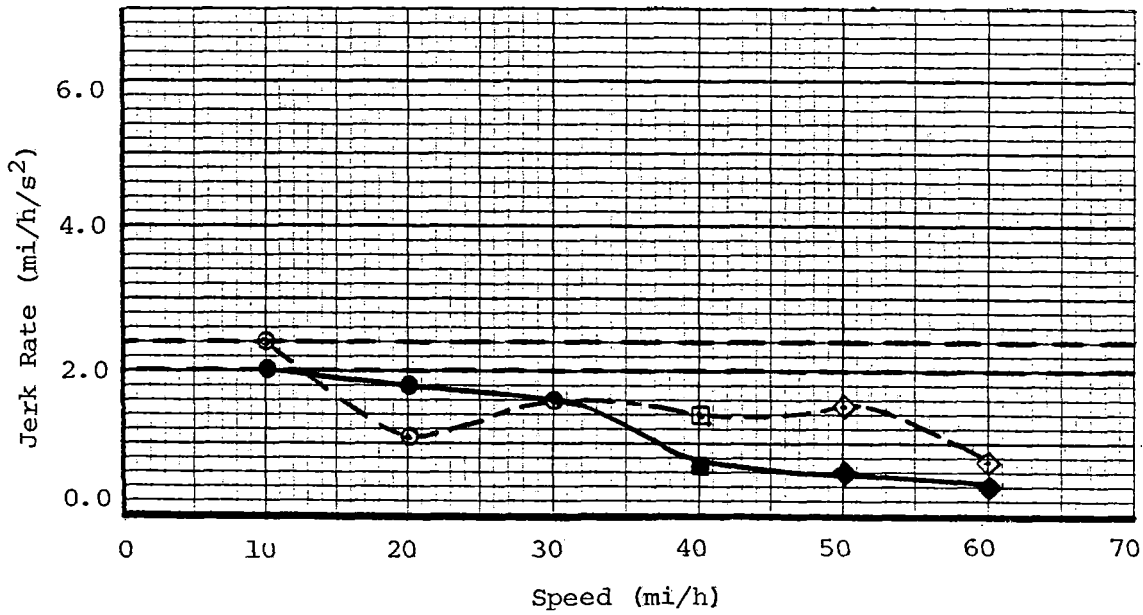
- The jerk rates associated with the transition from braking to acceleration are generally below the specification limit value of $2.0^{+0.4}$ mi/h/s². There are one or two exceptions at 10 mi/h where the highest value recorded was 3.6 mi/h/s². The jerk rate associated with the application of tractive effort shows a decreasing trend with increasing speed; this is to be expected, as the power available approaches the power required to sustain steady speed at the higher speeds.
- The jerk rates associated with the removal of propulsive tractive effort in the acceleration-to-brake mode change are generally high, with some values up to 6.0 mi/h/s² at speeds in excess of 30 mi/h. The actual changes in acceleration levels associated with these jerk rates, however, are small (0.5 mi/h/s or less) due to the small available tractive effort at these speeds. As a result, the overall effect on passenger comfort due to the jerk on removal of propulsive tractive effort is small and should not be considered with respect to the vehicle specification criteria.
- The jerk rates due to brake application are generally greater than the specification limit criteria of 2.0 mi/h/s², with values in the range 2.3 to 4.1 mi/h/s² for the conditions evaluated. Jerk rates show some consistent trends with speed, with peak values occurring in the 35 - 45 mi/h range. There were no discernable trends of jerk rate due to line voltage variation or operation from either car.

Transition times for the test runs at BR2 brake configuration and for the retest check runs at BR3 are found in tables 6-11 and 6-12, respectively. The vehicles met the transition time specification requirement of 0.3 s for the mode change from acceleration to brake and consistently recorded transition times of 0.20 to 0.25 s; transition times for the mode change from brake to propulsion were consistently in excess of the specification requirement of 0.5 s, with typical transition times in the 0.75 to 1.0 s range.

AW2	<u>Controller Position</u>	<u>Tractive Effort</u>	
750 V d.c.		Remove	Apply
Car #0109 Leading	B1/P2	○	●
BR2 Configuration	B2/P3	□	■
	B3/Full	◇	◆



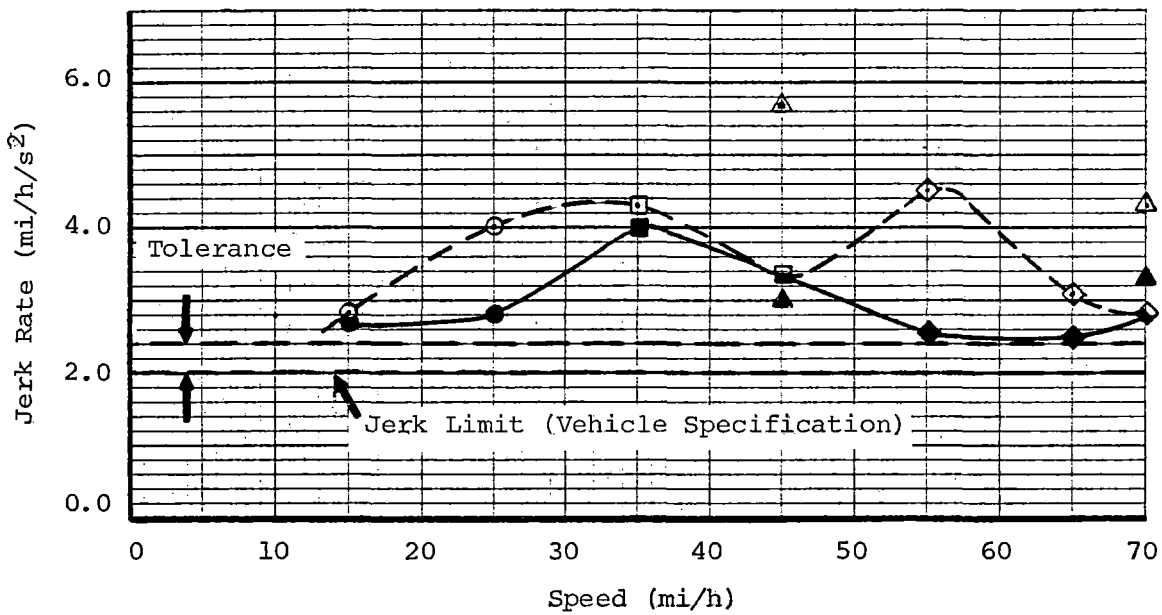
Acceleration to Brake Mode Change.



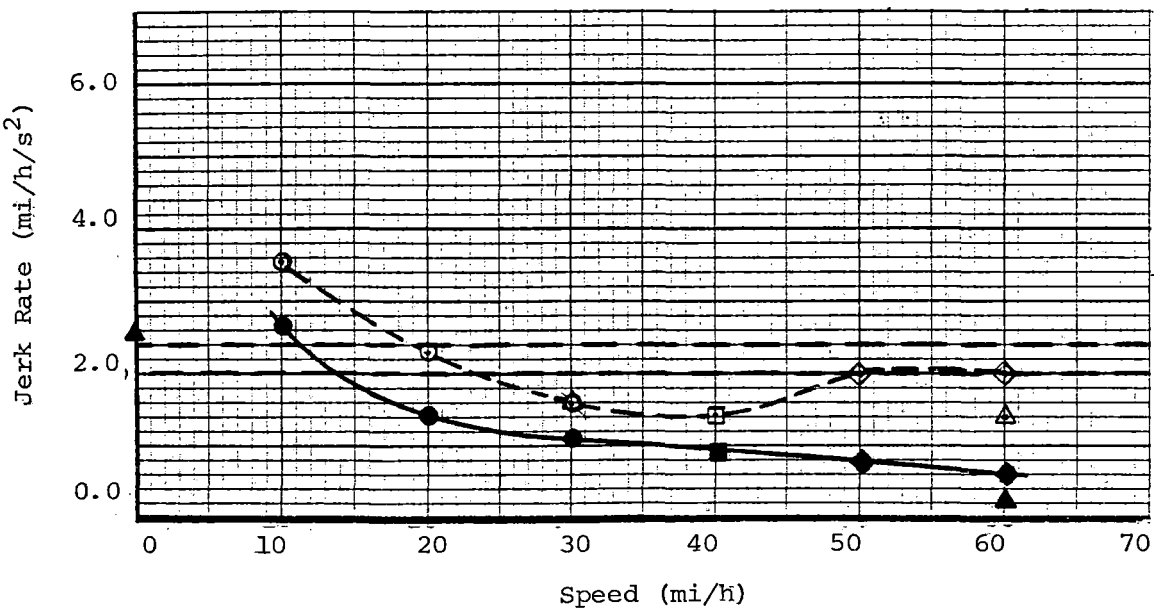
Brake to Acceleration Mode Change.

FIGURE 6-62. JERK RATES FOR PROPULSION SYSTEM MODE CHANGES.

	<u>Controller Position</u>	<u>Tractive Effort</u>	
AW2 Weight		Remove	Apply
Car #0110 Leading	B1/P2	○	●
BR2 Configuration	B2/P3	□	■
	B3/Full	◇	◆
BR3 Configuration.....	B3/Full	△	▲



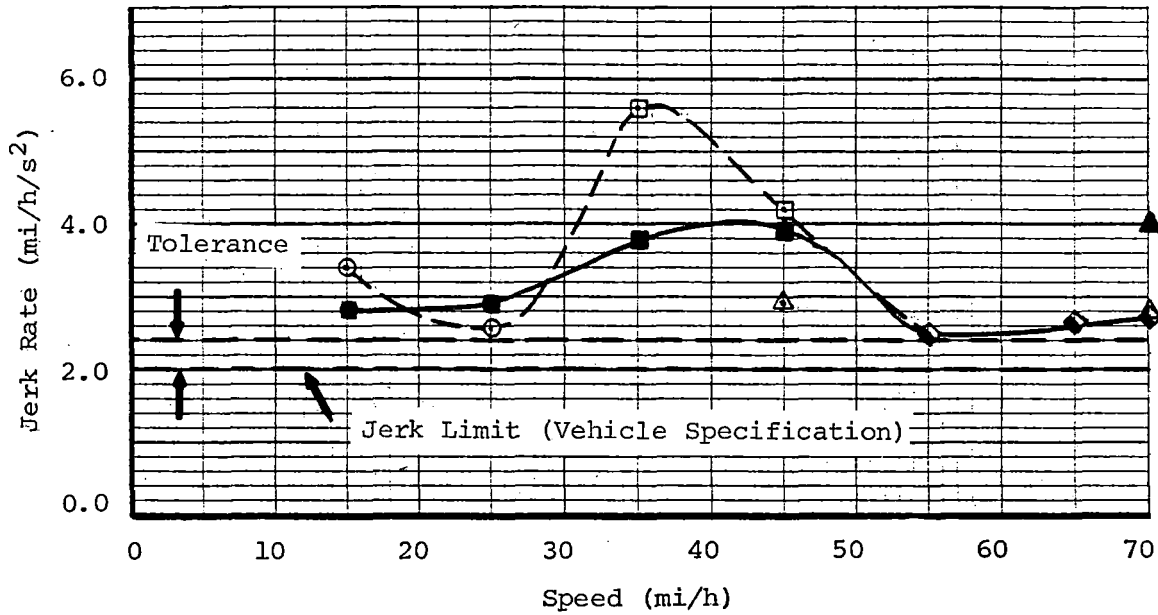
a. Acceleration to Brake Mode Change.



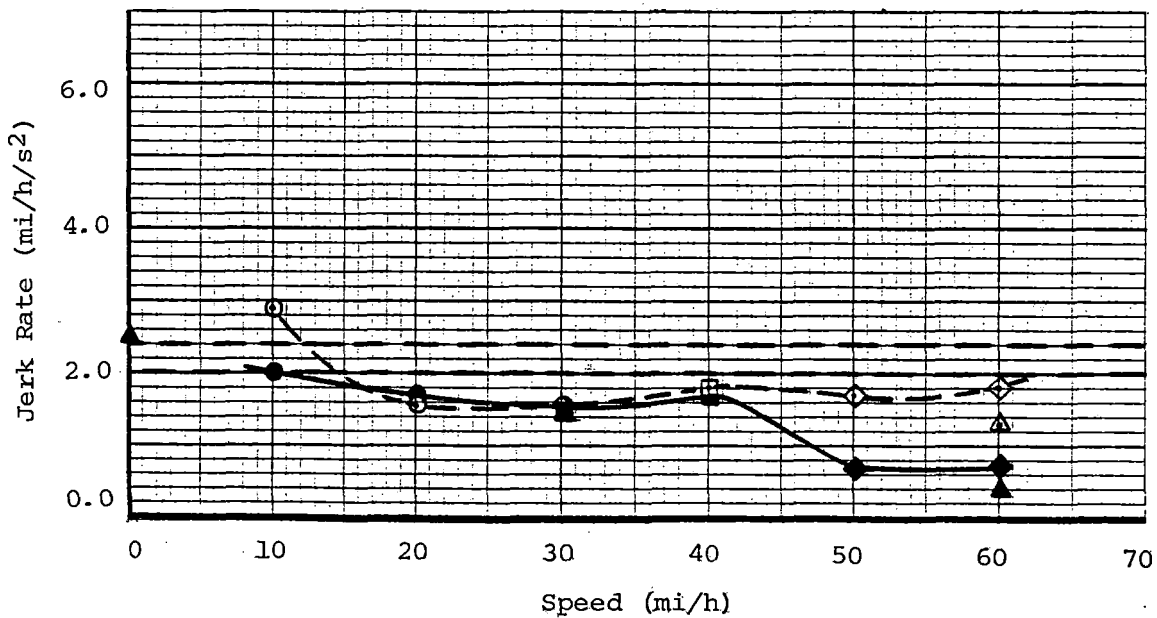
b. Brake to Acceleration Mode Change.

FIGURE 6-63. JERK RATES FOR PROPULSION MODE CHANGE, 750 V d.c.

	<u>Controller Position</u>	<u>Tractive Effort</u>	
		Remove	Apply
AW2 Weight		○	●
Car #0110 Leading	B1/P2	□	■
BR2 Configuration	B2/P3	◇	◆
	B3/Full	△	▲
BR3- Configuration.....	B3/Full		



a. Acceleration to Brake Mode Change.



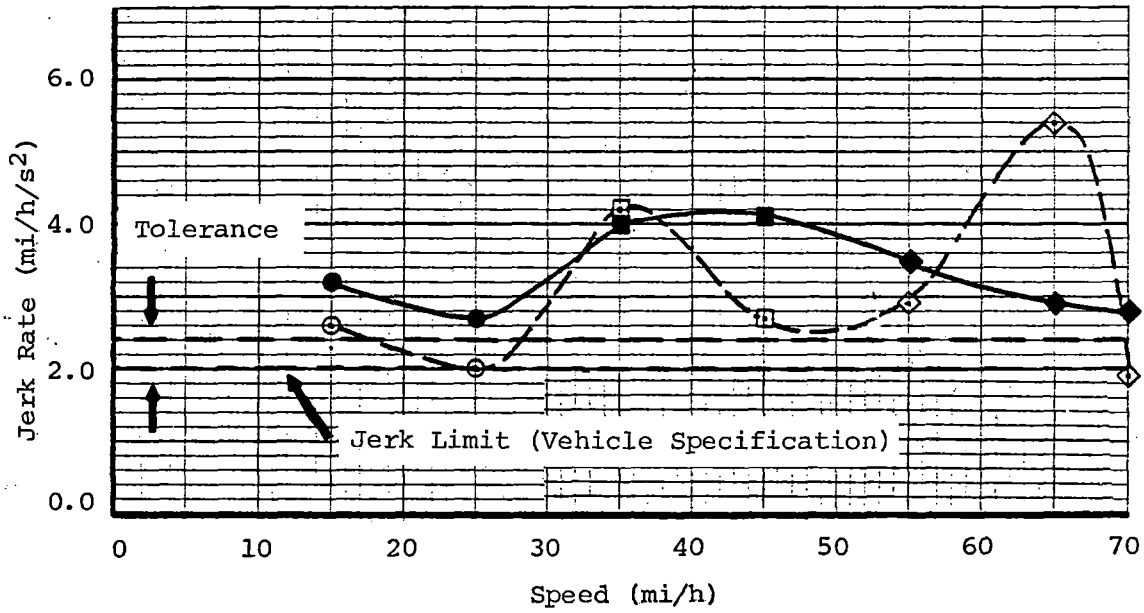
b. Brake to Acceleration Mode Change

FIGURE 6-64. JERK RATES FOR PROPULSION MODE CHANGE, 550 V d.c.

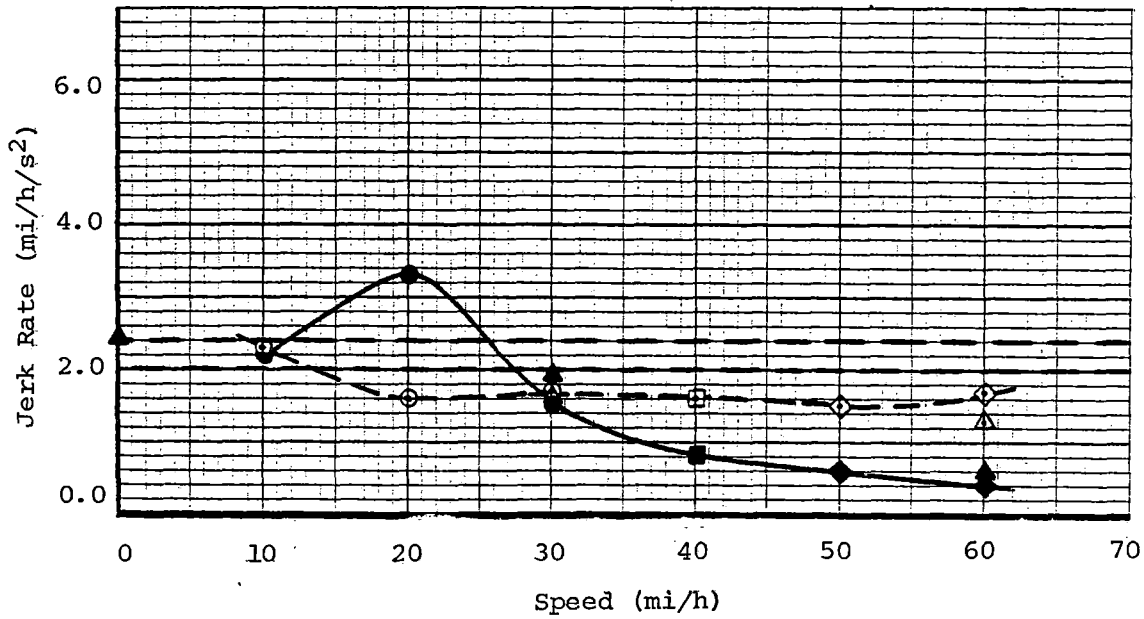
AW2
 800 V d.c.
 Car #0110 Leading
 BR2 Configuration

Controller Position
 B1/P2
 B2/P3
 B3/Full
 B3/Full Conf. BR3

Tractive Effort
 Remove Apply
 ○ ●
 □ ■
 ◇ ◆
 △



Acceleration to Brake Mode Change.



Brake to Acceleration Mode Change.

FIGURE 6-65. JERK RATES FOR PROPULSION MODE CHANGES, 800 V d.c.

TABLE 6-11. TRANSITION TIMES FOR MODE CHANGES, CONFIGURATION BR2.

Mode Change	Speed (mi/h)	Controller Position	Transition Time (s)			
			750 V d.c.*	750 V d.c.	550 V d.c.	800 V d.c.
Brake to	10	P2	0.8	0.35	0.75	0.8
	20	P2	0.8	0.75	0.7	0.8
	30	P2	1.0	0.9	0.85	1.0
Acceleration	40	P3	0.8	0.9	0.85	0.8
	50	Full	0.85	0.8	0.85	0.85
	60	Full	0.8	0.8	1.0	0.8
Acceleration	15	B1	0.25	0.25	0.25	0.25
	25	B1	0.2	0.25	0.25	0.2
	35	B2	0.25	0.3	0.25	0.25
	45	B2	0.25	0.25	0.2	0.25
to Brake	55	B3	0.25	0.25	0.25	0.25
	65	B3	0.2	0.25	0.25	0.2
	70	B3	0.25	0.25	0.25	0.25

* Car 0109 leading. All other data are for car 0110 leading.

TABLE 6-12. TRANSITION TIMES FOR MODE CHANGES, CONFIGURATION BR3.

Mode Change	Speed (mi/h)	Controller Position	Transition Time (s)			
			750 V d.c.*	750 V d.c.	550 V d.c.	825 V d.c.
Brake to	0	Full	0.95	0.95	0.95	1.0
Acceleration	30	Full	1.05	1.05	1.05	1.05
	60	Full	1.05	1.05	1.05	1.05
Acceleration	45	B3	0.25	0.25	0.25	0.25
	to Brake	70	B3	0.25	0.25	0.25

* Car 0109 leading. All other data are for car 0110 leading.

7.0 RIDE QUALITY

Ride quality testing was conducted on the two-car train to determine the vehicle ride characteristics as experienced by a passenger and to identify vibration induced in the vehicle body due to operation of the undercar equipment. Ride quality testing was conducted in order to determine the effects of the following:

- Component-induced vibration
- Speed
- Track construction
- Car weight
- Secondary suspension damping
- Train consist direction
- Vehicle acceleration
- Various braking modes

For component-induced vibration tests, acceleration data were recorded with eleven combinations of the vehicle auxiliary equipment operating. For ride quality testing, vibration data were recorded while the vehicles were operated at constant speeds at AW0 and AW3 weights, and with three secondary suspension damper configurations. The three configurations defined as R1, R2, and R3 are described in Section 3.13. Vibration data were also recorded while the vehicles were accelerated from 0 to 70 mi/h at a full acceleration rate, with R1 and R2 secondary suspension damper configurations. Vibration-acceleration data were also recorded while the vehicles were decelerated from 70 to 0 mi/h with the two secondary suspension damper configurations for blended and friction-only braking.

Six servo-type accelerometers were mounted on the carbody floor as shown in figure 7-1 for all ride quality testing. Two additional servo-type accelerometers were added over the rear truck centerline for an additional ride quality test at constant speeds which excited the vehicle modes. The electrical output of each accelerometer was low-pass filtered at 100 Hz, monitored on strip charts, and FM-recorded on magnetic tape. For each run, a minimum of 30 s of data were recorded for analysis.

A subset of the complete test data matrix was selected for data processing in order to limit the analysis to a manageable level. This subset was selected to provide enough representative cross sections to define the effects of the various test variables as outlined above.

The selected data parameters for the vehicle constant speed test conditions were reduced in a different manner than the selected data parameters for the vehicle acceleration and deceleration test conditions, as follows:

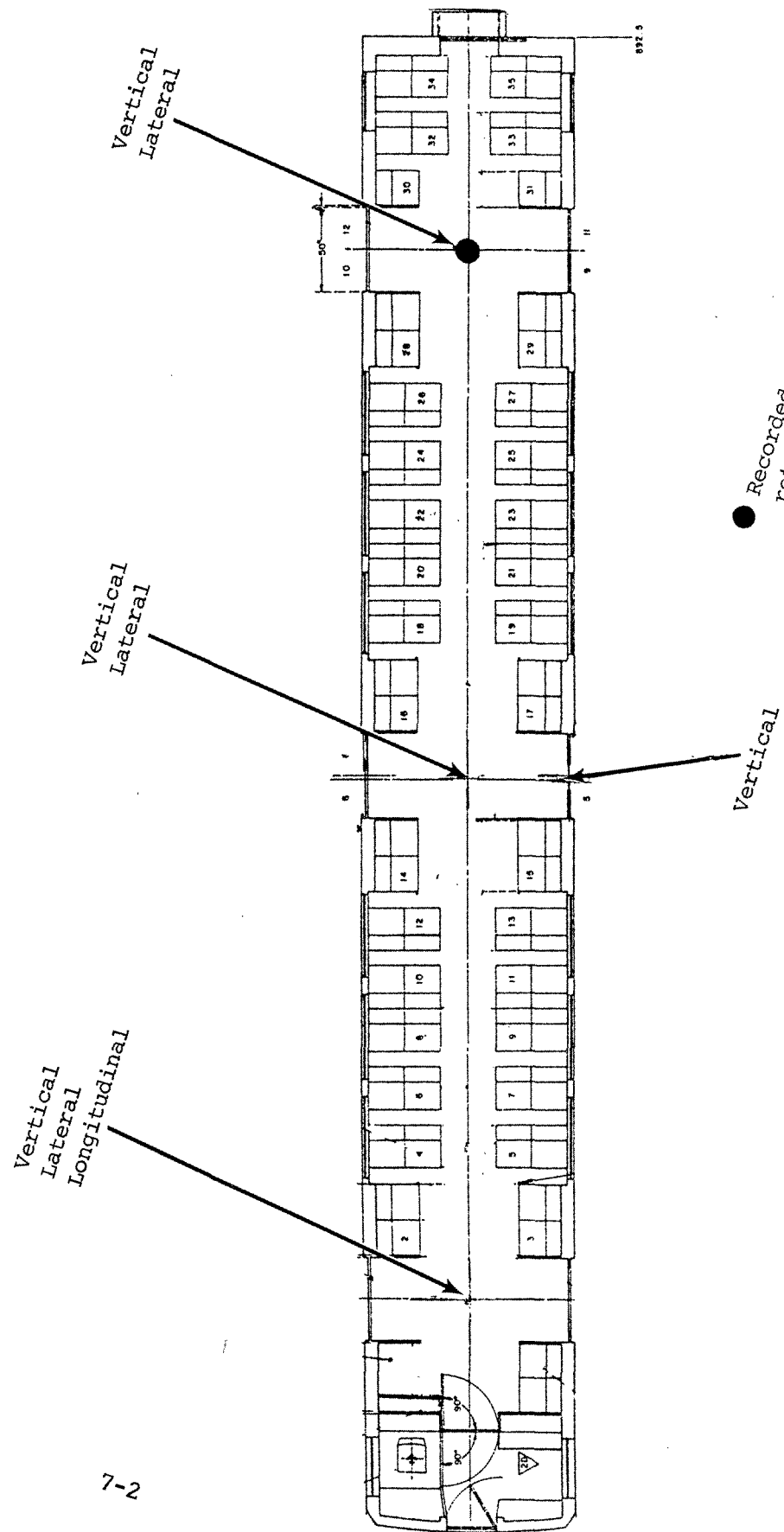


FIGURE 7-1. RIDE QUALITY ACCELEROMETER LOCATIONS.

- Since the vehicle body response at worst-speed conditions contains several significant frequencies, the analysis method described in the specification was not practical. Therefore, the data were digitized at 256 samples per second and processed to provide rms acceleration spectra plots using a Discrete Fourier Transform digital data processing technique. Four seconds of test data were selected for analysis at each stabilized speed. An equivalent filter bandwidth of 0.25 Hz was used in the analysis. The rms acceleration levels, within the filter bandwidth which resulted in the greatest amplitude at each body mode, were converted to an equivalent peak acceleration value and are shown in the following cross plots for the various test variables. Comparisons of the test data to the specification requirements were made.

The technique of converting the rms acceleration level in a single 0.25 Hz bandwidth to an equivalent average peak acceleration is a reasonable approximation of the average peak acceleration defined by the MARTA specification if the width of the structural response at the particular body mode falls within the 0.25 Hz filter bandwidth. A more widely accepted method of analysis, using 1/3 octave filtering, is defined in the International Standards Organization (ISO) standard for ride quality. However, this analysis procedure was not defined in the MARTA specification criteria.

- Digital filtering techniques were used to obtain frequency-weighted rms acceleration ride roughness values of the constant speed test data. The data were frequency-weighted for human sensitivity according to the ISO weighting curves shown in figure 7-2.
- The vehicle acceleration and deceleration test conditions resulted in a constantly changing forcing function to the carbody as the vehicle speed varied. Therefore, the response accelerations were not stationary and thus, the data were processed to provide rms acceleration versus vehicle speed plots. The data were processed through a 30 Hz low-pass filter with approximately 1 s averaging time using analog filtering techniques.

7.1 COMPONENT INDUCED VIBRATION

7.1.1 Test Objective

The objective of the component induced vibration test was to determine the vibration induced into the carbody floor by operation of the auxiliary equipment operating singly or in combinations, and to compare these vibration levels with specification criteria, which are:

"With the Transit Vehicle stationary, and with each individual auxiliary unit or other vibration-generating equipment operating, the vertical or horizontal vibrations on the floor, walls, seat frames, or any surface with which the passengers or the Operator can come in contact shall not exceed the following. This requirement shall also be met with all auxiliaries operating simultaneously:

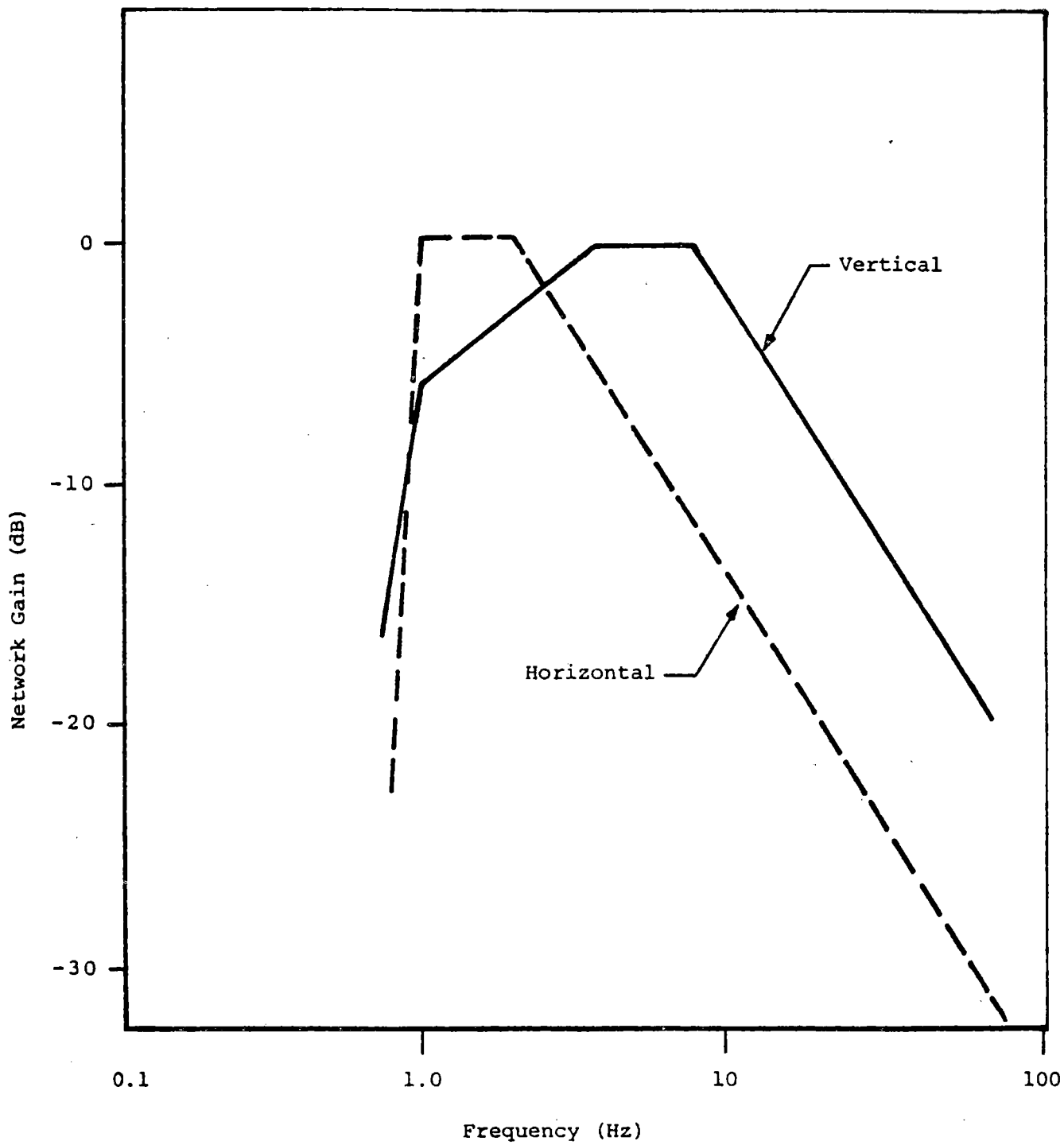


FIGURE 7-2. ISO WEIGHTING CURVES.

<u>Frequency, f (Hz)</u>	<u>Peak Acceleration (g's)</u>
zero to 1.4	0.0051 f ² (0.1" peak-to-peak displacement)
1.4 to 20	0.01
above 20	0.0005 f (0.03 inch per second peak velocity)"

7.1.2 Test Method

The car was stationary on level tangent track at approximately station 33 on the TTT. All testing was accomplished on car 0110 with equipment operating in combinations as shown in table 7-1.

7.1.3 Test Results

Vibrations for the carbody floor measurements showing the most significant acceleration levels were evaluated; i.e., the vertical and lateral accelerometers located on the floor centerline directly over the forward truck bolster (uncoupled end) and a vertical accelerometer located at the midcar floor centerline.

The accelerometer outputs were digitally processed to produce rms acceleration versus frequency plots (0-80 Hz). The test results presented in figures 7-3 and 7-4 show that the maximum component-induced vibration was approximately 37% of the specification requirements. The lateral vibration data were below the noise floor of the plot and therefore are not included. The highest vertical vibration observed was 0.008 g rms at 65 Hz over the forward truck, due to the operation of the traction motor (TM) blower.

7.2 SPEED EFFECT

7.2.1 Test Objective

The test objective was to determine the maximum vibration levels encountered due to vehicle operation at preselected constant speeds and at speeds which provided peak responses of the carbody dynamic modes. Test results are compared with specification requirements, which are:

"At all steady Transit Vehicle speeds from zero to 70 mph on tangent track the average vertical and lateral acceleration amplitudes measured on the floor over either truck pivot point and at the car center, shall not exceed the levels specified by the appropriate curve in figure 7-5. No peak acceleration value, when measured to include frequencies less than 30 Hz, shall exceed 0.15 g. The average acceleration amplitude shall be computed by dividing the sum of the peak-to-peak amplitudes of

TABLE 7-1. EQUIPMENT IN OPERATION DURING MEASUREMENTS OF COMPONENT-INDUCED VIBRATION.

Run No.	Aux Power System	Air Comp.	A/C Front Evap. Fan	A/C Rear Evap. Fan	A/C Front Cond.	A/C Rear Cond.	Traction Motor Fans	Doors Cycling
1	X							
2	X	X						
3	X		X					
4	X		X	X				
5	X		X	X	X	X		
6	X	X	X	X	X	X		
7	X						X	
8	X		X	X			X	
9	X		X	X	X	X	X	
10	X	X	X	X	X	X	X	
11	X	X	X	X	X	X	X	X

7-6

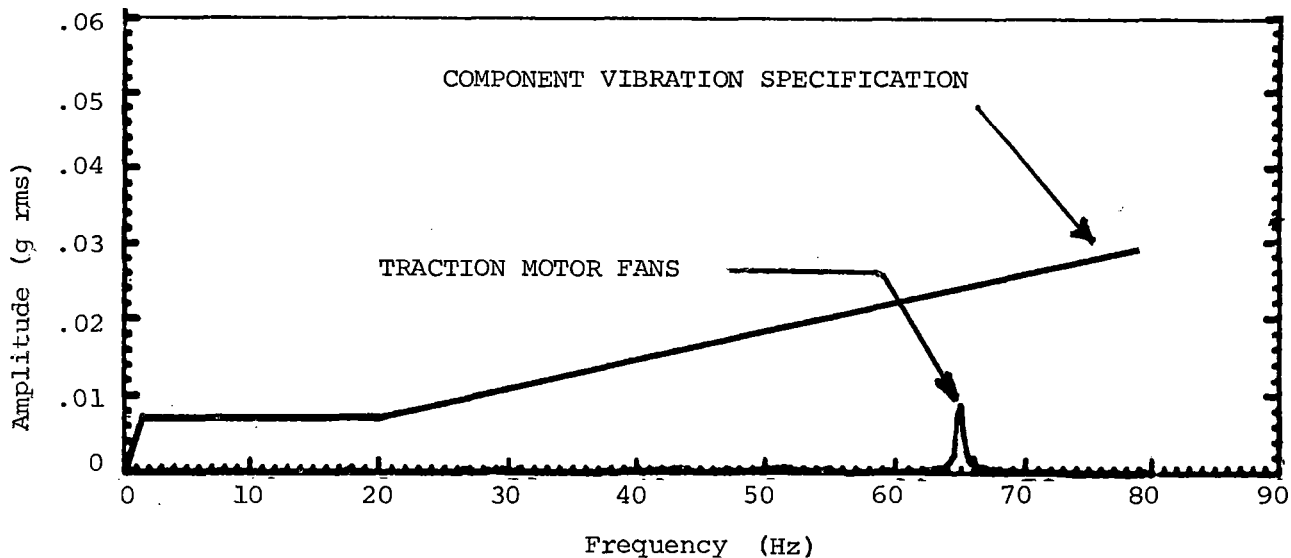


FIGURE 7-3. COMPONENT-INDUCED VIBRATION (VERTICAL) - FORWARD FLOOR CENTERLINE (OVER TRUCK PIVOT).

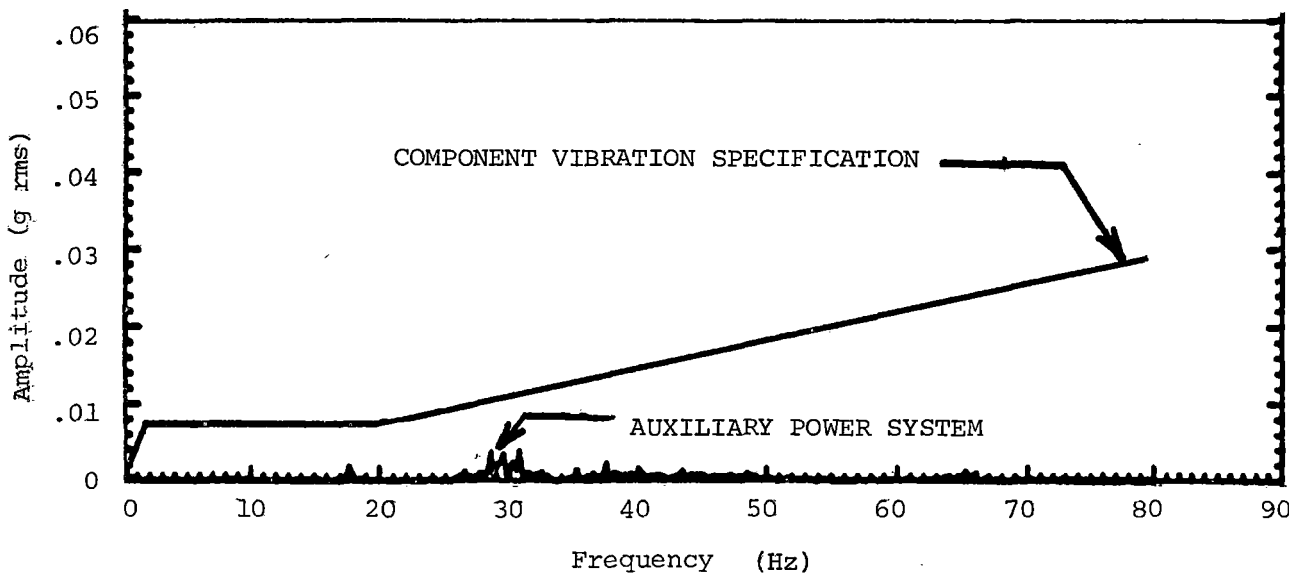


FIGURE 7-4. COMPONENT-INDUCED VIBRATION (VERTICAL) -- MIDFLOOR CENTERLINE

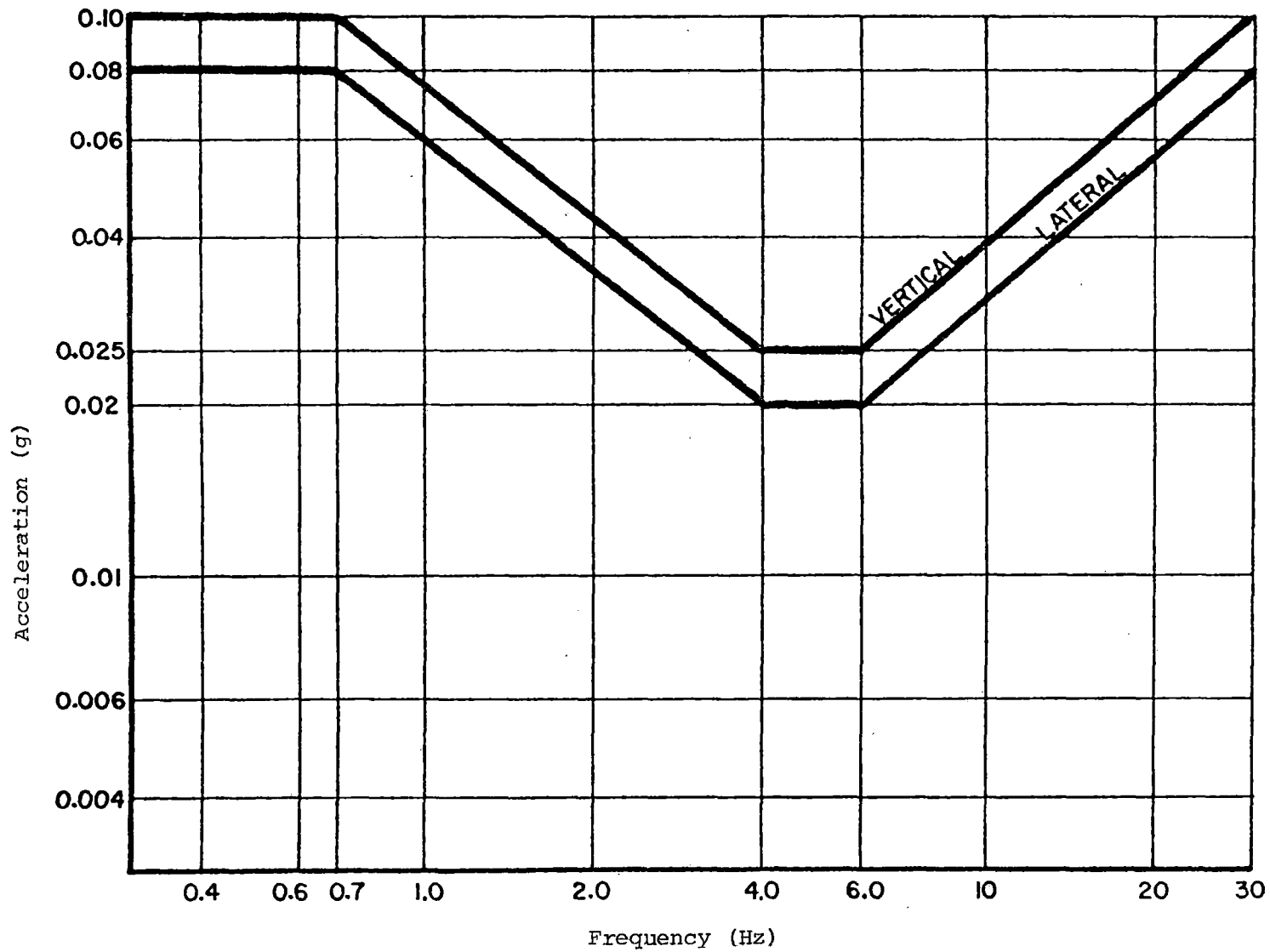


FIGURE 7-5. RIDE QUALITY CRITERIA.

the fundamental wave forms, measured over any five-second interval, by twice the number of fundamental cycles in the interval. The average frequency shall be obtained by dividing the number of cycles by five seconds."

7.2.2 Test Method

Vibration measurements were recorded while the two-car train was operating between stations 30 and 33 with car 0110 leading. All vibration measurements were recorded on car 0110. The train was accelerated to the desired test speed prior to reaching the start of the test zone and was held constant through the test zone.

The train was operated at speeds of 15, 35, 55, and 70 mi/h. Additionally, the train was accelerated at a very slow rate from standstill to 70 mi/h with an on-line recorder to determine the critical speeds at which the vehicle body modes were excited. The track and wheel geometry were used in conjunction with the vehicle shake test results (Section 9.0) shown in figure 7-6 to correlate 'blossoming' of individual sinusoidal frequencies on the chart recorders with vehicle body modes. Additional data were then acquired with the train operating through the test zone at each of the critical speeds identified from the slow acceleration test.

Test data were obtained at the critical speeds for the AW0 weight and R2 suspension configuration. Additional testing was conducted at speeds of 15, 35, 55, and 70 mi/h for vehicle configurations R1 and R2 at the AW3 weight. Testing was conducted with worn wheels of 32.5" diameter. The ride quality retest at the speeds critical to the vehicle modes was conducted with new wheels of 34" diameter. The increased wheel diameter resulted in a 5% increase in critical speed at which the vehicle modes were excited by wheel unbalance or flats, without significantly affecting ride quality levels at the critical speeds. Critical speeds related to track geometry were not affected by wheel diameter.

7.2.3 Test Results

The effects of vehicle speed on ride quality are presented in figures 7-7 through 7-11. Results show that the ride quality acceleration levels were highest when car and track geometry interactions caused perturbations at critical speeds which corresponded to carbody modal frequencies.

Increasing speed had a general tendency to increase the ride quality acceleration levels. The 15 mi/h data were of such low magnitude that they virtually all fell below the scale selected for the data presentation.

The ride quality levels at the vehicle critical speeds of 42, 44, and 52 mi/h exceeded the general increase in levels at the noncritical speeds of 35, 55, and 70 mi/h, as shown at the AW0 weight in figures 7-7 through 7-9. Each carbody mode responded at its maximum when a perturbation frequency corresponded with the resonant frequency of that mode. The AW3 carbody mode frequencies were approximately 84% of the AW0 frequencies.

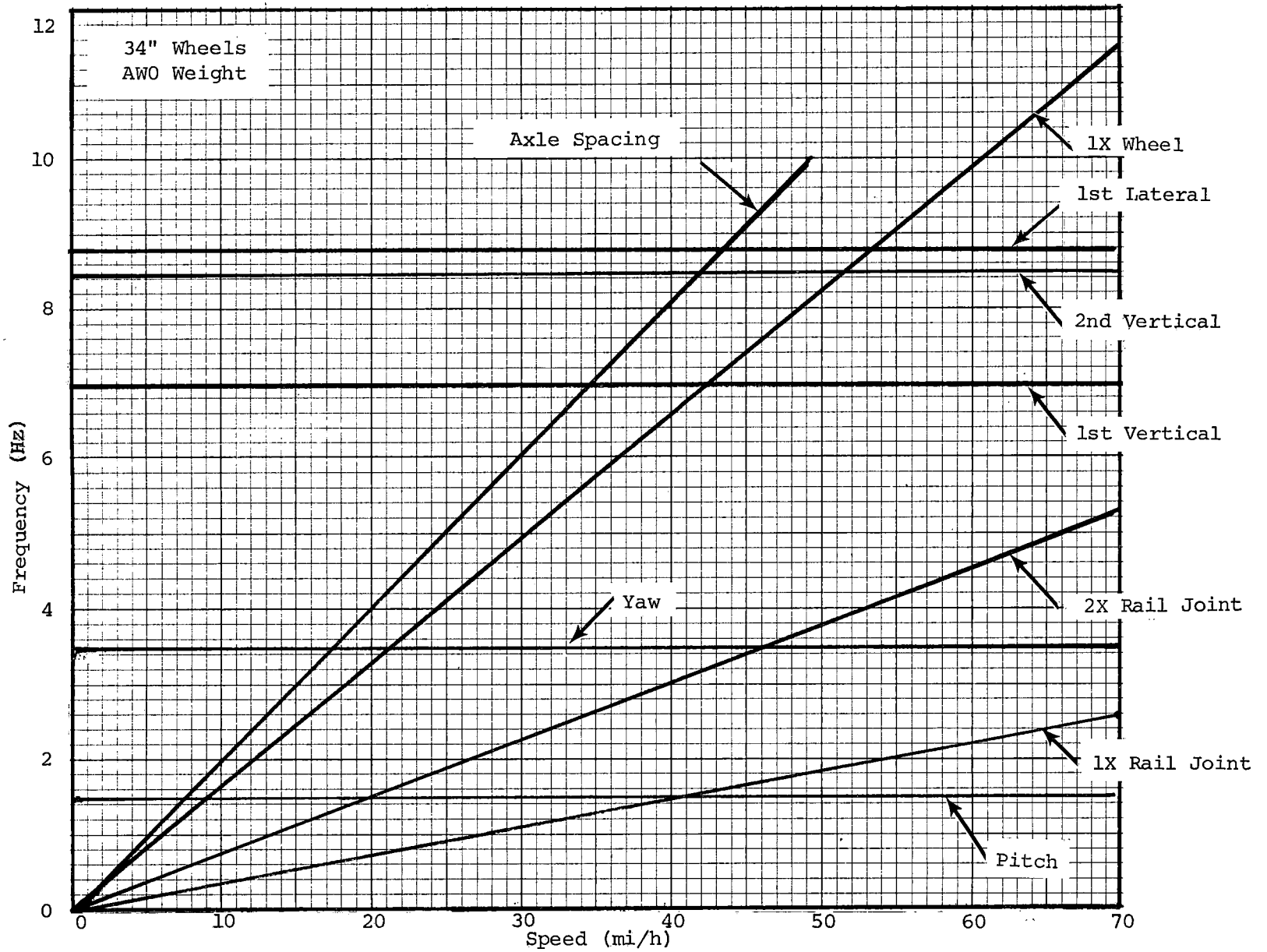


FIGURE 7-6. CARBODY MODE EXCITATION SPECTRUM.

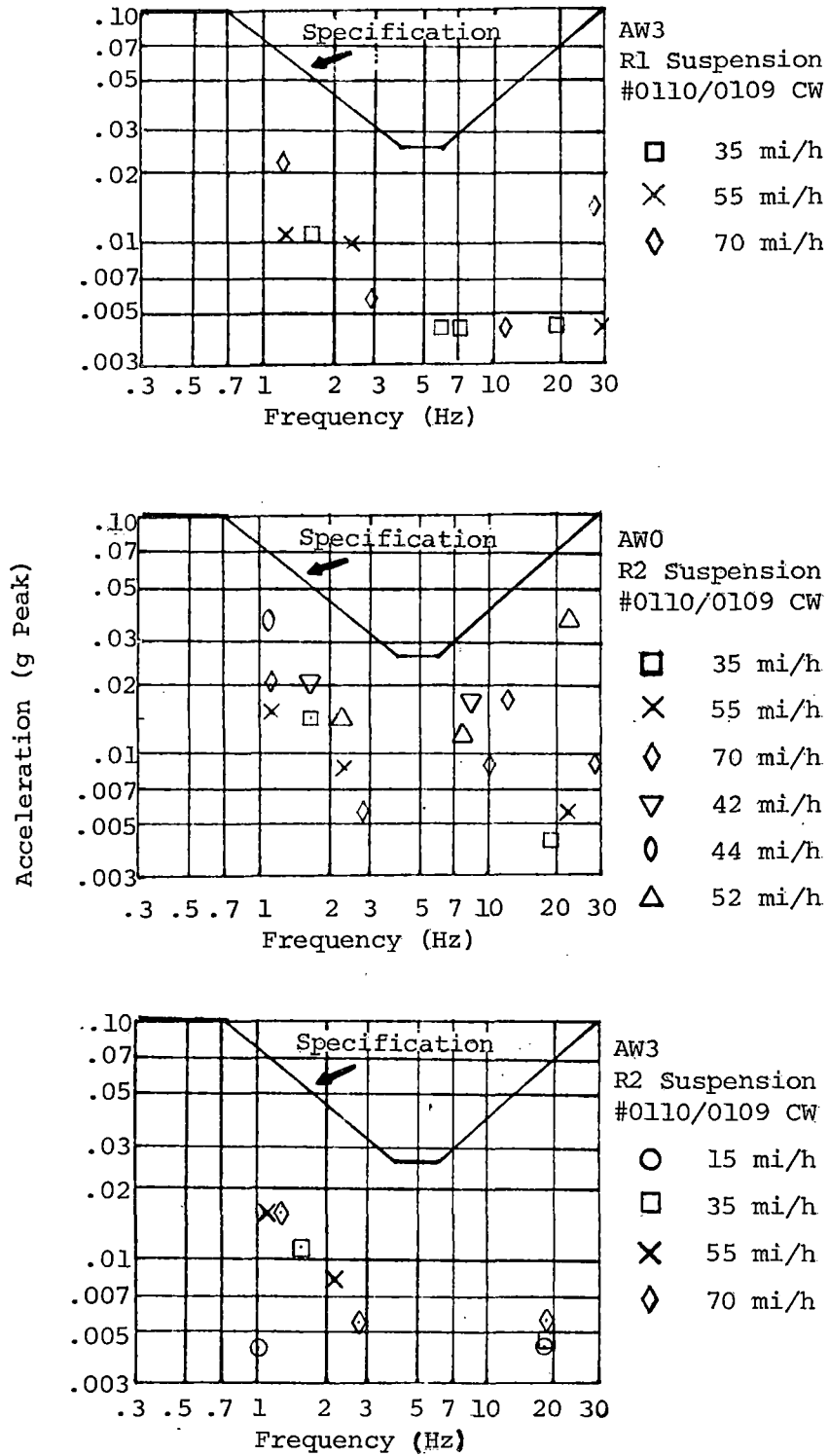


FIGURE 7-7. COMPARISON OF VERTICAL RIDE QUALITY TO VEHICLE SPECIFICATION, FORWARD CAR CENTERLINE.

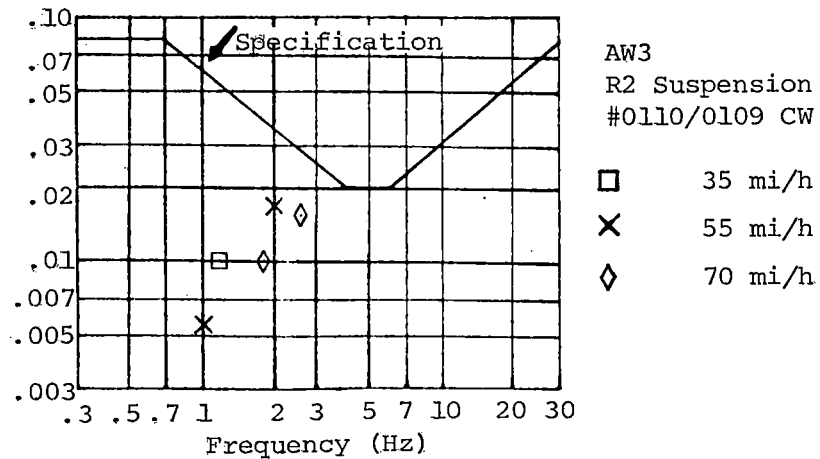
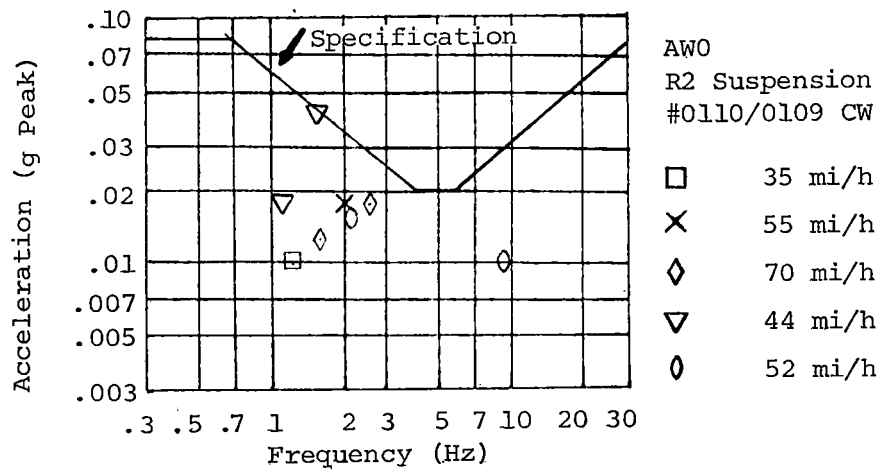
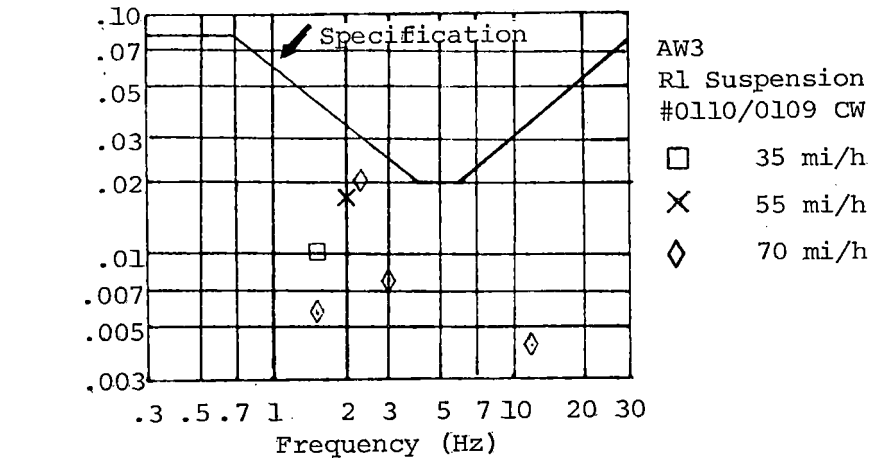


FIGURE 7-8. COMPARISON OF LATERAL RIDE QUALITY TO VEHICLE SPECIFICATION, FORWARD FLOOR CENTERLINE.

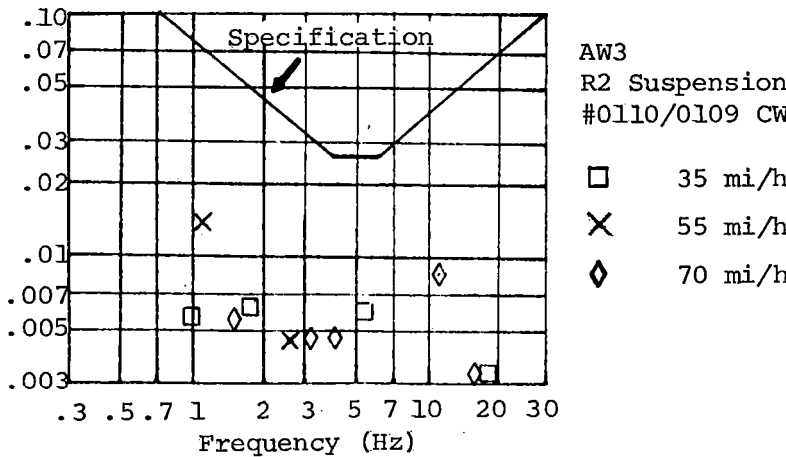
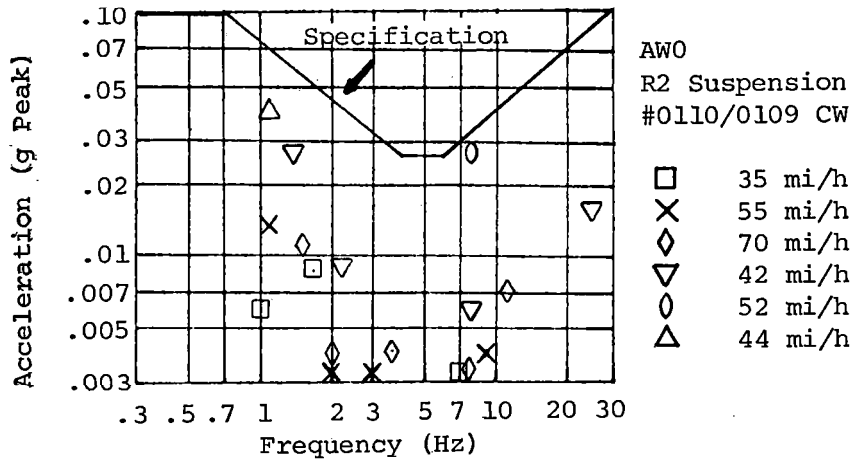
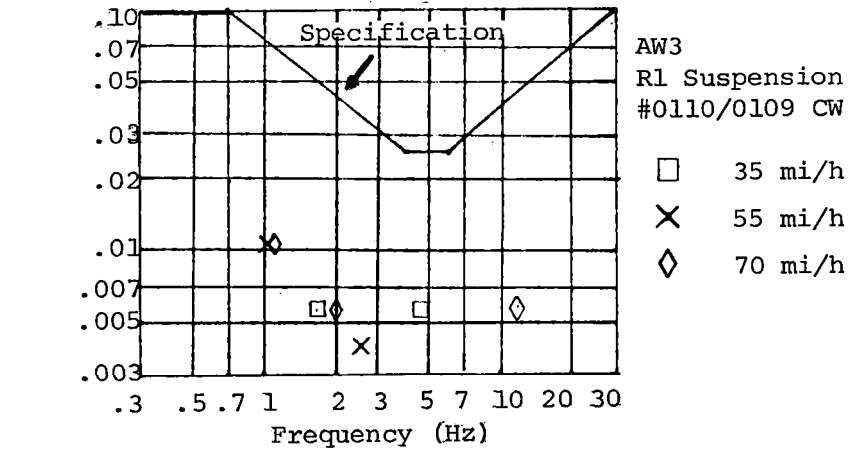


FIGURE 7-9. COMPARISON OF VERTICAL RIDE QUALITY TO VEHICLE SPECIFICATION, MIDFLOOR CENTERLINE.

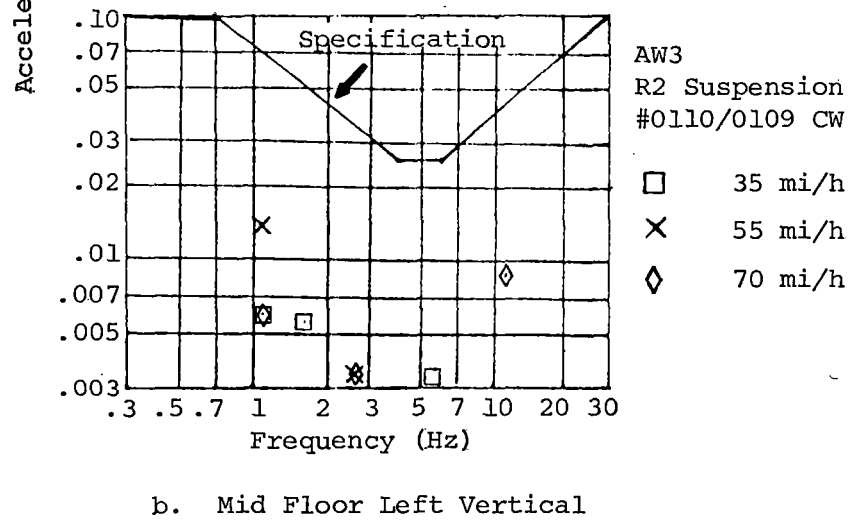
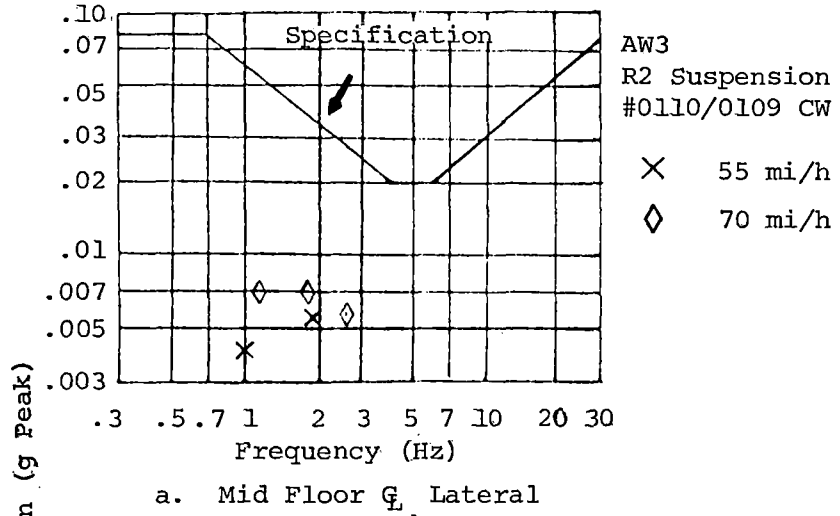
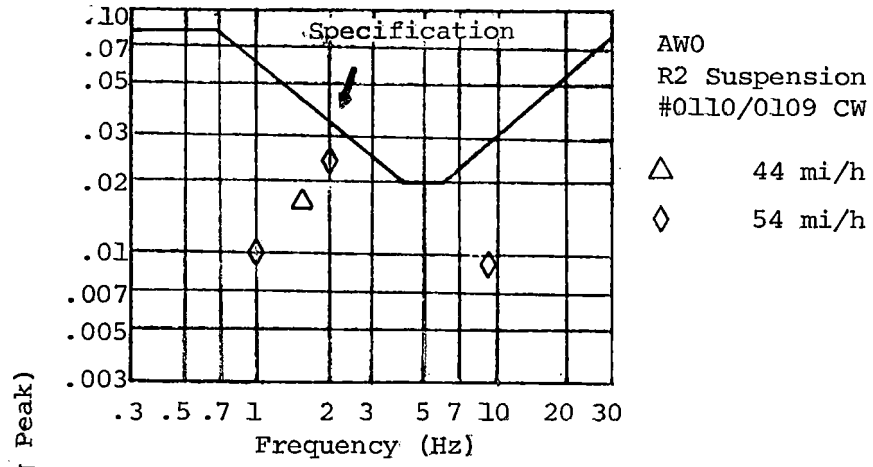
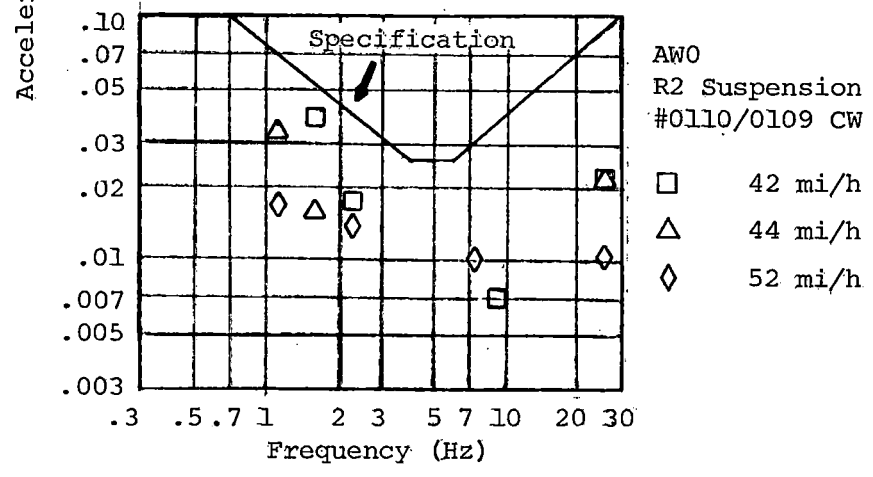


FIGURE 7-10. COMPARISON OF RIDE QUALITY TO SPECIFICATION - SPEED EFFECT.



a. Rear Floor C_L Lateral



b. Rear Floor C_L Vertical

FIGURE 7-11. COMPARISON OF RIDE QUALITY TO SPECIFICATION - SPEED EFFECT.

Fair correlation was obtained between the single car shake test modal frequencies and the modal frequencies of the two-car trains as identified from the slow acceleration speed sweep on the track. The single car and two-car train modal frequencies are compared in table 7-2.

The results of the slow acceleration speed sweep revealed that each body mode was excited at more than one discrete speed. In many cases, closely coupled modes would both be excited by a discrete speed. The critical test speeds were selected by reviewing the recorder charts to determine the speeds which resulted in the greatest response for each mode. In some cases, a speed change as small as 2 mi/h would separate peak responses of closely coupled modes.

The frequency-weighted rms acceleration ride roughness data presented in figures 7-12 and 7-13 also show a general increase in ride roughness with increase in noncritical speed. The ride roughness at the critical body mode speeds significantly exceeded the noncritical speed data, as shown for the AW0 weight configuration in figure 7-12, with differences of up to 0.02 g rms.

7.3 TRACK SECTION EFFECT

7.3.1 Test Objective

The objective was to determine the maximum vibration levels encountered during vehicle operation through the seven test sections on the TTT. The track rail and tie configuration for each track section were shown in figure 4-1. Track section VII, as defined for ride quality testing, is that portion of section I (from station 51 to station 5) where the spurs from the Urban Rail Building join the main TTT.

7.3.2 Test Method

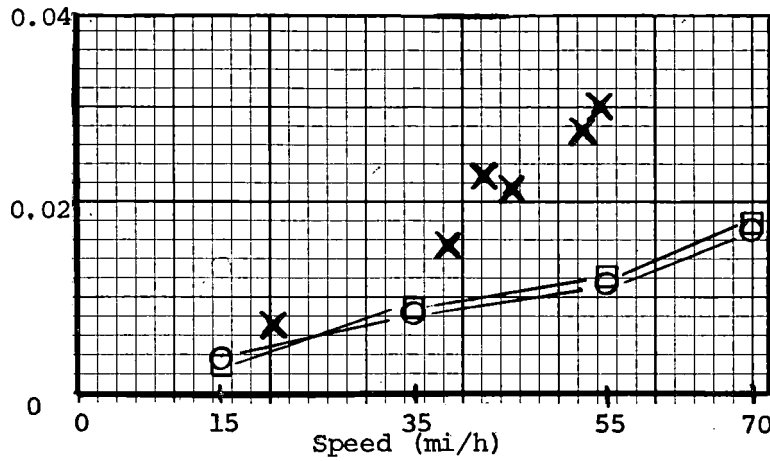
Vibration measurements were recorded while the two-car train was operating in a clockwise direction at 35 mi/h with car 0110 leading. All vibration measurements were recorded on car 0110. Test data were recorded for three vehicle configurations: AW0/R2, AW3/R1, and AW3/R2.

7.3.3 Test Results

The effect of track section construction on ride quality shown in figures 7-14 through 7-17 indicates body modal amplitude variations of up to 10:1 in the vertical direction through the various track sections with the midfloor left vertical acceleration varying from 0.0035 to 0.035 g peak at 7 Hz. The variation is greater in the vertical direction than it is in the lateral direction. Track sections II and VI exceeded the ride quality specification at the midcar vertical location for the AW3 weight configuration by approximately 0.01 g at the vertical bending mode (7 Hz), as shown in figures 7-16 and 7-17.

TABLE 7-2. CARBODY MODAL FREQUENCIES, AWO WEIGHT.

Mode	Shake Test, Single Car (Hz)	Track Sweep, Two-car Train (Hz)
Rigid Body Vertical	Not identified	1.1
Rigid Body Pitch	1.5	1.65
Rigid Body Yaw	3.5	1.95
1st Vertical	7.0	7.4
2nd Vertical	8.5	8.0
1st Lateral	8.75	8.7



R2 Suspension
#0110/0109 CW

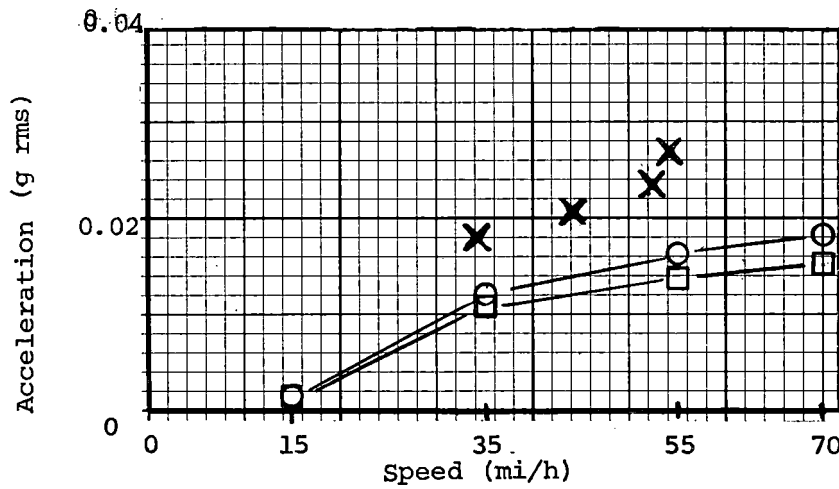
Weight

○ - AW0

□ - AW3

× - AW0
Critical Speeds

a. Forward Floor C_L Vertical



R2 Suspension
#0110/0109 CW

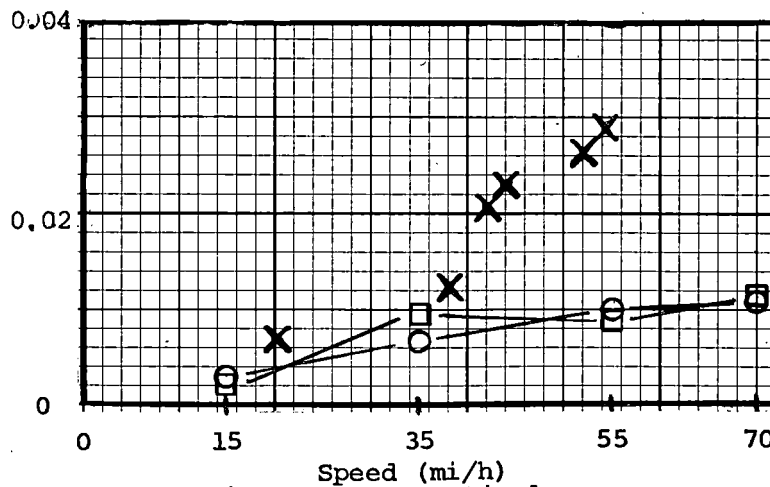
Weight

○ - AW0

□ - AW3

× - AW0
Critical Speeds

b. Forward Floor C_L Lateral



R2 Suspension
#0110/0109 CW

Weight

○ - AW0

□ - AW3

× - AW0
Critical Speeds

c. Mid Floor C_L Vertical

FIGURE 7-12. EFFECT OF VEHICLE SPEED ON RIDE ROUGHNESS.

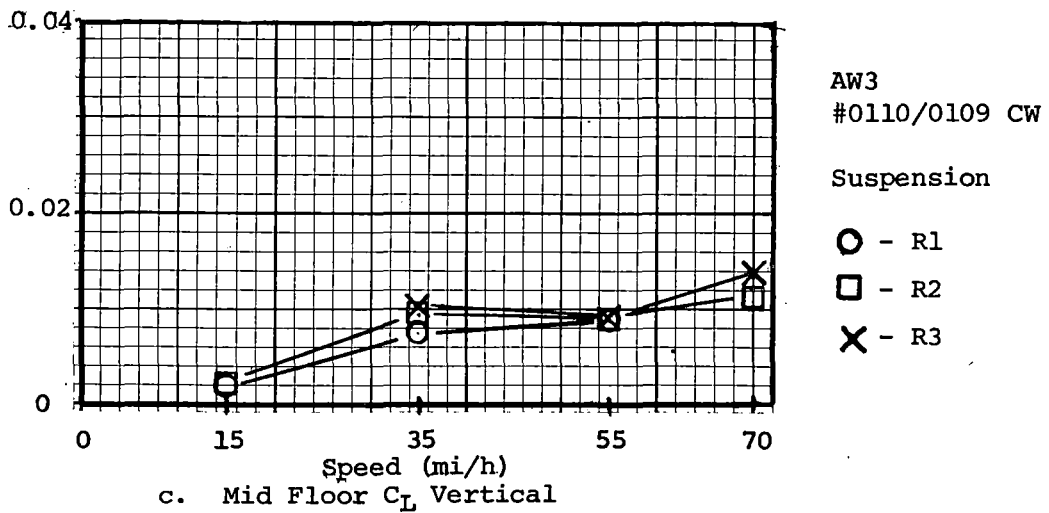
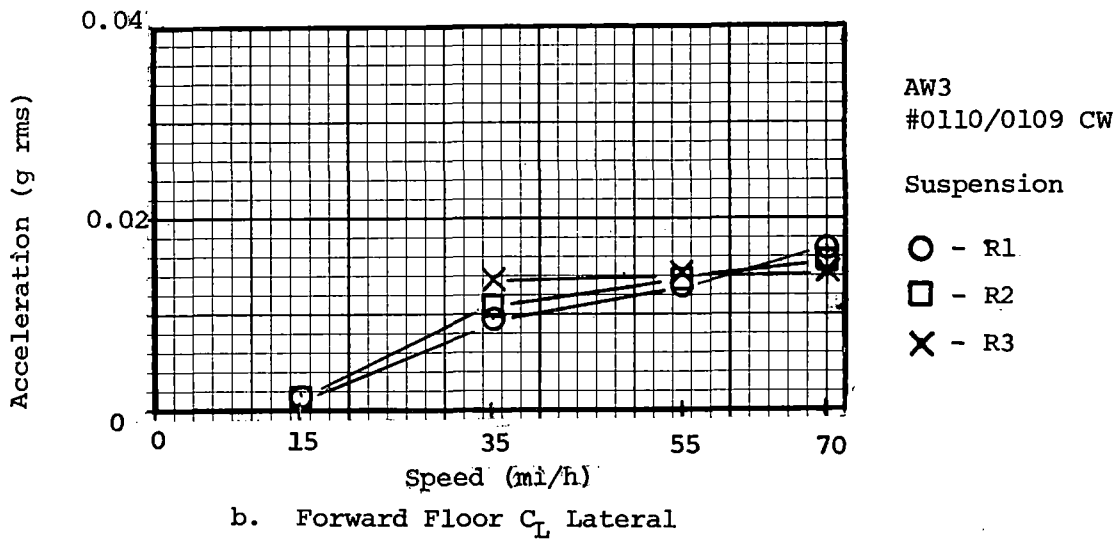
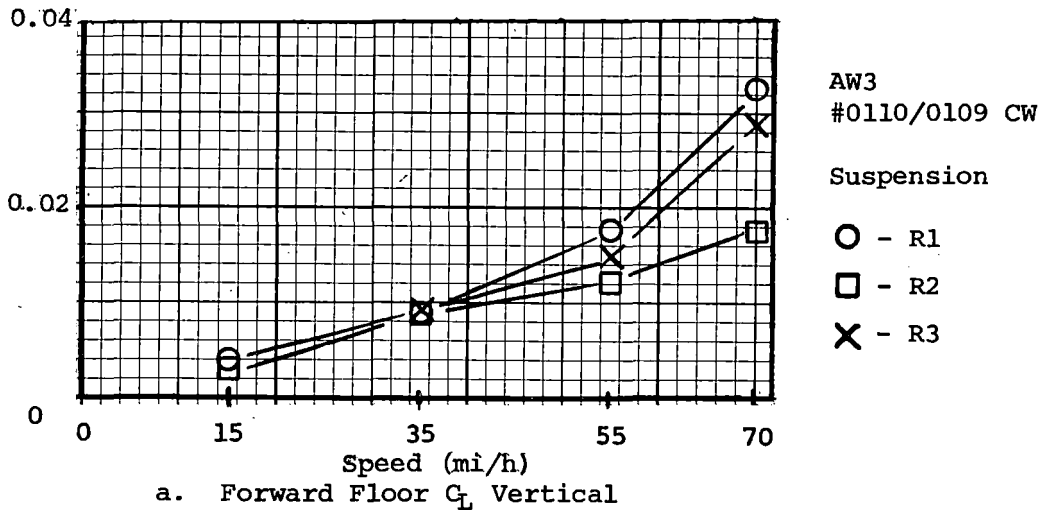


FIGURE 7-13. EFFECT OF VEHICLE SPEED ON RIDE ROUGHNESS.

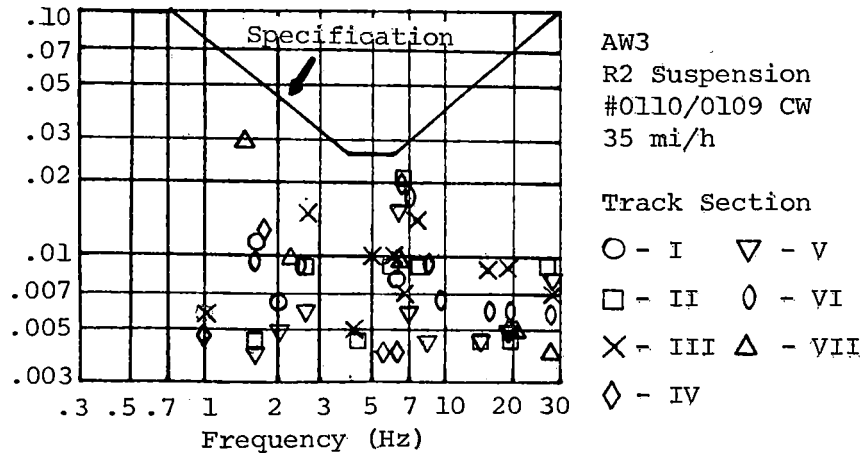
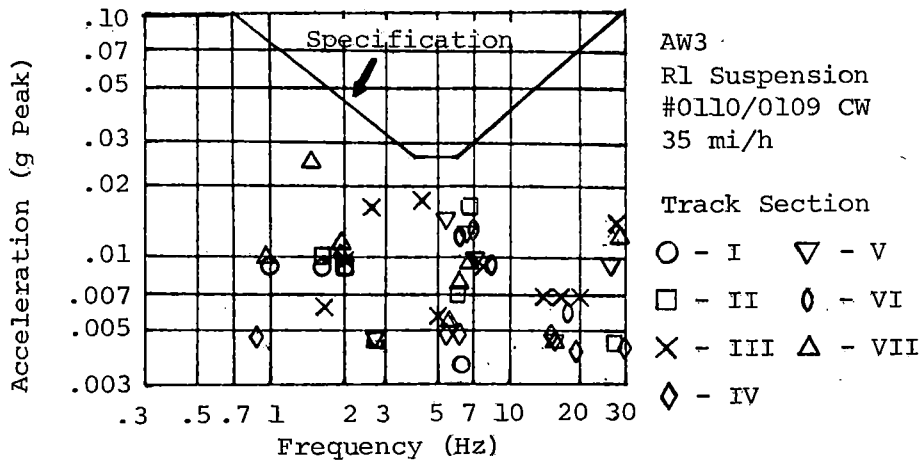
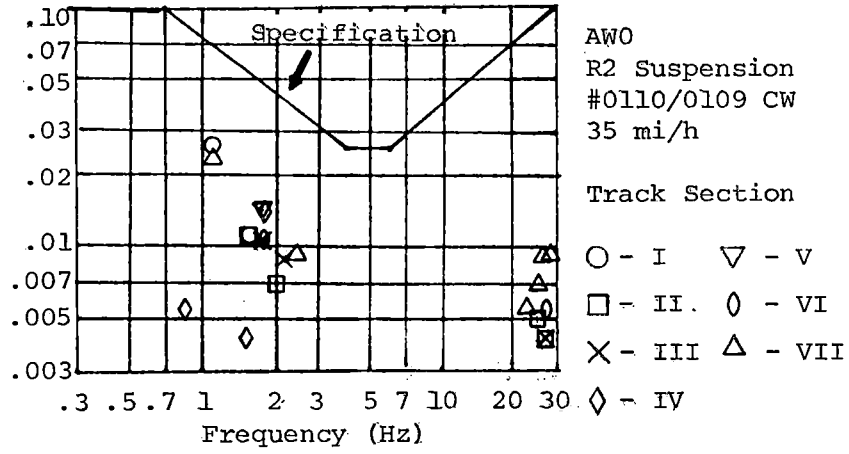


FIGURE 7-14. COMPARISON OF VERTICAL RIDE QUALITY TO VEHICLE SPECIFICATION - TRACK SECTION EFFECT, FORWARD FLOOR CENTERLINE.

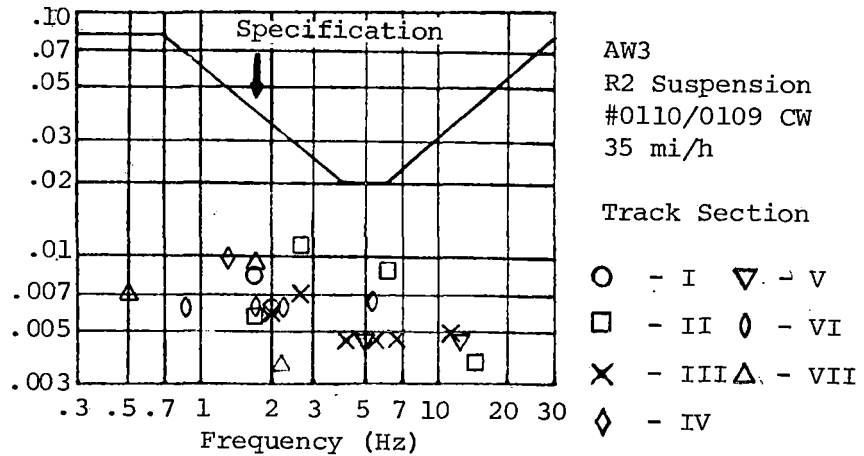
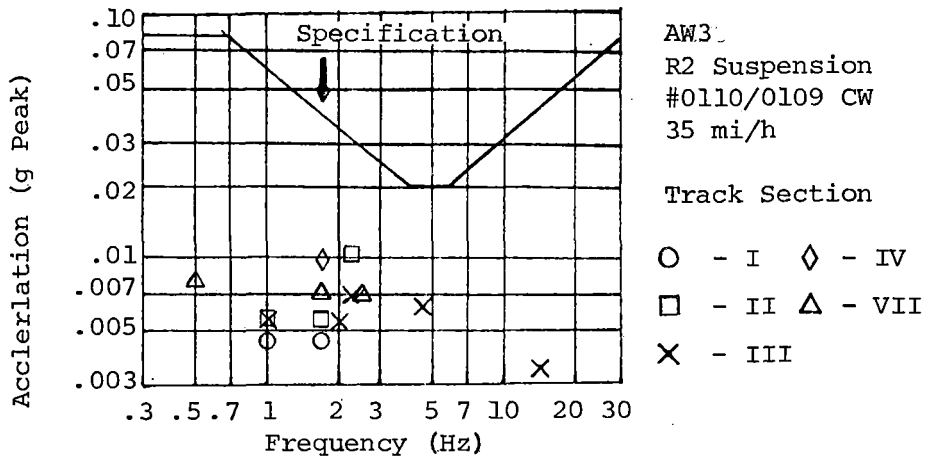
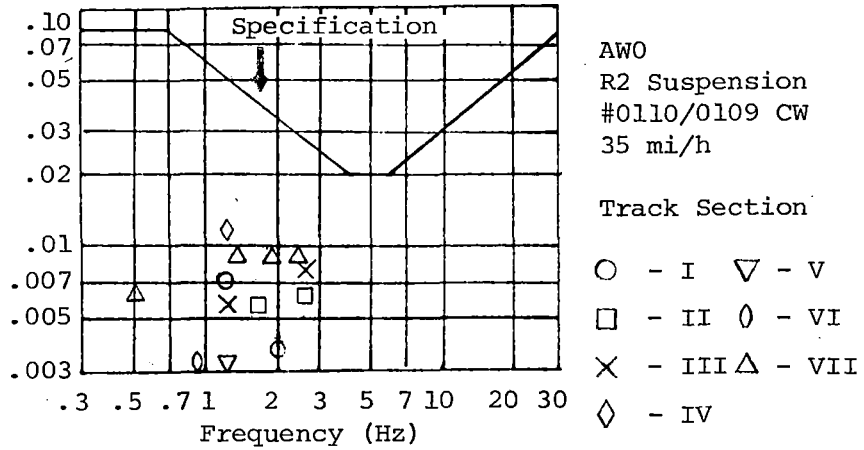


FIGURE 7-15. COMPARISON OF LATERAL RIDE QUALITY TO VEHICLE SPECIFICATION - TRACK SECTION EFFECT, FORWARD FLOOR CENTERLINE.

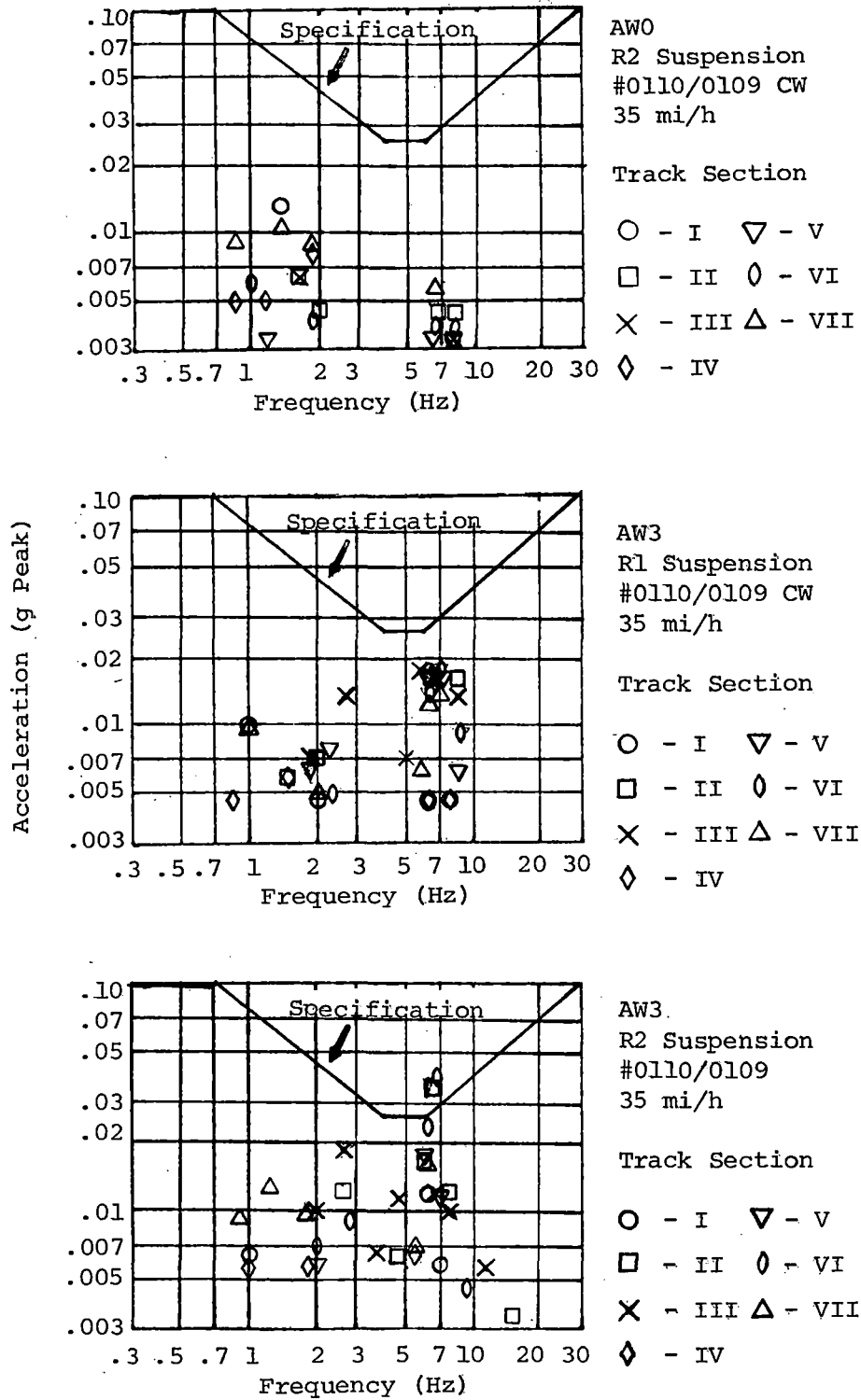
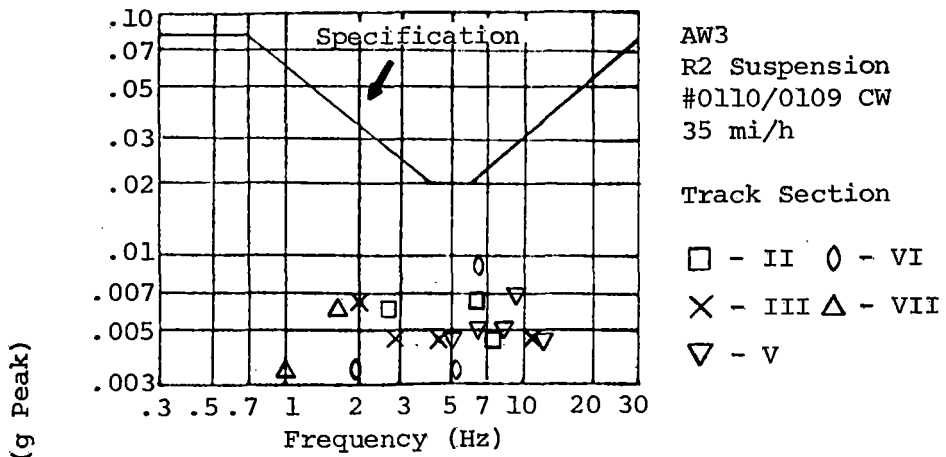
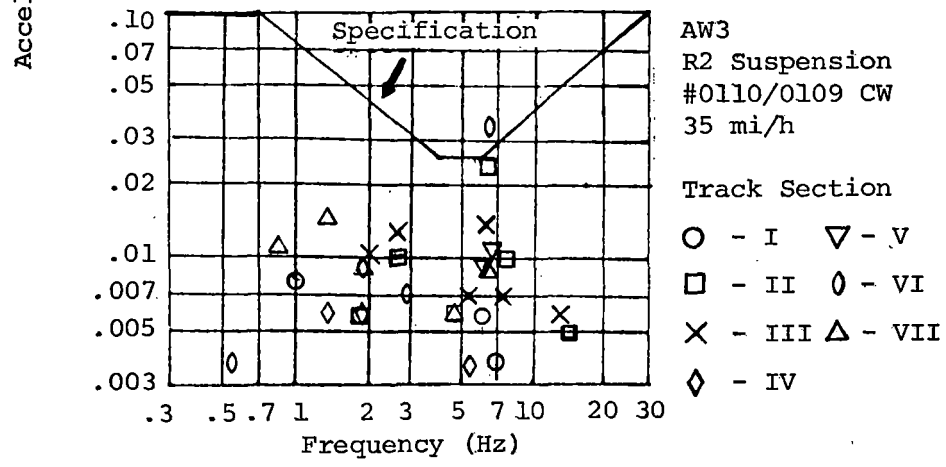


FIGURE 7-16. COMPARISON OF VERTICAL RIDE QUALITY TO VEHICLE SPECIFICATION - TRACK SECTION EFFECT, MIDFLOOR CENTERLINE.



a. Mid Floor G_L Lateral



b. Mid Floor Left Vertical

FIGURE 7-17. COMPARISON OF RIDE QUALITY TO VEHICLE SPECIFICATION - TRACK SECTION EFFECT.

It is significant to note on figures 7-14 and 7-16 that the AW0 weight configuration data in the 5 to 10 Hz frequency band show excellent isolation of the carbody on the suspension system at the carbody 1st and 2nd vertical bending frequencies of 7.4 and 8.0 Hz. Conversely, the equivalent AW3 weight data on figures 7-14 and 7-16 show that the carbody 1st and 2nd vertical bending modes of 6.2 and 6.8 Hz were being excited to levels which approached or exceeded the specification requirements. At the AW3 weight configuration, the carbody rolled over and the bolster/truck vertical stops came in contact when the car went around a curve, grounding out the secondary suspension system. Therefore, for the AW3 weight, the carbody vertical bending modes were excited to greater amplitudes by wheel and track perturbations through the grounded bolster.

The problem of grounding the vertical stops due to carbody roll when entering a curve or when exiting from a curve was investigated by a special test conducted between stations 26 and 30. Results of this test (figure 7-18) show that when the car operated from tangent to superelevated track, it rolled to the inside when entering the curve and grounded the bolster on the downstop. Conversely, when the car was parked on a curved section of track (4" superelevation), the air springs gradually adjusted the carbody such that the bolsters were level with the trucks. If the car was then accelerated around the curve, it remained level until it entered the straight section of track (no superelevation) at which time it rolled toward the outside until the bolster contacted the upstop (figure 7-18). The test data shown in figure 7-18 were recorded on the forward truck of car 0110 while in transition from tangent level to 4" superelevated curved track or vice-versa. The car was in the AW2 weight configuration.

The frequency-weighted rms acceleration ride-roughness data presented in figures 7-19 and 7-20 also show the significant increase in vertical ride roughness at AW3 through the curved sections of track from 0.01 g in Section IV to 0.039 g in Section VI. The suspension system centered the bolster on level sections of track even at the AW3 weight configuration and provided carbody isolation.

Grounding of the vertical stops while operating through a curved section of track did not have a significant effect on the lateral ride quality or ride roughness (as shown by the nearly constant amplitude of 0.01 g through all sections in figures 7-19 and 7-20).

Summarizing, we conclude that the vehicle had inadequate roll stiffness, or inadequate leveling valve response, to prevent the bolsters from contacting the downstops or upstops when entering or exiting superelevated track. The grounding of the bolster had a significant effect on the ride quality due to the increase in vertical acceleration levels transmitted to the carbody structure.

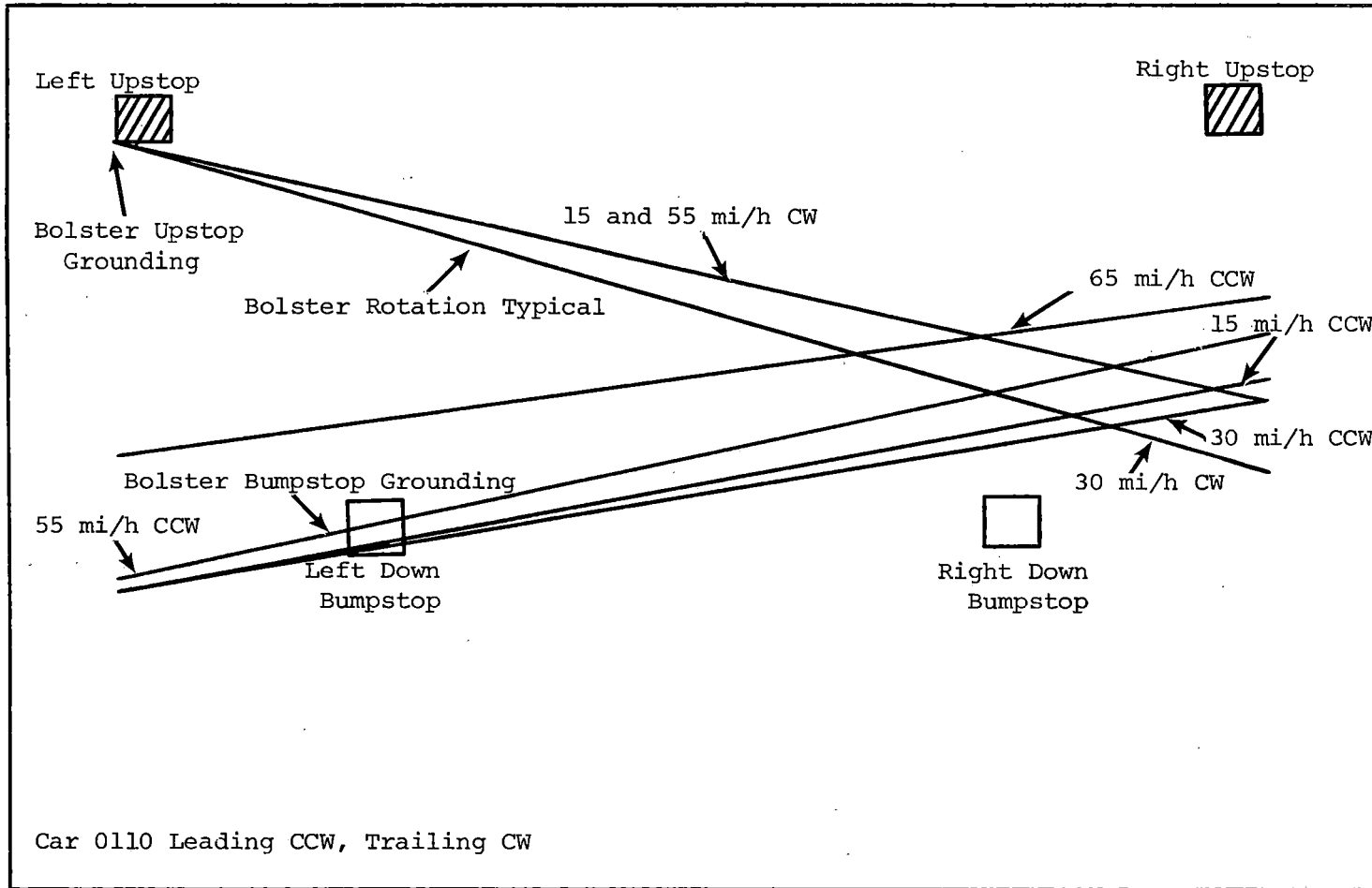
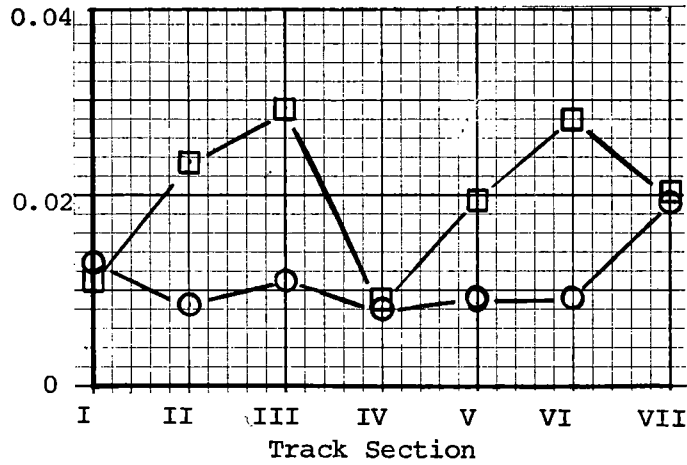
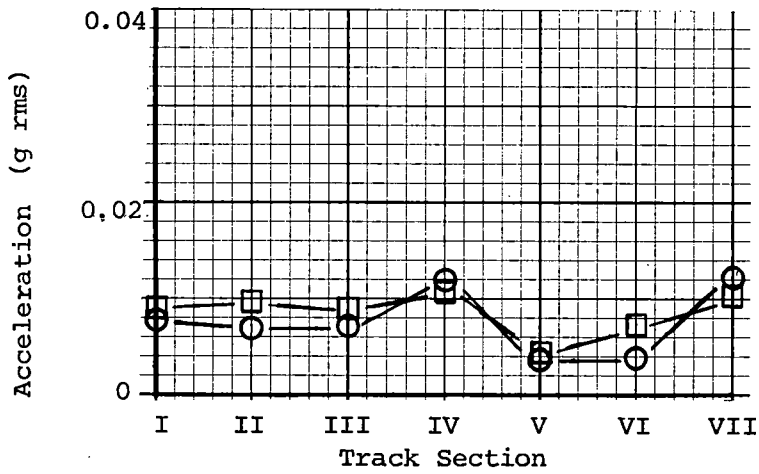


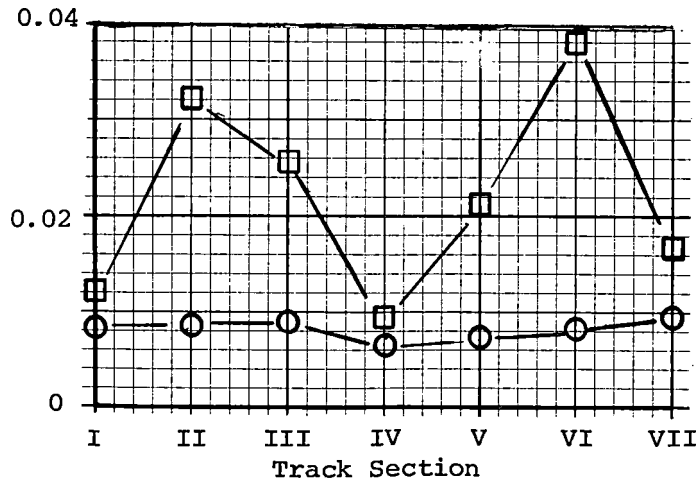
FIGURE 7-18. LEAD TRUCK BOLSTER GROUNDING.



a. Forward Floor ζ_L Vertical

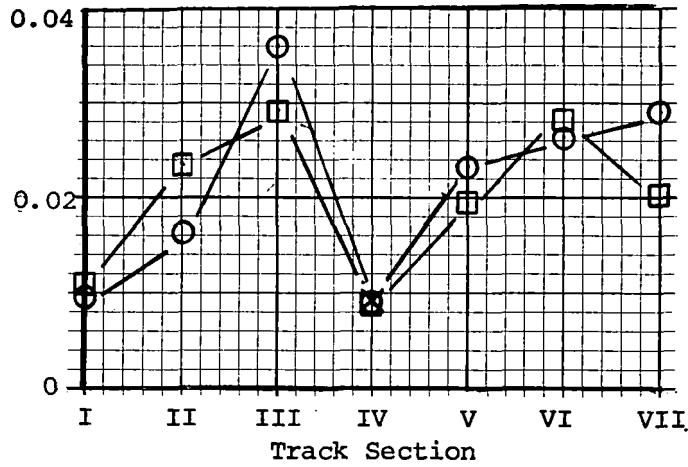


b. Forward Floor ζ_L Lateral

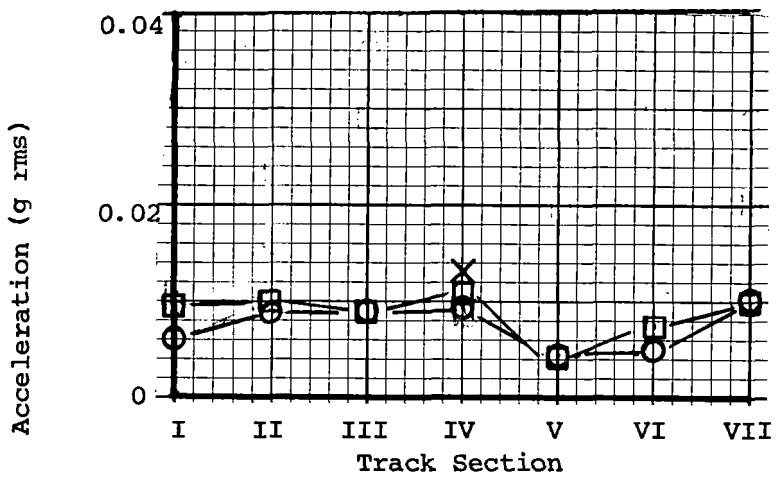


c. Mid Floor ζ_L Vertical

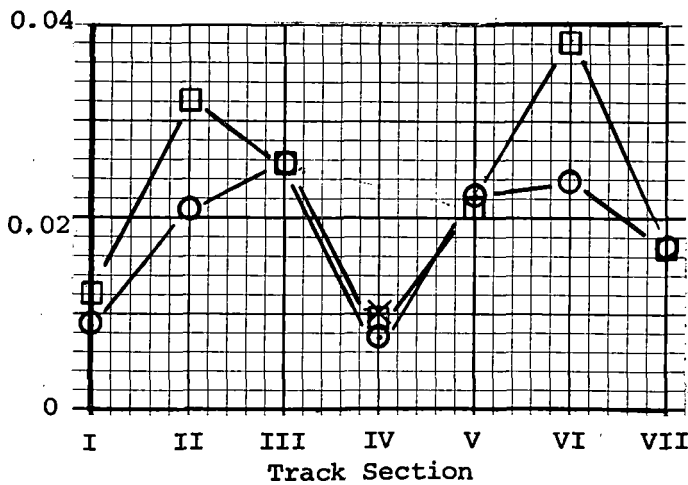
FIGURE 7-19. EFFECT OF TRACK SECTION ON RIDE ROUGHNESS.



a. Forward Floor C_L Vertical



b. Forward Floor C_L Lateral



c. Mid Floor C_L Vertical

FIGURE 7-20. EFFECT OF TRACK SECTION ON RIDE ROUGHNESS.

7.4 CAR WEIGHT EFFECT

7.4.1 Test Objective

The objective was to determine the effect of car weight on the ride quality vibration levels. Test results will be compared with the specification requirements, detailed in figure 7-5.

7.4.2 Test Method

Vibration measurements were recorded while the two-car train was operating at constant speeds between stations 30 and 33 with car 0110 leading. All vibration measurements were recorded on car 0110. The train was accelerated to the desired test speed prior to reaching the start of the test zone and was held constant through the test zone.

The train was operated at speeds of 15, 35, 55, and 70 mi/h. Test data were obtained with the R2 suspension system. Vibration measurements were also recorded while operating the two-car train clockwise around the TTT at 35 mi/h with car 0110 leading.

7.4.3 Test Results

The results showing the effect of the vehicle weight on ride quality (figures 7-21 through 7-24) show that there was no significant weight effect on ride quality. However, these data are presented for operation on straight track only; weight did have a significant effect in curves (paragraph 7.3.3).

The frequency-weighted rms acceleration ride roughness data (figures 7-25 and 7-26) also show that vehicle weight had no significant effect on ride quality on tangent track, but had a significant effect on vertical acceleration through curved sections. Vehicle weight had no noticeable effect on lateral ride roughness.

7.5 SUSPENSION EFFECT

7.5.1 Test Objectives

The objectives were to evaluate the effect of three configurations of vertical damping of the secondary suspension system, which were:

- Vertical damping provided by two hydraulic shock absorbers (identified as the R1 configuration).
- A second suspension configuration, identified as R2, which consisted of removing the hydraulic shock absorbers and providing air damping (by restricting the venturi in the air spring system).

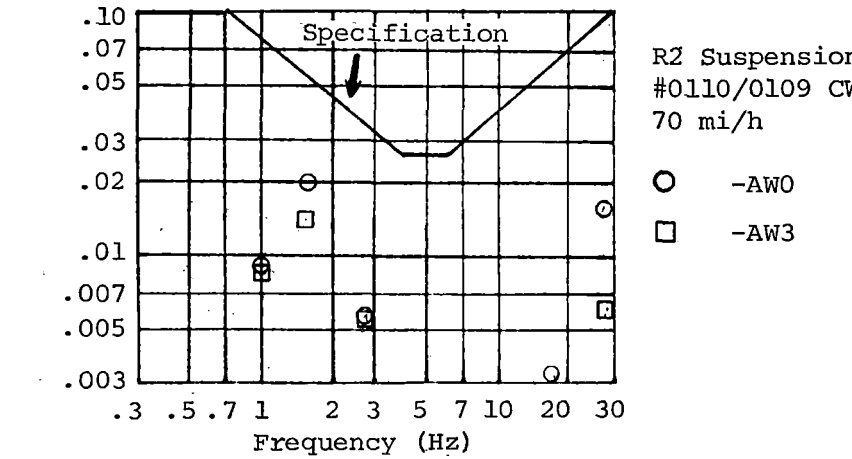
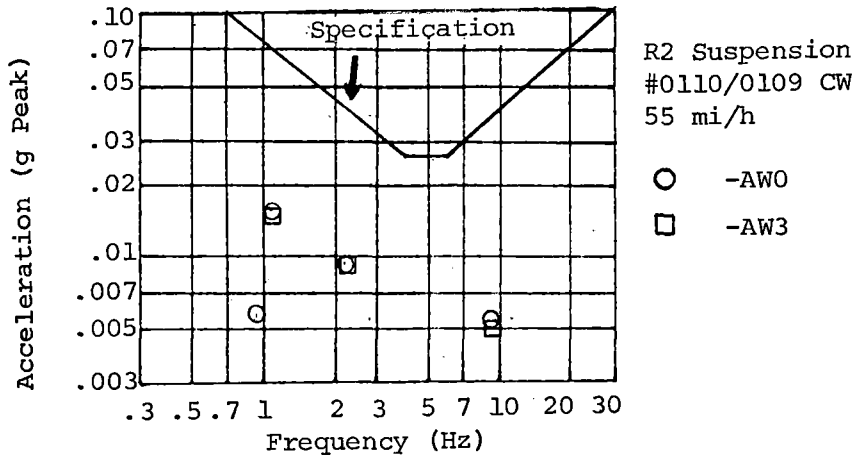
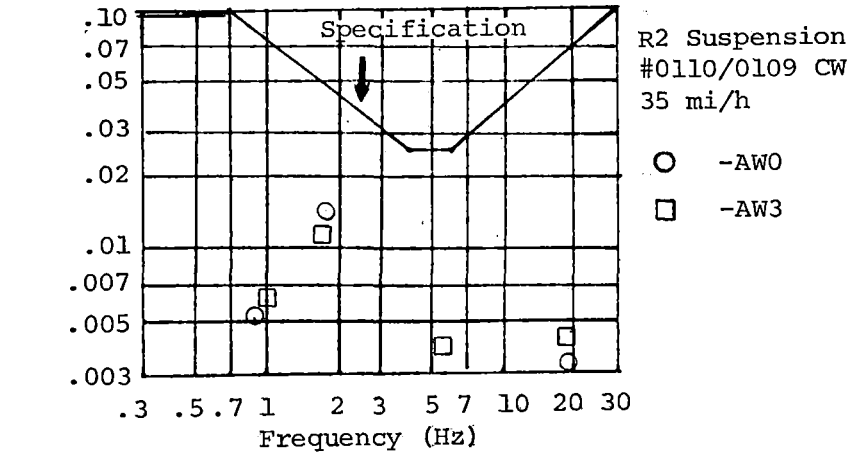


FIGURE 7-21. COMPARISON OF VERTICAL RIDE QUALITY TO VEHICLE SPECIFICATION - WEIGHT EFFECT, FORWARD FLOOR CENTERLINE.

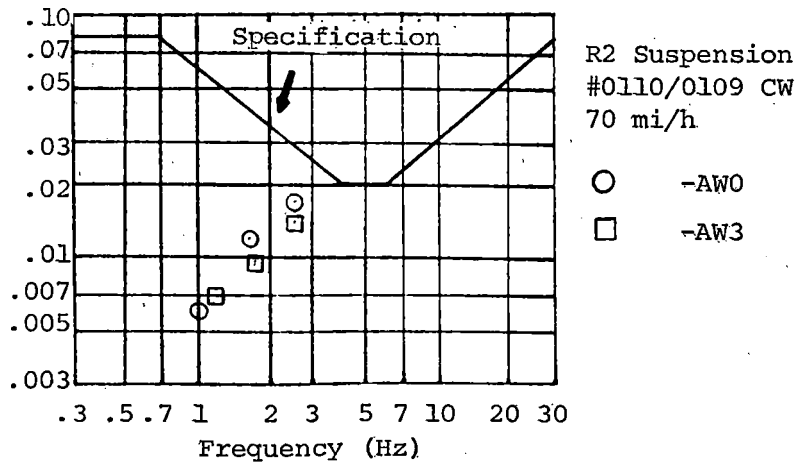
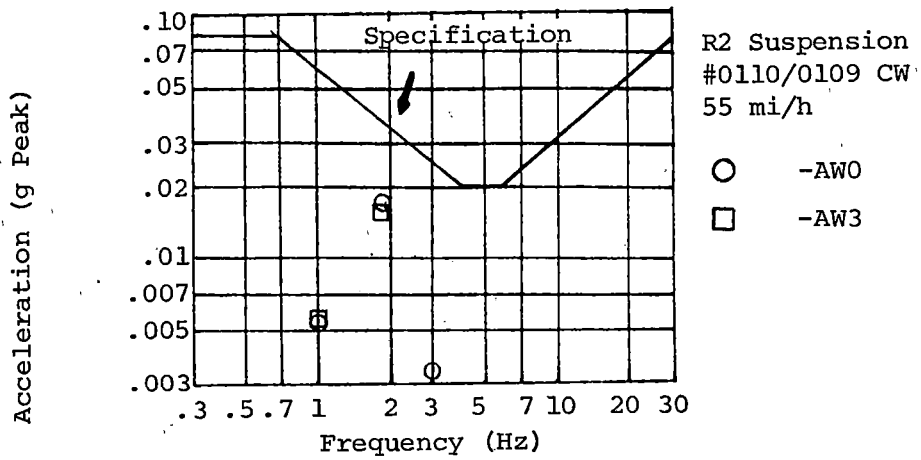
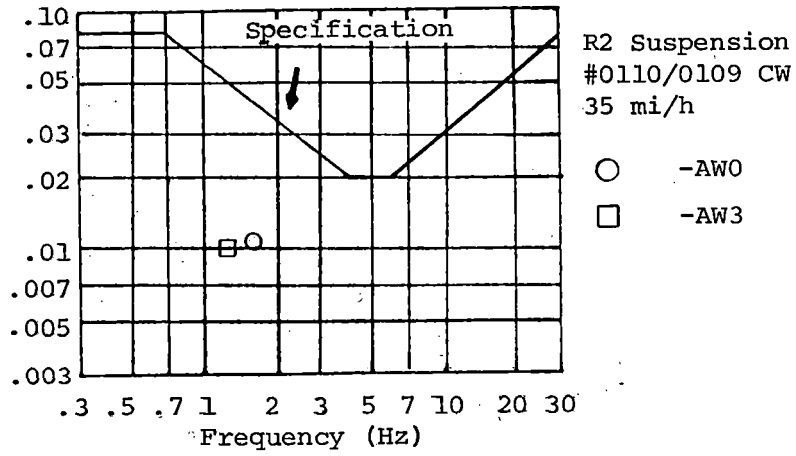


FIGURE 7-22. COMPARISON OF LATERAL RIDE QUALITY TO VEHICLE SPECIFICATION - WEIGHT EFFECT, FORWARD FLOOR CENTERLINE.

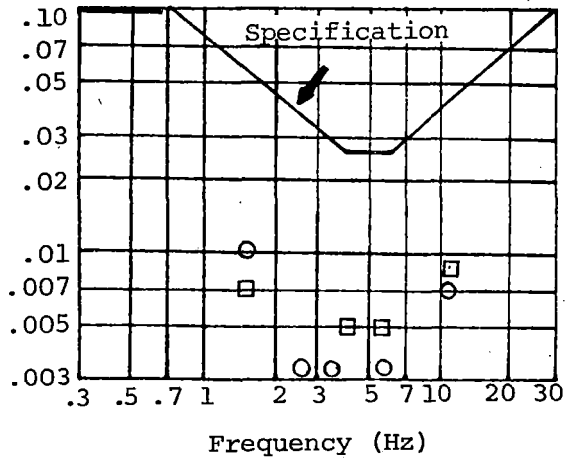
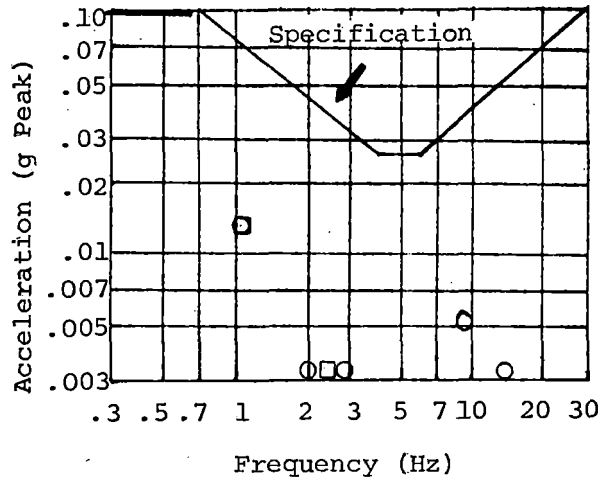
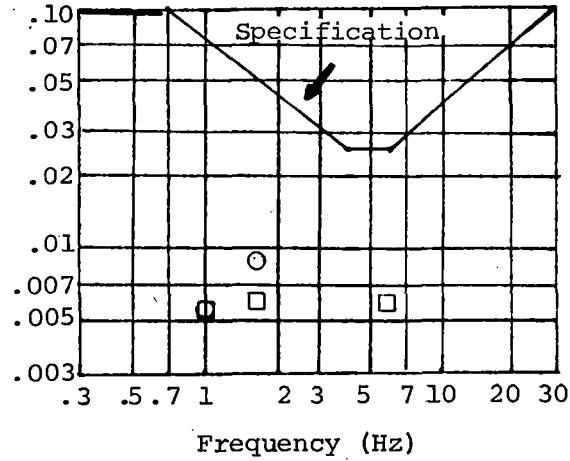
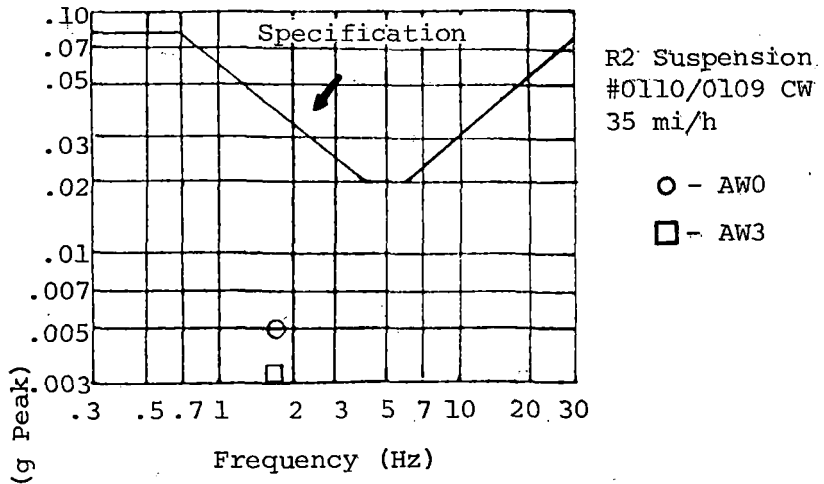
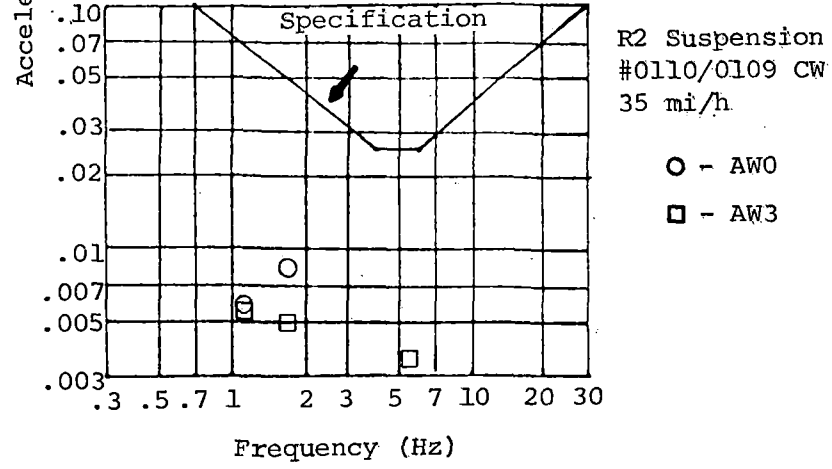


FIGURE 7-23. RIDE QUALITY TO SPECIFICATION COMPARISON (VERTICAL) WEIGHT EFFECT, MIDFLOOR CENTERLINE.



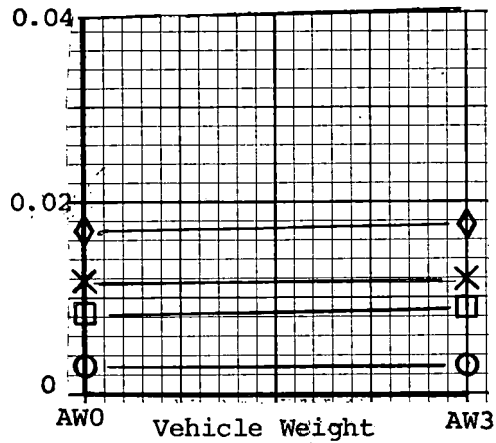
a. Mid Floor Lateral



b. Mid Floor Left Vertical

FIGURE 7-24. RIDE QUALITY SPECIFICATION COMPARISON - WEIGHT EFFECT.

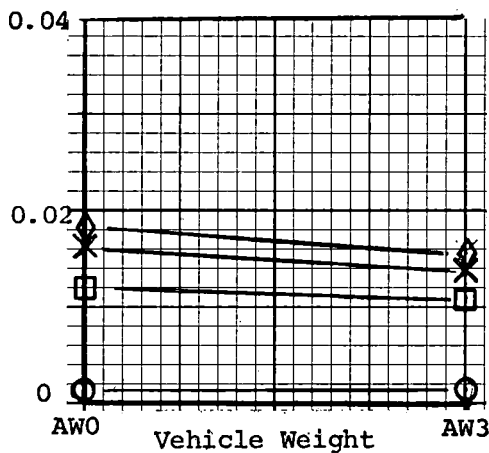
Acceleration (g rms)



R2 Suspension
#0110/0109 CW

- - 15 mi/h
- - 35 mi/h
- × - 55 mi/h
- ◇ - 70 mi/h

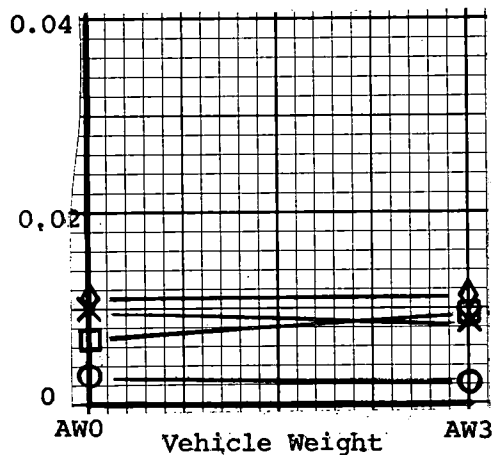
a. Forward Floor C_L Vertical



R2 Suspension
#0110/0109 CW

- - 15 mi/h
- - 35 mi/h
- × - 55 mi/h
- ◇ - 70 mi/h

b. Forward Floor C_L Lateral

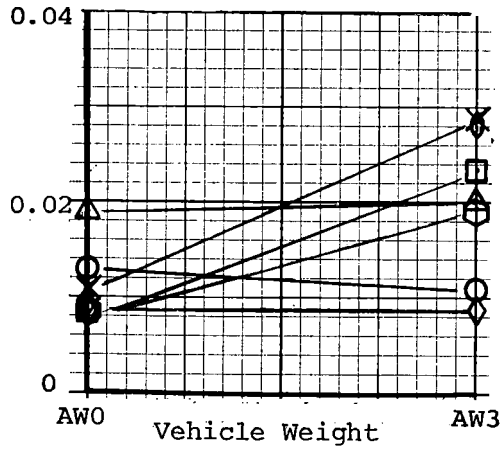


R2 Suspension
#0110/0109 CW

- - 15 mi/h
- - 35 mi/h
- × - 55 mi/h
- ◇ - 70 mi/h

c. Mid Floor C_L Vertical

FIGURE 7-25. EFFECT OF VEHICLE WEIGHT ON RIDE ROUGHNESS.

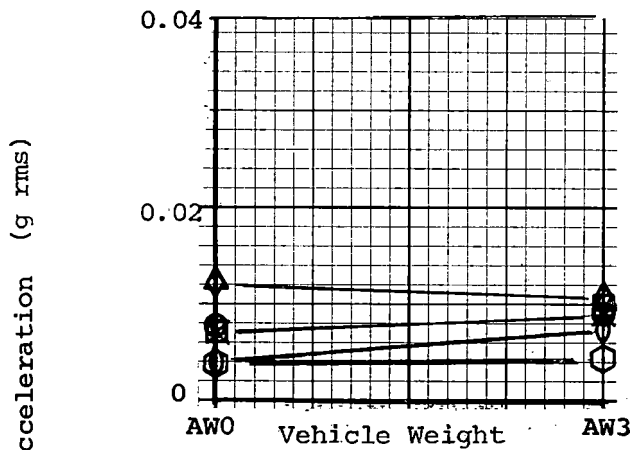


R2 Suspension
#0110/0109 CW
35 mi/h

Track Section

- - I ⬡ - V
- - II ◊ - VI
- × - III △ - VII
- ◇ - IV

a. Forward Floor Q_L Vertical

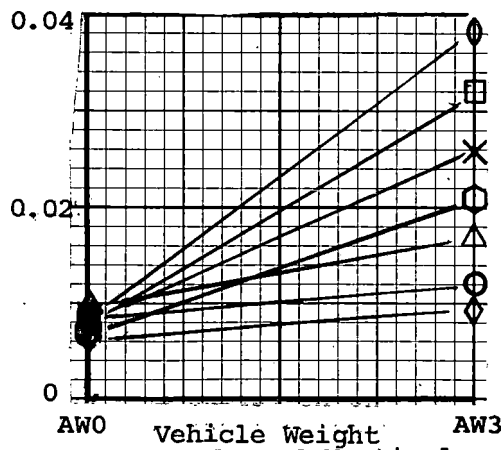


R2 Suspension
#0110/0109 CW
35 mi/h

Track Section

- - I ⬡ - V
- - II ◊ - VI
- × - III △ - VII
- ◇ - IV

b. Forward Floor Q_L Lateral



R2 Suspension
#0110/0109 CW
35 mi/h

Track Section

- - I ⬡ - V
- - II ◊ - VI
- × - III △ - VII
- ◇ - IV

c. Mid Floor Q_L Vertical

FIGURE 7-26. EFFECT OF VEHICLE WEIGHT ON RIDE ROUGHNESS.

- A third suspension configuration, identified as R3, which consisted of combining the hydraulic shock absorbers of configuration R1 with the air damping of configuration R2.

7.5.2 Test Method

Vibration measurements were recorded while the two-car train was operating between stations 30 and 33 with car 0110 leading. All vibration measurements were recorded on car 0110. The train was accelerated to the desired test speed prior to reaching the start of the test zone and was held constant through the test zone.

Constant test speeds of 15, 35, 55, and 70 mi/h were selected for each of the three suspension configurations. Vibration measurements were also recorded while operating the two-car train around the TTT at 35 mi/h in a clockwise direction with car 0110 leading. Data were obtained for AW0 and AW3 weight conditions with the R1 and R2 suspension configurations.

7.5.3 Test Results

The test results showing the effect of vertical damping of the secondary suspension system on ride quality are presented in figures 7-27 through 7-29. No significant difference was noted in ride quality as a result of suspension damping except at 26 Hz at 70 mi/h, where the R1 and R3 configuration vertical acceleration levels were two to three times the R2 configuration level at the forward floor centerline location (0.015 to 0.021 g rms compared to 0.006 g rms, respectively). There was no significant difference in lateral vibration.

The frequency-weighted rms acceleration ride roughness data (figure 7-30) also show no significant change in levels except at 70 mi/h at the forward centerline vertical location. Figure 7-31 shows a 50% increase in vertical ride roughness through track sections II and VI for the R2 configuration over the R1 configuration at the midcar centerline location. Typical levels were 0.02 to 0.024 g rms for configuration R1 compared to 0.032 to 0.38 g rms for configuration R2.

All data fell well below the specification requirements and it is concluded that all of the three configurations were satisfactory from a ride quality standpoint. The R2 configuration, which exhibited the best ride quality, has been selected for the revenue service vehicles.

7.6 DIRECTION EFFECT

7.6.1 Test Objective

The objective was to determine the effect of leading or trailing car location on the ride quality vibration levels. The prime ride quality data

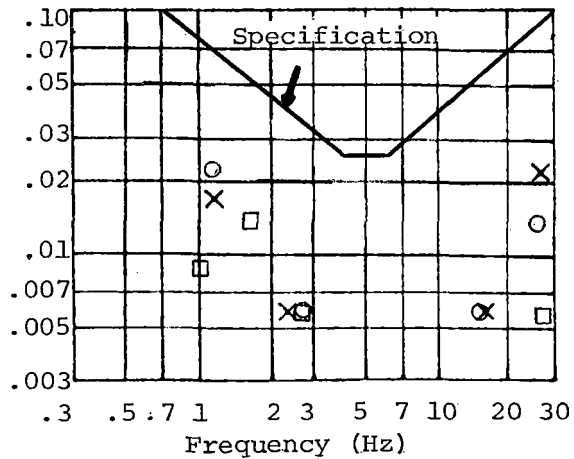
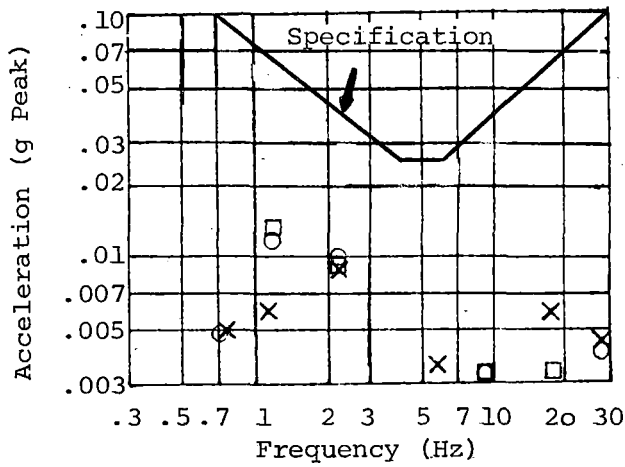
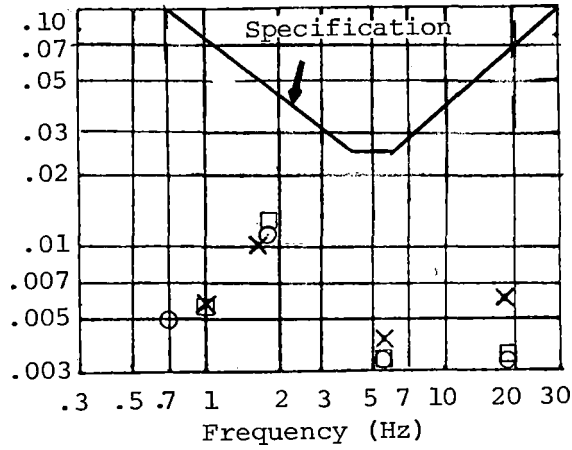


FIGURE 7-27. COMPARISON OF VERTICAL RIDE QUALITY TO VEHICLE SPECIFICATION - SUSPENSION EFFECT, FORWARD FLOOR CENTERLINE.

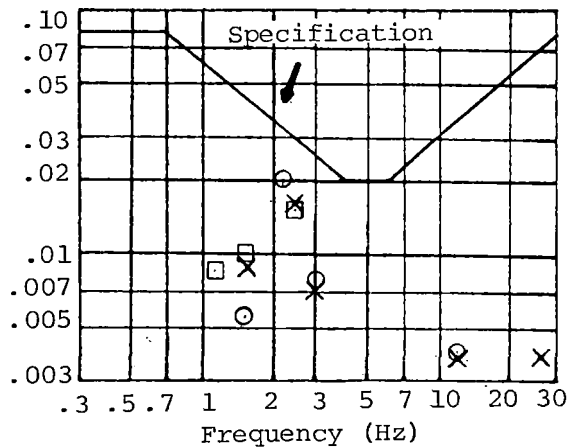
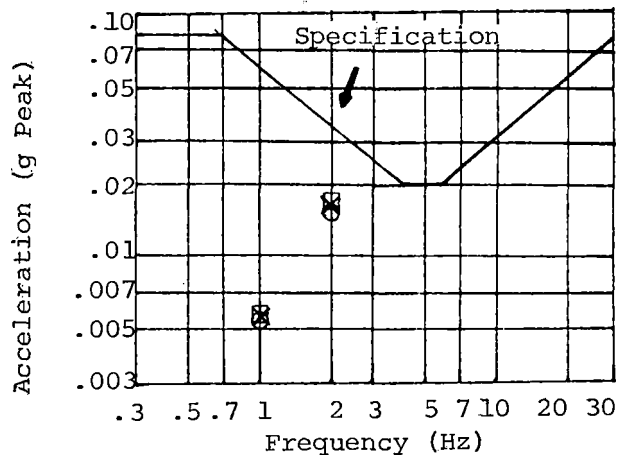
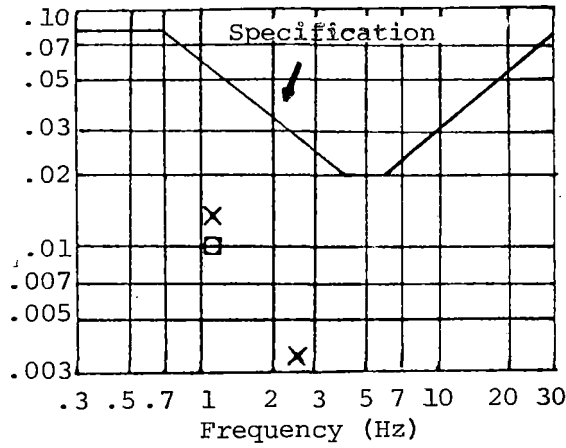


FIGURE 7-28. COMPARISON OF LATERAL RIDE QUALITY TO VEHICLE SPECIFICATION - SUSPENSION EFFECT, FORWARD FLOOR CENTERLINE.

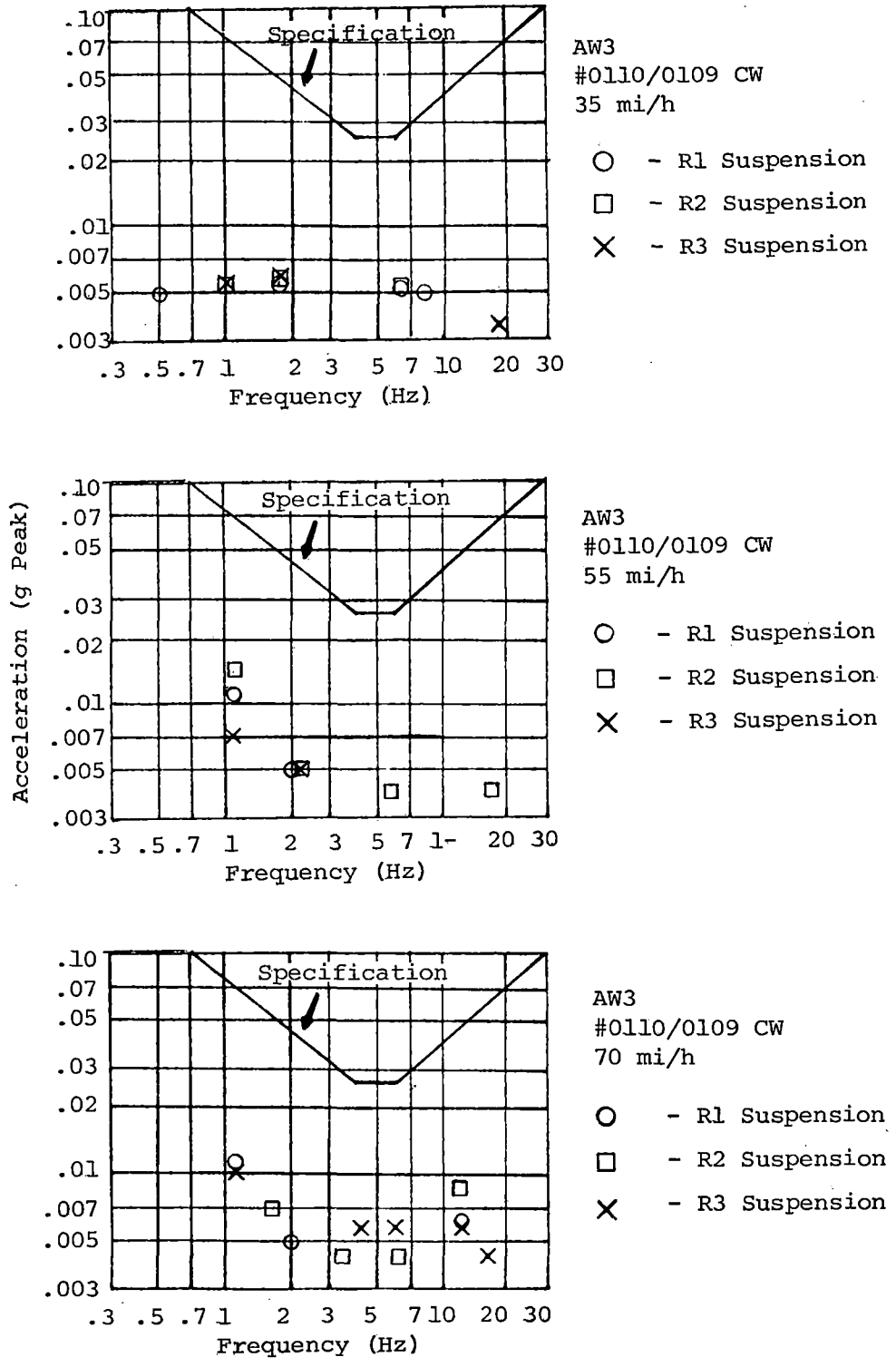


FIGURE 7-29. COMPARISON OF VERTICAL RIDE QUALITY TO VEHICLE SPECIFICATION - SUSPENSION EFFECT, MIDFLOOR CENTERLINE.

Acceleration (g rms)

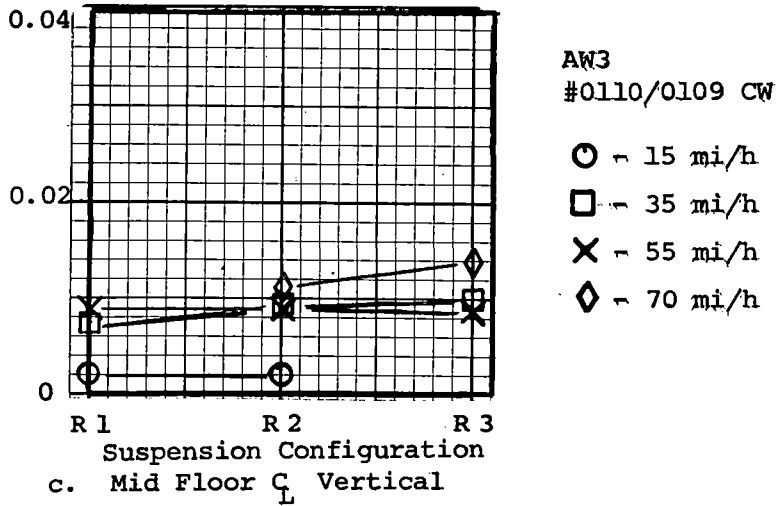
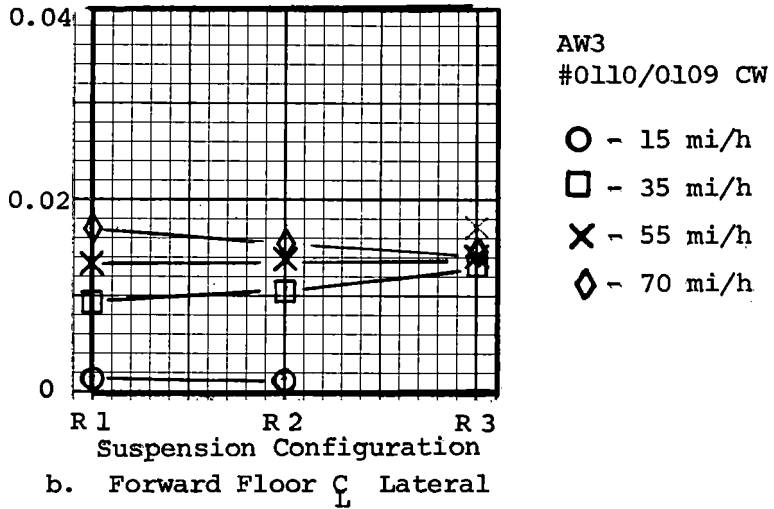
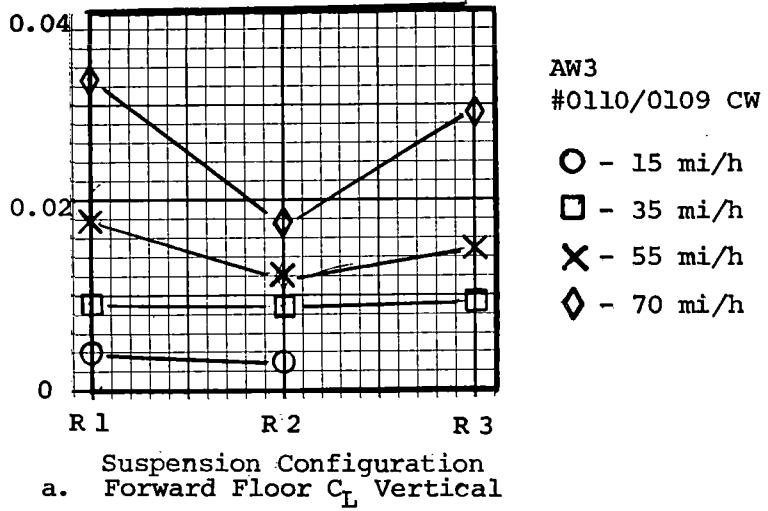


FIGURE 7-30. EFFECT OF SUSPENSION CONFIGURATION ON RIDE ROUGHNESS.

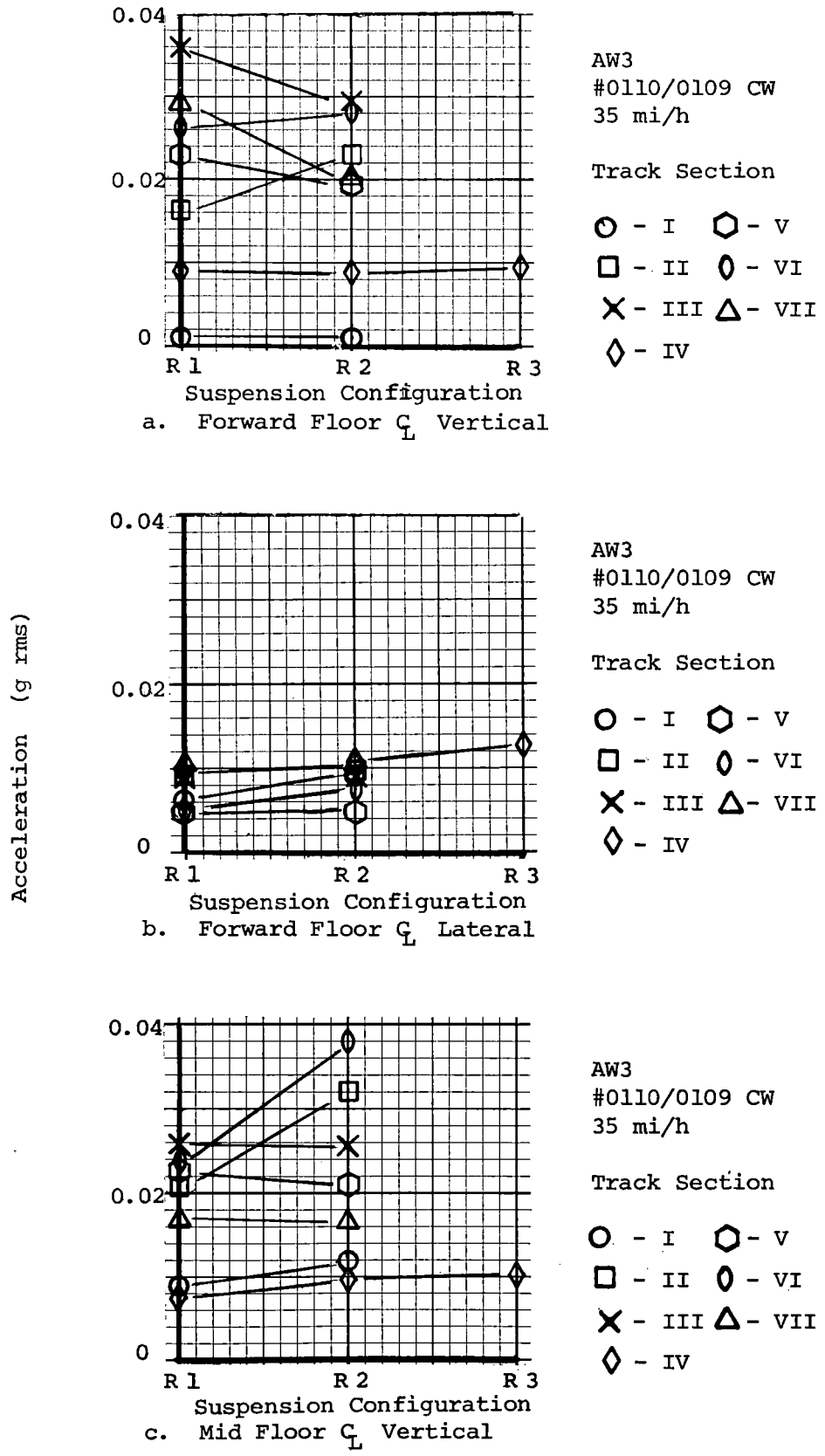


FIGURE 7-31. EFFECT OF SUSPENSION CONFIGURATION ON RIDE ROUGHNESS.

presented are for clockwise operation with car 0110 leading. In this section, ride quality levels obtained with car 0110 leading are compared to those obtained with car 0109 leading.

7.6.2 Test Method

Vibration measurements were recorded while the two-car train was operating between station 30 and station 33 (clockwise direction) at AW3 weight with R2 suspension configuration. All data were recorded on car 0110, whether leading or trailing.

The car was accelerated to the test speed prior to reaching the start of the test zone and then held constant through the test zone. Tests were conducted at constant speeds of 15, 35, 55, and 70 mi/h.

7.6.3 Test Results

The results, showing the effect of lead/trail car status in the train consist (figures 7-32 through 7-34), indicate a slightly higher level of vibration when the car is leading, but higher levels for the trailing car at 70 mi/h.

The frequency-weighted rms acceleration data (figure 7-35) show that the lateral data for the leading car were greater by nearly 35% (0.004 g rms) than for the trailing car. Differences in the vertical direction were less significant.

7.7 ACCELERATION, DECELERATION EFFECT

7.7.1 Test Objective

The objective was to determine the vibration rms acceleration levels at selected carbody floor locations as a function of car speed during full vehicle acceleration and full dynamic or friction-only braking.

7.7.2 Test Method

Vibration measurements were recorded during a full service acceleration and deceleration on the tangent level section of the TTT (stations 30 to 34). The acceleration runs were conducted by positioning the two-car train at station 30 with car 0110 leading for the clockwise runs or at station 34 with 0109 leading for the counterclockwise runs.

The full rate deceleration runs were conducted by accelerating the two-car train to 70 mi/h prior to entering the test zone at station 30 for the clockwise runs or station 34 for the counterclockwise runs. Deceleration runs were conducted for full service blended braking and full service friction-only braking. The following vehicle weight and suspension configurations were tested: AW3/R1, AW0/R2, and AW3/R2.

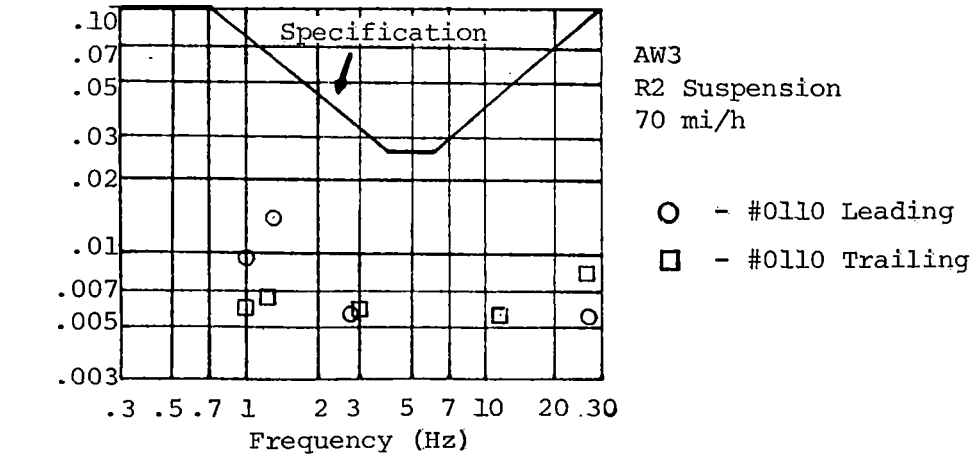
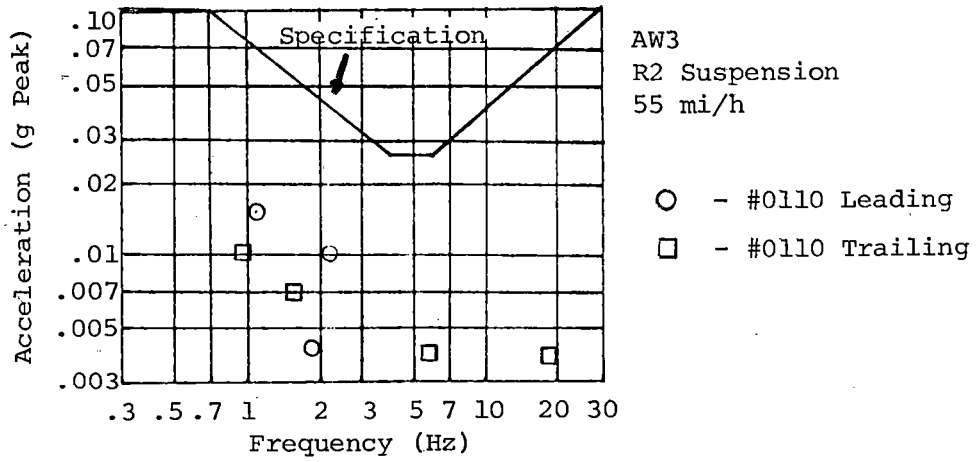
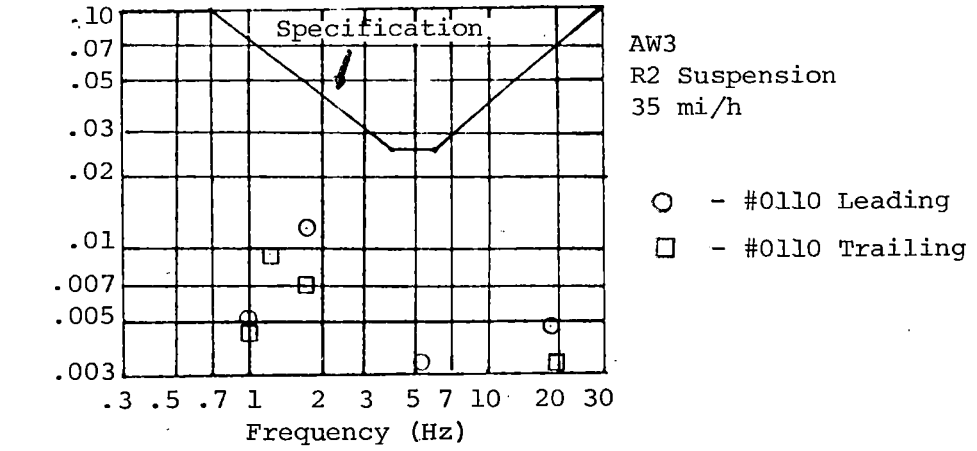


FIGURE 7-32. COMPARISON OF VERTICAL RIDE QUALITY TO VEHICLE SPECIFICATION - CONSIST DIRECTION EFFECT, FORWARD FLOOR CENTERLINE.

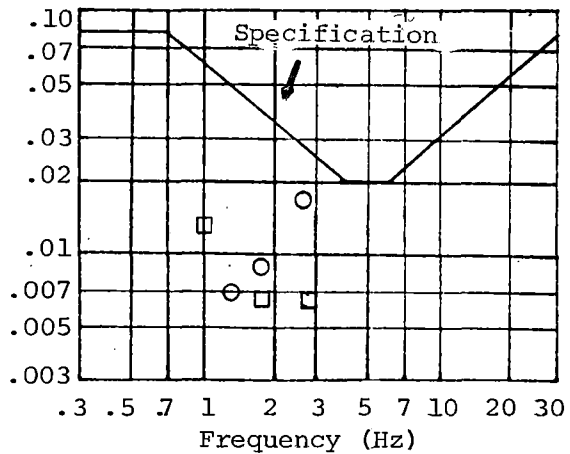
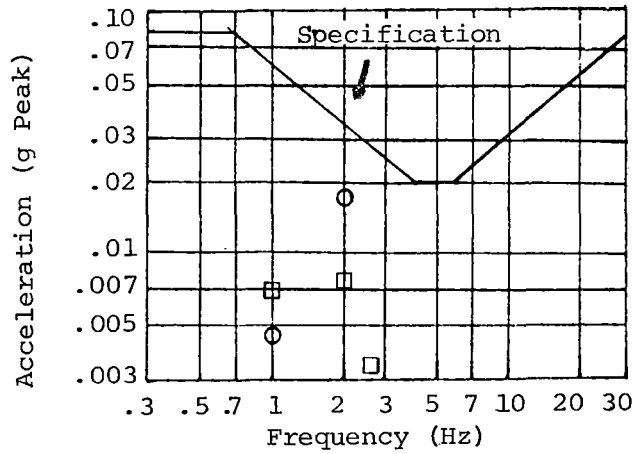
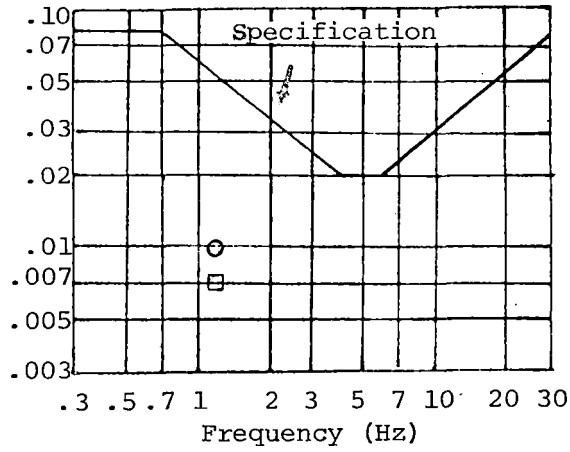


FIGURE 7-33. COMPARISON OF LATERAL RIDE QUALITY TO VEHICLE SPECIFICATION - CONSIST DIRECTION EFFECT, FORWARD FLOOR CENTERLINE.

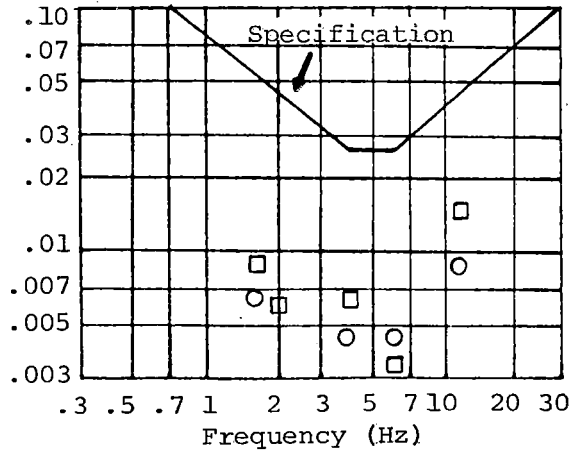
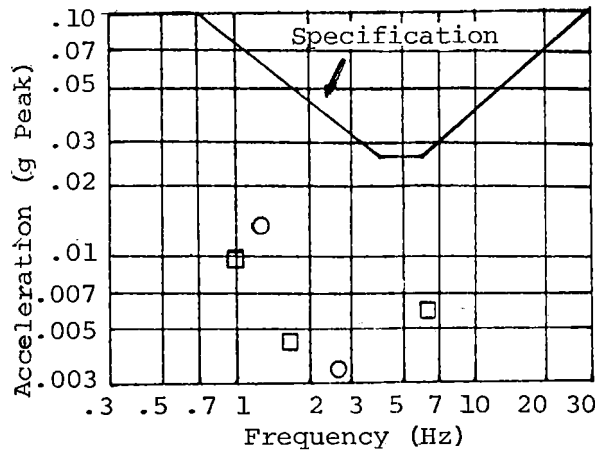
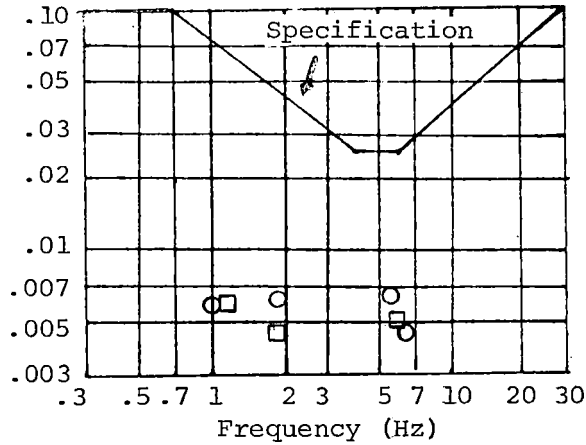
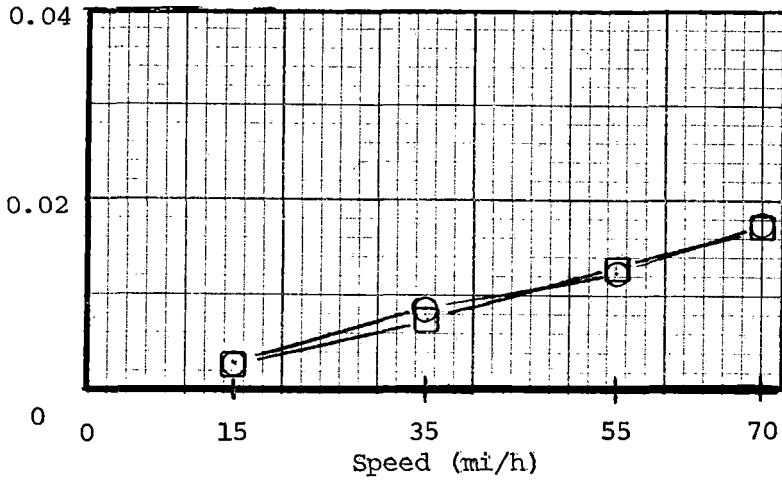


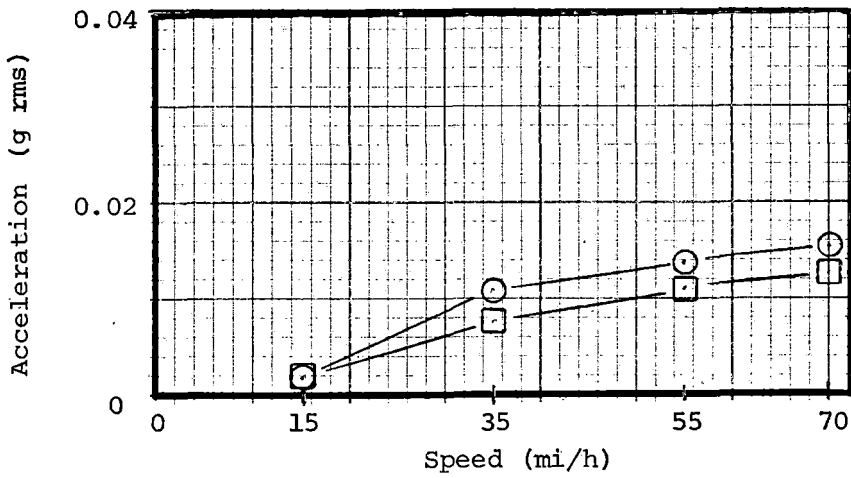
FIGURE 7-34. COMPARISON OF VERTICAL RIDE QUALITY TO VEHICLE SPECIFICATION - CONSIST DIRECTION EFFECT, MIDFLOOR CENTERLINE.



AW3
R2 SUSPENSION
Section IV

○ - #0110 Leading
□ - #0110 Trailing

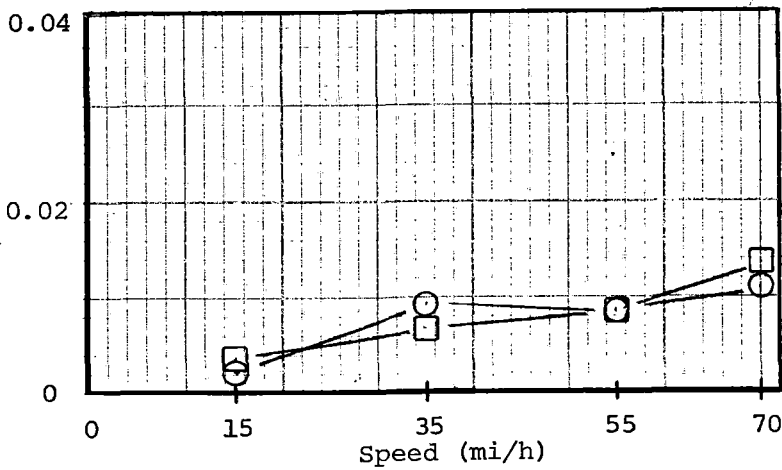
a. Forward Floor C_L Vertical



AW3
R2 Suspension
Section IV

○ - #0110 Leading
□ - #0110 Trailing

b. Forward Floor C_L Lateral



AW3
R2 Suspension
Section IV

○ - #0110 Leading
□ - #0110 Trailing

c. Mid Floor C_L Vertical

FIGURE 7-35. EFFECT OF VEHICLE DIRECTION ON RIDE ROUGHNESS.

7.7.3 Test Results

The results for the maximum acceleration runs (figures 7-36 through 7-40) are plots of rms acceleration versus vehicle speed. These data were processed by analog techniques through a 0-30 Hz bandwidth rms averaging filter with a 1-s averaging time window.

The data show that vehicle weight had no significant effect on the ride quality in the vertical direction. Vibration amplitudes at the AW3 weight in the lateral direction were significantly higher than at the AW0 weight below 20 mi/h. However, all lateral vibration amplitudes were below 0.05 g rms, which is acceptable.

The greatest vibration amplitudes occurred at the forward floor centerline vertical location (figure 7-36) where the vibration level reached 0.14 g rms for the R1 configuration. The amplitudes at all other locations were less than 0.06 g rms.

The vertical vibration amplitude at the forward floor centerline (figure 7-36) shows a gradual increase with increasing speed; more significant however is the change in amplitude due to the car leading or trailing the train. Above 50 mi/h, for example, the amplitude was up to 50% greater (0.09 g rms) when the instrumented car (0110) was trailing than when it was leading.

The suspension effect shows that the vibration amplitudes for the R2 suspension configuration were generally greater than those for the R1. However the R1 configuration gave the most severe vibration level at the forward floor vertical location (figure 7-36), where the level peaked at 0.14 g rms at 61 mi/h. The R2 suspension configuration was judged to provide the better overall ride quality because the vertical acceleration amplitudes did not exceed 0.06 g rms at any location.

The test results for the full service blended braking are presented in figures 7-41 through 7-45. The test results for the full service friction-only braking are presented in figures 7-46 through 7-50. The vibration amplitudes during blended and friction-only braking exhibited the same trends that were noted during maximum vehicle acceleration. Therefore, the above summarized results for the acceleration data are also applicable to the braking data results.

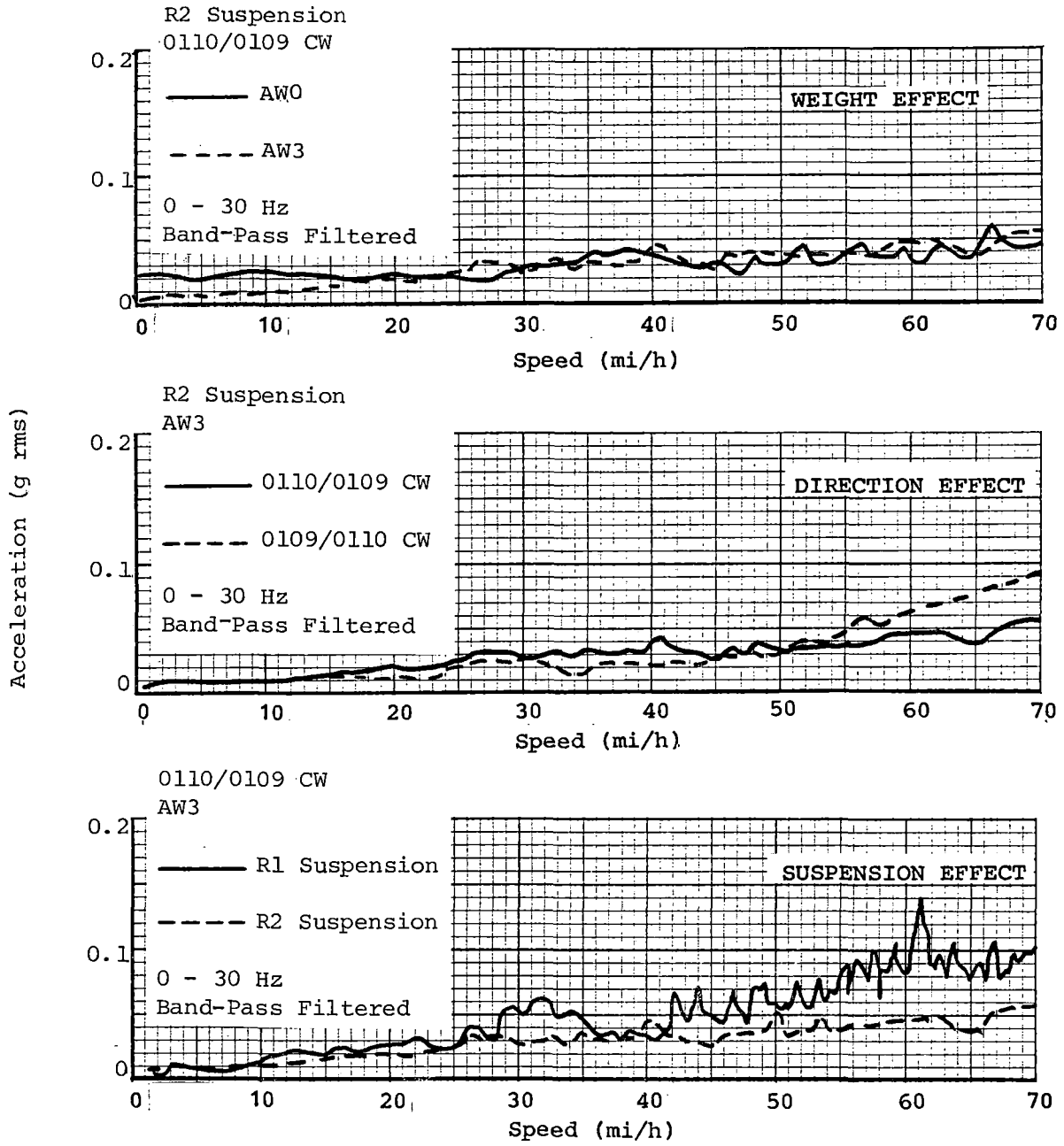


FIGURE 7-36. FORWARD FLOOR CENTERLINE - VERTICAL VIBRATION DURING MAXIMUM ACCELERATION.

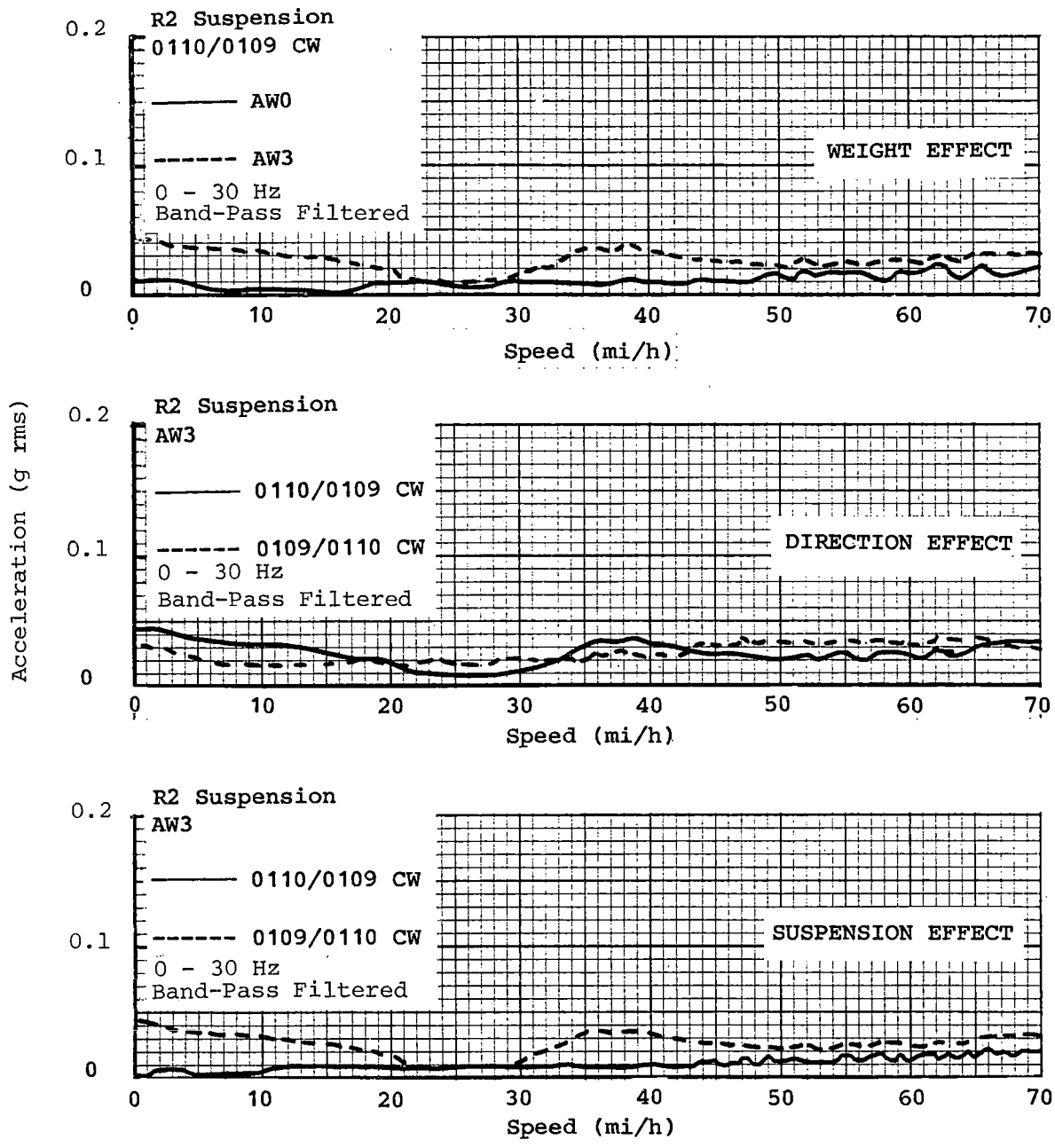


FIGURE 7-37. FORWARD FLOOR CENTERLINE LATERAL VIBRATION DURING MAXIMUM ACCELERATION.

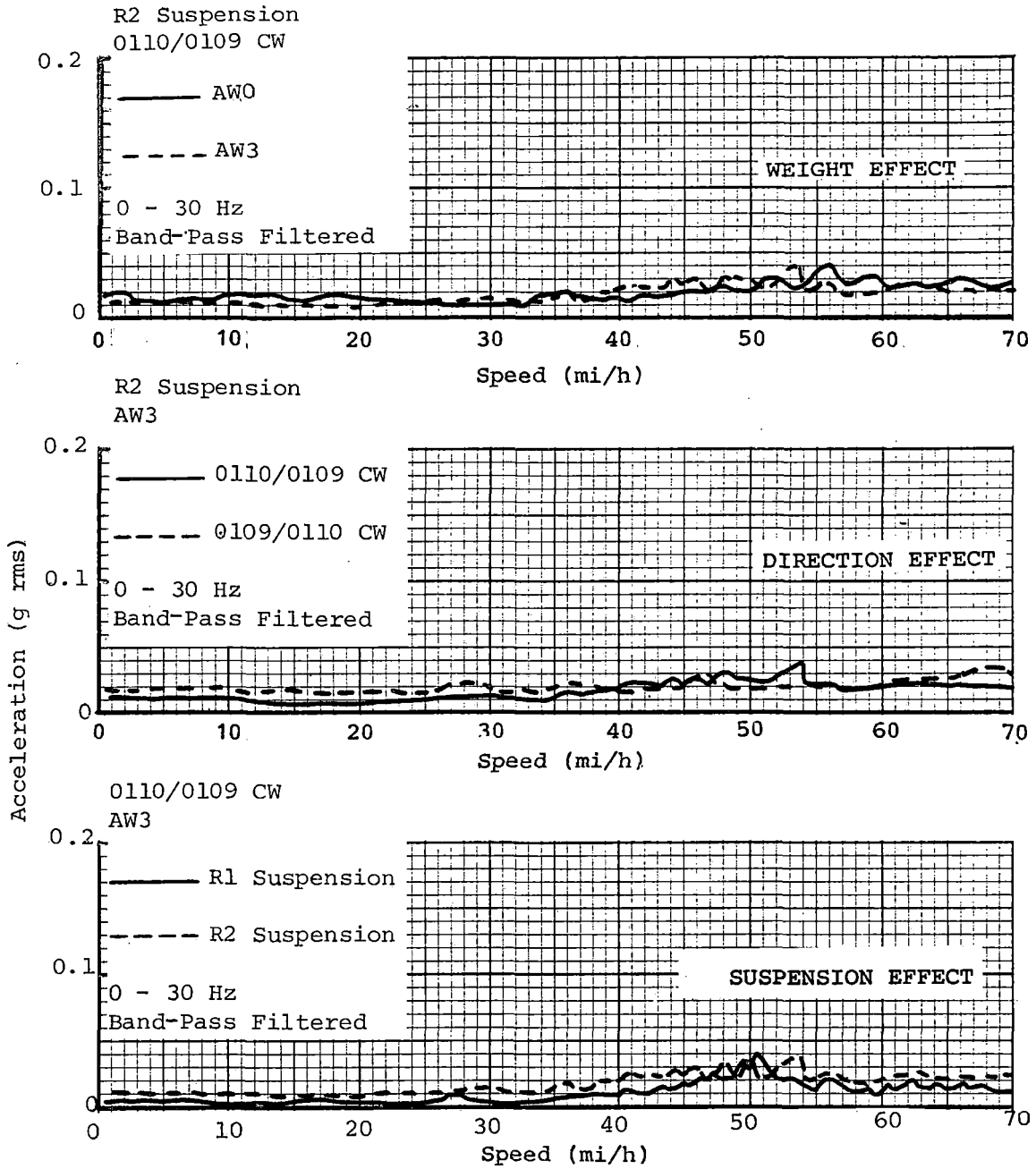


FIGURE 7-38. MIDFLOOR CENTERLINE - VERTICAL VIBRATION DURING MAXIMUM ACCELERATION.

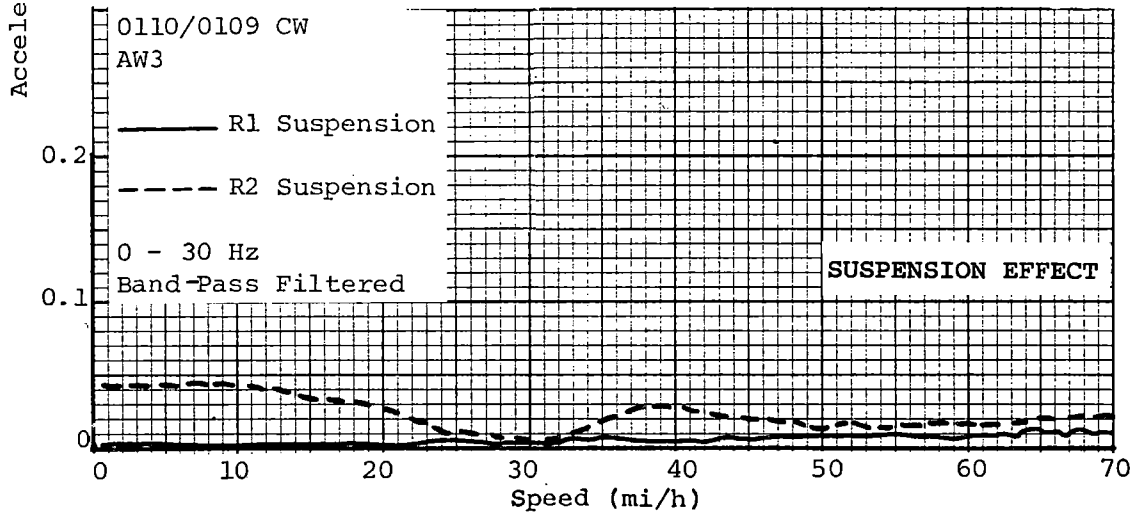
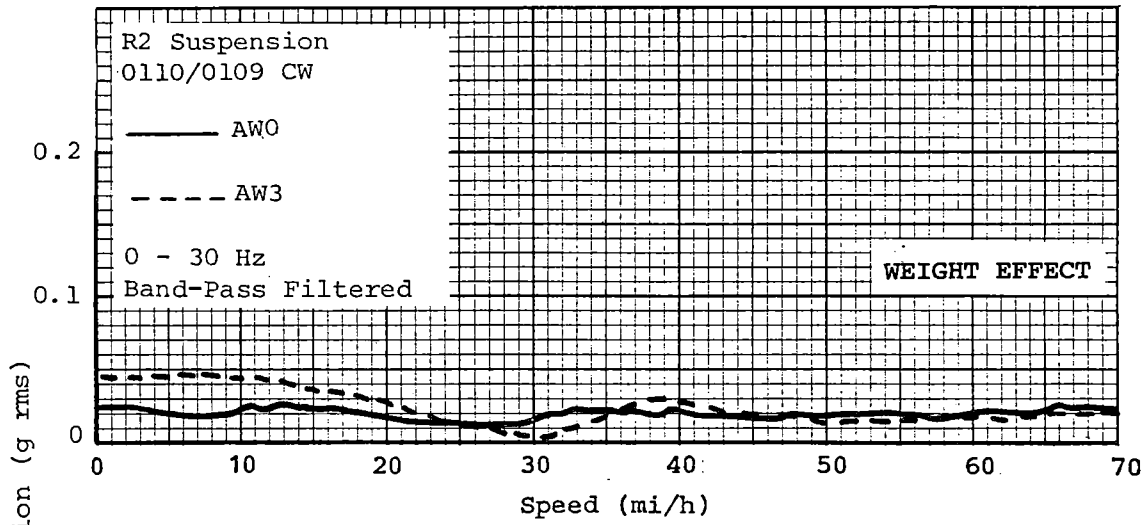


FIGURE 7-39. MIDFLOOR CENTERLINE - LATERAL VIBRATION DURING MAXIMUM ACCELERATION.

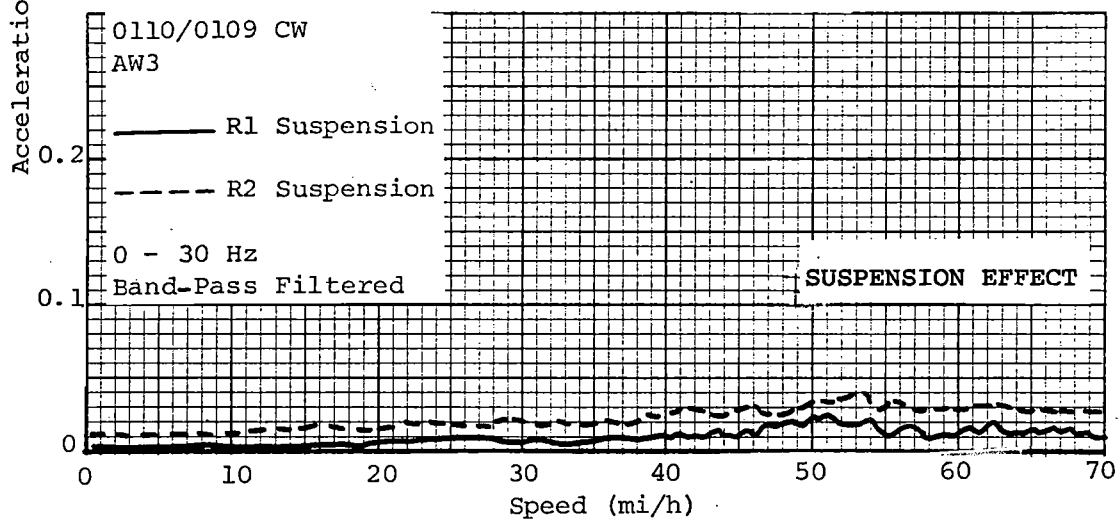
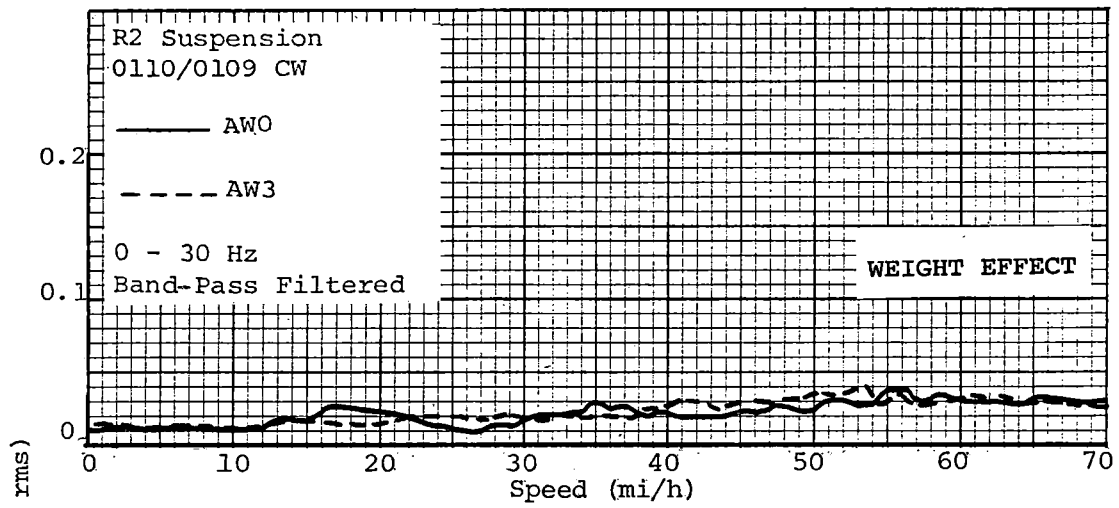


FIGURE 7-40. MIDFLOOR LEFT--VERTICAL VIBRATION DURING MAXIMUM ACCELERATION.

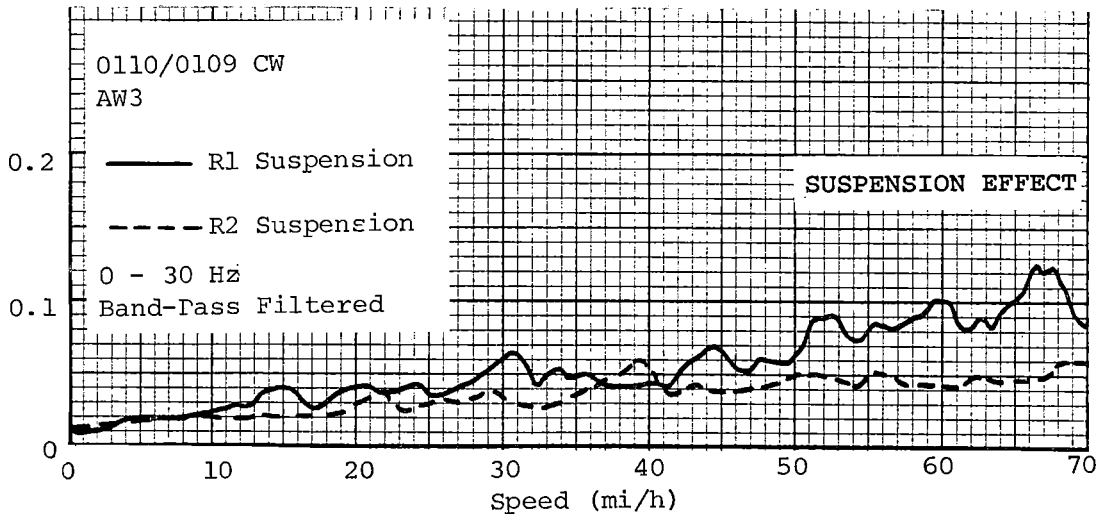
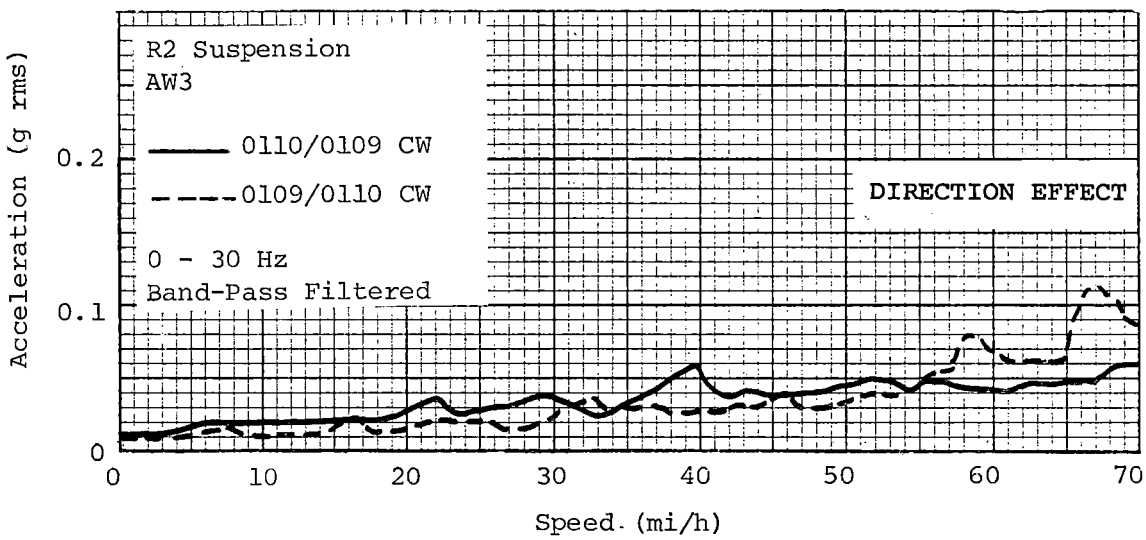
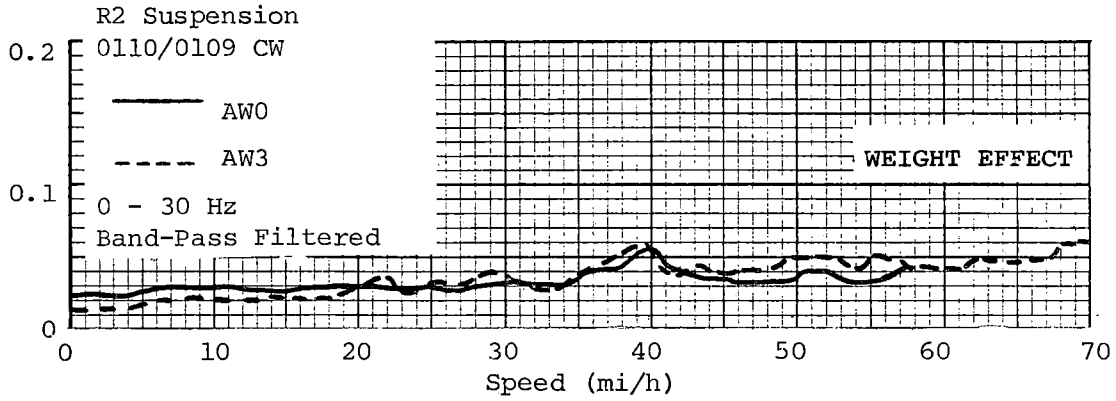


FIGURE 7-41. FORWARD FLOOR CENTERLINE - VERTICAL VIBRATION DURING FULL BLENDED BRAKING.

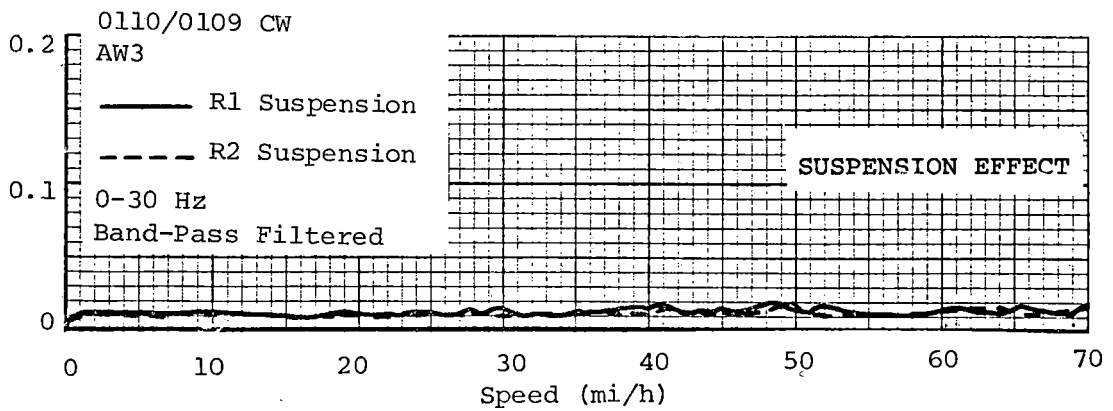
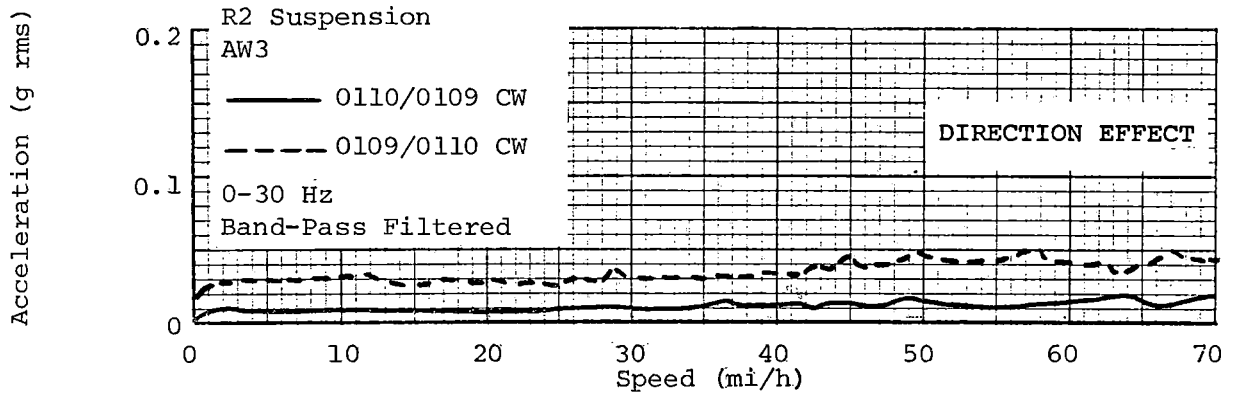
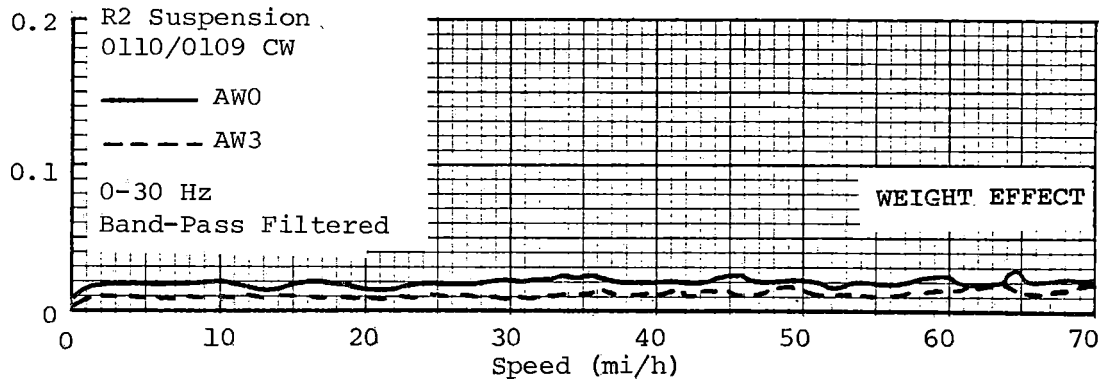


FIGURE 7-42. FORWARD FLOOR CENTERLINE - LATERAL VIBRATION DURING FULL BLENDED BRAKING.

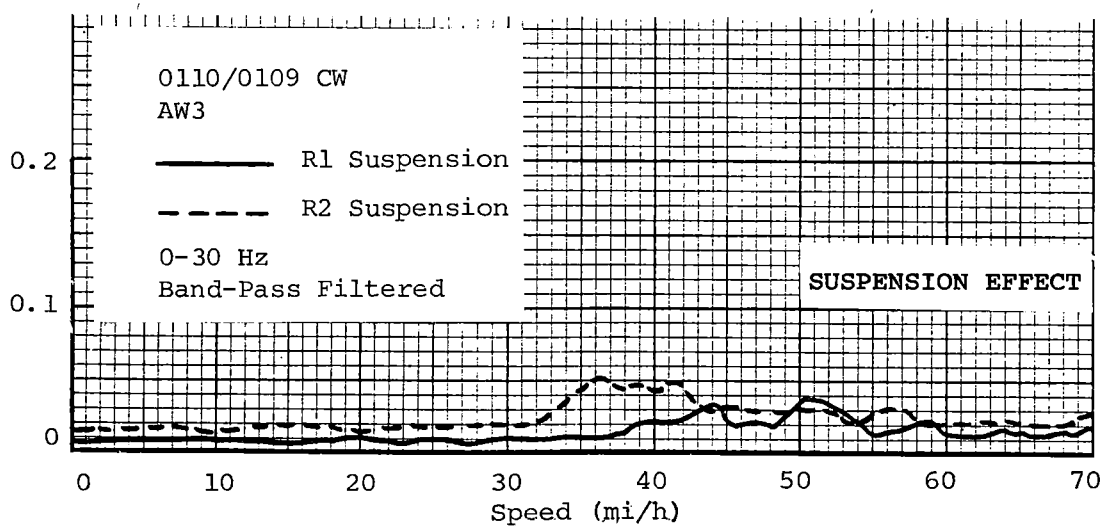
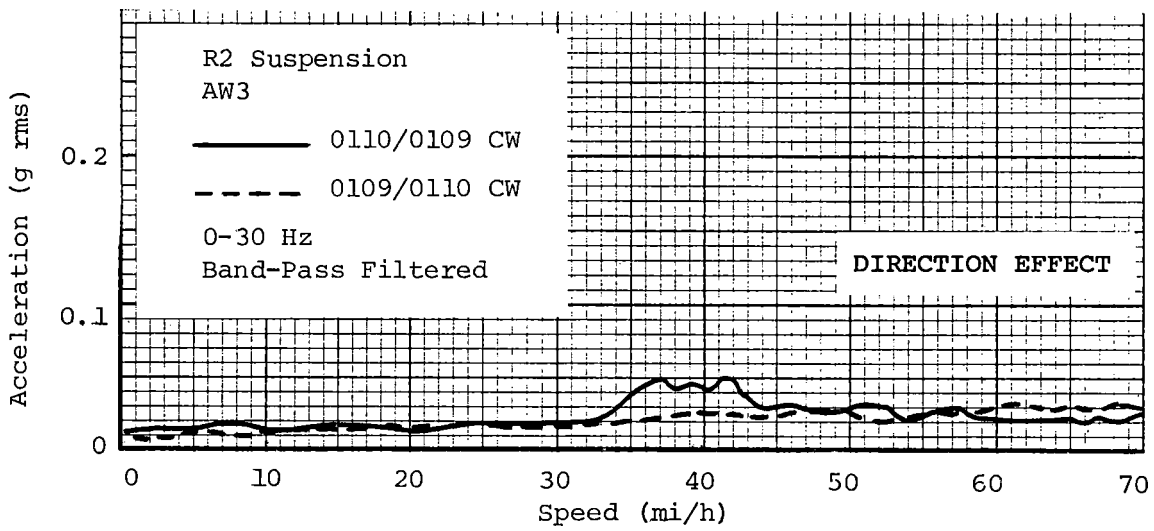
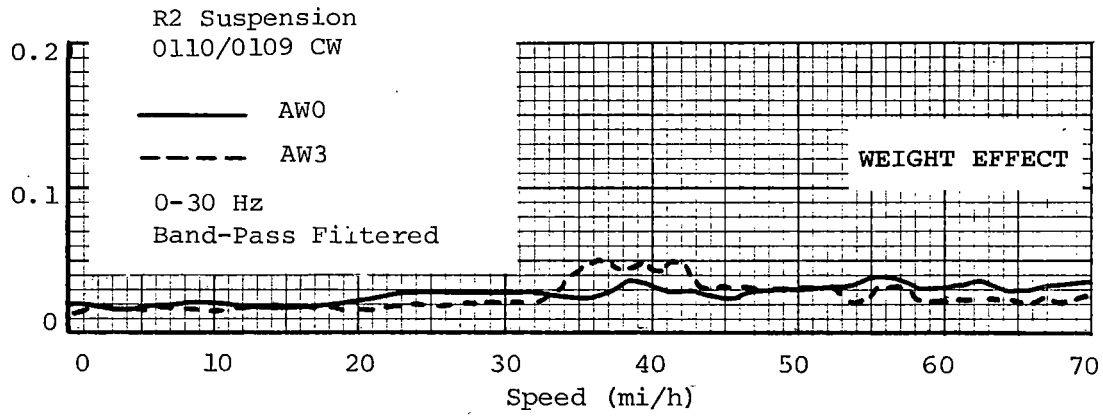


FIGURE 7-43. MIDFLOOR CENTERLINE--VERTICAL VIBRATION DURING FULL BLENDED BRAKING.

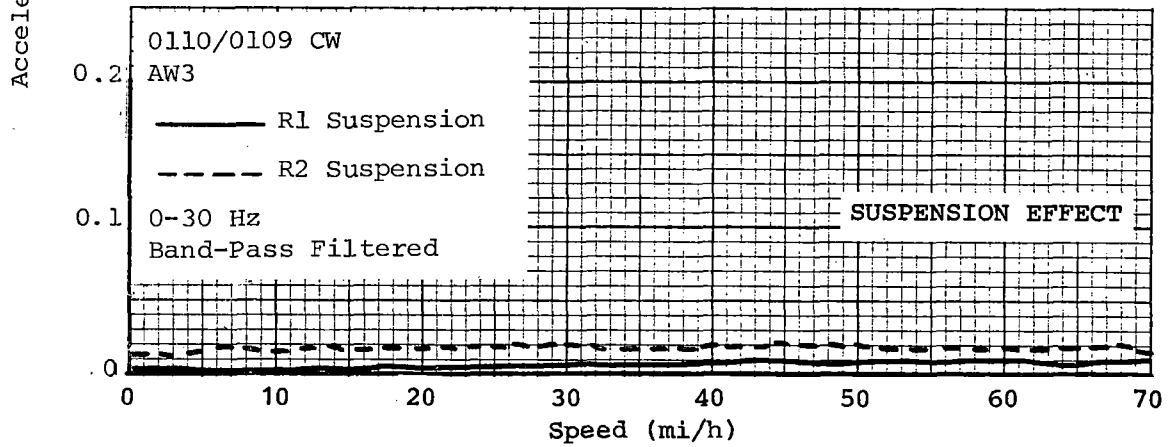
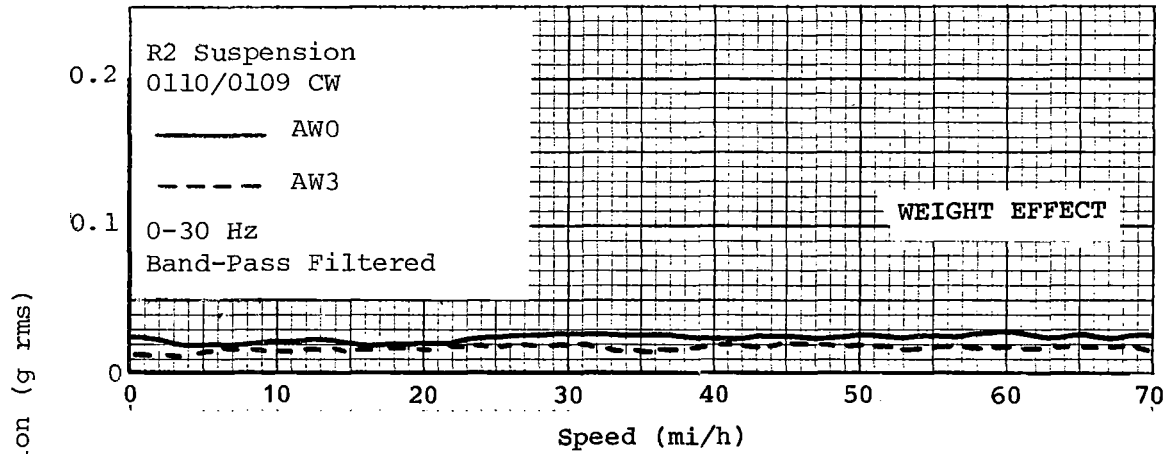


FIGURE 7-44. MIDFLOOR CENTERLINE--LATERAL VIBRATION DURING FULL BLENDED BRAKING.

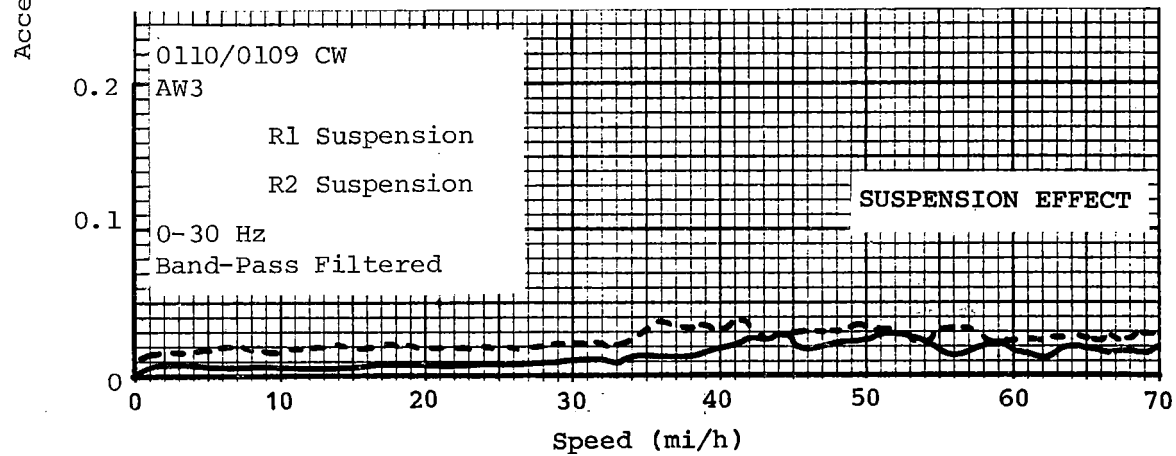
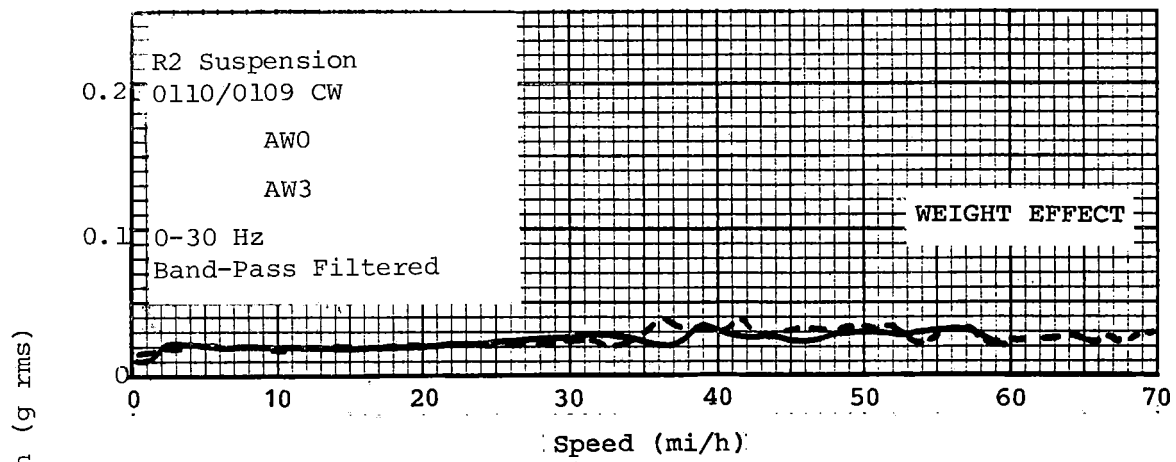


FIGURE 7-45. MIDFLOOR LEFT--VERTICAL VIBRATION DURING FULL BLENDED BRAKING.

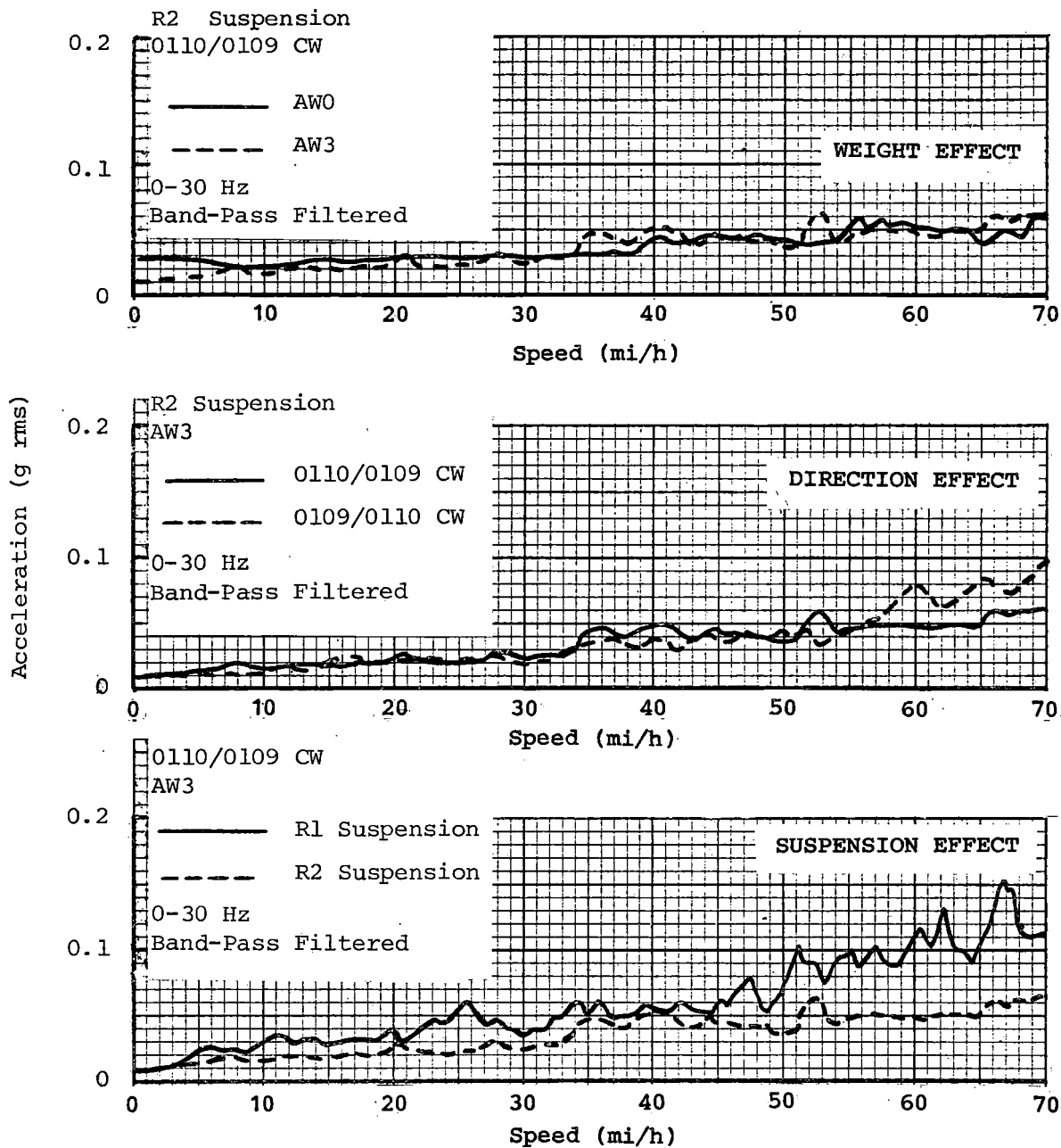


FIGURE 7-46. FORWARD FLOOR CENTERLINE--VERTICAL VIBRATION DURING FULL FRICTION-ONLY BRAKING.

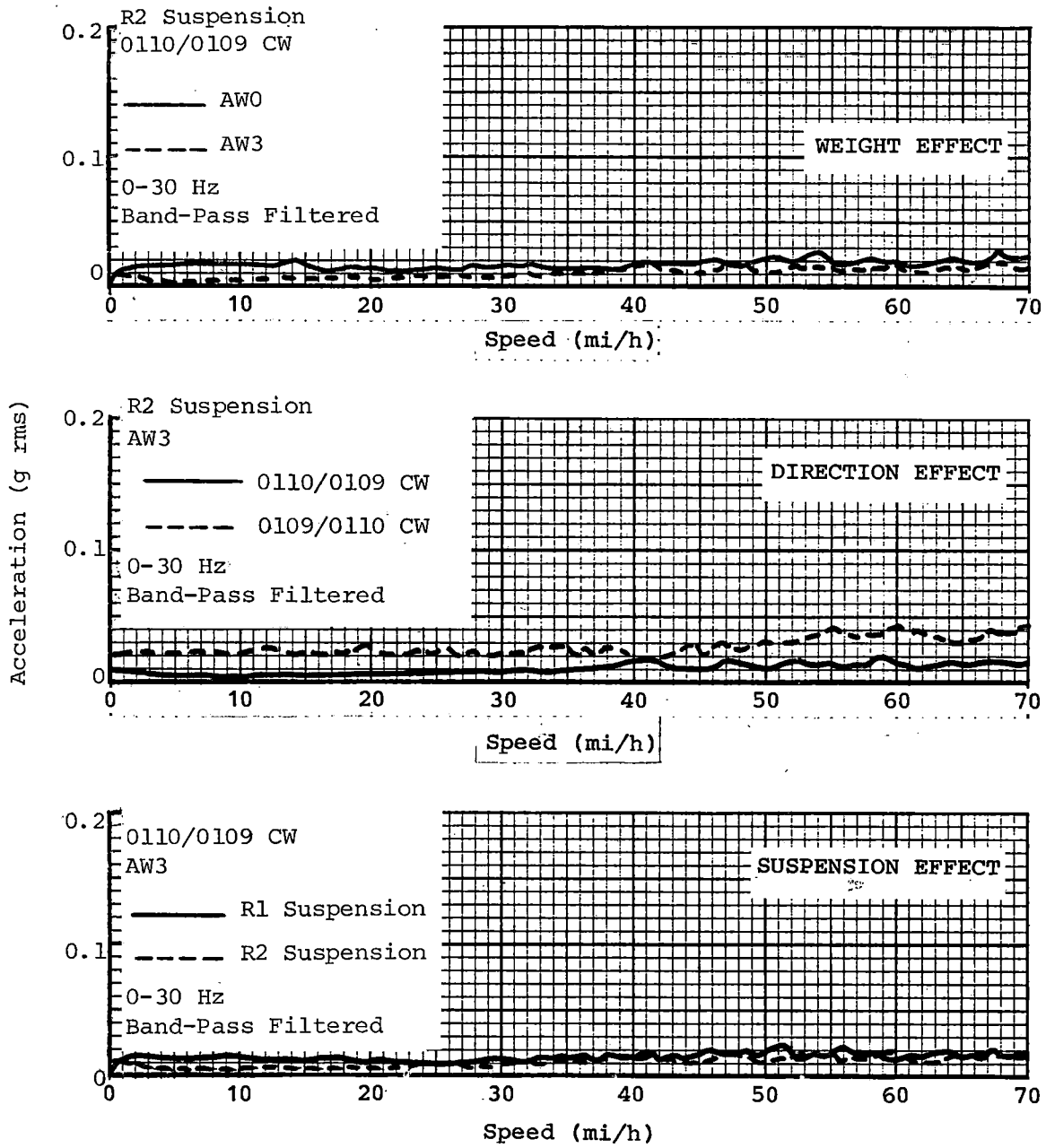


FIGURE 7-47. FORWARD FLOOR CENTERLINE--LATERAL VIBRATION DURING FULL FRICTION-ONLY BRAKING.

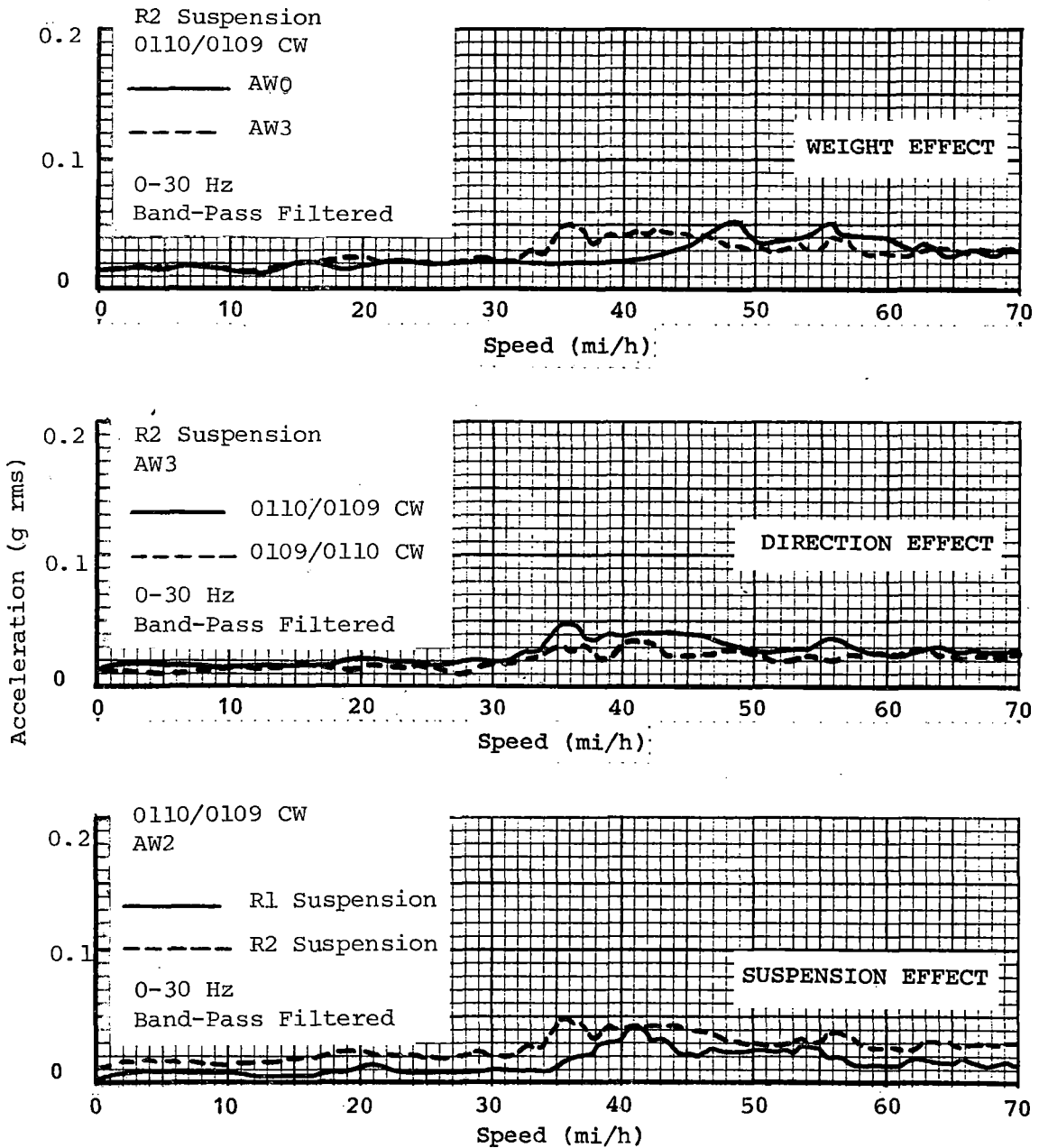


FIGURE 7-48. MIDFLOOR CENTERLINE--VERTICAL VIBRATION DURING FULL FRICTION-ONLY BRAKING.

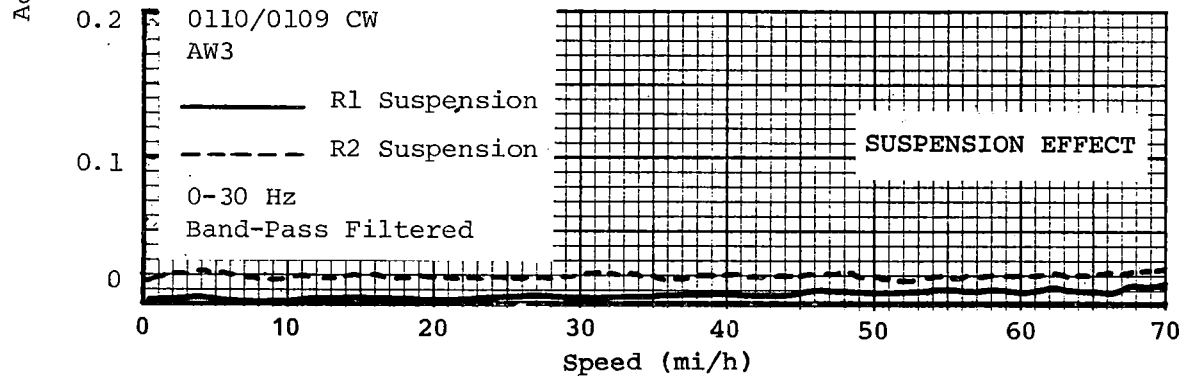
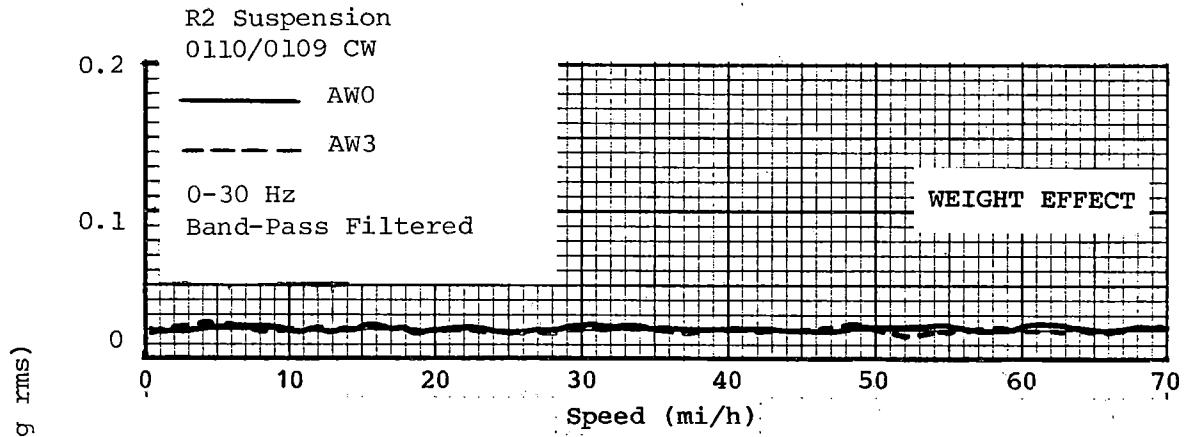


FIGURE 7-49. MIDFLOOR CENTERLINE--LATERAL VIBRATION DURING FULL FRICTION-ONLY BRAKING.

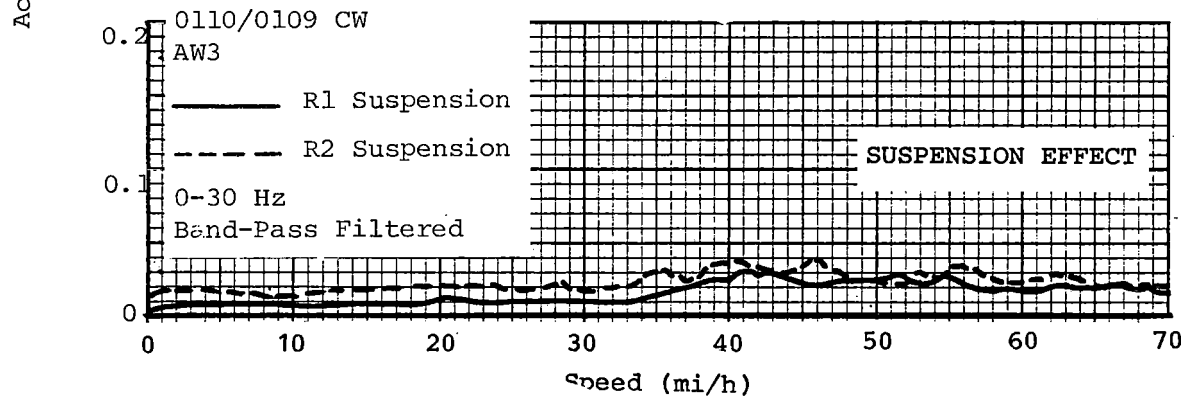
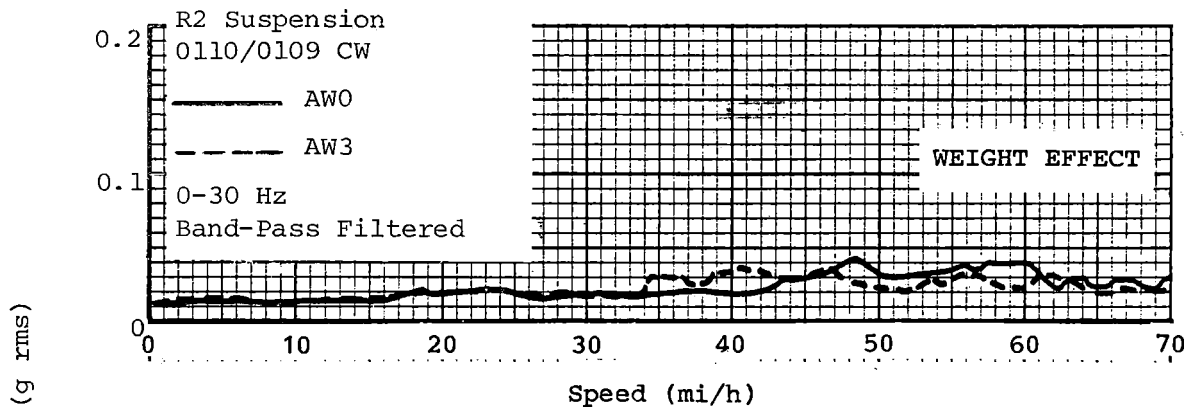


FIGURE 7-50. MIDFLOOR LEFT--VERTICAL VIBRATION DURING FULL FRICTION-ONLY BRAKING.

8.0 NOISE TESTS

The purpose of the noise tests was to measure the acoustic properties of the vehicles. The emphasis on the tests was to evaluate major noise characteristics, rather than to dwell on the noise emission of a particular piece of equipment or subsystem.

The tests involved measurements made both onboard the vehicles and at wayside. The onboard measurements comprised the bulk of the work, and investigated the noise environment as affected by the variables of speed, acceleration, deceleration, track construction, seat location, and auxiliary equipment operation. The wayside measurements were taken at a number of pass-by speeds and, in addition, the operation of a number of auxiliary equipment configurations was examined with the car stationary. In all, the onboard and wayside measurements have been grouped into seven categories; each category is addressed separately. Measurements have been compared wherever applicable to the acoustic requirements, as detailed in the vehicle specification.

A section is included which describes the acoustic instrumentation used, in particular for the onboard recording of noise made when the car was moving. For this test phase, the dynamic range of the noise signal was reduced by high-pass filtering before recording. Also included is a section on the analysis of the data with details of the 1/3 octave analysis equipment. Finally, a section of conclusions summarizes the most significant test findings.

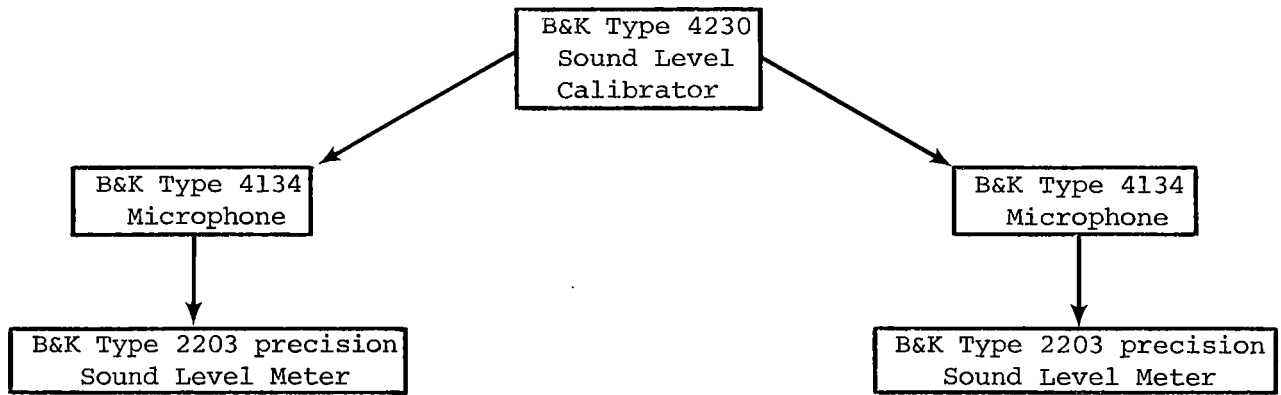
8.1 INSTRUMENTATION

The acoustic instrumentation was independent of other instrumentation, except that car speed was taken visually from the onboard car speedometer. The instrumentation can be divided into two groups--sound level indicating equipment and sound recording equipment. The first category was used to take 'A' weighted sound level readings; the second category was used for 1/3 octave analysis and to produce sound level time histories.

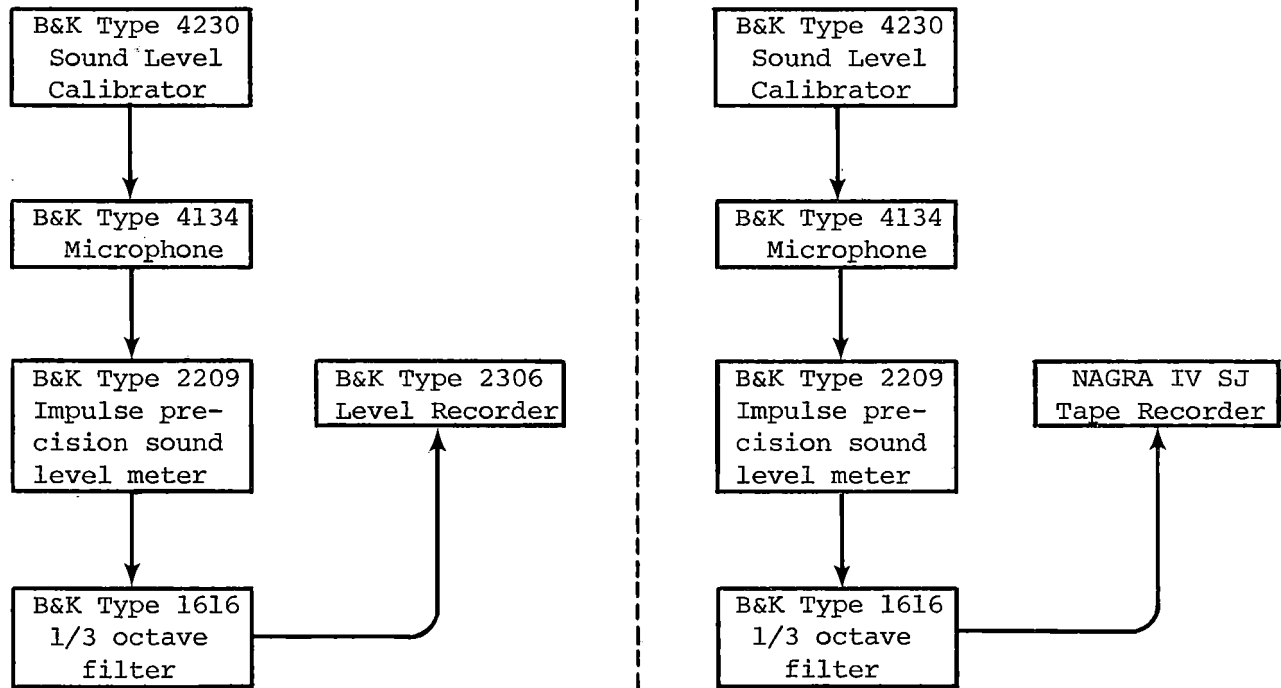
8.1.1 Sound Level Indicating Equipment

Manual readings were taken with two Brüel and Kjaer (B&K) 2203 Precision Sound Level meters fitted with B&K 4134 microphones (see figure 8-1). The sound level meters were set to the 'A' frequency weighting, and all readings were taken with the meter response set to 'Slow'. However in the case of pass-by measurements and for measurement of door operation noise levels, the meter response was set to 'Fast'. The sound measurement equipment was calibrated in the field before use, by means of a B&K 4230 Sound Level Calibrator which applied a 94 dB sound source at 1 kHz to the microphone.

In addition to the previous instrumentation, during the acceleration test and deceleration test, a B&K 2306 Level Recorder was connected to a B&K 2209 Sound Level Meter to produce 'A' weighted sound level strip charts in real time.



Equipment for 'A' frequency weighted sound level readings



Equipment for real time 'A' weighted strip charts

Recording equipment

FIGURE 8-1. ACOUSTIC INSTRUMENTATION.

8.1.2 Sound Recording Equipment

The measuring scheme for the tests is shown in figure 8-1. The use of the B&K 2209 sound level meter and B&K 1616 1/3 octave filter (upstream of the Nagra IV SJ recorder) was to reduce the dynamic range of the signal before recording. This was necessary because the sound onboard a moving transit vehicle has a broad band nature. The frequency spectrum shows significant components in both the infra-sound band (below 20 Hz) and the audio frequency band (from 20 Hz to 20 kHz). The frequency spectrum has very high levels at the low frequency end (of the order of 130 dB) and relatively low levels at the high frequency end (of the order of 30 dB). Because the Nagra IV SJ recorder has a dynamic range of 60 dB, it could not record the complete signal. Therefore, the low frequency infra-sound content of the signal was filtered out, such that only the audio frequency band content, which was of interest in this case, was recorded. The -3 dB point of the high pass filter was at 22.4 Hz, which corresponds to the shoulder of the 25 Hz center frequency 1/3 octave band.

The signal flow was as follows: The sound impinged on a B&K 4134 microphone, and the signal was amplified by the input amplifier of the B&K 2209 Sound Level Meter and then fed to the B&K 1616 1/3 Octave Filter, which was set in the 'Linear' mode. From the filter, the signal was returned to the B&K 2209 where it was amplified by the output amplifier and presented as an a.c. output. From there the signal was taken to the Nagra IV SJ recorder, where one channel was recorded at 'High Pass' with no frequency weighting, and the other channel (in parallel) recorded with 'A' weighting.

8.1.2.1 B&K 4134 Microphone. The B&K 4134 microphone was of the pressure response type and in general was oriented with the sound impinging perpendicularly to the normal of the pressure sensitive diaphragm. The pressure response type of microphone was selected over the free field microphone type because the free field type suffers a much more drastic loss of sensitivity for off-axis incidence; for these tests sound was to come from multiple and/or moving sources.

8.1.2.2 B&K 2209 Sound Level Meter. This instrument has excellent overload indicators, one for the input amplifier and a second for the output amplifier. The overload indicators will respond to either positive or negative peaks of a duration as short as 50 μ s and will continue to flash for about 1 s after overload. The dynamic range of the sound signal was first reduced in the input stage to the input amplifier. This input stage has two selectable high-pass settings: 2 Hz and 10 Hz. The 10 Hz setting was selected. The dynamic range of the signal was then further reduced in the B&K 1616 1/3 octave filter.

8.1.2.3 B&K 1616 1/3 Octave Filter. The B&K 1616 was not used as a selectable 1/3 octave bandpass filter, but was used in the 'Linear' mode. In this mode a high-pass filter of 100 db/Decade slope and a -3 dB point of 22.4 Hz were applied to the signal.

8.1.2.4 Nagra IV SJ Recorder. The sound signal was recorded in the 'Linear' mode on channel 1, and simultaneously 'A' frequency-weighted on channel 2.

8.1.2.5 B&K 4230 Sound Level Calibrator. This battery operated device provided a 94 dB, 1 kHz external sound signal and was used to calibrate the system from end to end.

8.2 ANALYSIS EQUIPMENT

Analysis of the recorded signals (figure 8-2) was accomplished in two areas, strip chart display of sound level with time, produced by a B&K Portable Graphic Level Recorder Type 2306, and 1/3 octave analysis, on a General Radio Type 1921 Real Time Analyzer. The level recorder had three output filter settings which were equivalent to sound level meter characteristic responses of 'Impulse', 'Fast', and 'Slow'. In addition, when used in the 'AC Log' mode, and with a 50 dB logarithmic potentiometer, the resulting strip chart had a 50 dB range and a linear scale. The 1/3 octave analyzer applied thirty 1/3 octave notch filters simultaneously to the signal and displayed the average rms level of each filter over selectable time windows. The 30 bands were from the 12.5 Hz band to the 10 kHz band, and when high-pass filtering had been applied to the signal, the 27 bands from the 25 Hz band to the 10 kHz band were valid. Averaging times up to 16 s were used if the signal remained steady over the interval. Since, in many cases, the spectra of sound produced by the vehicle were not constant with time, the practice of synthesizing 1/3 octave bands from narrow band analysis was not adopted.

8.3 TEST RESULTS

The characteristics of the acoustic properties were evaluated in the following seven areas:

- Equipment noise characteristics at wayside, stationary.
- Equipment noise characteristics onboard, stationary.
- Noise level variation with location onboard, 55 mi/h.
- Noise characteristic with steady speeds onboard, 0 to 70 mi/h.
- Noise characteristic under acceleration/deceleration onboard.
- Noise characteristic with track construction onboard, at 55 mi/h.
- Noise characteristic at steady speeds, at wayside, 0 to 70 mi/h.

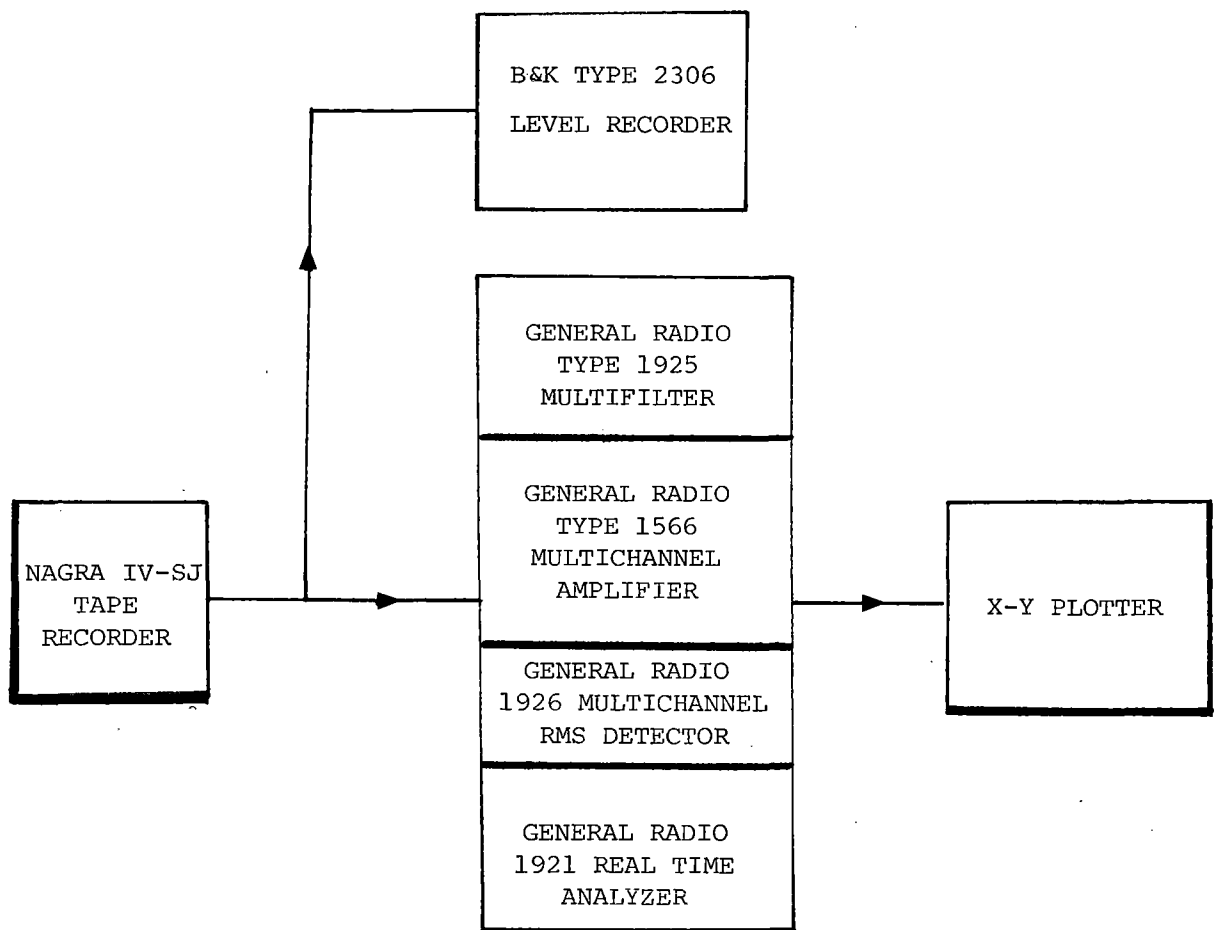


FIGURE 8-2. ANALYSIS EQUIPMENT.

Testing was conducted in three phases:

Phase 1--Preliminary test, car at AWO weight, cardboard protective covering on floor inside car 0109.

Phase 2--Major test, cars in empty condition as supplied to TTC.

Phase 3--Follow-up test, cars as in phase 2.

8.3.1 Equipment Noise Characteristics at Wayside, Car Stationary

8.3.1.1 Objective. The objective of the test was to obtain sound level values at a number of locations at the wayside as influenced by the operation of major pieces of onboard equipment. An additional objective was the identification of 1/3 octave frequency spectrum signatures from the equipment. The vehicle specification states that,

"...with the Transit Vehicle stationary on tie-and-ballast track, and with Transit Vehicle systems operating simultaneously under normal conditions, including the air conditioning system, propulsion motor blowers, and auxiliaries, except traction motors and gears, the noise level shall not exceed 50 dBA at 50 feet from track centerline for any location along either side of the Transit Vehicle."

8.3.1.2 Test Method. The vehicles were positioned on level tangent, tie and ballast track bed on the yard track with the third rail energized to 750 V d.c. Wayside noise was evaluated at twenty-four measurement locations around the car as shown in figure 8-3. Locations 1 thru 12 were 15' from the car centerline, and locations 13 thru 24 were 50' from the centerline. To comply with the vehicle specification requirements, microphone heights were set at axle level, which in general was 5' above the sandy terrain.

To assess the contribution of each major component of equipment to the sound level readings, the configurations shown in tables 8-1 and 8-2 were tested for A and B cars, respectively. The effects of the auxiliary power system, the front and rear air conditioning fans and compressors, the traction motor (TM) blowers, and the doors cycling were evaluated singly and in combinations. The air conditioning system was operated in its low speed mode.

Readings were taken on an individual car basis so that only one car was energized at one time. Readings were taken alongside car 0109 for the seven A car configurations, during which time car 0110 was deactivated. Then readings were taken alongside car 0110 for the eight B car configurations, during which time car 0109 was deactivated. Tape recordings were made at selected locations simultaneously with the above readings. Car configurations 1 through 5 were recorded with the sound level meter set to 'Slow' response; configurations 6 and 7 include the doors cycling and were recorded on 'Fast' response.

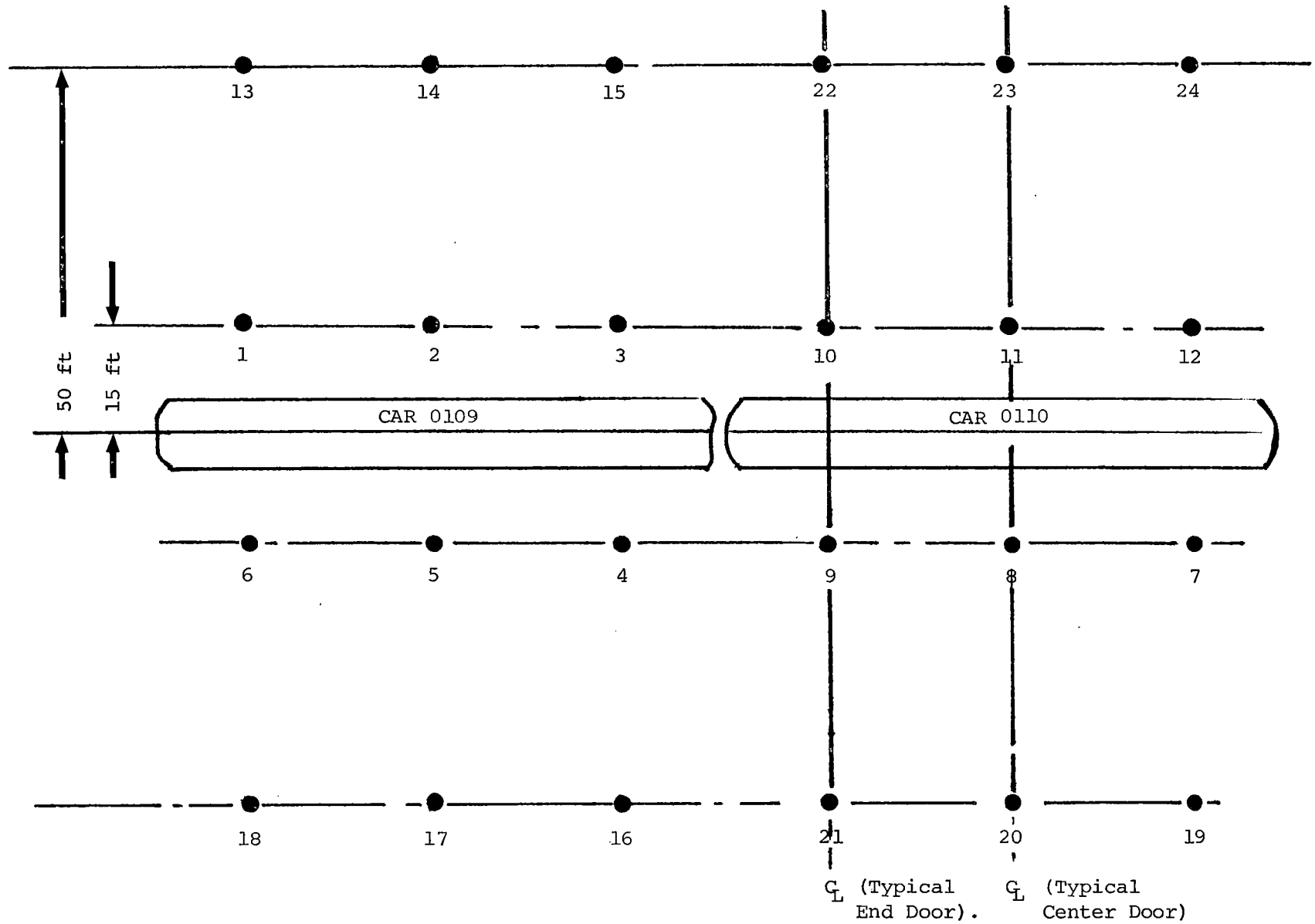


FIGURE 8-3. WAYSIDE MEASUREMENT LOCATIONS.

TABLE 8-1. EQUIPMENT OPERATING DURING A CAR WAYSIDE NOISE TESTS.

Config. No.	Aux Pwr Systems Equipment	A/C Front Evap Fan	A/C Rear Evap Fan	A/C Front Comp	A/C Rear Comp	Traction Motor Fans	Doors Cycling
1	X						
2	X	X	X				
3	X	X	X	X	X		
4	X					X	
5	X	X	X	X	X	X	
6	X						X
7	X	X	X	X	X	X	X

TABLE 8-2. EQUIPMENT OPERATING DURING B CAR WAYSIDE NOISE TESTS.

Config. No.	Aux Pwr Systems Equipment	Brake Air Comp	A/C Front Evap Fan	A/C Rear Evap Fan	A/C Front Comp	A/C Rear Comp	Traction Motor Fans	Doors Cycling
1	X							
1a	X	X						
2	X		X	X				
3	X		X	X	X	X		
4	X						X	
5	X	X	X	X	X	X	X	
6	X							X
7	X	X	X	X	X	X	X	X

8.3.1.3 Test Results - 'A' Weighted Sound Level Readings. Figures 8-4 through 8-12 show the 'A' weighted sound pressure level readings for the two cars in graphic form along with the maximum permissible limits set by the specification. The data show that the vehicle did not satisfy the specification in the following areas:

- Noise level at 50' from the car centerline with all systems operating exceeded the 60 dBA specification maximum at 10 of the 12 locations by an average of 2.25 dBA.
- Noise level at 15' from the car centerline with all systems operating exceeded the 65 dBA specification maximum at all 12 locations by an average of 5.0 dBA.
- Noise level at 15' from the car centerline also exceeded the specification maximum of 65 dBA with partial operation of equipment; i.e., with the auxiliary power system only, the levels exceeded specification at 4 of 12 locations by an average of 2.1 dBA.

However, car 0110 had an abnormally noisy out of balance APSE blower, so that the readings for this car would have been lower with equipment operating normally. Car 0109, however, did not satisfy requirements, even with equipment operating normally.

Figure 8-8 shows that when the TM blowers on car 0109 were energized (configuration 4), the average level increased 4.4 dBA over that when the APSE system only was energized (configuration 1). This compares to an average 1.0 dBA increase, when the air conditioning equipment on car 0109 was energized (configuration 3), over that of the APSE system only (configuration 1). In general, the underfloor blowers (APSE blower and TM blowers) contribute most to the 'A' weighted sound level readings.

8.3.1.4 Test Results - 1/3 Octave Analysis. Referring to the 'A' weighted sound levels shown in figures 8-4 through 8-12, it is apparent that the wayside noise with the car stationary was dominated by the contribution from the two TM blowers and the APSE blower on each car. The unweighted 1/3 octave spectra from this equipment for location 4 are shown in figure 8-13. The figure shows both the 1/3 octave spectrum from the APSE system and the 1/3 octave spectrum from the same location with the addition of the two traction motors energized. The salient 63 Hz band is not significant when 'A' weighted (the weighting is -26.2 dB at this frequency), but was sufficiently dominant along with its harmonics to be readily discernable to the ear. The APSE blower on car 0110 was abnormally noisy because of out of balance fan blades; the unweighted 1/3 octave spectra in figure 8-14 were produced at location 7 with this noisy blower and the TM blowers running. The figure shows five salient bands from the 63 Hz band to the 6.3 kHz band. The noisy blower on car 0110 prevented the production of clear frequency spectra from the air compressor. Also, because the auxiliary power supply was always energized and the APSE blower running, clear spectra from the other equipment on car 0109, which produced relatively low sound levels, were not possible.

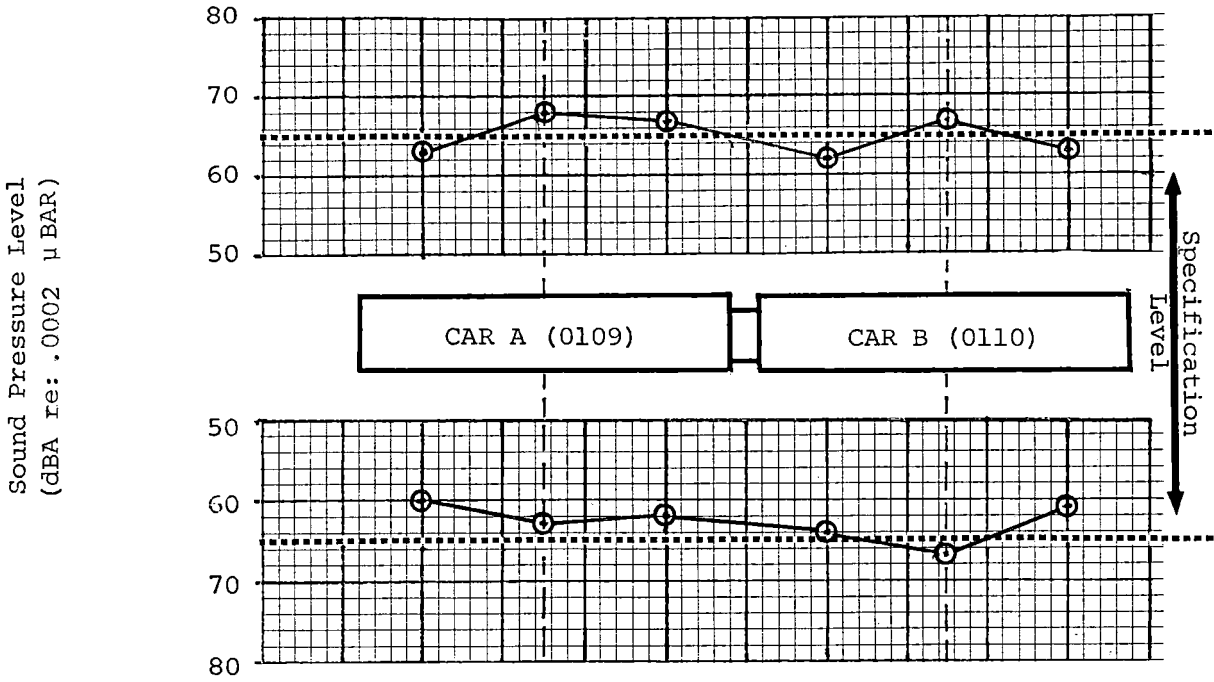


FIGURE 8-4. 'A' WEIGHTED WAYSIDE SOUND LEVELS 15' FROM TRACK CENTERLINE: CARS STATIONARY, CONFIGURATION 1.

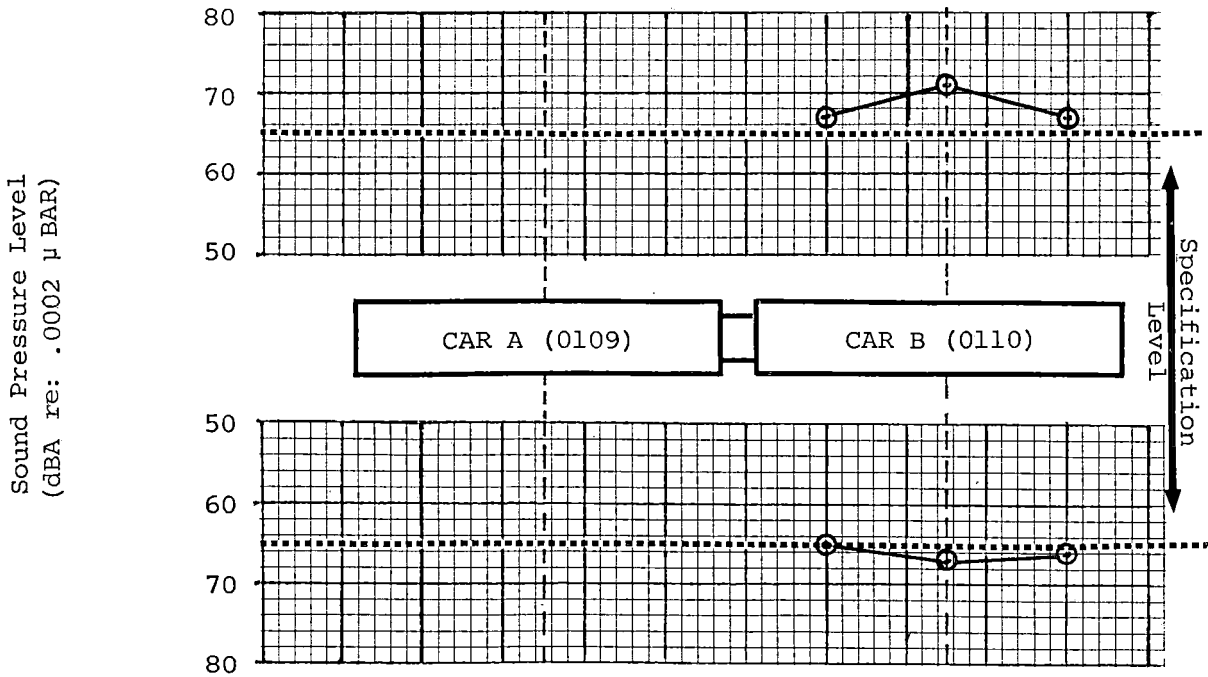


FIGURE 8-5. 'A' WEIGHTED WAYSIDE SOUND LEVELS 15' FROM TRACK CENTERLINE: CARS STATIONARY, CONFIGURATION 1a.

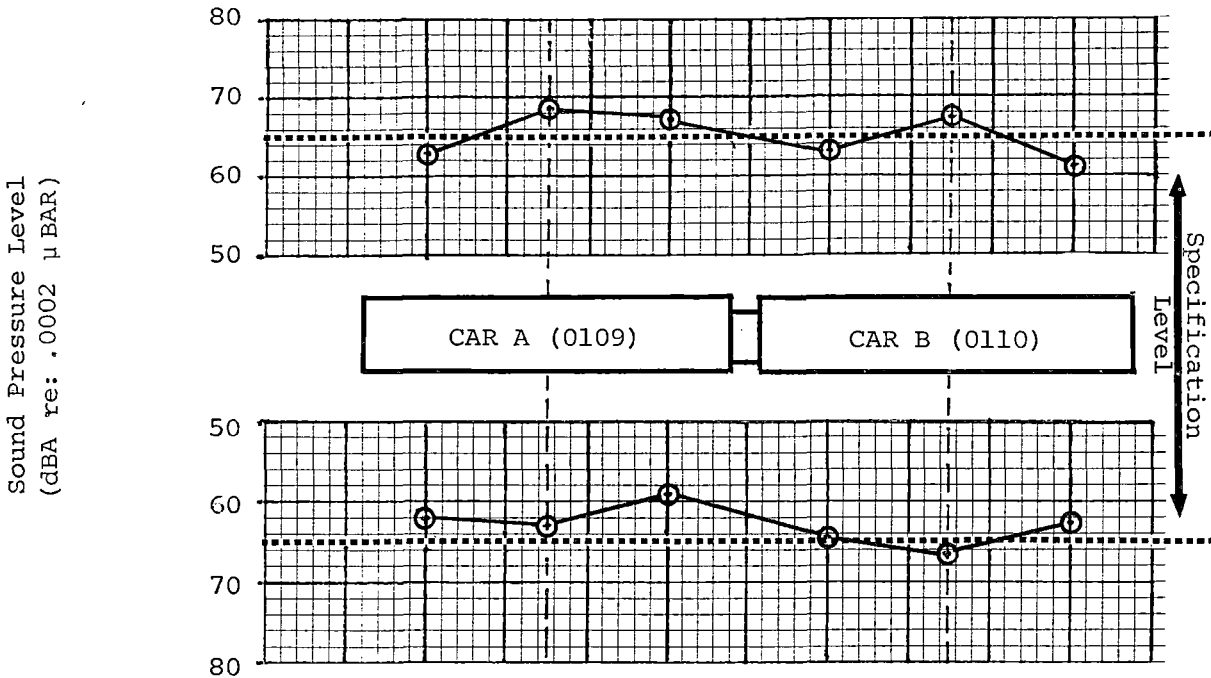


FIGURE 8-6. 'A' WEIGHTED WAYSIDE SOUND LEVELS 15' FROM TRACK CENTERLINE: CARS STATIONARY, CONFIGURATION 2.

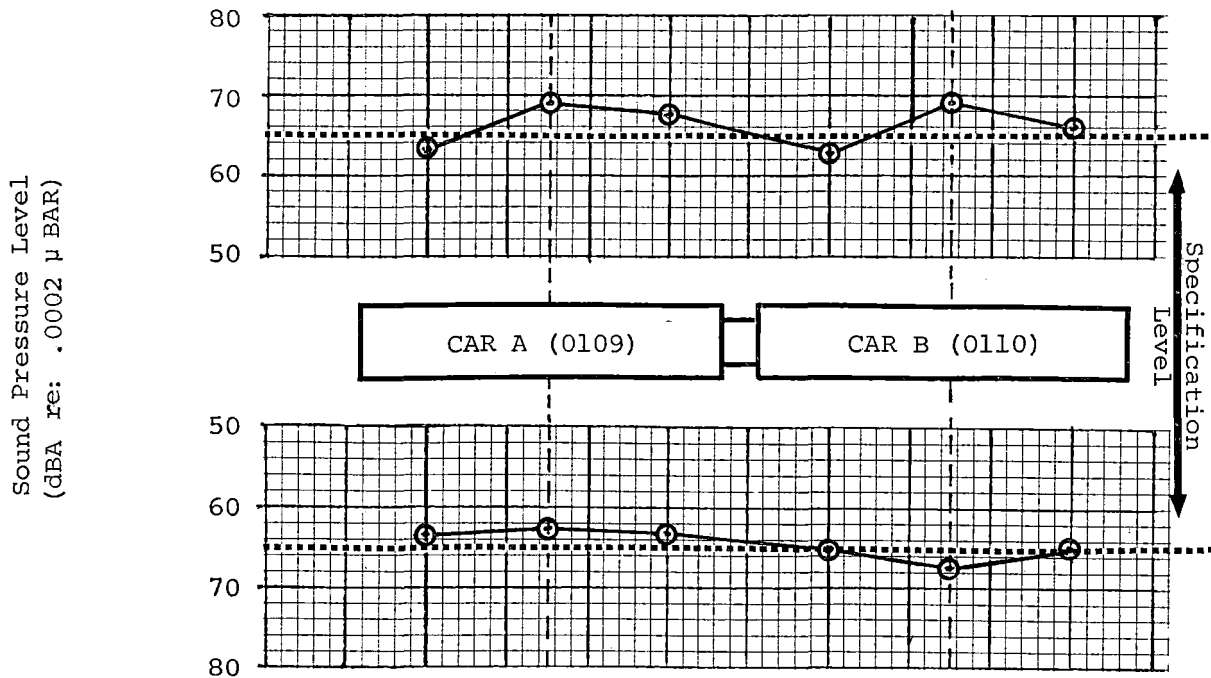


FIGURE 8-7. 'A' WEIGHTED WAYSIDE SOUND LEVELS 15' FROM TRACK CENTERLINE: CARS STATIONARY, CONFIGURATION 3.

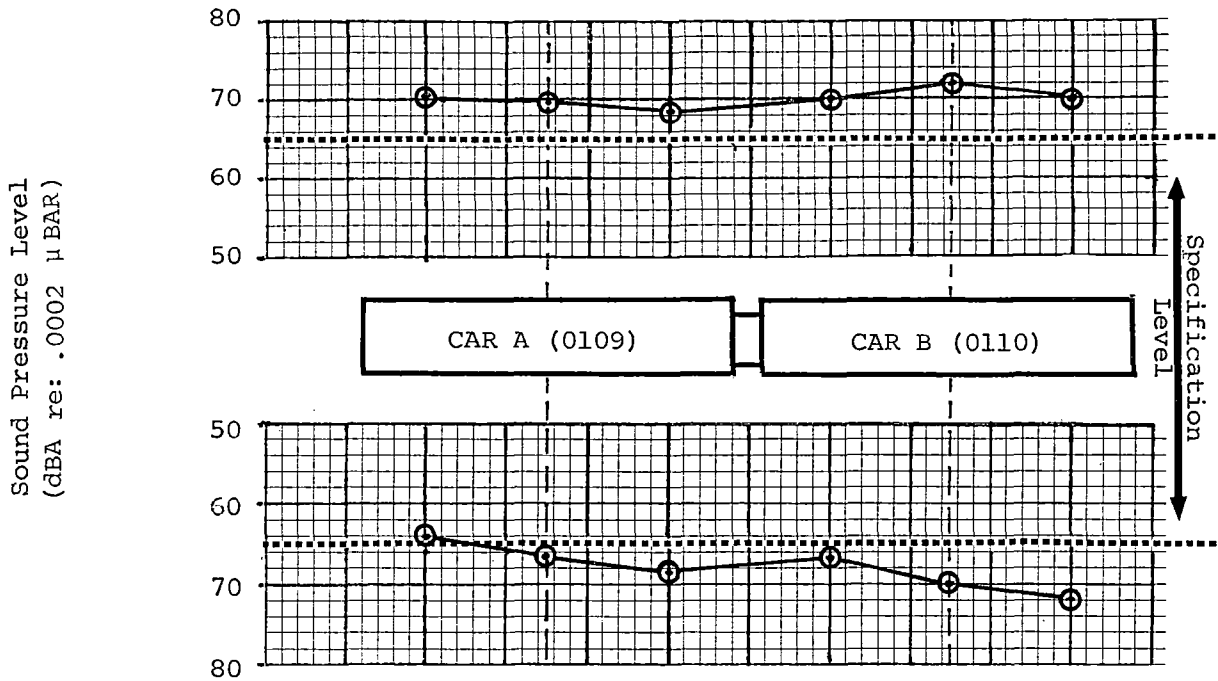


FIGURE 8-8. 'A' WEIGHTED WAYSIDE SOUND LEVELS 15' FROM TRACK CENTERLINE: CARS STATIONARY, CONFIGURATION 4.

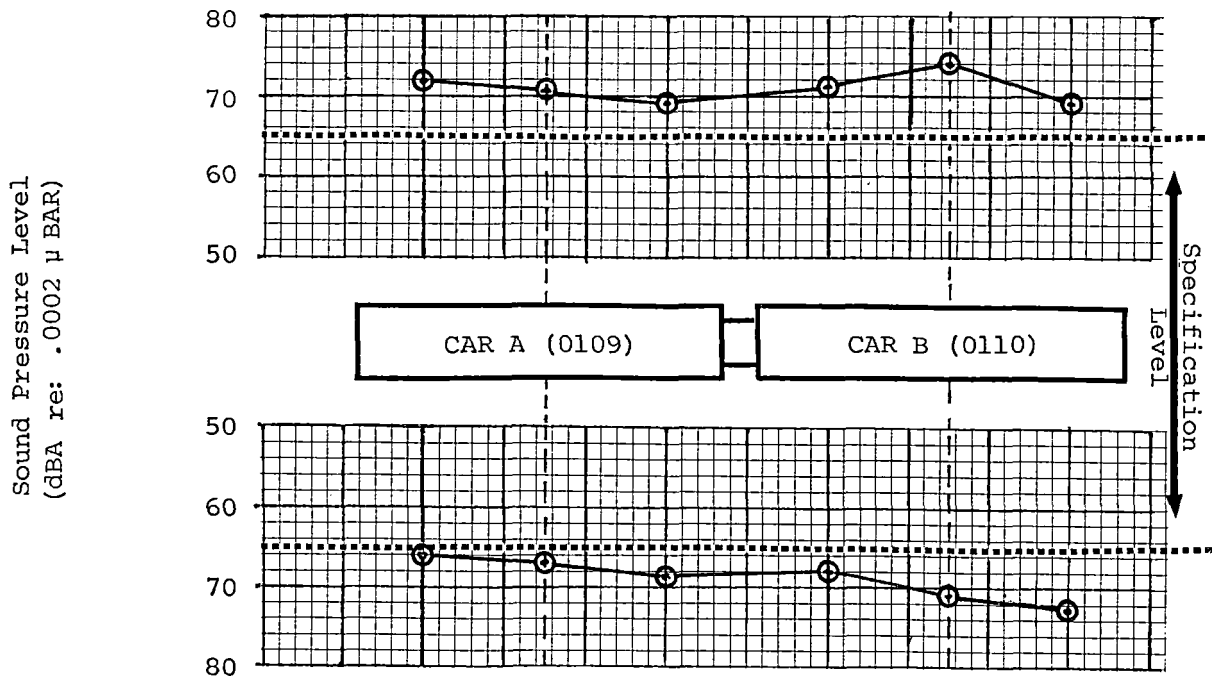


FIGURE 8-9. 'A' WEIGHTED WAYSIDE SOUND LEVELS 15' FROM TRACK CENTERLINE: CARS STATIONARY, CONFIGURATION 5.

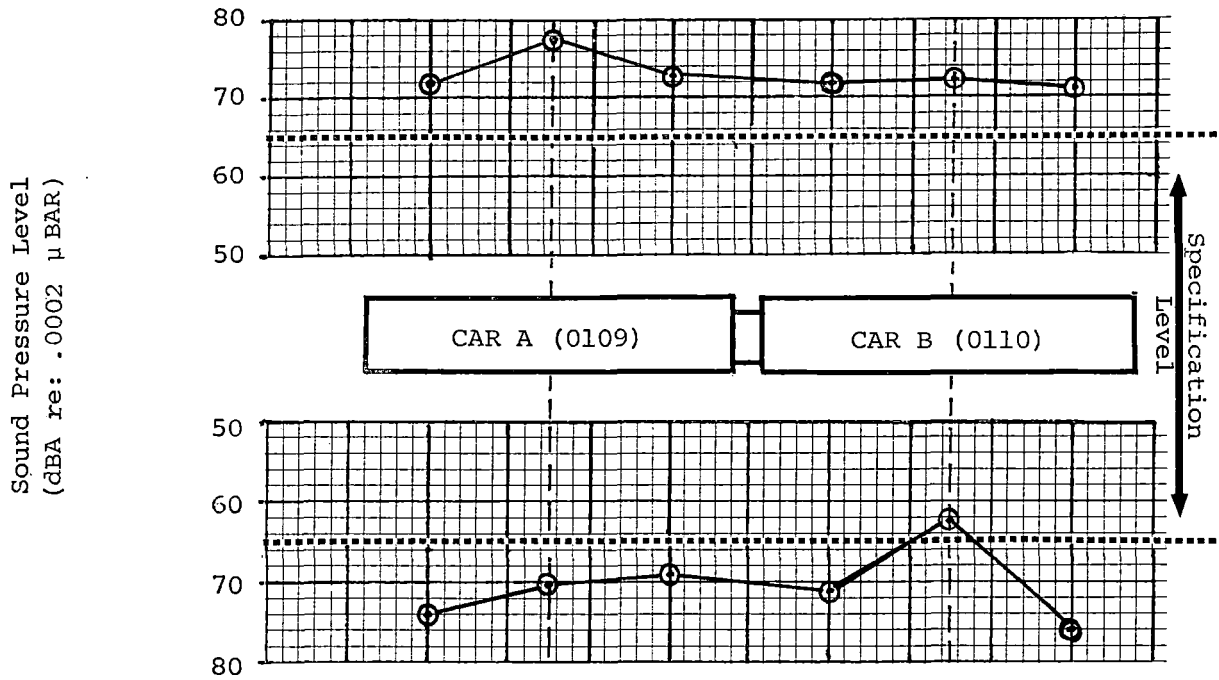


FIGURE 8-10. 'A' WEIGHTED WAYSIDE SOUND LEVELS 15' FROM TRACK CENTERLINE: CARS STATIONARY, CONFIGURATION 6.

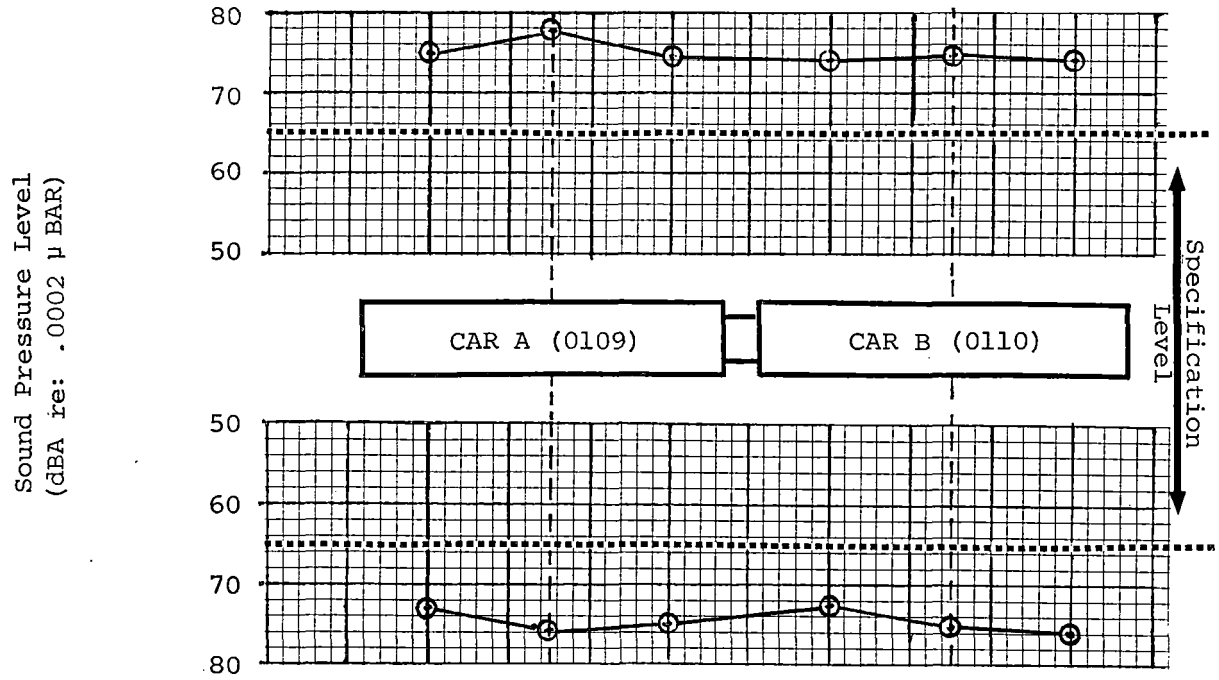


FIGURE 8-11. 'A' WEIGHTED WAYSIDE SOUND LEVELS 15' FROM TRACK CENTERLINE: CARS STATIONARY, CONFIGURATION 7.

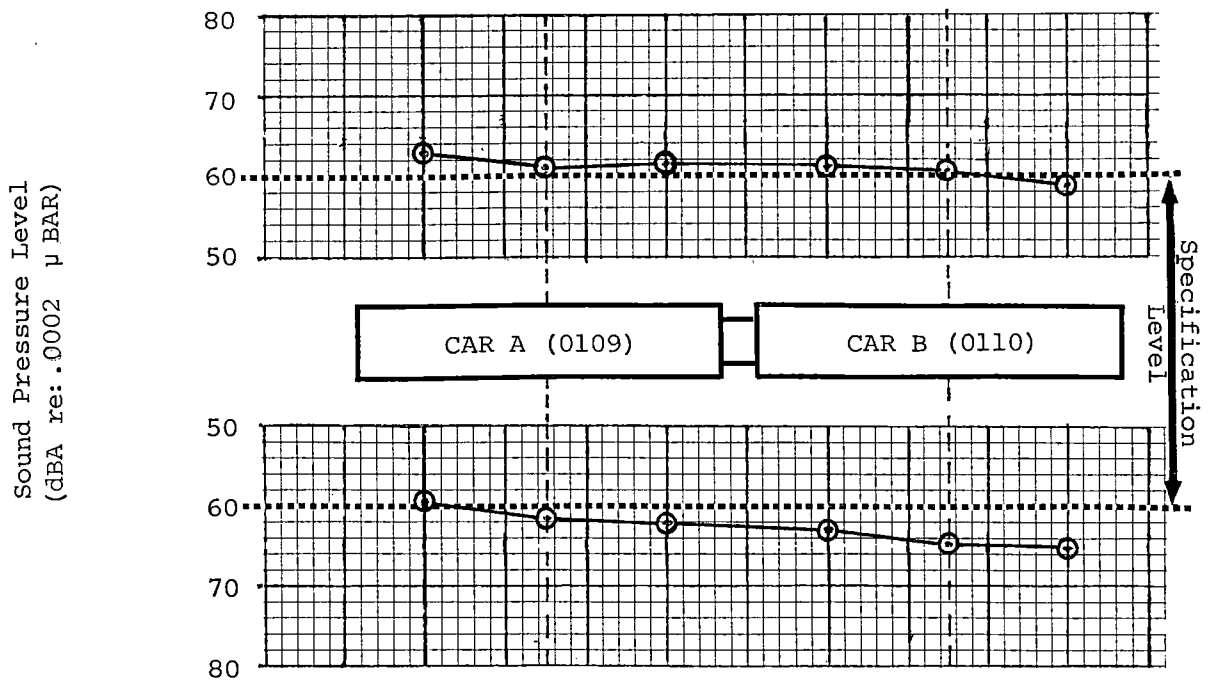


FIGURE 8-12. 'A' WEIGHTED WAYSIDE SOUND LEVELS 50' FROM TRACK CENTERLINE: CARS STATIONARY, CONFIGURATION 5.

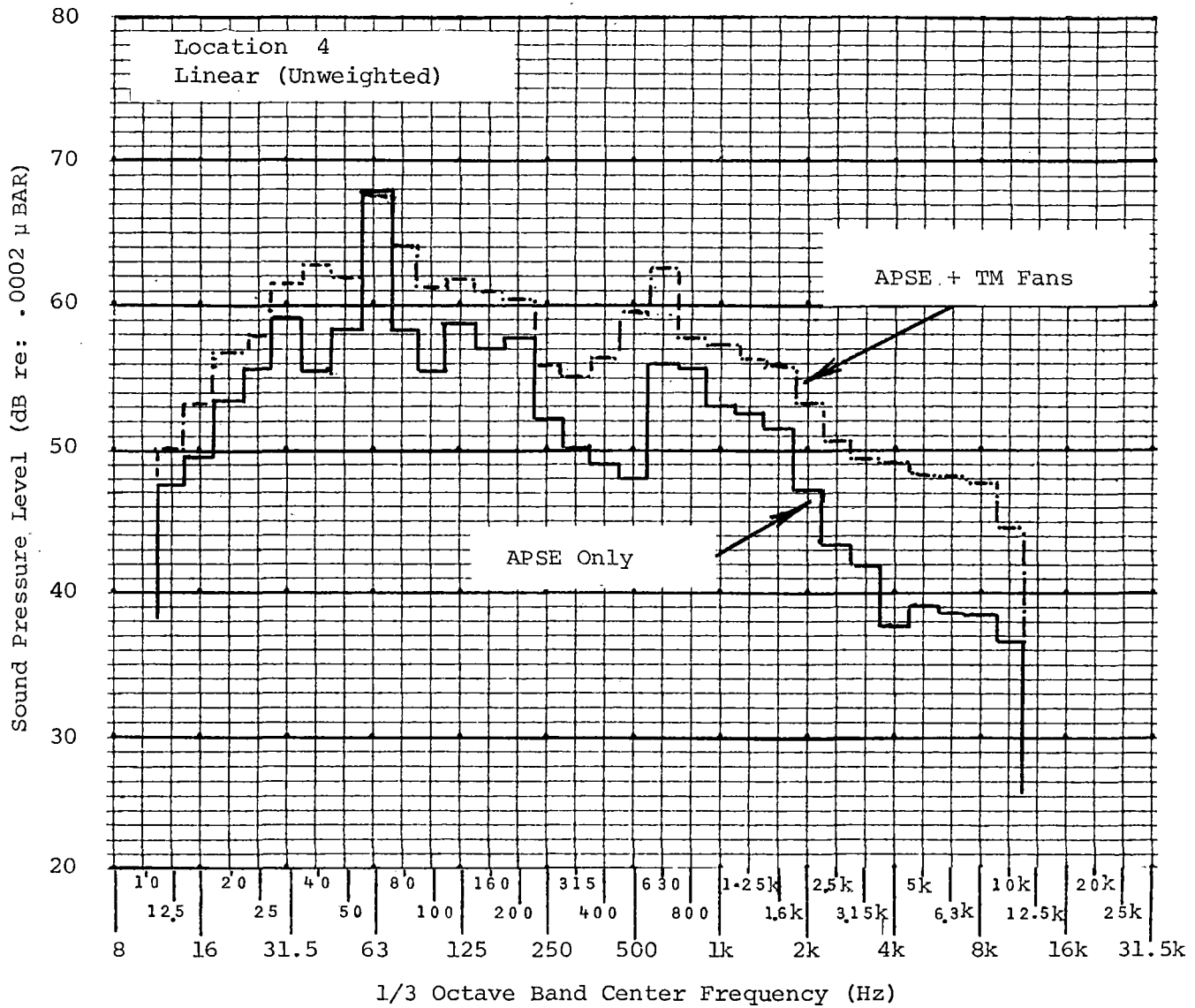


FIGURE 8-13. 1/3 OCTAVE SPECTRUM: WAYSIDE, CAR 0109 STATIONARY.

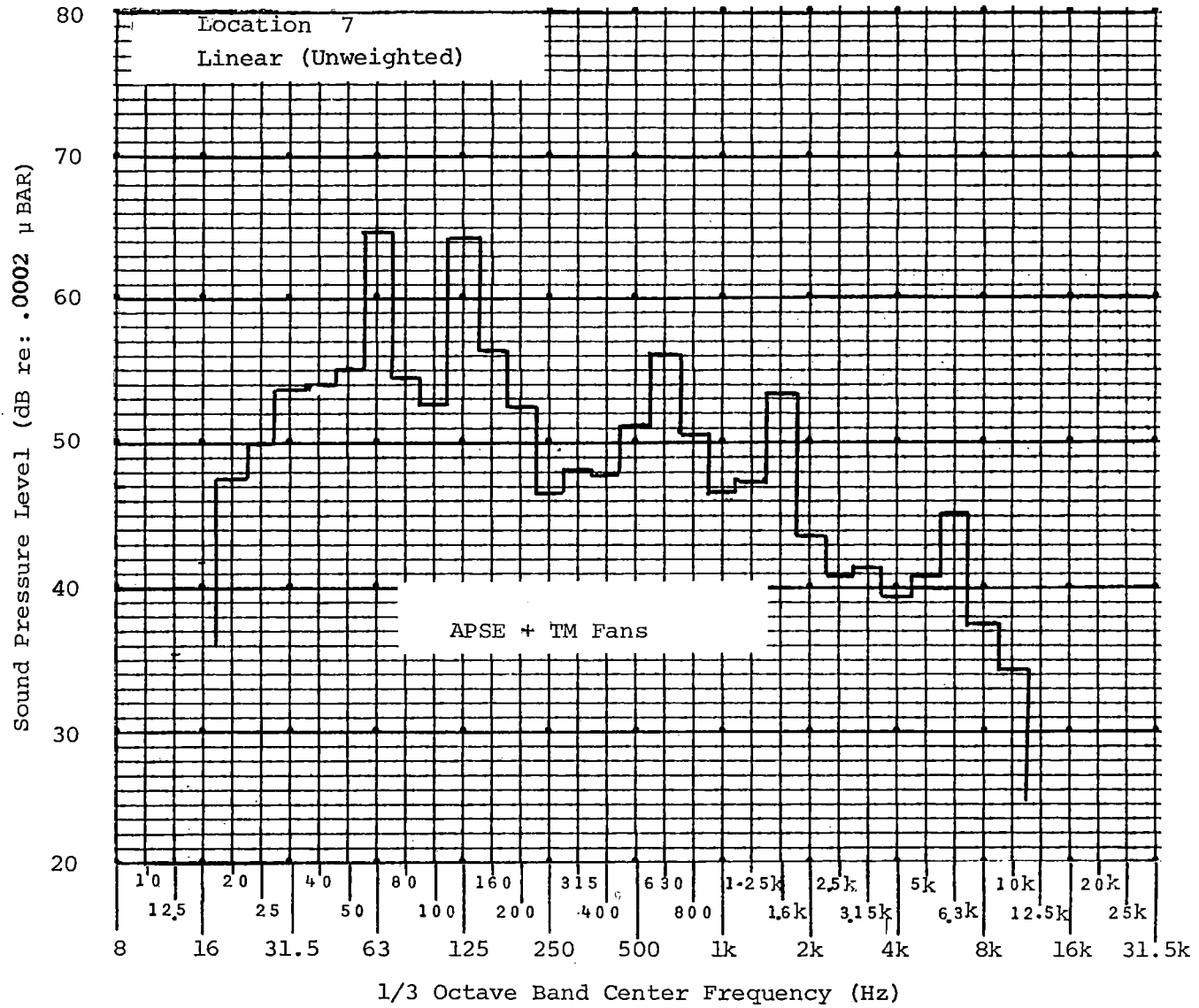


FIGURE 8-14. 1/3 OCTAVE SPECTRUM: WAYSIDE, CAR 0110 STATIONARY.

The frequency spectra in figure 8-13, produced by the APSE and TM fans, show that between the 12.5 Hz band to the 2 kHz band, the sound pressure level variation with frequency is fairly flat.

8.3.2 Interior Noise Characteristics, Car Stationary

8.3.2.1 Objectives. The objectives of the test were:

- To obtain sound level values at a number of locations onboard, as influenced by the operation of major pieces of equipment, and to identify 1/3 octave acoustic signatures from the equipment.
- To determine if the vehicle meets specification requirements for interior noise, which are:

"With auxiliary systems operating normally, the noise level at interior measurement locations shall not exceed 65 dBA in the stationary Transit Vehicle. With each individual auxiliary system operating normally and alone, the noise levels at all specified locations shall not exceed 60 dBA. If the specified sound level, one foot from the return register, cannot be achieved with commercially available fans, the Authority will grant relief in the sound criteria at this location by increasing permissible sound in this area up to 69 dBA.

Distinctive Vehicle Interior Noises and Pure Tones. Any identifiable, distinctive noises such as rasping, grinding, banging, knocking, rattling, and rapping, as measured at a distance not greater than six feet from the apparent noise source, shall be 5 dBA less than the noise level from Transit Vehicle equipment or Transit Vehicle operation in the absence of the identifiable, distinctive noise, or shall not exceed 5 dBA below the specified noise level, whichever is lower. Any pure tone or narrow-band tonal noises inside the Transit Vehicle, as measured at a distance not greater than six feet from the apparent noise source, shall be 5 dB less than the noise level from equipment or Transit Vehicle operation in the absence of the pure tone, as measured by using a 1/3 octave bandwidth, or shall not exceed 8 dBA below the specified noise level, whichever is lower."

8.3.2.2 Test Methods. The vehicles were positioned on level tangent tie-and-ballast track (yard track), with the third rail energized to 750 V d.c. Interior microphone locations are identified in figure 8-15. To assess the contribution of each major component of equipment to the sound level readings, the same configurations were tested as in the wayside tests (tables 8-1 and 8-2). As with the wayside tests, readings were taken on an individual car basis. Tape recordings were also made at selected locations and configurations.

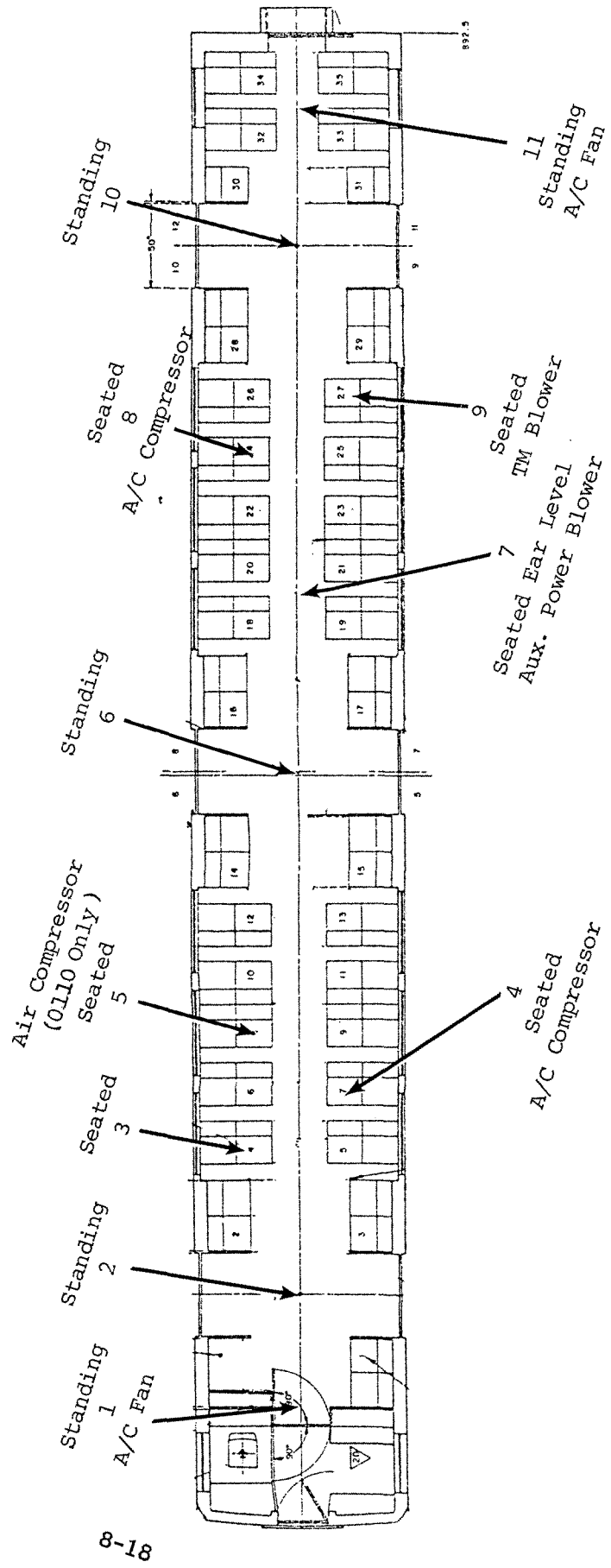


FIGURE 8-15. ONBOARD MEASUREMENT LOCATIONS, CARS STATIONARY.

8.3.2.3 Test Results - 'A' Weighted Sound Level Readings. Table 8-3 lists the 'A' weighted sound level readings. Results include:

- The most significant single contribution to onboard noise level (average of 63.6 dBA) was caused by the air conditioning equipment. This was most evident at each end of the cars, at a standing ear level beneath the fan outlets (see configuration 2, table 8-1).
- The sound levels at the air conditioning outlets locally exceeded the specified maximum of 65 dBA. This was mitigated by the specification relaxation to 69 dBA at the outlets themselves. The average sound level at the four locations just meets the above relaxed specification.
- The sound levels decreased unexpectedly by an average of 2.75 dBA when the air conditioning compressors were switched on, presumably because of the voltage drop characteristics of the equipment.
- With all equipment operating in car 0109, the noise levels at all of the 10 locations tested averaged 3.2 dBA below the specification maximum of 65 dBA.
- With all equipment operating in car 0110, the noise levels at seven of the eleven locations tested exceeded the specification maximum of 65 dBA by an average of 5.14 dBA.
- For locations remote from the air conditioning fan outlets, the contribution to noise levels from TM fans was approximately equal to that from air conditioning equipment.
- With the auxiliary power system operating alone, the noise levels at two of the eight locations tested averaged 1.25 dBA above the specification maximum of 60 dBA.
- With the auxiliary power energized and with doors on both sides of the car operating, the noise levels (excluding chime) at all six locations tested were, on average, 78.7 dBA.

8.3.2.4 Test Results - 1/3 Octave Analysis. The majority of 1/3 octave analyses in this section are from car 0109 because car 0110 had an abnormally noisy blower. The 1/3 octave unweighted spectra are shown in figure 8-16 for a recording made at ear level in the sitting position, in car 0109, location 7, with only the auxiliary power system on. The spectra, as with the stationary wayside noise, show a salient band at the 63 Hz center frequency. However, unlike the wayside frequency spectrum from the APSE, in which the band levels are fairly flat, 1/3 octave band levels in this case decrease rapidly above the 250 Hz band. It follows that there was poor acoustic isolation from the APSE blower at the low frequencies, but good isolation at higher frequencies. Also shown in the same figure are the 'A' weighted spectra from the 12.5 Hz band to the 800 Hz band. Above the 800 Hz band, the unweighted and 'A' weighted spectra are similar because the weighting values are only small. The figure shows that, at this location, the significant frequencies that contribute to the 'A' weighted meter readings lie in the 200, 250, and 315 Hz bands.

TABLE 8-3. 'A' WEIGHTED SOUND LEVELS; INTERIOR NOISE, STATIONARY CARS.

Car No.	Location In Car	Configuration									
		1 (dBA)	1a (dBA)	2 (dBA)	3 (dBA)	4 (dBA)	5 (dBA)	w/out chimes (dBA)		w/chimes (dBA)	
0 1 0 9	1*			70.5	63.5		64.5				104
	2*	51.5		62.5	57.5	60	63	81	91	81	96
	3					59	60				90
	4				57		61				87
	5										
	6*	58		62.5	60	58	60.5	76.5	94.5	77	96.5
	7	60.5		54	61.5	59.5	60.5				96.5
	8				57.5		61.5				91.5
	9					61	62.5				97.5
	10*	56		62	57.5	60	61	76.5	86.5	78	92.5
	11*			67.5	62		63.5				98.5
0 1 1 0	1*			69.5	64		70				105
	2*	52.5	52	61.5	57	70	73	80	94.5	80	95
	3					71	69.5				95
	4				59		69				94
	5		54.5				70.5				88
	6*	57	57	62	60	64	65	79.5	95.5	80.5	96.5
	7	62	59	62	61.5	63.5	64		92.5		85
	8				60.5		66				97
	9					63	64.5				95
	10*	52	52.5	61	56.5	65.5	65	79.5	92.5	80	90
	11*			68.5	69.5		73				100
Slow Meter Response							Fast Meter Response				

*Readings taken at standing ear level; others taken at seated ear level.

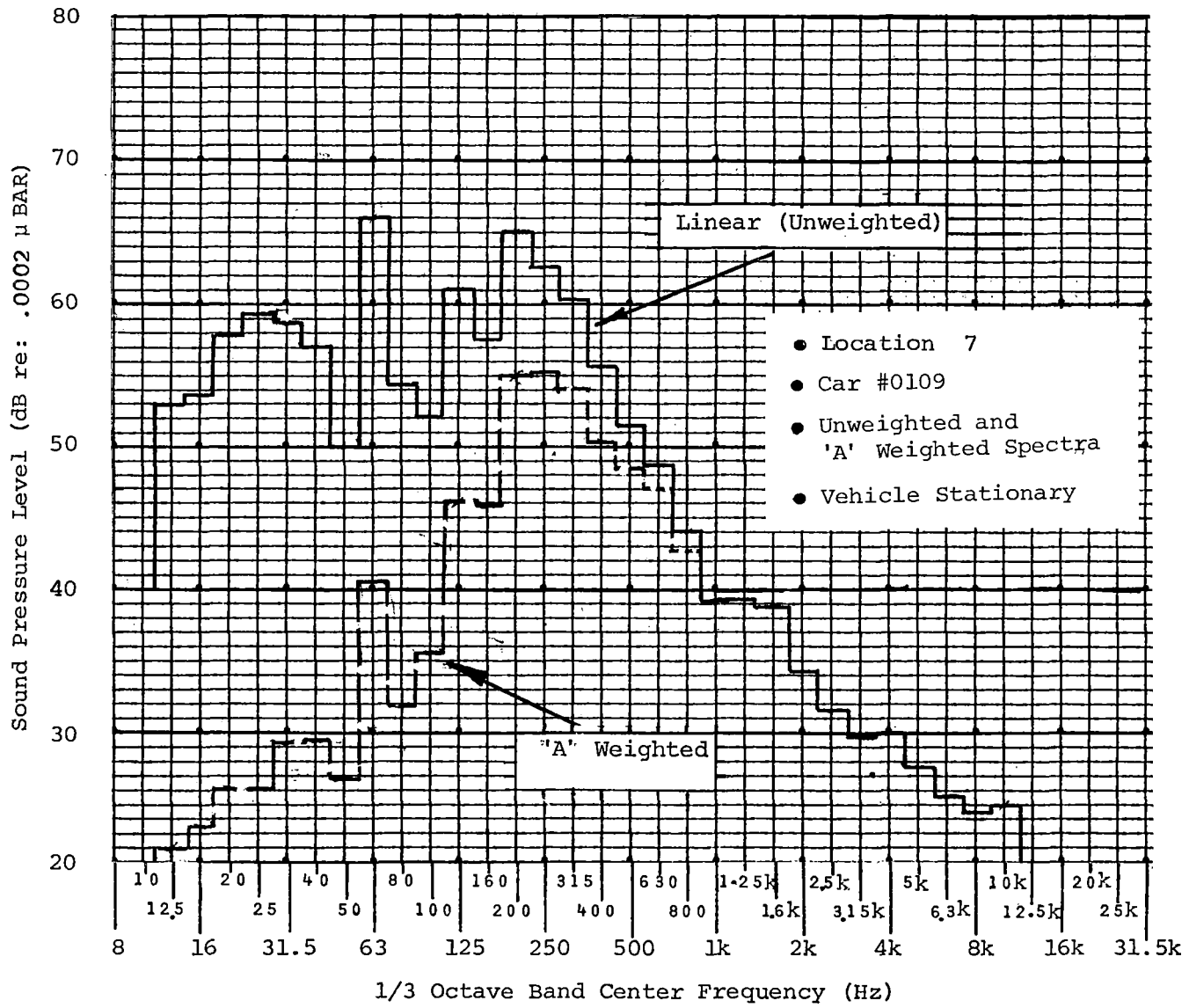


FIGURE 8-16. ONBOARD 1/3 OCTAVE SPECTRA: APSE ENERGIZED ONLY.

Although the salient 63 Hz band does not lie in the range addressed by the pure tone requirements of the vehicle specification; i.e., 300 Hz to 4 kHz, it is very prominent (12 and 16 dB, respectively, above adjacent bands) and is easily discernable to the ear.

The 1/3 octave unweighted spectra are shown in figure 8-17 for a recording made at ear level, in the standing position in car 0109 beneath the air conditioning outlet, location 1 with the APSE and air conditioning fan operating. Also shown in the same figure are the 'A' weighted spectra from the 12.5 Hz band to the 800 Hz band. The 'A' weighted spectra are fairly level from the 100 Hz band to the 1.6 kHz band, and the significant band that contributes to a dBA meter level reading is the 160 Hz band.

The 1/3 octave frequency spectrum produced by a TM blower can be seen in figure 8-18. The figure shows the unweighted spectra from the 12.5 Hz band to the 10 kHz band and shows the 'A' weighted spectrum from the 12.5 Hz band to the 800 Hz band. The recording was taken at a seat location over the front traction motor (location 3). The spectra show a very high 63 Hz band and a harmonic at the 125 Hz band. The 'A' weighted spectrum in figure 8-18 shows that the 63 Hz band was the greatest 'A' weighted 1/3 octave band and, along with the 200 to 500 Hz bands, contributed most to the 'A' weighted sound level readings taken at this location. The 63 Hz data show that the TM blowers had poor acoustic isolation in the low frequency range.

The spectra shown in figure 8-19 for all equipment operating were produced from a recording made in the standing position (location 6). The unweighted and 'A' weighted spectra are shown. Each spectrum contains the salient band at 63 Hz produced by the underfloor blowers, but above the 500 Hz band, the spectrum is probably produced by the above-floor air conditioning equipment. This is concluded because the band levels above the 500 Hz band are much higher than those produced by the underfloor equipment, even when the microphone was closer to the floor.

In general, the noise produced from the underfloor equipment is dominant in the lower frequencies and contains strong pure tones, but the noise produced from above-floor equipment is dominant in the higher frequencies and does not contain significant pure tones.

Unfortunately, car 0110 had an abnormally noisy APSE blower and, since this blower was running for all configurations, clear isolated spectra from the air compressor and other configurations were not possible. The linear and 'A' weighted spectra from a recording taken in car 0110 at location 3, with APSE and TM blowers energized (configuration 4), are shown in figure 8-20. The spectra show high salient bands at low frequencies but above the 500 Hz band they rapidly taper off (unlike the spectra obtained for the same equipment, running wayside, which show a broader shape). Again, this indicates that the vehicle attenuated high frequencies well, but not low frequencies.

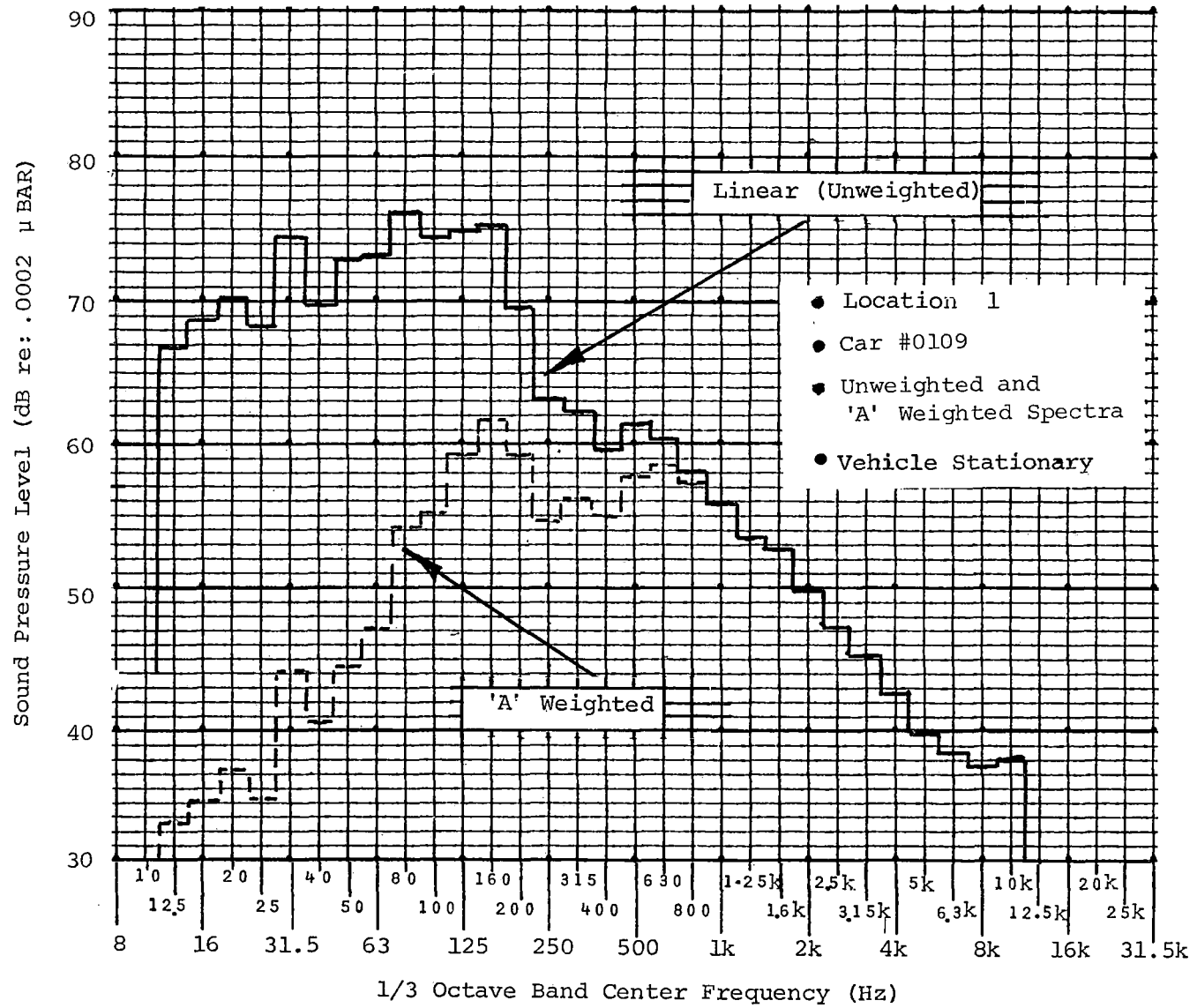


FIGURE 8-17. ONBOARD 1/3 OCTAVE SPECTRA:
BENEATH AIR CONDITIONING FAN OUTLET.

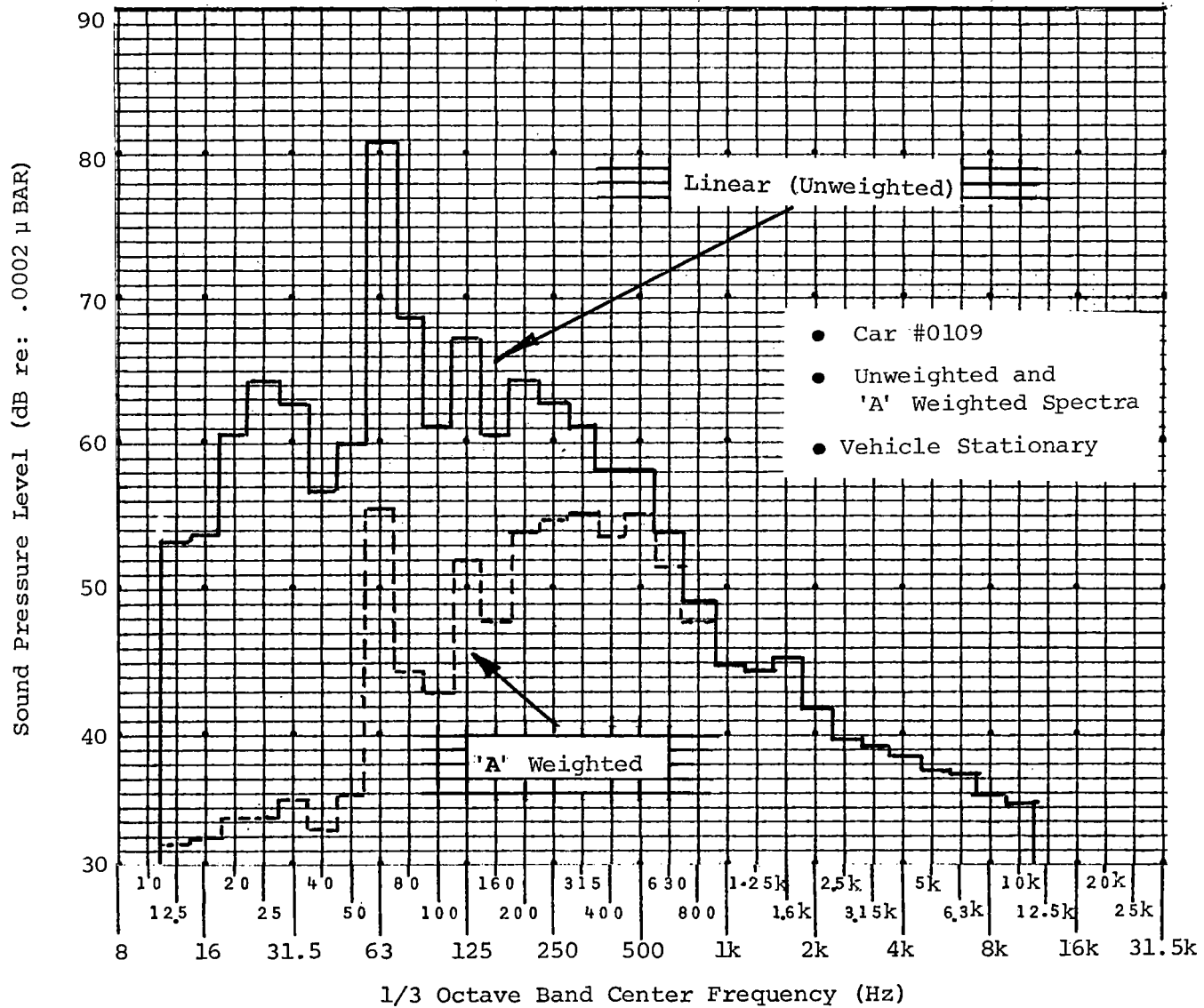


FIGURE 8-18. ONBOARD 1/3 OCTAVE SPECTRA: 'SEATED',
LOCATION 3 - APSE AND TM FANS ENERGIZED.

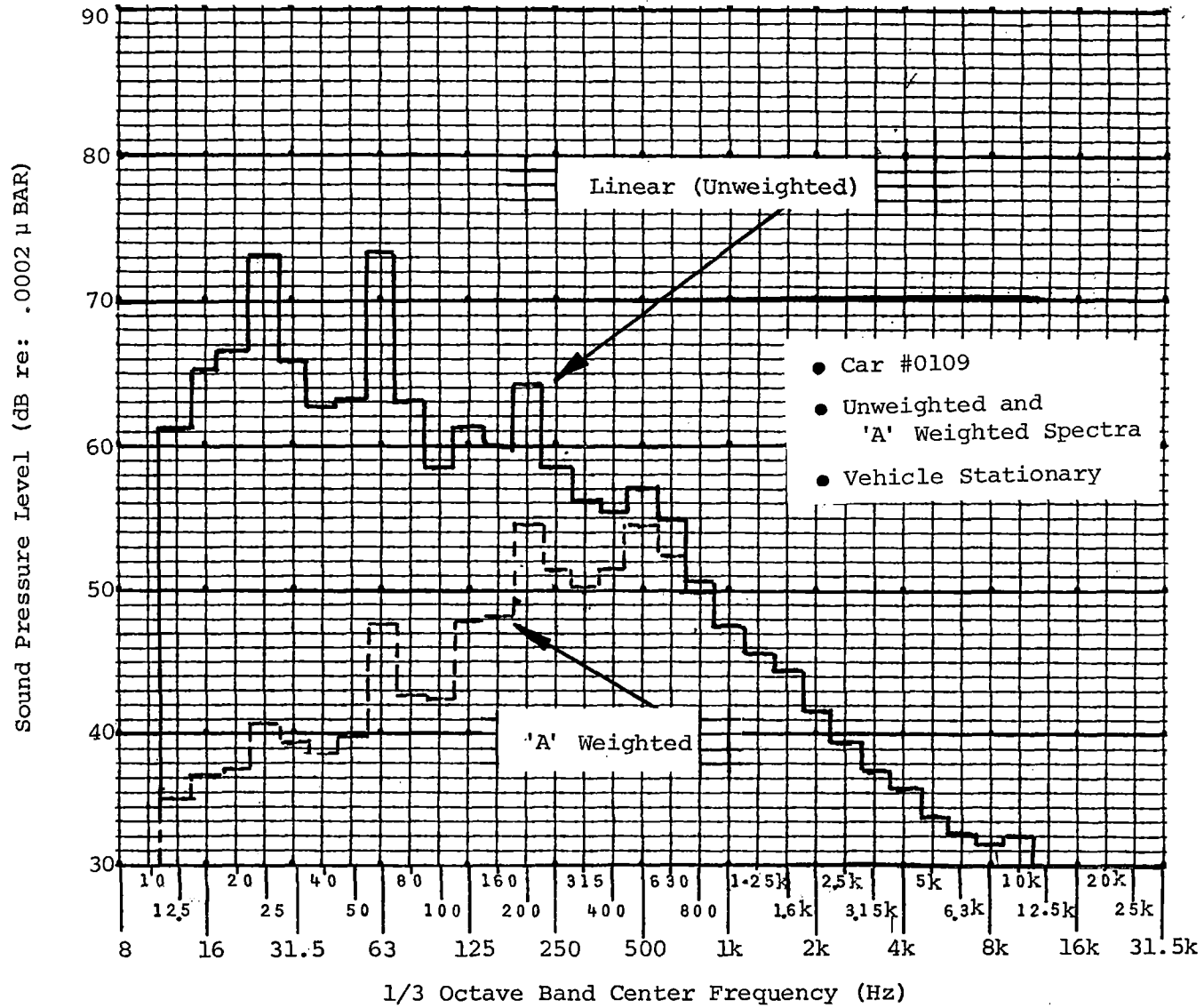


FIGURE 8-19. ONBOARD 1/3 OCTAVE SPECTRA: 'STANDING', CENTER OF CAR, AUXILIARY EQUIPMENT ENERGIZED.

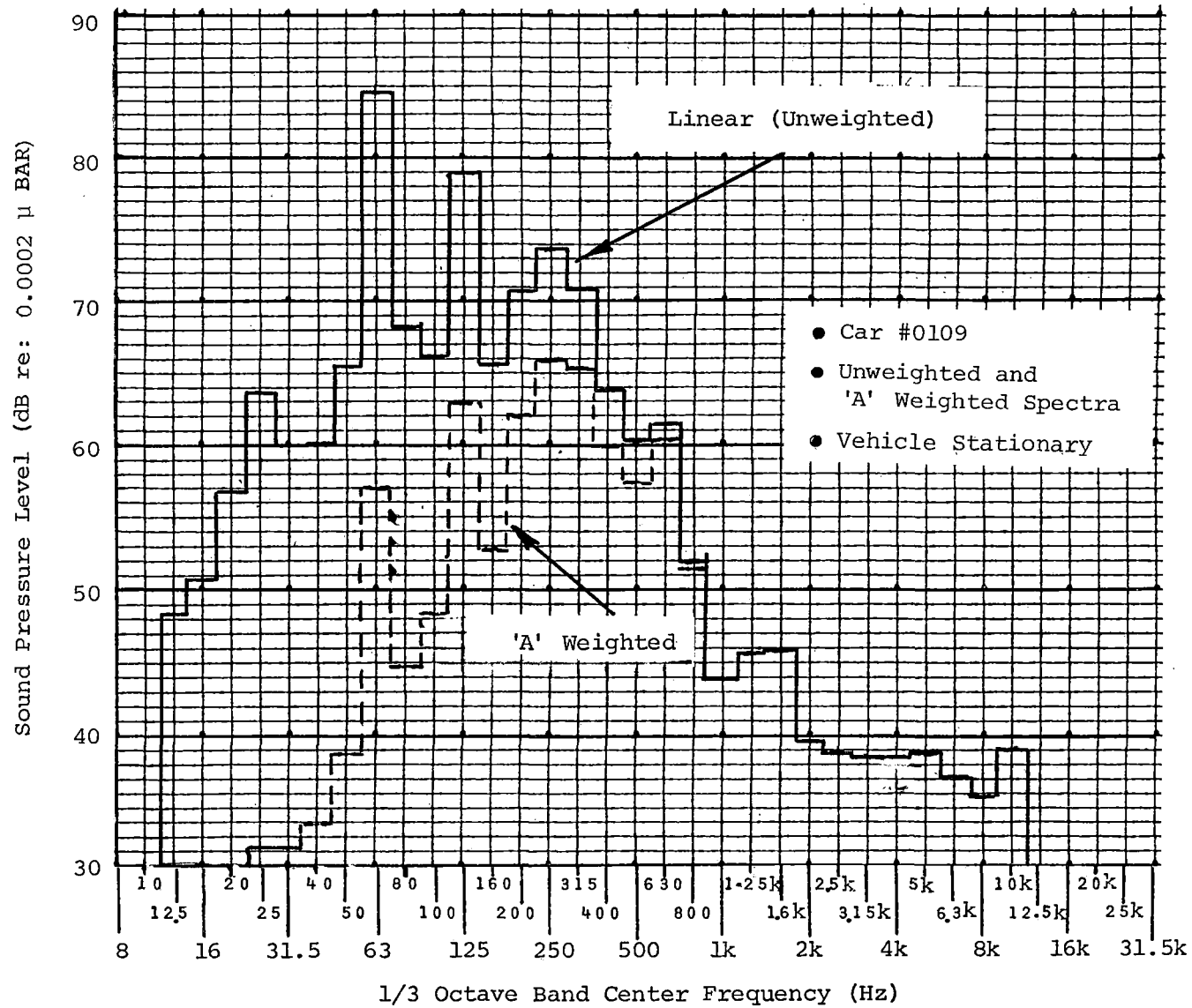


FIGURE 8-20. ONBOARD 1/3 OCTAVE SPECTRA: 'SEATED',
LOCATION 3 - APSE AND TM FANS ENERGIZED.

8.3.3 Noise Level Variation with Location Onboard, Car Travelling at 55 mi/h

8.3.3.1 Test Objective. The objective was to evaluate the acoustic characteristics for various locations in the car at 55 mi/h, and to compare those characteristics to the vehicle specification requirements, which are:

"The interior noise levels in a vehicle moving on tangent, tie-and-ballast track, with all systems operating, shall not exceed the values indicated by the solid curve in figure 8-21. Noise levels in the moving car shall be measured in a train of two Transit Vehicle minimum length, operating at: constant speeds, from 10 mi/h to 70 mi/h, in 10 mi/h increments; maximum acceleration, from rest to 70 mi/h; and normal braking, from 70 mi/h to rest."

8.3.3.2 Test Method. The train was run at a constant speed of 55 mi/h through the test section. The test section consisted of jointed rail on wood tie-and-ballasted roadbed (sections 30 - 33). 'A' weighted sound levels were measured at the 20 locations in car 0109 (figure 8-22). Data were taken with the sound level meter held at either seated ear level or standing ear level and the meter was set to 'Slow' response. The average meter reading over a period of 15 seconds was recorded.

8.3.3.3 Test Results - 'A' Weighted Sound Level Readings. The 'A' weighted sound pressure level readings for each location are shown in figure 8-22. From the data it was concluded that:

- The sound levels at the two locations at the center door were an average of 5.5 dBA below the specification maximum, which is 68.5 dBA for this location at 55 mi/h.
- The sound levels at the extreme ends, standing at the inner car door, and seated and standing in the operators cab area, were an average of 9 dBA below the specification maximum, 71 dBA for the ends of the car, at 55 mi/h.
- The most stringent specification requirement at 55 mi/h was the 68.5 dBA maximum for the center of the car. However, the sound level at all 20 locations tested was an average of 5.25 dBA below this value.
- The sound levels at all 20 locations spanned a range of 6.5 dBA, with a maximum of 67 dBA at the left rear doors.

The sound levels tended to be highest at the doors and toward the rear of the car, with the motorman's operating cab being among the quietest locations. This is probably due to the isolation provided by the doors, which separate the cab from the passenger compartment where the air conditioning outlet is located.

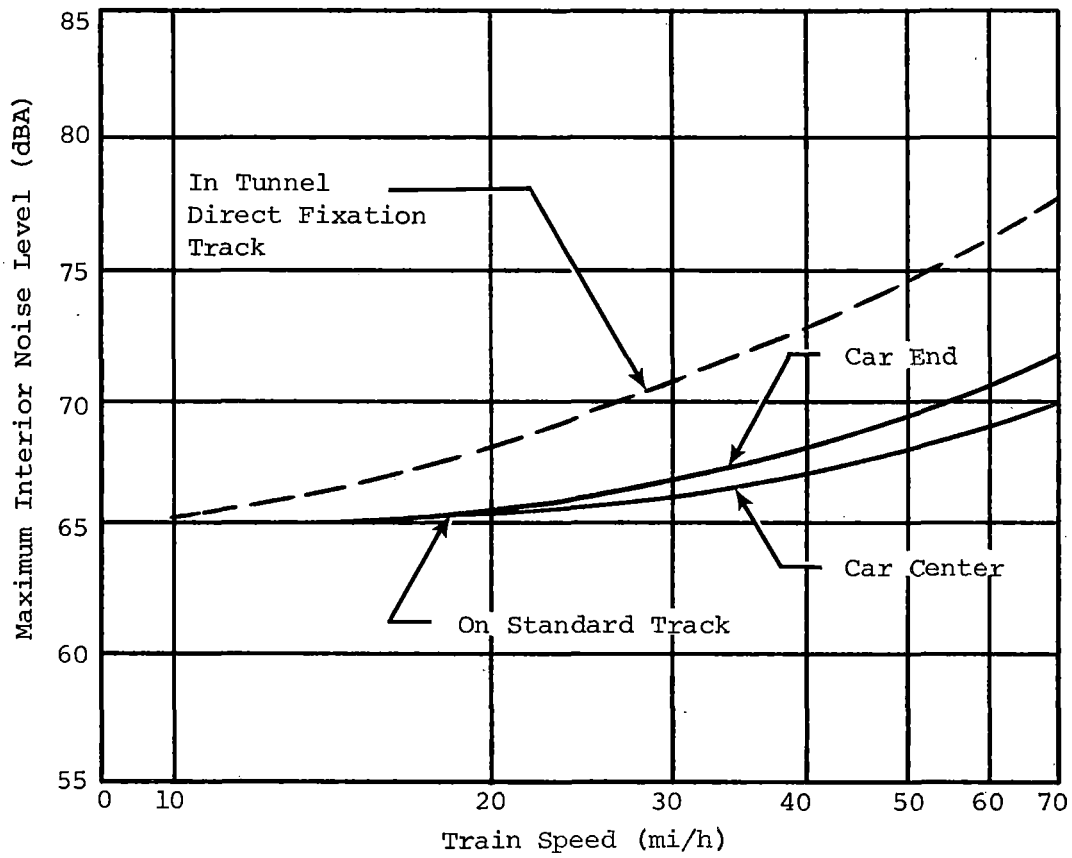


FIGURE 8-21. CAR INTERIOR NOISE LEVEL LIMITS.

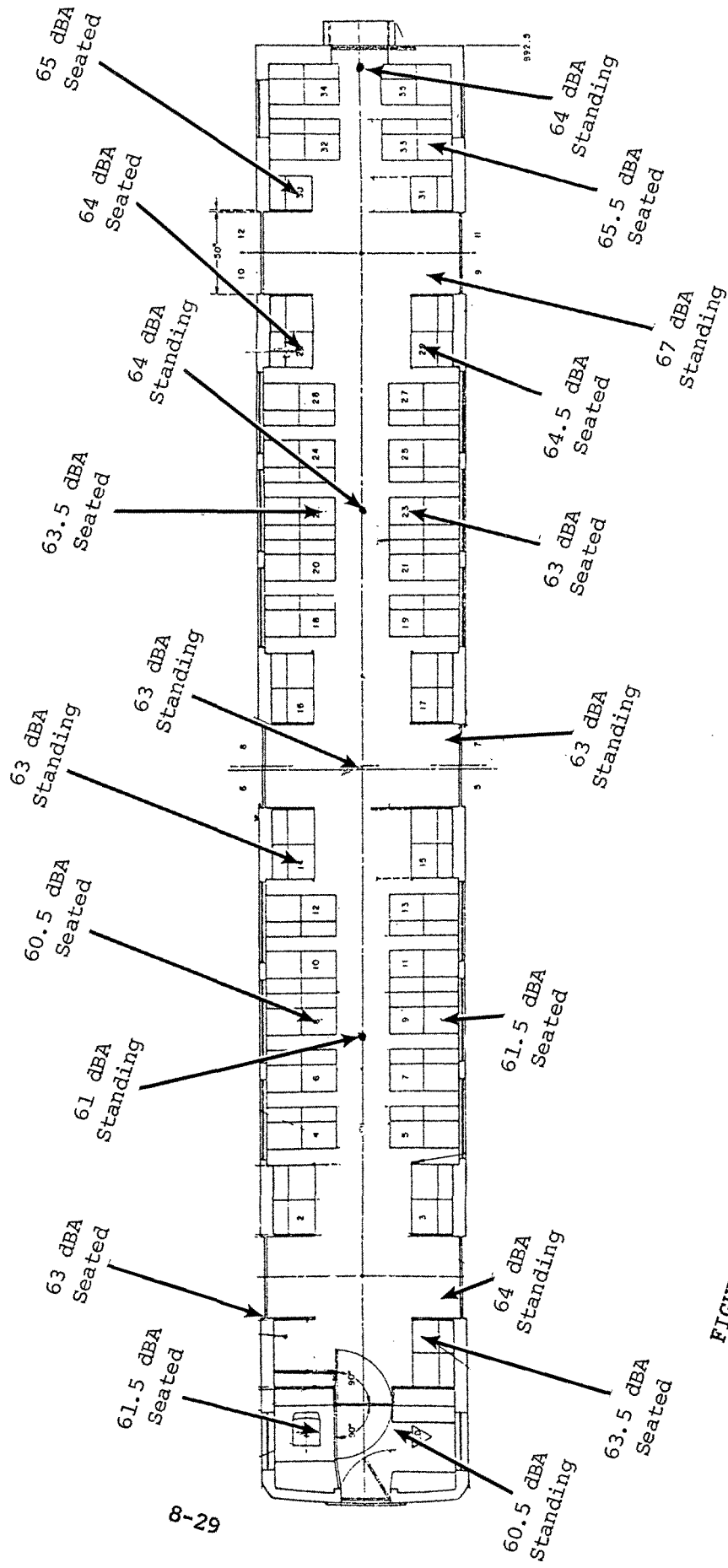


FIGURE 8-22. ONBOARD MEASUREMENT LOCATIONS, 'A' WEIGHTED SOUND LEVELS:
 CAR 0109 AT STEADY SPEED OF 55 mi/h.

8.3.4 Noise Characteristic at a Number of Steady Speeds, Onboard - 0-70 mi/h

8.3.4.1 Objective. The objective of the test was to determine the noise levels at a number of locations onboard the car, as influenced by steady speed. An additional objective was to identify the predominant 1/3 octave bands at each speed.

8.3.4.2 Test Method. The vehicles were run at five constant speeds over concrete tie and welded track (stations 33 to 42). The vehicle weight was AWO and the track energized to 750 V d.c. Sound levels were recorded in the motorman's cab and between the front, center, and rear doors, on the car centerline. Twenty 'A' weighted sound levels were taken on a B&K 2203 sound level meter with the meter characteristic set to 'Slow'. The average meter reading over a 15-s period was recorded. Tape recordings were made at selected locations for later analysis and were high-pass filtered at 22.4 Hz. Because car 0110 had an abnormally noisy blower, readings were only taken in car 0109. Interconnecting doors and the operator door were closed.

8.3.4.3 Test Results - 'A' Weighted Sound Level Readings. Table 8-4 lists the 'A' weighted sound level readings taken.

TABLE 8-4. 'A' WEIGHTED SOUND LEVELS ('SLOW' METER CHARACTERISTIC).

Speed (mi/h)	Motormans Cab (dBA)	Front Car Doors (dBA)	Center of Car (dBA)	Rear Car Doors (dBA)
0	57	60 (65)	62.5 (65)	62 (65)
15	58	61 (65.6)	63.5 (65.5)	63 (65.6)
35	58	62 (68)	63 (67)	63 (68)
55	60.5	63.5 (70.5)	63.5 (69)	64.5 (70.5)
70	65	65.5 (72)	64 (70)	66 (72)

NOTE: Figures in () are the maximum noise level limits set in the vehicle specification.

From these readings, the following are concluded:

- At no location or speed did the noise levels exceed the maximum permitted levels.
- On average, the levels were 4.8 dBA below the maximum permitted levels.

- Noise levels increased as the speed increased, and did so to the greatest extent at the ends of the car.
- 'A' weighted noise levels increased by only 1.5 dBA at the center of the car in the speed range 0 to 70 mi/h.

The very small increase in dBA level at the center of one car (as the speed increased) is addressed in the next section.

8.3.4.4 Test Results - 1/3 Octave Analysis and Time Histories. It was suspected that the 'A' weighted sound pressure levels did not increase significantly with speed because as speed increased, the contribution of wheel/rail noise transmitted into the car was small in comparison to the steady background noise from auxiliaries. The wheel/rail noise increase was in the high frequency range, which in this case did not contribute significantly to the 'A' weighted meter readings.

To test the above hypothesis, recordings made in the center of the car were analyzed. Figure 8-23 shows the 'A' weighted 1/3 octave spectra at 0 and 70 mi/h for the same location. The 1/3 octave bands in the figure show an increase in sound pressure level at 70 mi/h, except in the midrange about the 400 Hz band, where levels remained approximately the same.

The sound levels from the auxiliary equipment in the bands 250 Hz to 800 Hz are strong enough to effectively mask track and other noise at all speeds. Since, in this case, 250 Hz to 800 Hz bands are also the most significant in producing 'A' weighted sound levels, it follows that there will be little change of dBA reading with speed at this location.

8.3.5 Noise Characteristic Under Acceleration and Deceleration Onboard

8.3.5.1 Test Objective. The objective was to measure the 'A' weighted sound levels inside the cars, as influenced by acceleration and deceleration.

8.3.5.2 Test Method. The vehicles were accelerated from 0 to 70 mi/h on tangent level jointed rail, concrete ties, and ballasted track (section IV). 'A' weighted sound level readings were taken at one location in the standing position at ear level on the centerline of the car adjacent to seat 28 on car 0109. The meter characteristic was set to 'Slow' and the observers noted the average reading over a period of 2 seconds.

For the deceleration tests, two runs were made, one with friction brakes only and the other with blended brakes. An additional measurement location was used, seated at seat number 8. In addition, for both the acceleration and deceleration tests, 'A' weighted sound level versus time strip charts were made in real time, from a B&K type 2209 sound level meter connected to a B&K type 2306 level recorder. The pen writing was set to 16 mm/s (which corresponds to a meter characteristic of 'Slow').

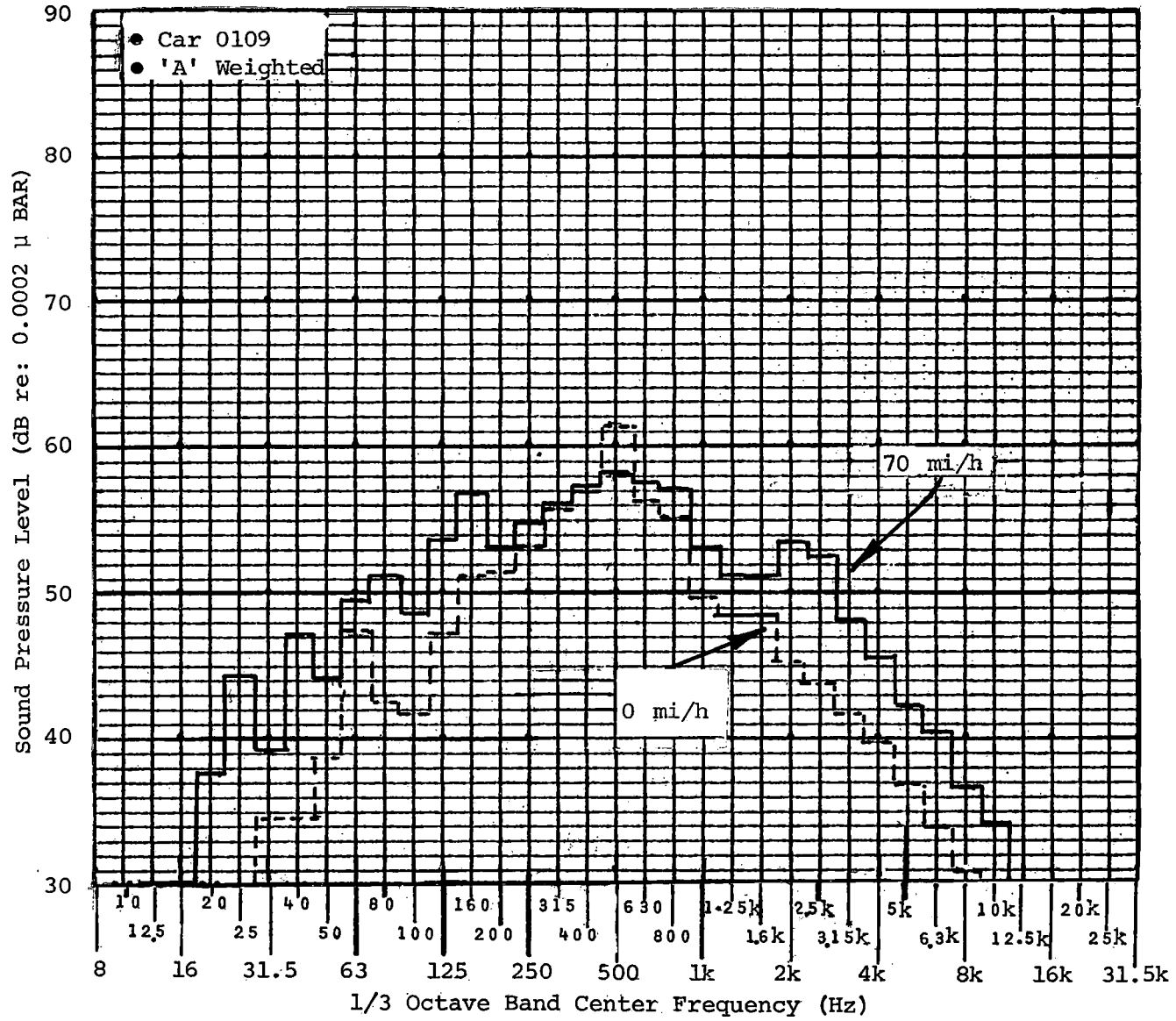


FIGURE 8-23. ONBOARD 1/3 OCTAVE SPECTRA: 'STANDING', CENTER OF CAR - AUXILIARIES ENERGIZED.

8.3.5.3 Test Results - Acceleration. The 'A' weighted sound level readings are presented graphically in figure 8-24 and the 'A' weighted sound level time history is shown in figure 8-25. The data show:

- 'A' weighted sound pressure levels were less than the specification maxima at all speeds.
- The levels changed very little with speed (62 to 65 dBA from 0 to 70 mi/h).
- There were no sound transients produced in the acceleration mode (the noise quality was steady throughout).
- The sound levels were similar to those produced in the vehicle at steady speeds.

8.3.5.4 Test Results - Deceleration. The 'A' weighted sound level readings are shown graphically in figure 8-26 and the 'A' weighted sound level time histories for both modes of braking are shown in figure 8-27. The data show:

- The sound level remained relatively constant. At the seat 28 location, for example, the level dropped from 64 dBA to 60 dBA while braking from 70 to 0 mi/h.
- There was little difference in sound levels between friction and blended braking.
- The sound levels differ little when compared with the steady-state sound levels.
- The sound levels measured were less than the specified maxima at the two locations.
- There is little difference in sound levels between acceleration and braking.

8.3.6 Noise Characteristic with Track Construction.

8.3.6.1 Test Objective. The objective was to determine the 'A' weighted sound levels inside the train as influenced by various constructions of track, while traveling at a steady speed of 55 mi/h.

8.3.6.2 Test Method. The vehicles were driven at a constant speed of 55 mi/h around the TTT. The driver was instructed to maintain speed of the vehicles, with as little recourse to heavy acceleration and braking as possible. 'A' weighted sound levels were measured with hand held meters for each separate track section at the midcar centerline, standing ear level.

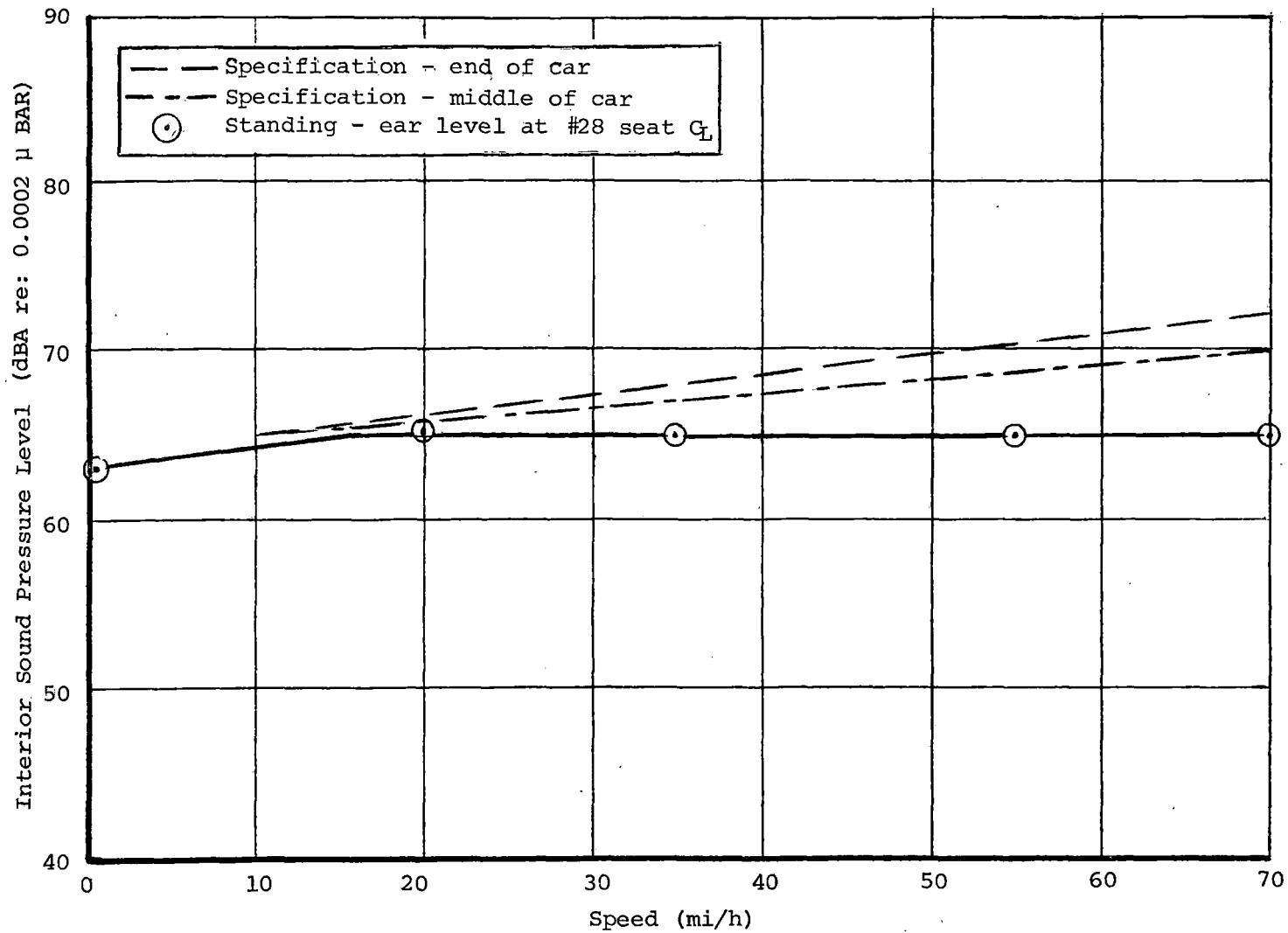
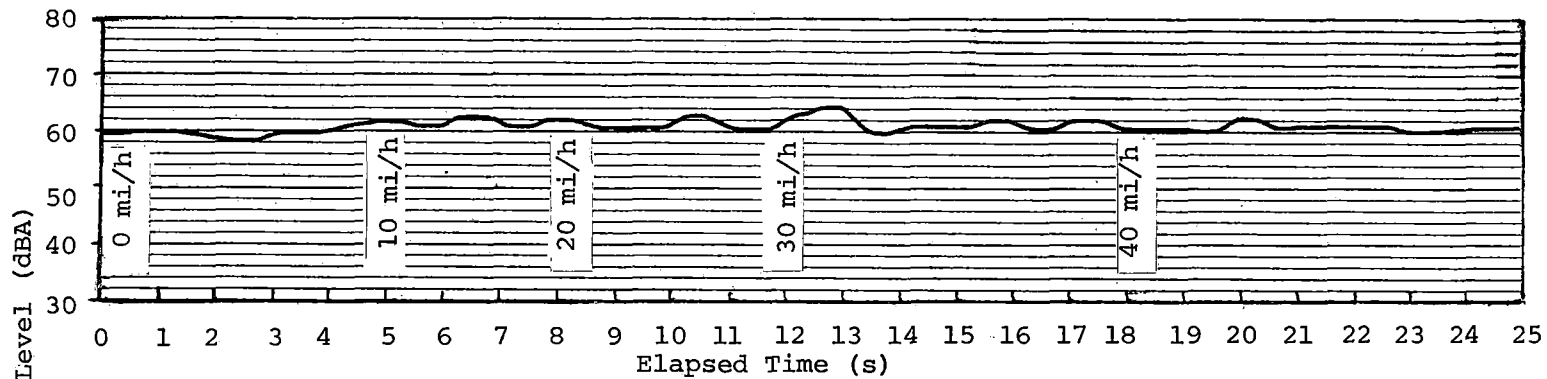


FIGURE 8-24. 'A' WEIGHTED SOUND LEVELS VS. SPEED:
CAR 0109 ACCELERATION.



NOTE: Writing speed is 16 mm/s ('Slow' meter characteristic)

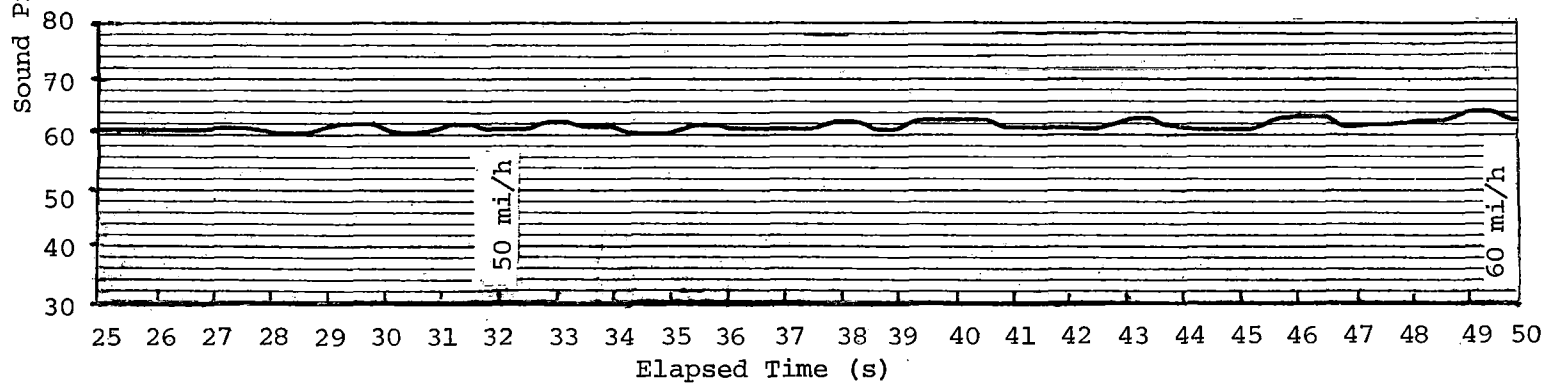


FIGURE 8-25. CAR 0109 (FULL POWER ACCELERATION: 0 TO 60 mi/h),
'A' WEIGHTED SOUND LEVEL TIME HISTORY.

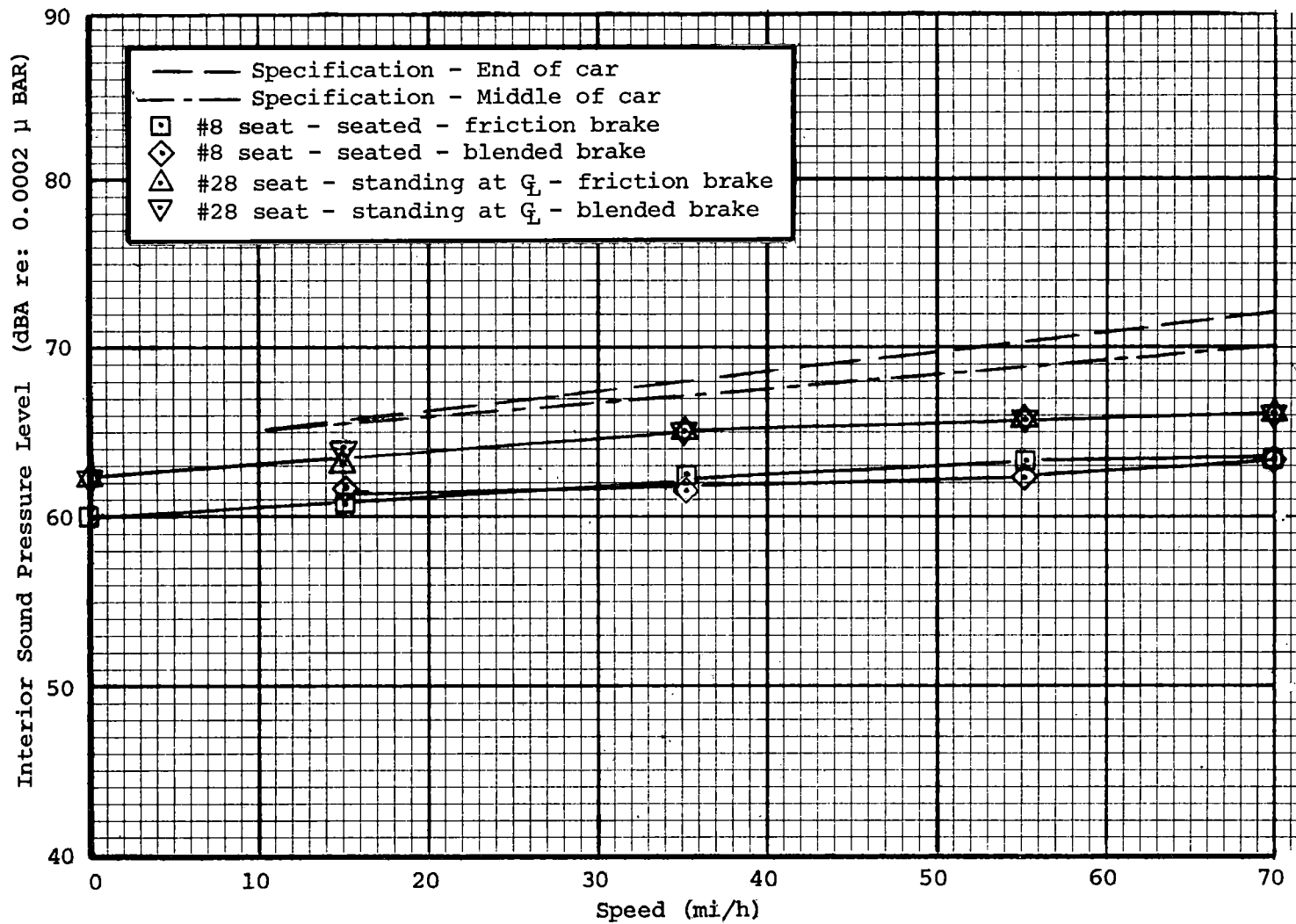
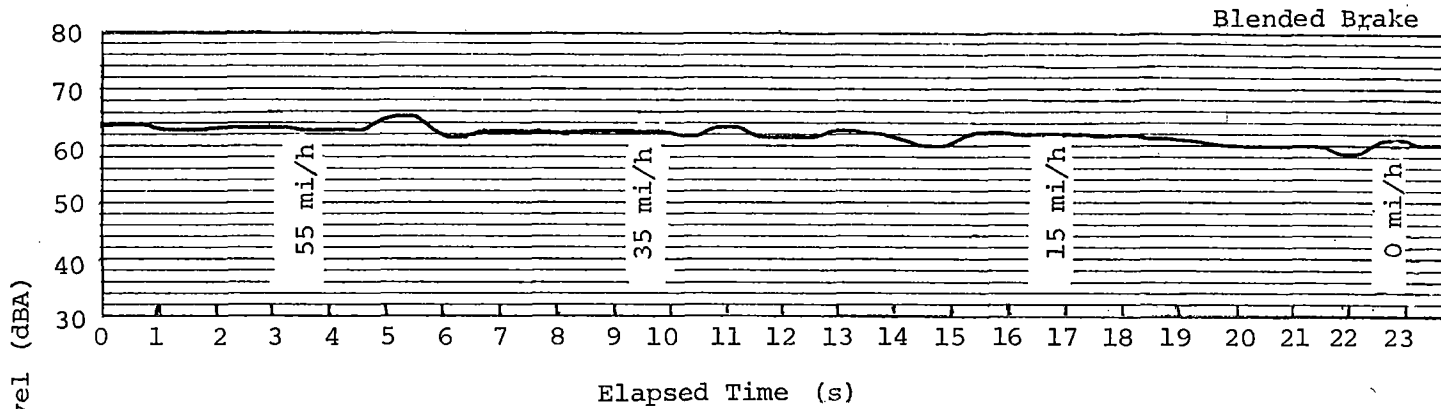


FIGURE 8-26. 'A' WEIGHTED SOUND LEVELS VS. SPEED:
CAR 0109 DECELERATION.



NOTE: Writing speed is 16 mm/s ('Slow' meter characteristic)

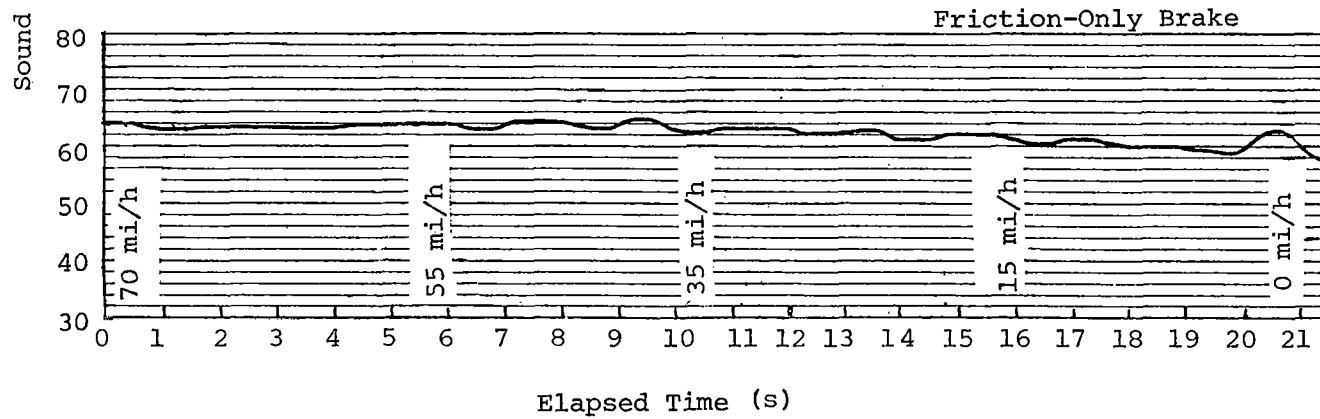


FIGURE 8-27. CAR 0109, 'A' WEIGHTED SOUND LEVEL TIME HISTORIES - BRAKING: BLENDED AND FRICTION-ONLY.

In addition, recordings were made at the same speed for a complete loop, again at the midcar centerline standing location. These recordings were replayed through a B&K type 2306 level recorder to produce 'A' weighted sound level versus time charts.

8.3.6.3 Test Results. The data for the hand-held meter reading are presented below in table 8-5.

TABLE 8-5. HAND-HELD METER READINGS, MIDCAR SOUND LEVELS, TRACK SECTIONS I THROUGH VII.

	Track Section						
	I	II	III	IV	V	VI	VII
Sound levels Midcar (dBA)	63	64	63.5	62.5	63	63	65

From the 'A' weighted sound level readings, it was concluded that there was little difference in sound level with track section. Track Section IV had the lowest level and Section VII had the highest. The span was 2.5 dBA.

The three 'A' weighted time histories presented in figure 8-28 are for the three major track types on the loop, i.e., Section III - jointed rail - wooden ties, Section II - welded rail - wooden ties, and Section V - welded rail - concrete ties. The time histories all have a pen writing speed of 250 mm/s (corresponding to a meter characteristic of 'Impulse'). Even at this high writing speed, the difference between track sections is almost indistinguishable. However, the effect of jointed rails does appear to produce slightly higher transient spikes than the other two sections.

The change in 'A' weighted sound level between coast and power can be seen in figure 8-29. The figure shows a 3 dBA change in level occurring at 55 mi/h in Section III. It was necessary to change controller mode from coast to power to brake, to maintain the approximately constant speed of 55 mi/h over the varying terrain of the test track. The 3 to 4 dBA change at the transition from coast to power is of the same magnitude as the difference in dBA level shown between sections in table 8-5.

The small difference in 'A' weighted levels, shown with track section, may in fact be due to power/coast changes occurring at random during the test. Because the deenergized car produced a 5 dBA lower sound level than the energized car at 55 mi/h, it is also concluded that the auxiliary noise effectively masked any track-section effect. This is supported by figure 8-30, which shows the 'A' weighted sound level time history at approximately 55 mi/h in a deenergized car. The trace shows the expected transients produced by track noise to be unlike the traces produced with auxiliaries (which are very much more steady) energized.

For large track discontinuities (crossing a switch, for example) the auxiliaries did not completely mask the noise. This is shown in figure 8-29,

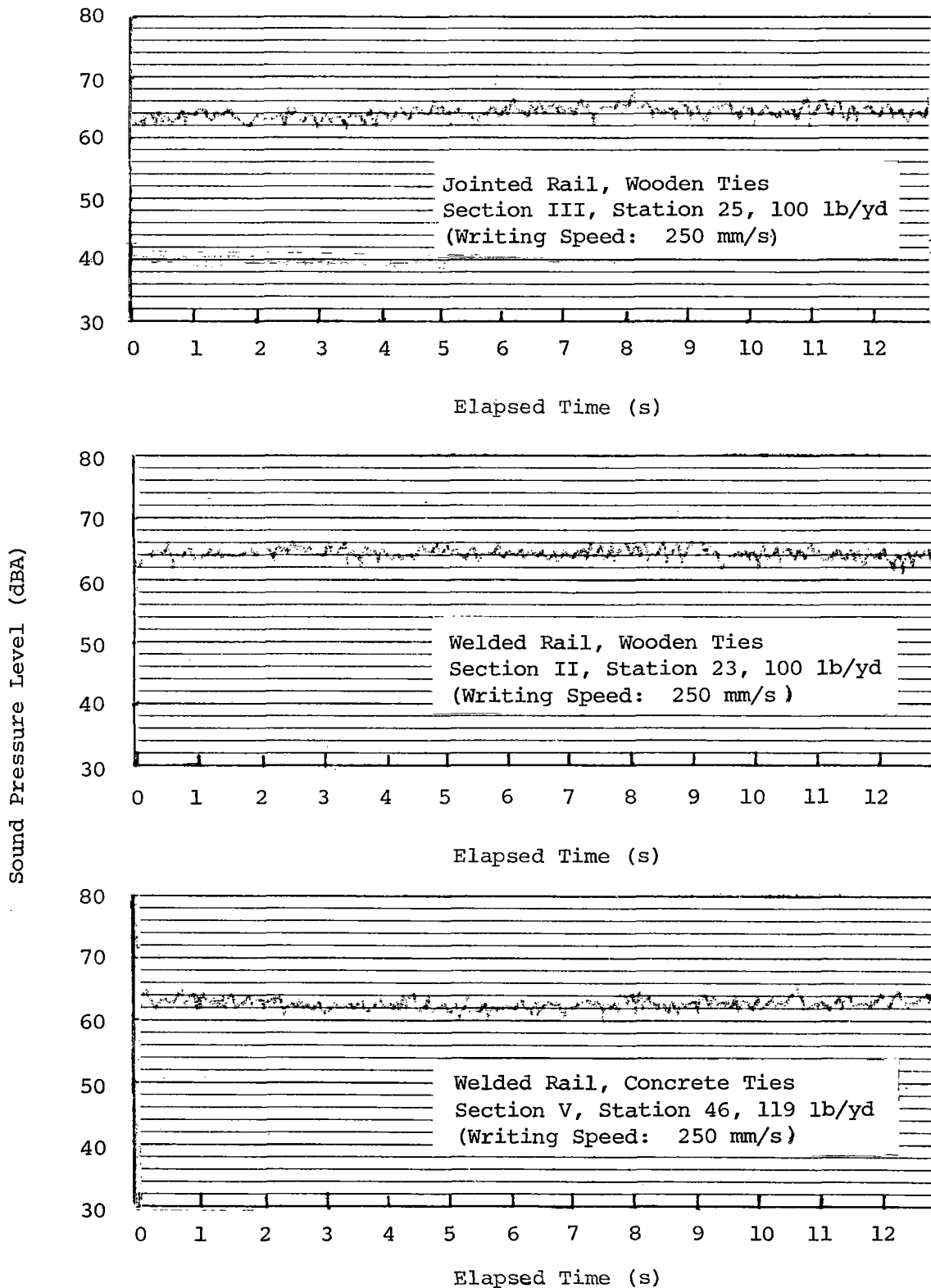


FIGURE 8-28. 'A' WEIGHTED SOUND LEVEL TIME HISTORIES AT 55 mi/h FOR THREE TRACK CONSTRUCTION TYPES, CAR 0109.

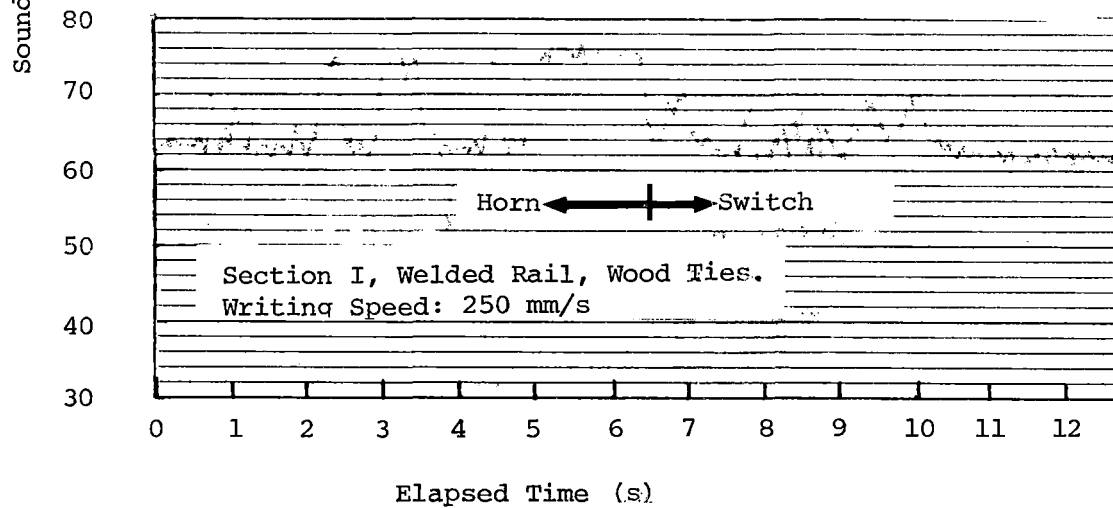
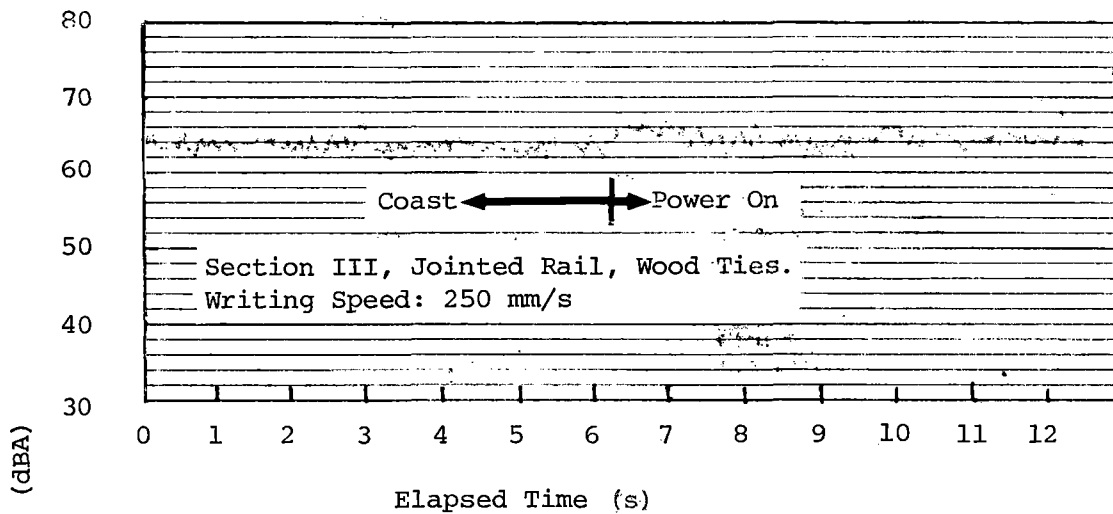
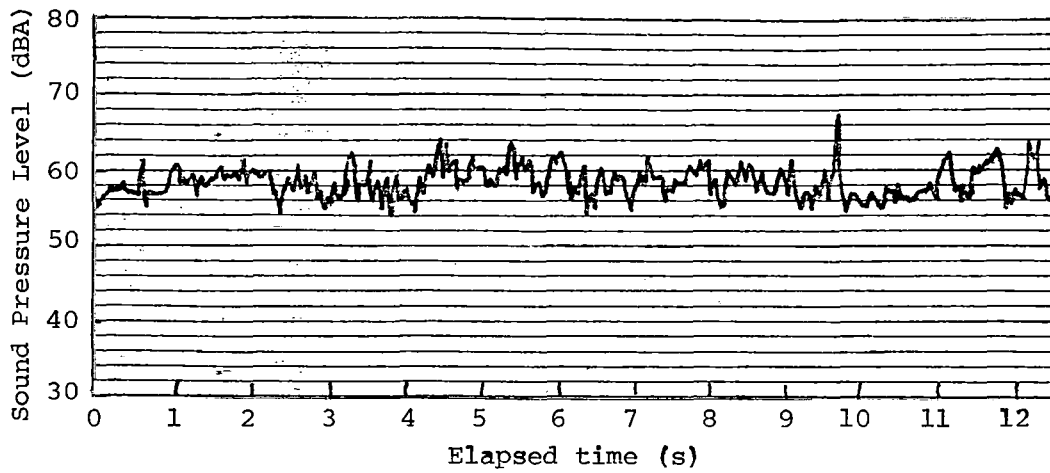


FIGURE 8-29. 'A' WEIGHTED SOUND LEVEL TIME HISTORIES AT 55 mi/h, SHOWING CHANGE FROM COAST TO POWER, AND CHANGE OVER SWITCH.



NOTE: Writing speed 250 mm/s ('Impulse' meter characteristic)
Data taken on track Section IV.

FIGURE 8-30. 'A' WEIGHTED SOUND LEVEL TIME HISTORY AT
55 mi/h, WITH AUXILIARIES DEENERGIZED.

where a switch produced a transient rise of 10 dBA (again at the 'Impulse' writing speed).

The 'A' weighted meter readings were taken with a meter characteristic of 'Slow'. The comparison between 'Slow', 'Fast', and 'Impulse' meter characteristics is shown in figure 8-31. The strip chart is produced from the same 12-s recording in Section III in 'Impulse', 'Fast', and 'Slow' meter characteristics.

8.3.7 Noise Characteristic with Steady Speeds, at Wayside 0 to 70 mi/h

8.3.7.1 Objective. The test objective was to measure the 'A' weighted sound levels at wayside, as influenced by pass-by speeds in the range 0 to 70 mi/h, and to compare these sound levels with the maxima specified in the vehicle specification, which are:

"With a two-vehicle train moving on tangent, tie-on-ballast track, the noise level 50' from track centerline shall not exceed the values indicated on figure 8-32. For this measurement, the fast sound level meter damping, or its equivalent, shall be used and the results shall be averaged for both directions of Transit Vehicle operation on the same track. The microphone shall be located in the plane of the axles, 50' from track centerline, on both sides of the vehicle."

8.3.7.2 Test Method. The vehicles were run at speeds of 15, 35, 55, and 70 mi/h in both clockwise and counterclockwise directions through the test section. The section consisted of welded rail, concrete ties, and a ballasted track. 'A' weighted sound pressure levels were measured 50' from track center, both inside and outside the test track loop. Tape recordings of the sound levels were also made. Data were taken during phases 1 and 2 of the test sequence.

8.3.7.3 Test Results - 'A' Weighted Sound Level Readings. Figure 8-32 shows the results in graphic form. As can be seen in the figure, the 'A' weighted sound levels exceeded the specification levels at 15, 55, and 70 mi/h speeds on the inside of the loop by an average of 1.67 dBA, while on the outside of the loop, the dBA sound levels were below specification by an average of 2.25 dBA for those three speeds.

Figures 8-33 and 8-34 show the dBA sound level variation inside and outside the loop with time, at various speeds as the train passed by. Although the test was run on welded rail, transient spikes of noise are apparent. This was audible when the wheels passed over some irregularity in the rails. Also noticeable is the sound of contact between the flanges and rail, even though the test was run on tangent track. In overlaying the data, the maximum levels were assumed to indicate the closest point of approach.

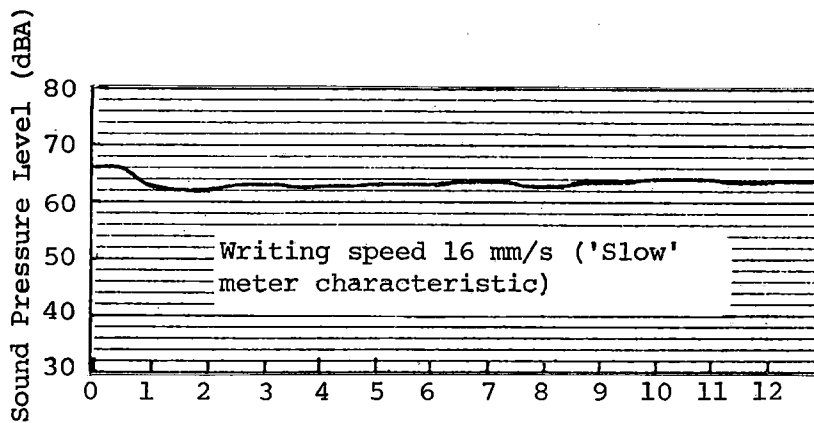
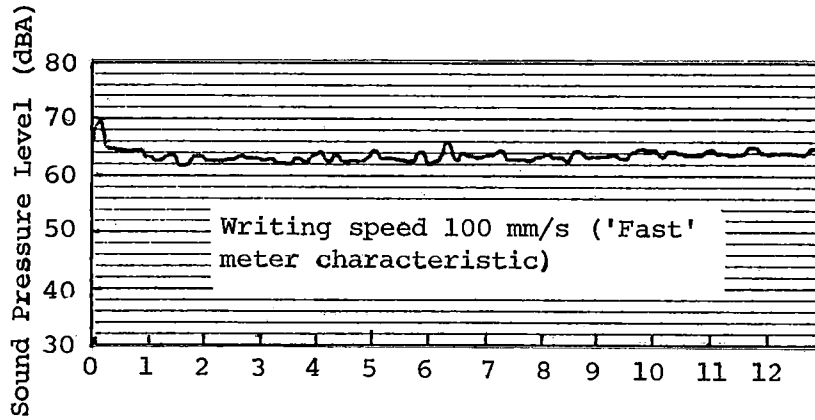
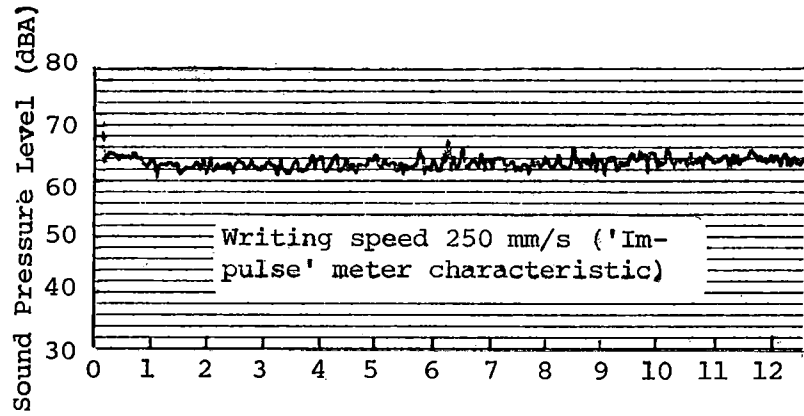


FIGURE 8-31. COMPARISON OF PEN WRITING SPEEDS EQUIVALENT TO METER CHARACTERISTICS AT SPEED OF 55 mi/h, TRACK SECTION III.

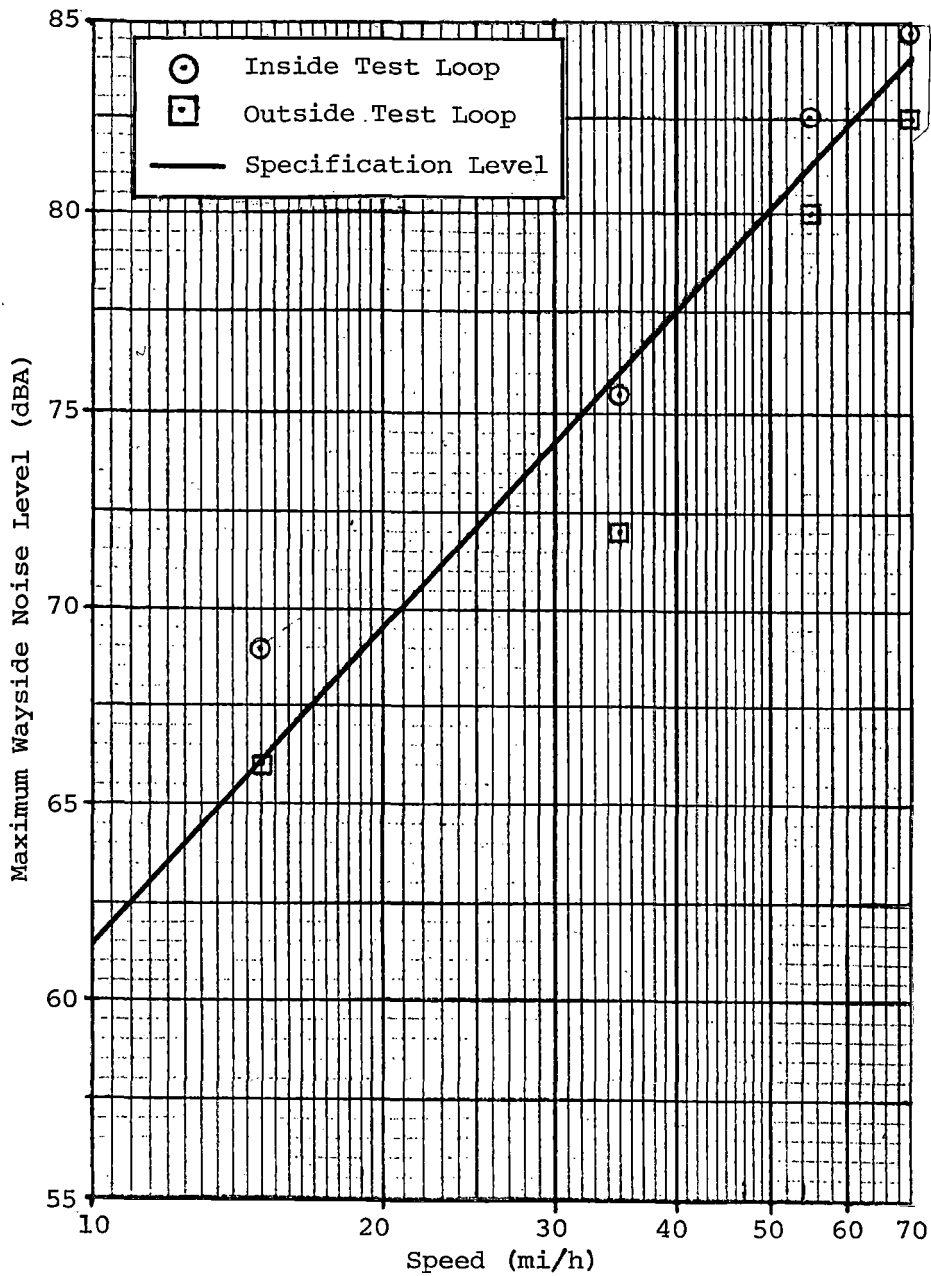


FIGURE 8-32. 'A' WEIGHTED SOUND LEVELS 50' FROM EACH SIDE OF TRACK, 4 PASS-BY SPEEDS.

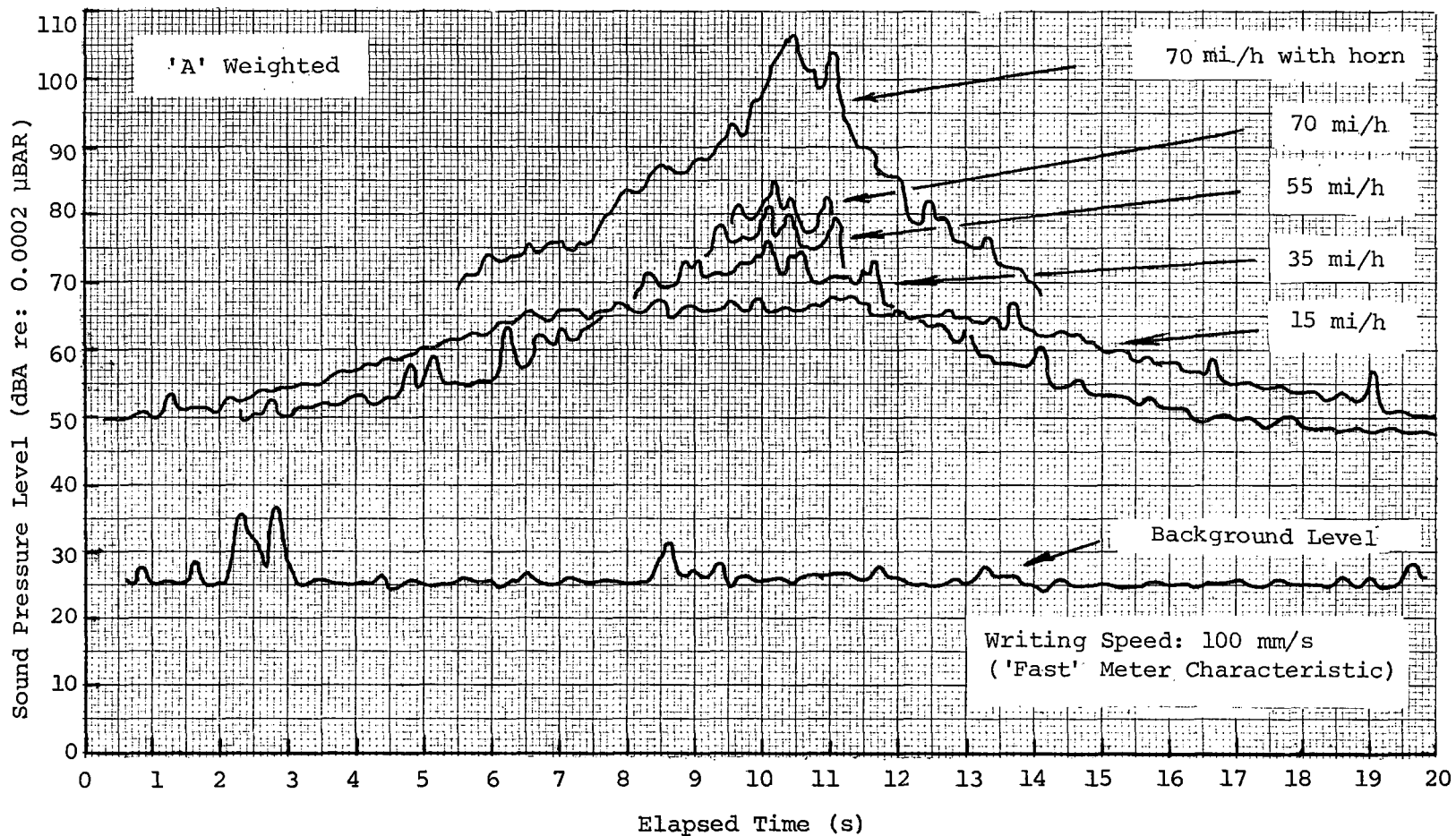


FIGURE 8-33. SOUND LEVEL TIME HISTORIES 50' ON INSIDE OF LOOP, 4 PASS-BY SPEEDS.

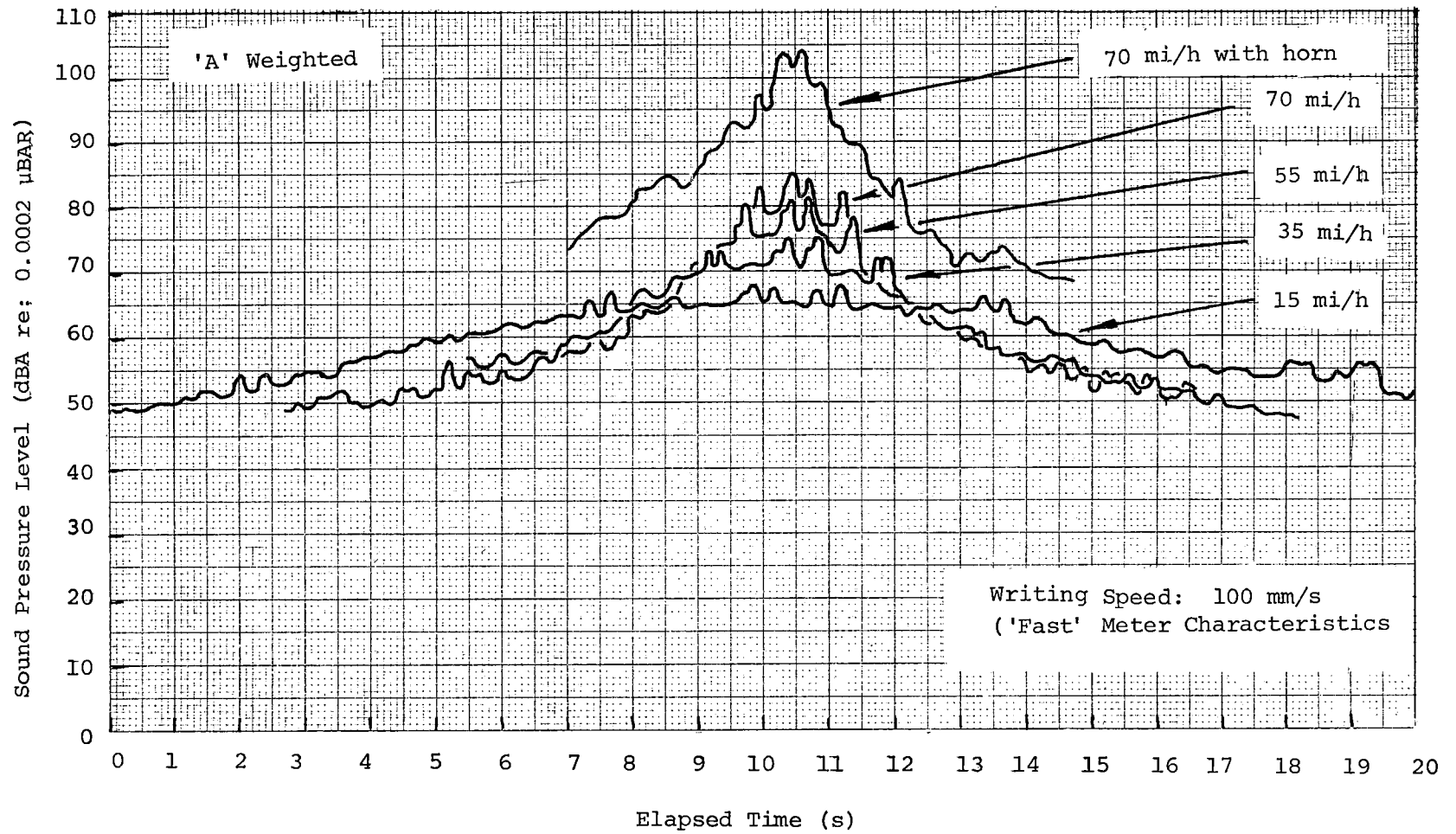


FIGURE 8-34. SOUND LEVEL TIME HISTORIES 50' ON OUTSIDE OF LOOP, 4 PASS-BY SPEEDS.

8.3.7.4 Test Results - 1/3 Octave Analysis. The 1/3 octave unweighted spectra for a typical 55 mi/h pass, 50' from track center, are shown in figure 8-35. The spectrum is from a 2-s period, approximately at the moment of pass-by.

The 1/3 octave band levels all lie within a small 10-20 dB span, and do not fall off at high or low frequencies. This broadness of the data was evident at all pass-by speeds. Also noticeable is the salient band at the 63 Hz center frequency. This is probably due to the TM blowers, and the effect is noticeable at other speeds.

8.4 CONCLUSIONS

The conclusions can be divided into the two areas of external noise and internal noise.

8.4.1 External Noise

With the vehicle stationary, the noise radiated from the vehicle is produced from the auxiliary equipment. It was concluded that:

- 'A' weighted sound pressure levels at 15' from the car centerline exceeded specification limits, both for individual equipment and for all equipment operating.
- The readings adjacent to car 0110 were not typical of a normal car because of abnormally noisy blowers.
- 'A' weighted sound pressure levels were similar in level for both sides of the cars.
- The noise from the auxiliary blower and TM blowers was strongly influenced by salient 1/3 octave bands in the low frequency area. The most significant band in this respect was the 63 Hz 1/3 octave band. This feature of the blowers made them very noticeable in the noise produced when all equipment was operating.

With the vehicle in the passing mode at steady speed, the noise radiated was a mixture of auxiliary noise and wheel/rail noise. It was concluded from the data that:

- The 'A' weighted sound pressure levels at 50' from the centerline of the cars fell close to, and in some cases slightly above, the maximum specification level allowed, and showed a steady increase in level with speed.
- The salient 63 Hz 1/3 octave band produced from the underfloor blower was noticeable in the spectra at all speeds.
- Flange squeal was audible at a number of speeds, even though the track was level and tangent.

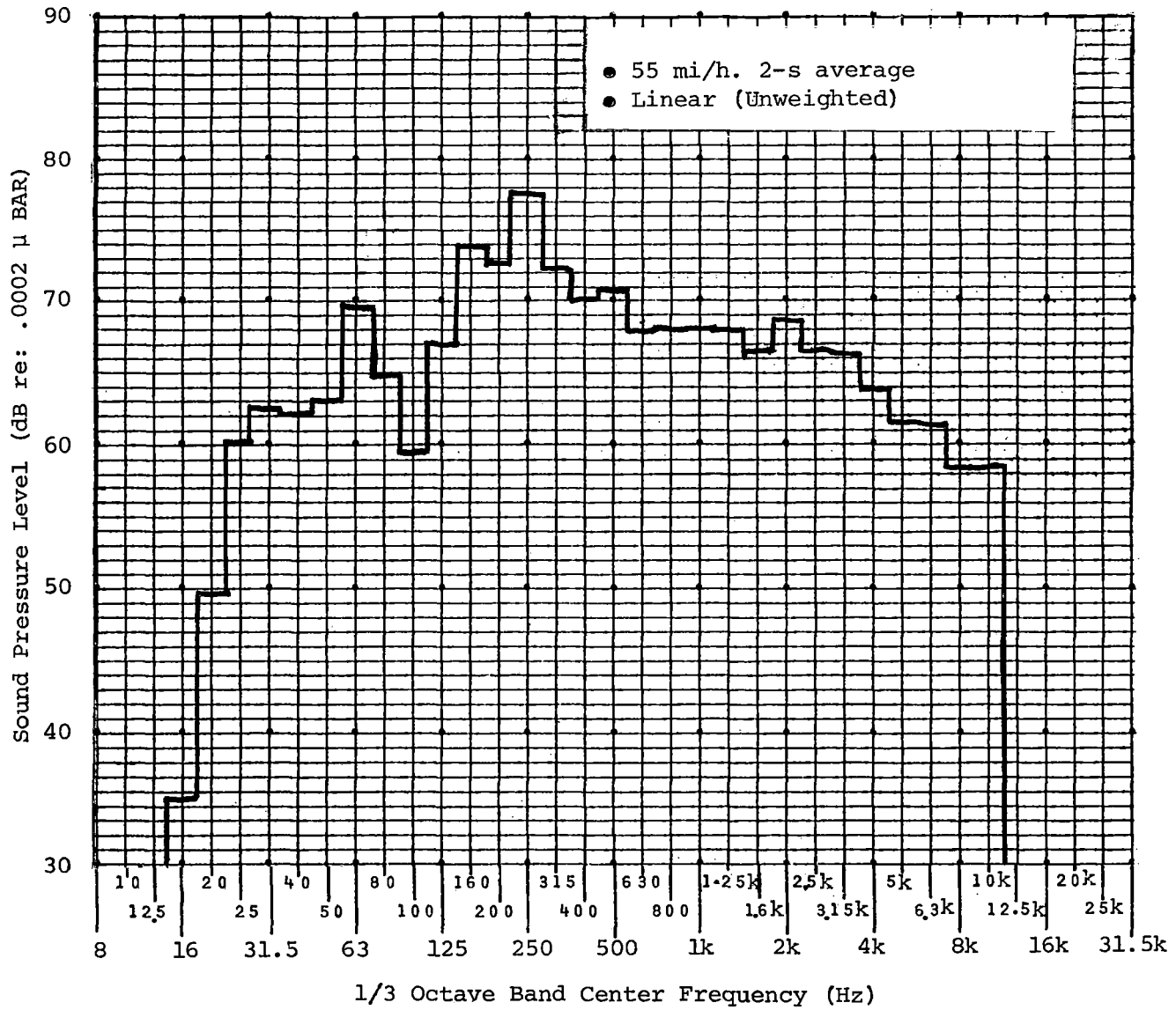


FIGURE 8-35. 1/3 OCTAVE SPECTRUM, WAYSIDE PASS-BY.

8.4.2 Internal Noise

In the vehicle stationary mode, the noise onboard was produced by auxiliary equipment. From the data it was concluded that:

- The interior was well isolated from underfloor equipment in the high frequency range but was poorly isolated in the low frequency range. This poor isolation transmitted the salient 63 Hz 1/3 octave band present in the noise spectra inside the car and was the most noticeable characteristic of the onboard noise environment.
- Although the air conditioning equipment outlets produced high 'A' weighted sound level readings, the spectra were broad and had excellent masking properties.
- Car 0110 exceeded the 'A' weighted sound pressure level specification limits in the majority of locations tested, but this deficiency is attributed to abnormally noisy blowers.

With the vehicle moving and auxiliaries on, it was concluded that:

- The vehicles were very well isolated from wheel/rail noise, to such an extent that the onboard noise environment was totally dominated by auxiliary equipment.
- 'A' weighted sound pressure levels effectively remained at the stationary values and at high speeds were still well below the specification limit.
- The vehicles produced approximately the same 'A' weighted sound pressure level, independent of acceleration, deceleration, constant speed, or track construction.
- The white noise produced by the air conditioning outlets provided good masking properties from other car noises and provided suitable conversation privacy.

Modification of the underfloor blowers to reduce low frequency transmission into the car would significantly improve the vehicles' acoustic environment.

9.0 DYNAMIC SHAKE TEST AND EQUIPMENT RESONANCE TESTS

9.1 DYNAMIC SHAKE TEST

9.1.1 Test Objective

The objective of the Dynamic Shake Test was to determine the carbody vertical, lateral, and torsional mode shapes and resonant frequencies. Carbody bending modes are excited in revenue service by periodic excitation forces produced by wheel and track irregularities. An understanding of carbody mode shapes and resonant frequencies, and their relationships to external excitation, can assist the analyst in the interpretation of ride quality test data and the definition of solutions to ride quality problem areas.

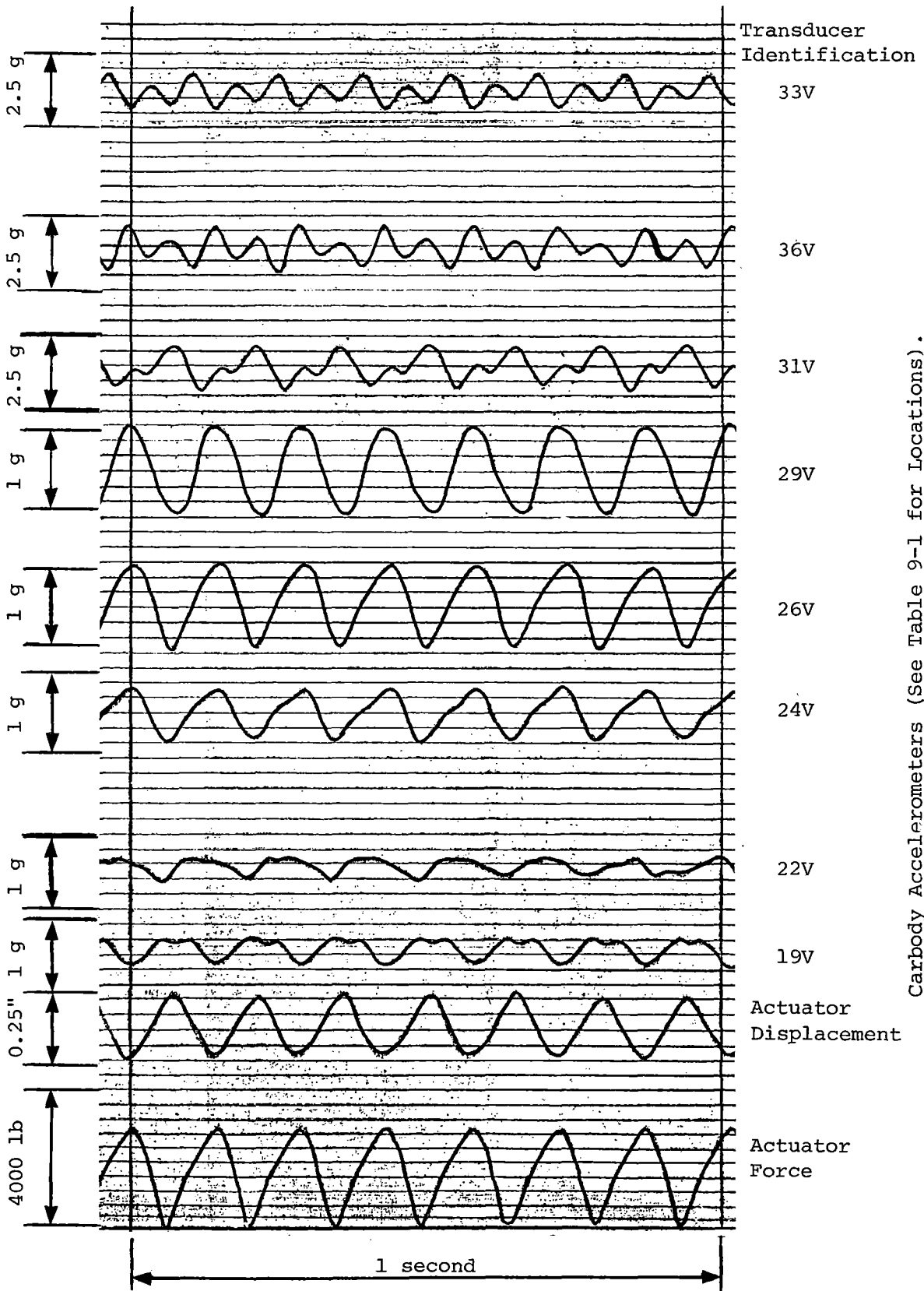
9.1.2 Test Method

These tests were conducted on car 0109 at the AWO (empty) weight. For each configuration, frequency sweeps of acceleration were obtained from 0.5 to 30.0 Hz at 0.1 Hz/s. To insure system integrity, the shaker and the accelerometers located adjacent to the shaker were monitored on a spectrum analyzer during each test run. Transfer functions and coherence plots were displayed on the analyzer screen and checked for phase and coherence. Oscillograph records were obtained in real time for 18 selected channels, depending on the mode of excitation (vertical, lateral, or torsional). Input force was monitored on the oscillograph paper for all three modes of excitation. Data were low-pass filtered at 125 Hz and recorded, both analog and digitally at 300 samples/s. In order to determine resonant frequencies and obtain mode shape information, the analog data were played back, low-pass filtered at 18 Hz, and displayed on an oscillograph. A typical oscillograph record, played back from the analog tape, is shown (figure 9-1) for the vertical excitation test run.

9.1.3 Instrumentation

Accelerometers were used to measure the dynamic response of the car and were mounted on plastic blocks which were glued to the carbody. The accelerometers used for determining the natural frequencies of the carbody are as listed in table 9-1. Transducer sensitivity, range, frequency response, and accuracy are provided in the table. A sketch of the location of the instrumentation on the car is shown in figure 9-2. A schematic of the signal conditioning and data acquisition system is shown in figure 9-3. The input force shaker was a servo-controlled hydraulic actuator, with force and displacement control electronics. A sinusoidal force of 2,000 lb amplitude was input for all test runs.

The actuator was attached to the rear of the car by means of a metal block bolted to the carbody at the anticlimber attachment point; (the anticlimber was removed). A load cell was installed between the actuator and



Carbody Accelerometers (See Table 9-1 for Locations).

FIGURE 9-1. TYPICAL SHAKE TEST ANALOG TRACES.

TABLE 9-1. EXCITATION TESTS

Location	Measurement Description	Expected Range
F-81	Actuator Loadcell	± 4 kip
D82	Actuator Displacement	± 2 "
19V	Car Floor, Front End Centerline (Vertical)	± 25 g
22V	Car Floor, Centerline (Vertical)	"
24V	Car Floor, Centerline (Vertical)	"
26V	Car Floor, Centerline (Vertical)	"
29V	Car Floor, Centerline (Vertical)	"
31V	Car Floor, Centerline (Vertical)	"
33V	Car Floor, Centerline (Vertical)	"
36V	Car Floor, Centerline (Vertical)	"
1L	Bottom Edge, North (N) Side (Lateral)	± 10 g

DATA ACQUISITION AND ANALYSIS.

Transducer Type	Range	Measurement Freq. Response (Hz)	Estimated Accuracy (%)
MTS	4 kip	0-125	±5
MTS	±2"	"	"
Endevco 2262-25	±25 g	"	"
"	"	"	"
"	"	"	"
"	"	"	"
"	"	"	"
"	"	"	"
"	"	"	"
"	"	"	"
"	±10 g	"	"

TABLE 9-1. EXCITATION TESTS, DATA ACQUISITION AND ANALYSIS (CONTINUED).

Location	Measurement Description	Expected Range	Transducer Type	Transducer Range	Measurement Freq. Response (Hz)	Estimated Accuracy (%)
4L	Bottom Edge, N. Side (Lateral)	±10 g	Endevco 2262-25	±10 g	0-125	±5
6L	Bottom Edge, N. Side (Lateral)	"	"	"	"	"
8L	Bottom Edge, N. Side (Lateral)	"	"	"	"	"
11L	Bottom Edge, N. Side (Lateral)	±25 g	"	±25 g	"	"
13L	Bottom Edge, N. Side	"	"	"	"	"
15L	Bottom Edge, N. Side (Lateral)	"	"	"	"	"
18L	Bottom Edge, N. Side (Lateral)	"	"	"	"	"
37V	Bottom Edge, South (S) Side (Vertical)	"	"	"	"	"
40V	Bottom Edge, S. Side (Vertical)	"	"	"	"	"
42V	Bottom Edge, S. Side (Vertical)	"	"	"	"	"
44V	Bottom Edge, S. Side (Vertical)	"	"	"	"	"

TABLE 9-1. EXCITATION TESTS, DATA ACQUISITION AND ANALYSIS (CONTINUED).

Location	Measurement Description	Expected Range	Transducer Type	Transducer Range	Measurement Freq. Response (Hz)	Estimated Accuracy (%)
47V	Bottom Edge, S. Side (Vertical)	±25 g	Endevco 2262-25	±25 g	0-125	±5
49V	Bottom Edge, S. Side (Vertical)	"	"	"	"	"
51V	Bottom Edge, S. Side (Vertical)	"	"	"	"	"
54V	Bottom Edge, S. Side (Vertical)	"	"	"	"	"

9-6

NOTE: See Figure 9-2 for exact accelerometer locations.

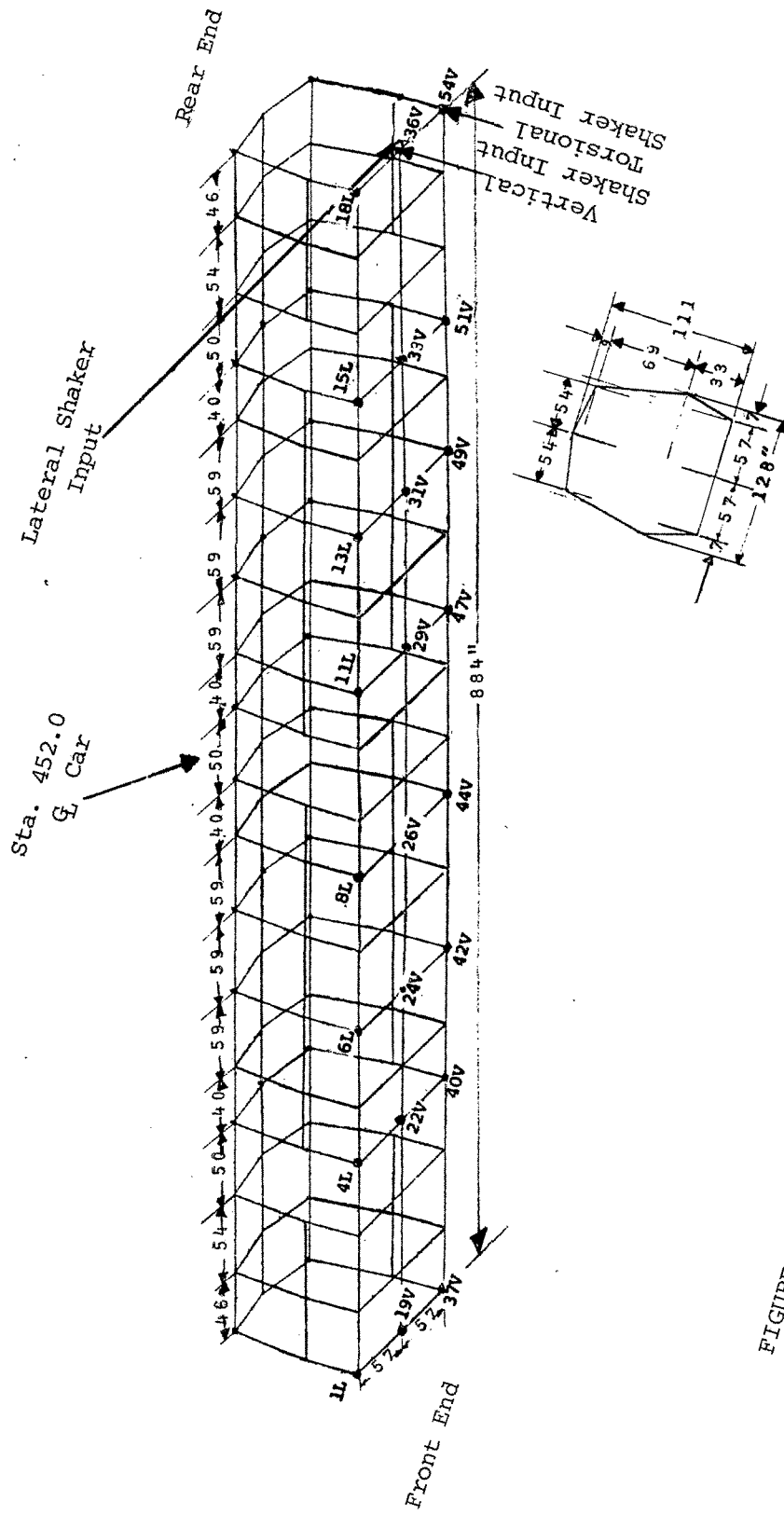


FIGURE 9-2. STRUCTURAL MODEL, SHOWING ACTUATORS AND ACCELEROMETER MEASUREMENT LOCATIONS.

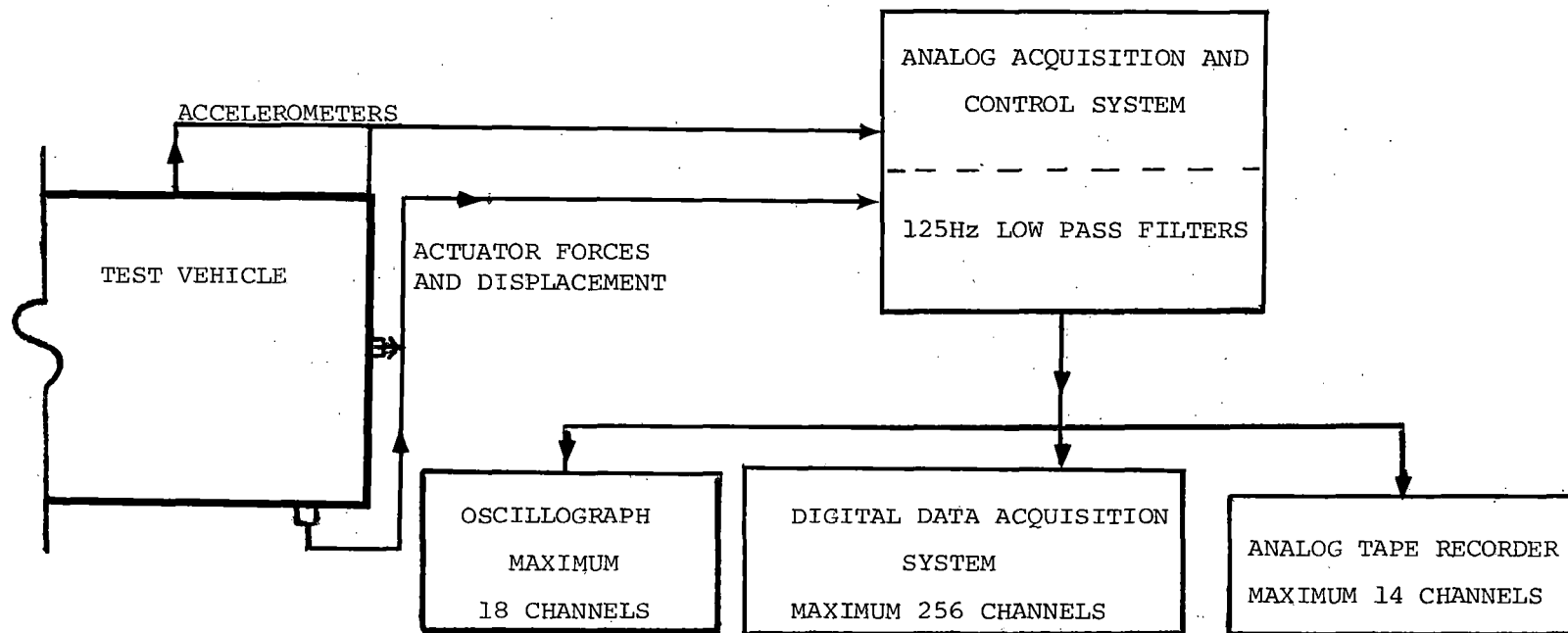


FIGURE 9-3. BLOCK DIAGRAM OF INSTRUMENTATION, SIGNAL CONDITIONING, AND DATA ACQUISITION SYSTEMS.

carbody to measure the excitation force. The vertical and lateral excitations were input through this metal block as shown in figure 9-4. The torsional excitation was induced through the jacking pad on the car left rear end corner and is also shown in the figure. Actual photographs of the lateral and torsional shaker attachments are shown in figure 9-5.

9.1.4 Test Results

Data used to evaluate the resonant frequencies were played back on an oscillograph from the analog tape made during the vertical shake test. Since the analog data were low-pass filtered at 18 Hz, it was possible to analyze phase and magnitude of accelerometer outputs with respect to the forcing function below 15 Hz. The same data were also low-pass filtered at 5 Hz to identify the rigid body pitch mode. Relative amplitudes in g were extracted for each channel for each mode, and the phase relationship of each channel with reference to the force signal was deduced. This information was used to plot the mode shapes. The channels available for analysis are shown in figure 9-2. The figure shows the carbody floor and the locations and distances of the accelerometers in terms of the car dimensions. The input actuator force is also shown and the arrows denote the direction of positive measurements. Analysis of the vertical shake test data show three significant modes, as summarized in figure 9-6. They were a rigid body pitch motion at 1.5 Hz, a first vertical bending mode at 7.0 Hz, and a second vertical bending at 8.5 Hz.

Data from the lateral and torsional modes of excitation were played back and low-pass filtered in a similar manner to the vertical excitation data. Two significant lateral modes and one torsional mode were identified and are shown in figure 9-7. The lateral modes identified were a rigid body yaw motion at 3.5 Hz and a first lateral bending mode at 8.75 Hz. The torsional mode appears to be that of first torsional bending at 12.5 Hz.

9.2 EQUIPMENT RESONANCE TESTS

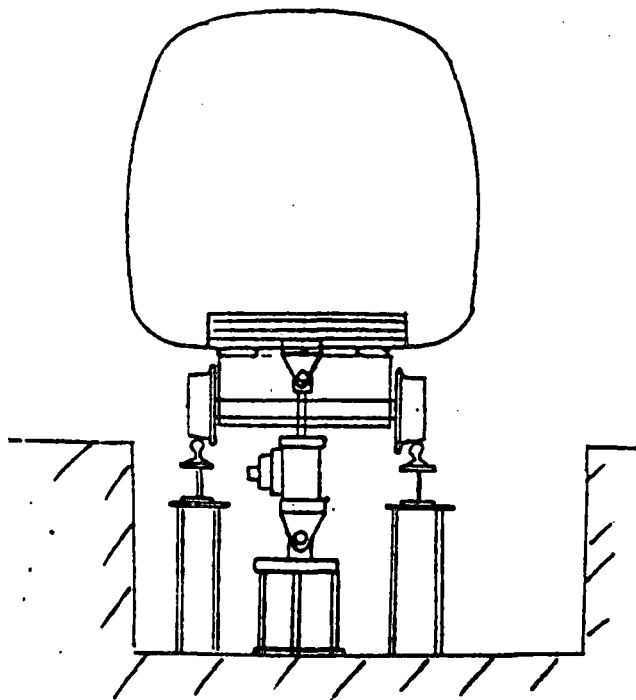
9.2.1 Objective

The objective of the equipment resonance tests was to ascertain critical resonant frequencies of the undercar equipment for the A car. The scope was limited to studying the effects of vertical and lateral excitation of the carbody on various items of equipment beneath the car. The information obtained could be used to troubleshoot structural problems of bracketry and fixtures used to attach equipment beneath the car, and hence reduce failure and damage of equipment during revenue service.

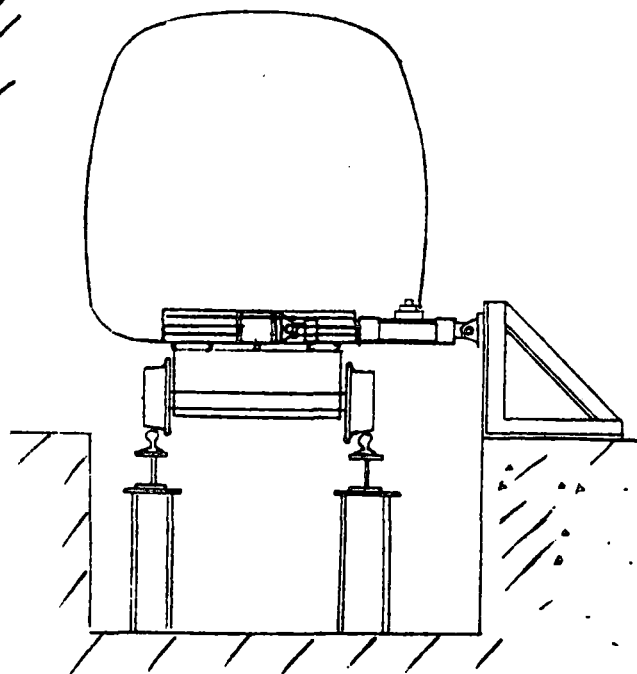
9.2.2 Test Method

The carbody was excited in the vertical and lateral directions using the same servo-controlled hydraulic actuator as for the carbody shake tests and

Views Looking Forward

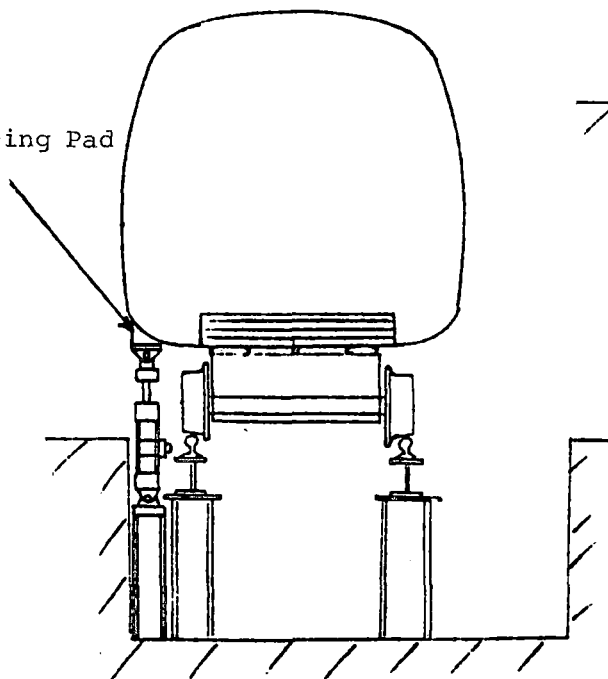


Vertical Body Excitation Mode



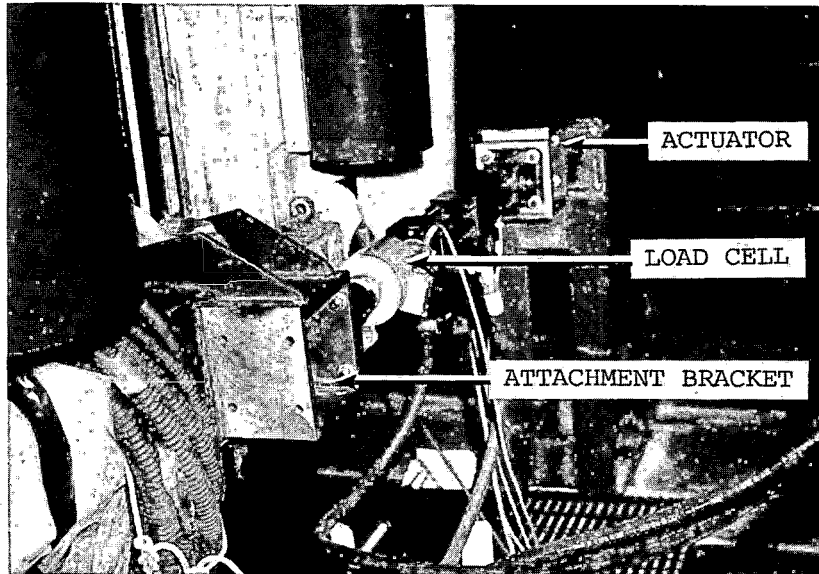
Lateral Body Excitation Mode

Jacking Pad

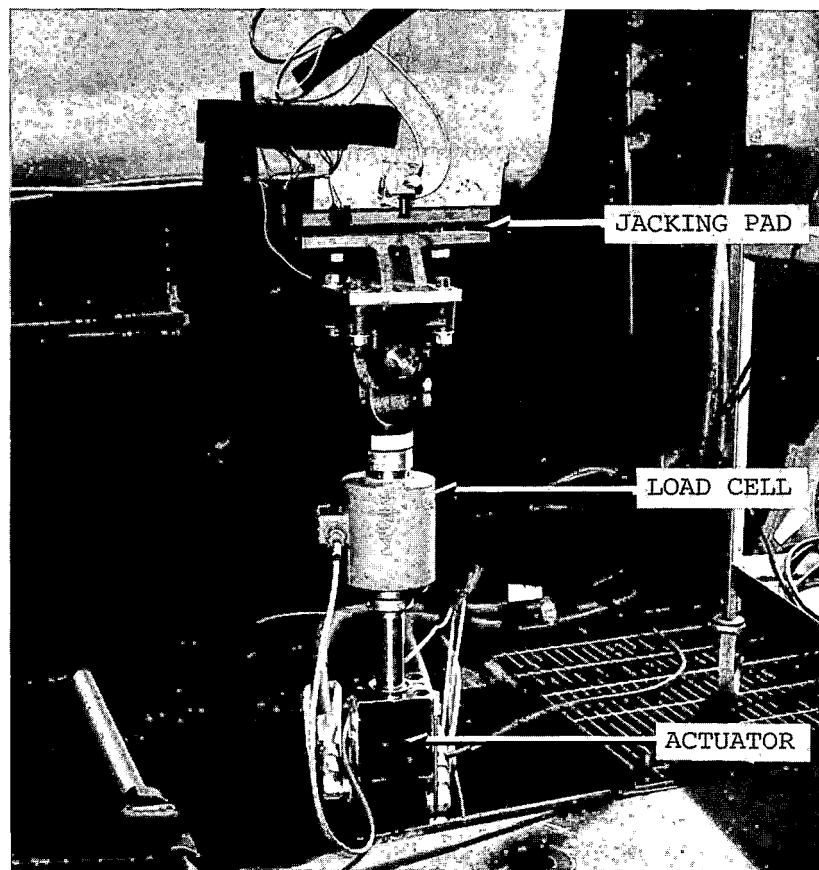


Torsional Body Excitation Mode

FIGURE 9-4. ACTUATOR LOCATIONS.

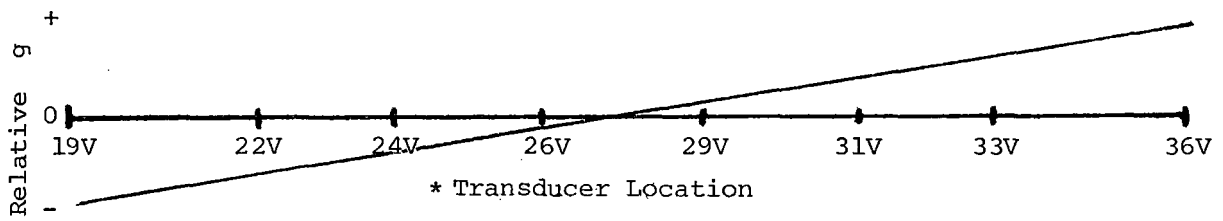


LATERAL EXCITATION TEST

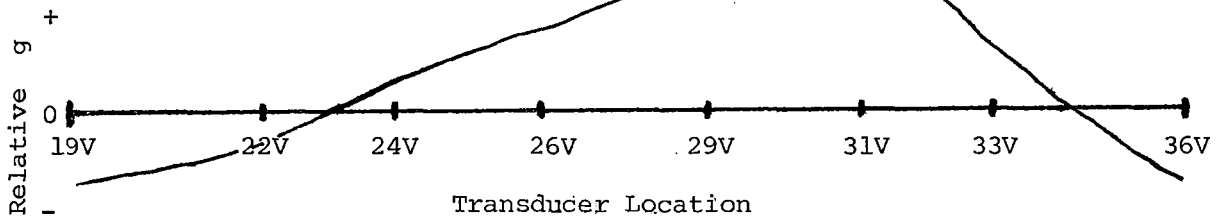


TORSIONAL EXCITATION TEST

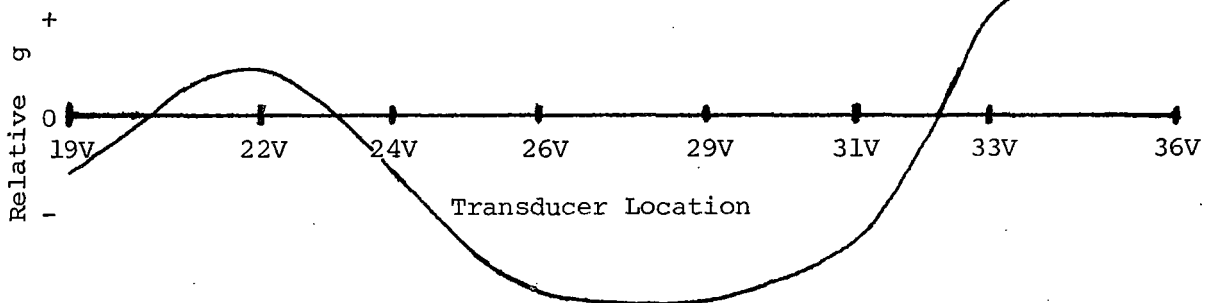
FIGURE 9-5. ACTUATOR ATTACHMENT.



Rigid Body Pitch (floor) 1.5 Hz



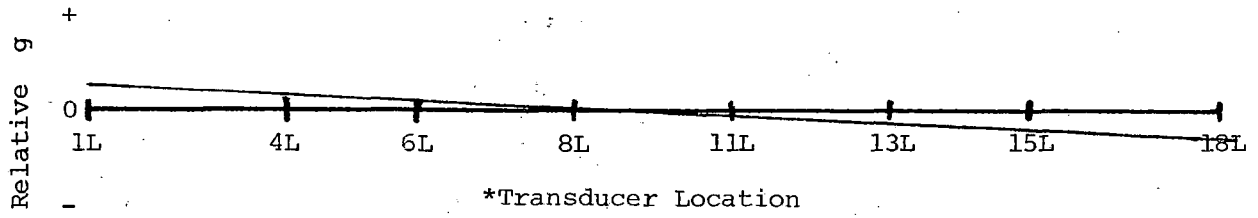
First Vertical Bending (floor) 7.0 Hz



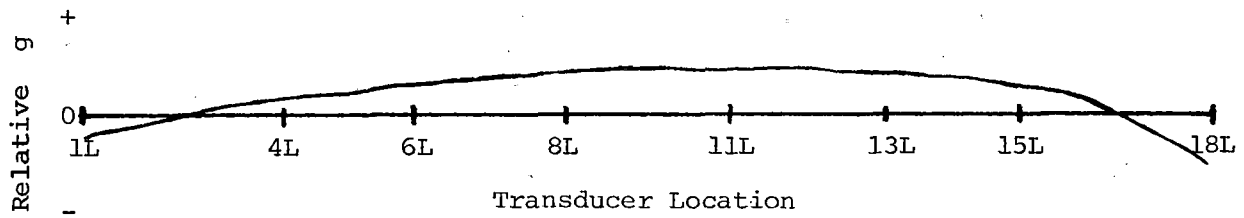
Second Vertical Bending (floor) 8.5 Hz

* See FIGURE 9-2.

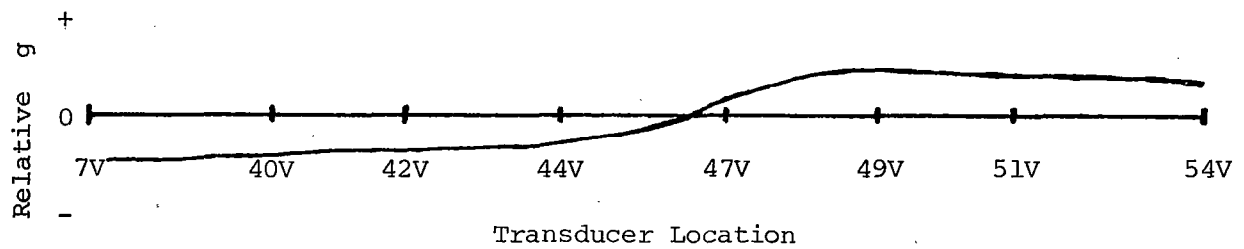
FIGURE 9-6. MODE SHAPES DUE TO VERTICAL EXCITATION, AWO CAR WEIGHT.



Rigid Body Yaw 3.5 Hz



First Lateral Bending 8.75 Hz



Torsional Bending 12.5 Hz

* See FIGURE 9-2.

AWO Vehicle Weight

FIGURE 9-7. MODE SHAPES DUE TO LATERAL AND TORSIONAL EXCITATION.

at the same locations, as detailed in figures 9-4 and 9-5. A random frequency, sinusoidal input force was used. The force was maintained at 2,000 lb amplitude over the frequency range of 0.5 to 30.0 Hz. Undercar equipment which had been observed to have resonant periods during the carbody shake test was instrumented with vertical and lateral accelerometers to determine resonant frequencies. This equipment included the front and rear air conditioning compressors, the ATC pickup coil, the resistor bank, the inductor, and the TM blower ballast resistor. Acceleration of the equipment was compared to adjacent floor locations by comparing the accelerometer outputs to determine the resonant periods of the bracketry or the resilient mountings.

9.2.3 Instrumentation

Selected carbody accelerometers were removed and placed on the undercar equipment in vertical and lateral orientations. Carbody accelerometers mounted on the floor centerline and side edges were kept in those positions, and their outputs were recorded as reference floor acceleration levels. All data were recorded digitally at 300 samples per second; in addition, analog tape and oscillograph records were made of undercar equipment acceleration data. A list of undercar equipment accelerometers and carbody reference accelerometers is given in table 9-2. The polarity of the transducer outputs, with respect to the direction of the force output, is noted by Z+, Y+ (positive, vertical and lateral) and Z-, Y- (negative, vertical and lateral). All accelerometers had a range of ± 10 g and an accuracy of $\pm 5\%$ of full scale. The signal conditioning and data acquisition system configurations were the same as for the Dynamic Shake Test.

9.2.4 Test Results

Analog oscillograph records were used to obtain frequencies where resonant conditions were noticed for each equipment item during sinusoidal vertical and lateral excitation tests. Digital analysis was used to determine whether the frequencies obtained from analog outputs were due to carbody resonance or equipment resonance. Modal analysis data were used for this purpose up to 15 Hz; the prime body modes were well below 15 Hz and no analysis was pursued above that frequency. Digital data recorded during the equipment resonance test were used to verify true equipment resonance; digital data from only the random excitation tests were analyzed for this purpose.

Digital time histories were converted into the frequency domain by taking Discrete Fourier Transforms (DFT) of 96 blocks of data (each block being equal to 1,024 points). Ensemble averaging was performed on these blocks; 192 ensembles were taken. Power Spectra of each channel were then obtained and used for analysis (a Power Spectrum being defined as a DFT, multiplied by its conjugate). Plots of these were reviewed for each channel to see if they exhibited frequency domain trends through the 0.5 to 30.0 Hz frequency range to determine whether a peak in an equipment accelerometer output spectrum was coincident with a peak in the carbody accelerometer spectrum. Equipment resonance thus influenced by carbody motion between 15 Hz to 30.0 Hz was excluded as not being a true equipment resonance.

TABLE 9-2. ACCELEROMETERS FOR UNDERCAR EQUIPMENT ANALYSIS.

Identification*/		
	Polarity	Vertical Excitation Transducer Locations
1.	19Z+	Floor Centerline, Carbody
2.	24Z+	Floor Centerline, Carbody
3.	31Z+	Floor Centerline, Carbody
4.	47Z+	Lower Edge Left Side, Carbody
5.	49Z+	Lower Edge Left Side, Carbody
6.	18Z-	Signal Coil (ATC Pickup Coil)
7.	19Z-	Air Conditioning Compressor, Front
8.	22Z-	Resistor Bank
9.	23Z-	Inductor Bank
10.	25Z-	Ballast Resistor
11.	27Z-	Air Conditioning Compressor, Rear

Identification*/		
	Polarity	Lateral Excitation Transducer Locations
1.	6Y+	Lower Edge Right Side, Carbody
2.	37Y-	Left Front Corner, Carbody
3.	47Y-	Lower Edge Left Side, Carbody
4.	49Y-	Lower Edge Left Side, Carbody
5.	17Y-	Signal Coil (ATC Pickup Coil)
6.	20Y-	Air Conditioning Compressor, Front
7.	21Y+	Resistor Bank
8.	24Y-	Inductor
9.	26Y-	Ballast Resistor
10.	28Y-	Air Conditioning Compressor, Rear

* See Figure 9-2.

Test results and analyses, both analog and digital, show various critical frequencies of individual equipment under the car and are summarized in table 9-3. The resonant frequencies of the undercar equipment examined are in the 10 to 13.5 Hz range for the vertical excitation, with harmonics at 24 and 28 Hz, respectively, for the inductor and ballast resistor. Lateral resonant frequencies were in the 11.3 to 20.4 Hz range. The prime periodic forcing functions which might excite equipment resonances are in the vertical direction due to wheel and rail joint irregularities; a secondary source could be the carbody first body bending mode. A once-per-revolution periodic input due to a wheel flat would require a speed of 61 mi/h to provide a 10 Hz forcing function; rail joint periodic input frequencies are a maximum of $5\frac{1}{2}$ Hz at 70 mi/h, the vehicles' top speed. Carbody first bending modal frequencies are 7 to 7.4 Hz for vertical mode and 8.7 Hz for the lateral mode.

We conclude that undercar equipment resonant frequencies are sufficiently far removed from likely sources of excitation that equipment resonance is unlikely to be a problem. Before any further conclusions could be drawn, further tests and analyses would be required to determine the frequency spectra and the levels of periodic excitation that could be expected in revenue service in Atlanta, and the amplification factors between input and response.

TABLE 9-3. CRITICAL FREQUENCIES FOR UNDERCAR EQUIPMENT.

Undercar Equipment	Critical Frequency (Hz)	
	Vertical	Lateral
Air Conditioning Compressor, Front	10	--
Resistor Bank	13.5	20.5
Inductor	12.3, 24	15
Ballast Resistor	11, 28	11.3
Air Conditioning Compressor, Rear	10	--
Signal Coil	--	14.5

10.0 CURVING

10.1 INTRODUCTION

During the early service life of the vehicles, MARTA indicated that the rate of wheel flange wear being experienced was higher than anticipated. In addition, MARTA observed that a small number of the trucks were experiencing wheel wear at a significantly greater rate than other trucks in the fleet, and that this was occurring asymmetrically.

The wheel wear (figure 10-1) appeared to be coming from two separate sources. The excessive tread wear was thought to be caused by a problem with the friction tread brake system; this particular problem is outside the scope of the work to be described in this section. The second source of wheel wear appeared as excessive wear of the wheel flanges; this problem was addressed in this phase of the test program.

The mechanism which causes excessive flange wear of wheels can also lead to increased rates of rail gage face wear in curves. There is evidence in Atlanta that significant high rail gage face wear is taking place in the curves. This wear is apparent, particularly on some of the curves in the yard at Avondale (figure 10-2) and on the 5.8° curve just outside of Georgia State Station.

The test program examined the behavior of the trucks during the negotiation of curves typical of those encountered in revenue service. During the test, modifications were made to the trucks and their effects were evaluated. These modifications were:

- The primary suspension bush, which surrounds the axle journal bearing, was modified in order to reduce its longitudinal stiffness to approximately one-third that of the standard bush.
- The wheel cross-sectional profile was changed from its standard AAR 1:20 to a Canadian National (CN), higher conicity CN-A profile.

The test results were compared with predictions from a mathematical model of the truck curving behavior. Subsequently, the model was used to examine the likely effect on wheel flange wear and rail gage face wear for a range of track parameter variations.

10.2 TEST OBJECTIVE

The objectives of the test program were:

- To investigate the behavior of the vehicle on sharply curved track, and to determine the effect on that behavior of modifications to the primary suspension and the wheel profiles.
- To compare the vehicle behavior to mathematical model predictions.



FIGURE 10-1. TYPICAL WORN WHEEL IN ATLANTA.



FIGURE 10-2. GAGE FACE WEAR IN AVONDALE YARD.

- To predict the effect of truck suspension and wheel profile changes on wheel wear rate using the mathematical model.

10.3 STATIC TESTS

In order to provide data for the mathematical model it was necessary to measure certain static truck parameters.

10.3.1 General

The tests carried out on the trucks were designed to measure parameters which were expected to have a significant effect on truck curving performance. The following parameters were determined:

- Primary suspension bush longitudinal stiffness.
- Primary suspension bush lateral stiffness.
- Primary suspension bush vertical stiffness.
- Secondary yaw pivot friction torque.
- Lateral and radial axle alinement.

As mentioned previously, the primary suspension bushes were modified, the main objective being to reduce the longitudinal stiffness to approximately one-third of its original value. The method of reducing the bush stiffness is described in section 3.13.2, and the final configuration of bush that was adopted is illustrated in figure 3-5. In order to determine the modified bush stiffness, measurements were made using a special test rig, shown in figure 10-3. The results obtained from this test were for a bush without the normal static vertical load applied, and it was also necessary to make stiffness measurements with the bushes installed in the truck.

The stiffness tests on the truck and the axle alinement measurements were made on three separate occasions. The first series was carried out with the standard primary suspension bush. The second was performed immediately after installation of the softened primary bushes, but before the track test had taken place. The final series of tests was carried out after the completion of the track tests.

10.3.2 Test Methods

10.3.2.1 Primary Suspension Bush Longitudinal Stiffness. One axle of the test truck was supported on an air bearing table, which allowed the axle to float free of the ground. A longitudinal force was applied at each wheel of the axle by means of the friction brake system. A load cell was placed between the brake actuator and the brake shoe in order to determine the relationship between brake cylinder pressure and brake shoe normal force.

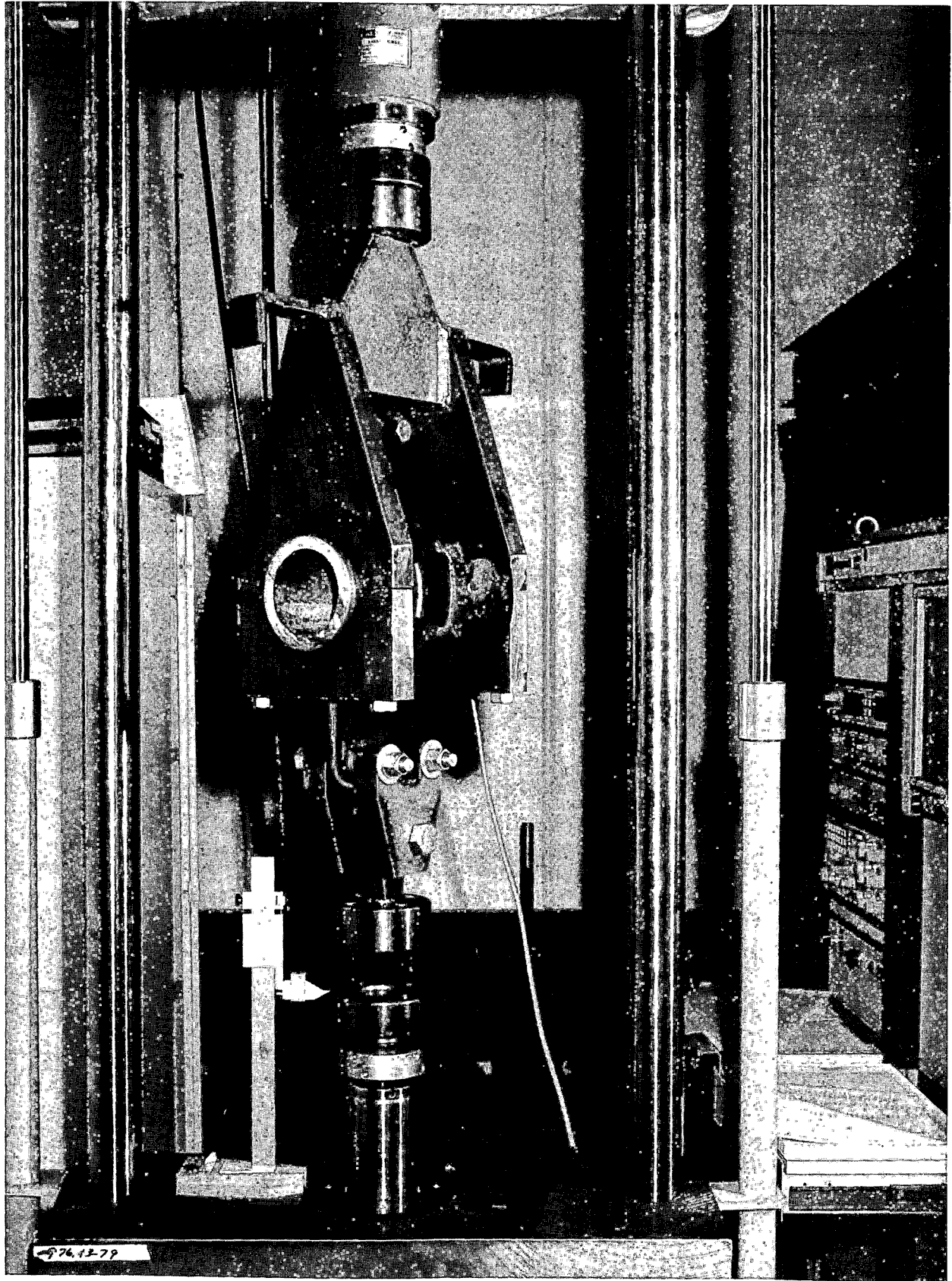


FIGURE 10-3. PRIMARY SUSPENSION BUSH STIFFNESS TEST RIG.

The brake cylinder pressure was measured using a pressure gage. The longitudinal displacements between the axle and the truck sideframe were measured using dial indicators and also the displacement transducers that were used to measure this displacement during the track tests.

With the axle floating free, pressure was applied to both brake actuators acting on that axle. The pressure was increased in increments up to a maximum of 75 psig, which is equivalent to a brake shoe force of 7,780 lb. The pressure was then reduced back to zero in increments. The stiffness was determined from the slope of the force/displacement data.

10.3.2.2 Primary Suspension Bush Lateral Stiffness. In order to apply a lateral force to the truck frame, the third rail current collection paddle assembly was removed and a fixture was bolted in its place. A cable was attached with a load cell in series, in order to determine the magnitude of the load being applied. Application of the load was made by using a chain hoist.

Lateral displacement between the truck frame and the axles was measured using dial gages and the primary lateral displacement transducers that were used in the track tests. Load was applied in increments up to a maximum of 6,000 lb and then decreased in increments back to zero. Stiffness was determined in the same manner as for the longitudinal tests.

10.3.2.3 Primary Suspension Bush Vertical Stiffness. Although the vertical stiffness of the primary bush does not have a significant effect on the curving behavior of the truck, it was important to know what change in vertical stiffness was taking place as a result of the modifications.

With the vehicle at AWO weight, each primary suspension bush carries a load of approximately 8,500 lb. The vertical stiffness test was carried out by relieving this load, using a jack under the primary suspension bush housing. A load cell was placed between the jack and the bush housing in order to determine the force being applied. The load was applied in increments up to the normal static load on the bush and then decreased in increments back to zero. Stiffness was determined from the slope of the load/deflection curve.

10.3.2.4 Secondary Yaw Pivot Friction Torque. Both axles of the truck were supported on a single air bearing table, which, when inflated, allowed the truck to yaw freely with respect to the ground. Equal and opposite lateral forces were applied at diagonally opposite corners of the truck frame. The forces were applied through a chain hoist and the magnitude of the forces was measured using a load cell. The angular position of the truck frame with respect to the carbody was measured using string potentiometers.

Air pressure was applied to the air bearing table until the truck was floating free of the ground. The lateral loads were then increased steadily until rotation of the truck took place. At this point, the magnitude of the applied load reduced. The breakaway torque could be determined from the maximum value reached.

10.3.2.5 Axle Alinement The two axles of the truck were supported on separate air bearing tables, which allowed the axles to float free of the ground. This permitted the primary longitudinal and lateral suspension of the truck to take up a position where the suspension elements were unstrained.

The method of testing was to first inflate the air bearing tables until the axles were floating and then to release the pressure and lower the axles to the ground. It was assumed that after this procedure was complete, the primary suspension remained unstrained.

The alinement of the axles was then measured using an optical technique. Figure 10-4 is a general view of the setup. An optical transit was used to enable very accurate measurements to be made, relative to an optical line of sight. Measurements were made of the lateral distance from two points on each wheel using precision-scribed scales. Figure 10-5 shows a close-up of the four scales in place. The two scales on each axle were placed as far apart longitudinally as was possible and in contact with points on the outside face of the wheel rim, which were known to lie on a line perpendicular to the axle centerline. From the four lateral dimensions it was possible to deduce the angular misalignment of the two axles with respect to one another. This test was repeated for each of the three suspension configurations.

10.3.3 Test Results

The parameters derived from the static tests and used in the mathematical model are presented in table 10-1. The values are shown for all four test configurations. Those parameters which were obtained from the static tests described in section 10.3.2 are marked with an asterisk in table 10-1. The load/deflection tests carried out on the truck present an elementary assessment of the primary suspension spring rates. For example, in the vertical direction, the primary suspension bushes were incrementally relieved of the vehicle load by jacking under each journal housing, and the vertical spring rates were derived from the linear portion of the load/deflection curve. Subsequent tests have shown that the spring rates are nonlinear, with increasing rates as the springs approach their load carrying limits. The values used here ignore such nonlinearities; the intent was to provide a parametric study to illustrate curving performance trends, rather than a qualitative assessment of truck parameters.

The axle misalignments for the three configurations are illustrated in figure 10-6. To aid in the interpretation of the misalignment data, it can be shown that the angular misalignments can be resolved into two misalignment components. These components can be considered as:

- o Equal and opposite angular misalignment of the axles, which is referred to as radial misalignment of the axles.
- o Angular misalignment having equal angles of the same sign.

This latter case, when the axles are parallel to each other but at an angle to the correct orthogonal position, is equivalent to a lateral displacement misalignment of one axle with respect to the other. The lateral displacement can be calculated by multiplying the angular misalignment in radians by the truck wheelbase.

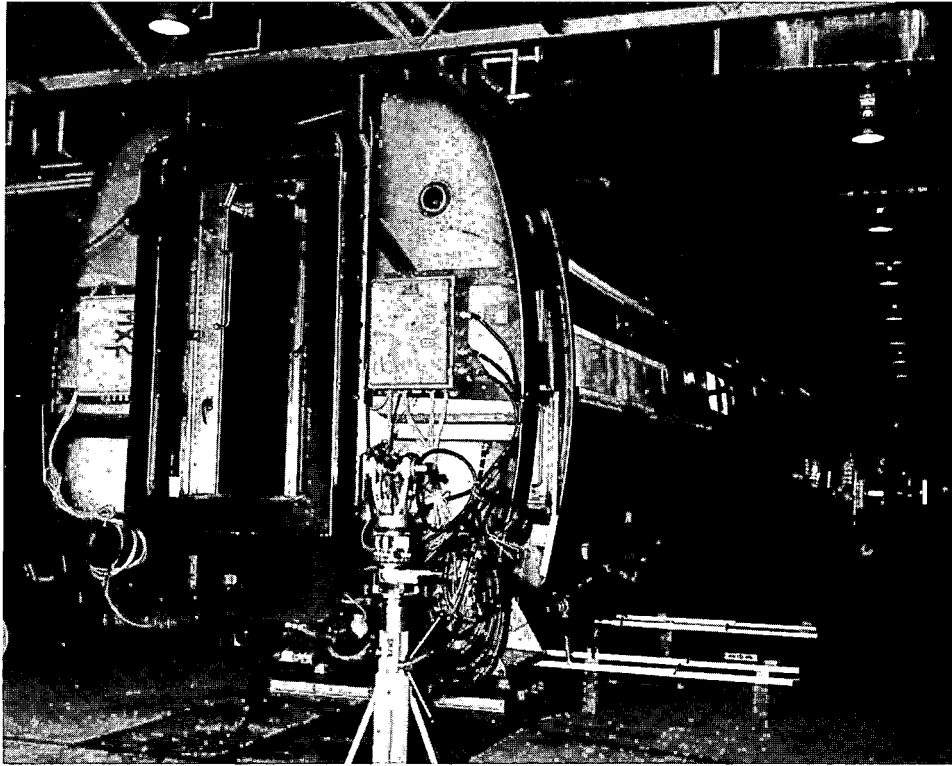


FIGURE 10-4. MEASURING AXLE ALINEMENT.

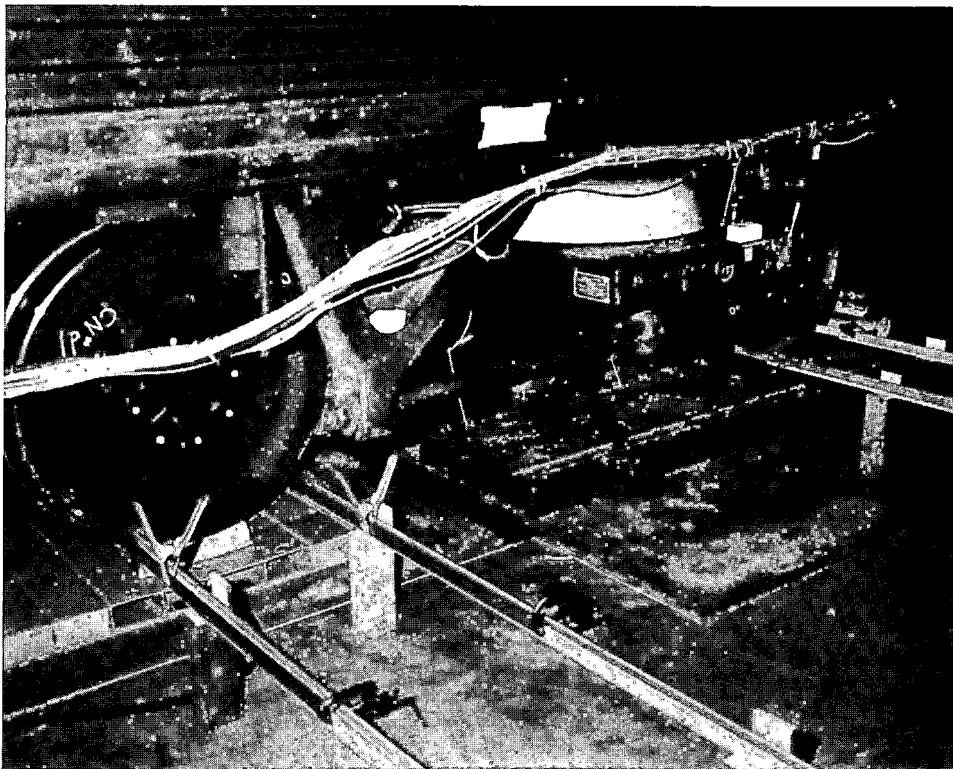
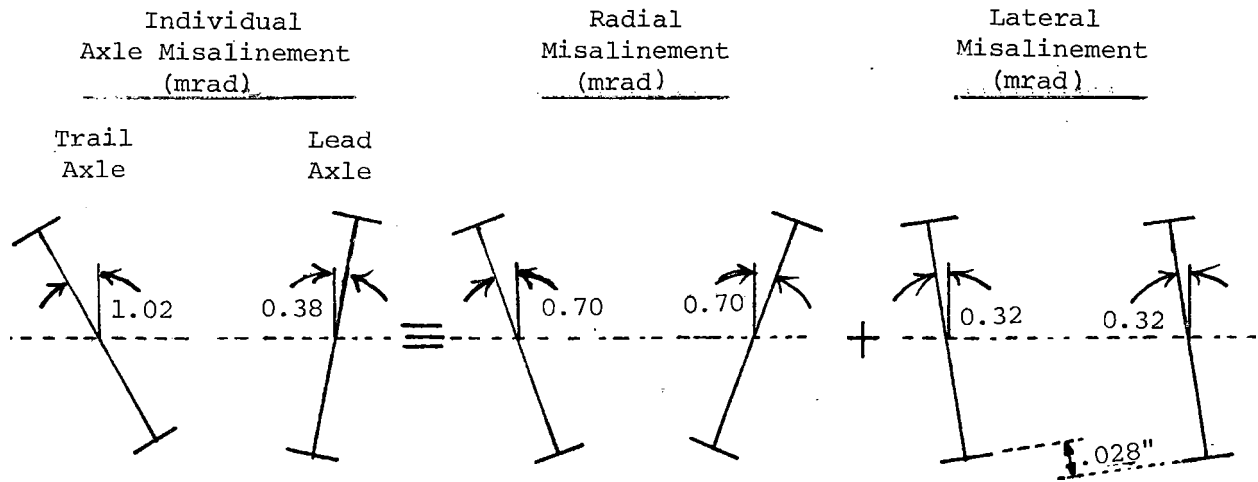


FIGURE 10-5. CLOSE-UP OF AXLE ALINEMENT MEASUREMENT.

TABLE 10-1. MARTA TRUCK PARAMETERS.

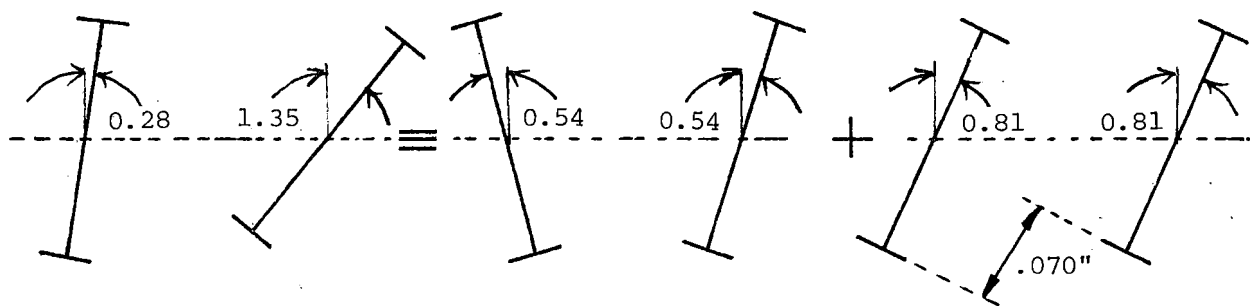
Truck Parameter	Vehicle Configuration			
	C1, AWO	C1, AW3	C2, AWO	C3, AWO
Truck Wheel Base (in)	87.0	87.0	87.0	87.0
Truck Pivot Spacing (in)	630.0	630.0	630.0	630.0
Primary Bush Lateral Spacing (in)	45.25	45.25	45.25	45.25
Vehicle Center of Gravity Height (in)	47.25	47.25	47.25	47.25
Wheel Radius (in)	16.34	16.34	16.34	15.91
Axle Load (lb)	21,100	29,700	21,100	21,000
Wheelset Mass (slugs)	125	125	125	125
Secondary Yaw Friction Torque (lb.ft)	5,680*	9,960*	5,680*	5,680*
Primary Bush Longitudinal Stiffness (lb/in)	150,000*	150,000*	50,000*	55,000*
Primary Bush Lateral Stiffness (lb/in)	65,500*	65,500*	26,250*	26,250*
Primary Bush Vertical Stiffness (lb/in)	100,000*	100,000*	57,500*	57,500*

* The values were derived from the static truck tests described in 10.3.2.



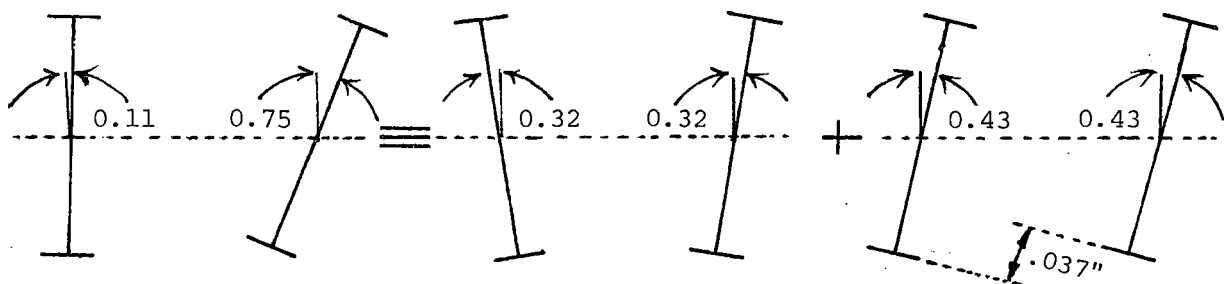
Misalignments with Unmodified Primary Suspension Bush.

(Configuration C1)



Initial Misalignments with Modified Primary Suspension Bush.

(Configuration C2)



Final Misalignments with Modified Primary Suspension Bush.

(Configuration C3)

FIGURE 10-6. TRUCK AXLE MISALIGNMENT.

10.4 TRACK TESTS

10.4.1 Test Instrumentation

The onboard instrumentation used for the curving tests was designed to measure the attitude that the truck adopted in a curve. The yaw angle of the truck with respect to the carbody was determined using two string potentiometers which measured the longitudinal displacement between the truck frame and the carbody. These measurements were made at two locations (figure 10-7), which were widely spaced in the lateral direction. The yaw angle could be determined by differencing the signals from these two transducers and dividing by the lateral distance between them.

The yaw angle of each axle with respect to the truck frame was measured using displacement transducers. Four transducers were used on the test truck, each transducer measuring the longitudinal displacement across one of the four primary suspension bushes (figure 10-8). The yaw angle was determined using the same technique as for the truck to carbody yaw angle.

The lateral displacement of each axle with respect to the truck frame was measured using a single displacement transducer per axle. The measurement was made between the outer race of the axle journal bearing and the truck frame journal bearing housing (figure 10-8).

The angle of attack of each axle with respect to the track was measured using a specially constructed frame. The frames were based on an AAR design and used many of the parts from previous AAR frames. The two frames mounted in the test truck (figure 10-9) are supported by bearings mounted on two small shafts extending from the axles. The frames thus follow the yaw attitude of the axles on which they are mounted. Each frame has two probes attached which rub against the gage face of the rail (figure 10-10). The displacement of each probe is measured using a string potentiometer. The output from these is used to calculate the angle of attack of the axle with respect to the track.

In addition to the above instrumentation, there were carbody and truck sideframe accelerometers, as well as truck to carbody vertical bumpstop displacement transducers. However, this part of the instrumentation was used for gaining information associated with the stability and curve entry tests. The results from these tests are not described here, as the responsibility for analysis and reporting rests with Neil K. Cooperrider and E. Harry Law of Acorn Associates, who are acting as engineering consultants to MARTA. Table 10-2 gives a complete list of instrumentation used in this test, measurement numbers, and other pertinent information.

The data acquisition consisted of parallel recording of data in both analog and digital form. The standard means of recording all data channels on FM tape was performed along with parallel recording of particular data channels on a digital data system located on test car DOTX 208 (Data Acquisition Vehicle). The digital system allowed most data reduction to be done immediately after the test runs were completed.

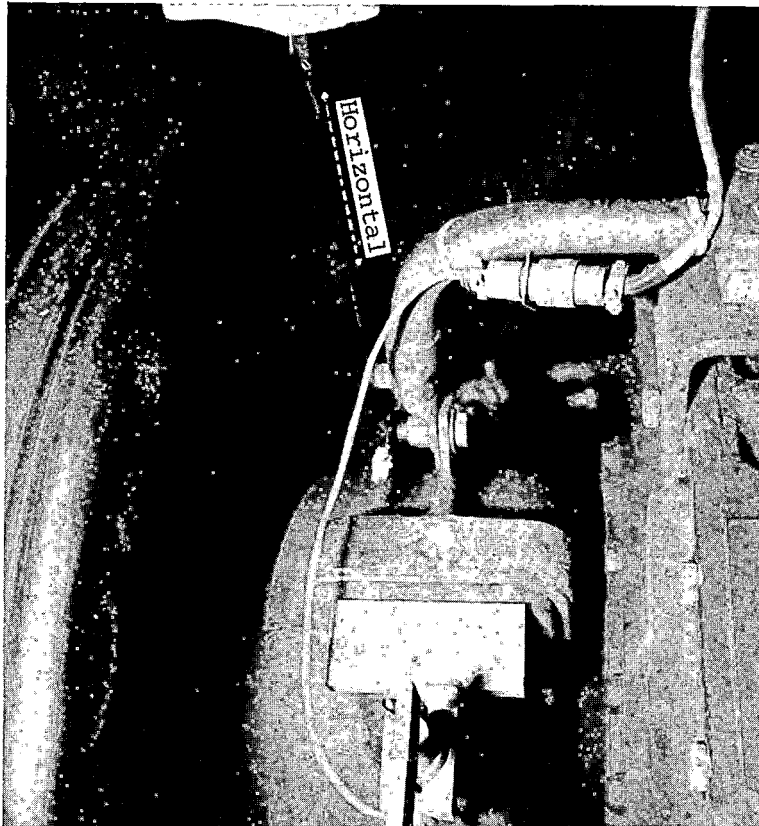


FIGURE 10-7. STRING POTENTIOMETER, TRUCK YAW ANGLE MEASUREMENT.

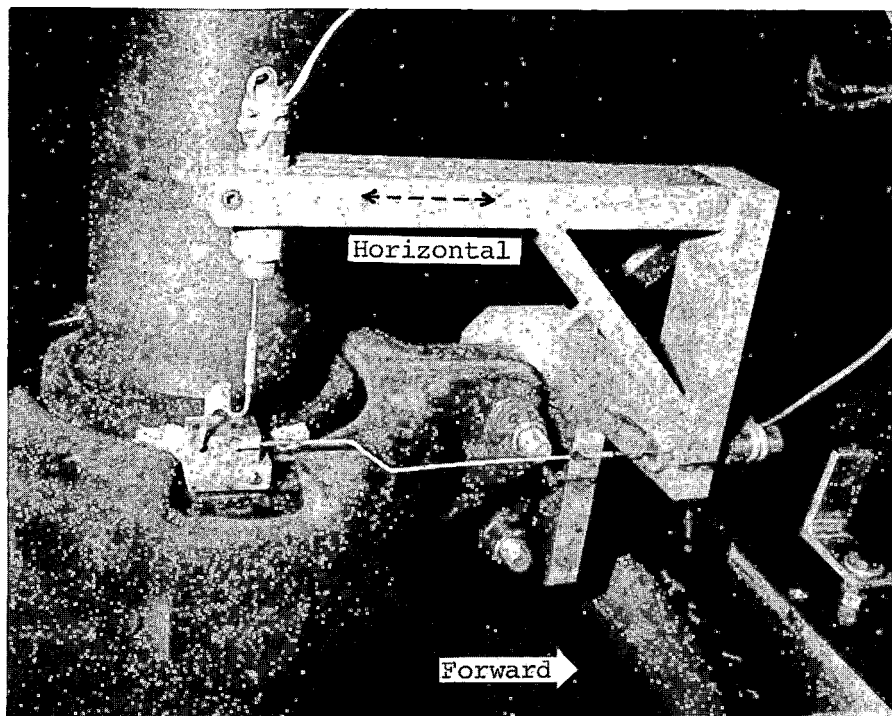


FIGURE 10-8. PRIMARY LONGITUDINAL AND LATERAL DISPLACEMENT MEASUREMENT.

10-12

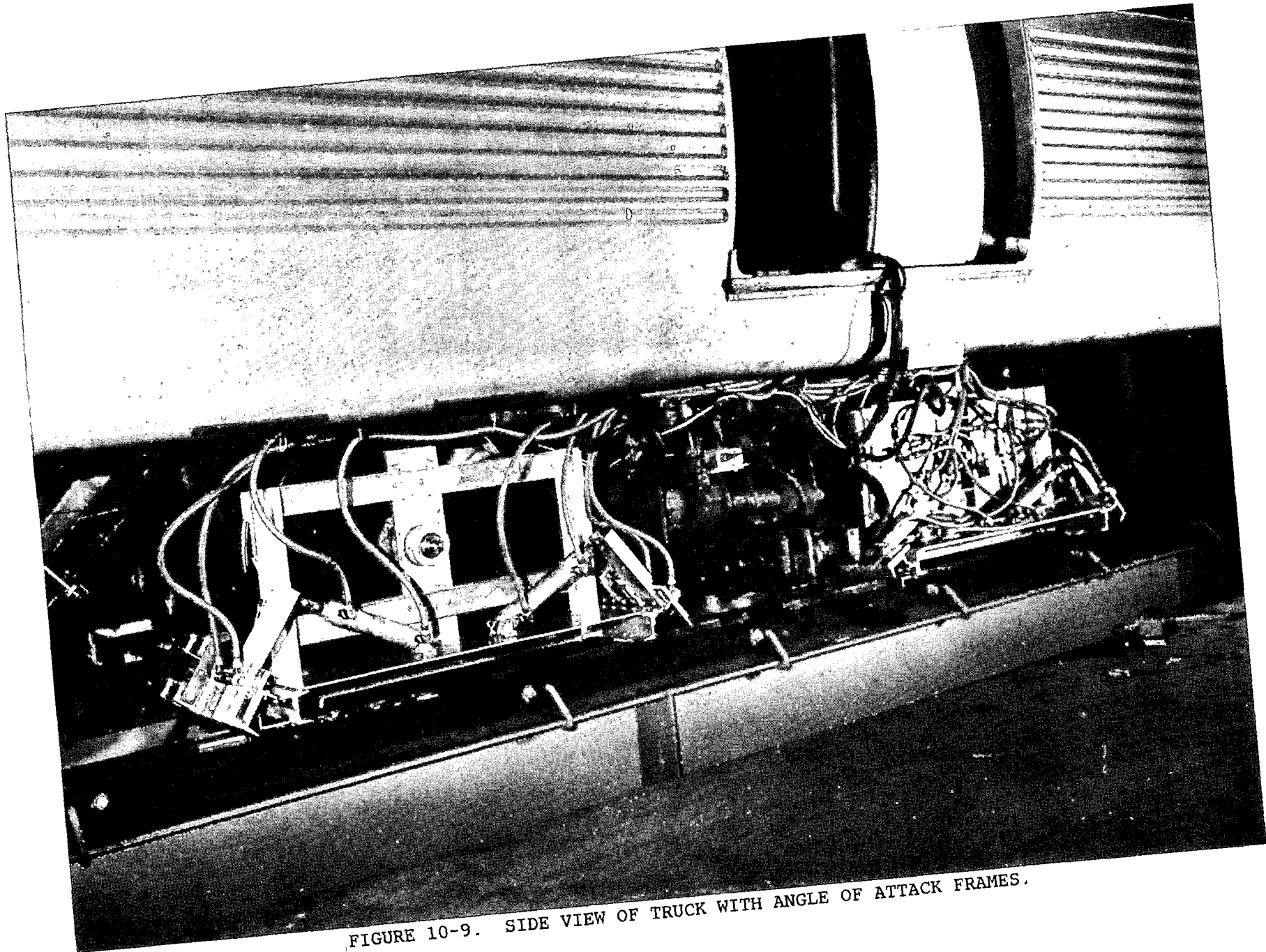


FIGURE 10-9. SIDE VIEW OF TRUCK WITH ANGLE OF ATTACK FRAMES.

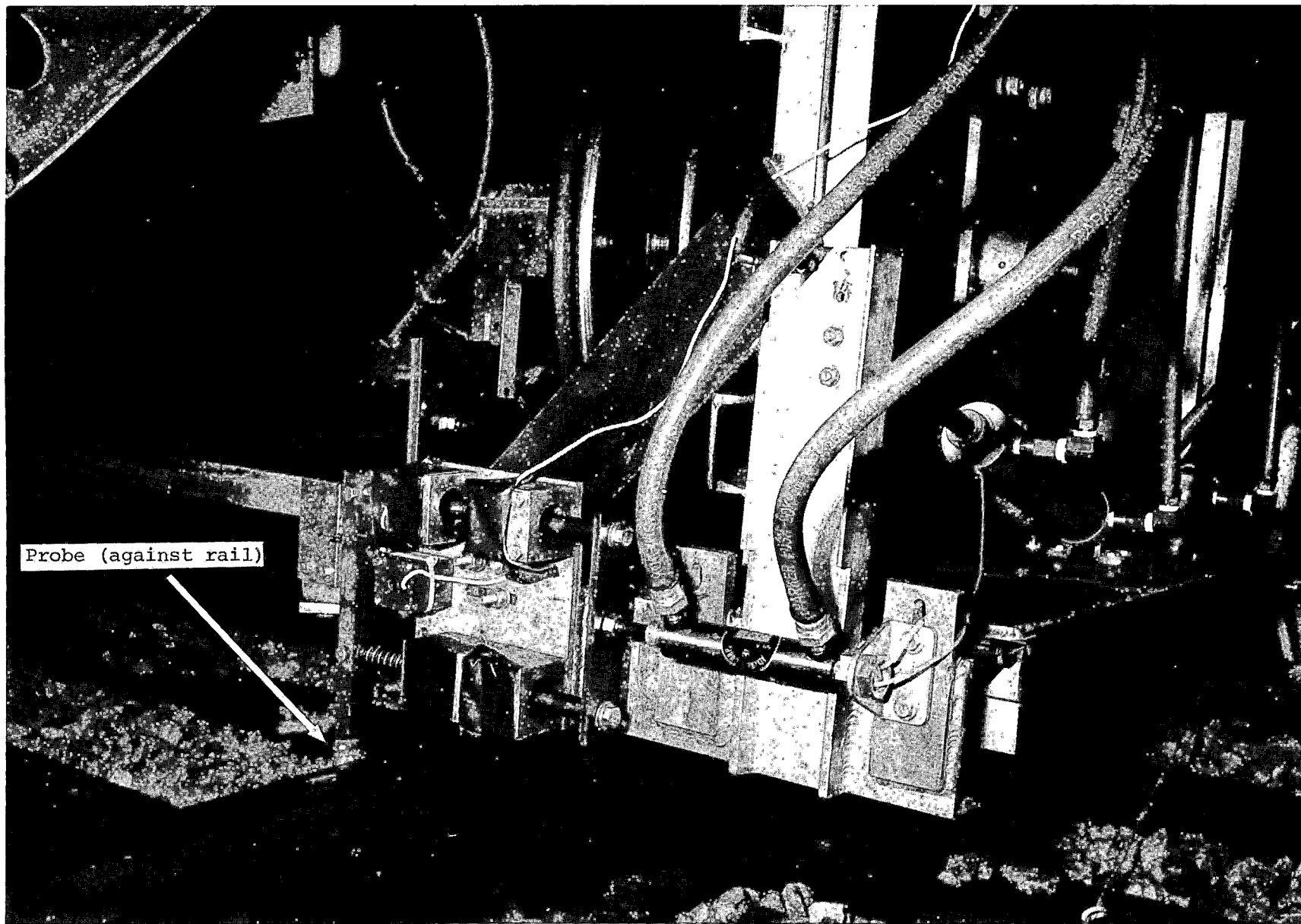


FIGURE 10-10. . . CLOSE-UP OF ANGLE OF ATTACK PROBE.

TABLE 10-2. INSTRUMENTATION SENSOR LISTING, CURVING/STABILITY.

Channel Number	Parameter	Standard		Sensor Type	Measurement Range	Maximum Cutoff Frequency
		Output Name	Measurement Number			
1	IRIG-B Time	T/A	01411	Time Code Generator	---	1 kHz
2	Truck Lateral Acceleration (Right Sideframe, Lead End)	ASF/A2	02206	Capacitance Accelerometer	± 5 g	63 Hz
3	Truck Lateral Acceleration (Right Sideframe, Trail End)	ASF/A6	02208	Capacitance Accelerometer	± 5 g	63 Hz
4	Truck Vertical Acceleration (Right Sideframe, Lead End)	ASF/A1	02205	Capacitance Accelerometer	± 5 g	63 Hz
5	Truck Vertical Acceleration (Left Sideframe, Lead End)	ASF/A3	02204	Capacitance Accelerometer	± 5 g	63 Hz
6	Body Lateral Acceleration (Car Centerline, Over Lead Truck)	AC/A2	02102	Servo Accelerometer	±0.5 g	63 Hz
7	Body Lateral Acceleration (Car Centerline, Over Trail Truck)	AC/A9	02109	Servo Accelerometer	±0.5 g	63 Hz
8	Body Vertical Acceleration (Car Right Side, Over Lead Truck)	AC/A7	02107	Servo Accelerometer	±0.5 g	63 Hz
9	Body Vertical Acceleration (Car Left Side, Over Lead Truck)	AC/A8	02108	Servo Accelerometer	±0.5 g	63 Hz
10	Body Vertical Acceleration (Car Right Side, Over Trail Truck)	AC/A10	02110	Servo Accelerometer	±0.5 g	63 Hz
11	Body Vertical Acceleration (Car Left Side, Over Trail Truck)	AC/A11	02111	Servo Accelerometer	±0.5 g	63 Hz
12	Body/Truck Vertical Displacement (Right Bump Stop)	STPD/C5	06105	Displacement Sensor	±2.5 in	63 Hz
13	Body/Truck Vertical Displacement (Left Bump Stop)	STPD/C4	06104	Displacement Sensor	±2.5 in	63 Hz
14	Body/Truck Lateral Disp. (Sideframe to Body, Lead Truck)	STPD/C3	06103	Displacement Sensor	±5.0 in	63 Hz
15	Body/Truck Long. Disp. (Sideframe to Body, Lead Truck Right)	STPD/C1	06101	Displacement Sensor	±1.5 in	63 Hz
16	Body/Truck Long. Disp. (Sideframe to Body, Lead Truck Left)	STPD/C2	06102	Displacement Sensor	±1.5 in	63 Hz
17	Primary Lateral Displacement (Lead Truck, Lead Axle-Left)	STPD/J1	06201	Displacement Sensor	±0.5 in	63 Hz
18	Primary Lateral Displacement (Lead Truck, Trail Axle-Right)	STPD/J4	06204	Displacement Sensor	±0.5 in	63 Hz
19	Primary Longitudinal Displacement (Lead Truck, Lead Axle-Right)	STPD/J3	06203	Displacement Sensor	±0.5 in	63 Hz
20	Primary Longitudinal Displacement (Lead Truck, Trail Axle-Right)	STPD/J5	06205	Displacement Sensor	±0.5 in	63 Hz
21	Primary Longitudinal Displacement (Lead Truck, Lead Axle-Left)	STPD/J2	06202	Displacement Sensor	±0.5 in	63 Hz
22	Primary Longitudinal Displacement (Lead Truck, Trail Axle-Left)	STPD/J6	06206	Displacement Sensor	±0.5 in	63 Hz
23	Wheel/Rail Lateral Displacement (Lead Axle, Lead Position)		06301	Displacement Sensor	±1.75 in	31.5 Hz
24	Wheel/Rail Lateral Displacement (Lead Axle, Trail Position)		06302	Displacement Sensor	±1.75 in	31.5 Hz
25	Wheel/Rail Lateral Displacement (Trail Axle, Lead Position)		06303	Displacement Sensor	±1.75 in	31.5 Hz
26	Wheel/Rail Lateral Displacement (Trail Axle, Trail Position)		06304	Displacement Sensor	±1.75 in	31.5 Hz
27	Speed	VS/A	01401	Electromagnetic Sensor	100 mph	10 Hz
28	ALD	ET/A	01423	IR Source	---	100 Hz

The digital data channels consisted of the various displacement measurements, which have been mentioned previously, along with reference data channels. The system allowed for determination of minimum, maximum, and mean values for each channel. These values were determined for each of the test zones for each test run. The data were low-pass filtered at 10 Hz and digitized at 30 samples per second.

The test zones were identified by a series of track location markers, Automatic Location Detectors (ALD's). The ALD system consisted of a modulated infra red light source, which detected its own signal reflected back into a receiver, tuned to respond to the modulation frequency. The track location markers consisted of thin, galvanized metal sheets with reflective tape on the upper face. These targets were placed at specified locations on each of the test tracks (FAST, Balloon Loop, and TTT). A speed signal was generated by the 9th-wheel speed system.

In addition to instrumentation onboard the test vehicle, trackside instrumentation was used at one of the test zones on the FAST track. The trackside instrumentation consisted of four sets of vertical and lateral force measurements on the high rail of Section 07 at the following specific tie locations; 07-0214, 07-0275, 07-0330, and 07-0399. These measurements were made using existing strain gage bridges.

10.4.2 Test Method

Previous experience with the wheel flange and rail gage face wear problem had indicated that, for this type of vehicle, significant rates of wheel and rail wear would occur only for curves of greater than approximately 3°.

The largest degree of curvature encountered during revenue service operations at Atlanta is 5.8° in the curve just outside of Georgia State Station. However, there are tracks in the yard at Avondale with more severe curvature. The TTT orientation and plan are shown in figure 4-1 and the track profile is shown in figure 4-2. The TTT has curves with a maximum curvature of only 1.5°. Therefore, it was necessary to carry out the majority of the curving tests on other test tracks. However, the tangent section of the TTT between stations 31 and 38 was used for the stability tests, and the north curve, 1.5° between stations 42 and 47, was used as one of the curving test zones.

The majority of the curving tests were carried out on the FAST track and on the Balloon Loop. These sites have curves in the range 3° to 7.4°, which are more typical of the curves encountered in Atlanta and also more typical of the curves encountered on other rapid transit routes. A general map showing the locations of the TTT, FAST track and Balloon Loop is shown in figure 4-3, and a detailed layout of the FAST track is shown in figure 4-4. The test zones used on FAST during the running tests were sections 03 (5° curve), 07 (5° curve), 13 (4° curve), 17A (5° curve), 17B (3° curve), and 20 (tangent). Two test zones were used on the Balloon Loop--a tangent zone between stations 306 and 307 and a curved zone from station 308.4 to 309.6. All the test zones were chosen as regions where the nominal values of track curvature and superelevation were thought to be constant. The actual values of curvature and superelevation were measured using a track geometry car, and the mean values determined for each curve are listed in table 10-3.

TABLE 10-3. DATA FOR CURVED TRACK TEST SITES.

Curved Track Section	Curvature (°)	Superelevation (in)	Gauge (in)
FAST Section			
03	5.2	3.4	56.9
07	5.2	3.8	57.0
13	4.1	3.0	56.6
17A	5.0	3.5	57.0
17B	3.2	1.8	56.9
Transit Test Track			
North Curve	1.5	4.4	56.8
Balloon Loop			
Main Curve	7.4	4.6	56.9

Each of the test zones was marked, at the beginning and end, with reflective ALD boards. Additional track side markers were used to indicate places where the angle of attack probes should be either raised or lowered. This was necessary because the angle of attack system is not capable of being run through switches or crossings without damage.

Neither the FAST track nor the Balloon Loop are equipped with a third rail current collection system and, therefore, the vehicles could not be run using their own power. The entire curving and stability test program was carried out using a diesel locomotive to provide the motive power. The test train consist is shown in figure 10-11. MARTA vehicle 0110 was the only test vehicle used and the truck at the A end of the car was instrumented in the manner described in section 10.4.1.

Before and after each day's testing, new zeros for the angle of attack measurements were established. This was achieved by placing a long straight-edge across the back of the flange of a wheel to which the two probes, fore and aft of that wheel, were clamped. In this position the apparent angle of attack was known and provided a datum for the measurements made during the running tests.

Unfortunately, it was found that significant changes took place between the data recorded at the beginning and end of the day. As a result, a different method for obtaining datum settings was used, not only for the angle of attack, but also for primary suspension yaw angle. The mean values of these parameters were obtained for the tangent track zones associated with each test site. These mean values were determined for both the forward and reverse direction of travel and the average of these wear values was calculated. This average value was then used as the zero datum.

For the truck angle of attack, the following method was used for determining the zero datum. The mean value of the truck yaw angle with respect to the carbody was calculated for the four different modes of operating around the Balloon Loop (the only test site for which the truck angle of attack was determined). These tests were performed in both clockwise and counterclockwise directions, forward and reverse. The average value of the four mean truck yaw angles was taken as the zero datum.

At each of the test sites a series of runs was made, during which the speed of the train was held as nearly constant as possible. The test procedure used during the running tests was as follows:

- On the TTT, runs were made in a forward direction (locomotive leading) proceeding in a clockwise direction over the tangent test zone and the 1.5° curve. Test speeds were in 10 mi/h increments from a minimum of 10 to a maximum of 70 mi/h.
- On the FAST track all runs were made in a forward direction in both clockwise and counterclockwise directions, over the full length of the track. Test speeds were in 10 mi/h increments from 10 to 40 mi/h and at 45 mi/h.
- The tests on the Balloon Loop were carried out over the tangent zone and the 7.4° curved test zone. Tests were performed clockwise and counterclockwise, and also in both forward and reverse directions.

10-18

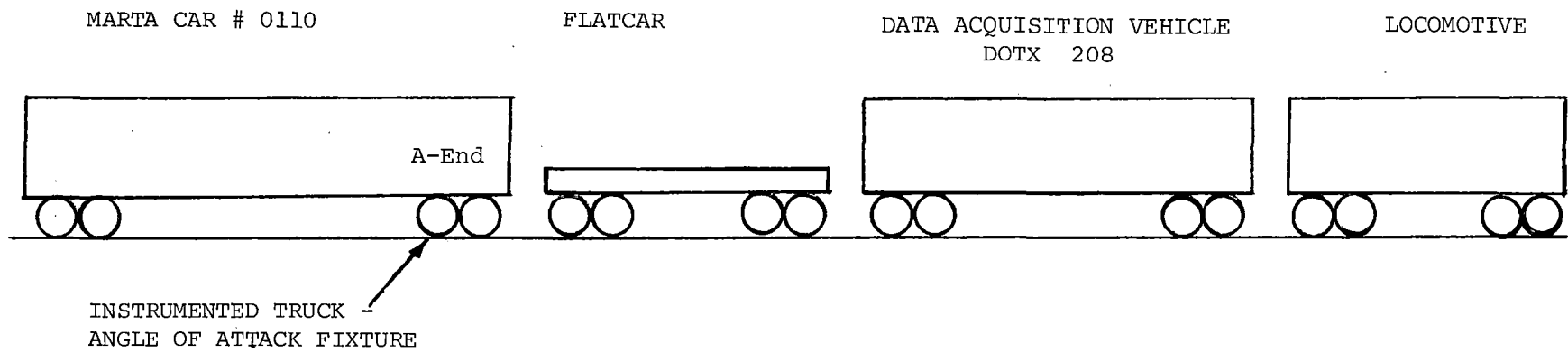


FIGURE 10-11. MARTA CURVING TEST, TRAIN CONSIST.

In addition to the data recorded from the onboard instrumentation, vertical and lateral force measurements were made at the four locations on the high rail of FAST section 07. The peak value of force as each axle passed was determined and an estimate of the likely steady-state force through the curve was made by averaging the peak values at the four locations.

The tests were run with three configurations, designated C1, C2, and C3, which are described in the following paragraphs:

C1 - The truck primary suspension is provided by cylindrical rubber bushings, which surround each axle journal bearing and are retained in a housing at each corner of the truck frame (figure 3-3). The journal housing and the primary bushing are split along the horizontal axis to enable removal of the axle from the truck frame (figure 3-4). The longitudinal stiffness of one of these bushings, as measured in the truck, was found to be 150,000 lb/in.

For the initial test configuration the wheels were reprofiled to AAR 1:20 profile. However, the vehicles had accumulated some mileage between this reprofiling operation and the commencement of the curving tests, and during this time some wear of the wheels had taken place. This wear is evident in figure 10-12, which shows the measured profiles compared with a new AAR 1:20 profile. These measurements were made using a British Rail designed wheel profilometer (figure 10-13). A companion machine for measuring rail profiles is shown in figure 10-14.

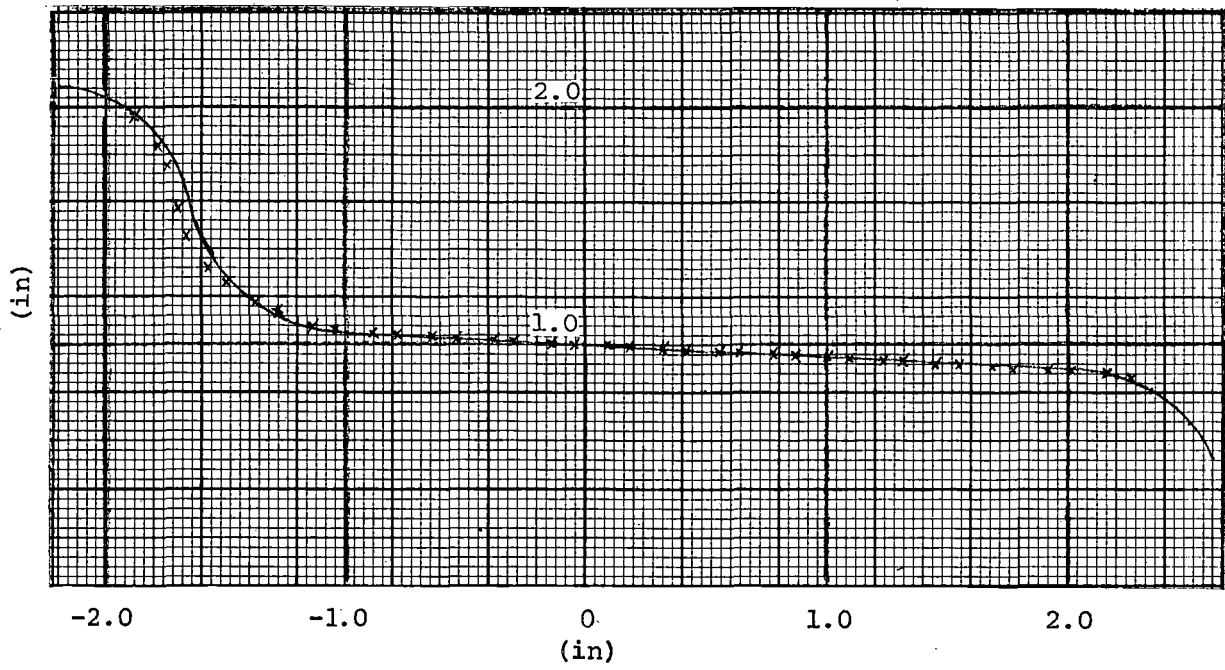
C2 - The rubber bushings described in C1 were subsequently modified in order to reduce their longitudinal stiffness to approximately one-third of the standard value. This was achieved by removing material from the bushings near to the horizontal axis. In their modified form, installed in the truck, the bush longitudinal stiffness was measured at 50,000 lb/in. The second test configuration used these modified bushings with the same wheel profiles as for configuration C1.

C3 - The modified bushings described in C2 were used for the third configuration, but when statically tested again, their stiffness had increased to 55,000 lb/in. The wheel profiles were changed from the standard AAR 1:20 to a CN-A wheel profile, which gave a higher conicity.

Tests were carried out with configuration C1 at AW0 and AW3 weight. Configurations C2 and C3 were tested only at the AW0 weight.

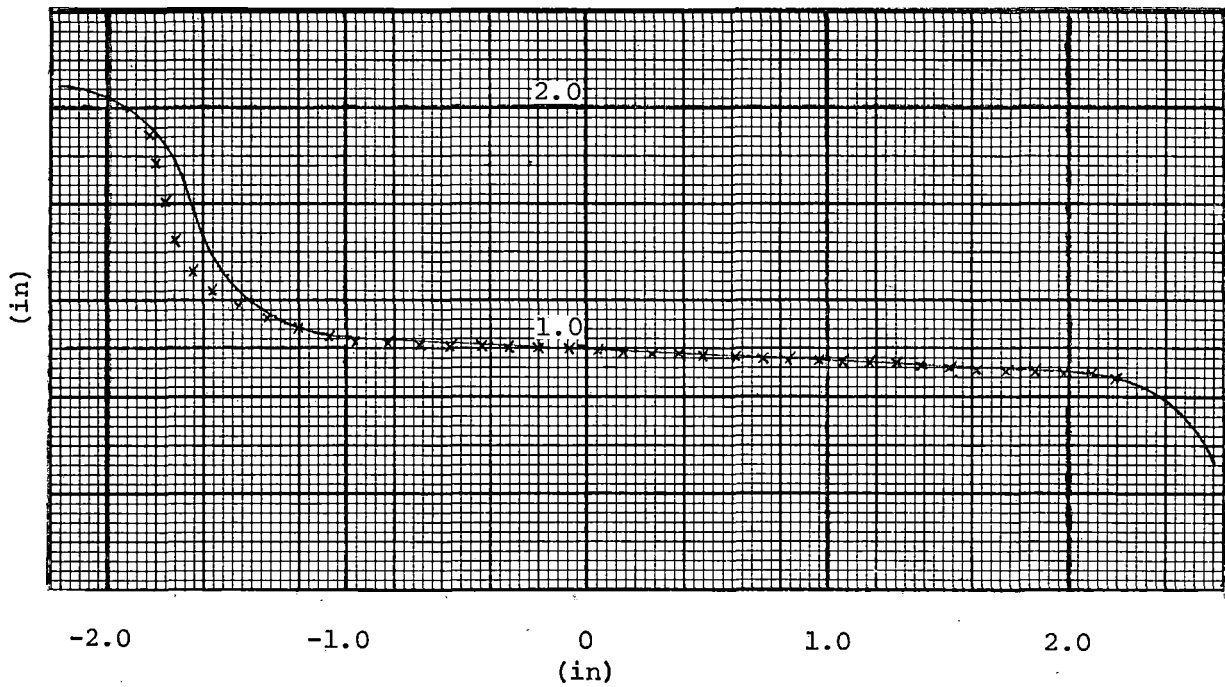
The wheel profiles were measured immediately before and after the tests in the C3 configuration had been completed. The profiles measured after the C3 tests are shown in figure 10-15 and compared with the design case CN-A profile.

Throughout the test program a number of problems were encountered. The major source of trouble was the angle of attack measuring system. The frame appeared to be a fairly sound design and gave very little trouble. However, the measuring probes attached to this frame suffered numerous problems. Typical of these were the following:



Left Wheel

x x x Configurations C1 and C2.
 _____ Design case profile.



Right Wheel

FIGURE 10-12. WHEEL PROFILE, CONFIGURATIONS C1 AND C2 COMPARED WITH DESIGN CASE AAR 1:20 PROFILE.

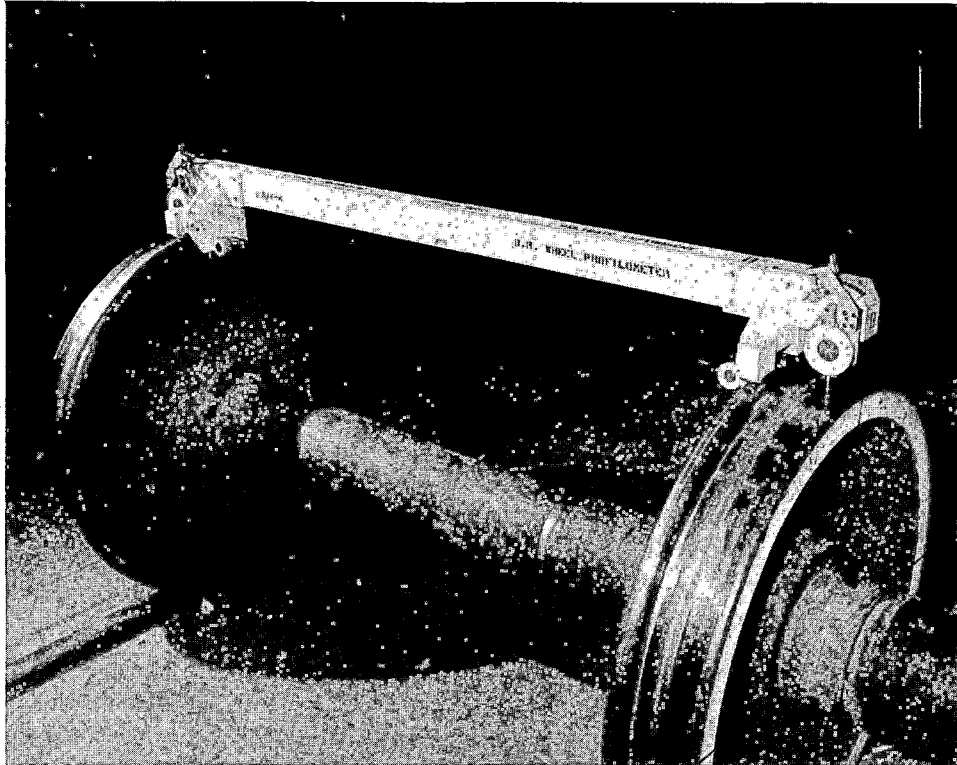


FIGURE 10-13. WHEEL PROFILOMETER.

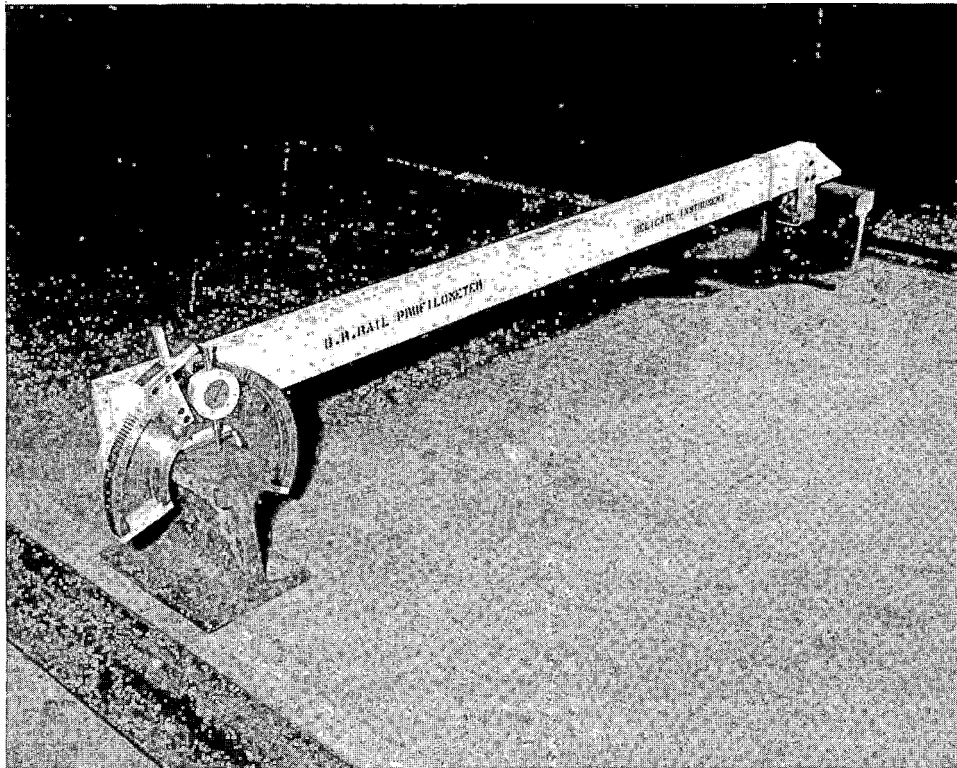
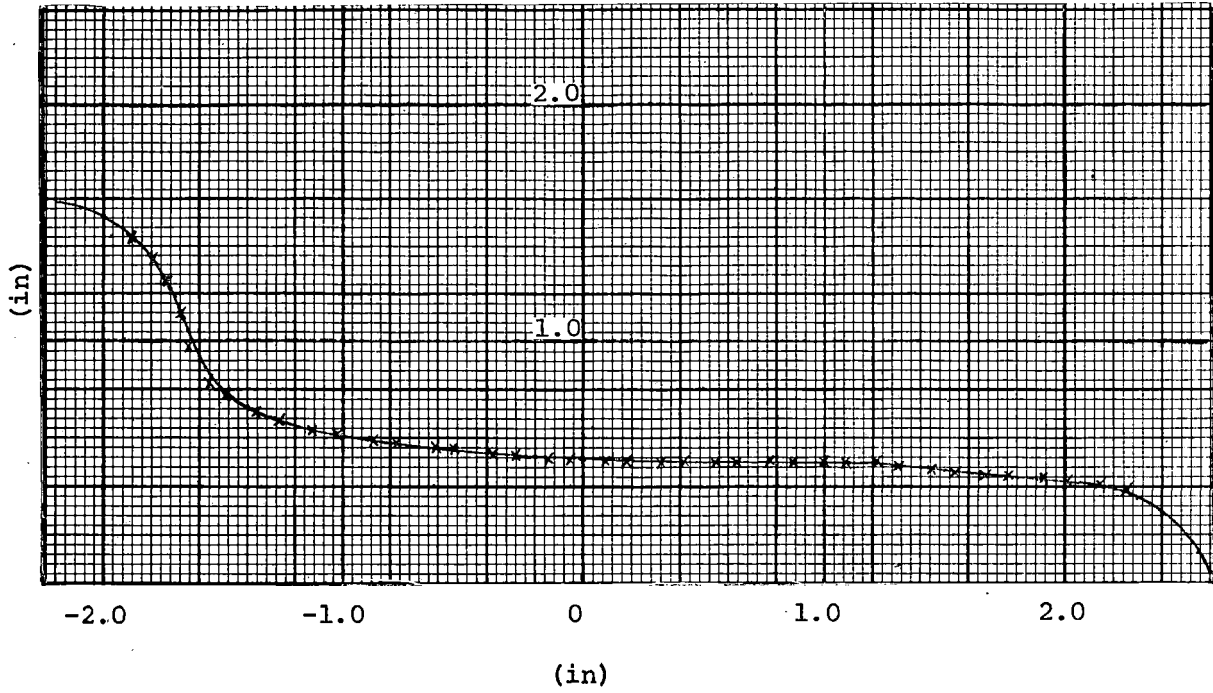


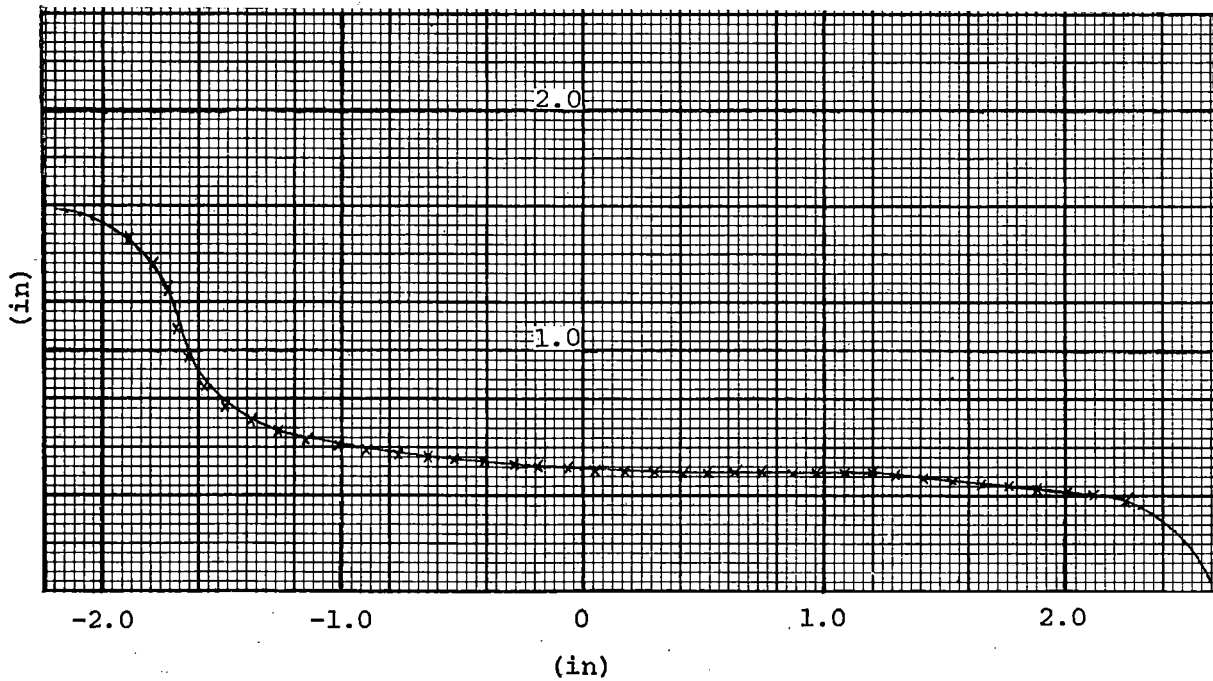
FIGURE 10-14. RAIL PROFILOMETER.



Left Wheel

x x x Configuration C3

_____ Design case profile.



Right Wheel

FIGURE 10-15. WHEEL PROFILE, CONFIGURATION C3 COMPARED WITH DESIGN CASE CN-A PROFILE.

- Probe arms breaking, due to longitudinal inputs, presumably at badly alined rail joints.
- Probe arms bending laterally, due to the lateral acceleration environment.
- Probe rubbing pads working loose and falling off, due to the acceleration environment.
- The attachment of the string to the probe arm from the string potentiometer failing, again due to the acceleration environment.

These and other failures were experienced mainly during the tests on the FAST track and, as a result, most of the data taken during the runs were of dubious value. The majority of the problems with the angle of attack system were encountered during the tests on the FAST track for the following reasons:

- The track quality on FAST is, in general, worse than the Balloon Loop and the TTT. Therefore, the acceleration environment experienced by the probe arms was higher.
- Tests on the FAST track were carried out at night. This made it difficult to properly correct problems that did occur.

10.4.3 Test Results and Comparison with Theoretical Predictions

The main test purpose was to produce data which could be compared with the predictions from a mathematical model of the vehicles' curving behavior. Given good correlation between the test results and the predictions, the mathematical model could then be used to predict the likely effect of a number of truck parameter changes on wheel and rail wear rate. The model was developed previously and has been tested extensively by comparing its predictions with the results from a number of test series using vehicles equipped with instrumented wheelsets. In all cases, very good agreement was obtained from the previous applications of this mathematical model, and those results are available.^{1 2}

The data required for the predictions are listed in table 10-1. Additional data required are the alinement of the axles (shown for the three configurations in figure 10-6) and the cross-sectional profiles of the truck wheels and the pair of rails on which they run. The two wheel profiles used during the test program have been described previously and are illustrated in figures 10-12 and 10-15.

¹ Elkins, J. A., and Gostling, R. J., "A General Quasi-Static Curving Theory for Railway Vehicles," Proceedings, 5th VSD-2nd IUTAM Symposium, Vienna, Sept., 1977.

² Elkins, J. A., and Eickhoff, B. M., "Advances in Non-Linear Wheel/Rail Force Prediction Methods and their Validation," presented at the ASME Winter Annual Meeting, New York, Dec., 1979, to be published by ASME.

The first test site that is considered is the Balloon Loop; a typical set of cross-sectional profiles for the two rails on the 7.4° curve is shown in figure 10-16. The crosses show the measured points, and the solid line is the original, unworn profile of a new 136 lb/yd rail section. The high rail exhibits a small amount of gage face wear of the type occurring in Atlanta; the low rail has a small amount of head wear. These wear patterns are typical of the wear experienced on the high and low rails of many sharp curves.

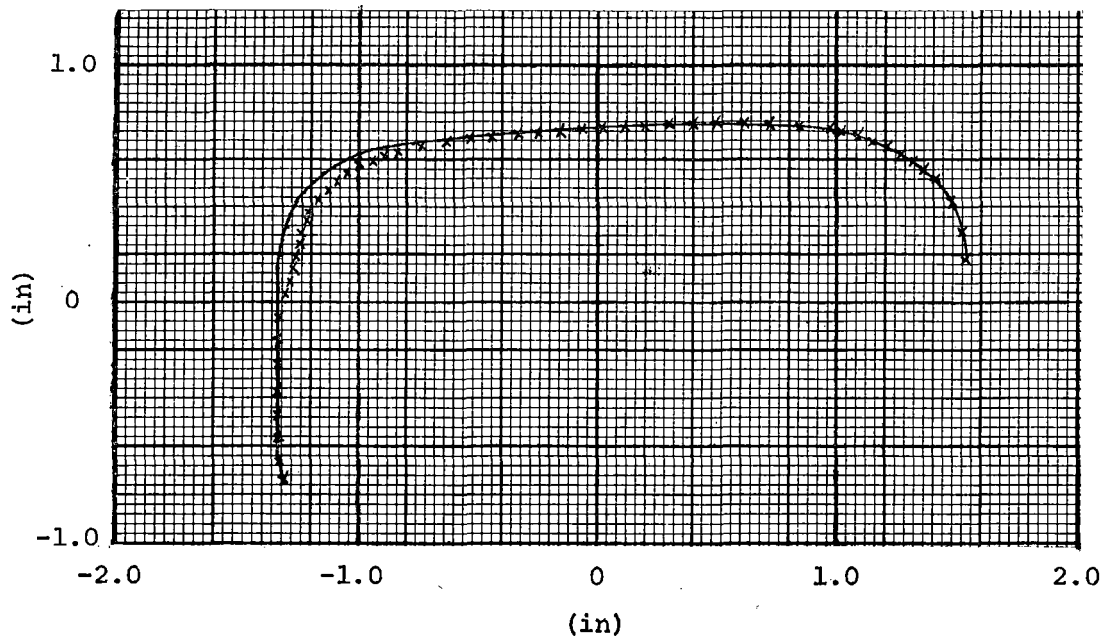
Figure 10-17 shows the mean value of the lead axle angle of attack, obtained from the Balloon Loop tests. Axle angle of attack is defined as the angle between the perpendicular to the axle axis of rotation and tangent to the curve at that location. The results from the four test cases are shown by the points on the graph; the lines show the predictions from the mathematical model. The results given are for the test truck in forward travel, both clockwise and counterclockwise around the loop, so that the curve appears as a right-hand curve in one case and a left-hand curve in the other.

A number of effects can be observed in this set of results. For all four test cases, the angles of attack for the left-hand curve are 2 to 3 mrad larger than for the right-hand curve. This effect is a direct result of the misalignment of the axles, which, in all cases, is such as to prefer the negotiation of a right-hand curve. It also can be seen that the reduction in primary longitudinal stiffness (configuration C2 compared with configuration C1) gives a 5 to 6 mrad reduction in angle of attack. However, it would appear from these results that the change in wheel profile from AAR 1:20 to CN-A (C3 compared with C2) is detrimental. In fact, this result is misleading, because configuration C3 had a smaller axle misalignment than C2 and, in addition, by the time C3 was tested, the longitudinal stiffness of the modified primary suspension bush had increased by approximately 10%. Without the use of the mathematical model, which permits these effects to be separated out later, erroneous conclusions could be made.

Another effect apparent in these results is the tendency for the lead axle angle of attack to decrease with increasing speed. This was so for all four cases that were tested.

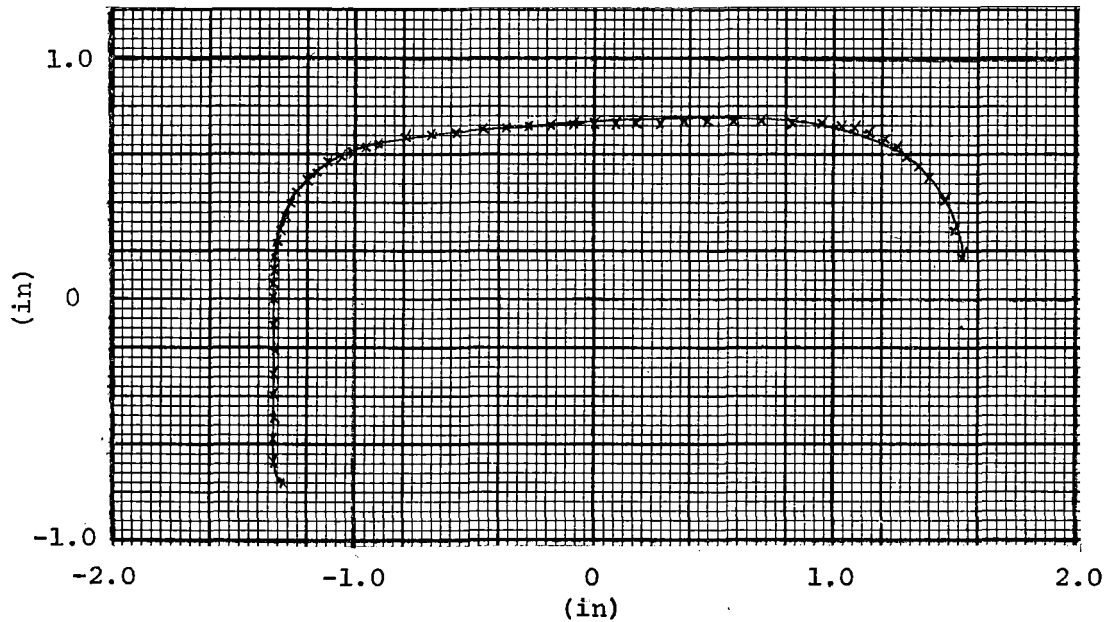
Figure 10-18 shows the corresponding mean value of the truck frame angle of attack for the same four test cases on the Balloon Loop. Truck frame angle of attack is defined as the angle between the longitudinal centerline of the track and the tangent to the curve, at a point midway between the two angles. The results show that the reduction in primary longitudinal stiffness reduced not only the lead axle angle of attack by 5 to 6 mrad, but also the truck frame angle of attack by 1 to 4 mrad. The reduction in lead axle angle of attack being achieved can be attributed, half, to the reduction in truck angle of attack and, half, to the increased primary longitudinal suspension displacement (which gives an increased yaw angle of the axle with respect to the truck frame).

The mean value of the yaw angle of the lead primary suspension is shown in figure 10-19. Suspension yaw angle is defined as the yaw angle between the axle and the truck frame. These results show that an increased yaw angle is being obtained with the softened bush, 4 mrad compared to 1 mrad. The apparent inferior performance of the CN-A profile, as compared with the AAR 1:20 (C3 compared with C2), is also shown. The results for the trailing axle



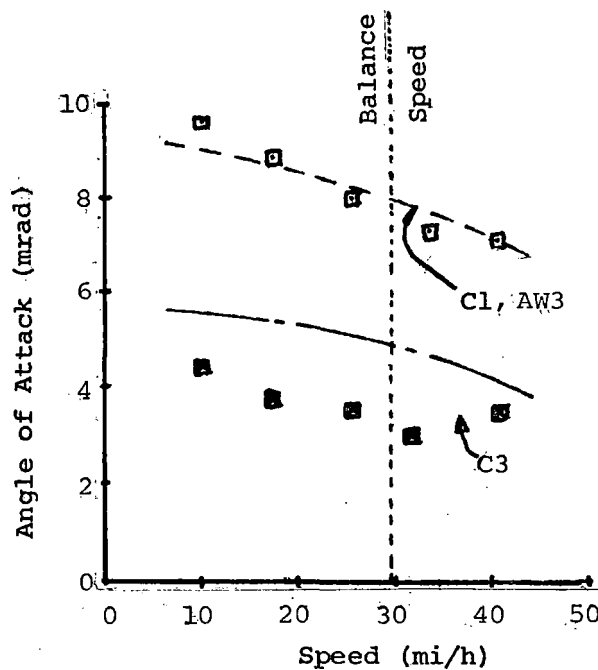
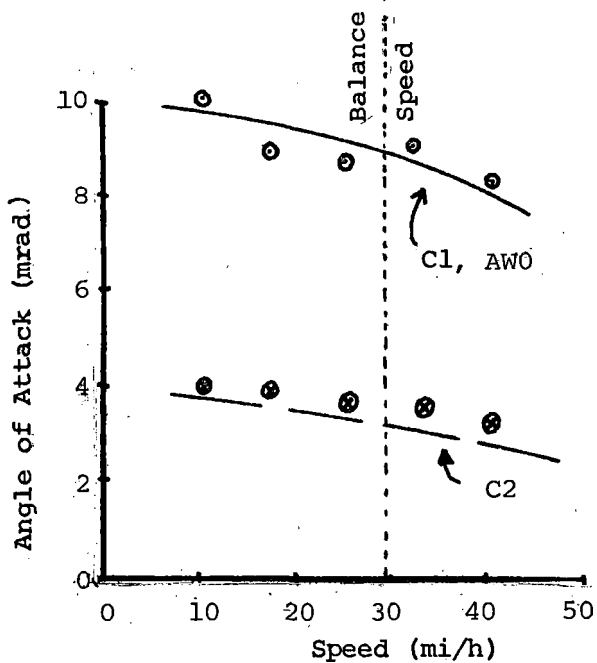
High Rail

x x x Balloon Loop
 _____ Design case profile.

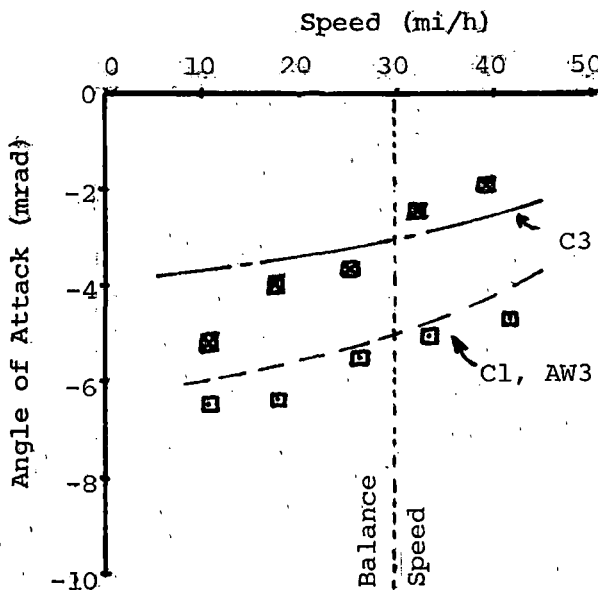
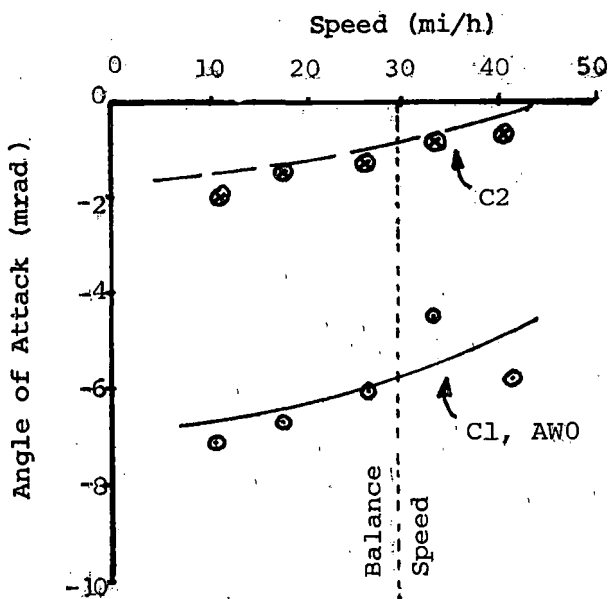


Low Rail

FIGURE 10-16. TYPICAL RAIL PROFILES FOR BALLOON LOOP COMPARED WITH DESIGN CASE 136 lb/yd RAIL.



LEFT-HAND CURVE

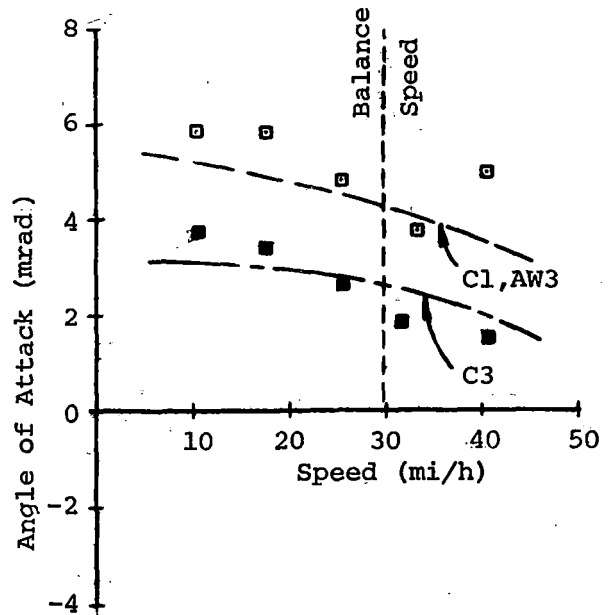
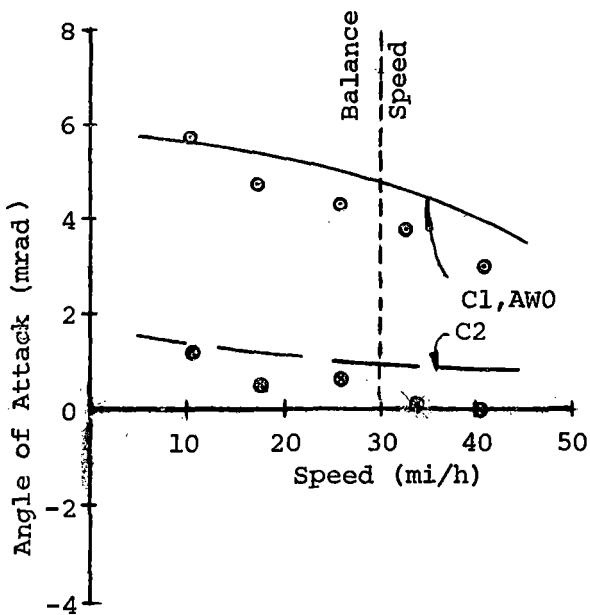


RIGHT-HAND CURVE

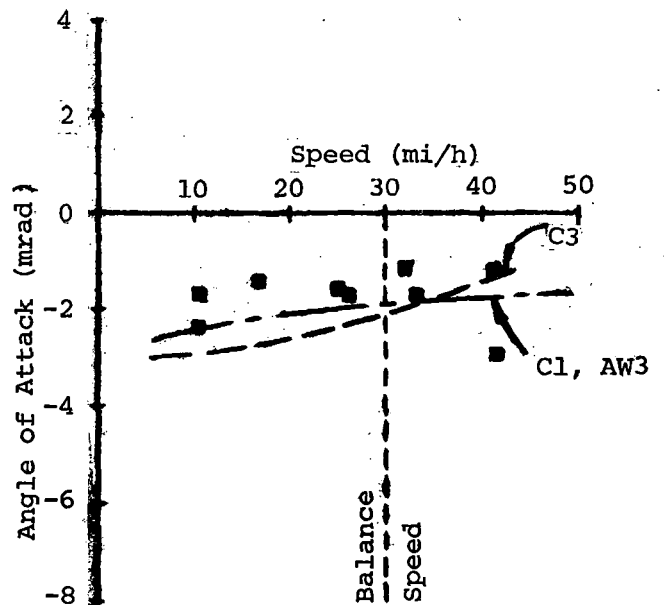
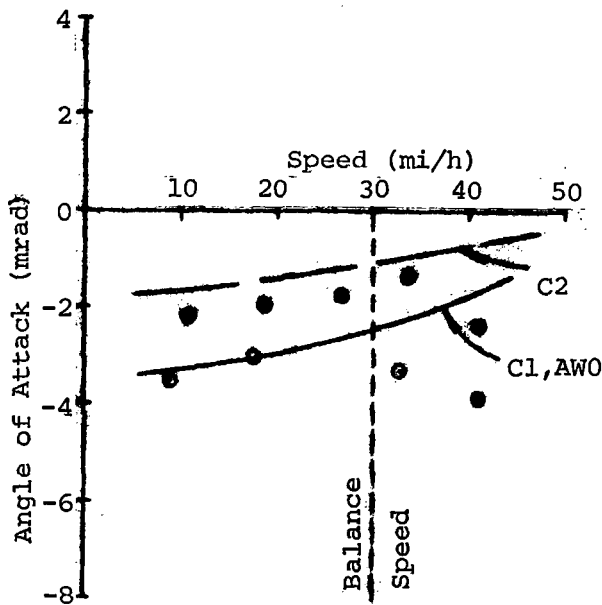
Legend: C1= Configuration C1
 C2= Configuration C2
 C3= Configuration C3
 AW0, AW3 = Vehicle Weights

Symbols = Test Data
 Lines = Computer Predictions

FIGURE 10-17. LEAD AXLE ANGLE OF ATTACK VS. SPEED (BALLOON LOOP 7.4° CURVE).



LEFT-HAND CURVE



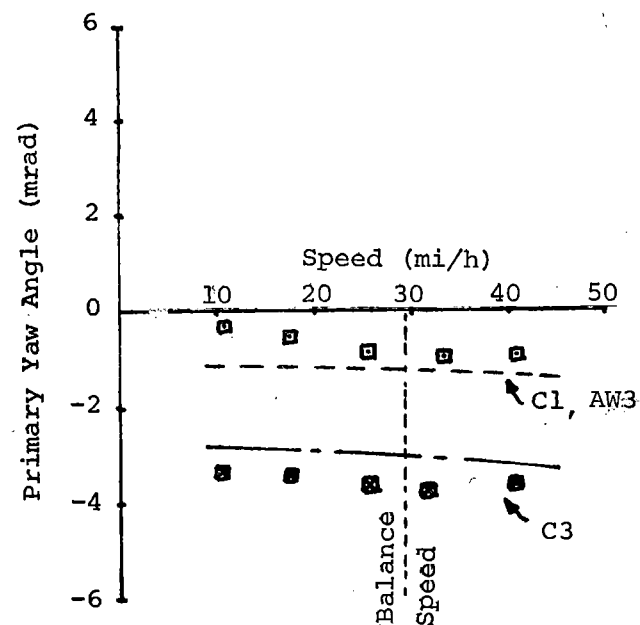
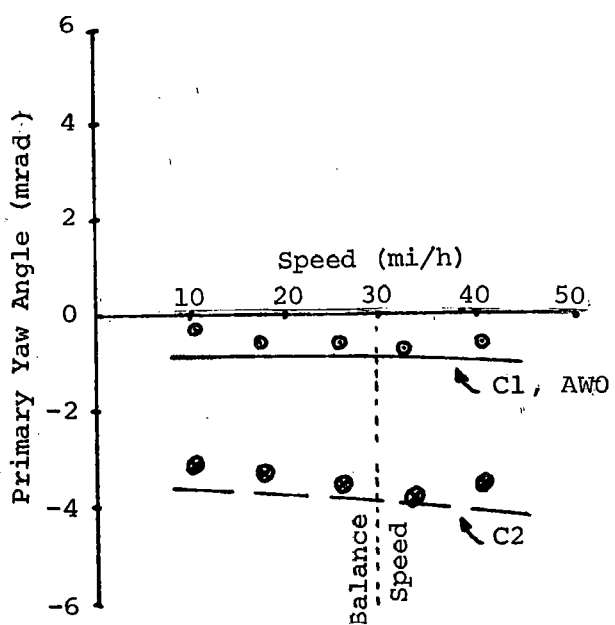
RIGHT-HAND CURVE

Legend :

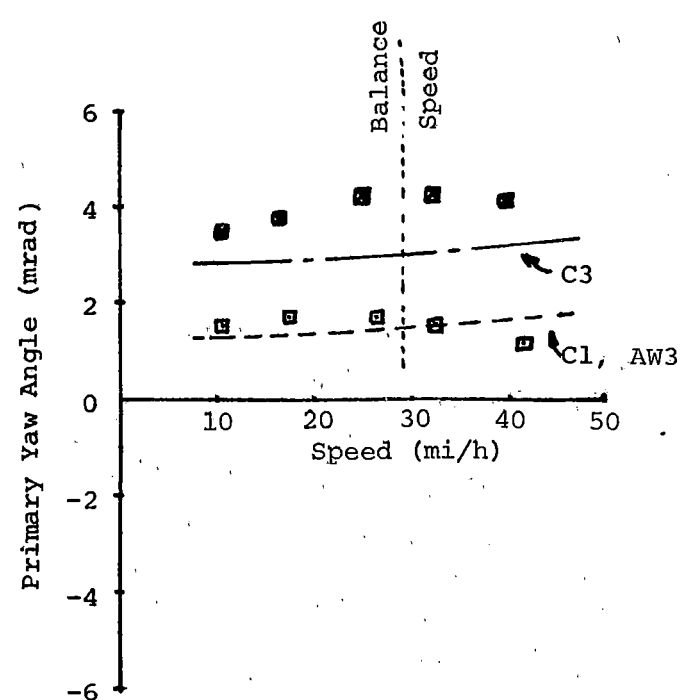
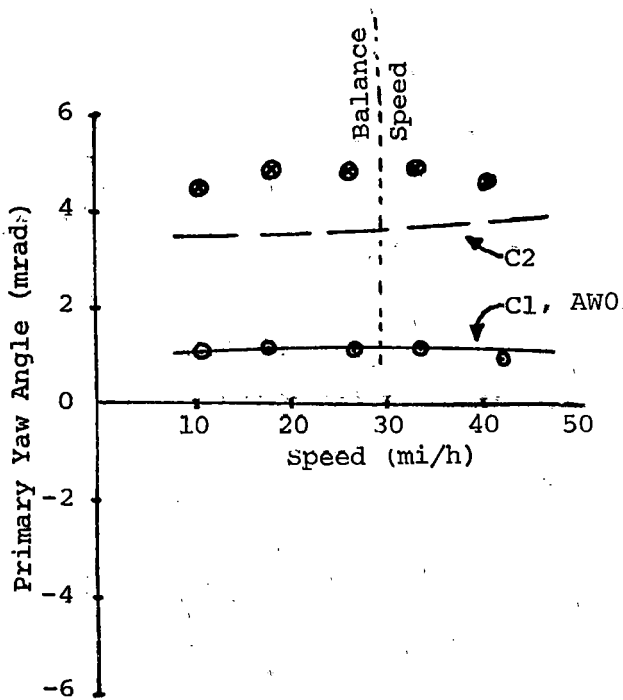
- C1 = Configuration C1
- C2 = Configuration C2
- C3 = Configuration C3
- AW0, AW3 = Vehicle Weights

- Symbols = Test Data
- Lines = Computer Predictions

FIGURE 10-18. TRUCK ANGLE OF ATTACK VS. SPEED (BALLOON LOOP, 7.4° CURVE).



LEFT-HAND CURVE



RIGHT-HAND CURVE

Legend: C1 = Configuration C1 Symbols = Test Data
 C2 = Configuration C2 Lines = Computer Predictions
 C3 = Configuration C3
 AW0, AW3 = Vehicle Weights

FIGURE 10-19. LEADING AXLE PRIMARY YAW DISPLACEMENT (BALLOON LOOP, 7.4° CURVE).

are shown in figure 10-20. It can be seen that the suspension yaw angles for lead and trail axles are approximately constant with speed, which implies that the longitudinal steering forces being generated between wheel and rail are approximately constant with speed.

The curving diagrams in figures 10-21 and 10-22 show the behavior of the truck for the four test cases, in right-hand and left-hand curving situations around the Balloon Loop. These diagrams are drawn with vehicle dimensions reduced 50 times, curve radius reduced 2,500 times, and flangeway clearance full size, so that yaw rotations are multiplied by 50 and become clearly visible. This method of illustrating the curving behavior is very useful for showing at a glance the attitudes adopted by the various test configurations when running at the balance speed for the curve. It can be seen that the trailing axle almost invariably runs in a radial position. The leading axle usually has a significant angle of attack, with the outside wheel in flange contact with the gage face of the high rail. As a result, it is the leading axle that is responsible for the vast majority of the wear that takes place on the gage face of the high rail, the crown of the low rail, and the flange of the wheel.

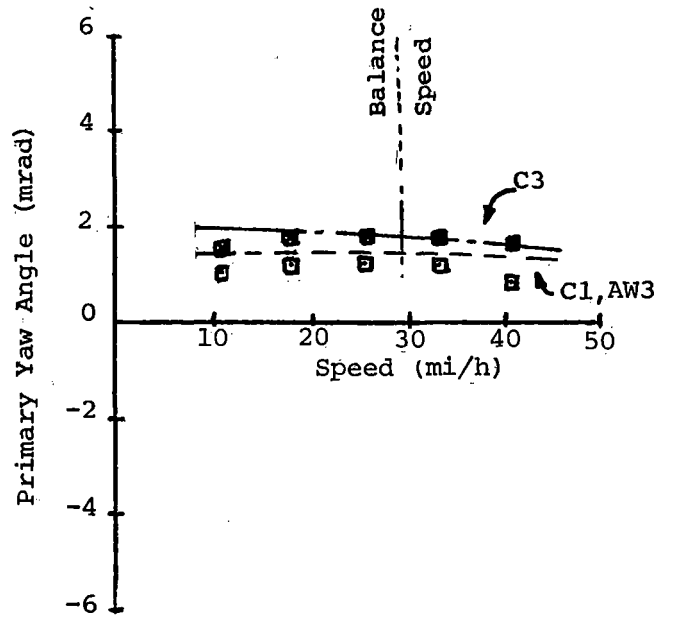
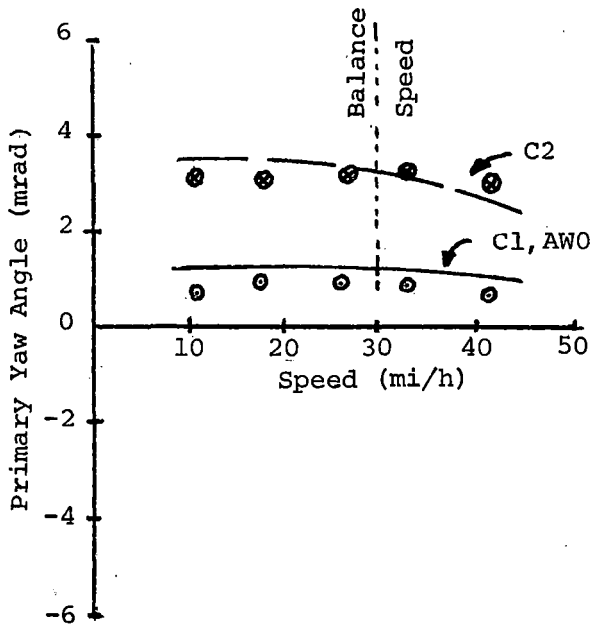
These diagrams show quite clearly the reduced angle of attack of the truck frame and the leading axle, due to the reduction in primary longitudinal stiffness. Also shown, when comparing the left-hand and right-hand curve situation, is the significantly worse behavior on left-hand curves, due to the axle misalignments.

The next test site to be considered is section 07 on FAST. Figure 10-23 illustrates typical rail cross-sectional profiles for this 5.2° curve. Quite substantial gage face wear is evident on the high rail. The low rail appears to have a most peculiar wear pattern when compared with its new shape, but this is due to the fact that these rails have been transposed and ground. The results (figure 10-24) presented come from the strain gaged high rails and show the lateral force on the high rail due to the leading axle of the test truck.

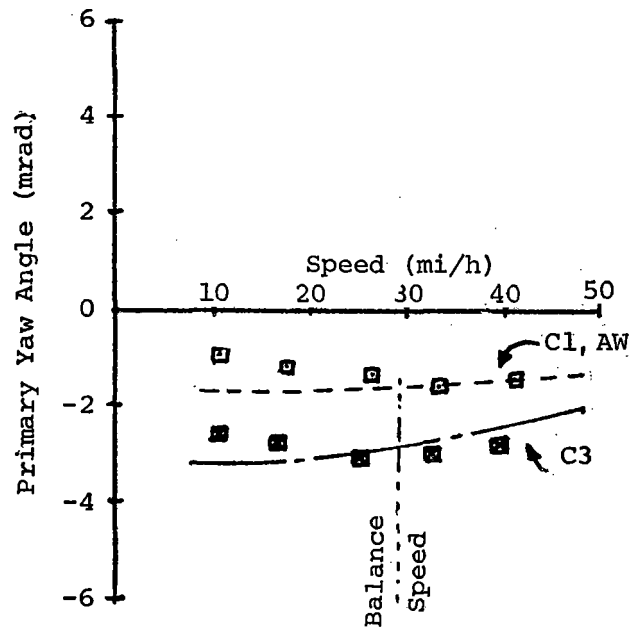
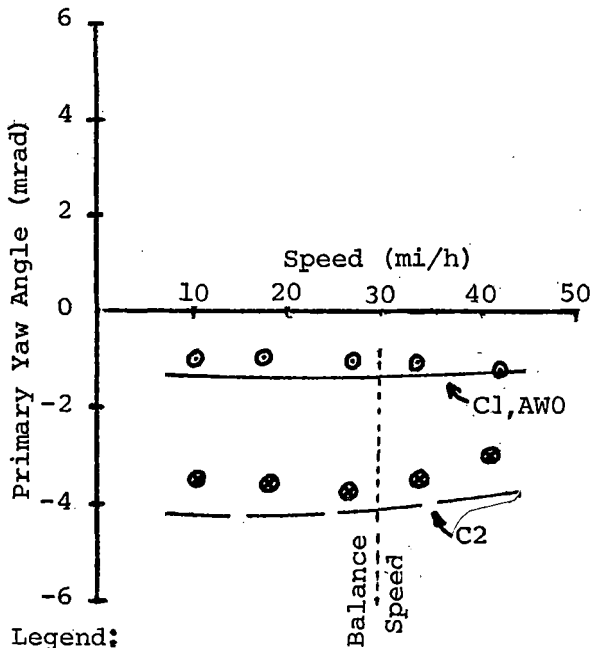
The values of lateral force were obtained in the following manner. The maximum output for each lateral force bridge, due to the passage of an axle, was measured. The values for the axles passing each of the four measurement locations were then averaged to obtain the values presented in figure 10-24. Only values for the leading axle are shown, as they were always much larger than the values for the trailing axle.

Again, the format is the same as for the previous test results, with the points representing the test results and the lines the theoretical predictions. A lateral force reduction of approximately one-third is obtained as a result of the reduction in longitudinal stiffness. The CN-A profile appears to give slightly lower forces than the AAR 1:20. The change from AW0 to AW3 weight with the standard suspension (C1) increased lateral forces by approximately 1,000 lb throughout the speed range.

The third set of results is from the 1.5° north curve on the TTT and is shown in figures 10-25, 10-26, and 10-27. Apart from showing qualitative agreement between the test results and the theoretical predictions, these results indicate the small magnitude of all the test results on a 1.5° curve, as compared with the 5.2° and 7.4° curves.



LEFT-HAND CURVE



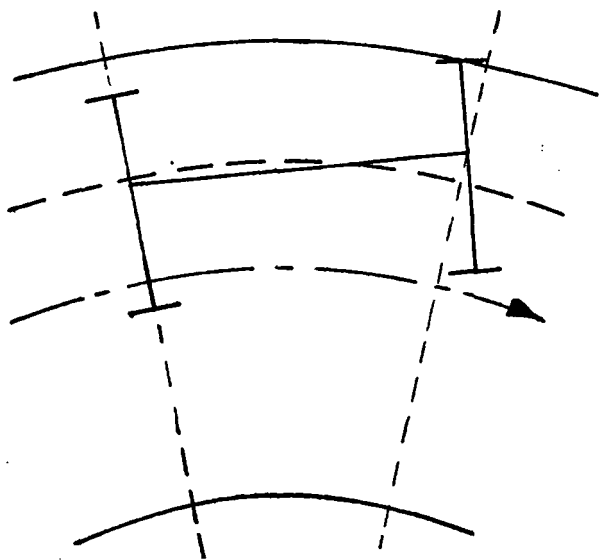
RIGHT-HAND CURVE

Legend:

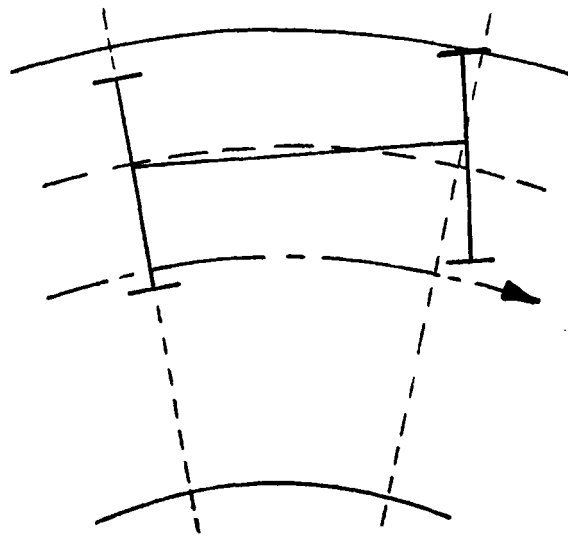
- C1 = Configuration C1
- C2 = Configuration C2
- C3 = Configuration C3
- AW0, AW3 = Vehicle Weights

- Symbols = Test Data
- Lines = Computer Predictions

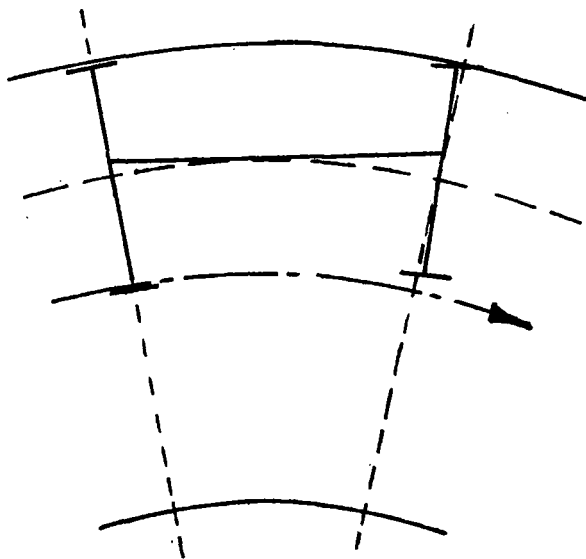
FIGURE 10-20. TRAILING AXLE PRIMARY YAW DISPLACEMENT (BALLOON LOOP, 7.4° CURVE).



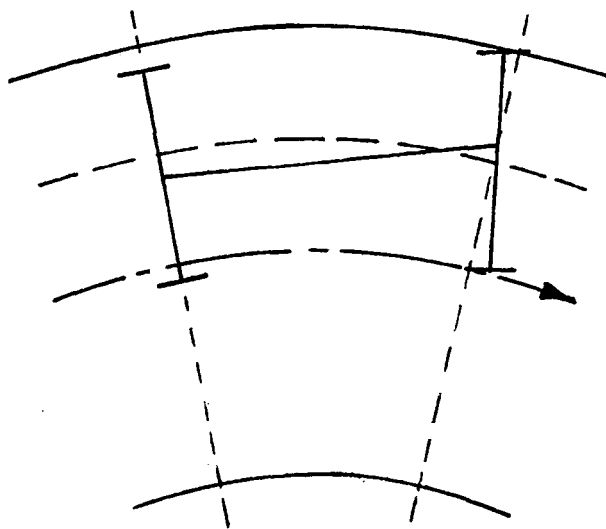
Configuration C1, AW0



Configuration C1, AW3

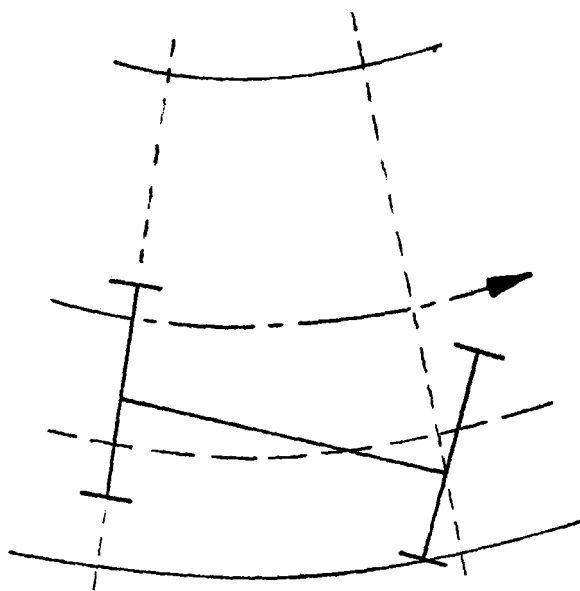


Configuration C2, AW0

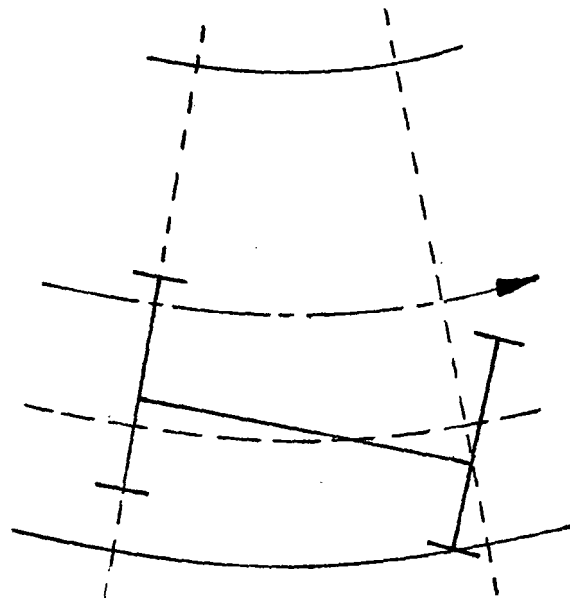


Configuration C3, AW0

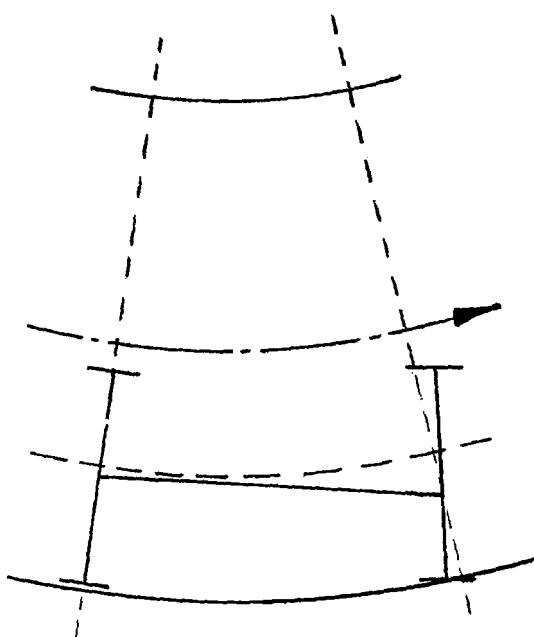
FIGURE 10-21. TRUCK CURVING DIAGRAMS (BALLOON LOOP, 7.4° CURVE, RIGHT HAND).



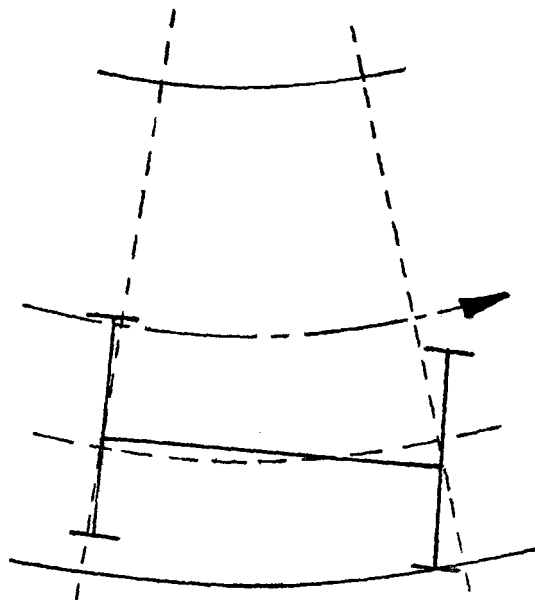
Configuration C1, AW0



Configuration C1, AW3

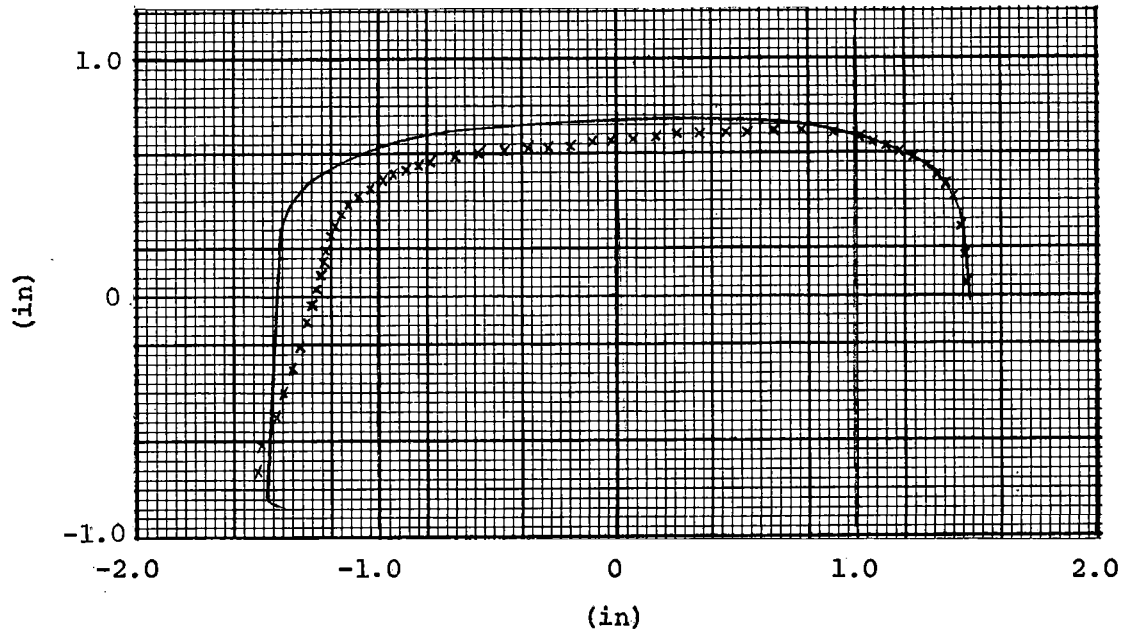


Configuration C2, AW0



Configuration C3, AW0

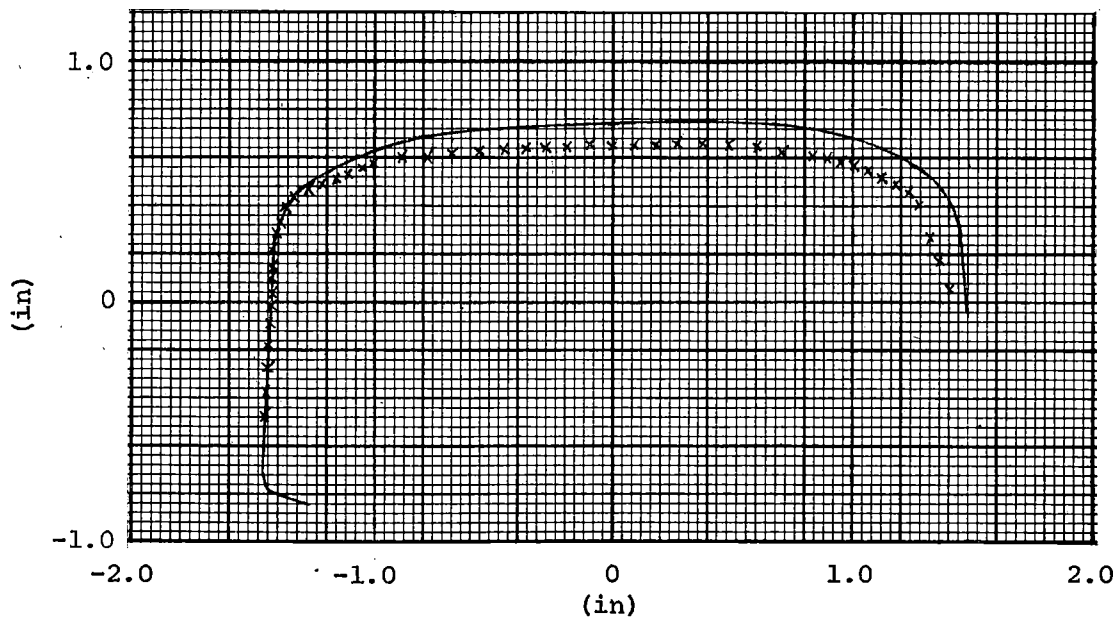
FIGURE 10-22. TRUCK CURVING DIAGRAMS (BALLOON LOOP, 7.4° CURVE, LEFT HAND).



High Rail

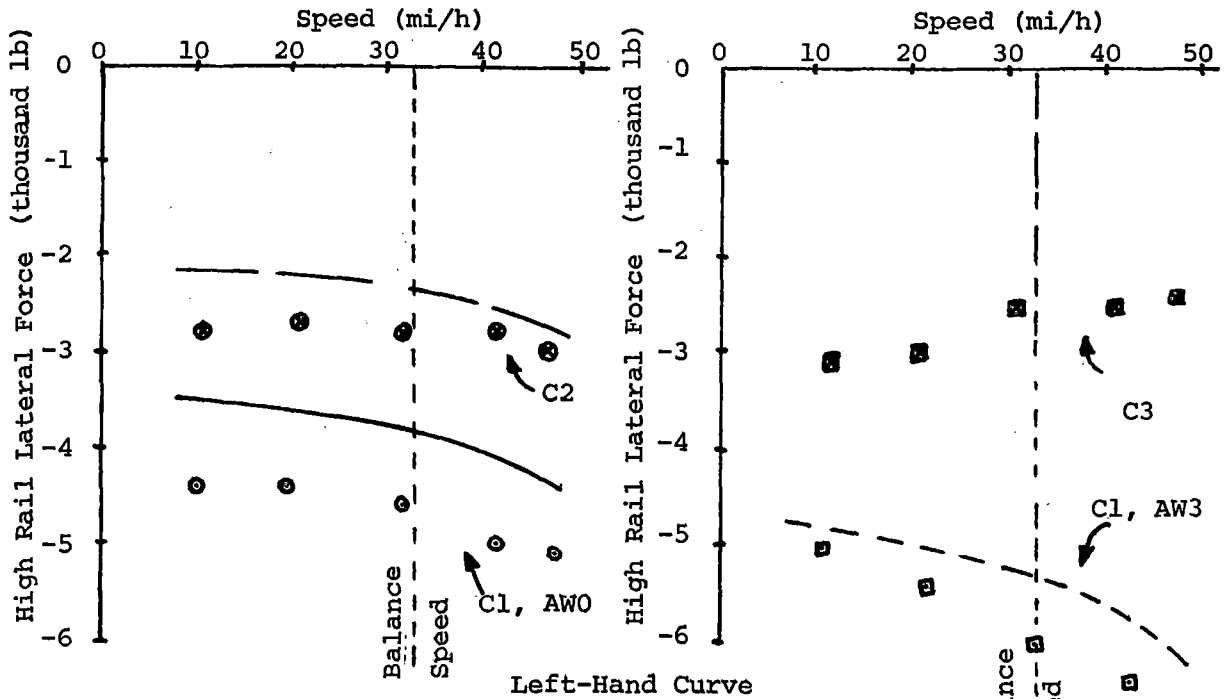
x x x FAST Section 07

_____ Design case profile.



Low Rail

FIGURE 10-23. TYPICAL RAIL PROFILES FOR FAST SECTION 07 COMPARED WITH DESIGN CASE 140 lb/yd RAIL.



Legend

- C1 = Configuration C1 Symbols = Test Data
- C2 = Configuration C2 Lines = Computer Predictions
- C3 = Configuration C2
- AW0, AW3 = Vehicle Weights

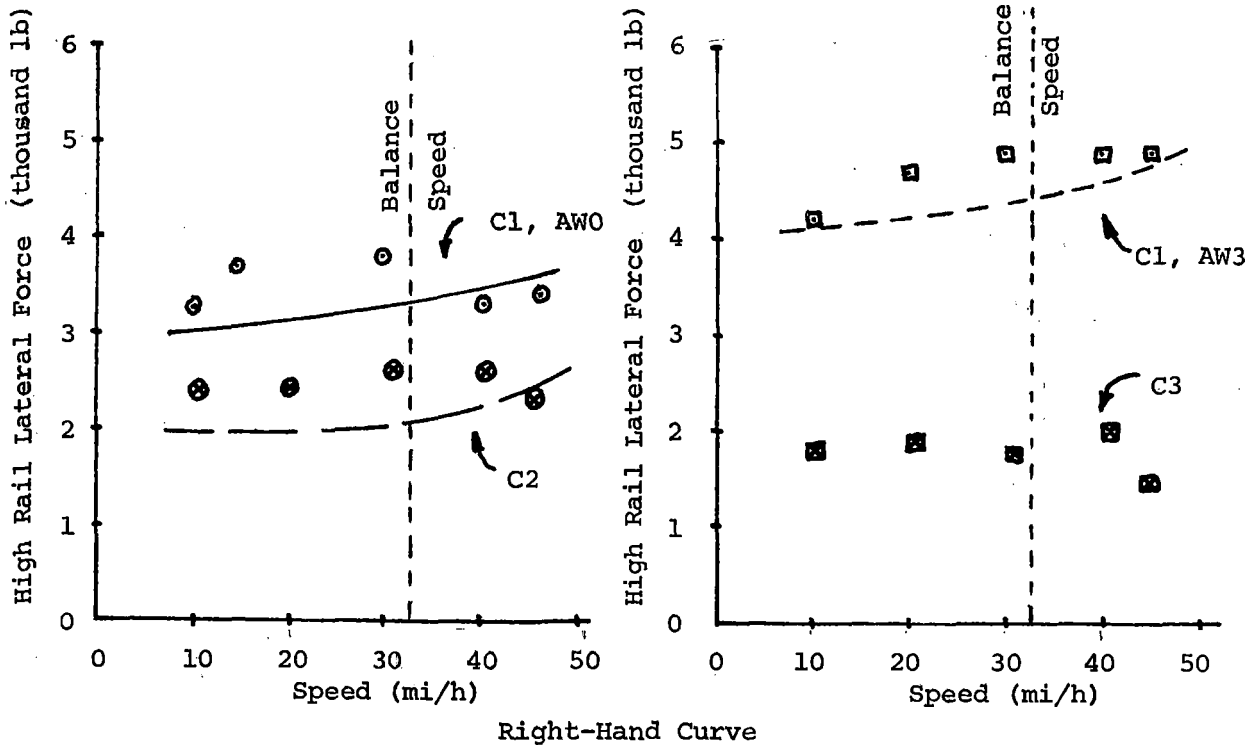


FIGURE 10-24. LEADING AXLE HIGH RAIL LATERAL FORCE VS. SPEED (FAST SECTION 07, 5.2° CURVE).

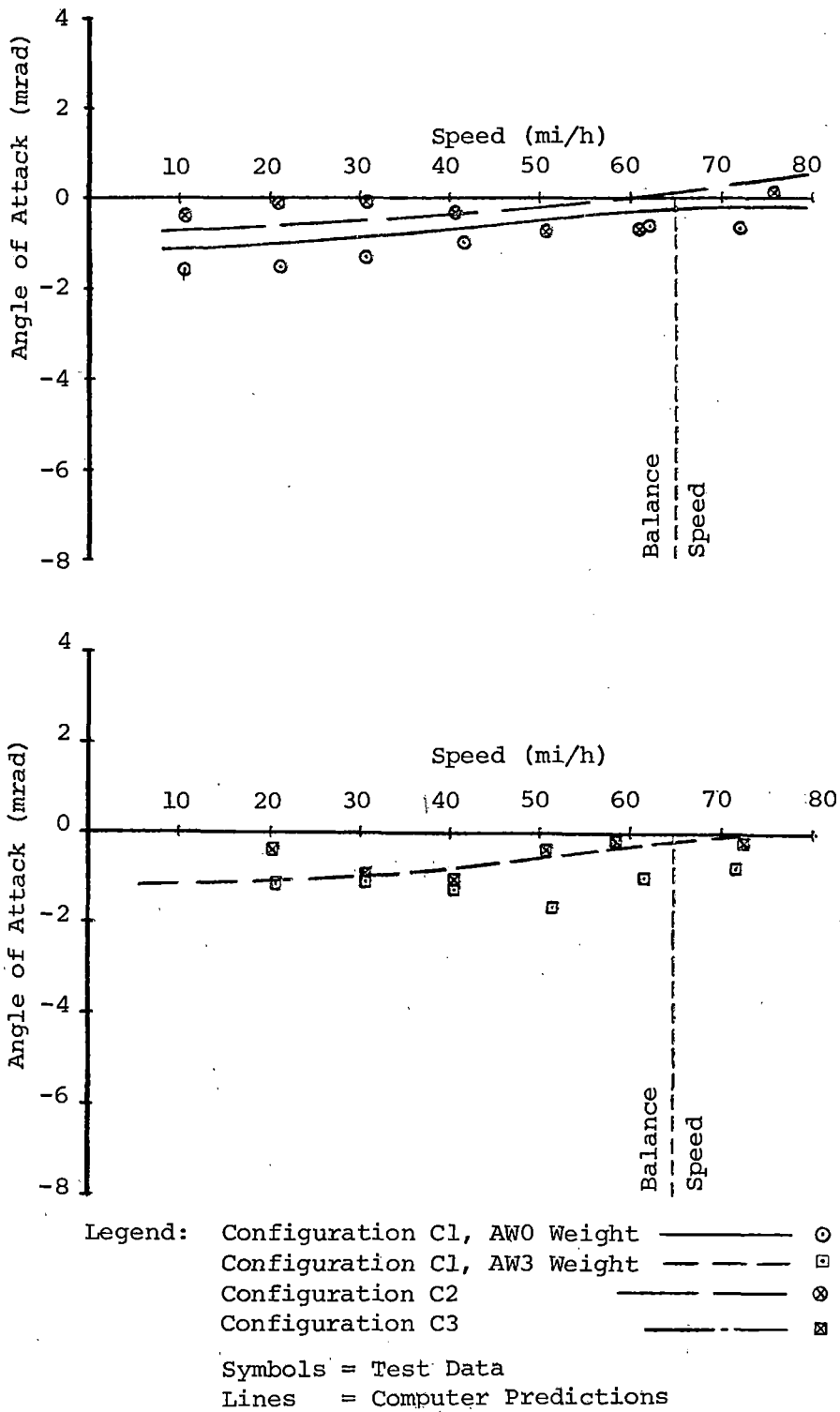
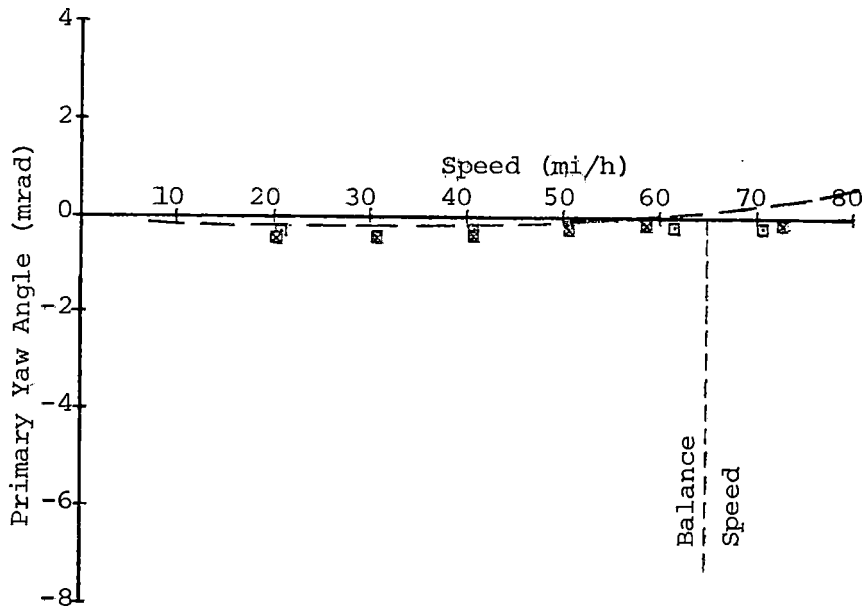
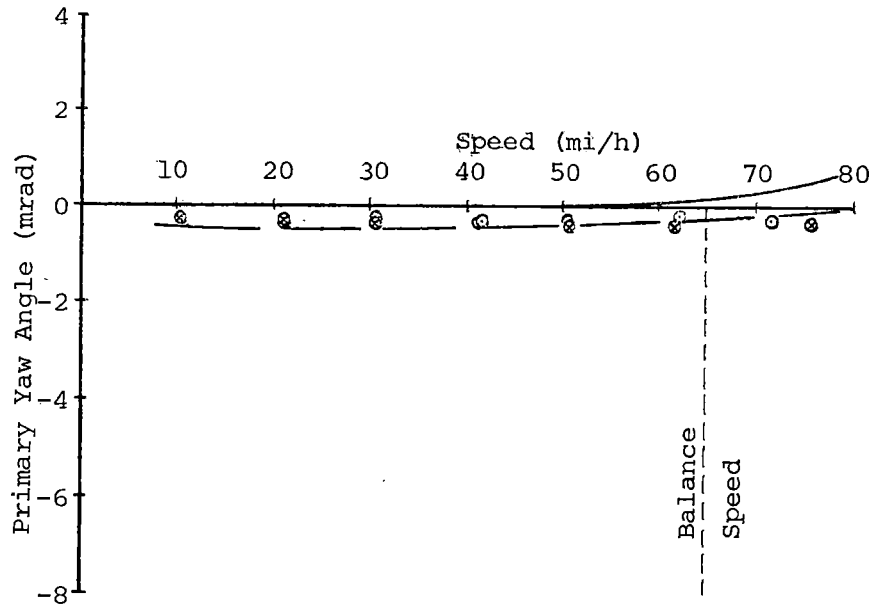


FIGURE 10-25. LEADING AXLE ANGLE OF ATTACK VS. SPEED (TTT, 1.5° RIGHT-HAND CURVE).



Legend: Configuration C1, AW0 Weight ——— ○
 Configuration C1, AW3 Weight - - - - □
 Configuration C2 ——— ⊗
 Configuration C3 ——— ⊠
 Symbols = Test Data
 Lines = Computer Predictions

FIGURE 10-27. TRAILING AXLE PRIMARY YAW DISPLACEMENT VS. SPEED (TTT, 1.5° RIGHT-HAND CURVE).

As well as showing the various effects described in the preceding text, the test results are generally in reasonable agreement with the theoretical results. This fact, in addition to the good agreement obtained with previous test results using instrumented wheelsets, gives confidence in the use of the mathematical model for making predictions of the effects of various truck parameter changes on the truck curving performance.

The following results are theoretical predictions for a perfectly aligned truck at AWO weight running at the balance speed for the curve:

- Figure 10-28 shows angle of attack of the leading axle as a function of track curvature, for primary longitudinal stiffness of 150,000 and 50,000 lb/in, and for wheel/rail friction coefficients of 0.4 and 0.6.
- Figure 10-29 shows the high rail lateral force due to the leading axle, again for primary longitudinal stiffness of 150,000 and 50,000 lb/in, and wheel/rail friction coefficients of 0.4 and 0.6.

These theoretical results summarize the effect on angle of attack and high rail lateral force of the reduction in primary longitudinal stiffness that was made in going from configuration C1 to C2. The results are shown for wheel/rail friction coefficients of 0.4, which is probably typical of values that would be found on sharp curves in Atlanta, and 0.6, which is typical of the values found during testing at the TTC.

10.5 WEAR INDEX PREDICTIONS

The wear index predictions which follow are based on the premise that rates of wheel and rail wear can be related in some way to the force and creepage which take place between the wheels and rails. Previous work carried out in this country has suggested that rates of rail gage face wear and wheel flange wear are proportional to the flange force multiplied by the angle of attack. However, this hypothesis seems to completely ignore the effects of longitudinal force and creepage.

Work is currently in progress at a number of places to relate the wear of wheels and rails to some form of wear index. Some early results have already been obtained from a series of small scale laboratory wear experiments.³ Figure 10-30 is reproduced from a report of those experiments and shows the kind of relationship that seems to exist between wear rate and the rate of energy dissipated in the contact zone. The results of this study are presented in the form of a wear index which is proportional to the rate of energy dissipation in the contact patch between the wheel and rail. However, in order to relate this to actual rates of wheel and rail wear it would be necessary to have available the full-scale equivalent of figure 10-30. At the present time this information is not available, so it is not possible to make quantitative predictions of the effect on wear rate of a given parameter

³ Bolton, P. J.; Clayton, P.; and McErven, I. J., "Wear of Rail and Tyre Steels under Rolling/Sliding Conditions," presented at the ASME/ASLE Conference in San Francisco, August, 1980, to be published by ASLE.

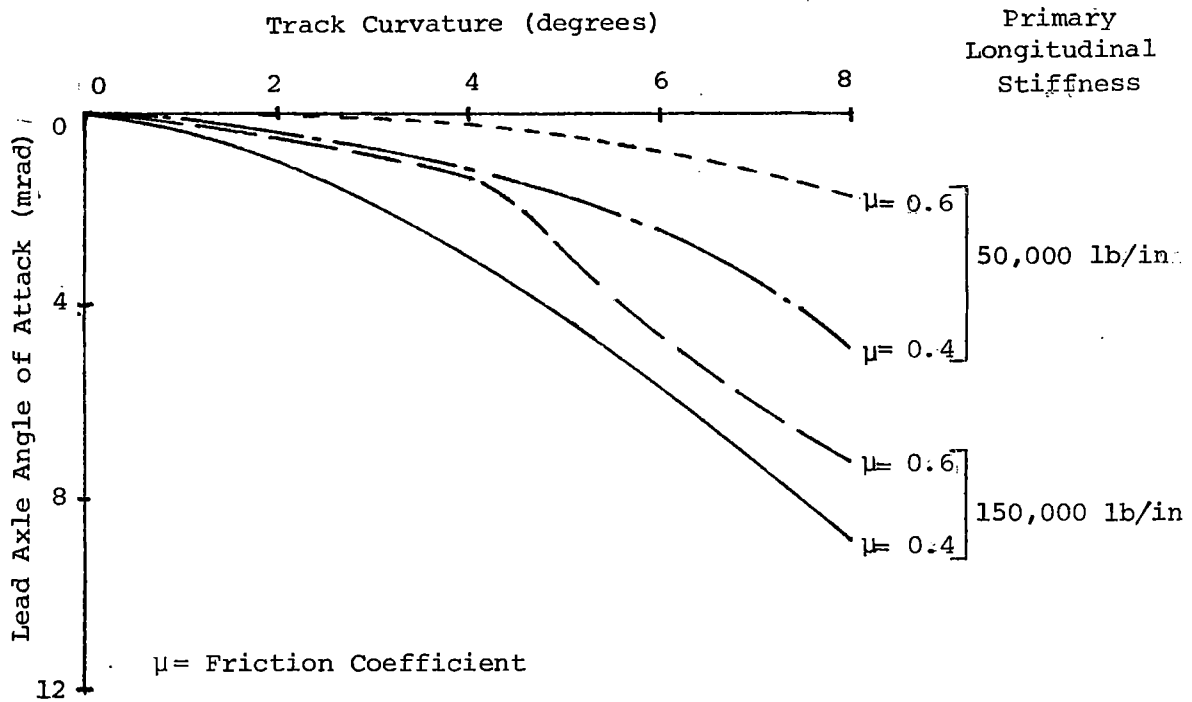


FIGURE 10-28. THEORETICAL LEAD AXLE ANGLE OF ATTACK VS. TRACK CURVATURE.

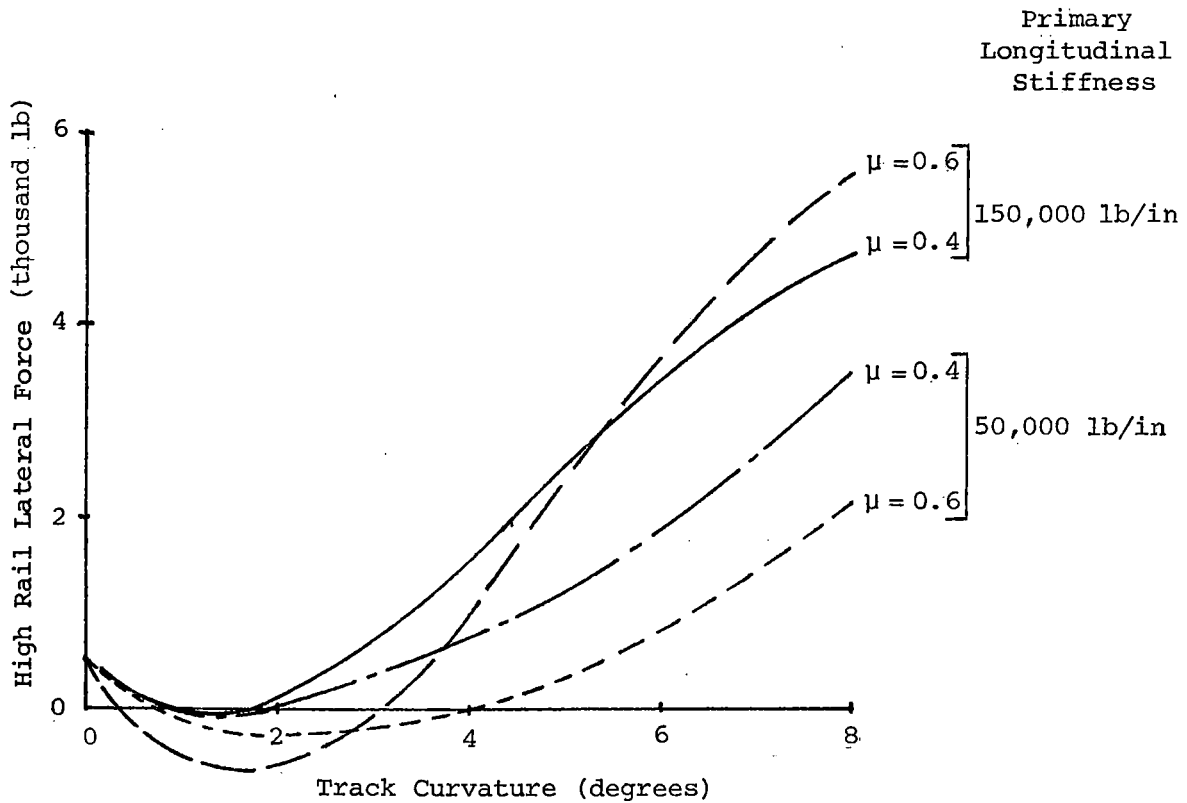


FIGURE 10-29. THEORETICAL HIGH RAIL LATERAL FORCE VS. TRACK CURVATURE.

10-40

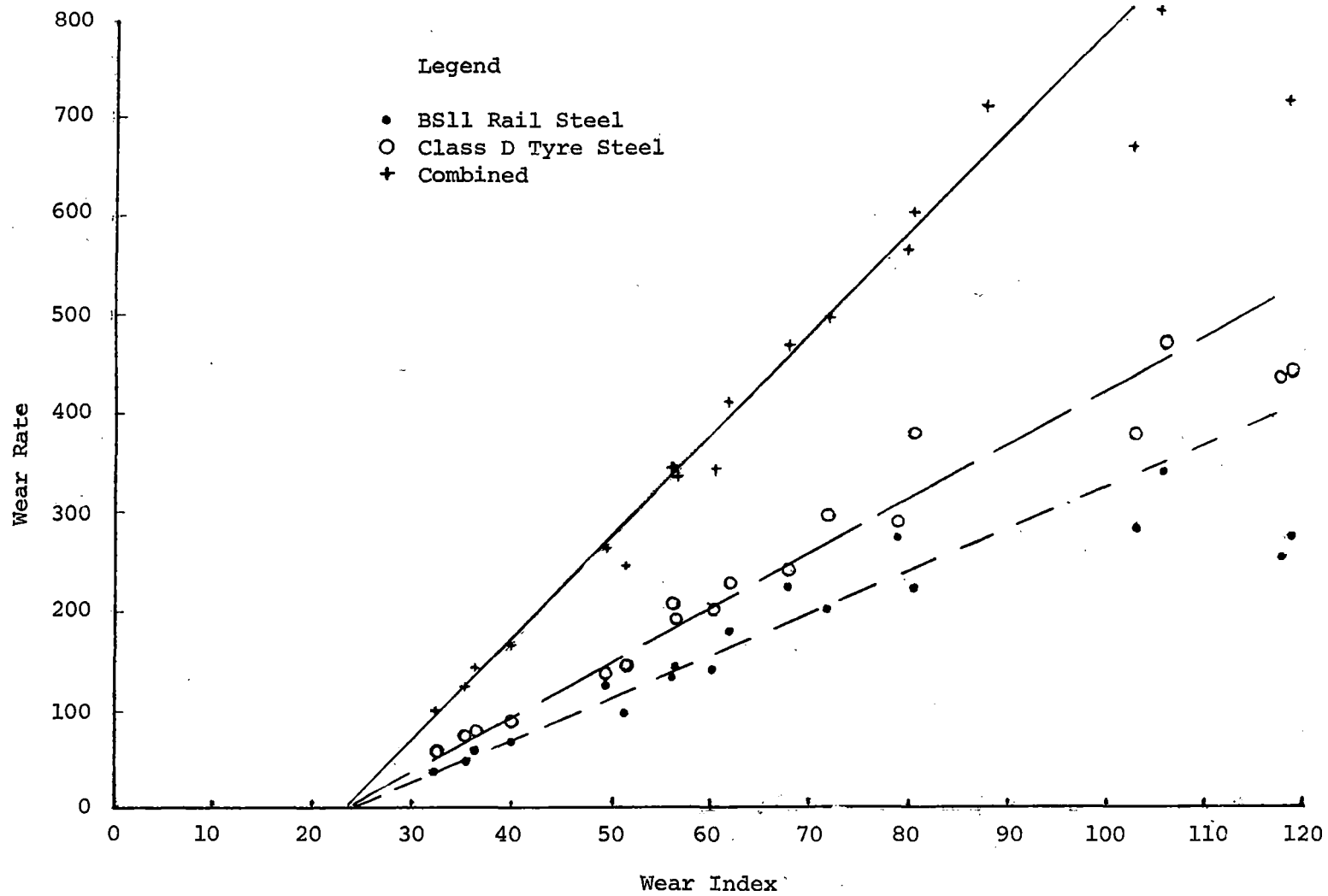


FIGURE 10-30. SAMPLE WEAR RATE VS. WEAR INDEX FROM LABORATORY EXPERIMENT.

change. However, if the shape of the full-scale relationship (wear index and wear rate) agrees with figure 10-30; i.e., no significant wear occurs until a certain threshold value is exceeded, followed by a regime wherein wear rate is proportional to wear index values which exceed the threshold, it can be said that the improvements indicated by the wear index graphs are, in all cases, conservative.

All of the results that follow are in the form of graphs of wear index against track curvature and show the theoretical effects of various truck parameter changes. In figures 10-31 and 10-32, the result of reducing the primary longitudinal stiffness is shown. Figure 10-31 is for a wheel/rail friction coefficient of 0.4, and figure 10-32 for a friction coefficient of 0.6. The reductions in wear that could be expected from a reduction in primary longitudinal stiffness from 150,000 to 50,000 lb/in are clearly shown. The effect of a further reduction to 25,000 lb/in is also shown.

All of the results that follow are for the standard suspension with AAR 1:20 wheel profiles and a wheel/rail friction coefficient of 0.4, unless otherwise stated. Figures 10-33 and 10-34 show the predicted effect of the two components of axle misalignment. Figure 10-33 illustrates the very significant effect of the radial misalignment, whereas figure 10-34 shows the almost insignificant effect of the lateral misalignment component. It should be noted that the difference in diagonal dimensions between axle box centers is a measure only of the lateral component of misalignment, and no measure at all of the radial component. It is, therefore, of dubious value as a measure of the detrimental effects of misalignment.

The radial misalignment is almost certainly the cause of the severe asymmetric wear occurring on a small number of the trucks in Atlanta. The test truck, which is known to be one of the trucks experiencing high rates of asymmetric wear, was found to have much larger radial misalignment than the other trucks on the two MARTA vehicles sent to the TTC, see table 10-4.

TABLE 10-4. TRUCK RADIAL AND LATERAL MISALIGNMENT.

Truck	Misalignment	
	Radial (mrad)	Lateral (in)
109A	- 0.06	- 0.111
109B	0.17	0.015
110A	0.70	- 0.028
110B	- 0.15	0.011

Consider now the case where the primary suspension bush longitudinal stiffness has been reduced to 50,000 lb/in and the same range of radial and lateral misalignments exists. Figures 10-35 and 10-36 show again that the lateral component is not important, but that radial misalignments, although causing less wear than with the stiff bushing, still have a degrading effect.

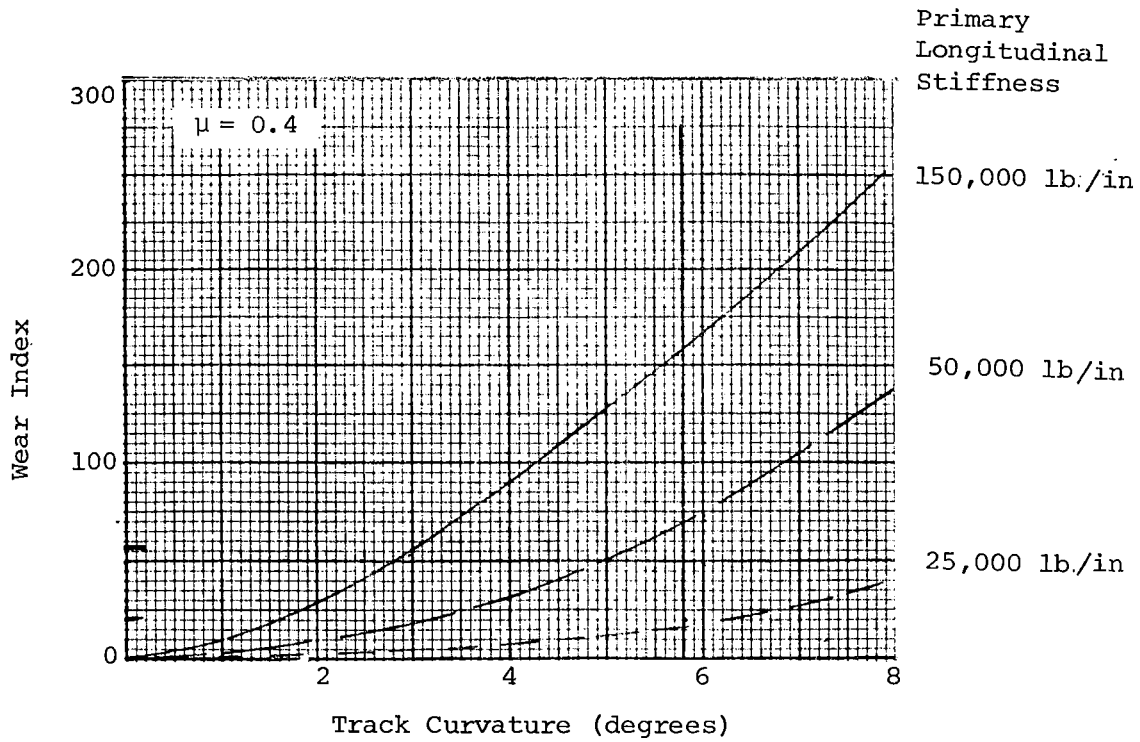


FIGURE 10-31. PREDICTED EFFECT OF PRIMARY LONGITUDINAL STIFFNESS ON WEAR INDEX

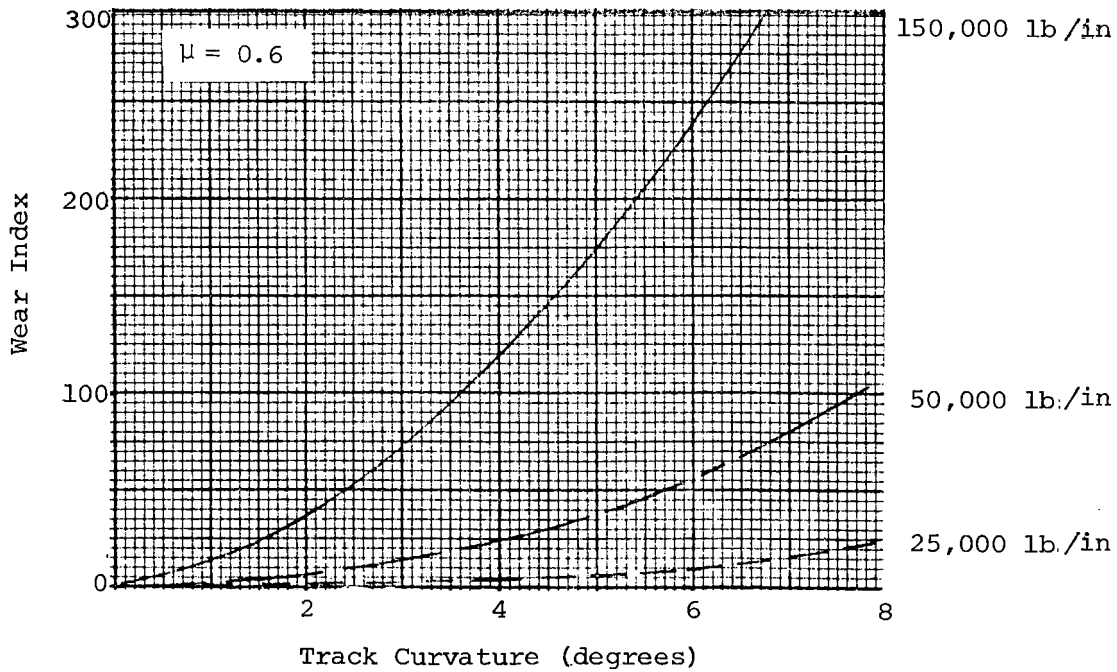


FIGURE 10-32. PREDICTED EFFECT OF PRIMARY LONGITUDINAL STIFFNESS ON WEAR INDEX

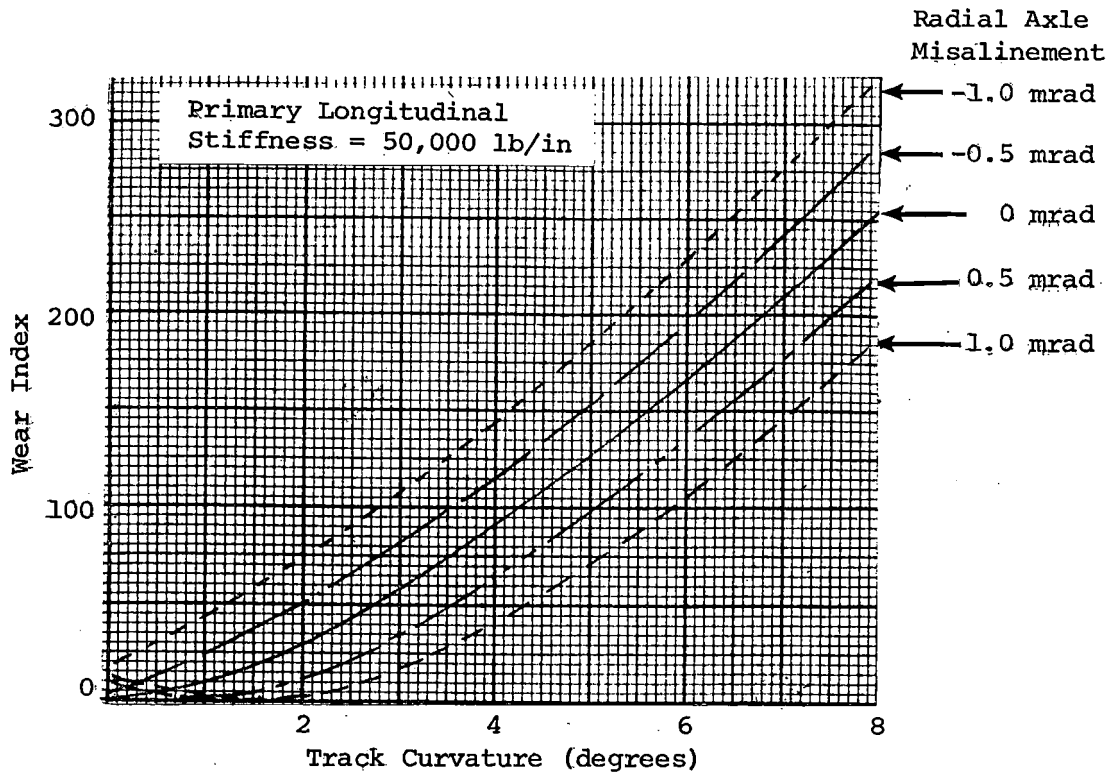


FIGURE 10-33. PREDICTED EFFECT OF RADIAL AXLE MISALIGNMENT ON WEAR INDEX,

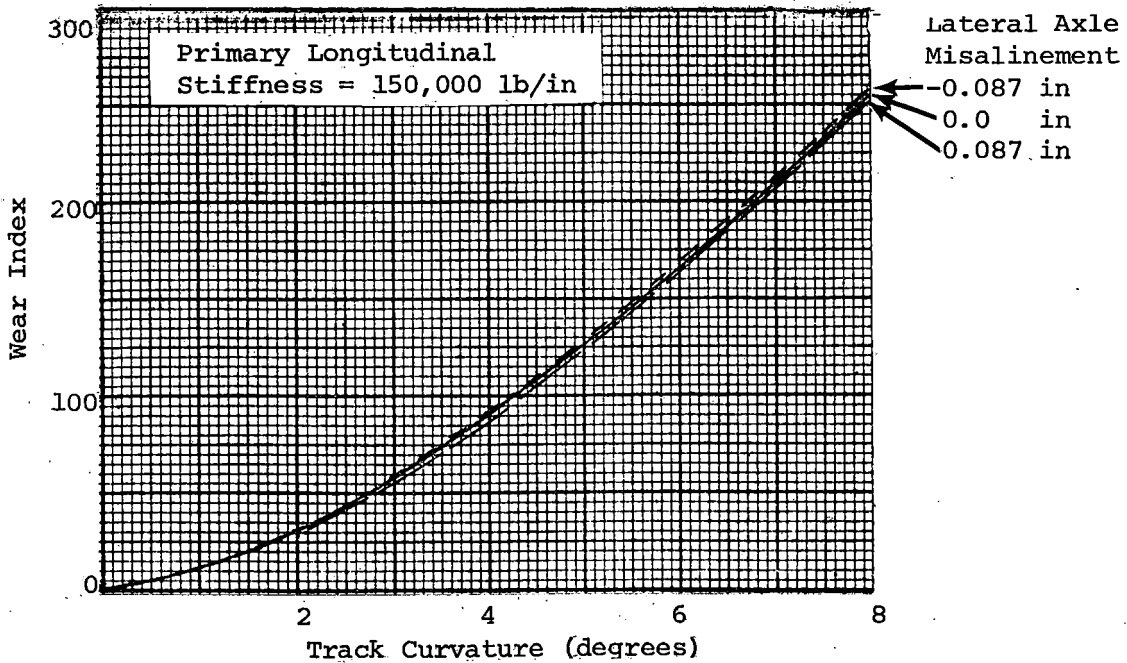


FIGURE 10-34. PREDICTED EFFECT OF LATERAL AXLE MISALIGNMENT ON WEAR INDEX.

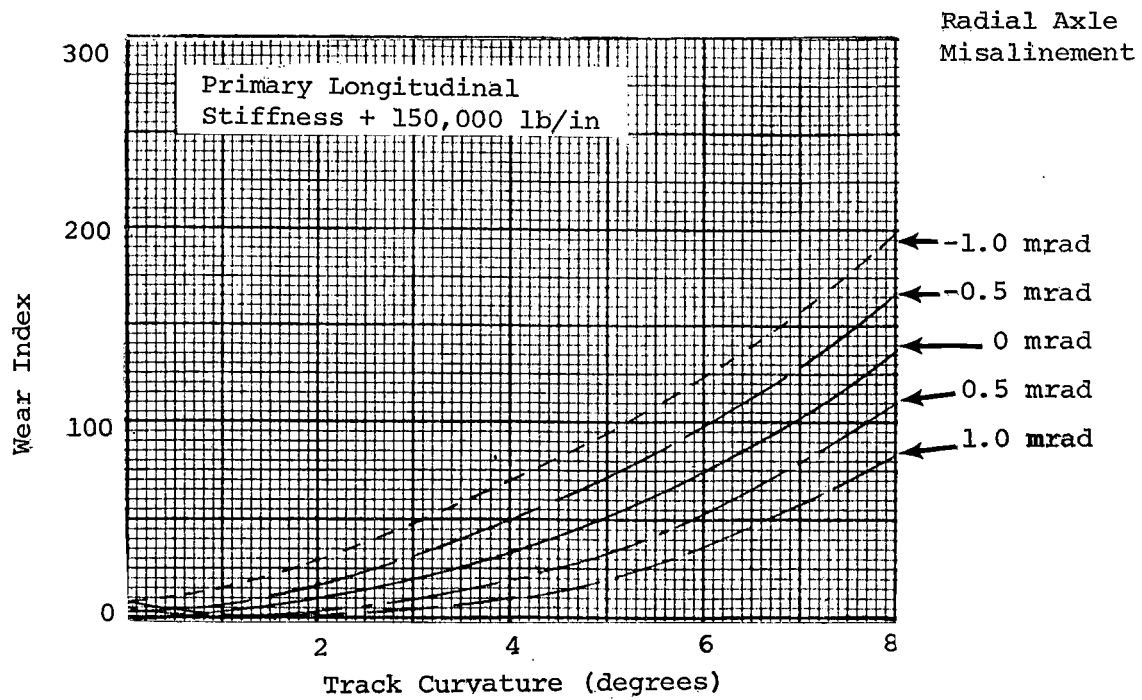


FIGURE 10-35. PREDICTED EFFECT OF RADIAL AXLE MISALIGNMENT ON WEAR INDEX.

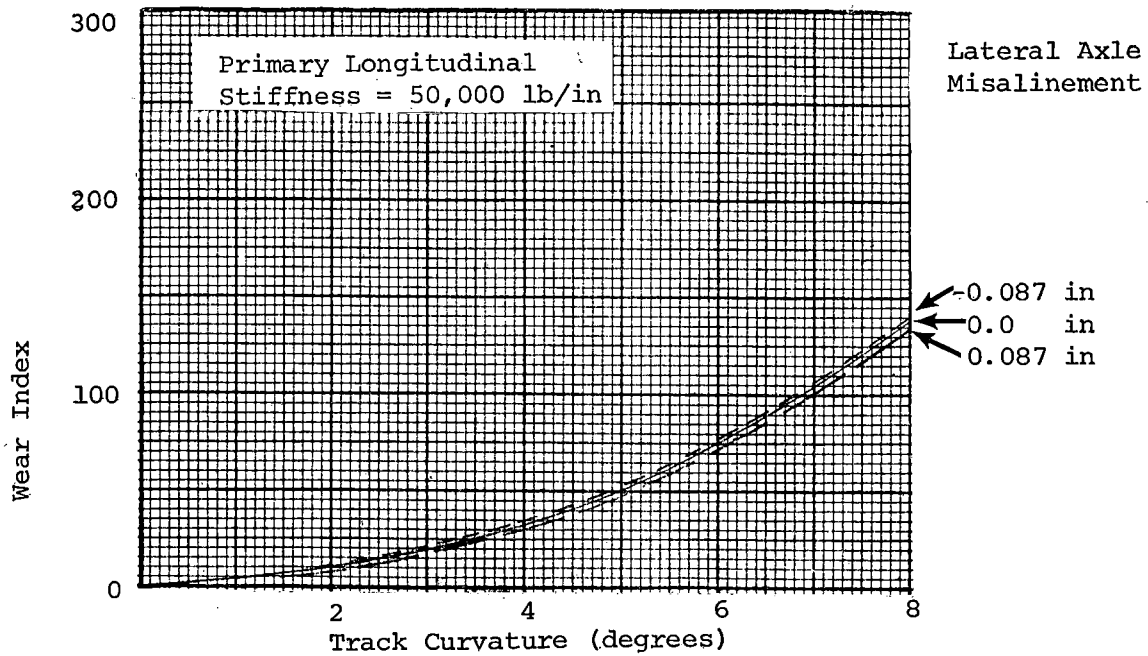


FIGURE 10-36. PREDICTED EFFECT OF LATERAL AXLE MISALIGNMENTS ON WEAR INDEX.

Figures 10-37 and 10-38 show what happens when the vehicle weight is changed from AW0 to AW3. For the stiff bush (figure 10-37), the increased axleload is slightly detrimental, whereas for the softened bush (figure 10-38), the increased axleload is slightly beneficial.

In figure 10-39 the theoretical result of changing from AAR 1:20 to CN-A wheel profiles is seen. Despite the results from the Balloon Loop, which seemed to show that the CN-A was significantly worse, although there were certain mitigating factors, we now see that in fact the CN-A is marginally better.

Figure 10-40 shows the predicted effect of the yaw pivot friction, which acts between the truck frame and the carbody as a result of the friction side bearers. It should be noted that these results are for the case where the maximum pivot friction torque is applied. In practice, due to dynamic motion of the truck during its passage through a curve, the level of pivot torque will reduce considerably from this value. For a particular truck being tested, the mean pivot torque in a curve is reduced to approximately one-third of its maximum static value.⁴ When this is taken into account, it can be seen that the effect of yaw pivot friction torque on wear index is relatively small.

The curving test program was performed without traction or braking torques being applied to the axles of the truck. Figures 10-41 and 10-42 show for the stiff and soft bush, respectively, the theoretical result of applying traction and braking torques of a magnitude sufficient to cause acceleration or retardation rates on level track of 3 mi/h/s, which is the maximum service rate. It can be seen that propulsive torque caused more wear than for the coasting case, and braking torque caused less.

The 5.8° curve just outside of Georgia State Station is on a 3% gradient, such that vehicles accelerate under traction up the gradient away from the station, and are under braking down the gradient into the station. Examination of the rails indicates that the gage face wear on the high rail, on the line out of the station, is greater than that on the line into the station. This seems to substantiate the trend shown in figure 10-41.

The final graph (figure 10-43) shows the predicted effect of speed around the curve. This seems to be a relatively minor effect, with increasing speed apparently causing slightly less wear. This result is probably due to the reduction in angle of attack that occurs with increasing speed, which was illustrated in figure 10-40 for the Balloon Loop tests.

It must be made clear that the results of this study are based on a theoretical wear index. For reasons that are stated in section 10.5, it is not possible at this time to use the theoretical wear index as an absolute quantitative measure of wheel or rail wear rate. In order to do so would require full-scale experimental data relating wear rate to wear index. However, it is estimated that the threshold value of wear index, above which significant wear would occur, lies in the range equivalent to 1.5° to 3° of

⁴ Pollard, M. G., "The Development of Cross-Braced Freight Bogies," Rail International, September, 1979, pp. 735, 758.

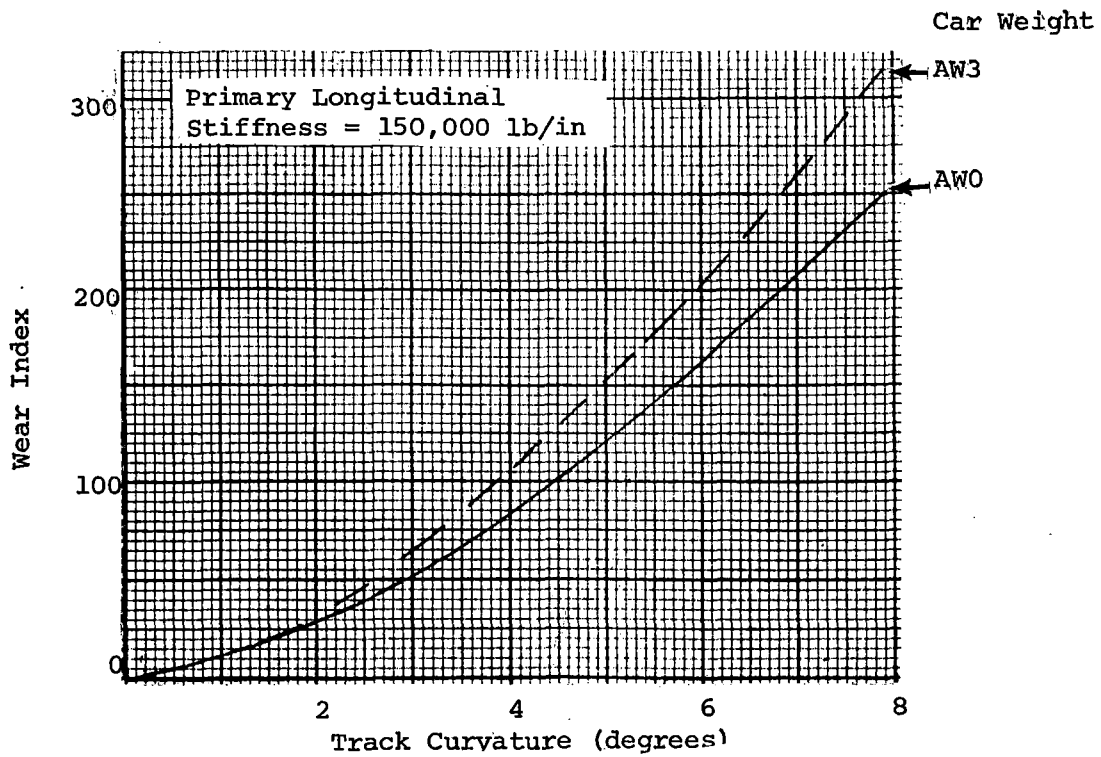


FIGURE 10-37. PREDICTED EFFECT OF CARBODY WEIGHT ON WEAR INDEX.

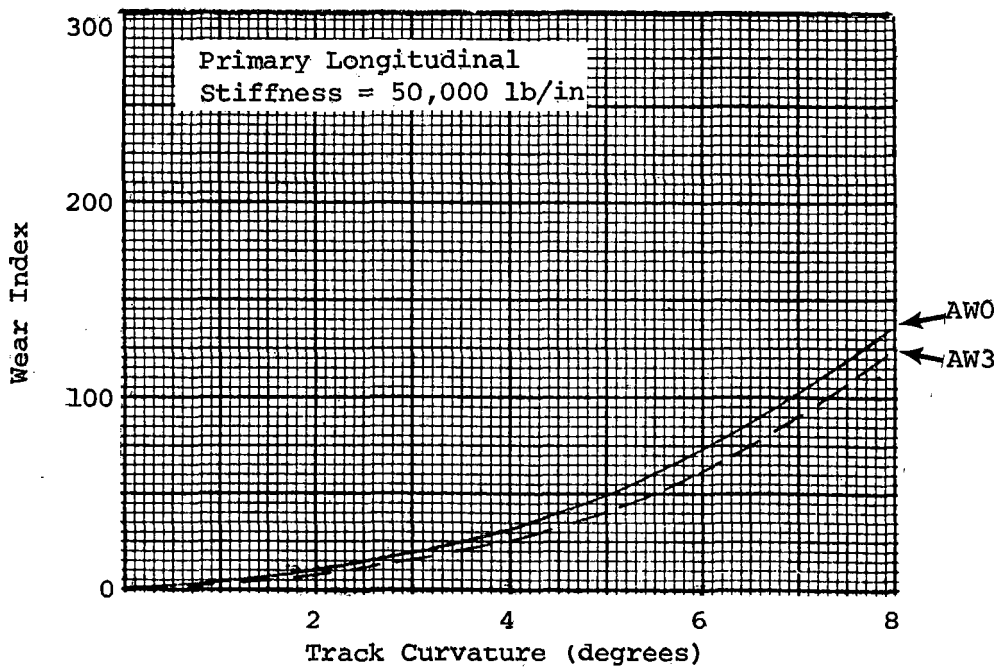


FIGURE 10-38. PREDICTED EFFECT OF CARBODY WEIGHT ON WEAR INDEX.

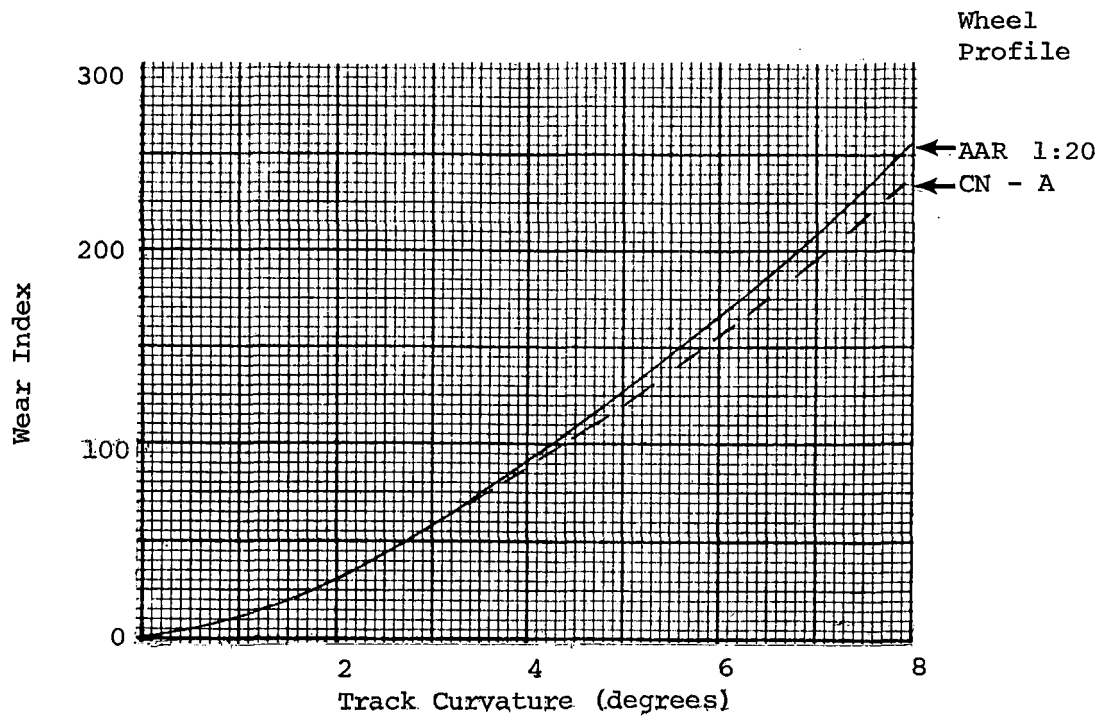


FIGURE 10-39. PREDICTED EFFECT OF WHEEL CROSS-SECTIONAL PROFILE ON WEAR INDEX.

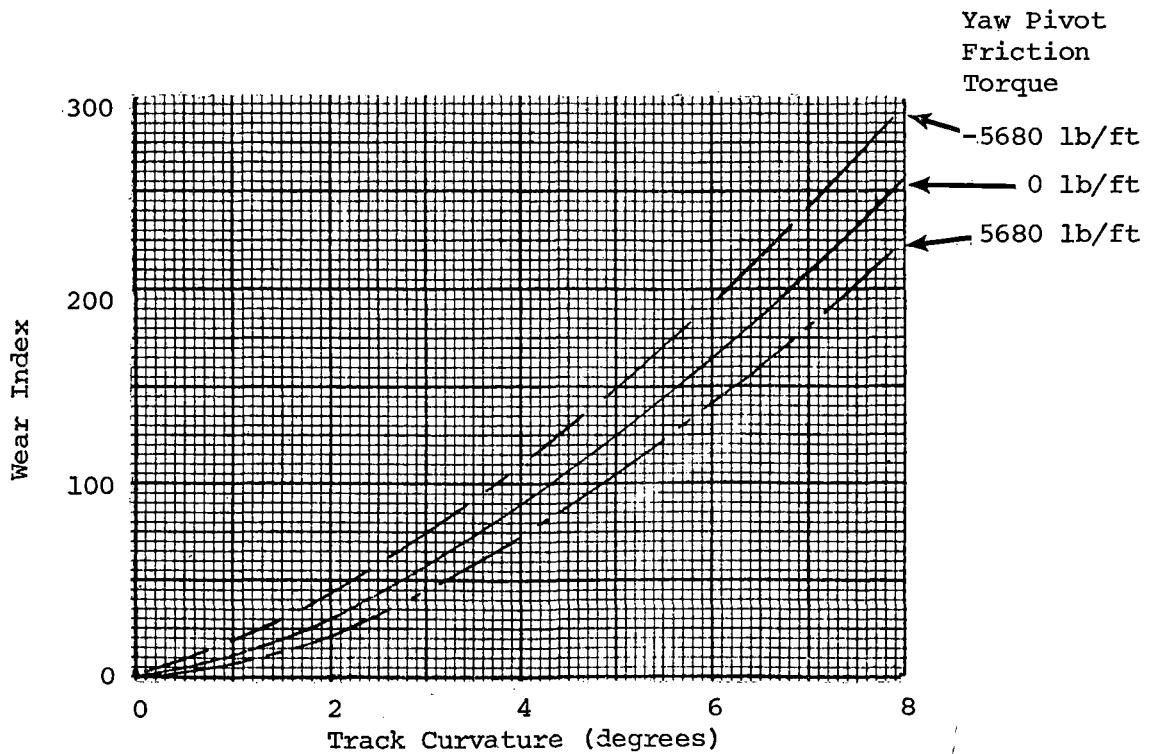


FIGURE 10-40. EFFECT OF TRUCK CARBODY YAW PIVOT FRICTION TORQUE ON WEAR INDEX.

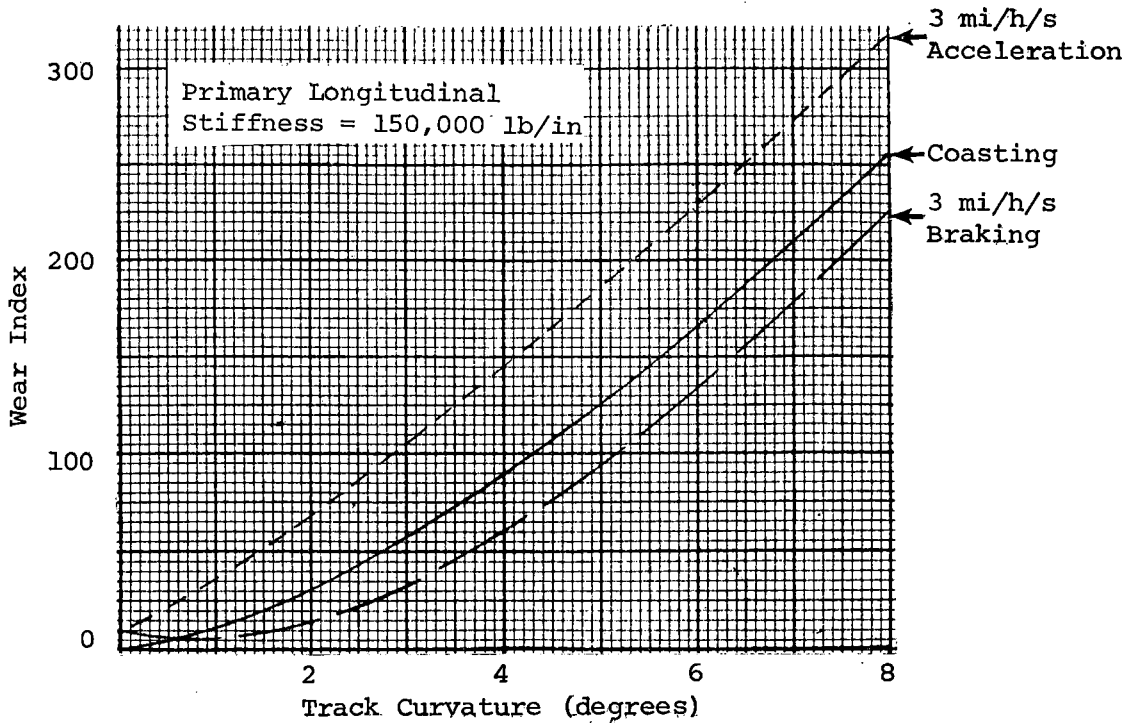


FIGURE 10-41. EFFECT OF TRACTION AND BRAKING ON WEAR INDEX.

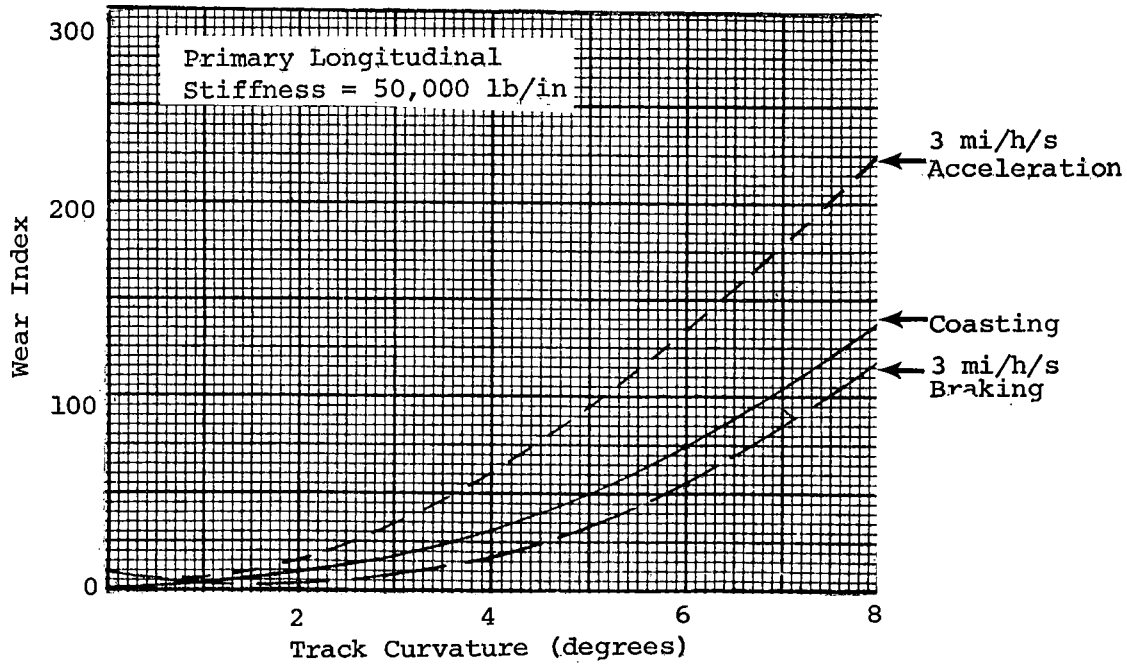


FIGURE 10-42. EFFECT OF TRACTION AND BRAKING ON WEAR INDEX.

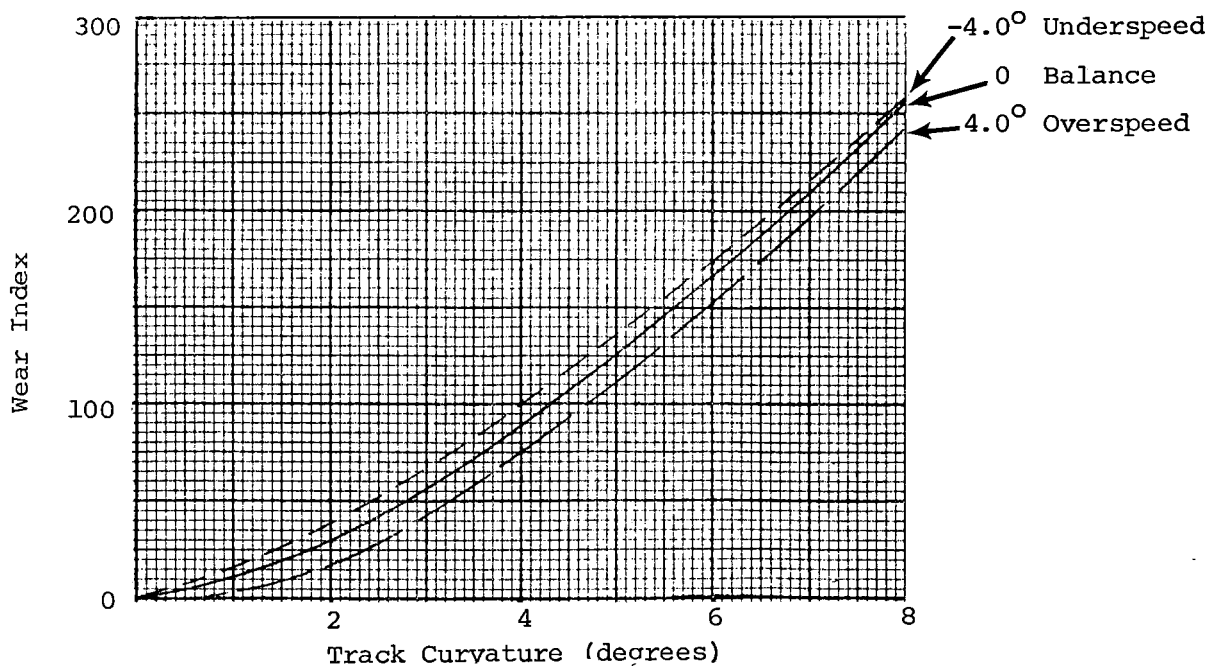


FIGURE 10-43. EFFECT OF CANT DEFICIENCY ON WEAR INDEX.

track curvature for the standard MARTA vehicle. This implies a wear index threshold value of between 20 and 55 (see figure 10-31).

If we assume that the wear index threshold lies in the range from 20 to 55, then figure 10-31 indicates that the wear rate on a 5.8° curve with a primary longitudinal stiffness of 50,000 lb/in would be 15-35% of the wear rate with a stiffness of 150,000 lb/in. For smaller curvatures, the improvements would be even greater.

10.6 CONCLUSIONS AND RECOMMENDATIONS

There are two major conclusions that appear from this work:

Very significant reductions in the rate of wheel flange wear, high rail gage face wear, and low rail crown wear can probably be achieved by reducing the longitudinal stiffness of the primary suspension bush on the trucks of the vehicles. If there were no other constraints, then the limiting value of stiffness would be that which gave truck hunting at a speed which is a reasonable margin above the maximum operating speed. Tests to ascertain the proximity of truck hunting were carried out, along with the tests described in this report, but the results of those tests are being reported separately. However, for the purpose of these conclusions it is sufficient to report that with the soft primary bush, there was no evidence of an approach to hunting at a speed of 70 mi/h.

Therefore, if there were no other considerations, the longitudinal stiffness of the bush could be reduced to a value even lower than the 50,000 lb/in. There are at least two problems associated with a further reduction in stiffness. The friction braking system used on the vehicles has a limited amount of brake actuator piston travel when a brake application is made. With a very low longitudinal bush stiffness, this piston travel can be used up before the required brake shoe force has been developed. This problem could be overcome by using a soft bush which has a limited travel. The other problem is to produce a modified bush design, within the constraint of the existing bush dimensions, that will achieve the required low longitudinal stiffness over an extended period of service.

The second major conclusion is that the radial misalignment of the two axles within a truck can have a significant detrimental effect on the rates of wheel and rail wear. This effect can be mitigated, to some extent, by adopting a low longitudinal stiffness bush. However, even with the 50,000 lb/in stiffness, the effects of radial misalignment are still significant. This problem could be overcome by better quality control of axle alignment during the manufacturing process, or the incorporation of appropriate adjustment capabilities in the trucks.

On the evidence of this work, the possibility of modifying the wheel profile from AAR 1:20 to CN-A does not seem to offer a very large reduction in the rates of wheel and rail wear.

As a result of this series of tests and the subsequent analysis of the test results, the following recommendations are made:

- The longitudinal stiffness of the primary suspension bush should be reduced to no more than 50,000 lb/in. If this causes problems with the friction brake system, the stroke of bush within which the stiffness is 50,000 lb/in should be limited to an amount sufficient to allow the brake system to operate properly. Initially, the modification should be made to two of the trucks of a two-car set. This could be done on either one or a small number of car sets. The rates of wheel wear, on the modified and unmodified trucks, could then be monitored over an extended period of time. This would enable a direct measurement to be made of the effect of the proposed modification.
- Radial misalignments between the two axles of a truck should be limited to 0.35 mrad, or 1.2 minutes.
- A further experiment should be carried out to obtain data relating wear index to rates of wheel and rail wear.

11.0 ELECTROMAGNETIC INTERFERENCE

11.1 INTRODUCTION

The MARTA cars are equipped with a d.c. propulsion control system that uses a solid-state chopper. The propulsion equipment is located underneath the carbody, and emits strong magnetic fields that can interfere with ATC systems. These systems employ audio frequency signals, using the running rails to transmit signals between the car and the track. The mechanism by which the magnetic fields couple with the ATC system involves the circuit comprised of the car wheel axles, the running rails, and the ATC signal circuit bonds to the running rails. This configuration only exists as the vehicle passes over the bond, and it is only during this interval (when the bond is between the innermost axles) that the circuit is susceptible to induction.

A means of measuring the magnitude and frequency of the voltages induced in the impedance bond of the ATC circuit has been recommended.^{1 2} The vehicle passing over the bond is simulated by testing the vehicle in a stationary position using a variable length sensing loop under the car in a plane parallel to the rails. (See figures 11-1, 11-2, and 11-3.) In this test, one side of the coil is fastened to the top of the rail parallel to and directly below one of the innermost axles. The two sides joining the axle side are placed adjacent to the base of the running rails. The fourth side of this loop is placed at various fixed distances from the axle side of the loop, as shown in figure 11-4. This concept is a simulation of the vehicle approaching and crossing the circuit bond or leaving and crossing the bond. With the help of this method, different revenue line operational modes such as varying speeds, acceleration, or braking can be examined under controlled conditions. In addition, the effect of having the wheels insulated from the rails and currents flowing in the rails can be studied.

11.2 TEST OBJECTIVES

The objective of the electromagnetic interference (EMI) tests was twofold. It was desirable to obtain test data that could be used by MARTA and others to investigate any potential EMI problem. The intent was also to develop test procedures, techniques, and data analyses. Because of the large amount of data that would be acquired in a test of this type, tests were restricted to one operating condition - that is, the auxiliaries operating and the propulsion level set at P3.

¹ Frasco, Louis A., "Rail Transit Vehicle EMC Testing," Proc. of AAR/IEEE/AREA Symposium, Railroad EMC Working Group, January 1981.

² Frasco, Louis A.; Gagon, Robert; and Holstrom, F. Ross, "Electromagnetic Compatibility of Advanced Propulsion Systems," Intl. Conf., Advanced Propulsion Systems for Urban Rail Vehicles, Washington, D.C., February 1980.

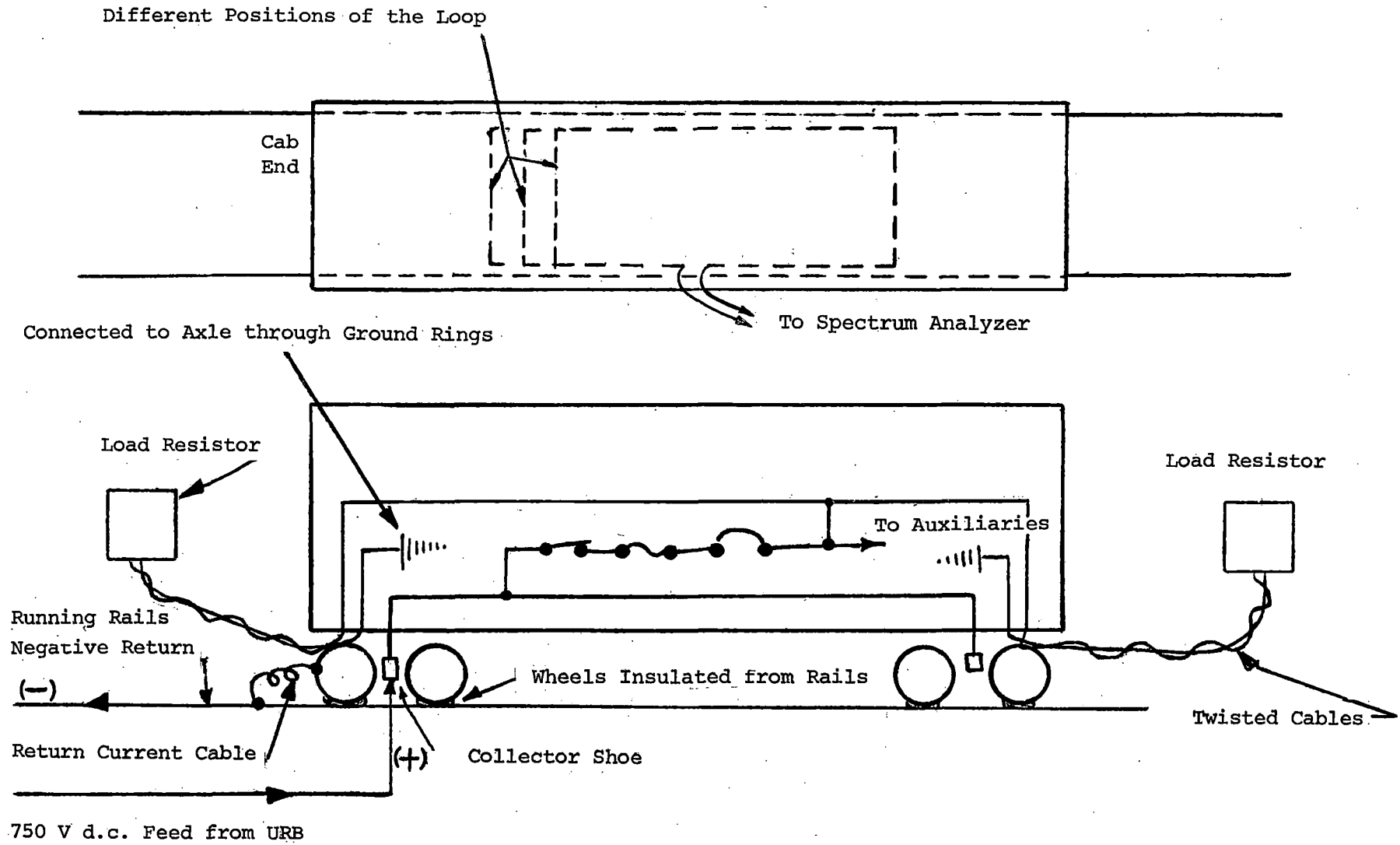


FIGURE 11-1. TEST CONFIGURATION: ISOLATED CARBODY, NO RETURN CURRENT UNDER CAR.

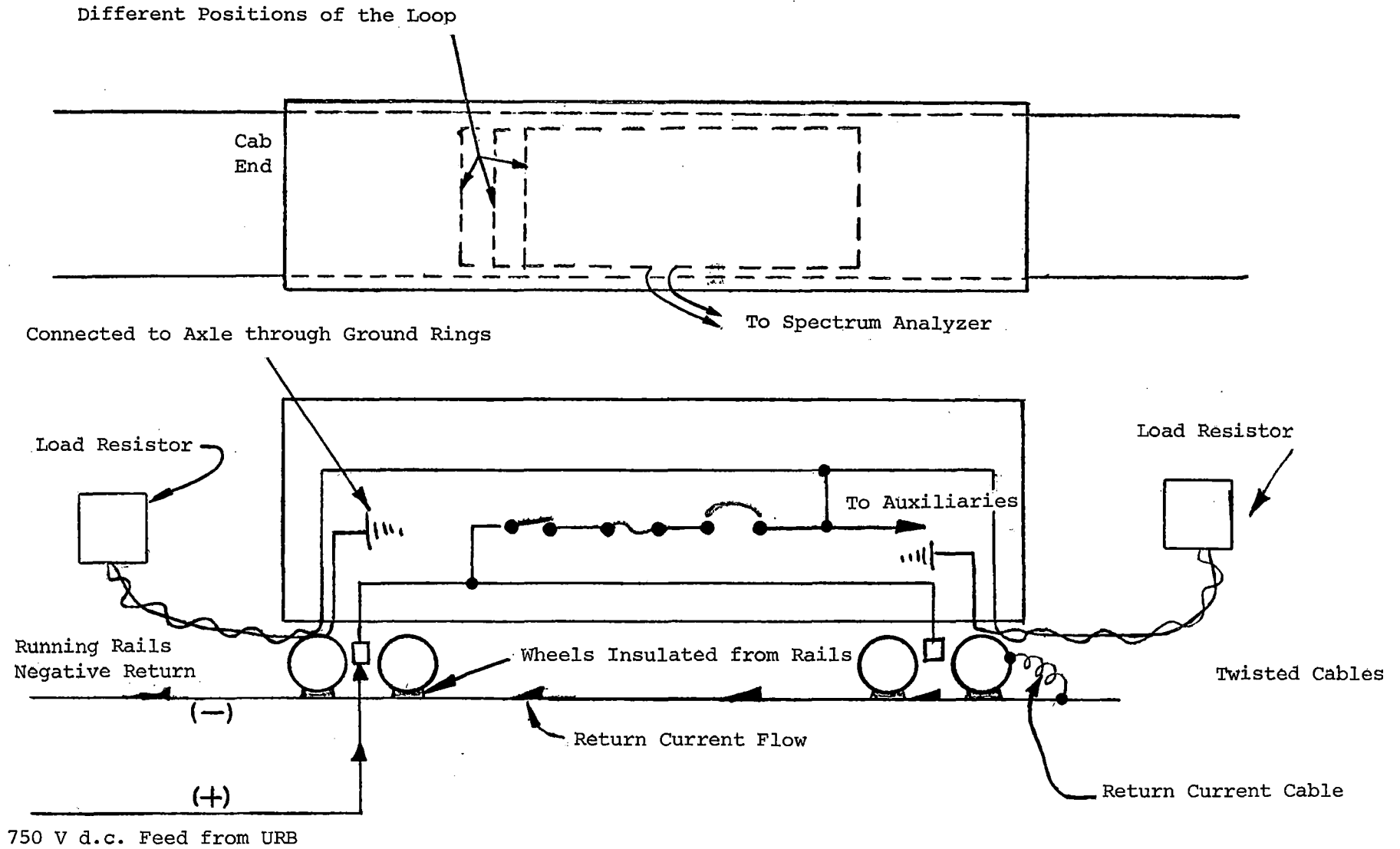


FIGURE 11-2. TEST CONFIGURATION: ISOLATED CARBODY, RETURN CURRENT UNDER CAR.

11-4

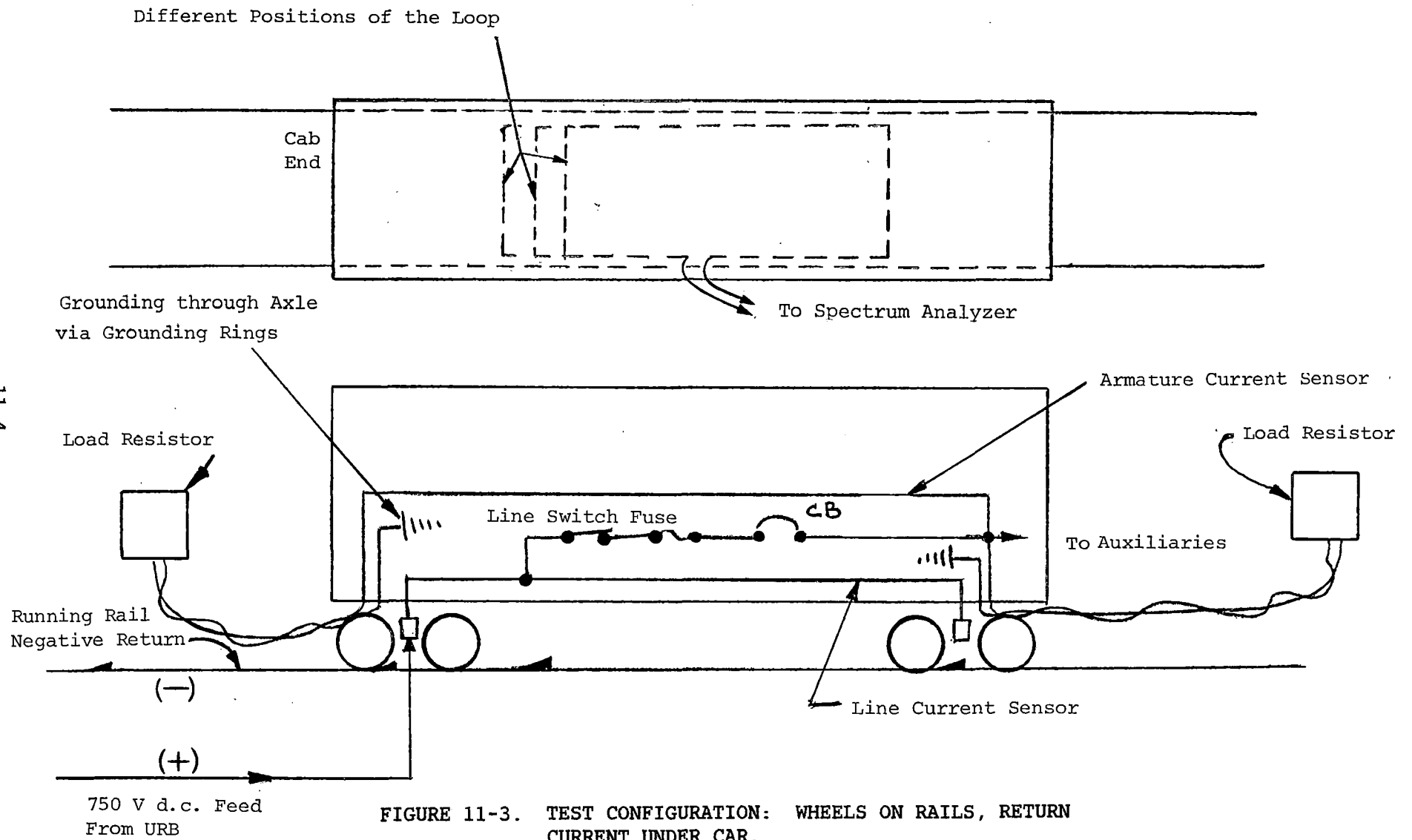


FIGURE 11-3. TEST CONFIGURATION: WHEELS ON RAILS, RETURN CURRENT UNDER CAR.

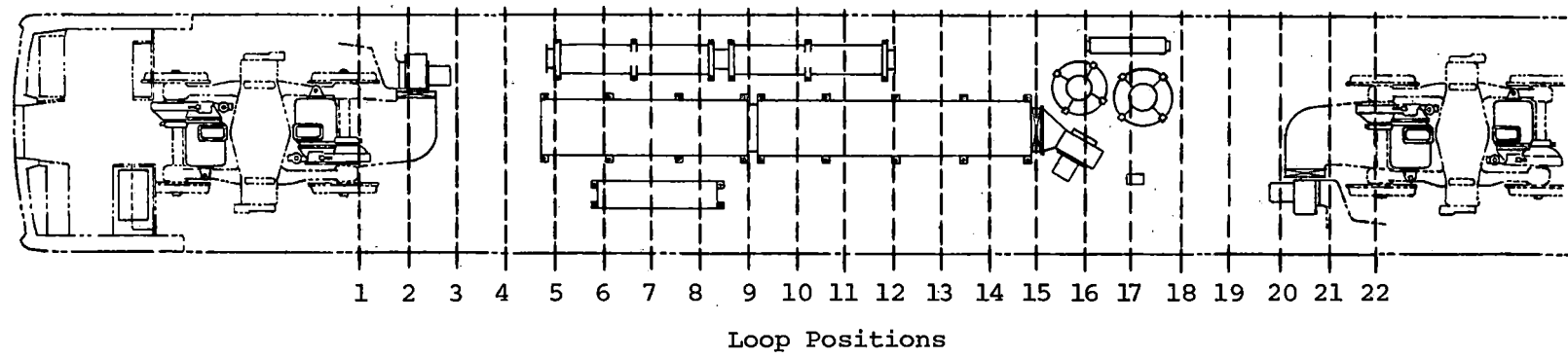


FIGURE 11-4. LOOP POSITIONS RELATIVE TO PROPULSION COMPONENTS.

Tests were conducted as follows:

- Case I, wheels insulated from the rails, with no return current flowing in the rails.
- Case II, wheels insulated from the rails, with return current permitted to flow in the rails.
- Case III, wheels in contact with the rails, with return current permitted to flow in the rails.

11.3 TEST PROCEDURES

By varying the length of the loop toward the rear wheels (front wheel end of the loop being fixed), voltages induced in the loop would simulate an approaching car moving over a fixed loop. With the controller in P3 position and the propulsion chopper connected to a fixed load, repeatable data were assured, because the chopper ran at nearly constant frequency and duty cycle.

For all tests, the carbody height above rails was normal (44", ± 1 "). The traction motor armatures were disconnected at both trucks and the equivalent load resistors were substituted at each end of the car. All cables to the resistors were run as twisted pairs in order to minimize induction into the other circuits.

The search coil data were obtained by feeding the voltage induced in the test loop to a real-time dual channel spectrum analyzer. Results, as shown in figure 11-5, were recorded on an x-y plotter with the magnitude of each component displayed in decibels relative to 1 V rms.

11.3.1 Isolated Carbody, No Return Current Under Car

The test configuration, as illustrated in figure 11-1, was with the wheels insulated from the running rails. A return current cable was clamped to one of the front wheels so that the return current did not flow through the portion of rails under the car. The power was fed to one collector shoe only. Figure 11-4 shows positions of the test loop placed under the car, in relationship to the undercar components. The test loop was placed in the largest loop configuration and power was applied. Data were collected with all auxiliaries running, and then with the propulsion controller in the P3 position and all auxiliaries running. The test was repeated for different loop positions, and frequency spectra plots were obtained for each configuration.

11.3.2 Isolated Carbody, Return Current Under Car

The test configuration is illustrated in figure 11-2. The return current cables were clamped to the rear wheels of the rear truck so that the return current flowed forward through the running rails under the car. The

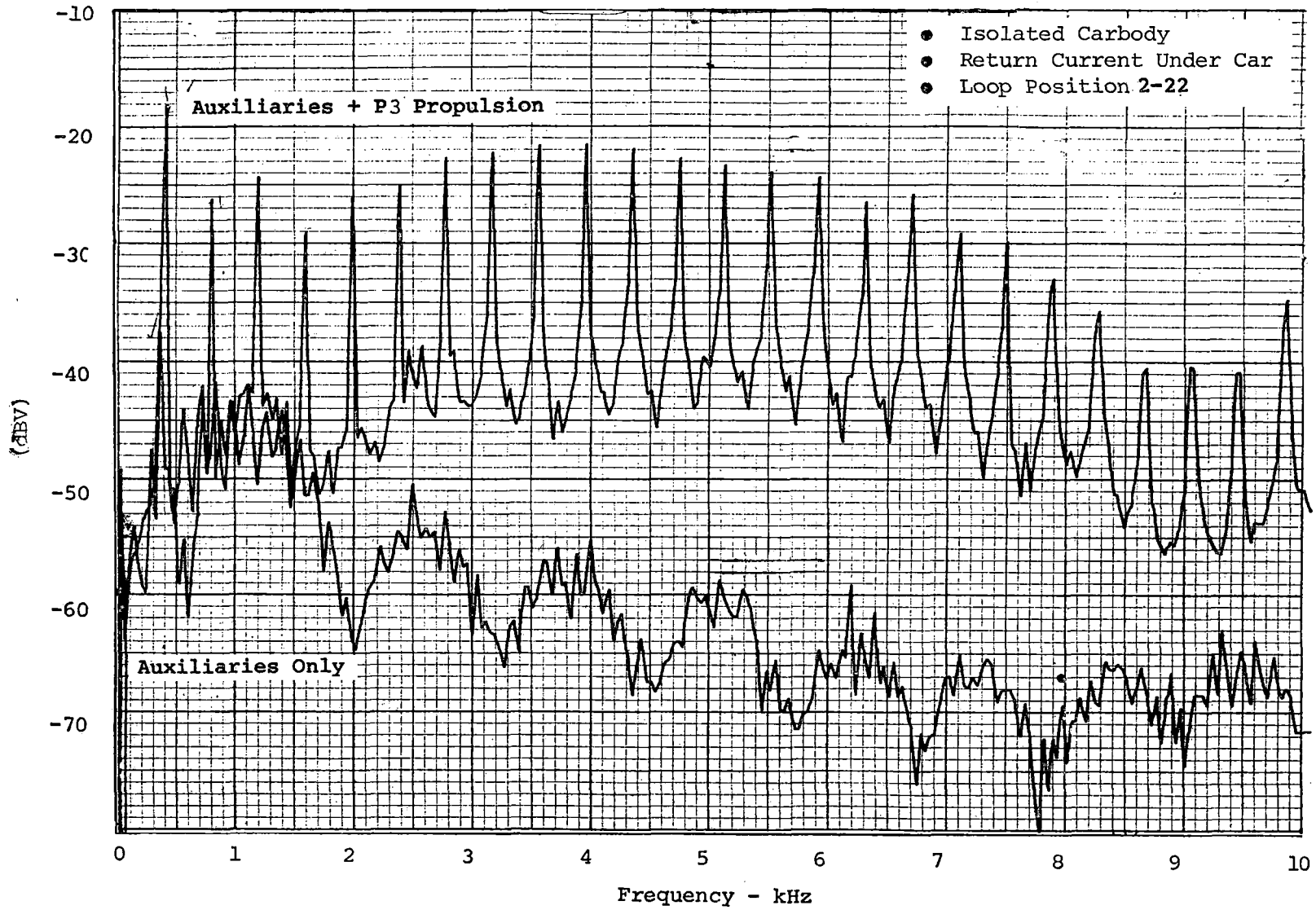


FIGURE 11-5. UNDERCAR INDUCED VOLTAGE, AMPLITUDE AND FREQUENCY DISTRIBUTION.

power was fed to one collector shoe only. The loop positions and data collection were as for the previous test series.

11.3.3 Wheels on Rails, Return Current Under Car

This test series was similar to the previous series except that the wheels were not insulated from the running rails, as shown in figure 11-3. Hence, the return current path was through axles, wheels, and running rails. The loop positions and data collection were as for the previous test series.

11.4 DATA ANALYSIS

All of the frequency related data were acquired in the form of spectral plots. From these plots, the voltages corresponding to the fundamental and to all harmonics through the 25th were obtained and tabulated in the order of the harmonic number and the variable coil side position. See tables 11-1, 11-2, and 11-3.

For all search coil tests, the fixed coil side was at position 22. Differences in the voltage levels were calculated for adjacent coil positions and each frequency component of the coil voltages. These voltages are the equivalent of voltages that would be obtained by a single search coil of fixed dimensions located with the coil sides at the even numbered positions. For example, the difference between signal voltages of the fundamental component for coil positions 2-22 and 4-22 (as tabulated in table 11-1) is: $178 - 168 = 10$. This is equivalent to having a fixed dimension coil with sides at 2 and 4. A more easy reference can be obtained by using the position of the center of the coil. In the case cited, the equivalent fixed dimension search coil is located at position 3.

These adjacent coil voltage differences are presented for each test series in tables 11-4, 11-5, and 11-6 by harmonic number and coil center position. These voltage differences represent changes in the magnetic flux that link the circuit formed by the vehicle axle, the rails, and the bond connection between the rails as the vehicle passes over the bond. The changes in the voltage - that is, the voltage differences - fairly represent the modulation of the voltage as it passes the bond.

To estimate the modulation rate, the fundamental, second, and third harmonic voltage differences have been plotted as a function of search coil position along the car (see figure 11-6). It can be seen that the modulation rate is approximately the same for all frequency components; the voltage differences have the same trend.

Restricting the discussion to the fundamental component only and using figure 11-6c, it can be seen that there is only one net change for a 300 mV sensitivity per car passing, and two per car passing for a 200 mV change. Using the coil width, it is possible to estimate the frequency of occurrence. However, the data only represent changes between adjacent search coil posi-

TABLE 11-1. SEARCH COIL FUNDAMENTAL AND HARMONIC VOLTAGES (mV): CASE I -
WHEELS INSULATED FROM RAILS AND NO RETURN CURRENT IN THE RAILS.

Harmonic Number	Coil Side Position									
	2	4	6	8	10	12	14	16	18	20
1*	178	168	422	138	355	211	427	385	126	29
2	72	79	191	63	158	100	129	132	37	11
3	28	18	23	15	36	81	158	115	33	6
4	40	32	81	28	84	67	150	129	30	6
5	49	43	106	36	112	49	53	53	6	2
6	41	50	126	40	112	63	79	84	21	5
7	53	45	112	38	141	50	100	75	12	3
8	71	79	178	69	178	100	40	39	15	5
9	67	84	204	63	182	94	58	35	19	7
10	63	71	182	71	166	75	65	47	12	5
11	79	87	174	65	207	111	47	45	14	5
12	78	98	204	65	204	110	36	22	16	7
13	63	87	200	69	166	77	56	29	14	6
14	71	75	145	60	174	97	50	29	19	4
15	67	81	162	56	174	91	22	21	16	6
16	45	67	145	42	119	60	34	12	12	5
17	45	40	91	36	94	62	23	12	6	3
18	40	44	71	29	91	57	15	15	8	3
19	19	40	71	25	63	32	15	14	6	2
20	15	25	56	19	35	28	20	14	3	2
21	16	21	18	17	47	25	18	12	6	1
22	10	23	33	11	35	14	14	15	6	2
23	8	15	27	6	18	15	17	16	2	1
24	9	18	25	11	36	17	24	16	6	1
25	5	23	42	10	13	13	24	15	6	2

* Fundamental frequency = 400 Hz.

TABLE 11-2. SEARCH COIL FUNDAMENTAL AND HARMONIC VOLTAGES (mV): CASE II - WHEELS INSULATED FROM RAILS AND RETURN CURRENT IN THE RAILS.

Harmonic Number	Coil Side Position									
	2	4	6	8	10	12	14	16	18	20
1*	126	126	211	229	316	295	372	376	85	23
2	50	62	100	107	141	96	110	111	29	8
3	60	13	15	28	45	69	141	122	20	4
4	36	29	54	69	106	63	162	141	21	4
5	50	47	94	91	138	42	69	50	2	3
6	56	51	85	89	114	63	101	81	15	5
7	74	56	91	100	164	37	110	79	8	3
8	78	72	126	141	200	79	58	25	10	5
9	83	72	126	129	162	74	48	29	13	5
10	84	56	94	95	146	50	63	40	7	3
11	81	62	110	117	174	65	49	32	7	4
12	73	65	100	119	155	66	24	11	12	5
13	69	58	87	94	141	53	40	27	11	4
14	65	44	75	106	172	63	51	29	7	6
15	62	50	93	127	158	75	32	17	13	6
16	48	44	79	94	119	56	22	9	12	5
17	52	29	59	85	141	54	33	17	6	3
18	35	32	68	100	123	60	30	21	8	4
19	32	31	63	66	63	41	21	20	8	3
20	41	23	34	37	79	28	11	5	4	1
21	17	14	36	50	74	33	28	15	4	2
22	9	18	32	35	26	17	23	20	6	2
23	10	11	14	21	36	13	19	19	2	-
24	9	17	29	32	22	20	10	5	4	2
25	33	19	32	11	46	-	28	16	5	1

* Fundamental frequency = 400 Hz.

TABLE 11-3. SEARCH COIL FUNDAMENTAL AND HARMONIC VOLTAGES (mV): CASE III - WHEELS IN CONTACT WITH RAILS AND RETURN CURRENT IN THE RAILS.

Harmonic Number	Coil Side Position									
	2	4	6	8	10	12	14	16	18	20
1 [*]	105	138	182	422	282	309	417	234	178	56
2	62	78	78	178	123	91	108	100	63	19
3	17	18	25	71	32	62	155	141	44	13
4	32	35	56	133	71	56	160	153	46	12
5	62	69	72	182	102	48	65	63	8	5
6	66	72	62	141	95	54	98	85	28	10
7	56	63	81	209	100	45	101	81	15	5
8	63	72	90	229	150	81	53	48	22	11
9	79	79	79	224	150	76	58	30	30	12
10	66	75	79	193	126	71	79	56	19	9
11	65	78	98	260	168	95	65	62	21	13
12	79	91	94	272	155	98	35	38	30	15
13	84	98	84	226	141	78	61	44	25	11
14	67	78	105	282	168	98	78	56	19	12
15	68	78	94	263	164	94	45	44	28	15
16	74	84	69	184	123	66	29	11	25	10
17	60	66	72	182	107	71	44	28	13	8
18	36	41	69	180	107	65	38	29	16	9
19	43	44	35	93	79	39	21	23	13	5
20	40	44	35	87	39	39	11	8	6	3
21	22	24	35	94	47	31	32	17	7	4
22	8	7	14	33	36	11	21	18	7	2
23	14	14	14	36	18	13	7	20	2	2
24	8	6	12	35	27	11	8	15	6	3
25	13	16	16	30	16	14	26	13	6	-

* Fundamental frequency = 400 Hz.

TABLE 11-4. EQUIVALENT DIFFERENTIAL, COIL FUNDAMENTAL AND HARMONIC VOLTAGES (mV) - CASE I.

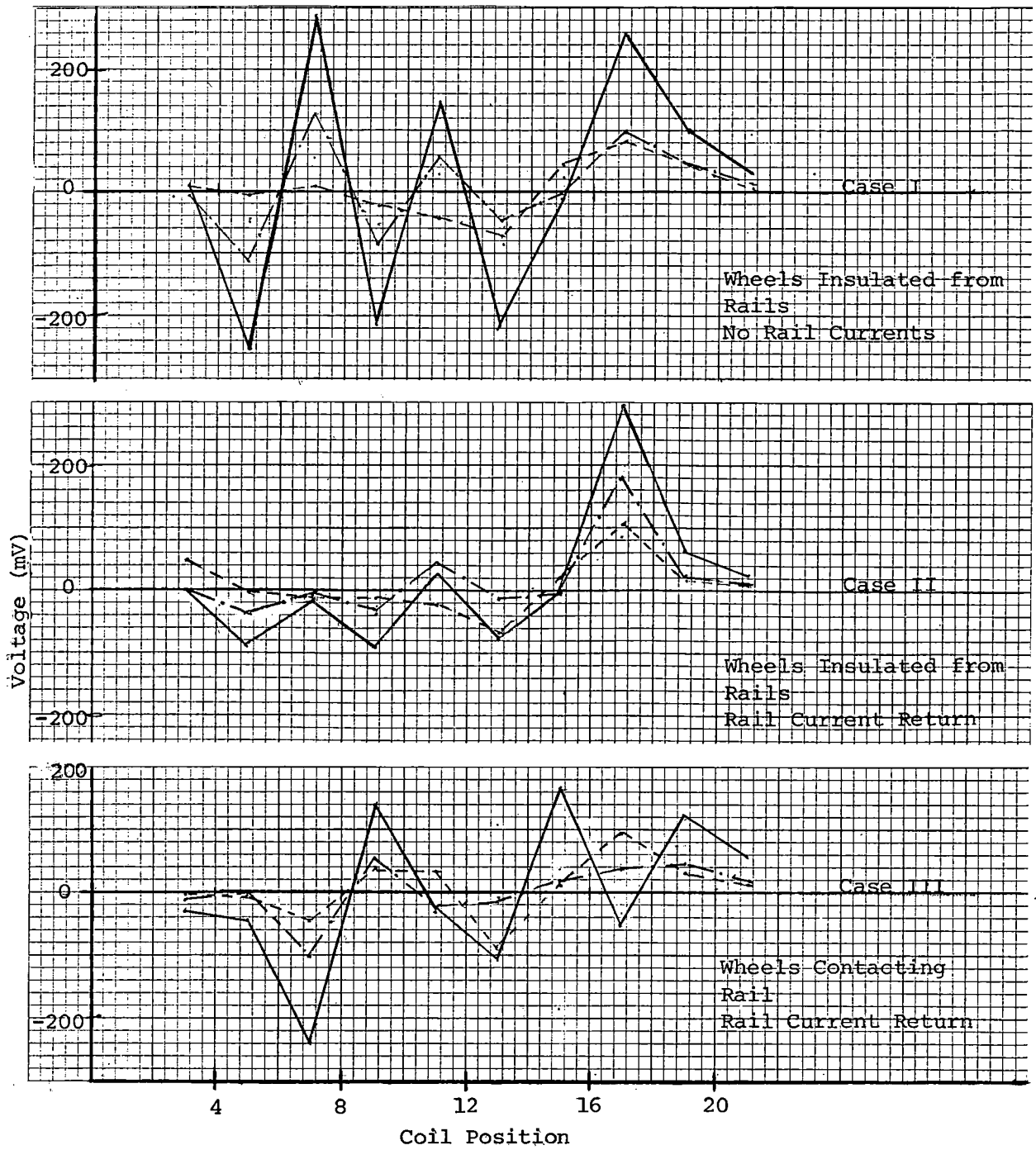
Harmonic Number	Coil Side Position									
	3	5	7	9	11	13	15	17	19	21
1	10	-254	284	-217	144	-216	-12	259	97	29
2	-7	-112	128	-95	58	-29	-3	95	26	11
3	10	-5	8	-21	-45	-77	43	82	27	6
4	8	-49	53	-56	17	-83	21	99	24	6
5	6	-63	70	-76	63	-4	0	47	4	2
6	-9	-76	86	-72	49	-16	-5	63	16	5
7	8	-67	74	-103	91	-50	25	63	9	3
8	-9	-99	109	-109	78	60	1	24	10	5
9	-17	-120	141	-119	84	36	23	14	12	7
10	-8	-111	111	-95	91	10	18	35	7	5
11	-8	-87	89	-142	96	64	2	31	9	5
12	-20	-106	139	-139	94	74	14	6	9	7
13	-24	-113	131	-97	89	21	27	15	8	6
14	-4	-70	85	-114	77	47	21	10	15	4
15	-14	-81	106	-118	83	69	1	5	10	6
16	-22	-78	103	-77	59	26	22	0	7	5
17	-5	-51	55	-58	32	39	11	6	3	3
18	-4	-27	42	-62	34	42	0	7	5	3
19	-21	-31	46	-38	31	16	1	8	4	2
20	-10	-31	47	-16	7	8	6	11	1	2
21	-5	3	1	-30	22	7	6	6	5	1
22	-13	-10	22	-24	21	0	-1	9	4	2
23	-7	-12	21	12	3	-2	+1	14	1	1
24	-9	7	14	25	19	-7	8	+10	5	1
25	-18	19	32	1	0	-11	0	9	4	2

TABLE 11-5. EQUIVALENT DIFFERENTIAL, COIL FUNDAMENTAL AND HARMONIC VOLTAGES (mV) - CASE II.

Harmonic Number	Coil Side Position									
	3	5	7	9	11	13	15	17	19	21
1	-0	-85	-18	-87	21	-77	-4	291	62	23
2	-12	-38	-7	-34	45	-14	-1	82	21	8
3	47	-2	-13	-17	-24	-72	19	102	16	4
4	11	-25	-15	-87	43	-99	21	120	17	4
5	3	-47	3	-49	96	-27	19	48	-1	3
6	5	-34	-4	-47	51	-38	19	66	10	5
7	28	-45	-9	-60	123	73	31	71	5	3
8	6	-58	-10	-60	121	21	33	15	5	5
9	9	-58	10	-40	86	26	19	16	8	5
10	28	-38	-1	-35	80	-13	23	33	4	3
11	19	-48	-	-60	105	16	17	25	3	4
12	8	-35	-20	-30	84	42	13	-1	7	5
13	11	-29	-6	-47	87	13	13	16	7	4
14	21	-31	-35	-60	107	12	22	22	1	6
15	12	-43	-37	-28	83	43	15	4	7	6
16	4	-35	-15	-29	67	34	13	-3	6	5
17	23	-30	-26	-56	87	21	16	11	3	3
18	3	-36	-32	-23	63	30	9	13	4	4
19	1	-32	-3	3	22	20	1	12	5	3
20	18	-11	-3	-42	51	17	6	1	3	1
21	-2	-22	-14	-24	41	5	13	11	2	2
22	-9	-14	-3	9	9	6	3	14	4	2
23	-1	-3	-7	-15	23	-6	-	17	2	-
24	-8	-12	-4	10	2	10	5	1	2	2
25	14	-13	21	-35	46	-28	12	11	4	1

TABLE 11-6. EQUIVALENT DIFFERENTIAL, COIL FUNDAMENTAL AND HARMONIC VOLTAGES (mV) - CASE III.

Harmonic Number	Coil Side Position									
	3	5	7	9	11	13	15	17	19	21
1	-33	-44	-240	140	-27	-108	183	-56	19	56
2	-16	-	-100	55	32	-17	8	37	44	19
3	-1	-7	-46	+39	-30	-93	14	97	31	13
4	-3	-21	-79	62	15	-104	7	107	34	12
5	-7	-3	-110	80	54	-17	2	55	3	5
6	-6	10	-79	86	41	-56	13	57	18	10
7	-7	-18	-128	109	55	-55	10	66	10	5
8	-9	-18	-139	79	69	28	7	22	11	11
9	-	-	-145	74	74	18	28	-	18	12
10	-9	-4	-116	67	55	-8	23	27	10	9
11	-13	-20	-162	92	73	30	3	41	8	13
12	22	-3	-170	117	57	63	-3	8	15	15
13	-14	14	-142	58	63	17	17	19	14	11
14	-10	22	-177	114	70	20	22	37	7	12
15	-10	16	-169	99	70	49	1	16	13	15
16	-10	15	-115	61	57	37	18	-14	15	10
17	-6	-6	-110	75	36	27	16	15	5	8
18	-5	-28	-121	73	42	27	11	13	7	9
19	-1	-9	-58	14	40	18	-2	10	8	5
20	-4	-9	-52	48	-	20	11	2	3	3
21	-2	-11	-59	47	16	7	15	10	3	4
22	1	7	-19	-3	28	-10	3	11	5	2
23	-	-	22	18	5	6	-11	18	-	2
24	2	-6	-23	9	16	5	-3	9	3	3
25	-3	-	-14	14	2	-12	13	7	6	-



Legend: — Fundamental (400 Hz)
 - - - Second Harmonic (800 Hz)
 - · - · Third Harmonic (1,200 Hz)

FIGURE 11-6. EQUIVALENT SEARCH COIL DIFFERENTIAL VOLTAGES.

tions. Because of the wide spacing (~42"), there may be more voltage differences per car length than indicated in the figure. This aliasing effect can be eliminated by using coils with less change in width for each measurement. As a rough order of magnitude, if one cycle of modulation occurred every 5' of car length, a modulation rate of 0.3 Hz/mi/hr car velocity could conceivably occur. This is within the modulation band of 2 to 30 Hz in use in some train detection systems. However, these systems use a carrier frequency that is much higher than the 400, 800, and 1,200 Hz components discussed here.

Consider the case where the carrier frequency could be on the order of 3 kHz. Referring to tables 11-3 and 11-6, the carrier frequency maximum voltages are 109 and 229 mV for the carrier frequencies of 2.8 and 3.2 kHz, respectively. The maximum modulation voltages for the same two frequencies are 128 and 139 mV. If the ATC networks were tuned to this frequency band and sensitive to voltages of this magnitude, then interference between the propulsion system and the ATC could conceivably occur.

11.5 TEST RESULTS

The data acquired during these tests have been reduced to table form for comparison with test data acquired by others in actual revenue service or in controlled experiments. The analysis of test data tends to support the hypothesis that the EMI from chopper controlled transit vehicles can emulate control signals used in ATC systems. If the systems are sensitive to the voltage levels acquired by these tests, intermittent pickup of relays could occur.

No significant conclusions can be drawn from comparing the data for the three test cases, except that the carrier voltage magnitudes are about the same for all cases. There does appear to be some redistribution of magnetic flux for each case. The tests were run at different times, and the anomalies in the propulsion control may be of such significance that identical chopper frequencies and dwell times were not attained.

12.0 FAULT CLEARING TESTS

12.1 TEST OBJECTIVES

The objectives of these tests were to determine the effectiveness of the onboard protective devices under severe fault conditions, for the following faults:

- Traction motor armature fault.
- PCE blower motor fault.
- VLC output fault.
- LVPS fault.
- A/B car circuit breaker short (output side).
- Third rail collector shoe grounding through shoe fuse, knife switch open.
- Grounding through main fuse and knife switch, circuit breaker CB1 open.
- Grounding output of circuit breaker CB1, main fuse, and knife switch.

12.2 TEST METHODS

A short circuit between the running rails and the car frame was applied instantaneously at each location described in table 12-1. The location was connected to the rail by means of a 500 MCM cable and a 500 A contactor, which was closed to simulate the short circuit. Fault current was measured using a 5,000 A resistive shunt connected on the ground side of the contactor. Voltage across the main contacts of the contactor (which is the same voltage as across the device under test) was measured using a 200:1 voltage divider; the third rail line voltage was also measured using a similar voltage divider.

12.2.1 Test Locations

The first five tests were conducted at the rear of the URB, using an 800 kVA rectifier as the power source. The last three were conducted on the TTT at stations 33 and 30, using substation No. 2 as the power source. Short-circuit fault locations for all tests were as per table 12-1.

12.3 TEST RESULTS

All tests were performed on the A car and the following data were recorded on an oscillograph at a paper speed of 2 meters per second:

TABLE 12-1. INDUCED SHORT CIRCUIT FAULT LOCATIONS.

Test No.	Location of Short Circuit	Protective Device	System Protected	Backup Protection	Test Circuit Diagram
1	Armature circuit	Chopper, CB1	Propulsion	CB1	Figure 12-1
2	Auxiliary blower	Auxiliary CB*	Auxiliary	VLC fuse	Figure 12-3
3	VLC output	Fuse	Auxiliary	CB1	Figure 12-5
4	LVPS output	Fuse	LVPS	CB1	Figure 12-7
5	A/B car CB (input and output)	CB	LVPS	A/B car CB	Figure 12-9
6	Between collector shoes	Shoe fuses	3rd rail collector	Substation	Figure 12-10
7	Main fuse output terminal	Main fuse	3rd rail input circuit	Shoe fuses/substation	Figure 12-13
8	Main circuit breaker output terminal	CB1	Propulsion	Shoe/main fuse	Figure 12-15

* Circuit breaker.

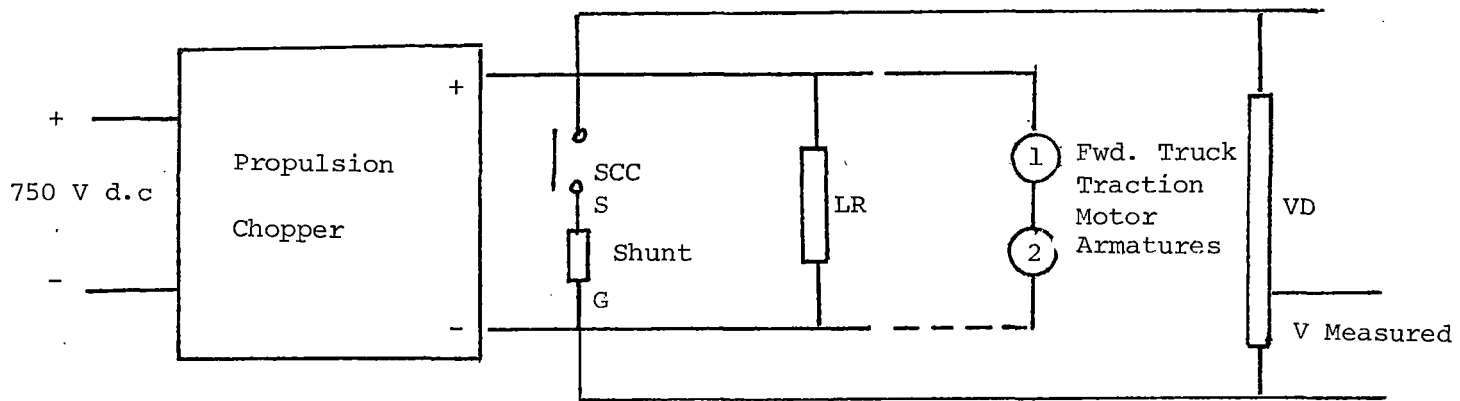
- Supply voltage
- Fault current
- Time
- Voltage across the device under test

The test procedures and test results are detailed below and summarized in table 12-2.

- Traction Motor Armature Fault. For this test the traction motors were disconnected from the propulsion system and were replaced by equivalent load resistors (simulating motor armature resistance). The controller handle was placed in position P3. When the armature current (I_a) was stabilized to about 450 A, the short-circuit contactor was closed (refer to figure 12-1 for the test circuit diagram), thus shorting out the load resistor which simulated the rear truck traction motor armature. The armature current immediately fell to zero and then pulsed between zero and approximately 100 A (refer to figure 12-2), indicating the proper functioning of the propulsion chopper protection. During that time, the quick shutdown (QSD), tractive effort pause (TE PAUSE), $I_a=0$, and traction error (TE) lights flashed continuously until the controller handle was moved to the 'Coast' position. When the fault was removed (keeping the controller in P3 position), the armature current returned to its normal level. There was no latching QSD, and cab fault lights were not illuminated.
- PCE Blower Motor Fault. For this test, the car auxiliaries were running normally. When the short-circuit contactor was closed, the blower motor stopped running and smoke began to appear from the series running resistors (refer to figures 12-3 and 12-4 for the test circuit diagram and current and voltage waveforms). The circuit breaker HCBI did not trip. When the fault was removed by opening the short-circuit contactor, the blower motor restarted. If the fault had not been removed, current would probably have continued to flow through the ballast resistor until it burned out. The short-circuit current (through the resistor) was approximately 43 A; the power dissipated was about 28 kW.
- VLC Output Fault (On VLC Contactor, KVLC). For this test, the car auxiliaries were kept running normally. The short-circuit contactor was closed and the circuit breaker (CBI) tripped due to the activation of the differential current relay (KDC); refer to figure 12-5 for test circuit diagram. The VLC fuse blew and the 10 output filter capacitor fuses blew. The peak fault current was 172 A and lasted for about 100 ms; refer to figure 12-6 for the voltage and current waveforms. When the blown fuses were replaced, the VLC performed normally.
- LVPS Fault (Output Terminal of Battery Contactor). For this test the car auxiliaries were running normally. When the short-circuit contactor was closed, it caused a QSD to occur immediately, mainly due to the fact that the battery contactor (K-BATT), the line contactor (KLS), and the ECE lost their power supply (refer to figure 12-7 for the test circuit diagram and figure 12-8 for voltage and current waveforms). Dropout of

TABLE 12-2. SUMMARY OF FAULT CLEARING TEST RESULTS.

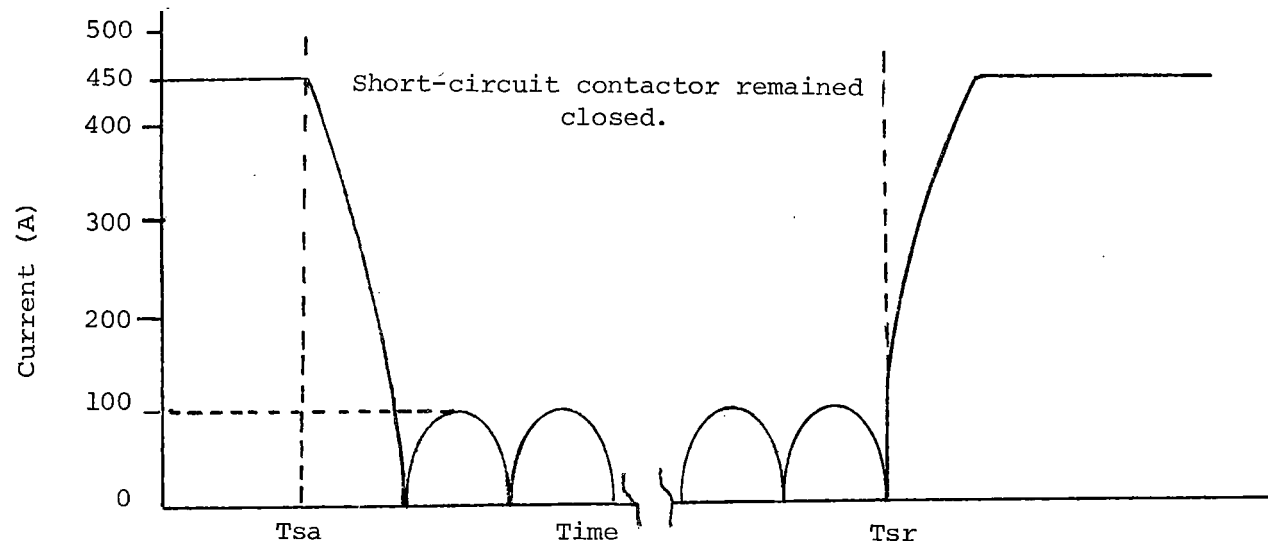
Test No.	Test Description	Results
1	Traction Motor Armature Fault	QSD, TE PAUSE, $I_a=0$, and TE lights flashed continuously as long as the fault condition existed. Armature current returned to normal when the fault was removed.
2	PCE Blower Motor Fault	Circuit breaker HCBl did not trip. Ballast resistor became hot and produced smoke. Blower restarted when the fault was removed.
3	VLC Output Fault	VLC fuse blown; also all output filter capacitor fuses blown. VLC performed normally when the fault was removed and all fuses replaced.
4	LVPS Fault	Fault caused QSD condition.
5	A/B Car Circuit Breaker	When input side was shorted with auxiliaries running, it caused a QSD but battery breaker did not trip. When test was repeated with auxiliaries not running, battery circuit breaker tripped. When the output side was shorted with auxiliaries running, the breaker A/B car circuit tripped but did not cause a QSD condition.
6	Third Rail Collector Grounding Through Shoe Fuse	When the short circuit was applied 3,000' from the substation, the shoe fuse did not blow but substation circuit breaker tripped. When the test was repeated at 600' from the substation, both shoe fuses blew simultaneously and the substation also tripped. 'Fuse Blown' indicator on the car also operated.
7	Grounding Through Main Fuse and Knife Switch (Circuit Breaker Open)	At Station 33 the main fuse did not blow but the substation tripped. At Station 30, the main fuse blew.
8	Grounding Through Circuit Breaker, Main Fuse, and Knife Switch	When the short circuit was applied, the CB1 tripped and the substation also tripped.



- Notes:
- 750 V d.c. - Supply from 800 kVA rectifier
 - SSC - Short circuit contactor, 5000 A rating
 - Shunt - 5000 A resistive shunt to measure short circuit current
 - LR - Load resistor equivalent of two traction motor armatures in series
 - VD - 200:1 voltage divider to measure armature voltage
- Refer to Figure 12-2 for propulsion chopper current profile.

FIGURE 12-1. TRACTION MOTOR ARMATURE FAULT PROTECTION, TEST CIRCUIT.

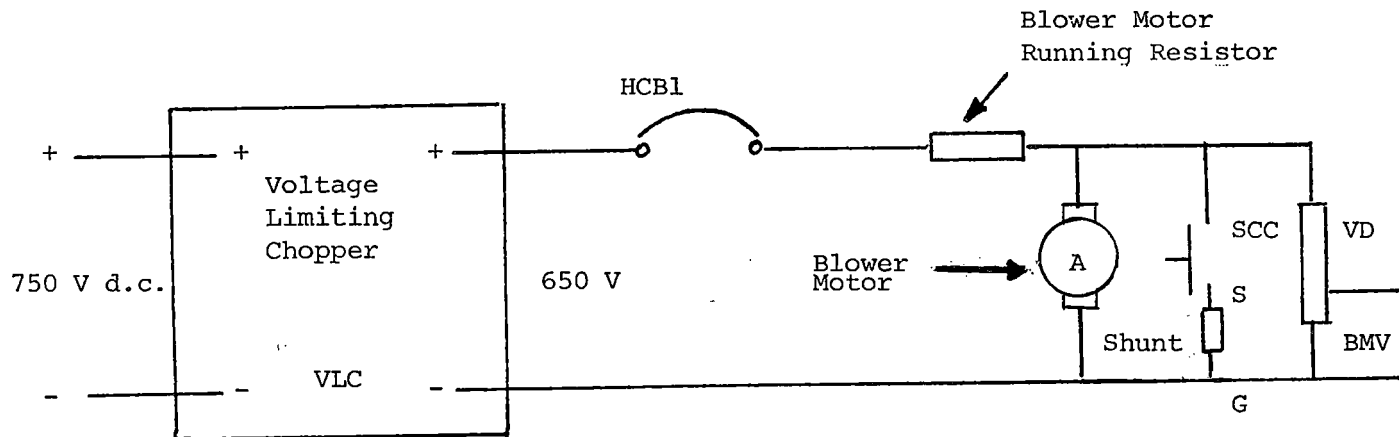
Tsa - short applied
Tsr - short removed



Notes: Master controller in P3 position.

Refer to Figure 12-1 for the test circuit diagram.

FIGURE 12-2. ARMATURE FAULT CURRENT PROFILE.

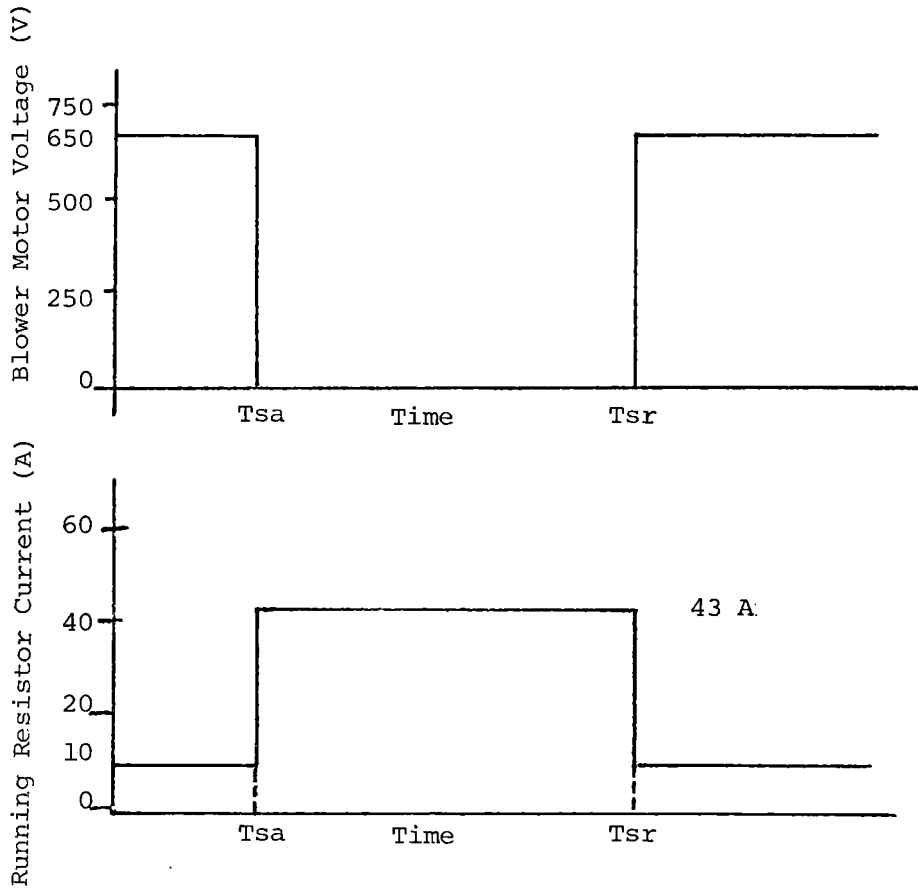


- Notes:
- SSC - Short-circuit contactor, 5000 A rating
 - BMV - Blower motor voltage
 - Shunt - Resistive shunt to measure short-circuit current
 - VD - Voltage divider to measure BMV
 - HCBl - Contact breaker HCBl

Signal for short-circuit current measurement was taken across the shunt at points S and G.

Refer to Figure 12-4 for blower motor output short-circuit current and voltage waveforms.

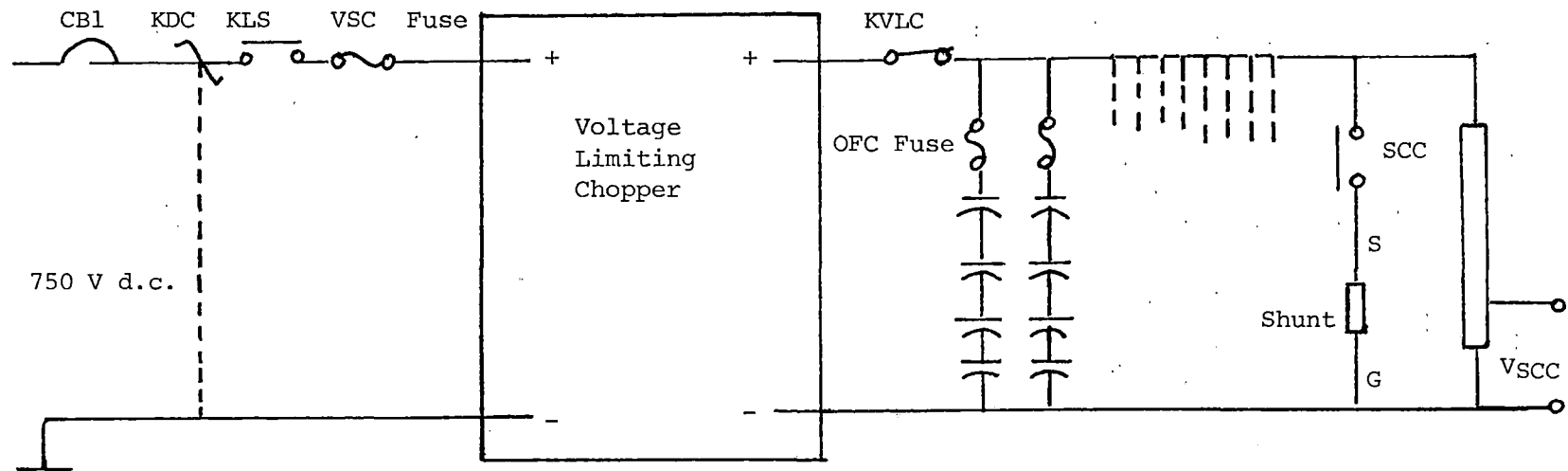
FIGURE 12-3. PCE BLOWER MOTOR FAULT PROTECTION, TEST CIRCUIT.



Notes: Tsa - short applied
 Tsr - short removed

Refer to Figure 12-3 for test circuit diagram.

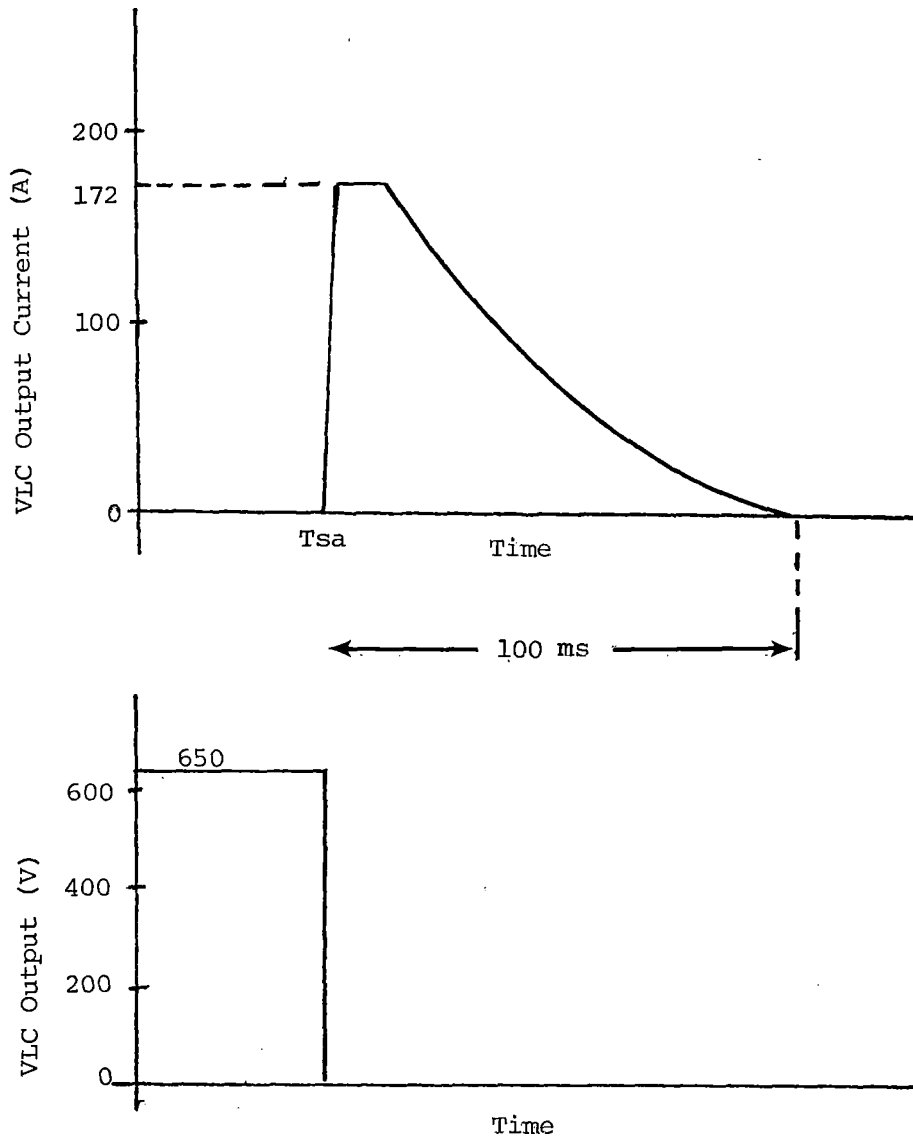
FIGURE 12-4. PCE BLOWER MOTOR SHORT-CIRCUIT CURRENT AND VOLTAGE WAVEFORMS.



- Notes:
- SCC - short circuit contactor, 5000 A rating
 - 750 V d.c. - supply from 800 kVA rectifier
 - OFC - output filter capacitor
 - Shunt - 5000 A/50 mV resistive shunt to measure short-circuit current
 - VD - 200:1 voltage divider to measure VLC output voltage
 - KVLC - break relay KVLC
 - KDC - differential current relay
 - KLS - line contactor

Refer to Figure 12-6 for VLC output voltage and current waveforms during test.

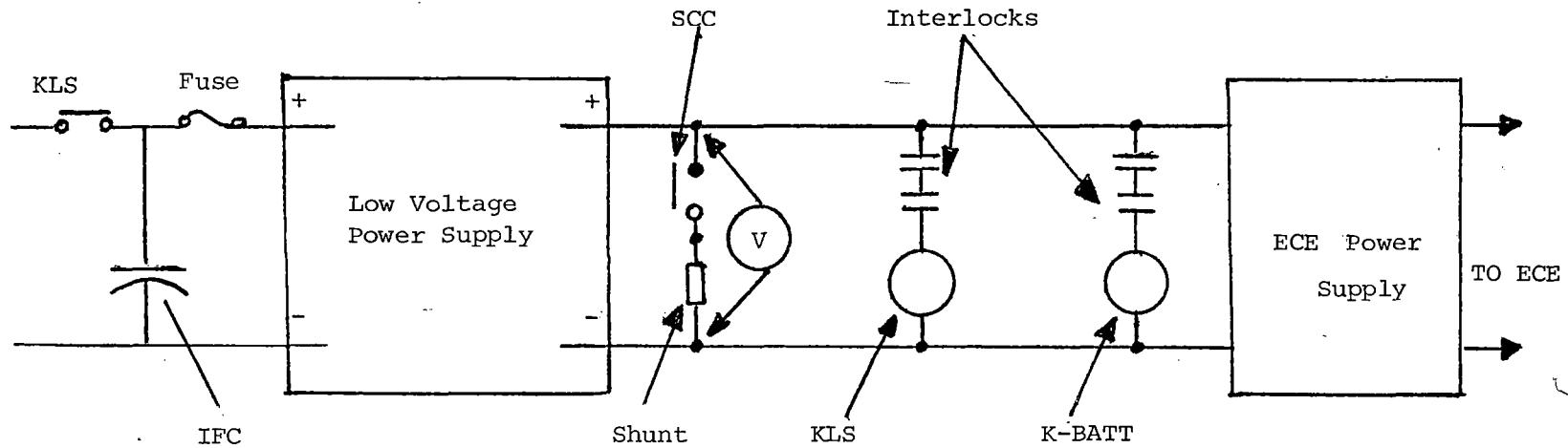
FIGURE 12-5. VLC OUTPUT FAULT PROTECTION, TEST CIRCUIT.



Note: T_{sa} - short applied

Refer to Figure 12-5 for test circuit diagram.

FIGURE 12-6. VLC OUTPUT FAULT CURRENT AND VOLTAGE WAVEFORMS.



Notes:

750 V d.c. - supply from 800 kVA rectifier

IFC - input filter capacitor

Shunt - resistive shunt to measure short-circuit current

ACC - short-circuit contactor, 5000 A rating

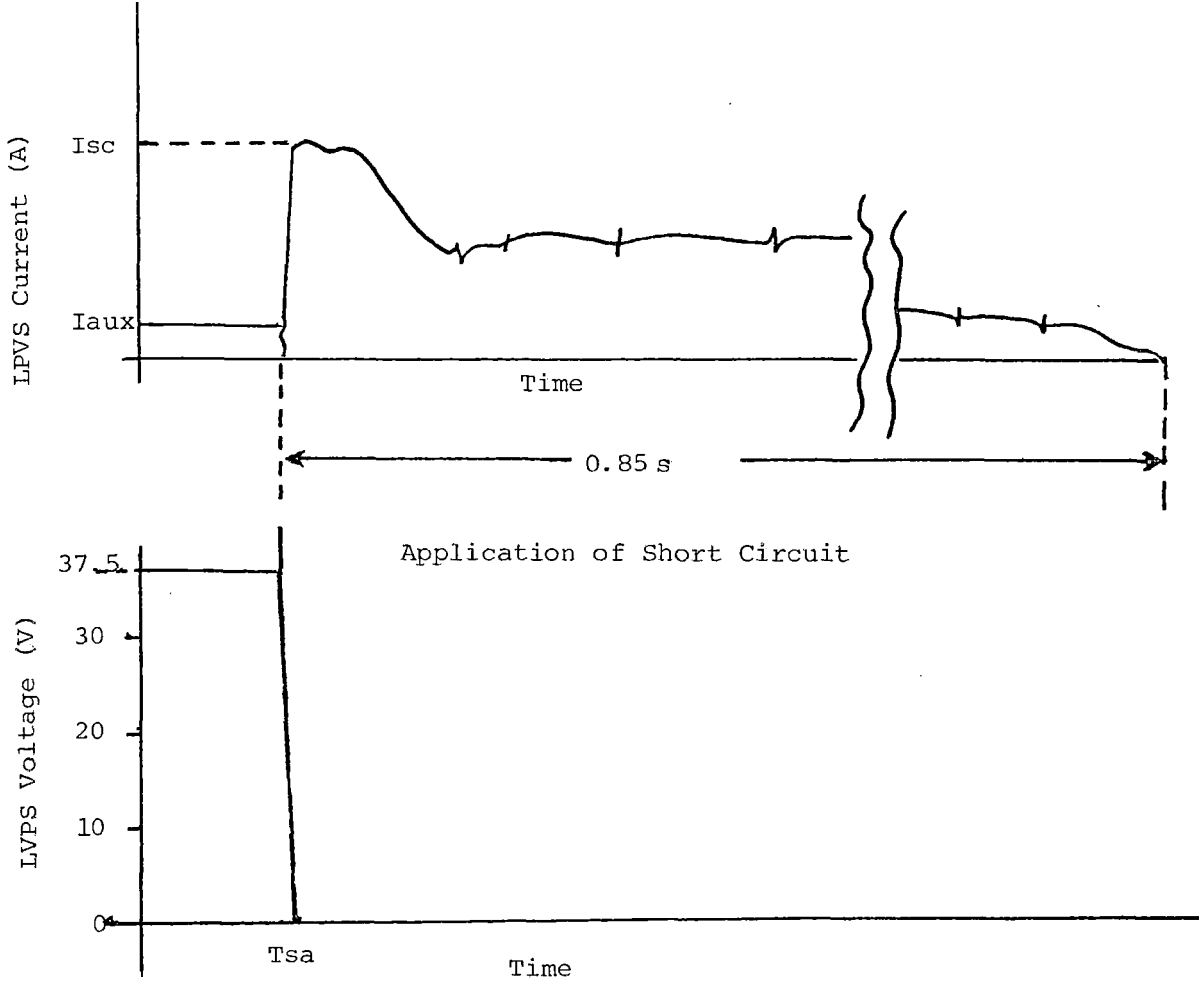
K-BATT - battery contactor

KLS - line contactor

ECE - Electronic Control Equipment

Refer to Figure 12-8 for output current and voltage waveforms.

FIGURE 12-7. LVPS OUTPUT FAULT PROTECTION, TEST CIRCUIT.



Notes: I_{sc} - short-circuit current
 I_{aux} - auxiliaries

Refer to Figure 12-7 for the LVPS fault protection test circuit.

FIGURE 12-8. LVPS OUTPUT FAULT CURRENT AND VOLTAGE WAVEFORMS.

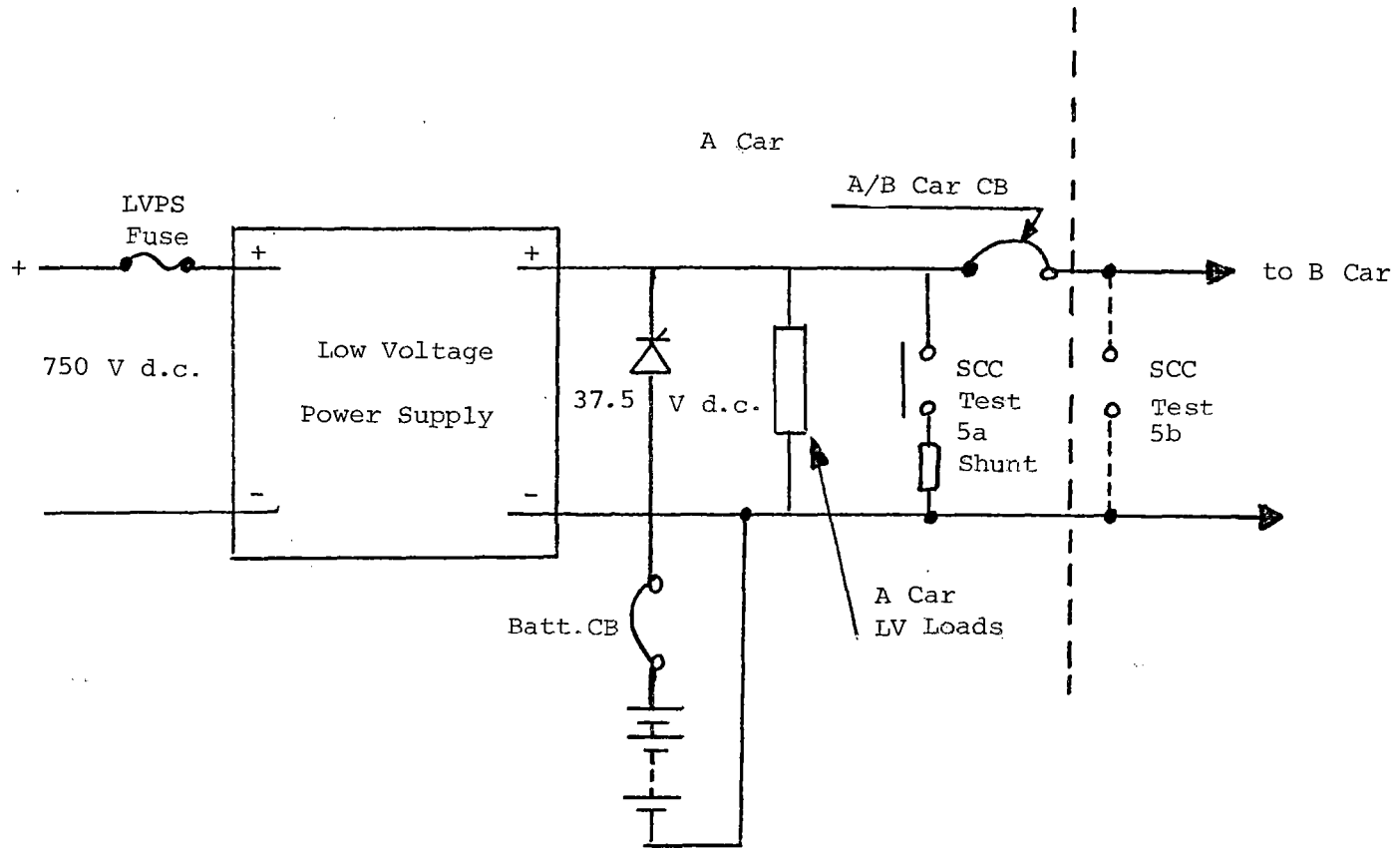
KLS removed the line voltage input to LVPS, but the short-circuit current continued to flow till the energy stored in the input filter capacitor was dissipated (approximately 0.85 s).

- A/B Car Circuit Breaker. This test was conducted in two ways: a short circuit was applied to the input side and the output side of this circuit breaker (refer to figure 12-9 for test circuit diagram). When the input side was shorted with the vehicle auxiliaries running, it caused a QSD; the battery breaker did not trip. When the test was repeated (auxiliaries not running), the battery circuit breaker tripped immediately. When the output side of the A/B car circuit breaker was shorted with auxiliaries running, the circuit breaker tripped but did not cause a QSD condition or any other fault condition on the car.
- Third Rail Collector Grounding Through Shoe Fuse. For this test, the car was positioned approximately 3,000' from substation No. 2, on jointed track, with one collector shoe on the third rail and the other in the rail gap. When a short circuit was applied to the collector shoe located in the third rail gap, the substation circuit breaker was tripped; the shoe fuse did not blow (refer to figure 12-10 for the test circuit diagram). The maximum fault current was approximately 12,000 A and lasted for about 115 ms. (Refer to figure 12-11 for current and voltage waveforms.)

When the car was then moved closer to the substation (approximately 600' away from the single-ended power feed), the test was repeated and both shoe fuses blew simultaneously. The maximum current was approximately 20,400 A; the voltage surge on the third rail was about 3 kV. Sparks were emitted from the end of the fuses, and the 'Fuse Blown' indicator operated as designed. The substation also tripped on overload. Refer to figure 12-12 for current and voltage waveforms.

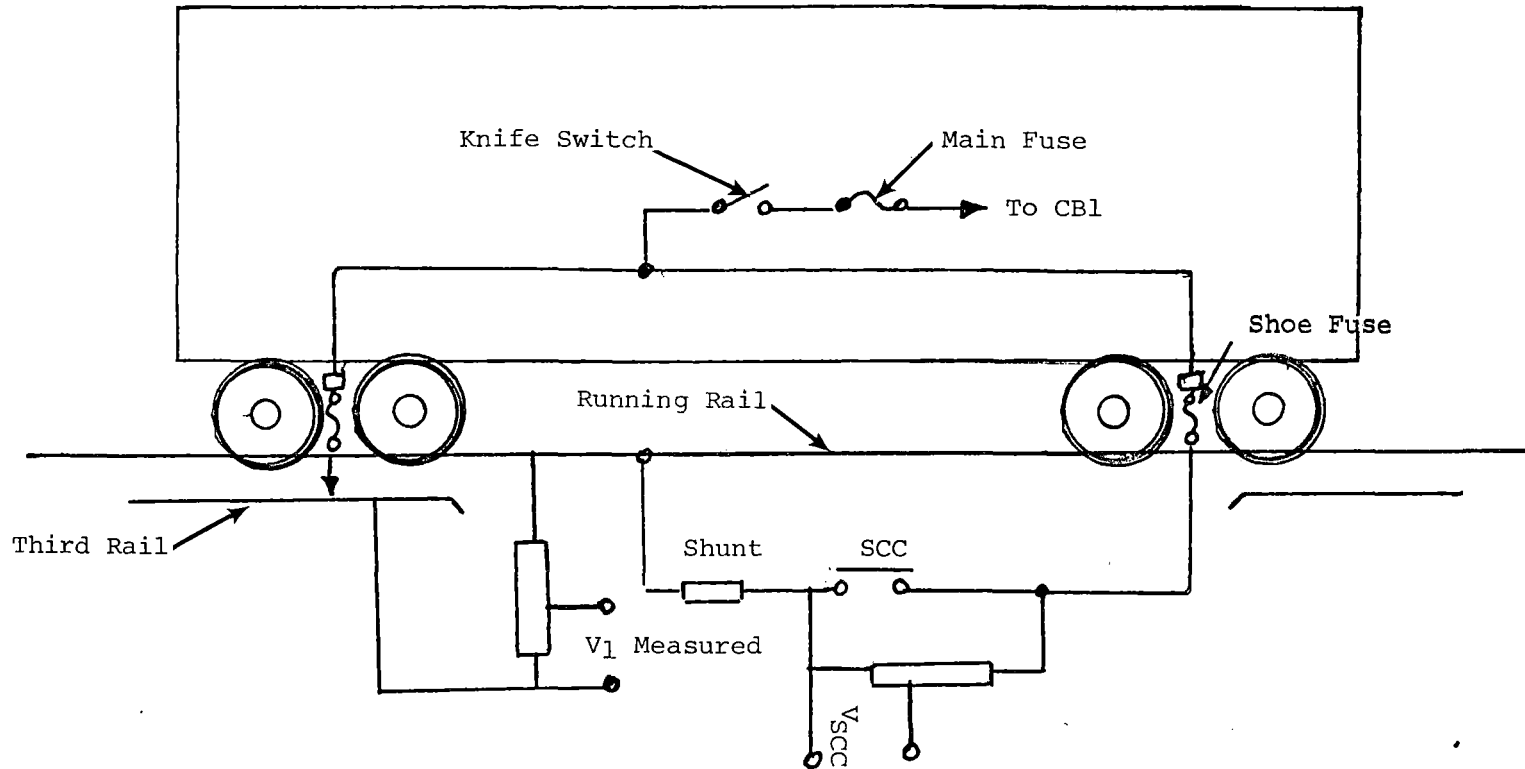
- Grounding Through Main Fuse and Knife Switch, Circuit Breaker Open. For this test, a short circuit was applied (refer to figure 12-13 for the test circuit diagram) through the short-circuit contactor at station 33. The main fuse did not blow, but the substation tripped out on overload. The same test was conducted at station 30 and, in this case, the main fuse blew. The maximum current was approximately 21,000 A. Maximum surge voltage was approximately 3 kV. The 'Fuse Blown' indicator operated as designed; the fuse case became hot (approximately 220°F), but there was no apparent damage to the enclosure. The third rail voltage, short-circuit contactor voltage, and current trends are shown in figure 12-14.
- Grounding Through Circuit Breaker, Main Fuse, and Knife Switch. For this test, the output terminal of circuit breaker CB1 was disconnected from the car's power circuitry and was connected to the short-circuit contactor only (refer to figure 12-15 for test circuit diagram). When the short circuit was applied, the CB1 tripped and the substation also tripped on overload. The maximum fault current was approximately 6,000 A when tested at station 33, and approximately 11,000 A at station 30. Maximum surge voltage was approximately 3 kV.

When the car control system was energized after short-circuit application, the monitor panel showed a QSD condition caused by a KDC trip.



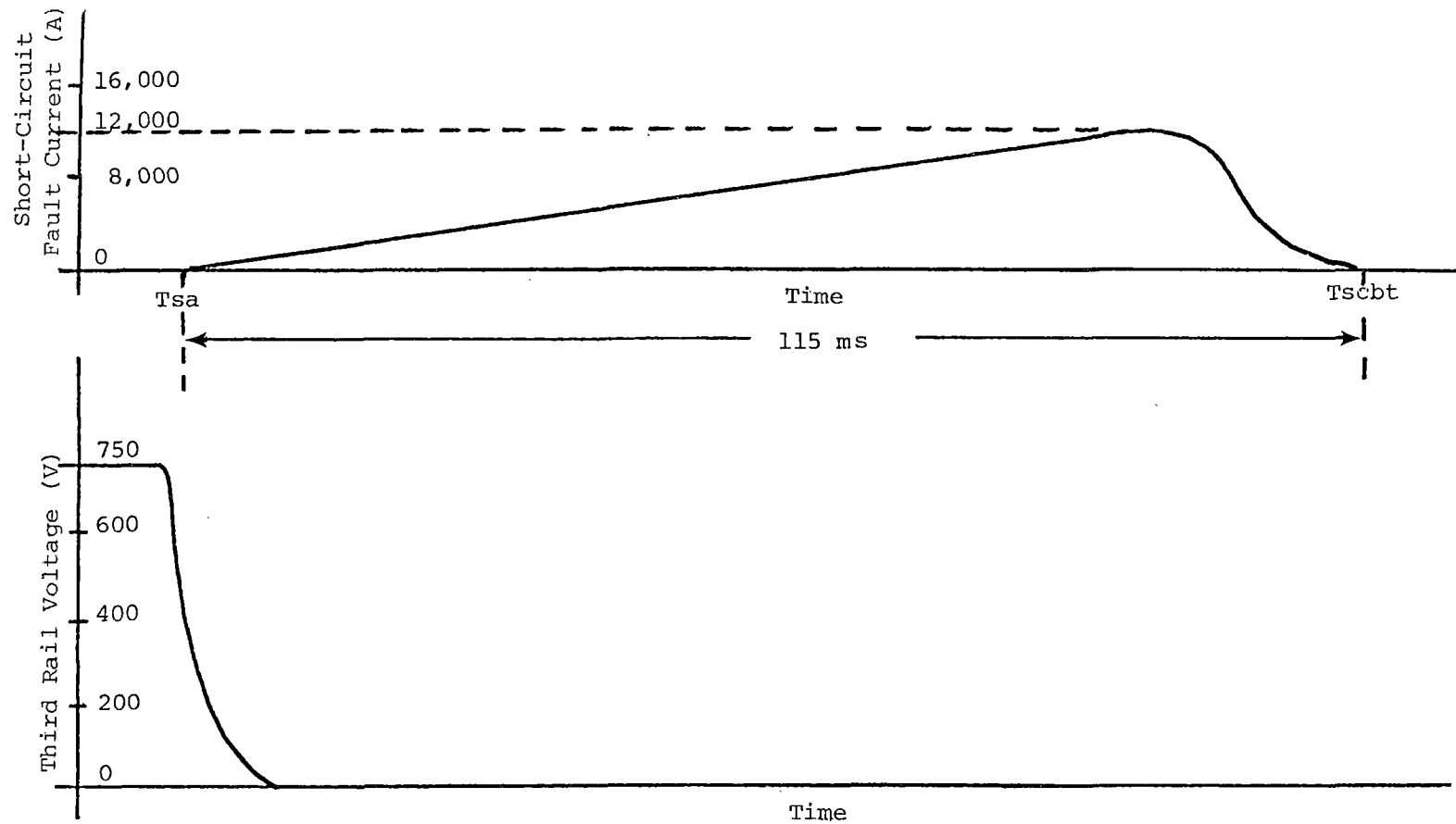
- Notes:
- 750 V d.c. - supply from 800 kVA rectifier.
 - SCC - short-circuit contactor, 5000 A rating
 - Shunt - resistive shunt to measure short-circuit current

FIGURE 12-9. A/B CAR CB INPUT AND OUTPUT SIDE SHORT CIRCUIT, TEST CIRCUIT.



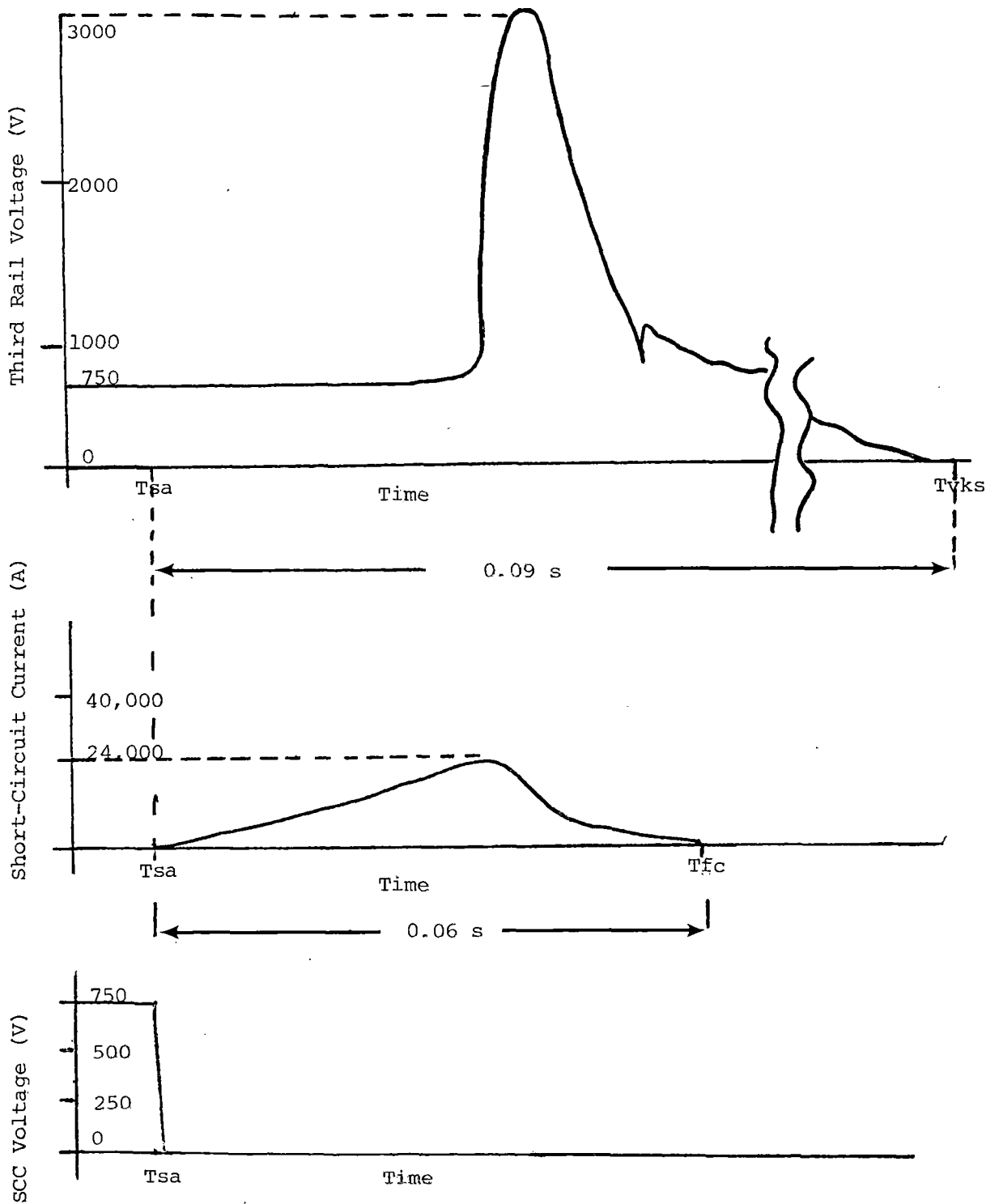
Note: Refer to figures 12-11 and 12-12 for current and voltage wave forms at Station 33 and Station 30, respectively.

FIGURE 12-10. THIRD RAIL COLLECTOR SHOE GROUNDING THROUGH SHOE FUSE, WITH KNIFE SWITCH OPEN.



NOTES: T_{sa} - short applied
 T_{scbt} - substation CB tripped
 Refer to Figure 12-10 for test circuit diagram.

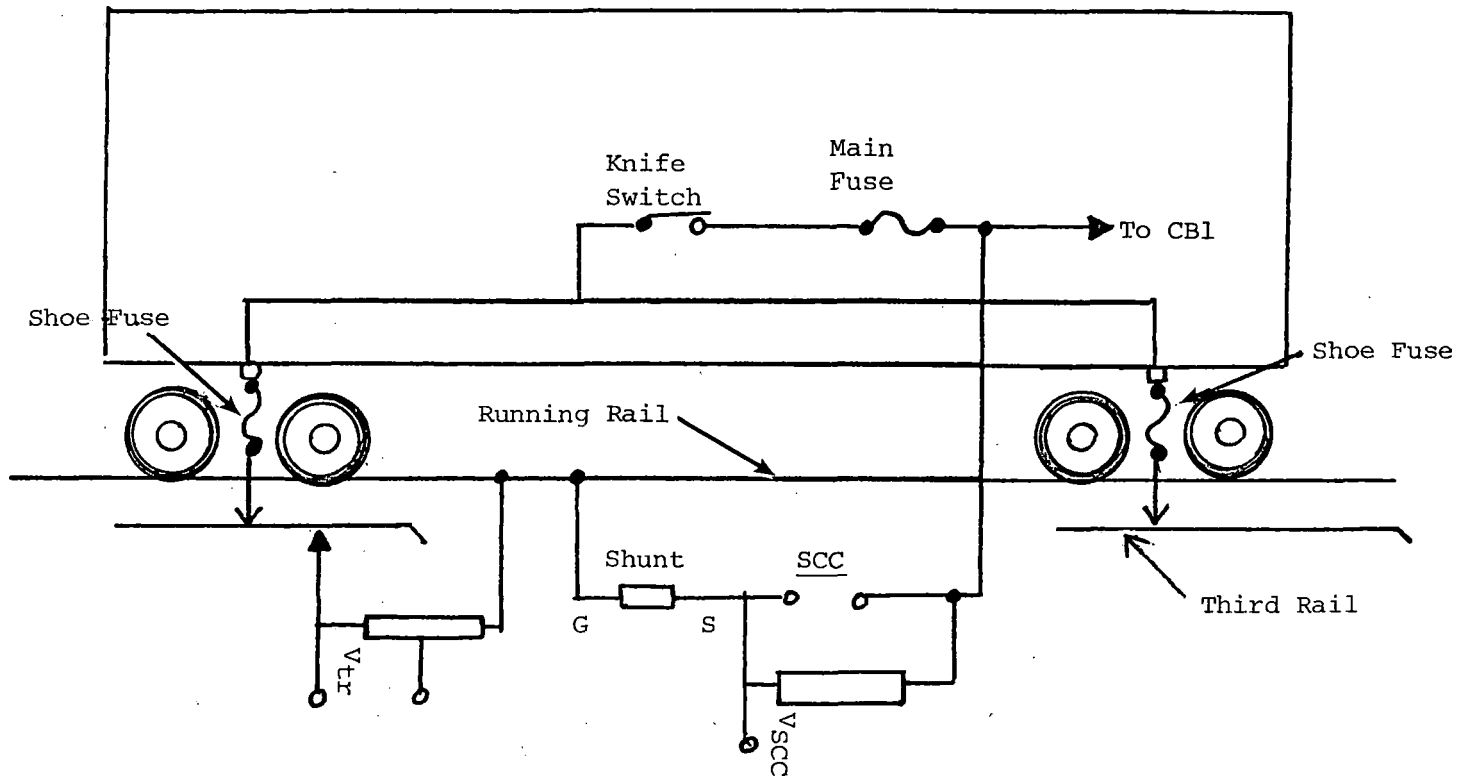
FIGURE 12-11. VOLTAGE AND CURRENT WAVEFORMS (STATION 33),
 THIRD RAIL COLLECTOR SHOE GROUNDING TEST.



Notes: T_{sa} - short applied
 T_{fc} - fuse cleared
 T_{vks} - voltage kick subsided

Refer to Figure 12-10 for test circuit diagram.

FIGURE 12-12. VOLTAGE AND CURRENT WAVEFORMS (STATION 30),
 COLLECTOR SHOE GROUNDING TEST.



- Notes:
- SCC - short-circuit contactor, 5000 A rating
 - Shunt - resistive shunt to measure short-circuit current
 - V_{SCC} - voltage across SCC
 - V_{tr} - voltage across third rail

Refer to Figure 12-14 for current and voltage waveforms at Station 30.

FIGURE 12-13. THIRD RAIL COLLECTOR SHOE GROUNDING THROUGH MAIN FUSE, KNIFE SWITCH, AND SHOE FUSE.

12-20

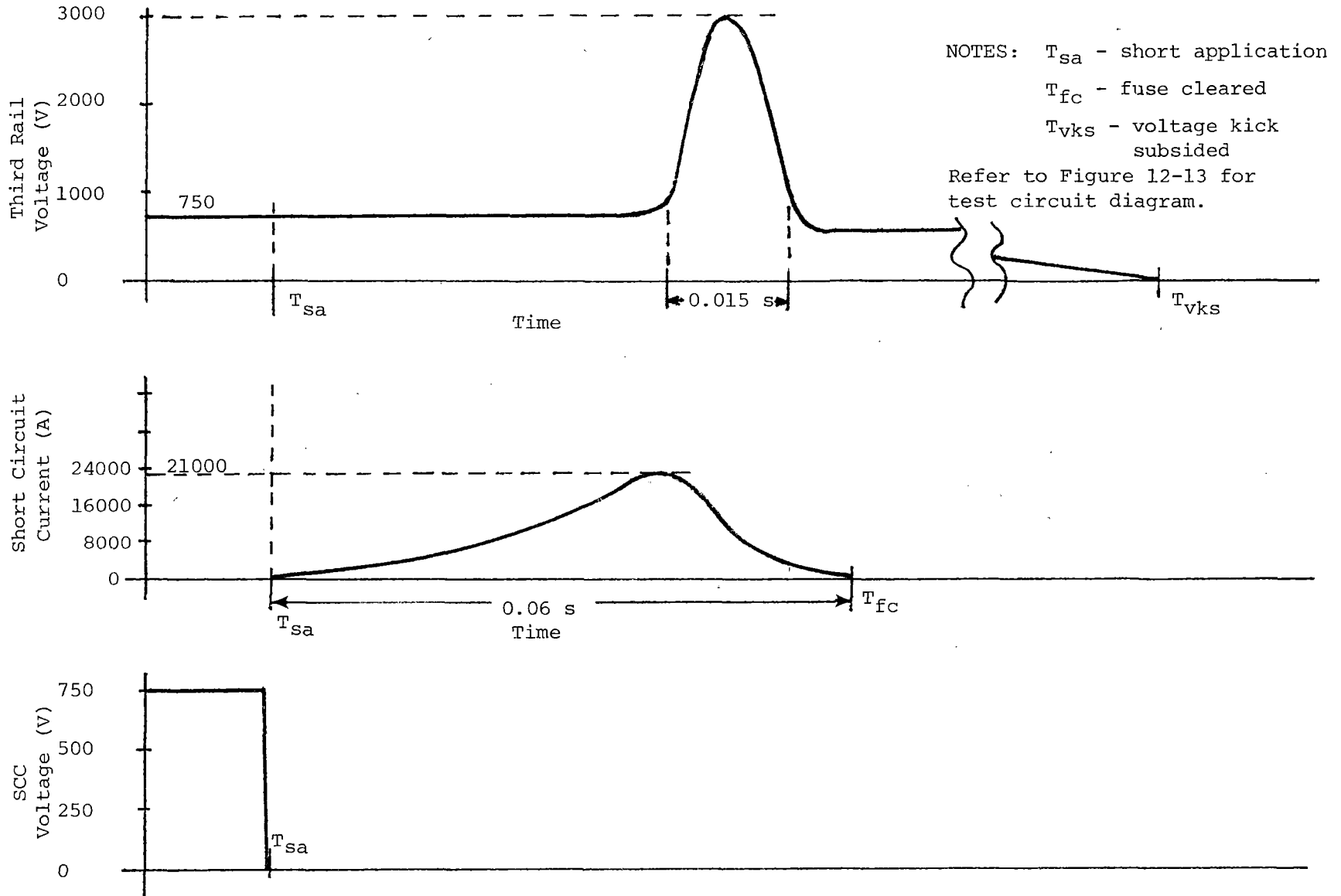
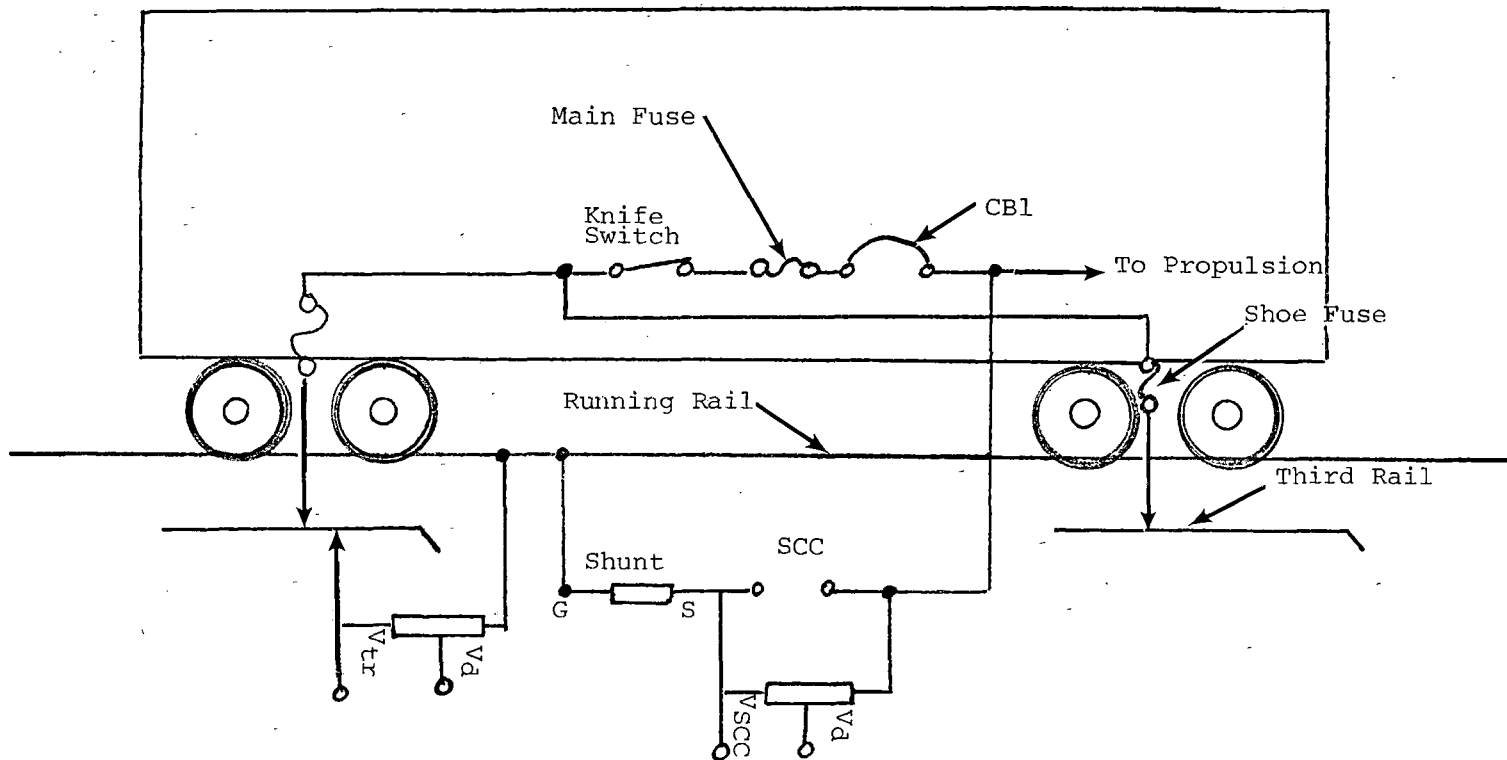


FIGURE 12-14. VOLTAGE AND CURRENT WAVEFORMS AT STATION 30 - THIRD RAIL COLLECTOR SHOE GROUNDING THROUGH MAIN FUSE AND KNIFE SWITCH.



- Notes:
- SCC - short circuit contactor, 5000 A rating
 - Shunt - resistive shunt (5000 A/50 mV) to measure short-circuit current
 - VSCC - voltage across SCC
 - Vtr - voltage across third rail
 - Vd - voltage divider for voltage measurements

FIGURE 12-15. THIRD RAIL COLLECTOR SHOE GROUNDING THROUGH CIRCUIT BREAKER, MAIN FUSE, KNIFE SWITCH, AND SHOE FUSE.

13.0 RADIO FREQUENCY INTERFERENCE

A complete set of radio frequency interference tests were conducted on the MARTA transit vehicle by the consulting firm of Radiation Sciences Incorporated of Skippack, PA. Results of their tests are documented in test reports, as follows:

1. Inductive Emission of the Metropolitan Atlanta Rapid Transit Authority (MARTA) Vehicle Electrical Power Subsystem, Rail-to-Rail Voltage Measurements, RSI Test Report No. 811E, Contract No. DTRS 57-80-80497.
2. Electromagnetic Emissions of the Metropolitan Atlanta Rapid Transit Authority (MARTA) Vehicle Electrical Systems, Electric and Magnetic Field Measurements, RSI Test Report No. 812 E, Contract No. DTRS 57-80-80497.

APPENDIX A

INSTRUMENTATION, DATA ACQUISITION, AND DATA PROCESSING

This appendix describes the onboard instrumentation sensors, the data acquisition system, and the data processing techniques used to acquire and process data. The system described is that which is common to the standardized tests; i.e., all performance tests, energy consumption, train resistance, and ride quality tests. Other engineering tests which have individual instrumentation requirements, such as noise, electromagnetic interference tests, the Dynamic Shake Test, and the curving performance test, have their instrumentation systems described separately in their respective report areas.

1.0 INSTRUMENTATION

1.1 INTRODUCTION

The instrumentation requirements for the test program were divided into six basic groups according to the type of test to be performed:

- Performance (acceleration, deceleration, energy consumption, train resistance, spin/slide efficiency)
- Vehicle dynamics (ride quality, component induced vibration)
- Noise (wayside and onboard)
- Curving and truck stability
- Dynamic Shake Test
- Electromagnetic interference

1.2 PERFORMANCE TESTS

The performance test objectives were met by using a combination of built-in sensors inherent to the propulsion system design and special purpose sensors mounted on the cars. The sensor signals were obtained from the onboard test panel located in the operator cab of each car above the ECE cabinet. The signal outputs were buffered at the test panel to prevent overloading or otherwise distorting them.

The following sensors were mounted on the cars to supplement the signals obtained from the test panel:

- Brake cylinder pressure transducers for the front and rear truck of each car.
- A servo accelerometer mounted on the floor of car 0110 to measure vehicle acceleration and deceleration.
- A ninth wheel assembly mounted on the rear truck of car 0110 to give an accurate speed and distance signal. This assembly allows a sprung, damped suspension to push a wheel of known diameter against the rail head. A gear wheel mounted on the wheel together with a magnetic pickup provide a signal output with 60 pulses per revolution of the wheel; by conditioning and counting these pulses, outputs are provided which are proportional to speed and distance and unaffected by vehicle wheel slips.
- Track location information was provided by a series of steel targets mounted on the track crossties at 1,000 ft intervals, in conjunction with a capacitive displacement sensor mounted on the lead truck of car

0110. Detection of a steel target gave a momentary output from the displacement sensor and was then annotated on the chart records and on the voice channel of the analog tape recorder to identify the specific track station.

- Twenty-nine thermocouples were installed at undercar locations on equipment likely to be subjected to heat from brake resistor banks, to meet the test objectives of the duty cycle test program. They were monitored separately on a data logger; specific locations of these thermocouples are detailed in Section 6.3, Duty Cycle.

The measurement number, standard output name, and sensor description for each particular performance test and analog tape are listed in tables A-1 through A-7. The sensor requirements were derived from the recommended 'Standard Outputs' for performance testing detailed in the General Vehicle Test Procedure¹ in conjunction with the signal descriptions provided in the Garrett-Airesearch Study Guide Manuals for the MARTA car propulsion system.

1.3 VEHICLE DYNAMICS

Accelerometers were installed on the carbody, and accelerometers and displacement transducers were installed on the lead truck of car 0110, to meet the requirements of several ride quality and vehicle dynamic stability objectives. While analysis of all of the sensors was not undertaken for any one test objective, the sensors were active and were recorded on the analog tape; they are therefore described and documented here to present a complete picture of the data available for any future analysis effort. The sensors installed on the car addressed two major objectives, which are described in the two paragraphs below:

1.3.1 Evaluation of Ride Quality Within the Carbody

A series of servo accelerometers were mounted on the floor of the carbody, at the centerline over the lead truck, at the centerline and left side at a midcar location, and at the centerline over the trailing truck. Vertical and lateral accelerations were measured at each longitudinal station, together with longitudinal acceleration at the lead truck position.

1.3.2 Detection of Truck Dynamic Instability

Truck hunting was considered to be a possible explanation for the wheel/rail wear problems experienced by MARTA, and was the subject of a curve entry and stability study conducted concurrently with the curving test program described in Section 10.0.; the study was conducted for Cooperrider and Law, of Acorn Associates, and will be reported separately. The sensors were in place during the ride quality test program. A brief description is included here to document the data available on the analog tapes for the potential

¹ General Vehicle Test Plan (GVTP) for Urban Rail Transit Cars, Report No. UMTA-MA-06-0025-75-14.

TABLE A-1. PERFORMANCE INSTRUMENTATION, SENSOR LISTING (BY DATA TAPES AND TEST SERIES, AS CITED)

CHANNEL NUMBER	PARAMETER	STANDARD OUTPUT NAME	MEASUREMENT NUMBER	SENSOR TYPE	MEASUREMENT RANGE	MAXIMUM CUTOFF FREQUENCY
1	IRIG-B Time	T/A	01411	Time Code Generator	---	1 KHz
2	Armature Current (A-Car, Forward Truck)	IAF	01103	Hall Effect Sensor	1000 Amps	100 Hz
3	Armature Current (A-Car, Rear Truck)	IAR	01104	Hall Effect Sensor	1000 Amps	100 Hz
4	BRK 1 #1 Trainline Current (A-Car)	BRK1#1	01118	Current Sensor	1 Amp	100 Hz
5	BRK 1 #2 Trainline Current (A-Car)	BRK1#2	01119	Current Sensor	1 Amp	100 Hz
6	Line Current (A-Car)	I LINE	01102	Hall Effect Sensor	1500 Amps	100 Hz
7	Line Voltage	E LINE	01101	Resistive Divider	1500 Volts	100 Hz
8	Armature Current (B-Car, Forward Truck)	IAF	01108	Hall Effect Sensor	1000 Amps	100 Hz
9	Armature Current (B-Car, Rear Truck)	IAR	01109	Hall Effect Sensor	1000 Amps	100 Hz
10	EP Valve Current (A-Car)	EP VALVE	01120	Derived Signal	1 Amp	100 Hz
11	EP Valve Current (B-Car)	EP VALVE	01121	Derived Signal	1 Amp	100 Hz
12	Line Current (B-Car)	I LINE	01107	Hall Effect Sensor	1500 Amps	100 Hz
13	Vehicle Acceleration	AP/A	02001	Servo Accelerometer	±5.4 MPHPS	3.15 Hz
14	Vehicle Speed	VS/A1	01402	Electromagnetic Sensor	100 MPH	100 Hz
15	P-Signal	CS/B	01301	Current Sensor	100%	100 Hz
16	Brake Tractive Effort Command/Jerk Limited (A-Car)	BTECJL#1	01122	Derived Signal	100%	100 Hz
17	Calculated Tractive Effort (A-Car)	TECALC	01124	Derived Signal	100%	100 Hz
18	Brake Tractive Effort Command/Jerk Limited (B-Car)	BTECJL#1	01123	Derived Signal	100%	100 Hz
19	Calculated Tractive Effort (B-Car)	TECALC	01125	Derived Signal	100%	100 Hz
20	Event	ET/A1	01422	Switch	---	---
21	Vehicle Speed (9th Wheel)	VS/A	01401	Electromagnetic Sensor	100 MPH	100 Hz
22	Distance	D/A	01421	Pulse Generator	10 Ft/Step	50 Hz
23	Brake Cylinder Pressure (A-Car, Rear Truck)	BCP/AR	01202	Strain Gage	75 PSIG	100 Hz
24	Brake Cylinder Pressure (B-Car, Forward Truck)	BCP/BF	01203	Strain Gage	75 PSIG	100 Hz
25	Brake Cylinder Pressure (A-Car, Forward Truck)	BCP/AF	01201	Strain Gage	75 PSIG	100 Hz
26	Brake Cylinder Pressure (B-Car, Rear Truck)	BCP/BR	01204	Strain Gage	75 PSIG	100 Hz
27	Tape Speed Reference	---	---	---	---	---
28	Voice	---	---	---	---	---

NOTE: THIS LISTING ACCOMPANIES TAPES #6564-004
6564-005

TEST SERIES: P-4001-TT

TABLE A-2. PERFORMANCE INSTRUMENTATION, SENSOR LISTING (BY DATA TAPES AND TEST SERIES, AS CITED).

CHANNEL NUMBER	PARAMETER	STANDARD OUTPUT NAME	MEASUREMENT NUMBER	SENSOR TYPE	MEASUREMENT RANGE	MAXIMUM CUTOFF FREQUENCY
1	IRIG-B Time	T/A	01411	Time Code Generator	---	1 KHz
2	Armature Current (A-Car, Forward Truck)	IAF	01103	Hall Effect Sensor	1000 Amps	100 Hz
3	Armature Current (A-Car, Rear Truck)	IAR	01104	Hall Effect Sensor	1000 Amps	100 Hz
4	BRK 1 #1 Trainline Current (A-Car)	BRK1#1	01118	Current Sensor	1 Amp	100 Hz
5	BRK 1 #2 Trainline Current (A-Car)	BRK1#2	01119	Current Sensor	1 Amp	100 Hz
6	Line Current (A-Car)	I LINE	01102	Hall Effect Sensor	1500 Amps	100 Hz
7	Line Voltage	E LINE	01101	Resistive Divider	1500 Volts	100 Hz
8	Armature Current (B-Car, Forward Truck)	IAF	01108	Hall Effect Sensor	1000 Amps	100 Hz
9	Armature Current (B-Car, Rear Truck)	IAR	01109	Hall Effect Sensor	1000 Amps	100 Hz
10	EP Valve Current (A-Car)	EP VALVE	01120	Derived Signal	1 Amp	100 Hz
11	EP Valve Current (B-Car)	EP VALVE	01121	Derived Signal	1 Amp	100 Hz
12	Line Current (B-Car)	I LINE	01107	Hall Effect Sensor	1500 Amps	100 Hz
13	Vehicle Acceleration	AP/A	02001	Servo Accelerometer	±5.4 MPHPS	3.15 Hz
14	Vehicle Speed	VS/A1	01402	Electromagnetic Sensor	100 MPH	100 Hz
15	P-Signal	CS/B	01301	Current Sensor	100%	100 Hz
16	Brake Tractive Effort Command/Jerk Limited (A-Car)	BTECJL#1	01122	Derived Signal	100%	100 Hz
17	Calculated Tractive Effort (A-Car)	TECALC	01124	Derived Signal	100%	100 Hz
18	Brake Tractive Effort Command/Jerk Limited (B-Car)	BTECJL#1	01123	Derived Signal	100%	100 Hz
19	Calculated Tractive Effort (B-Car)	TECALC	01125	Derived Signal	100%	100 Hz
20	Spin/Slide Indication (A-Car)	ANY S/S	01126	Derived Signal	Digit On/Off	100 Hz
21	Spin/Slide Indication (B-Car)	ANY S/S	01127	Derived Signal	Digit On/Off	100 Hz
22	Distance	D/A	01421	Pulse Generator	10 Ft/Step	50 Hz
23	Brake Cylinder Pressure (A-Car, Rear Truck)	BCP/AR	01202	Strain Gage	75 PSIG	100 Hz
24	Brake Cylinder Pressure (B-Car, Forward Truck)	BCP/BF	01203	Strain Gage	75 PSIG	100 Hz
25	Brake Cylinder Pressure (A-Car, Forward Truck)	BCP/AF	01201	Strain Gage	75 PSIG	100 Hz
26	Brake Cylinder Pressure (B-Car, Rear Truck)	BCP/BR	01204	Strain Gage	75 PSIG	100 Hz
27	Tape Speed Reference	---	---	---	---	---
28	Voice	---	---	---	---	---

NOTE: THIS LISTING ACCOMPANIES TAPE #6564-005
 6564-006
 6564-004

TEST SERIES: P-3001-TT P-3002-TT
 P-3003-TT P-3004-TT
 P-2001-TT P-2001-TT
 SPEN-QTP-01

TABLE A-3. PERFORMANCE INSTRUMENTATION, SENSOR LISTING (BY DATA TAPES AND TEST SERIES, AS CITED).

CHANNEL NUMBER	PARAMETER	STANDARD OUTPUT NAME	MEASUREMENT NUMBER	SENSOR TYPE	MEASUREMENT RANGE	MAXIMUM CUTOFF FREQUENCY
1	IRIG-B Time	T/A	01411	Time Code Generator	---	1 KHz
2	Armature Current (A-Car, Forward Truck)	IAF	01103	Hall Effect Sensor	1000 Amps	100 Hz
3	Armature Current (A-Car, Rear Truck)	IAR	01104	Hall Effect Sensor	1000 Amps	100 Hz
4	Field Flux Feedback (A-Car, Front Truck Fields)	ØFBF	01105	Hall Effect Sensor	100%	100 Hz
5	Field Flux Feedback (A-Car, Rear Truck Fields)	ØFBR	01106	Hall Effect Sensor	100%	100 Hz
6	Line Current (A-Car)	I LINE	01102	Hall Effect Sensor	1500 Amps	100 Hz
7	Line Voltage	E LINE	01101	Resistive Divider	1500 Volts	100 Hz
8	Armature Current (B-Car, Forward Truck)	IAF	01108	Hall Effect Sensor	1000 Amps	100 Hz
9	Armature Current (B-Car, Rear Truck)	IAR	01109	Hall Effect Sensor	1000 Amps	100 Hz
10	Field Flux Feedback (B-Car, Front Truck Fields)	ØFBF	01110	Hall Effect Sensor	100%	100 Hz
11	Field Flux Feedback (B-Car, Rear Truck Fields)	ØFBR	01111	Hall Effect Sensor	100%	100 Hz
12	Line Current (B-Car)	I LINE	01107	Hall Effect Sensor	1500 Amps	100 Hz
13	Vehicle Acceleration	AP/A	02001	Servo Accelerometer	±5.4 MPHPS	3.15 Hz
14	Vehicle Speed	VS/A1	01402	Electromagnetic Sensor	100 MPH	100 Hz
15	P-Signal	CS/B	01301	Current Sensor	100%	100 Hz
16	Drive Contactor (A-Car)	KDR	01112	Contact Closure	Digit Hi/Lo	100 Hz
17	Field Contactor (A-Car, 'A' Direction)	KFA	01114	Contact Closure	Digit Hi/Lo	100 Hz
18	Field Contactor (A-Car, 'B' Direction)	KFB	01116	Contact Closure	Digit Hi/Lo	100 Hz
19	Drive Contactor (B-Car)	KDR	01113	Contact Closure	Digit Hi/Lo	100 Hz
20	Field Contactor (B-Car, 'A' Direction)	KFA	01115	Contact Closure	Digit Hi/Lo	100 Hz
21	Field Contactor (B-Car, 'B' Direction)	KFB	01117	Contact Closure	Digit Hi/Lo	100 Hz
22	Distance	D/A	01421	Pulse Generator	10 Ft/Step	50 Hz
23	Tractive Effort Pause (A-Car)	TE PAUSE	01128	Derived Signal	Digit Hi/Lo	100 Hz
24	Tractive Effort Pause (B-Car)	TE PAUSE	01129	Derived Signal	Digit Hi/Lo	100 Hz
25	Brake Cylinder Pressure (A-Car, Forward Truck)	BCP/AF	01201	Strain Gage	75 PSIG	100 Hz
26	Brake Cylinder Pressure (B-Car, Rear Truck)	BCP/BR	01204	Strain Gage	75 PSIG	100 Hz
27	Tape Speed Reference	---	---	---	---	---
28	Voice	---	---	---	---	---

NOTE: THIS LISTING ACCOMPANIES TAPE #6564-004
6564-006

TEST SERIES: SPEN-QTP-01
SPEN-QTP-02
SPEN-QTP-04
P-2001-TT
P-3003-TT

TABLE A-4. PERFORMANCE INSTRUMENTATION, SENSOR LISTING (BY DATA TAPES AND TEST SERIES, AS CITED).

CHANNEL NUMBER	PARAMETER	STANDARD OUTPUT NAME	MEASUREMENT NUMBER	SENSOR TYPE	MEASUREMENT RANGE	MAXIMUM CUTOFF FREQUENCY
1	IRIG-B Time	T/A	01411	Time Code Generator	---	1 KHz
2	Line Voltage	E LINE	01101	Resistive Divider	1500 Volts	100 Hz
3	Line Current (A-Car)	I LINE	01102	Hall Effect Sesor	1500 Amps	100 Hz
4	Armature Current (A-Car, Forward Truck)	I AF	01103	Hall Effect Sensor	1000 Amps	100 Hz
5	Armature Current (A-Car, Rear Truck)	I AR	01104	Hall Effect Sesor	1000 Amps	100 Hz
6	Field Flux Feedback (A-Car, Front Truck Fields)	ØFBF	01105	Hall Effect Sensor	100%	100 Hz
7	Field Flux Feedback (A-Car, Rear Truck Fields)	ØFBR	01106	Hall Effect Sensor	100%	100 Hz
8	Traction Motor Armature Voltage Feedback (A-Car)	V EMF FB	01130	Resistive Divider	1500 Volts	100 Hz
9	Brake Resistor Current (A-Car)		01132	Current Probe	2000 Amps	100 Hz
10	Line Current (B-Car)	I LINE	01107	Hall Effect Sensor	1500 Amps	100 Hz
11	Armature Current (B-Car, Forward Truck)	I AF	01108	Hall Effect Sensor	1000 Amps	100 Hz
12	Armature Current (B-Car, Rear Truck)	I AR	01109	Hall Effect Sensor	1000 Amps	100 Hz
13	Field Flux Feedback (B-Car, Forward Truck)	ØFBF	01110	Hall Effect Sensor	100%	100 Hz
14	Field Flux Feedback (B-Car, Rear Truck)	ØFBR	01111	Hall Effect Sensor	100%	100 Hz
15	Traction Motor Armature Voltage Feedback (B-Car)	V EMF FB	01131	Resistive Divider	1500 Volts	100 Hz
16	Forward Field Current (B-Car)		01133	Hall Effect Sensor	31.5 Amps	100 Hz
17	Drive Contactor (B-Car)	KDR	01113	Contact Closure	Digit Hi/Lo	100 Hz
18	P-Signal	CS/B	01301	Current Probe	100%	100 Hz
19	Vehicle Speed	VS/A1	01402	Electromagnetic Sensor	100 MPH	100 Hz
20	Distance	D/A	01421	Pulse Generator	10 Ft/Step	50 Hz
21	Event	ET/A1	01422	Switch	---	---
22	Brake Cylinder Pressure (A-Car, Forward Truck)	BCP/AF	01201	Strain Gage	75 PSIG	100 Hz
23	Brake Cylinder Pressure (A-Car, Rear Truck)	BCP/AR	01202	Strain Gage	75 PSIG	100 Hz
24	Brake Cylinder Pressure (B-Car, Forward Truck)	BCP/BF	01203	Strain Gage	75 PSIG	100 Hz
25	Brake Cylinder Pressure (B-Car, Rear Truck)	BCP/BR	01204	Strain Gage	75 PSIG	100 Hz
26	ALD	ET/A2	01423	Displacement Sensor	---	100 Hz
27	Tape Speed Reference	---	---	---	---	---
28	Voice	---	---	---	---	---

NOTE: THIS LISTING ACCOMPANIES TAPE #6564-006

TEST SERIES: PC-5011-TT

TABLE A-5. PERFORMANCE INSTRUMENTATION, SENSOR LISTING (BY DATA TAPES AND TEST SERIES, AS CITED).

CHANNEL NUMBER	PARAMETER	STANDARD OUTPUT NAME	MEASUREMENT NUMBER	SENSOR TYPE	MEASUREMENT RANGE	MAXIMUM CUTOFF FREQUENCY
1	IRIG-B Time	T/A	01411	Time Code Generator	---	1 KHz
2	Axle #1 Speed (B-Car)	VS/B1	01406	Electromagnetic Sensor	100 MPH	10 Hz
3	Axle #2 Speed (B-Car)	VS/B2	01407	Electromagnetic Sensor	100 MPH	10 Hz
4	Axle #3 Speed (B-Car)	VS/B3	01408	Electromagnetic Sensor	100 MPH	10 Hz
5	Axle #4 Speed (B-Car)	VS/B4	01409	Electromagnetic Sensor	100 MPH	10 Hz
6	Vehicle Speed (9th Wheel)	VS/A	01401	Electromagnetic Sensor	100 MPH	10 Hz
7	Line Voltage	E LINE	01101	Resistive Divider	1500 Volts	100 Hz
8	Armature Current (B-Car, Forward Truck)	IAF	01108	Hall Effect Sensor	1000 Amps	100 Hz
9	Armature Current (B-Car, Rear Truck)	IAR	01109	Hall Effect Sensor	1000 Amps	100 Hz
10	Field Flux Feedback (B-Car, Front Truck Fields)	ØFBF	01110	Hall Effect Sensor	100%	100 Hz
11	Field Flux Feedback (B-Car, Rear Truck Fields)	ØFBR	01111	Hall Effect Sensor	100%	100 Hz
12	Line Current (B-Car)	I LINE	01107	Hall Effect Sensor	1500 Amps	100 Hz
13	Vehicle Acceleration	AP/A	02001	Servo Accelerometer	±5.4 MPHPS	3.15 Hz
14	Vehicle Speed (A-Car)	VS/A1	01402	Electromagnetic Sensor	100 MPH	10 Hz
15	P-Signal	CS/B	01301	Current Sensor	100%	100 Hz
16	Vehicle Speed (B-Car)	VS/B	01403	Electromagnetic Sensor	100 MPH	100 Hz
17	Tractive Effort Pause (B-Car)	TE PAUSE	01129	Derived Signal	Digit Hi/Lo	100 Hz
18	Tractive Effort/Load Weigh/Jerk Limited (B-Car)	TE LW JL	N/A	Derived Signal	100%	100 Hz
19	Calculated Tractive Effort (B-Car)	TECALC	01125	Derived Signal	100%	100 Hz
20	EP Valve Command #2 (B-Car)	EP VALVE CMD #2	N/A	Derived Signal	1 Amp	100 Hz
21	EP Valve Command #1 (B-Car)	EP VALVE CMD #1	N/A	Derived Signal	1 Amp	100 Hz
22	Distance	D/A	01421	Pulse Generator	10 Ft/Step	100 Hz
23	Slide Condition Detection (B-Car, Front Truck)	DUMP F	N/A	Derived Signal	Digit Hi/Lo	100 Hz
24	Brake Cylinder Pressure (B-Car, Front Truck)	BCP/BF	01203	Strain Gage	75 PSIG	100 Hz
25	Slide Condition Detection (B-Car, Rear Truck)	DUMP R	N/A	Derived Signal	Digit Hi/Lo	100 Hz
26	Brake Cylinder Pressure (B-Car, Rear Truck)	BCP/BR	01204	Strain Gage	75 PSIG	100 Hz
27	Tape Speed Reference	---	---	---	---	---
28	Voice	---	---	---	---	---

NOTE: THIS LISTING ACCOMPANIES TAPE #6564-007

TEST SERIES: P-2011-TP
P-3011-TP

TABLE A-6. PERFORMANCE INSTRUMENTATION, SENSOR LISTING (BY DATA TAPES AND TEST SERIES, AS CITED)

CHANNEL NUMBER	PARAMETER	STANDARD OUTPUT NAME	MEASUREMENT NUMBER	SENSOR TYPE	MEASUREMENT RANGE	MAXIMUM CUTOFF FREQUENCY
1	IRIG-B Time	T/A	01411	Time Code Generator	---	1 KHz
2	Armature Current (A-Car, Forward Truck)	IAF	01103	Hall Effect Sensor	1000 Amps	100 Hz
3	Armature Current (A-Car, Rear Truck)	IAR	01104	Hall Effect Sensor	1000 Amps	100 Hz
4	Field Flux Feedback (A-Car, Front Truck Fields)	ØFBF	01105	Hall Effect Sensor	100%	100 Hz
5	Field Flux Feedback (A-Car, Rear Truck Fields)	ØFBR	01106	Hall Effect Sensor	100%	100 Hz
6	Line Current (A-Car)	I LINE	01102	Hall Effect Sensor	1500 Amps	100 Hz
7	Line Voltage	E LINE	01101	Resistive Divider	1500 Volts	100 Hz
8	Armature Current (B-Car, Forward Truck)	IAF	01108	Hall Effect Sensor	1000 Amps	100 Hz
9	Armature Current (B-Car, Rear Truck)	IAR	01109	Hall Effect Sensor	1000 Amps	100 Hz
10	Field Flux Feedback (B-Car, Front Truck Fields)	ØFBF	01110	Hall Effect Sensor	100%	100 Hz
11	Field Flux Feedback (B-Car, Rear Truck Fields)	ØFBR	01111	Hall Effect Sensor	100%	100 Hz
12	Line Current (B-Car)	I LINE	01107	Hall Effect Sensor	1500 Amps	100 Hz
13	Vehicle Acceleration	AP/A	02001	Servo Accelerometer	±5.4 MPHPS	100 Hz
14	Vehicle Speed	VS/A1	01402	Electromagnetic Sensor	100 MPH	100 Hz
15	P-Signal	CS/B	01301	Current Sensor	100%	100 Hz
16	ALD	ET/A2	01423	Displacement Sensor	---	100 Hz
17	Field Contactor (A-Car, 'A' Direction)	KFA	01114	Contact Closure	Digit Hi/Lo	100 Hz
18	Field Contactor (A-Car, 'B' Direction)	KFB	01116	Contact Closure	Digit Hi/Lo	100 Hz
19	Dirve Contactor (B-Car)	KDR	01113	Contact Closure	Digit Hi/Lo	100 Hz
20	Field Contactor (B-Car, 'A' Direction)	KFA	01115	Contact Closure	Digit Hi/Lo	100 Hz
21	Vehicle Speed (9th Wheel)	VS/A	01401	Electromagnetic Sensor	100 MPH	100 Hz
22	Distance	D/A	01421	Pulse Generator	10 Ft/Step	100 Hz
23	Tractive Effort Pause (A-Car)	TE PAUSE	01128	Derived Signal	Digit Hi/Lo	100 Hz
24	Tractive Effort Pause (B-Car)	TE PAUSE	01129	Derived Signal	Digit Hi/Lo	100 Hz
25	Brake Cylinder Pressure (A-Car, Front Truck)	BCP/AF	01201	Strain Gage	75 PSIG	100 Hz
26	Brake Cylinder Pressure (B-Car, Rear Truck)	BCP/AR	01204	Strain Gage	75 PSIG	100 Hz
27	Tape Speed Reference	---	---	---	---	---
28	Voice	---	---	---	---	---

NOTE: THIS LISTING ACCOMPANIES TAPE #6564-008

TEST SERIES: P-2001-TT

TABLE A-7. PERFORMANCE INSTRUMENTATION, SENSOR LISTING (BY DATA TAPES AND TEST SERIES, AS CITED).

CHANNEL NUMBER	PARAMETER	STANDARD OUTPUT NAME	MEASUREMENT NUMBER	SENSOR TYPE	MEASUREMENT RANGE	MAXIMUM CUTOFF FREQUENCY
1	IRIG-B Time	T/A	01411	Time Code Generator	---	1 KHz
2	Armature Current (A-Car, Forward Truck)	IAF	01103	Hall Effect Sensor	1000 Amps	100 Hz
3	Armature Current (A-Car, Rear Truck)	IAR	01104	Hall Effect Sensor	1000 Amps	100 Hz
4	Field Flux Feedback (A-Car, Front Truck Fields)	ØFBB	01105	Hall Effect Sensor	100%	100 Hz
5	ALD	ET/A2	01423	Displacement Sensor	---	100 Hz
6	Line Current (A-Car)	I LINE	01102	Hall Effect Sensor	1500 Amps	100 Hz
7	Line Voltage	E LINE	01101	Resistive Divider	1500 Volts	100 Hz
8	Armature Current (B-Car, Forward Truck)	IAF	01108	Hall Effect Sensor	1000 Amps	100 Hz
9	Armature Current (B-Car, Rear Truck)	IAR	01109	Hall Effect Sensor	1000 Amps	100 Hz
10	Field Flux Feedback (B-Car, Front Truck Fields)	ØFBB	01110	Hall Effect Sensor	100%	100 Hz
11	Field Flux Feedback (B-Car, Rear Truck Fields)	ØFBR	01111	Hall Effect Sensor	100%	100 Hz
12	Line Current (B-Car)	I LINE	01107	Hall Effect Sensor	1500 Amps	100 Hz
13	Vehicle Acceleration	AP/A	02001	Servo Accelerometer	±5.4 MPHPS	100 Hz
14	Vehicle Speed	VS/A1	01402	Electromagnetic Sensor	100 MPH	100 Hz
15	P-Signal	CS/B	01301	Current Sensor	100%	100 Hz
16						
17	Field Contactor (A-Car, 'A' Direction)	KFA	01114	Contact Closure	Digit Hi/Lo	100 Hz
18	Field Contactor (A-Car, 'B' Direction)	KFB	01116	Contact Closure	Digit Hi/Lo	100 Hz
19	Dirve Contactor (B-Car)	KDR	01113	Contact Closure	Digit Hi/Lo	100 Hz
20	Field Contactor (B-Car, 'A' Direction)	KFA	01115	Contact Closure	Digit Hi/Lo	100 Hz
21	Vehicle Speed (9th Wheel)	VS/A	01401	Electromagnetic Sensor	100 MPH	100 Hz
22	Distance	D/A	01421	Pulse Generator	10 Ft/Step	100 Hz
23	Brake Cylinder Pressure (A-Car, Rear Truck)	BCP/AR	01202	Strain Gage	75 PSIG	100 Hz
24	Brake Cylinder Pressure (B-Car, Front Truck)	BCP/BF	01203	Strain Gage	75 PSIG	100 Hz
25	Brake Cylinder Pressure (A-Car, Front Truck)	BCP/AF	01201	Strain Gage	75 PSIG	100 Hz
26	Brake Cylinder Pressure (B-Car, Rear Truck)	BCP/AR	01204	Strain Gage	75 PSIG	100 Hz
27	Tape Speed Reference	---	---	---	---	---
28	Voice	---	---	---	---	---

NOTE: THIS LISTING ACCOMPANIES TAPE #6564-008

TEST SERIES: P-3002-TT P-3003-TT
P-3004-TT P-2001-TT
P-4001-TT

user. A series of sensors were mounted on the front truck of car 0110 to measure truck rotation, bump stop travel, and axle journal and sideframe accelerations.

String pot type displacement transducers were mounted between the car-body and the truck sideframes to measure longitudinal and lateral displacements, from which truck rotation angles could be computed. String pots were also mounted between the truck sideframes and the bolster to measure bump stop travel on each side of the truck. Vertical and lateral accelerations of the lead axle of the truck were sensed with piezo resistive type accelerometers mounted on the journal bearing sleeves. Vertical and lateral accelerations of the truck sideframes were sensed with capacitance type accelerometers mounted at the front and rear of the sideframes.

The lists of sensors recorded for each test series and analog tape of the ride quality test program (with standard output name and measurement number) are to be found in tables A-8, A-9 and A-10. Photographs and sketches detailing the exact location of the sensors are available on file at TTC.

TABLE A-8. RIDE QUALTY INSTRUMENTATION, SENSOR LISTING (BY DATA TAPES AND TEST SERIES, AS CITED).

CHANNEL NUMBER	PARAMETER	STANDARD OUTPUT NAME	MEASUREMENT NUMBER	SENSOR TYPE	MEASUREMENT RANGE	MAXIMUM CUTOFF FREQUENCY
1	IRIG-B Time	T/A	01411	Time Code Generator	---	1 KHz
2	Body Vertical Acceleration (Car CL Floor, Over Lead Truck)	AC/A1	02101	Servo Accelerometer	±0.5 g	100 Hz
3	Body Lateral Acceleration (Car CL Floor, Over Lead Truck)	AC/A2	02102	Servo Accelerometer	±0.5 g	100 Hz
4	Body Longitudinal Acceleration (Car CL Floor, Over Lead Truck)	AC/A3	02103	Servo Accelerometer	±0.5 g	100 Hz
5	Body Vertical Acceleration (Car CL Floor, Middle Car)	AC/A4	02104	Servo Accelerometer	±0.5 g	100 Hz
6	Body Lateral Acceleration (Car CL Floor, Middle Car)	AC/A5	02105	Servo Accelerometer	±0.5 g	100 Hz
7	Body Vertical Acceleration (Car Floor, Middle Car-Left)	AC/A6	02106	Servo Accelerometer	±0.5 g	100 Hz
8	Journal Vertical Acceleration (Lead Truck, Lead Axle-Right)	AJ/A1	02201	Piezo Accelerometer	± 10 g	1 KHz
9	Journal Lateral Acceleration (Lead Truck, Lead Axle-Right)	AJ/A2	02202	Piezo Accelerometer	± 3 g	1 KHz
10	Journal Vertical Acceleration (Lead Truck, Lead Axle-Left)	AJ/A3	02203	Piezo Accelerometer	± 10 g	1 KHz
11	ALD (Automatic Location Detector)	ET/A2	01423	Displacement Sensor	---	10 Hz
12	Vehicle Speed	VS/A1	01402	Electromagnetic Sensor	100 MPH	10 Hz
13	P-Signal	CS/B	01301	Current Sensor	100%	10 Hz
14	Vehicle Acceleration	AP/A	02001	Servo Accelerometer	±5.4 MPHPS	3.15 Hz
15	Distance	D/A	01421	Pulse Generator	10 Ft/Step	100 Hz
16	Speed (9th Wheel)	VS/A	01401	Electromagnetic Sensor	100 MPH	10 Hz
17	Event	ET/A1	01422	Switch	---	---
27	Tape Speed Reference					
28	Voice					

NOTE: THIS LISTING ACCOMPANIES TAPES #6564-001
#6564-002

TEST SERIES: R-0010-TT
R-1101-TT
R-2001-TT
R-3001-TT

TABLE A-9. RIDE QUALTY INSTRUMENTATION, SENSOR LISTING (BY DATA TAPES AND TEST SERIES, AS CITED).

CHANNEL NUMBER	PARAMETER	STANDARD OUTPUT NAME	MEASUREMENT NUMBER	SENSOR TYPE	MEASUREMENT RANGE	MAXIMUM CUTOFF FREQUENCY
1	IRIG-B Time	T/A	01411	Time Code Generator	---	1 KHz
2	Body Vertical Acceleration (Car CL Floor, Over Lead Truck)	AC/A1	02101	Servo Accelerometer	±0.5 g	100 Hz
3	Body Lateral Acceleration (Car CL Floor, Over Lead Truck)	AC/A2	02102	Servo Accelerometer	±0.5 g	100 Hz
4	Body Longitudinal Acceleration (Car CL Floor, Over Lead Truck)	AC/A3	02103	Servo Accelerometer	±0.5 g	100 Hz
5	Body Vertical Acceleration (Car CL Floor, Middle Car)	AC/A4	02104	Servo Accelerometer	±0.5 g	100 Hz
6	Body Lateral Acceleration (Car CL Floor, Middle Car)	AC/A5	02105	Servo Accelerometer	±0.5 g	100 Hz
7	Body Vertical Acceleration (Car Floor, Middle Car-Left)	AC/A6	02106	Servo Accelerometer	±0.5 g	100 Hz
8	Journal Vertical Acceleration (Lead Truck, Lead Axle-Right)	AJ/A1	02201	Piezo Accelerometer	± 10 g	1 KHz
9	Journal Lateral Acceleration (Lead Truck, Lead Axle-Right)	AJ/A2	02202	Piezo Accelerometer	± 3 g	1 KHz
10	Journal Vertical Acceleration (Lead Truck, Lead Axle-Left)	AJ/A3	02203	Piezo Accelerometer	± 10 g	1 KHz
11	Truck Vertical Acceleration (Right Sideframe, Lead End)	ASF/A1	02205	Capacitance Accelerometer	± 5 g	1 KHz
12	Truck Lateral Acceleration (Right Sideframe, Lead End)	ASF/A2	02206	Capacitance Accelerometer	± 5 g	1 KHz
13	Truck Vertical Acceleration (Left Sideframe, Lead End)	ASF/A3	02204	Capacitance Accelerometer	± 5 g	1 KHz
14	Truck Vertical Acceleration (Left Sideframe, Trail End)	ASF/A4	02209	Capacitance Accelerometer	± 5 g	1 KHz
15	Truck Vertical Acceleration (Right Sideframe, Trail End)	ASF/A5	02207	Capacitance Accelerometer	± 5 g	1 KHz
16	Truck Lateral Acceleration (Right Sideframe, Trail End)	ASF/A6	02208	Capacitance Accelerometer	± 5 g	1 KHz
17	Body/Truck Long. Disp. (Sideframe to Body, Lead Truck-Right)	STPD/C1	06101	Displacement Sensor	±2.5 Inches	25 Hz
18	Body/Truck Long. Disp. (Sideframe to Body, Lead Truck-Left)	STPD/C2	06102	Displacement Sensor	±2.5 Inches	25 Hz
19	Body Truck Lateral Disp. (Sideframe to Body, Lead Truck)	STPD/C3	06103	Displacement Sensor	±1.5 Inches	25 Hz
20	Bolster/Truck Vertical Disp. (Left Bump Stop)	STPD/C4	06104	Displacement Sensor	±2.5 Inches	25 Hz
21	Bolster/Truck Vertical Disp. (Right Bump Stop)	STPD/C5	06105	Displacement Sensor	±2.5 Inches	25 Hz
22	Vehicle Speed	VS/A	01401	Electromagnetic Sensor	100 MPH	10 Hz
23	Distance	D/A	01421	Pulse Generator	10 Ft/Step	50 Hz
24	Event	ET/A1	01422	Switch	---	---
25	ALD	ET/A2	01423	Displacement Sensor	---	10 Hz
26	Vehicle Acceleration	AP/A	02001	Servo Accelerometer	±5.4 MPHPS	3.15 Hz
27	Tape Speed Reference	---	---	---	---	---
28	Voice	---	---	---	---	---

NOTE: THIS LISTING ACCOMPANIES TAPES #6584-002
6564-003

TEST SERIES: R-1101-TT
R-2001-TT
R-3001-TT

TABLE A-10. RIDE QUALITY INSTRUMENTATION, SENSOR LISTING (BY DATA TAPES AND TEST SERIES, AS CITED).

CHANNEL NUMBER	PARAMETER	STANDARD OUTPUT NAME	MEASUREMENT NUMBER	SENSOR TYPE	MEASUREMENT RANGE	MAXIMUM CUTOFF FREQUENCY
1	Voice	---	---	---	---	---
2	Armature Current (A-Car, Forward Truck)	IAF	01103	Hall Effect Sensor	1000 Amps	100 Hz
3	Armature Current (A-Car, Rear Truck)	IAR	01104	Hall Effect Sensor	1000 Amps	100 Hz
4	Armature Current (B-Car, Forward Truck)	IAF	01108	Hall Effect Sensor	1000 Amps	100 Hz
5	Armature Current (B-Car, Rear Truck)	IAR	01109	Hall Effect Sensor	1000 Amps	100 Hz
6	Line Current (A-Car)	I-LINE	01102	Hall Effect Sensor	1500 Amps	100 Hz
7	Line Voltage	E-LINE	01101	Resistive Divider	1500 Volts	100 Hz
8	Vehicle Acceleration	AP/A	02001	Servo Accelerometer	±5.4 MPHPS	3.15 Hz
9	Speed (9th Wheel)	VS/A	01401	Proximity Sensor	100 MPH	10 Hz
10						
11	ALD	ET/A	01422	Displacement Sensor	---	100 Hz
12	Distance	D/A	01421	Pulse Generator	10 Ft/Step	10 Hz
13	Brake Cylinder Pressure (A-Car, Front Truck)	BCP/AF	01201	Strain Gage	100 PSIG	100 Hz
14	Brake Cylinder Pressure (A-Car, Trail Truck)	BCP/AR	01202	Strain Gage	100 PSIG	100 Hz
15	Brake Cylinder Pressure (B-Car, Front Truck)	BCP/BF	01203	Strain Gage	100 PSIG	100 Hz
16	Brake Cylinder Pressure (B-Car, Trail Truck)	BCP/BR	01204	Strain Gage	100 PSIG	100 Hz
17	Body Vertical Acceleration (Car CL Floor, Over Lead Truck)	AC/A1	02101	Servo Accelerometer	±0.5 g	100 Hz
18	Body Lateral Acceleration (Car CL Floor, Over Lead Truck)	AC/A2	02102	Servo Accelerometer	±0.5 g	100 Hz
19	Body Longitudinal Acceleration (Car CL Floor, Over Lead Truck)	AC/A3	02103	Servo Accelerometer	±0.5 g	100 Hz
20	Body Vertical Acceleration (Car CL Floor, Middle Car)	AC/A4	02104	Servo Accelerometer	±0.5 g	100 Hz
21	Body Lateral Acceleration (Car CL Floor, Middle Car)	AC/A5	02105	Servo Accelerometer	±0.5 g	100 Hz
22	Body Vertical Acceleration (Car Floor, Middle Car-Left)	AC/A6	02106	Servo Accelerometer	±0.5 g	100 Hz
23	Body Vertical Acceleration (Car CL Floor, Over Trail Truck)	AC/A12	02112	Servo Accelerometer	±0.5 g	100 Hz
24	Body Lateral Acceleration (Car CL Floor, Over Trail Truck)	AC/A9	02109	Servo Accelerometer	±0.5 g	100 Hz
25						
26	Event	ET/A	01423	Switch	---	---
27	Tape Speed Reference	---	---	---	---	---
28	IRIG-B Time	T/A	01411	Time Code Generator	---	1 KHz

NOTE: THIS LISTING ACCOMPANIES TAPE #6564-009

TEST SERIES: R-2010-TT

2.0 DATA ACQUISITION

The onboard analog data acquisition system for the performance and ride quality tests consisted of signal conditioning, filters, strip chart recorders, and one 28-track tape recorder. A schematic of the basic system is shown in figure A-1. The data acquisition system, as implemented onboard the vehicle, is shown in figures A-2 and A-3 (onboard test panel).

2.1 SIGNAL CONDITIONING AND MONITORING ELECTRONICS

The signal conditioning system, an ENDEVCO 4470 unit, provided excitation voltages for transducers, sensors, and for preconditioning circuits. The 4470 also provided amplification as required to normalize all analog signals to a ± 5 V level. The SM-1 signal monitor provides real-time static monitoring (digital multimeter) and dynamic monitoring (oscilloscope) of any analog data signals. The signal conditioning system is described below, and the signal monitoring system is described in detail in a standard instrumentation manual.²

The 4470 has 35 separate channels, each of which is composed of a modular unit and a plug-in mode card. Seven rack adapters provide for mounting of the modules in a standard 19" rack, five modules per adapter, and provide interconnections for power, signal input, signal output, and monitor and calibration functions. The modular unit is a package containing circuit instrument power supply, calibration circuits, and interconnections for each plug-in mode card.

The mode card contains circuit components designed for a specific type of signal conditioning. Conditioning functions of the measurement system are all routed through the mode card, and the function of a particular module is 'specialized' by the card installed. Any module can be used to perform any conditioning function by installing the appropriate card. Cards may have a standard circuit configuration or a custom circuit. The block diagram and interconnection of the cards are shown in figure A-1.

2.2 SIGNAL FILTERING ELECTRONICS

An Ithaco type 4113 system was used to enhance the signal-to-noise ratio of the measurement systems and to minimize signal 'aliasing' during digitization. The system is made up of 32 separate channels of low-pass filter networks. Each channel is switch-selectable between 4-pole Bessel (linear phase delay) or 4-pole Butterworth (maximum flat amplitude response) filter characteristics. The cutoff frequency of each channel can be varied from 1 Hz to 1 MHz. Each of the separate filters (Ithaco 4113M101) is an integral

² General Vehicle Test Instrumentation Manual, Report No. UMTA-MA-06-0025-77-17.

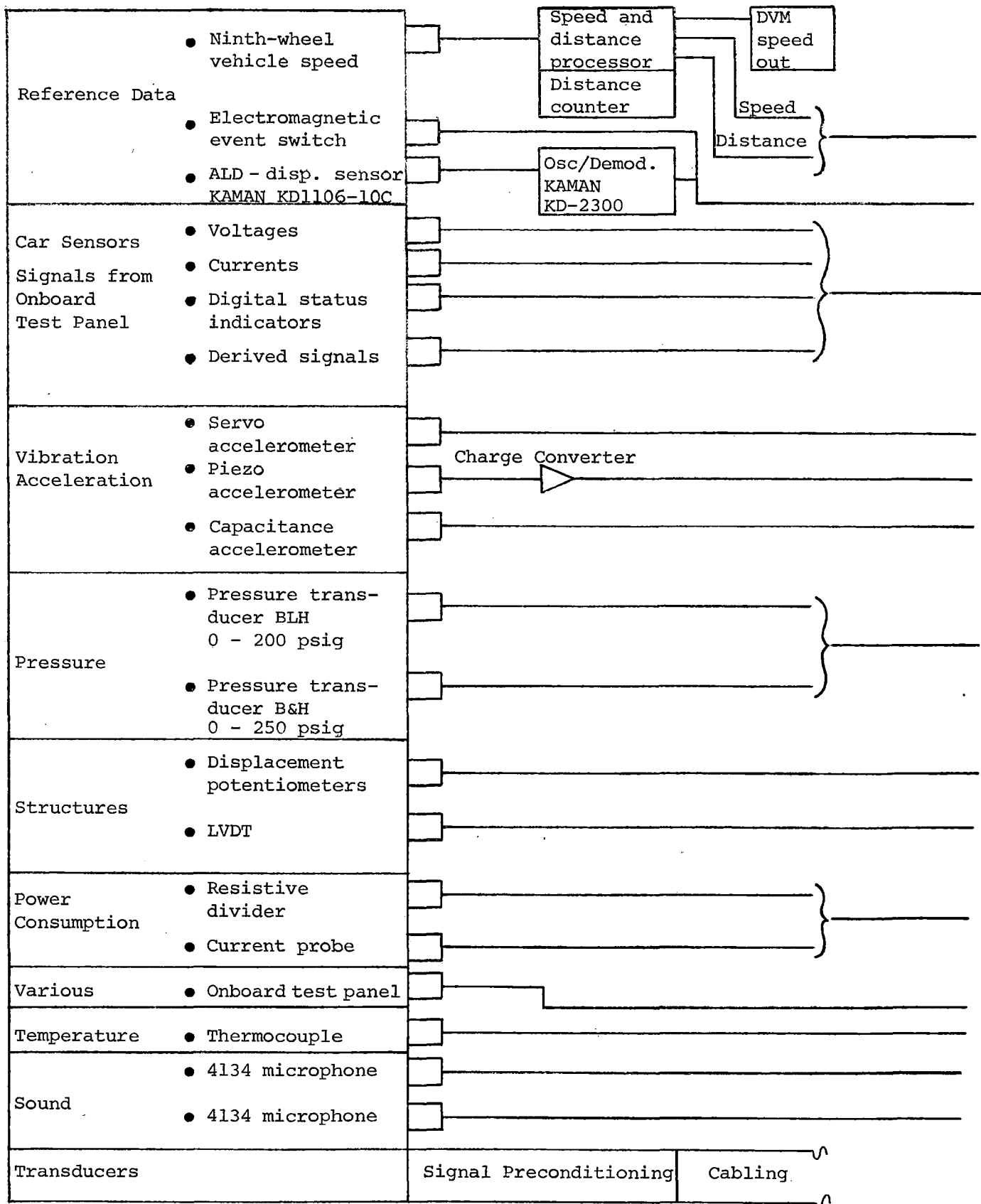
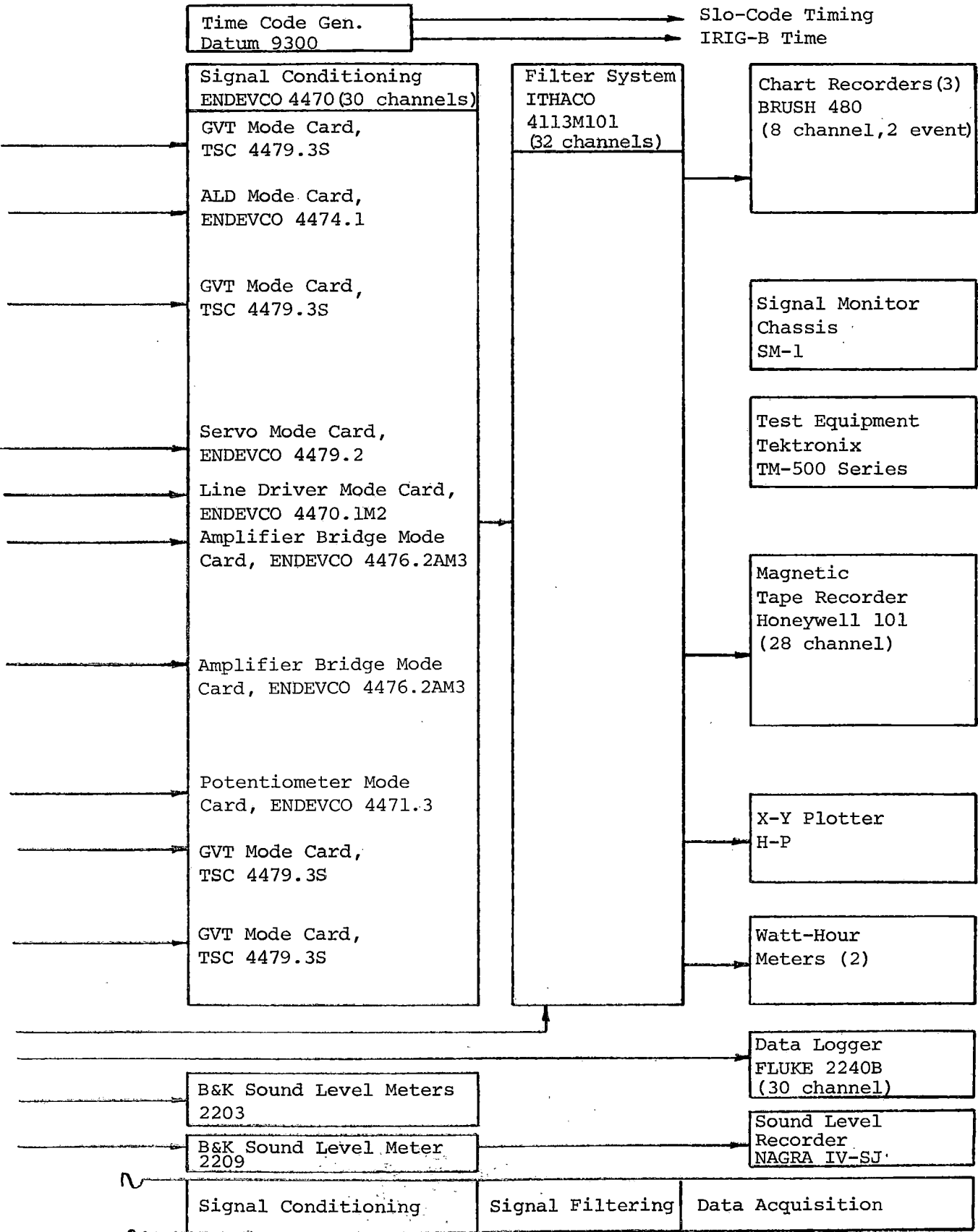


FIGURE A-1. BLOCK DIAGRAM, DATA ACQUISITION SYSTEM.



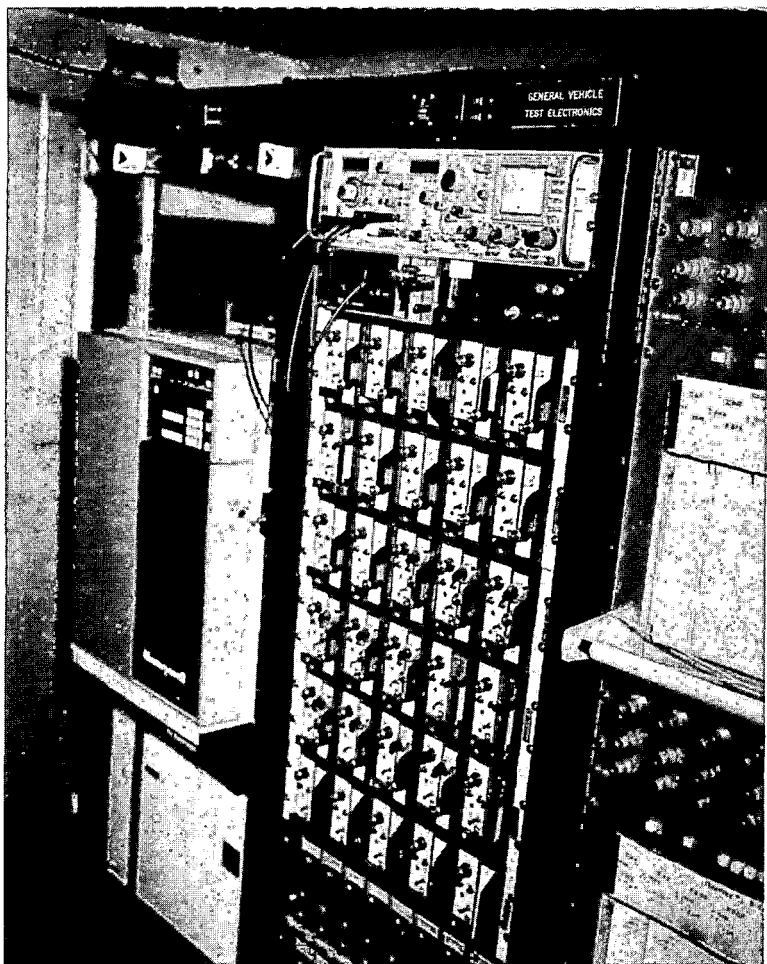


FIGURE A-2. GENERAL VEHICLE TEST ELECTRONICS.

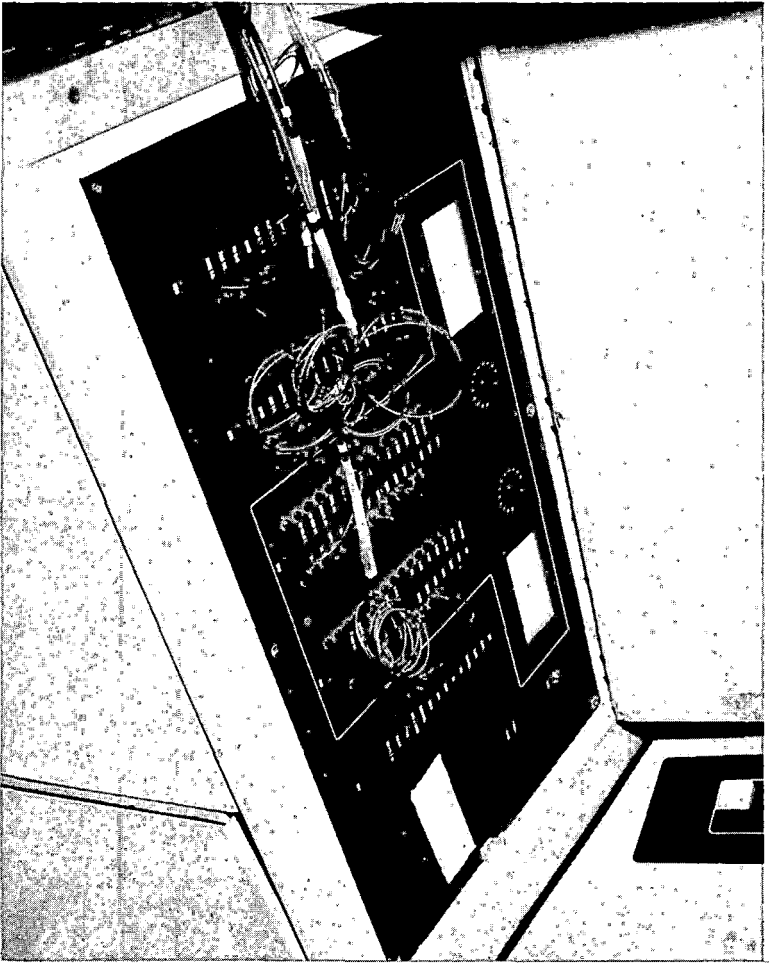


FIGURE A-3. MARTA ONBOARD TEST PANEL.

modular unit. Eight of these modules were installed in a rack-mounted adapter which provided a common a.c. power input, switch, indicator lamp, and fuse.

2.3 STRIP CHART RECORDERS

The strip chart recorders that were used to monitor test progress online consisted of three Brush model 480 8-channel recorders.

2.4 TAPE RECORDER

The analog tape recorder used was a Honeywell model 101 portable magnetic tape recorder/reproducer with microcomputer control. The tape heads were 28 track, IRIG configuration.

The tape recorder setup for testing is listed in table A-11.

TABLE A-11. TAPE RECORDER CONFIGURATION.

Track No.	Record/Reproduce	Data
1	Direct	IRIG-B time code
2-26	FM	Data channels
27	FM (Shorted input to record center frequency as a reference signal)	
28	Voice	Voice

Note: The FM data channels were set for signal full-scale = 40% deviation, at a tape speed of 1-7/8 in/s. The center frequency was 3.375 kHz with +40% = 4.725 kHz and -40% = 2.025 kHz.

2.5 X-Y PLOTTER

A Hewlett-Packard 70048 X-Y analog plotter was onboard the cars during the performance test phase, to plot acceleration/deceleration versus speed from conditioned inputs from the data acquisition system.

2.6 NINTH WHEEL SPEED AND DISTANCE PROCESSOR

The ninth wheel speed and distance processor was fabricated by Garrett-Airesearch, Inc. The unit provides excitation for an electromagnetic sensor mounted on the ninth wheel assembly under the car, and in turn receives pulses from the sensor caused by a 60 tooth gear wheel (attached to the ninth wheel) rotating in its magnetic field. As the wheel rotates, the sensor produces a pulsed signal whose frequency is proportional to the rotational speed of the wheel. The processor accepts this signal and produces an analog output voltage proportional to speed, together with a staircase function distance signal. The circuitry within the processor can apply scaling factors to suit the circumference of the ninth wheel and the number of pulses per revolution from the toothed gear wheel. The staircase distance signal is comprised of a series of ten additive step functions which reset to zero output voltage after every tenth step. A scaling factor can be set in the processor to equate each step to 0.1', 1', or 10'.

2.7 ENERGY CONSUMPTION WATT-HOUR METER

Energy consumption data were acquired during the test program by means of a watt-hour chassis, designed and constructed at the TTC. The chassis used an analog multiplier to provide an output, from scaled voltage inputs of voltage and current sensors, proportional to instantaneous power consumption. The output of the multiplier was then integrated with respect to time by an integrating voltage-frequency converter. This device produced a pulse frequency proportional to applied voltage. Each pulse represented an increment of energy, the sum of which represented total energy. Output from the frequency converter was then conditioned in a divider/counter driver circuit, using three scaleable counters and a monostable multivibrator. This driver circuit acted as a pulse stretcher to increase the pulse width to the 20-ms minimum required to drive a 6-digit mechanical counter (one for each car of a married pair), which totalled power consumption over the duration of a test run.

A functional description of the system³ and a circuit diagram of the watt/hour meter chassis⁴ are maintained by the TTC.

³ "Functional Description of Watt-Hour Meter," Memo IE/DG/76-109, Transportation Test Center, November 23, 1976.

⁴ "Drawing Number SK-RDL-4255," Transportation Test Center, January 4, 1977.

3.0 DATA PROCESSING

The following paragraphs describe the methods used to select data slices of interest for post-test data processing, and the analog and digital data presentation techniques used for the data in this report.

3.1 DIGITAL PROCESSING

3.1.1 Data Selection

Up to 27 channels of analog data were recorded with an IRIG time code on magnetic tape onboard the test vehicle. Selected data were simultaneously recorded on three strip chart recorders, also on the vehicles; these were used to assure the quality of the data, to monitor the progress of the test, and to make engineering judgements to direct the course of the test. At least once during the test day, the data recorded on magnetic tape, together with the calibration levels for each channel, were played back through the strip chart recorders to ensure that the signal levels were as expected.

Time slices of data to be analyzed were selected by reviewing the strip chart and noting the start and stop times of the period of interest, using the 'Slow Code' binary time code on the chart to determine the time of day of the record. The analog tapes were then forwarded to TTC Data Processing for digitizing, with tape logs detailing the start and stop times required and the data channels of interest.

3.1.2 Performance Data

The performance data which were treated digitally were digitized at a rate of 32 samples per second and converted to engineering units. The digitized output was assembled on tape for further processing on a DEC 11/60 computer. An optional engineering unit listing was available at this stage for direct use by the analyst, and for validation of the conversion process. Channels of interest were extracted from the tape and placed on file in the 11/60 computer. From the files they were accessed and processed using the Data Reduction System (DRS) software package to produce report quality graphics. A performance data processing flow chart is shown in figure A-4.

3.1.3 Ride Quality Data

The ride quality data to be processed digitally were digitized at 256 samples/s from time slices selected by the analyst from the chart records of the test. Data for processing on the DEC 11/60 computer were assembled on a digital tape from which selected channels were extracted and placed in file. From here the data were processed and analyzed interactively using the DRS software. The data could be examined in the time domain (time histories) or

the frequency domain using Fast Fourier Transform algorithms. Conversion of the digital tape format from 1,600 bits/in to 800 bits/in was used to make the data compatible with the Varian V76 computer, which allowed the use of the TTC DRS software. This allowed access to further processing techniques to compute rms, average acceleration values, and acceleration weighted in the frequency domain for human whole-body response to vibration, to International Standards Organization standards.⁵ Weighting acceleration data in this manner is a technique used to enhance those frequencies present which have the most adverse effect on the human body. A flow chart of the ride quality data processing methods is shown in figure A-5.

3.2 ANALOG DATA PROCESSING

3.2.1 Performance Data

Performance acceleration and deceleration versus speed plots were obtained directly onboard the cars using scaled analog inputs to an X-Y plotter. The plotter was patched in parallel with the tape recorder and the chart recorders, allowing data plots to be produced as the test runs were conducted. Scaling of the plotter was obtained directly from the check calibration of the longitudinal accelerometer for the acceleration input, and from an oscillator input to the speed and distance processor representing a known speed for the vehicle speed input.

3.2.2 Ride Quality Data

Selected ride quality data channels were processed using analog techniques, post-test. The analog tapes were played back on a tape recorder and the channel of interest was fed into an rms averaging filter network; the signal was averaged over a 1-s time window and plotted versus vehicle speed on an X-Y plotter.

⁵ Guide for the Evaluation of Human Exposure to Whole-Body Vibration, ISO2631-1978(E) TC-108.

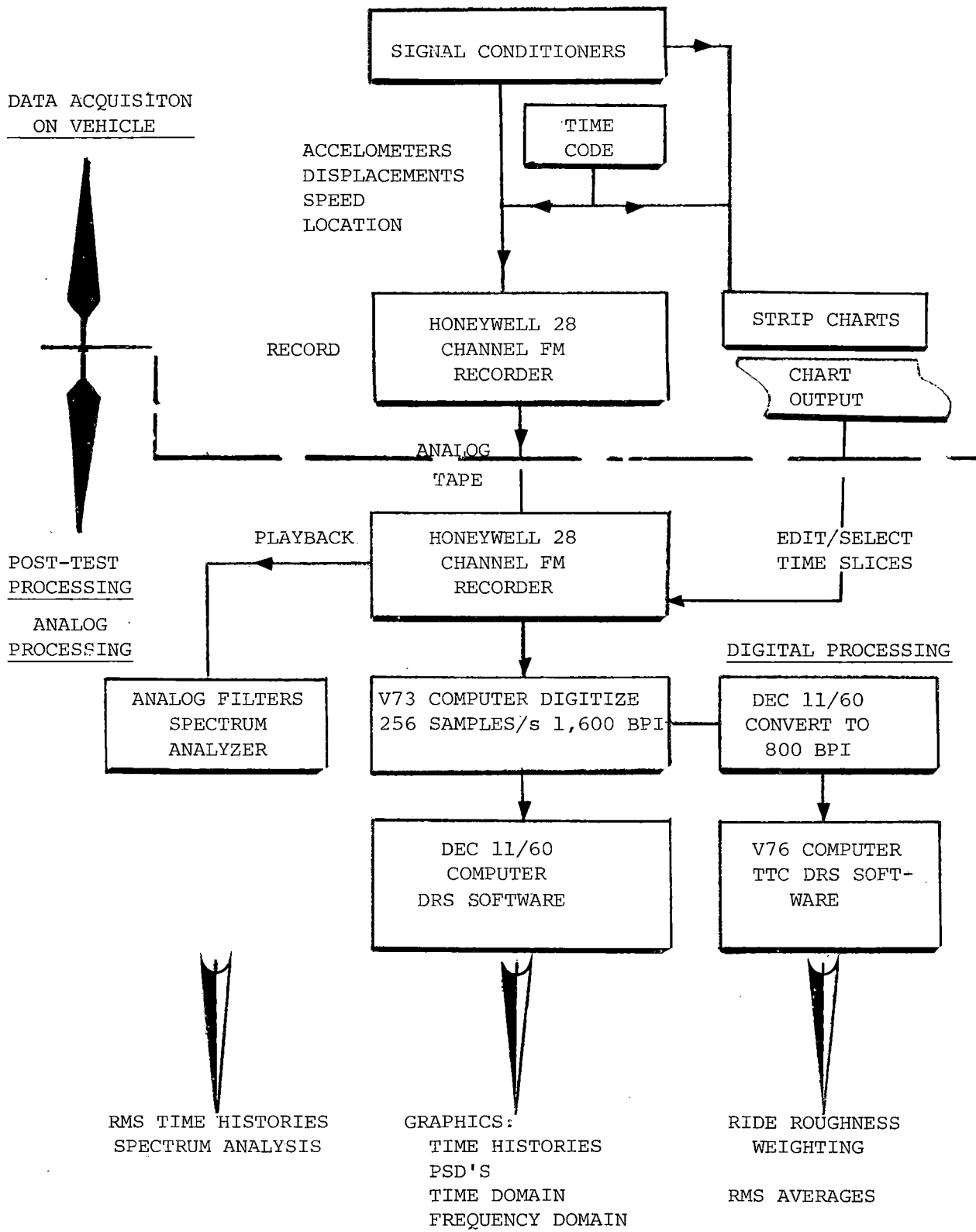


FIGURE A-5. RIDE QUALITY DATA PROCESSING FLOW CHART.